NBSIR 83-2742 (R)

Photonuclear Data-Abstract Sheets 1955 - 1982 Volume II (Lithium-Boron)

U.S. DEPARTMENT OF COMMERCE
National Bureau of Standards
National Measurement Laboratory
Center for Radiation Research
Washington, D.C. 20234

July 1983

DEPARTMENT OF COMMERCE
ONAL BUREAU OF STANDARDS

NBSIR 83-2742

PHOTONUCLEAR DATA—ABSTRACT SHEETS 1955 - 1982 VOLUME II (LITHIUM-BORON)

E. G. Fuller, Henry Gerstenberg

U.S. DEPARTMENT OF COMMERCE
National Bureau of Standards
National Measurement Laboratory
Center for Radiation Research
Washington, D.C. 20234

July 1983

U.S. DEPARTMENT OF COMMERCE, Malcolm Baldrige, *Secretary*
NATIONAL BUREAU OF STANDARDS, Ernest Ambler, *Director*

TABLE OF CONTENTS

Photonuclear Data-Abstract Sheets
1955-1982

I. Introduction

As used in connection with this collection of data-abstract sheets, the term photonuclear data is taken to mean any data leading to information on the electromagnetic matrix element between the ground state and excited states of a given nuclide. The most common types of reactions included in this compilation are: (e,e'), (γ,γ), (γ,γ'), (γ,n), (γ,p), etc. as well as ground-state particle capture reactions, e.g. (α,γ_0). Two reactions which fit the matrix element criterion are not included in the compilation because of their rather special nature. These are heavy particle Coulomb excitation and the thermal neutron capture reaction (n,γ_0). While the energy region of particular interest extends from 0 to 150 MeV, papers are indexed which report measurements in the region from 150 MeV to 4 GeV. Most of the experiments listed are concerned with the excitation energy range from 8 to 30 MeV, the region of the photonuclear giant resonance.

The hierarchical grouping of the photonuclear data-abstract sheets within the file is by: 1. Target Element, 2. Target Isotope, and 3. by the Bibliographic Reference Code assigned to the paper from which the data on the sheet were abstracted. In this file, colored pages are used to mark the beginning and end of the sheets for each chemical element. A brief historical sketch of the element is given on the divider sheet marking the start of each section; the information for this sketch was derived from references such as the Encyclopaedia Britannica. In those cases where the sheets for a given element make up a major part of a volume, colored pages are also used to delineate sections pertaining to the individual isotopes of the element. Each of the sections of the file, as delineated by two colored divider sheets, represents a 27 year history of the study of electromagnetic interactions in either a specific nuclide or a specifc element.

The data-abstract sheets are filed under the element and/or isotope in which the ground-state electromagnetic transition takes place. For example, the abstract sheet for a total neutron yield measurement for a naturally occurring copper sample would appear in the elemental section of the copper file. On the other hand, a measurement of the ^{62}Cu 9.73 minute positron activity produced in the same sample by photons with energies below the three-neutron separation energy for ^{65}Cu (28.68 MeV) would be filed with the sheets for ^{63}Cu. Similarly a measurement of the ground-state neutron capture cross section in ^{12}C would be filed under ^{13}C while the corresponding ground-state alpha-particle capture cross section would be filed under ^{16}O.

At the end of this volume there is a master list of the abbreviations that have been used in the index section of the abstract sheets. The listings are those used in the final published index, Photonuclear Data Index, 1973-1981, NBSIR 82-2543, issued in August 1982 by the U. S. Department of Commerce, National Bureau of Standards, Washington, DC 20234. In some cases two notations are entered for the same quantity. The second entry is the abbreviation that was used in one or more of the earlier published editions of the index.

# LITHIUM
Z=3

Lithium was discovered in 1817 by J. A. Arfredson in Sweden while analyzing the mineral petalite. The name lithium (from the Greek, *lithos*, "stone") was proposed by Jons Jacob Berzelius, a Swedish chemist and one of the founders of modern chemistry.

Ref. F. Heinrich, R. Rubin
Helva. Phys. Acta 28, 185 (1955)

Elem. Sym.	A	Z
Li*		3

Method
betatron; BF_3 counters

Ref. No.
55 He 1 | EGF

Reaction	E or ΔE	E_o	Γ	$\int \sigma dE$	Jπ	Notes
Li(γ,n)	Bremss					* 7.5% of Li^6 Measured: $A(E_G) = \frac{\int_0^{E_G} \sigma_{Li}(E)N_\gamma(E)dE}{\int_0^{E_G} \sigma_{Cu}(E)N_\gamma(E)dE}$ Cu and Li intercepted same brem angle Used Spencer method to get σ from activation curve. In Figure 4, $E_T(\gamma,2n) \simeq$ 12.5 MeV - no correction made for this. In Figure 5, σ(γ,p) from Rubin and Walter [Helva. Phys. Acta 27, 163 (1954)] - measure activity of He^3.

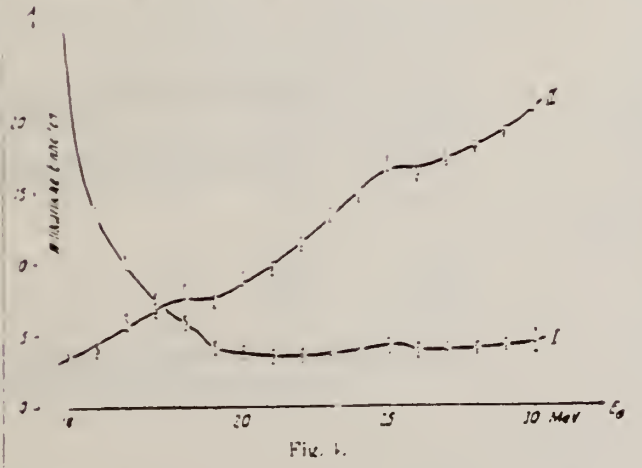

Fig. 4.

Curve I gives $A(E_G)$; Curve II gives the neutron yield curve for Li.

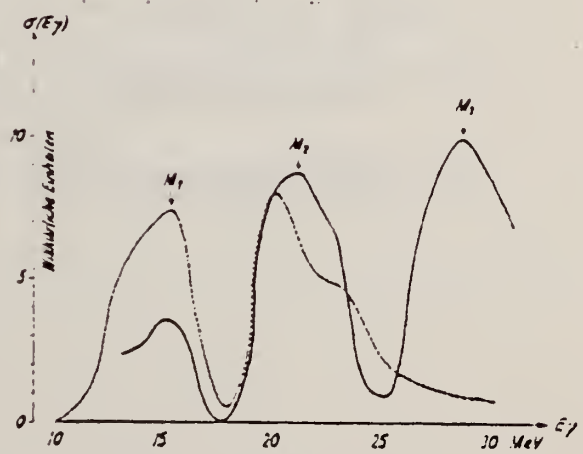

Fig. 5.

Neutron production cross section for Li.

REF.

A.C. Odian, P.C. Stein, A. Wattenberg, B.T. Feld, and R. Weinstein
Phys. Rev. 102, 338 (1956)

ELEM. SYM.	A	Z
Li		3

METHOD

Synchrotron; plastic scintillator proton telescope, liquid scintillator neutron detector, also integrating neutron detector

REF. NO.	
56 Od 1	NVB

REACTION	RESULT	EXCITATION ENERGY	SOURCE		DETECTOR		ANGLE
			TYPE	RANGE	TYPE	RANGE	
G,NP	RLX	140-260	C	340	TEL-D	70-125	DST

NP COINCIDENCE

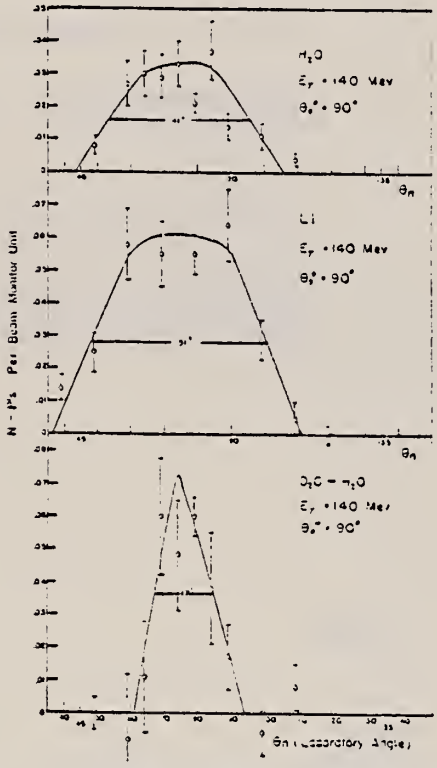

FIG. 2. Variation of neutron-proton coincidences with neutron angle. Gamma-ray energy is 140 Mev.

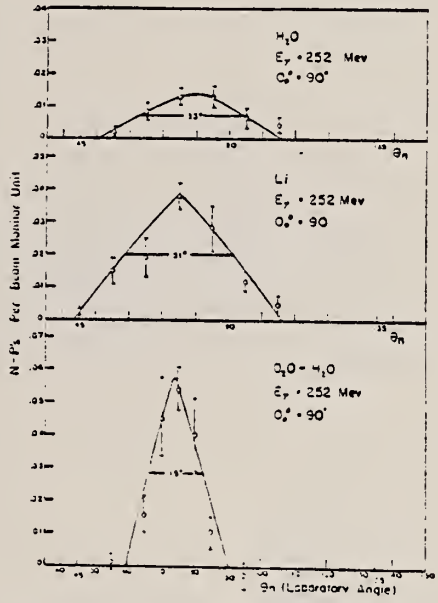

FIG. 3. Variation of neutron-proton coincidences with neutron angle. Gamma-ray energy is 252 Mev.

REF.

A.C. Odian, P.C. Stein, A. Wattenberg, B.T. Feld, and R. Weinstein
Phys. Rev. 102, 838 (1956)

ELEM. SYM.	A	Z
Li		3

METHOD

REF. NO. 56 Od 1 NVB

REACTION	RESULT	EXCITATION ENERGY	SOURCE TYPE	SOURCE RANGE	DETECTOR TYPE	DETECTOR RANGE	ANGLE

NP COINCIDENCE

at E_γ = 200 MeV,

$$\frac{(N-P)_{Li}}{(N-P)_{Dt}} = 0.85 \pm 0.10$$

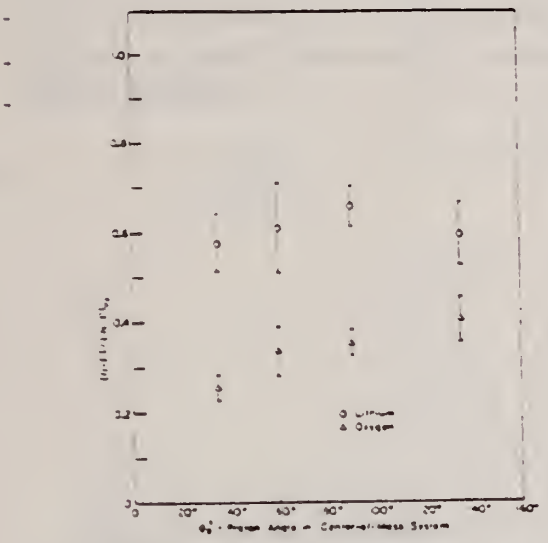

FIG. 6. Angular distribution of photoneutron proton pairs from lithium and oxygen relative to deuterium. $E_\gamma = 260$ Mev.

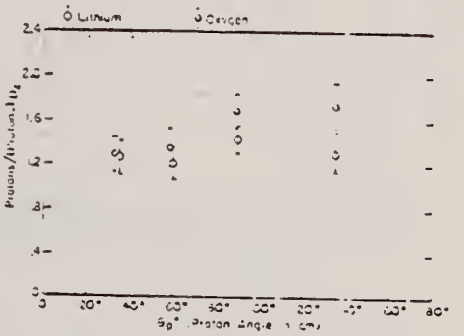

FIG. 7. Proton rates for oxygen and lithium relative to deuterium for various laboratory angles.

TABLE II. Summary of data[a] for lithium and oxygen. $E_\gamma = 260$ Mev; $\theta_p^* = 90°$; $\theta_p = \theta_\gamma = \theta_{lab} = 76°$; $E_p = 129$ Mev; $E_\gamma = 129$ Mev.[b]

Substance	Run[a]	P/M	$(N-P)/M$	$(N-P)/P$
Li	1	5.42	0.214	0.0430
	2	5.42	0.244	0.0450
	3	6.07	0.257	0.0423
	Av	5.84	0.248	0.0441
O_2	1	7.00	0.142	0.0203
	2	7.00	0.142	0.0203
	3	7.35	0.130	0.0178
	Av	7.18	0.145	0.0201

[a] Large counter up close (10 in.).
[b] Each run corresponds to about 2000 monitor units.

REF.

M. O. Barton, J. H. Smith
Phys. Rev. 110, 1143 (1958)

EL EM. SYM.	A	Z
Li		3

METHOD

Betatron; ion chamber monitor; plastic scintillator proton telescope; liquid scintillator neutron detector

REF. NO. 58 Ba 3 NVB

REACTION	RESULT	EXCITATION ENERGY	SOURCE		DETECTOR		ANGLE
			TYPE	RANGE	TYPE	RANGE	
G.NP	RLX	150-280	C	280	TEL-D	60-160	DST

NP COINC., PSPC

$$\left(\frac{d\sigma}{d\Omega}\right)_{np} = (7.05 \pm 1.0)\left(\frac{d\sigma}{d\Omega}\right)_{d}$$

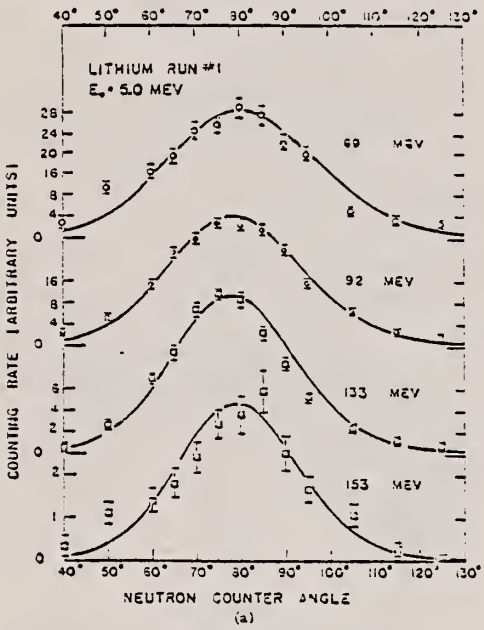

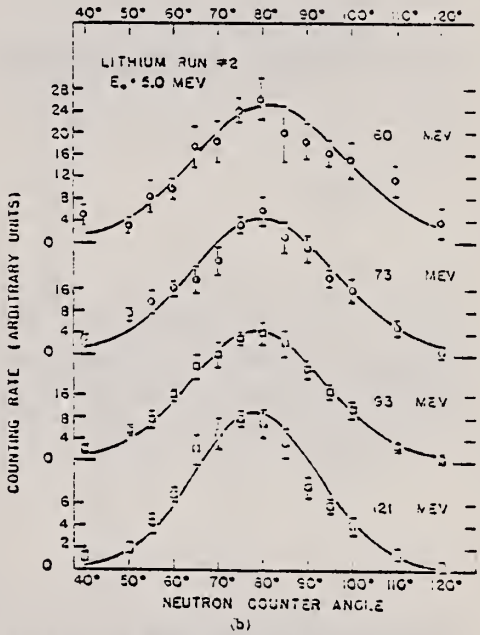

FIG. 8. Lithium coincidence counting rate vs angle of the neutron counter.

(continued)

REF.

M. O. Barton, J. H. Smith
Phys. Rev. 110, 1143 (1958)

ELEM. SYM.	A	Z
Li		3

METHOD

REF. NO.	
58 Ba 3	NVB

REACTION	RESULT	EXCITATION ENERGY	SOURCE		DETECTOR		ANGLE
			TYPE	RANGE	TYPE	RANGE	

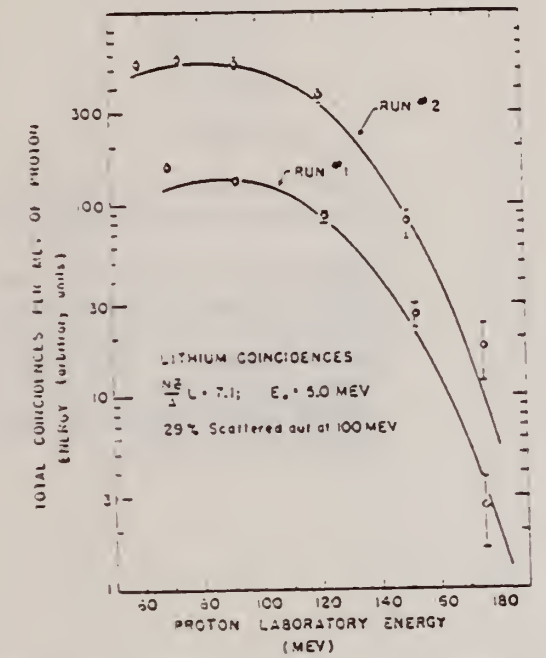

FIG. 10. Total coincident counts per Mev of proton energy from lithium as the proton laboratory energy.

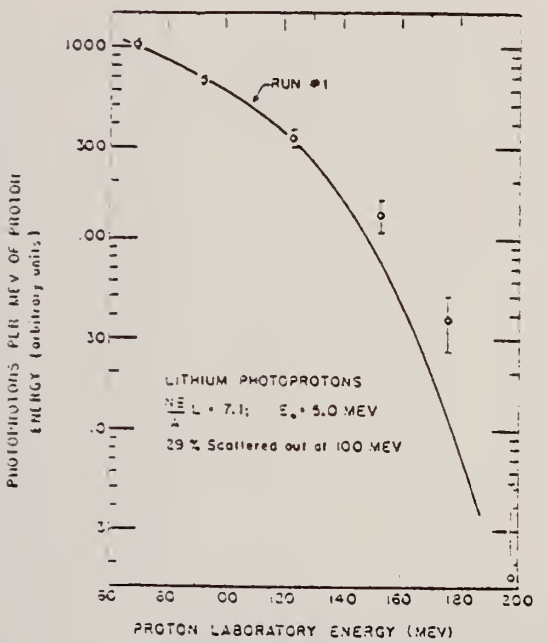

FIG. 12. Total proton counts per Mev of proton energy from lithium as the proton laboratory energy. During the second lithium run, insufficient data were taken to justify a separate curve.

Ref. T.W. Rybka, L. Katz
Phys. Rev. 110, 1123 (1958)

Elem. Sym.	A	Z
Li		3

Method BF_3 neutron counter, ion chamber; 8cm Lucite

Ref. No. 58 Ry 1 | EH

Reaction	E or ΔE	E_o	Γ	$\int \sigma dE$	Jπ	Notes
(γ,n)	Bremss. 5 - 23.6	16.8	9.3	0.018 MeV-mb		σ_{max} = 2.3 mb
$Li^6(\gamma,np)He^4$						E_{th} = 3.61±0.15
$Li^6(\gamma,p)He^5$						4.64±0.08
Li^6 level						5.24±0.05
$Li^6(\gamma,n)Li^5$						5.73±0.05
$Li^7(\gamma,n)$						7.30±0.04
Li^7 level						9.66±0.04

Neutrons come from breakup of He^5; all these energies come from "breaks"

Magnitude of cross section much smaller than that obtained by Goldemberg and Katz [Can. J. Phys. 32, 49 (1954)]. This results from using 583 to obtain no. r/erg and changing the screening cnnstant in the Schiff formula.

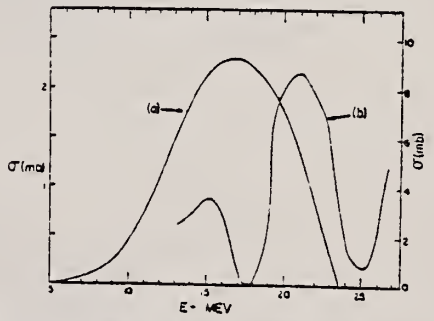

FIG. 2. (a) Cross-section curve obtained from the yield curve of Fig. 1. (b) The cross section obtained by Heinrich and Rubin; its ordinate scale is on the right-hand side.

Curve "(b)" - Heinrich and Rubin, Helv. Phys. Acta 28, 186 (1955).

Ref. C. Whitehead, W.R. McMurray, M.J. Aitken, N. Middlemas, C.H. Collie
Phys. Rev. 110, 941 (1958)

Elem. Sym.	A	Z
Li		3

Method: counter telescope; Bremss.

Ref. No.: 58 Wh 2 EH

Reaction	E or ΔE	E_0	Γ	$\int \sigma dE$	Jπ	Notes
Li(γ,p)	Bremss.					
	37					
	96					

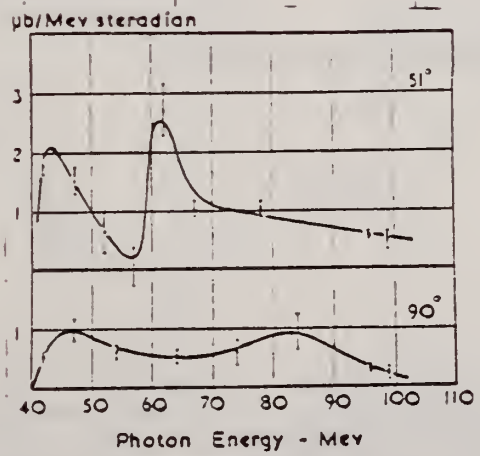

FIG. 14. Cross sections for the production of 37-Mev photoprotons from lithium.

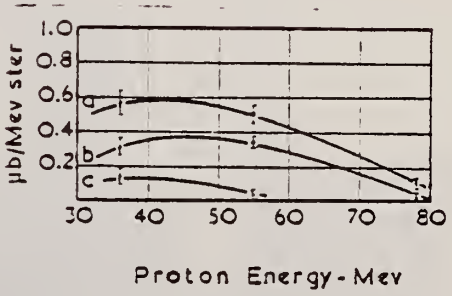

FIG. 15. Energy spectra of photoprotons from lithium produced by 96-Mev photons (a) 51°, (b) 90°, and (c) 129

Ref.

R.W. Fast, P.A. Flournoy, R.S. Tickle, W.D. Whitehead
Phys. Rev. 118, 535 (1960)

Elem. Sym.	A	Z
Li		3

Method

70 MeV Synchrotron; BF_3 ctrs.

Ref. No. 60 Fa 1 JH

Reaction	E or ΔE	E_o	Γ	$\int \sigma dE$	Jπ	Notes
(γ,xn)	11.5-565	19 ± 4		$0.101 \pm .001 \left|{}^{56}_{11}\right.$ MeV-barns $.093 \left|{}^{50}_{11}\right.$ $.039 \left|{}^{25}_{11}\right.$		σ_{max}(19 MeV) = 3.2 ± 0.8 mb. No correction for (γ,2n), (γ,np) contributions. 1063

1063

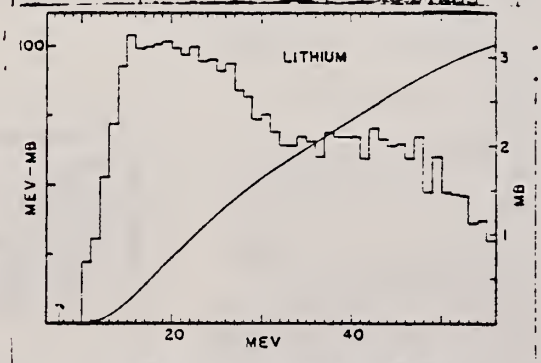

FIG. 7. Cross section and integrated cross section for lithium reaction as functions of energy.

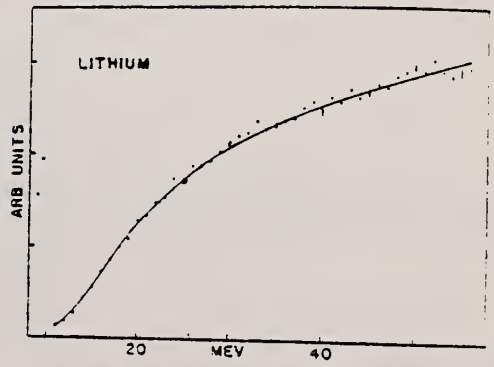

FIG. 8. Integrated reduced cross section for the reaction Li(γ, n)

Ref.		Elem. Sym.	A	Z
	L.A. Kul'chitskii, V. Presperin Zhur. Eksp. i Teoret. Fiz. 39, 1001 (1960) Soviet Phys. JETP 12, 696 (1961)	Li		3

Method	Ref. No.
90 MeV Synchr.; proton recoil counter telescopes	60 Ku 2 – JH

Reaction	E or ΔE	E_0	Γ	$\int \sigma dE$	Jπ	Notes
(γ,n) (γ,p)	Bremss.; $E_{\gamma max}$=90Mev					Relative yields in table below are per nuclear neutron, normalized to Li In Figure 3, caption: "neutral spectrum" is "neutron spectrum".

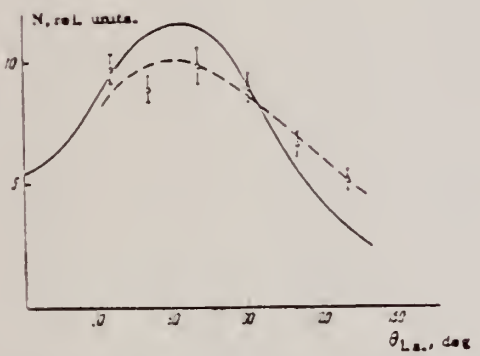

FIG. 1. Angular distribution of l.s. of neutrons of energy ⩾ 10 Mev from Li. Solid curve – calculated from the data of reference 2, dashed curve – interpolation of the experimental data.

Element	Relative neutron yield	Element	Relative neutron yield
Li	1.00±0.05	Cu	0.37±0.02
Be	1.22±0.09	Cd	0.35±0.[illegible]
O	0.74±0.05	I	0.39±0.[illegible]
Al	0.49±0.03	Bi	0.41±0.[illegible]
Ca	0.33±0.02		

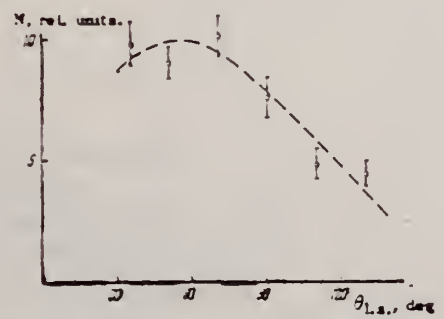

FIG. 2. Angular distribution of ⩾ 18-Mev neutrons from Li. Dashed curve – interpolation of experimental data.

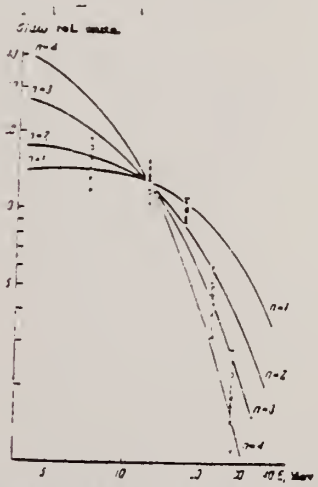

FIG. 3. Energy distribution of recoil protons in the rear crystal of "telescope" in the case of neutrons from lithium: ○ – for 35°, × – for 130°. The solid curves have been calculated under the assumption that the neutral spectrum has a [illegible]

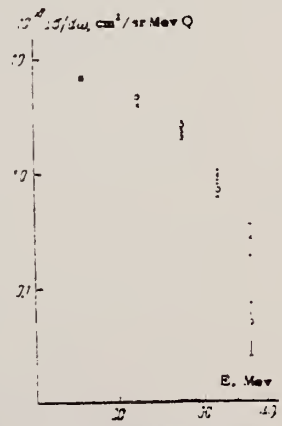

FIG. 4. Energy distribution from Li($\theta_{l.s.}$ = 75°); × – of neutrons, ○ – of protons.

REF.

M. Masuda
J. Phys. Soc. 16, 1801 (1961)

ELEM. SYM.	A	Z
Li		3

METHOD

Betatron; proton angular distribution; ZnS scintillator

REF. NO.	
61 Ma 2	NVB

REACTION	RESULT	EXCITATION ENERGY	SOURCE		DETECTOR		ANGLE
			TYPE	RANGE	TYPE	RANGE	
G,XP	NΦX	10 - 21	C	21	SCI-I	1 - 10	DST

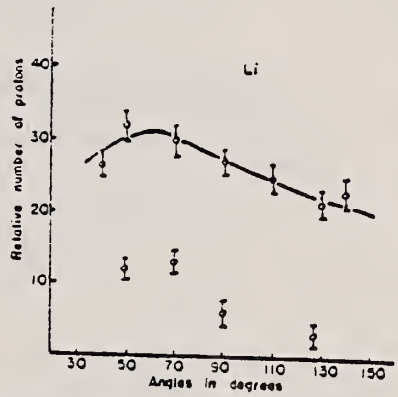

Fig. 4. Angular distribution of photo-protons from lithium for maximum excitation energy of 21 MeV. The smooth curve drawn by the least square has the form,

$$1+0.25\sin^2\theta(1+0.90\cos\theta)^2 .$$

The white dots quoted from the result of Whitehead[13], for excitation with 96 MeV are shown for comparison.

Ref 12: R. Rubin and M. Walker: Helv. Phys. Acta 27, 163 (1954)

Ref. A.S. Belousov, S.V. Rusakov, E.I. Tamm
Zhur. Eksp. i Teoret. Fiz. 43, 813 (1962);
Soviet Phys. JETP 16, 576 (1963)

Elem. Sym.	A	Z
Li		3

Method: Synchrotron; magnetic spectrometer; emulsions

Ref. No.: 62 Be 1 + BG

Reaction	E or ΔE	E_o	Γ	$\int \sigma dE$	Jπ	Notes
Li (γ,D)	160 200 240 260					Main contribution to photodeutron production is made by the energy region below 160 MeV. Directions at 23-57° with respect to beam: $3.8 \leq E_D \leq 9.6$ $7.6 \leq E_p \leq 10.0$

$E_{\gamma\ max}$, MeV	Y_1/Y_p
160	0.061±0.009
200	0.073±0.012
240	0.098±0.012
260	0.092±0.012

Ref.		Elem. Sym.	A	Z
	S. Costa, F. Ferrero, S. Ferroni, B. Minetti, C. Molino, R. Malvano Phys. Letters 6, 286 (1963)	Li		3

Method	Ref. No.	
100 MeV Synchrotron; 4π neutron detector; calculated integrated cross sections - fitted with polynomial of degree -	63 Co 3	RCF

Reaction	E or ΔE	E_o	Γ	$\int \sigma dE$	$J\pi$	Notes
(γ, xn)						$\sigma_b = \int \frac{\sigma(E)}{E} dE$ gets $\langle \bar{\nu}_p \cdot \bar{\nu}_n - \bar{\nu}_n \cdot \bar{\nu}_{n1} \rangle$ $= (R_c^2 - R_p^2 - \frac{3}{\pi^2} \frac{\hbar c}{e^2} \sigma_b \frac{A-1}{A^2}) x \frac{2}{A-2}$ See "Boron" for plots of this and $\int \sigma dE / 60\ NZ/A$

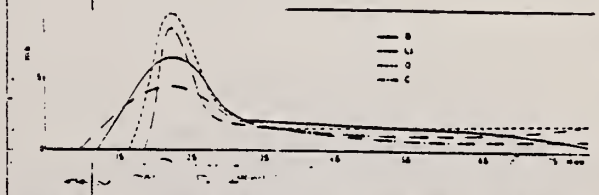

Figure 1: Photoneutron cross sections for several light elements versus γ-ray energy.

Ref.	Elem. Sym.	A	Z
Y.S.Kim, F.F.Liu, F.J.Loeffler, T.R.Palfrey,Jr. Phys.Rev. 129, 1362 (1963)	Li		3

Method	Ref. No.	
335 MeV Synch-scintillation counter telescope	63Ki1	B G

Reaction	E or ΔE	E_o	Γ	$\int \sigma dE$	Jπ	Notes
(γ,p)	$E_{\gamma max}$ = 335					Data corrected for: nuclear absorption, γ attenuation, multiple scattering in target, multiple scattering in counter, pion contamination. Photoproton cross section found proportional to NZ/A (NZ probability of having np pair) over angular and energy region examined. (Z = 3, 4, 5, 6) Differential cross section data given. T_p = proton energy (Figure 2)

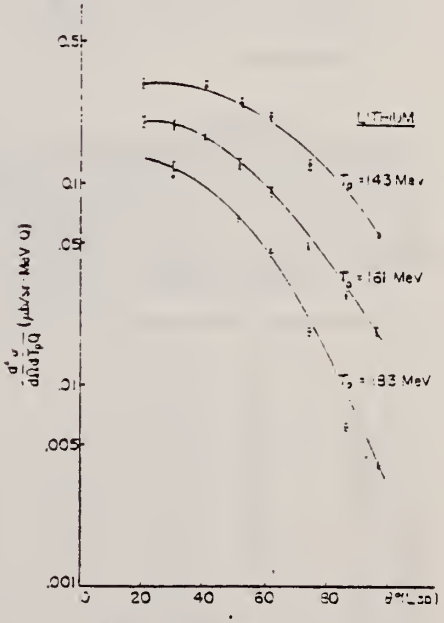

FIG. 2. Differential cross sections for photoproton production from lithium

REF.

L.A. Kulchitskii, Yu.M. Volkov, V.P. Denisov, V.I. Ogurtsov
Izv. Akad. Nauk SSSR 27, 1412 (1963)

EL EM. SYM.	A	Z
Li		3

METHOD: Proton, triton cross sections; energy and angular distributions

REF. NO.: 63 Ku 2 | NVB

REACTION	RESULT	EXCITATION ENERGY	SOURCE		DETECTOR		ANGLE
			TYPE	RANGE	TYPE	RANGE	
G,P	ABX	10-30	C	30			DST
G,T	ABX	12-27	C	30			DST

G-WDTH

Таблица 1

Коэффициенты угловых распределений фотопротонов, аппроксимированных по формуле $a + b \sin^2\theta\,(1 + p\cos\theta)^2$

Интервал энергии, MeV	b/a	p	Интервал энергии, MeV	b/a	p
3,8—4,2	0,35±0,06	0,4	7,7—8,3	0,70±0,14	0,36
4,3—4,9	—0,20±0,05	—	8,6—9,2	3,50±0,45	0,08
5,2—5,7	0,31±0,07	0,25	9,4—10,0	0,75±0,14	0,24
5,8—6,4	1,75±0,20	0,135	10,2—10,8	0,78±0,14	0,23
6,6—7,2	1,65±0,18	0,20	11,0—12,1	1,45±0,30	0,00

(protons)

Таблица 2

Коэффициенты угловых распределений фототритонов, аппроксимированных по формуле $a + b \sin^2\theta\,(1 + p\cos\theta)$

Интервал энергии, MeV	a/b	p	Интервал энергии, MeV	a/b	p
6,7—7,2	—0,07±0,12	—0,05	11,8—12,6	0,50±0,15	—0,30
7,4—8,4	0,15±0,15	—0,20	7,5—15*	0,40±0,07	—
8,6—11,4	0,03±0,08	—0,05			

(tritons)

* Из работы [6].

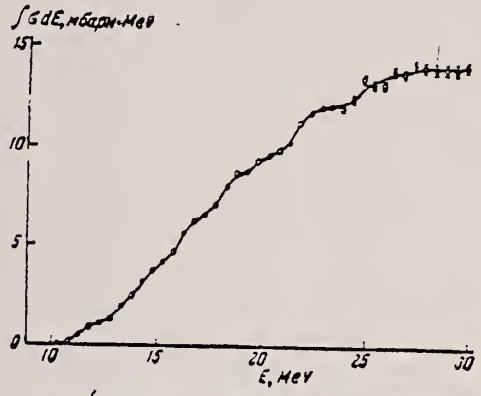

(proton integrated cross section

Рис. 4. Интегральное сечение реакции $Li^7(\gamma, p)He^4$

(protons) Таблица 6

Рассчитанные угловые распределения фотопротонов, испускаемых ядром Li^7 при дипольном поглощении γ-квантов

Спин конечного состояния ядра I_c	Спин канала реакции $S = I_c \pm 1/2$	Спин возбужденного состояния I	Относительный орбитальный момент протона, L	Угловое распределение
0+	1/2	1/2	0	const
1+	1/2	3/2	2	$1-0{,}43\sin^2\theta$
1+	1/2	5/2	2	$1+\sin^2\theta$
1+, 2+	3/2	1/2	2	const
1+, 2+	3/2	3/2	0	const
1+, 2+	3/2	3/2	2	const
1+, 2+	3/2	5/2	2	$1+0{,}25\sin^2\theta$
2+, 3+	5/2	3/2	2	$1+0{,}6\sin^2\theta$
2+, 3+	5/2	5/2	0	const
2+, 3+	5/2	5/2	2	$1-0{,}19\sin^2\theta$
3+	7/2	3/2	2	$1-0{,}54\sin^2\theta$
3+	7/2	5/2	2	$1-0{,}35\sin^2\theta$
0−, 1−	1/2	1/2	1	const
0−, 1−	1/2	3/2	1	$1-0{,}43\sin^2\theta$
1−, 2−	3/2	1/2	1	const
1−, 2−	3/2	3/2	1	$1+0{,}70\sin^2\theta$
1−, 2−	3/2	5/2	1	$1+0{,}57\sin^2\theta$
2−, 3−	5/2	3/2	1	$1-0{,}02\sin^2\theta$
2−, 3−	5/2	5/2	1	$1-0{,}055\sin^2\theta$

(tritons) Таблица 5

Рассчитанные угловые распределения фототритонов ядра Li^7

Мультипольность γ-перехода, δ	Спин возбужденного состояния, I	Относительный орбитальный момент тритона и α-частицы, L	Угловое распределение
E1	5/2	2	$1+\sin^2\theta$
	3/2	2	$1-0{,}43\sin^2\theta$
	1/2	0	const
M1	5/2	3	$1+\sin^2\theta$
	3/2	1	$1-0{,}43\sin^2\theta$
	1/2	1	

(protons) Таблица 7

Интегральные сечения для протонов и тритонов и радиационные ширины наблюдаемых уровней Li^7

Энергия уровней, MeV	$\int \sigma_i(E)\,dE$ (MeV·мбарн) для протонов	$\int \sigma_i(E)\,dE$ (MeV·мбарн) для тритонов	Γ_γ, keV
11,0	1,20	—	0,6
14,1	2,80	1,60	1,9
16,1	2,90	1,50	2,5
18,0	3,05	1,50	3,2
19,6	1,30	1,60	3,2
21,5	2,90	1,50	4,7
23,5	2,30	1,60	5,1
25	1,05	1,80	5,7

(continued)

EL EM. SYM.	A	Z
Li	9	3

METHOD

REF. NO. 63 Ku 2

REACTION	RESULT	EXCITATION ENERGY	SOURCE		DETECTOR		ANGLE
			TYPE	RANGE	TYPE	RANGE	

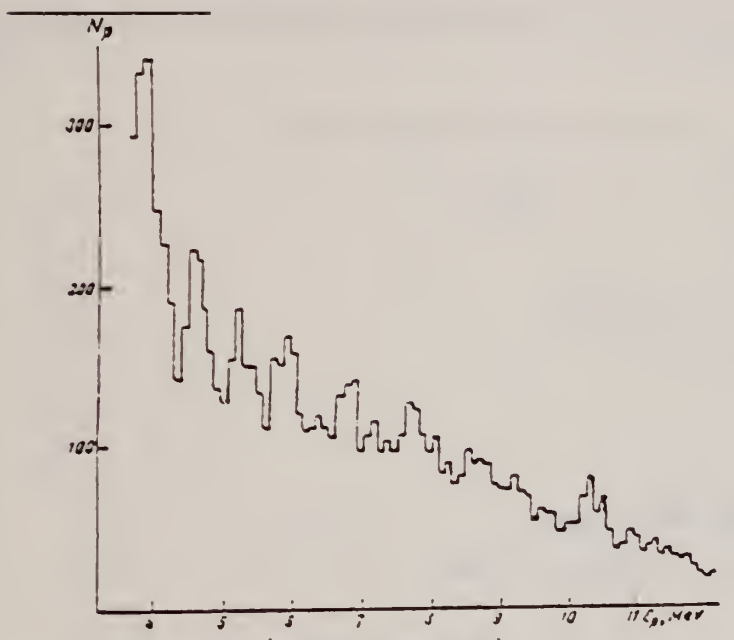

(proton spectrum)

Рис. 1. Экспериментальный спектр протонов, полученный при фоторасщеплении Li^7 тормозным излучением с $E_{тмакс}$ = 30 MeV. По оси ординат отложено суммарное число протонов на двух телескопах

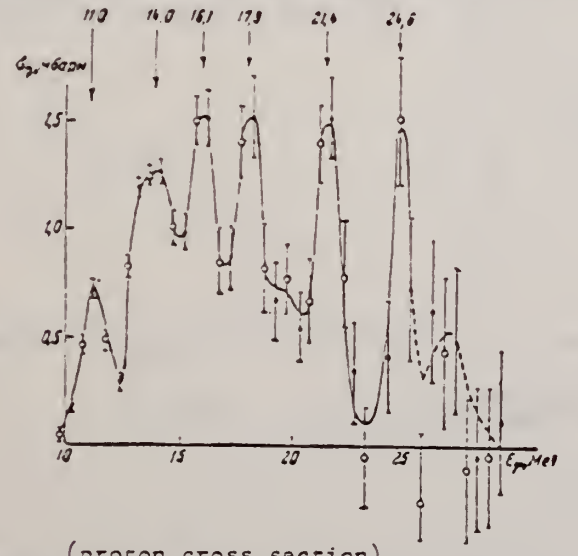

(proton cross section)

Рис. 2. Дифференциальное сечение реакции Li^7 (γ, p) He^6, измеренное по β-активности He^6

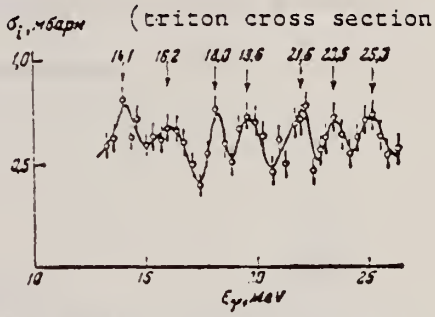

Рис. 3. Сечение реакции Li^7 (γ, t) He^4, полученное из спектра фототритонов

REACTION	RESULT	EXCITATION ENERGY	SOURCE TYPE	SOURCE RANGE	DETECTOR TYPE	DETECTOR RANGE	ANGLE
G, XN	ABX	THR-19	C	-19	BF3-I		4 PI

System A 7.0 cm paraffin moderator
B 1.5 cm " "

1062

System B should respond essentially to neutrons having energies below 0.6 MeV.

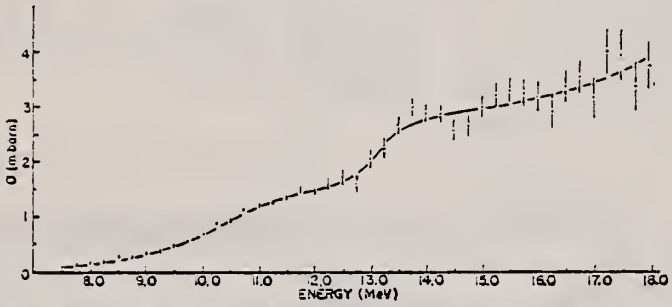

Fig. 3. Photoneutron cross section curve for natural lithium; System A, bin width Δ = 1.0 MeV.

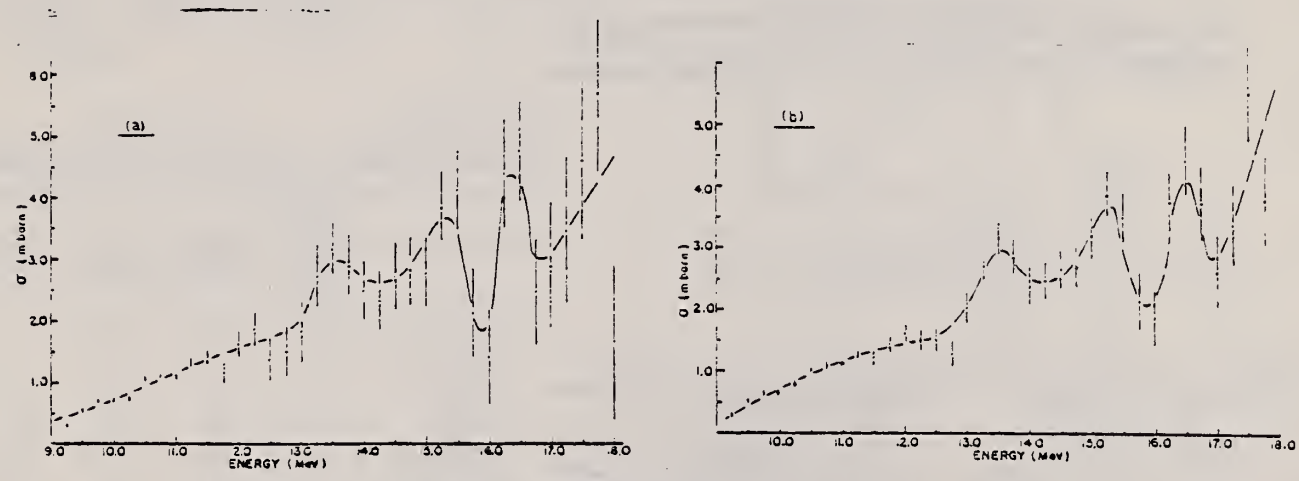

Fig. 4. Photoneutron cross section curve for natural lithium; System A, bin width Δ = 0.5 MeV. (a) Unsmoothed data. Curve (b) Smoothed data (see text).

(continued)

METHOD | REF. NO. 64 A1 1 | JOC

REACTION	RESULT	EXCITATION ENERGY	SOURCE TYPE	SOURCE RANGE	DETECTOR TYPE	DETECTOR RANGE	ANGLE

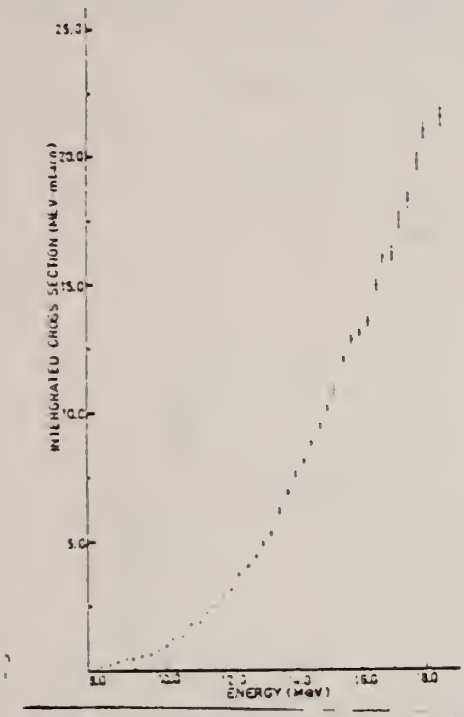

Fig. 5. Integrated photoneutron cross section curve for natural lithium; System A, bin width Δ = 0.5 MeV.

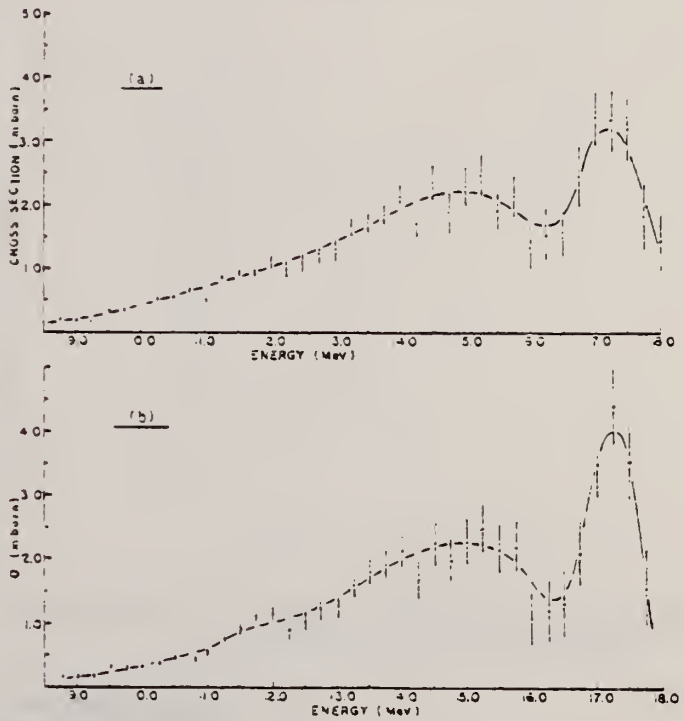

Fig. 6. Slow neutron cross section curve for natural lithium; System B, bin width Δ = 1.0 MeV. (a) Unsmoothed data, (b) smoothed data (see text).

(continued)

REACTION	RESULT	EXCITATION ENERGY	SOURCE		DETECTOR		ANGLE
			TYPE	RANGE	TYPE	RANGE	

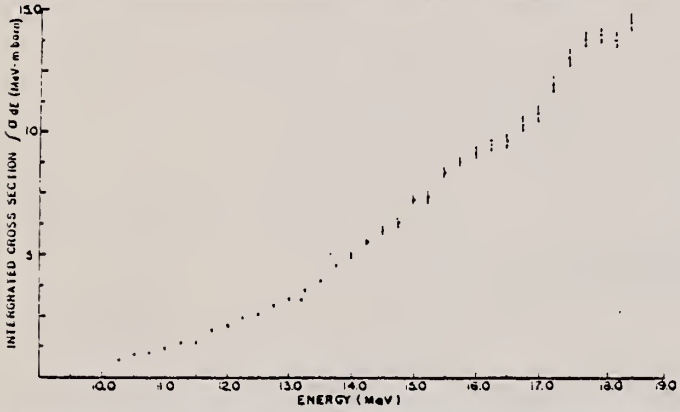

Fig. 7. Slow neutron integrated cross section curve for natural lithium; system B, bin width Δ = 1.0 MeV.

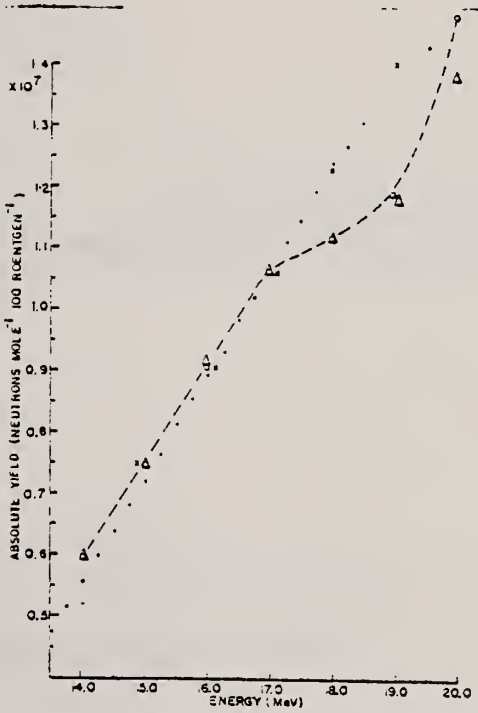

Fig. 8. Comparison of photoneutron yield curve (system A) with those obtained in previous experiments. O present experiment, C Romanowski and Voeiker, Δ Heinrich and Rubin, × Goldemberg and Katz.
Data from the various experiments were normalised to a common value at 17 MeV.

(continued)

REACTION	RESULT	EXCITATION ENERGY	SOURCE		DETECTOR		ANGLE
			TYPE	RANGE	TYPE	RANGE	

TABLE 2

High energy ^{7}Li levels (energy in MeV)

Reaction Ref.	^{7}Li(γ, t) [16]	^{7}Li(γ, t) [16, 17]	^{7}Li(γ, n) [3]	^{7}Li(γ, n) Present work	^{7}Li(γ, p) [20]
	9.3	9.6	9.6		
			10.8		
		11.7			
			12.4		12.5
		13.5		13.6	13.5
			14.0		14.3
				15.3	
	16.7	16.2		16.5	
			17.5		
	21.5				
	23.5				

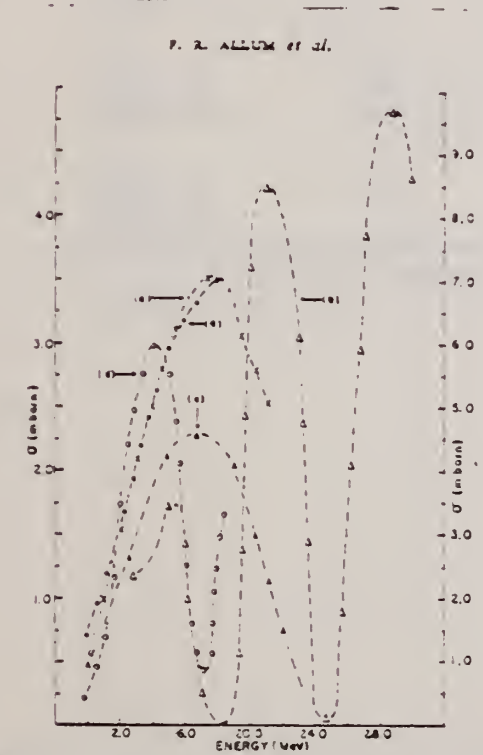

Fig. 9. Comparison of photoneutron cross section curve (system A) with those obtained in previous experiments. (a) × Goldemberg and Katz, (b) J Heinrich and Rubin, (c) ▲ Ryoka and Katz, (d) ○ Romanowski and Voelker, ○ present experiment.
The scale on the left hand side is appropriate to curves (a), (c), (d) and (e) while that on the right hand side refers to the experiment of Heinrich and Rubin.

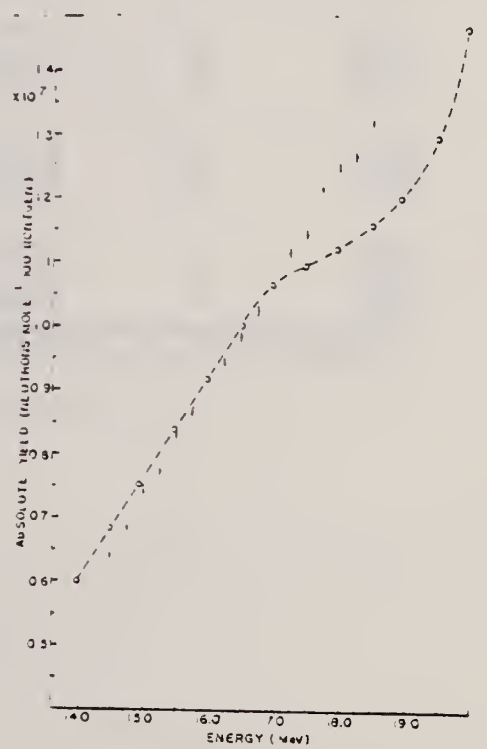

Fig. 10. Comparison of the photoneutron yield curve from system B(E, greater than 14 MeV) with the yield curve obtained by Romanowski and Voelker. (Curves normalised at 17 MeV). ○ present experiment, ○ Romanowski and Voelker.

REF.

J. Goldemberg, W.C. Barber, F.H. Lewis, Jr., J.W. Walecka
Phys. Rev. 134, B1022 (1964)

ELEM. SYM.	A	Z
Li		3

METHOD: Linac

REF. NO.: 64 Go 3 | NVB

REACTION	RESULT	EXCITATION ENERGY	SOURCE		DETECTOR		ANGLE
			TYPE	RANGE	TYPE	RANGE	
E,E/	ABX	4	D	40-70	MAG-D		180

EMF

TABLE I. Data on $M1$ transitions.

	q MeV/c	Cross section[a]	Reference	$\lvert(J_f\lvert\lvert T_1^{max}(q)\rvert\rvert J_i)\rvert^2\ (1/q^2)$ (10^{-3})	$\lvert(J_f\lvert\lvert T_1^{max}(q)\rvert\rvert J_i)\rvert^2$ [10^{-4}(MeV/c)$^{-4}$]
		15.1-MeV level in C^{12}			
Photons	15.1	(2.05±0.27)	8	0.044	(0.19 ±0.025)
Electrons	68	(2.0 ±0.3)	this work	0.55	(0.12 ±0.018)
Electrons (160°)	68	(2.6 ±$_{0.10}^{0.12}$)	5	0.69	(0.15 ±$_{0.022}^{0.025}$)
Electrons	93	(2.0 ±0.3)	this work	0.87	(0.10 ±0.015)
Electrons	125	(1.5 ±0.25)	this work	1.10	(0.07 ±0.012)
		3.56-MeV level in Li^6			
Photons	3.56	(0.92±$_{0.11}^{0.13}$)	b	0.014	(1.10 ±$_{0.13}^{0.16}$)
Electrons	76	(3.0 ±0.45)	this work	2.0	(0.33 ±0.057)
Electrons	106	(1.55±0.23)	this work	2.1	(0.19 ±0.029)
Electrons	136	(0.90±0.14)	this work	2.0	(0.11 ±0.017)
		11.6-MeV level in Si^{28}			
Photons	11.6	(9.3 ±2.6)	c	0.016	(1.2 ±0.32)
Electrons	71.5	(3.5 ±1.4)	d	0.92	(0.18 ±0.07)
Electrons	88.4	(3.0 ±0.75)	this work	1.2	(0.15 ±0.038)
Electrons	129.4	(1.3 ±0.45)	this work	1.5	(0.09 ±0.022)
		11-MeV level in Mg^{24}			
Photons	11	(13.1 ±3.8)	c	0.02	(1.7 ±0.50)
Electrons	83	(4.4 ±0.88)	6	1.5	(0.22 ±0.044)
Electrons	97	(3.5 ±0.70)	this work	1.6	(0.1 ±0.034)
Electrons	129	(1.8 ±0.36)	this work	1.3	(0.031±0.016)

[a] In units of 10^{-27} MeV-cm^2 for photons and 10^{-28} cm^2/sr for electrons.
[b] L. Cohen and R. A. Tobin, Nucl. Phys. 14, 243 (1960).
[c] A. B. de Nercy, Ann. Phys. (Paris) 6, 1379 (1961).
[d] R. D. Edge and G. A. Peterson, Phys. Rev. 128, 2750 (1962).

REF. G. E. Manuzio, G. Ricco and M. Sanzone
Nuovo Cimento 42B, 348 (1966)

ELEM. SYM.	A	Z
Li		3

METHOD
32 MeV Betatron

REF. NO. 66 Ma 1 JDM

REACTION	RESULT	EXCITATION ENERGY	SOURCE		DETECTOR		ANGLE
			TYPE	RANGE	TYPE	RANGE	
G,T	ABX	10 - 28	C	32	TEL-D	4 - 16	90
G,P	SPC	10 - 28	C	32	TEL-D	4 - 16	90
G,D	SPC	10 - 28	C	32	TEL-D	4 - 16	90

29c

Tables compare cross section peaks found in this and other work.

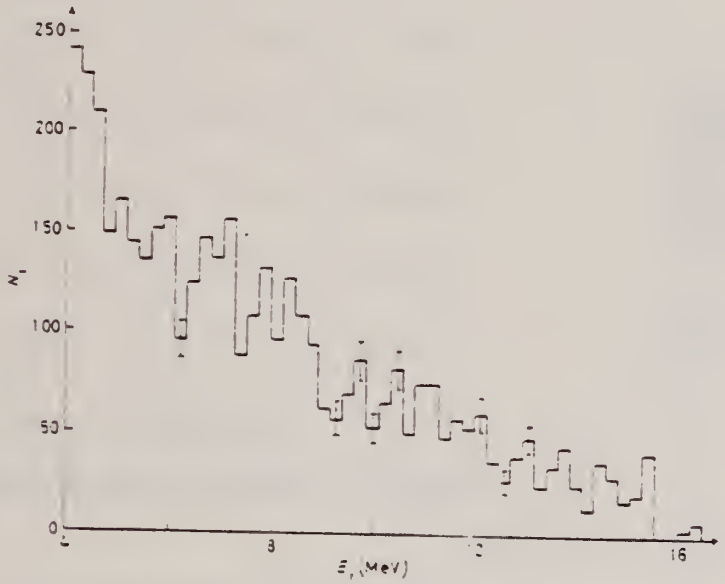

Fig. 1. – Spectrum of phototritons from ^{7}Li produced by 32 MeV bremsstrahlung.

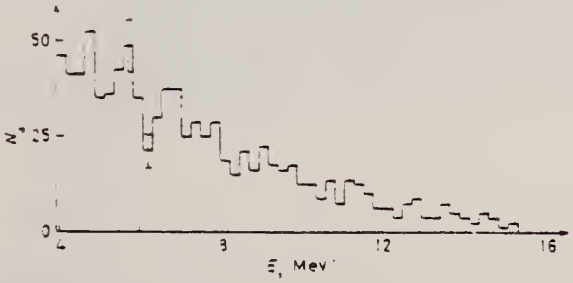

Fig. 3. – Spectrum of photodeuterons from ^{7}Li produced by 32 MeV bremsstrahlung.

(continued)

REF.

G. E. Manuzio, G. Ricco and M. Sanzone
Nuovo Cimento 42B, 348 (1966)

ELEM. SYM.	A	Z
Li		3

METHOD

32 MeV Betatron

REF. NO.

66 Ma 1 - JDM

REACTION	RESULT	EXCITATION ENERGY	SOURCE		DETECTOR		ANGLE
			TYPE	RANGE	TYPE	RANGE	

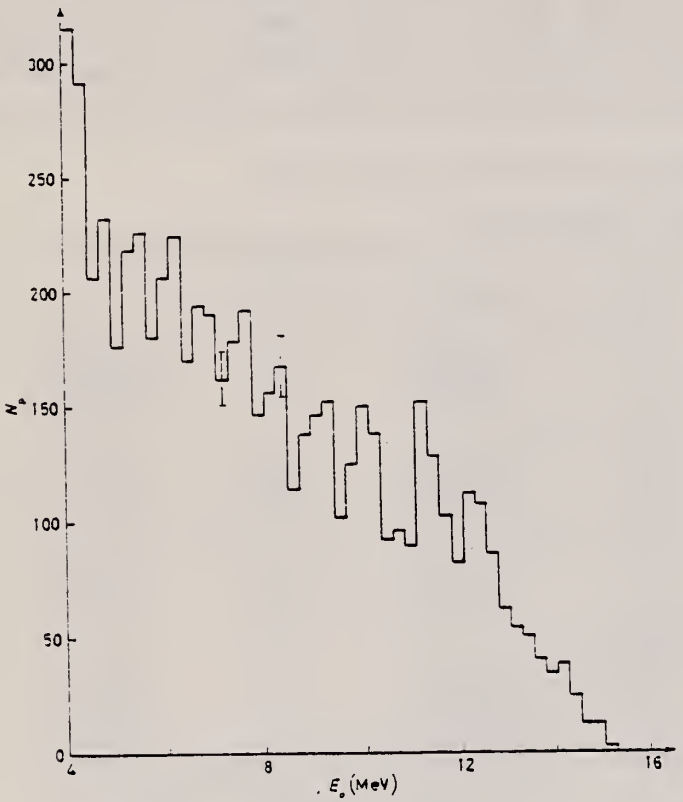

Fig. 3. – Spectrum of photoprotons from ^{7}Li produced by 32 MeV bremsstrahlung.

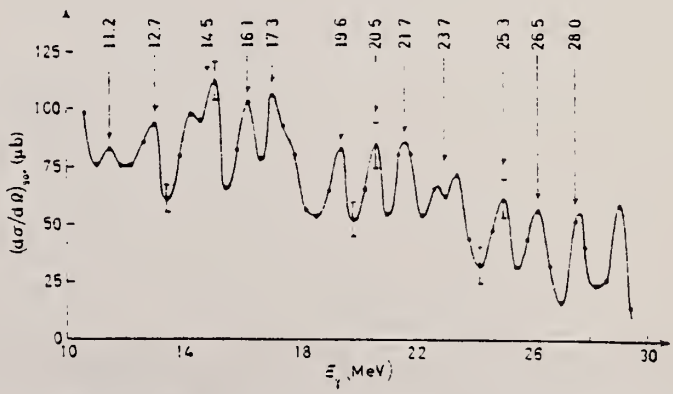

Fig. 4. – Differential cross-section at 90° of the ^{7}Li(γ, n)^{6}He reaction in the γ-ray energy range between 10 and 28 MeV.

REF.	ELEM. SYM.	A	Z
N. N. Kaushal, E. J. Winhold, P. F. Yergin, H. A. Medicus and R. H. Augustson Phys. Rev. 175, 1330 (1968)	Li		3

METHOD	REF. NO.	
	68 Ka 1	- HMG

REACTION	RESULT	EXCITATION ENERGY	SOURCE		DETECTOR		ANGLE
			TYPE	RANGE	TYPE	RANGE	
G,N	ABX	50-85	C	55,85	TOF-D	10-85	67
							(67.5)

NEUT ENGY SPEC

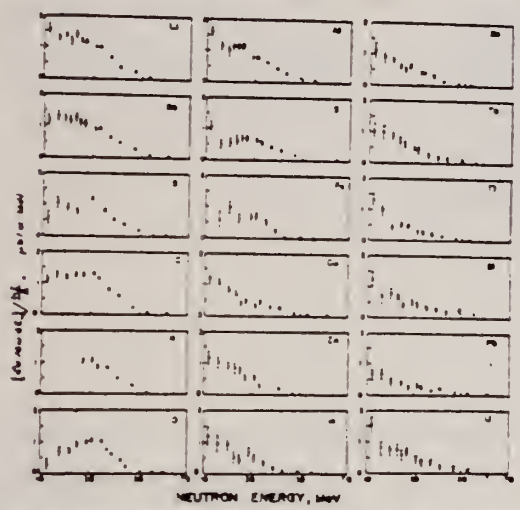

FIG. 6. Observed neutron spectra due to 55–85-MeV difference photon spectra. The effective cross sections have been divided by NZ/A.

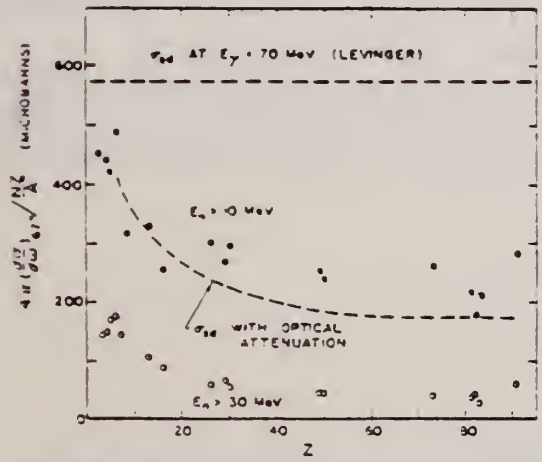

FIG. 7. Effective cross sections for production of fast neutrons with energies greater than 10 MeV (solid circles) and 30 MeV (open circles) by the 55–85-MeV photon difference spectrum. The dashed curves are modified quasideuteron model predictions as discussed in the text.

TABLE I. Comparison of present cross-section values in mb for production of high-energy photoneutrons by 55–85-MeV photons with measured cross sections $\sigma(\gamma,Tn)$, also in mb, for total photoneutron production. The present cross-section values are uncertain by 8 to 10% because of counting statistics and normalization errors; in addition all values depend on an absolute normalization in terms of the deuteron photodisintegration cross section, which is known to about 10% at these energies.

Target	$4\pi(d\sigma/d\omega)_{90°}$ (E_n > 10 MeV) [Present experiment]	$\sigma(\gamma,Tn)$ Jones and Terwilliger[a]	$\sigma(\gamma,Tn)$ Costa *et al.*[b]	Other results
Li	0.75		1.0	
Be	1.0	2.7	2.3	2.3[c]
B	1.0		1.4	
C	1.5	1.3	1.4	2.4[d]
O	1.3		1.6	
Al	2.8	5.5	4.6	8[d]
S	2.1		4.4	6.5[d]
Fe	4.2	16	12	
Cu	4.3	20	19	
Zn	4.4		15	
In	7.4			
Sn	7.0			
Ta	10.7	95		
Tl	10.7			
Pb	8.3	100		
Bi	13			
U	16	65		

[a] Average cross sections between 55 and 85 MeV, as read from Figs. 4 and 5 of Ref. 4.
[b] $\int_{\omega_{th}}^{\omega_{max}} \sigma_{tot} dE - \int_{\omega_{th}}^{\omega_{max}} \sigma_{tot} dE/50$, as taken from Fig. 4 of Ref. 5 and Table I of Ref. 6.
[c] S. Costa, L. Pasqualini, G. Piragino, and L. Roasio, Nuovo Cimento 42, 306 (1966).
[d] G. Bishop, S. Costa, S. Ferroni, R. Malvano, and G. Ricco, Nuovo Cimento 42, 144 (1966).

REF.

Yu. P. Antufyev, V. L. Agranovich, V. B. Ganenko, V. S. Kuzmenko, I.I. Miroshnichenko, P.V. Sorokin
Ukr. Fiz. 14, 496 (1969)

ELEM. SYM.	A	Z
Li		3

METHOD

REF. NO.	
69 An 8	hmg

	REACTION	RESULT	EXCITATION ENERGY	SOURCE		DETECTOR		ANGLE
				TYPE	RANGE	TYPE	RANGE	
1)	E,P	RLY	THR-999	C	999	MAG-D		DST
2)	E,D	RLY	THR-999	C	999	MAG-D		DST
3)	E,T	RLY	THR-999	C	999	MAG-D		DST

The differential cross-sections of (γ, p), (γ, d) and (γ, t) reactions on carbon for 700 and 1200 MeV maximum energies of photons and energy distributions of the secondary particles were measured at 30, 60 and 120° of particle emission angles. Excitation function for protons with the energy of 97 MeV is given for the maximum incident photon energy from 400 to 1300 MeV. Deuteron to proton and triton to deuteron yield ratios for various nuclei are also shown.

Experiment was carried out at the Kharkov linear accelerator. The particles were detected by scintillation counters after a magnetic spectrometer.

Possible mechanisms of the high energy photon-nuclei interactions are discussed. (3 Figs).

1) 999 = 1 GEV, REL P/D
2) 1.3 GEV, REL P/D, D/T
3) 999 = 1 GEV, REL D/T

Таблица 2

	θ°	$\left[\frac{d^2\sigma_d(2p)}{d\Omega d\nu}\Big/\frac{d^2\sigma_p(p)}{d\Omega d\nu}\right]\cdot 10^4$	$\left[\frac{d^2\sigma_t(3p)}{d\Omega d\nu}\Big/\frac{d^2\sigma_d(2p)}{d\Omega d\nu}\right]\cdot 10^4$
Li^7	60	1,94±0,19	2,1±0,3
	120	0,8±0,08	0,9±0,13
C^{12}	60	2,2±0,2	1,8±0,3
	120	—	—
Ta^{181}	60	3,1±0,3	2,8±0,4
	120	1,89±0,2	1,85±0,28

Yu. P. Antuf'ev, V. L. Agranovich, V. B. Ganenko, V. S. Kuz'menko, I. I. Miroshnichenko, and P. V. Sorokin
Yad. Fiz. 13, 473 (1971); Sov. J. Nucl. Phys. 13, 265 (1971)

Li		3

METHOD

REF. NO. 71 An 1 hmg

REACTION	RESULT	EXCITATION ENERGY	SOURCE		DETECTOR		ANGLE
			TYPE	RANGE	TYPE	RANGE	
G,P	SPC	41-999	C	700,999	TEL-D	25-400	DST
G,D	SPC	46-999	C	700,999	TEL-D	25-400	DST

999= 1.2 GEV, REL D/P

Table I. Values of the parameter τ, MeV

Target	E_0 = 700 MeV										E_0 = 1200 MeV					
	Protons					Deuterons					Protons			Deuterons		
	30°	40°	60°	100°	120°	40°	60°	100°	120°		30°	40°	120°	30°	40°	120°
Li	46	42	34	30	27	28	24	22	21	20		45	28		27	24
Be	48	43	36	30	27	28	28	24	22	19		45	28		27	24
C	50	44	38	30	26	34	33	29	23	19	60	48	35	37	34	22
Si		43			28		27			22		46	35		28	25
Cu												45	29		27	24
Ta					28					21		45	34		27	24
Pb											54		29	36		22

Yield of protons 30-400 MeV, deuterons 30-200 MeV.

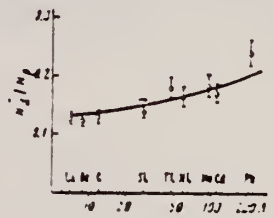

FIG. 4. The ratios N_d/N_p as a function of target-nucleus mass number A at an angle $\theta = 60°$ for E_0 = 1200 MeV. Solid curve – $A^{0.13}$.

The measured secondary-particle spectra for kinetic energies $T > 30$ MeV are well described by the expression

$$d^2\sigma / d\Omega dTQ = \text{const}\, T \exp(-T/\tau). \qquad (1)$$

which is identical to the formula for the evaporation process.[4] In Table I we have given the values of the parameter τ for the nuclei studied, at various angles. The accuracy in determination of τ is about 10%.

Yu. P. Antuf ev, V. L. Agranovich, V. B. Ganenko, V. S. Kuz menko, I. I. Miroshnichenko, P. V. Sorokin, and S. V. Shalatskii
Yad. Fiz. 15, 643 (1972)
Sov. J. Nucl. Phys. 15, 357 (1972)

Li		3

METHOD

REF. NO. 72 An 3 hmg

REACTION	RESULT	EXCITATION ENERGY	SOURCE		DETECTOR		ANGLE
			TYPE	RANGE	TYPE	RANGE	
G,T	RLY	83-999	C	999	MAG-D		DST
G,P	RLY	34-999	C	999	MAG-D		DST
G,D	RLY	100-999	C	999	MAG-D		DST

999=1.1 GEV

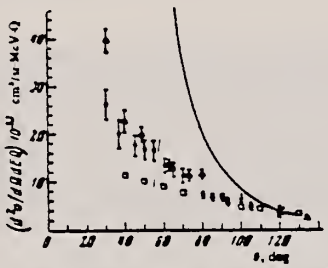

FIG. 3. Angular dependence of the yield of tritons with momentum 680 MeV/c (E_T = 80 MeV) from Li^7 for E_0 = 1100 MeV. Solid curve—calculation with Eq. (7). Points: □—210-MeV/c protons, Δ—90-MeV deuterons, ●—tritons.

REF. P. Dougan and W. Stiefler
Z. Physik 265, 1 (1973)

ELEM. SYM.	A	Z
Li		3

METHOD

REF. NO. 73 Do 9 egf

REACTION	RESULT	EXCITATION ENERGY	SOURCE		DETECTOR		ANGLE
			TYPE	RANGE	TYPE	RANGE	
G,XP	ABY	90-400	C	400	TEL-D		DST

Table 2. Lithium. Bremsstrahlung endpoint energy: 400 MeV. Differential cross-sections in microbarns/sterrad · MeV · eq. quantum. Quoted errors: statistical in percent

Energy	Angle								
	14	22	30	40	50	60	74	90	110
86.4		1.93 1.9	1.70 1.8	1.18 1.8	0.879 2.0	0.651 2.2	0.509 2.2	0.372 2.1	0.262 2.6
103.7		1.59 2.3	1.23 2.2	0.830 2.3	0.623 2.6	0.492 2.7	0.360 2.8	0.268 2.6	0.169 3.5
110.3	1.54 2.1	1.29 2.1	1.12 2.2	0.775 2.2	0.543 3.0	0.453 2.2	0.339 2.1	0.237 2.3	0.144 2.6
120.3		1.07 2.8	0.829 2.7	0.601 2.7	0.446 3.0	0.381 3.0	0.290 3.1	0.183 3.1	0.105 4.4
132.4	1.04 2.6	0.797 2.3	0.649 3.0	0.462 2.9	0.379 3.8	0.312 2.7	0.232 2.7	0.144 3.1	0.0753 3.7
153.3	0.599 3.5	0.514 3.6	0.400 3.8	0.345 3.4	0.287 4.4	0.227 3.2	0.159 3.3	0.0734 4.4	0.0335 5.7
172.4	0.417 3.3	0.367 2.9	0.326 2.4	0.265 2.4	0.207 2.6	0.179 2.9	0.101 3.3	0.0382 5.9	
189.2	0.292 4.2	0.258 3.6	0.251 2.9	0.192 3.0	0.158 3.1	0.124 3.6	0.0576 4.6	0.0173 8.9	
206.0	0.200 5.0	0.185 4.3	0.183 3.4	0.149 3.4	0.100 3.9	0.0635 4.3	0.0265 6.8	0.00797 13.0	
224.6	0.198 4.4	0.156 3.7	0.134 3.6	0.0953 4.6	0.0858 5.3				
240.9	0.115 6.1	0.109 4.6	0.0936 4.5	0.0656 6.0	0.0435 7.8				
257.2	0.0943 6.6	0.0713 5.6	0.0556 5.3	0.0387 3.0	0.0202 11.3				

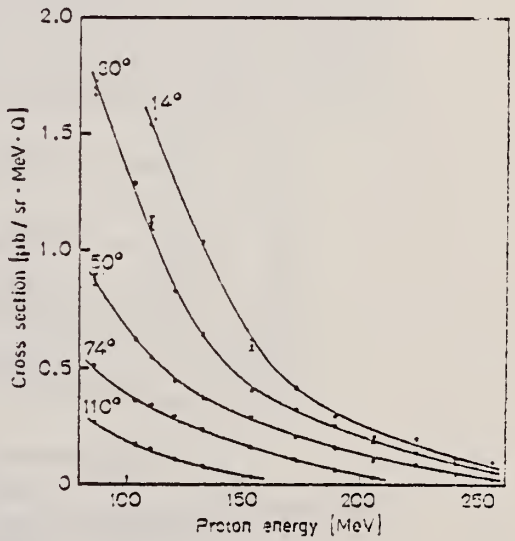

Fig. 2. Energy distributions of protons from lithium irradiated with bremsstrahlung of 400 MeV maximum energy for selected proton emission angles. Note that in this and similar figures, error bars have not in general been drawn. This has been done partly to improve the clarity of the drawings and partly because the statistical errors are so small as to be negligible on the scale of the drawing

(continued)

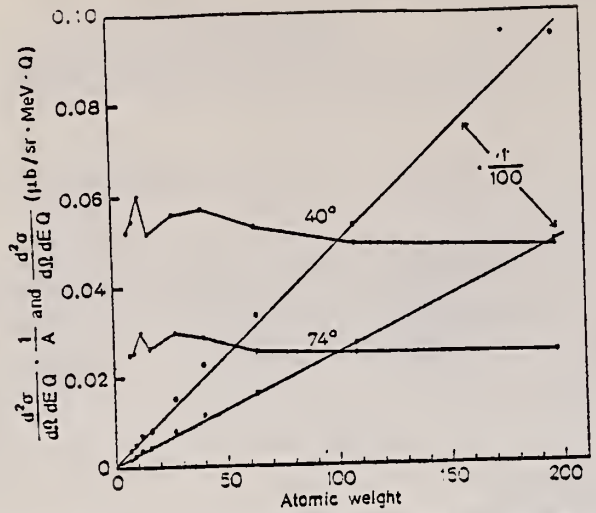

Fig. 9. In this figure, the straight lines show the experimental cross-sections at 40° and 74° for $E_p = 150$ MeV. The other curves are the same cross-sections divided by atomic weight

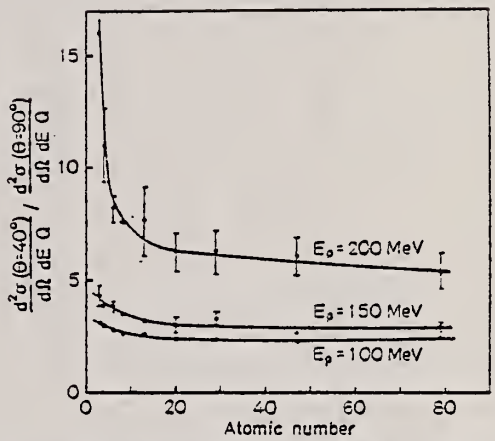

Fig. 6. The ratios of the experimental cross-sections at 40 and 90 degrees for selected proton energies as a function of atomic number

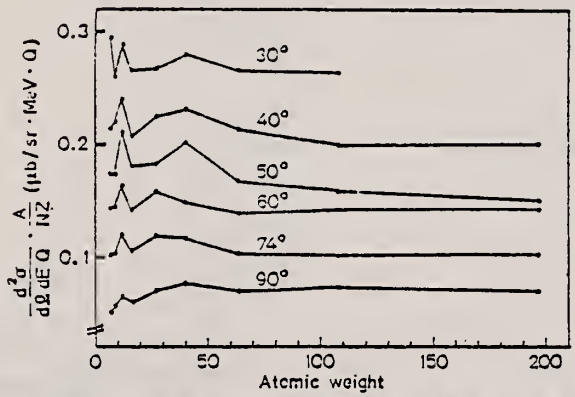

Fig. 8. Experimental cross-sections at various angles for $E_p = 150$ MeV divided by NZ/A plotted as a function of atomic weight

REF. J. Ahrens, H.B. Eppler, H. Gimm, M. Kroning, P. Riehn, A. Zieger and B. Ziegler
Phys. Lett. 52B, 43 (1974)

ELEM. SYM.	A	Z
Li		3

METHOD

REF. NO. 74 Ah 8 egf

REACTION	RESULT	EXCITATION ENERGY	SOURCE		DETECTOR		ANGLE
			TYPE	RANGE	TYPE	RANGE	
G,MUT	ABX	15-220	C	300	MGC-D		4PI

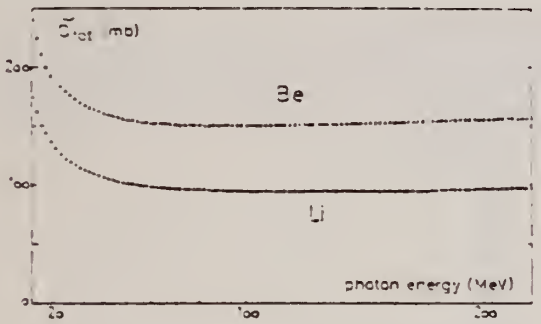

Fig. 1. The total photon absorption cross section σ_{tot} for Li and Be. One standard deviation of the statistical error is by far smaller than the size of the symbols.

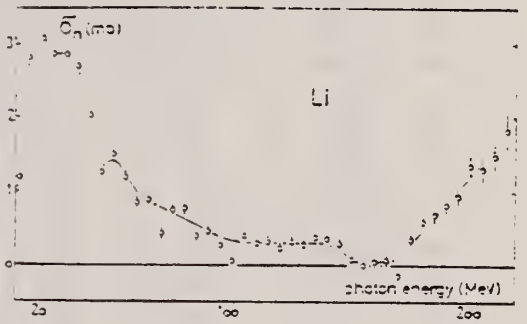

Fig. 2. The total photonuclear cross section σ_n for Li. The error bars indicate one standard deviation in counting statistics from the second spectrometer [2]. The dotted lines indicate uncertainties arising from counting statistics in the normalizing instrument [2]. This error can only cause structures at least 10 % wide in energy. The full line was drawn by hand.

Table 1
Absorber characteristics and relevant errors

	Li	Be
diameter (cm)	1.983 ± 0.002	2.029 ± 0.001
weight (g)	331.40 ± 0.15	716.340 ± 0.03
length (cm)	200.1	120.72
density (g/cm^3)	0.53613	1.943
impurities	0.024 %	0.448 %

REF. J. Ahrens, H. Borchert, K.H. Czock, H.B. Eppler, H. Gimm, H. Gundrum, M. Kroning, P. Riehn, G. Sita Ram, A. Zieger, and B. Ziegler
Nucl. Phys. A251, 479 (1975)

ELEM. SYM.	A	Z
Li		3

METHOD

REF. NO.	
75 Ah 3	egf

REACTION	RESULT	EXCITATION ENERGY	SOURCE		DETECTOR		ANGLE
			TYPE	RANGE	TYPE	RANGE	
G,MU-T	ABX	10-210	C	140-275	MGC-D		4PI

912+

TABLE 2

The moments of the experimental nuclear cross section distributions integrated from 10 MeV to the energy E, and their statistical errors

	E (MeV)	$\sum_{-2}$ (mb/MeV)	±(%)	$\sum_{-1}$ (mb)	±(%)	$\sum_{0}$ (mb·MeV)	±(%)	$\sum_{+1}$ (b·MeV²)	±(%)	$\sum_{+2}$ (b·MeV³)	±(%)
Li	100	0.196	1.1	4.64	1.0	143	1.7	5.82	3.1	305	5
	140	0.197	1.1	4.79	1.0	161	1.9	8.03	3.4	577	5
	210	0.198	1.1	5.03	1.0	206	2.0	16.60	3.7	2220	5
Be	100	0.192	2.5	5.19	1.5	173	2.0	7.11	3.4	362	5
	140	0.194	2.5	5.33	1.5	189	2.1	9.09	3.6	600	6
	210	0.195	2.5	5.58	1.5	236	2.1	17.80	3.5	2240	5
C	100	0.313	1.7	8.81	1.1	291	1.6	12.00	2.9	630	4
	140	0.316	1.7	9.18	1.2	334	2.2	17.10	5	1250	7
O	100	0.580	1.6	14.50	1.3	432	2.0	16.00	4	748	8
	140	0.585	1.6	15.10	1.3	508	2.5	25.20	5	1880	8
Al	100	1.10	1.8	25.70	1.5	739	2.6	27.9	5	1400	8
	140	1.11	1.8	26.3	1.7	807	3.9	36.4	9	2450	16
Ca	100	2.22	1.2	45.5	1.5	1120	3.6	34.9	9	1430	18
	140	2.23	1.2	46.8	1.7	1290	4.6	56.6	11	3710	19

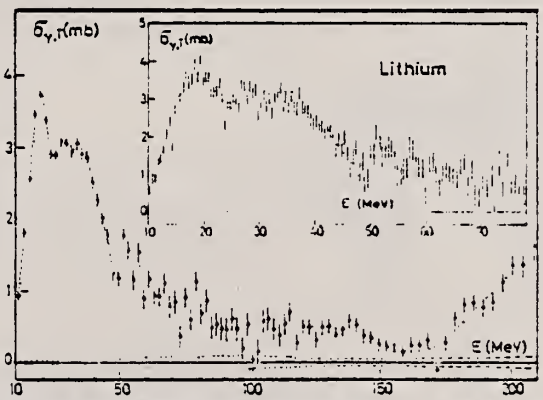

Fig. 2. Total photonuclear cross section for natural Li. The error bars indicate one standard deviation of counting statistics from the main spectrometer. The dashed lines along the abscissa indicate the uncertainty due to counting statistics in the normalizing spectrometer. Oscillations of the base line within this area are possible, the period of these oscillations, however, must not be smaller than 10% in photon energy. The dashed and dotted lines through the cross section values have been drawn to guide the eye.

REF. M. K. Leung, J. J. Murphy, II, Y. M. Shin, D. M. Skopik
Can. J. Phys. 55, 252 (1977)

ELEM. SYM.	A	Z
Li		3

METHOD

REF. NO. 77 Le 1 hmg

REACTION	RESULT	EXCITATION ENERGY	SOURCE		DETECTOR		ANGLE
			TYPE	RANGE	TYPE	RANGE	
E,HE	ABX	5- 15	D	24	MAG-D		90
				(23.8)			

1059

Tritons resulting from the electrodisintegration of ^{7}Li have been measured at 90° for an incident electron energy of 23.8 MeV over an energy range which ensured that only tritons emitted in the two-body channel were detected. The electrodisintegration cross sections were converted to equivalent photodisintegration data and compared to earlier results. Large discrepancies are observed. It is found that the (γ,^{3}H) channel contributes appreciably to the electric dipole sum rule for ^{7}Li.

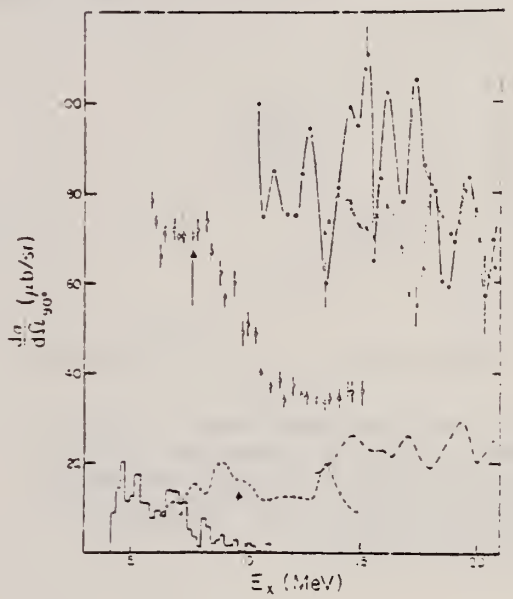

FIG. 1. The 90° differential cross section for the reaction ^{7}Li(γ,^{3}H)^{4}He. ○, this experiment; ———, Erdös *et al.* (1954); ▲, Seeser (1970); — Miwa and Yamanouchi (1960); – – –, Denisov and Kul'chitskii (1967); ⊕, Manuzio *et al.* (1966); and ×, Kul'chitskii and Volkov (1963). Error bars show statistical uncertainties.

BRAMBLETT, R. L., BERMAN, B. L., KELLY, M. A., CALDWELL, J. T., and FULTZ, S. C. 1973. Proc. Int. Conf. on Photonuclear Reactions and Applications, Asilomar Conference Grounds, Pacific Grove, CA (E. O. Lawrence Livermore Laboratory, University of California, Livermore, CA), p. 175.

CHONG, K. F., PHENNEGER, M. C., SHIN, Y. M., SKOPIK, D. M., and TOMUSIAK, E. L. 1974. Nucl. Phys. A, 218, 43.

DENISOV, V. P. and KUL'CHITSKII, L. A. 1967. Sov. J. Nucl. Phys. 5, 344.

ERDÖS, P., STOLL, P., WACHTER, M., and WATAGHIN, V. 1954. Nuovo Cimento, 12, 638.

GREGORY, A. G., SHERWOOD, T. R., and TITTERTON, E. W. 1962. Nucl. Phys. 32, 543.

KUL'CHITSKII, L. A. and VOLKOV, YU. M. 1963. Sov. Phys.-JETP, 17, 750.

MANUZIO, G. E., RICCO, G., and SANZONE, M. 1966. Nuovo Cimento B, 42, 343.

MIWA, M. and YAMANOUCHI, M. 1960. J. Phys. Soc. Japan, 15, 942.

SEESER, J. W. 1970. Ph.D. thesis, University of Missouri (Unpublished).

SHIN, Y. M., SKOPIK, D. M., and MURPHY, J. J. 1975. Phys. Lett. B, 55, 297.

SKOPIK, D. M., SHIN, Y. M., PHENNEGER, M. C., and MURPHY, J. J. 1974. Phys. Rev. C, 9, 531.

REF. D.M. Skopik, J. Asai, E.L. Tomusiak, J.J. Murphy II
Phys. Rev. C20, 2025 (1979)

ELEM. SYM.	A	Z
Li		3

METHOD

REF. NO. 79 Sk 3 hg

REACTION	RESULT	EXCITATION ENERGY	SOURCE		DETECTOR		ANGLE
			TYPE	RANGE	TYPE	RANGE	
E,T	ABX	5-50	D	20-50	MAG-D		DST

Differential and total cross sections for the $^7Li(\gamma,t)^4He$ reaction were measured. Both real and virtual photons were used in the experiment and gave self-consistent results. The data show a broad resonance indicating the presence of positive parity states near 8 MeV excitation in ^7Li. A calculation using an α-^3H cluster model of ^7Li was also performed. Poor agreement is found between the calculation and experimental results.

VIRT PHOT ANALYSIS

(1) Measured ^4He particles above 14.5 MeV

(2) $\int_{THR}^{50} \sigma(\gamma,t)dE = 8.1$ MeV mb

(3) $\int \sigma(\gamma,t)dE$ for low energy resonance is 6.2 MeV mb and Breit-Wigner fit gives Γ=7.2 MeV centered at E_r=7.7 MeV

(4) Target 92.4% ^7Li, 7.6% ^6Li

[NUCLEAR REACTIONS $^7Li(\gamma,t)^4He$, measured $\sigma(E;E_\alpha,\theta_\alpha)$ and $(E;E_t,\theta_t)$ calculated ^3H-α cluster model cross section.]

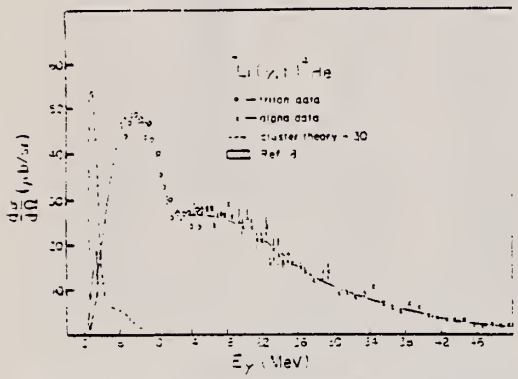

FIG. 2. The 90° cross section for the (γ,t) and (γ,α) reactions. The $^7Li(\gamma,t)^4He$ measurement is indicated by the open circles, while the $^7Li(\gamma,\alpha)^3H$ measurement is indicated by the crosses. The dashed line is the result of the theory described in the text. The solid line is only meant to guide the eye.

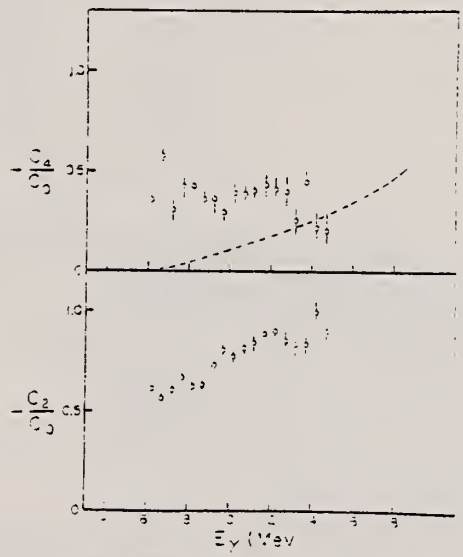

FIG. 3. Even Legendre coefficients found by least-squares fitting the data to Eq. (4). The dashed line indicates the $E2$ strength in our α-^3H cluster model.

(continued)

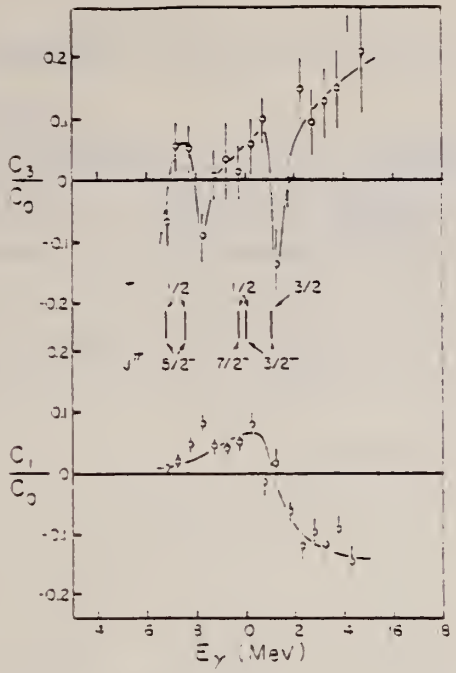

FIG. 4. Odd Legendre coefficients. The location of the known negative parity states in ^{7}Li are indicated

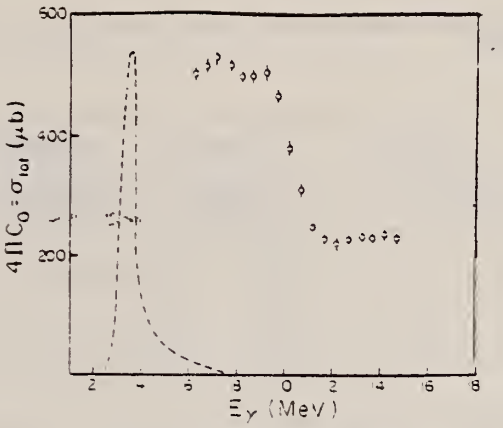

FIG. 5. The total cross section determined from the angular distribution data. The dashed line is the theory divided by 30.

REF. B. Bellinghausen, A. Christ, H.J. Gassen, G. Goerigk, R. Muller, G. Noldeke, T. Reichelt, H. Stanek, P. Stipp
Nucl. Phys. A358, 373c (1981)

ELEM. SYM.	A	Z
Li		3

METHOD

REF. NO. 81 Be 3 hg

REACTION	RESULT	EXCITATION ENERGY	SOURCE		DETECTOR		ANGLE
			TYPE	RANGE	TYPE	RANGE	
G,PIO	ABX	280-386	C	300-450	MGP-D		0

Abstract: π^0 photoproduction on ^{3}He, Li(nat) and ^{9}Be has been measured under small angles in the P_{33} resonance region.

Table 1
Cross sections as function of energy and momentum transfer

K_{max}	K	q	$d\sigma/d\Omega^*$ in ub/sterad		
MeV	MeV	fm^{-1}	^{3}He	Li(nat)	^{9}Be
300	280	0.27	12.4 ± 1.5	21.0 ± 2.4	23.6 ± 2.7
320	296	0.27	14.6 ± 1.5	26.9 ± 2.1	34.4 ± 2.7
370	334	0.26	14.3 ± 1.5	24.9 ± 2.0	31.0 ± 2.6
390	361	0.23	10.0 ± 1.1	21.1 ± 1.6	24.5 ± 1.8
450	386	0.27	7.7 ± 1.1	22.7 ± 2.3	22.8 ± 2.3

LI
A=4

LI
A=4

LI
A=4

REF.

W. L. Imhof, F. J. Vaughn, L. F. Chase, Jr., H. A. Grench and M. Walt
Nucl. Phys. 59, 81-88 (1964)

ELEM. SYM.	A	Z
Li	4	3

METHOD

$He^3(p,\gamma)Li^4$ Van de Graaff

REF. NO.	
64 Im 1	JOC

REACTION	RESULT	EXCITATION ENERGY	SOURCE		DETECTOR		ANGLE
			TYPE	RANGE	TYPE	RANGE	
P,G	ABY		D	0 - 3	NAI-D		90
				(.5 - 2.6)			

NØ LI4 FØUND

TABLE 1
Upper limits to the cross sections

Reaction	Bombarding energy (MeV)	Half-life interval (sec)	Upper limit to cross section (cm^2)
$H^3(n,\gamma)H^4$	thermal	3×10^{-4}–10^4	6×10^{-30}
$H^3(n,\gamma)H^4$	thermal	10^3 –10^5	1×10^{-30}
$H^3(n,\gamma)H^4$	0.030–1.2	3×10^{-3}–10^3	6×10^{-32}
$H^3(n,\gamma)H^4$	0.030–1.2	10^3 –10^5	1×10^{-32}
$H^3(d,p)H^4$	2.5	10^{-1}–10^3	3×10^{-32}
$He^3(p,\gamma)Li^4$	0.5	3×10^{-4}–4×10^{-3}	9×10^{-34}
$He^3(p,\gamma)Li^4$	1.3	3×10^{-4}–10^{-1}	2×10^{-34}
$He^3(p,\gamma)Li^4$	1.3	10^{-1}–10^3	6×10^{-34}
$He^3(p,\gamma)Li^4$	2.4	10^{-1}–10^3	8×10^{-34}
$He^3(p,\gamma)Li^4$	2.6	3×10^{-4}–10^{-1}	2×10^{-33}
$He^3(d,n)Li^4$	0.5	3×10^{-4}–4×10^{-4}	3×10^{-33}
$He^3(d,n)Li^4$	0.7	4×10^{-4}–10^3	4×10^{-33}
$He^3(d,n)Li^4$	2.3	10^{-4}–10^{-1}	4×10^{-33}
$He^3(d,n)Li^4$	2.3	10^{-1}–10^3	8×10^{-33}

Based on search for Li^4 β-activity

$\sigma \leq 4\times10^{-32}$ cm^2, based on search for directly observed γ-rays with NaI.

LI
A=5

LI
A=5

LI
A=5

REF. W. Buss, W. Del Bianco, H. Waffler and B. Ziegler
Nucl. Phys. A112, 47 (1968)

ELEM. SYM.	A	Z
Li	5	3

METHOD

REF. NO. 68 Bu 1 EGF

REACTION	RESULT	EXCITATION ENERGY	SOURCE		DETECTOR		ANGLE
			TYPE	RANGE	TYPE	RANGE	
D,G	ABX	16-17	D	0-1	NAI-D	6-18	DST

TABLE 1
Measured angular distributions

ϑ	0°	30°	60°	90°	120°
E_d = 480 keV	5450±93	5681±97	5591±95	5577±95	
E_d = 1025 keV	3410±80	3519±84	3729±85	3725±85	3787±87

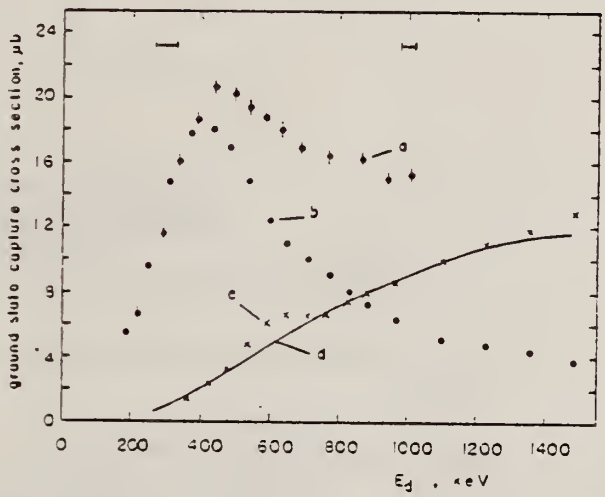

Fig. 7. The $^3He(d,\gamma)^5Li$ reaction. Curve a — ground state cross section (this experiment), curve b — resonance part of the capture cross section (the energy dependence was assumed to be the same as that of the $^3He(d,p)^4He$ reaction) curve c — difference between resonance part and total cross section (direct part); curve d — calculated direct component of capture cross section.

REF. W. Del Bianco, F. Lemire, R. J. A. Lévesque, and J. M. Poutissou
Can. J. Phys. 46, 1585 (1968)

ELEM. SYM.	A	Z
Li	5	3

METHOD

REF. NO. 68 De 2 egf

REACTION	RESULT	EXCITATION ENERGY	SOURCE		DETECTOR		ANGLE
			TYPE	RANGE	TYPE	RANGE	
HE,G	ABX	17-21	D	2-12	NAI-D	7-20	90

HE= HE3

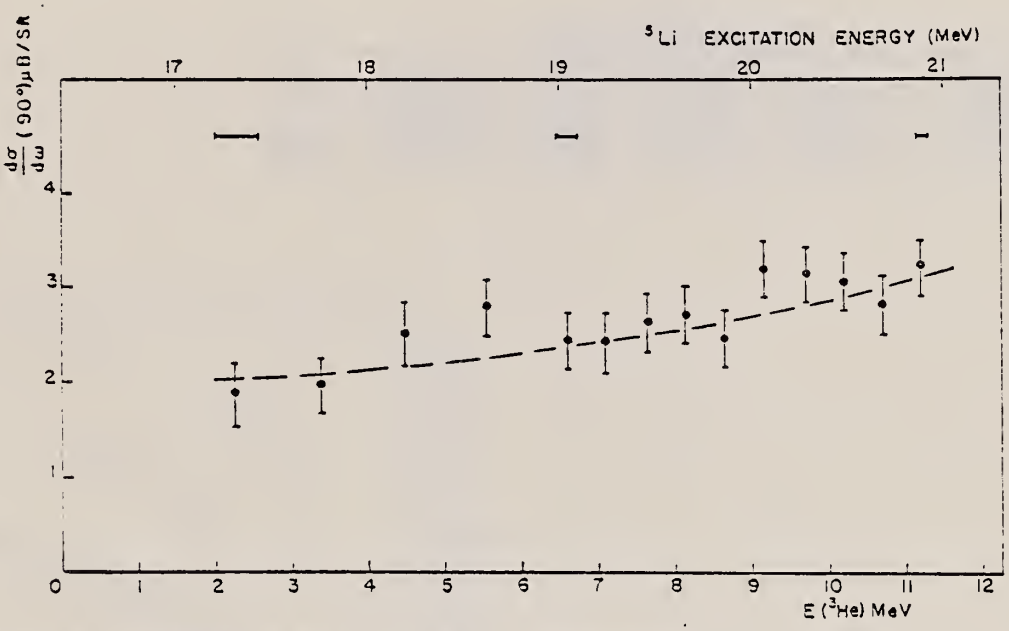

FIG. 2. 90° differential cross section of the D(^{3}He, γ)^{5}Li reaction for transitions to the ground and first excited states of ^{5}Li.

REF. L. Kraus, M. Suffert and D. Magnac-Valette
Nucl. Phys. A109, 593 (1968)

ELEM. SYM.	A	Z
Li	5	3

METHOD

REF. NO. 68 Kr 1

- EGF

REACTION	RESULT	EXCITATION ENERGY	SOURCE		DETECTOR		ANGLE
			TYPE	RANGE	TYPE	RANGE	
D,G	ABX	16-19	D	2-6	NAI-D	10-20	DST

J-PI: 3/2+

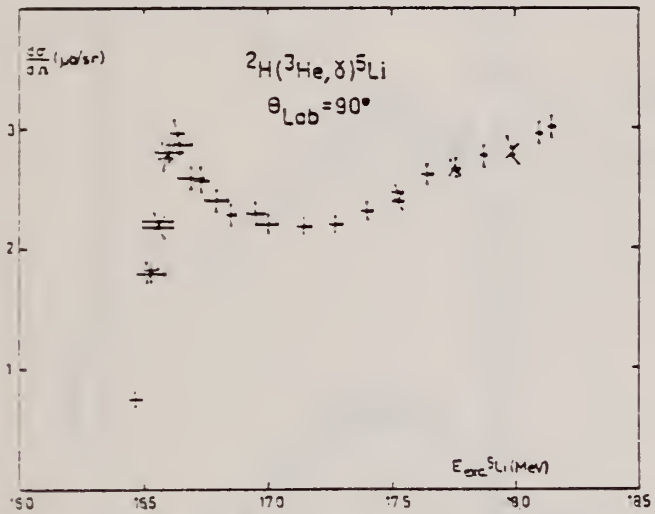

Fig. 3. Section efficace différentielle à 90° de la réaction $^2H(^3He,\gamma)^5Li$ en fonction de l'énergie d'excitation dans ^5Li, au centre de la cible. Les barres horizontales indiquent la dispersion en énergie due à l'épaisseur de la cible. L'erreur indiquée pour la section efficace ne tient pas compte de l'erreur possible sur l'étalonnage absolu (valeur maximum estimée ±30 %).

TABLEAU I

Section efficace totale au sommet de la résonance

Réaction	$^5Li^*$ (MeV)	$\sigma(\mu b)$
$^2H(^3He,\gamma)^5Li$	16.633	37.3±1.4
$^3He(d,\gamma)^5Li$	16.630	38.3±1.4

prises entre 1 et 5 MeV. Dans ce cas, les spectres obtenus se différencient de celui de la fig. 1 par la présence d'un bruit de fond de basse énergie dû aux neutrons produits

(continued)

REF. L. Kraus, M. Suffert and D. Magnac-Valette
Nucl. Phys. A109, 593 (1968)

ELEM. SYM.	A	Z
Li	5	3

METHOD

REF. NO.	
68 Kr 1	- EGF

DETECTOR		ANGLE
TYPE	RANGE	

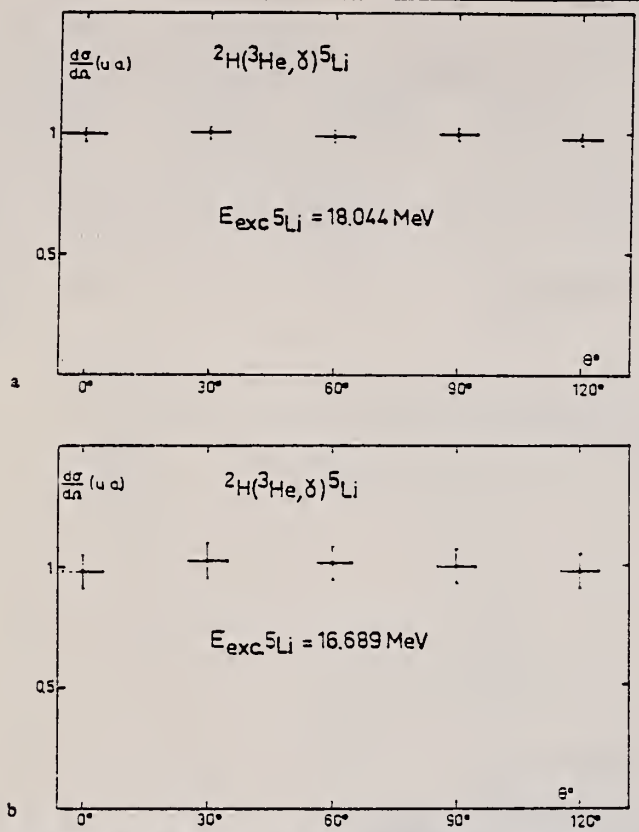

Fig. 4. Distributions angulaires des photons émis dans la réaction $^2H(^3He,\gamma)^5Li$. La correction de l'effet Doppler est faite. Les barres horizontales représentent l'angle d'ouverture du cône de détection. Les mesures sont faites à $^5Li^*$ = 16.689 MeV (a) et à $^5Li^*$ = 18.044 MeV (b).

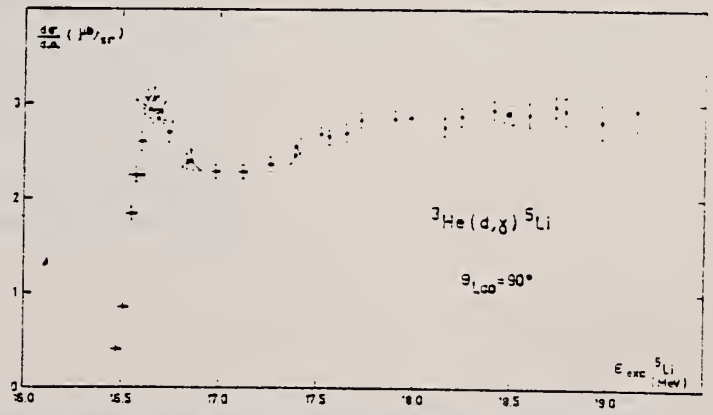

Fig. 5. Section efficace différentielle à 90° de la réaction $^3He(d,\gamma)^5Li$ en fonction de l'énergie d'excitation dans ^5Li au centre de la cible. Les barres horizontales sur certains points représentent l'étalement en énergie dû à l'épaisseur de la cible gazeuse.

REF. H. Schroder and W. Mausberg
Z. Physik 235, 234 (1970)

ELEM. SYM.	A	Z
Li	5	3

METHOD

REF. NO. 70 Sc 3 egf

REACTION	RESULT	EXCITATION ENERGY	SOURCE TYPE	SOURCE RANGE	DETECTOR TYPE	DETECTOR RANGE	ANGLE
HE.G	ABX	18-21	D	4-12	NAI-D		DST
		(17.8-21.1)					

HE=HE3

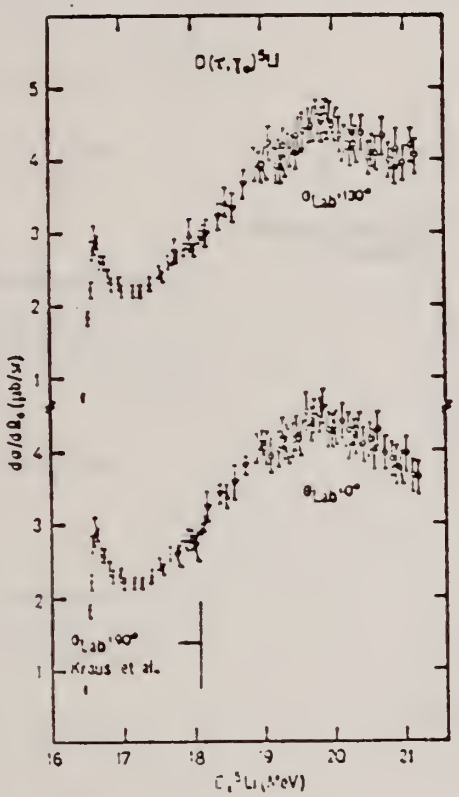

Fig. 2. Excitation curves of the reaction $D(\gamma, \gamma_0)^5Li$ at θ_{Lab} 0° and 130°. The circles and triangles represent measurements taken in different runs

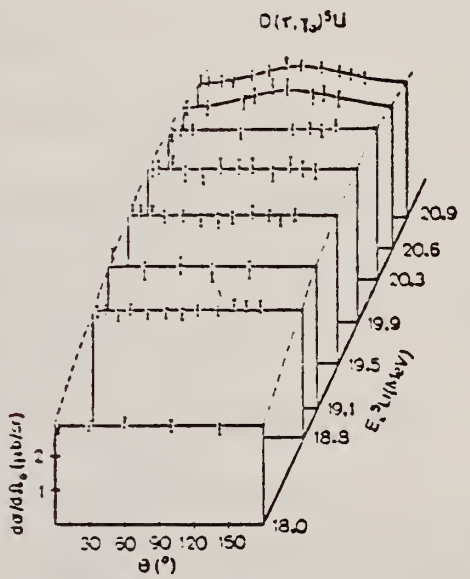

Fig. 3. Angular distributions of the γ-radiation from the reaction $D(\gamma, \gamma_0)^5Li$

(continued)

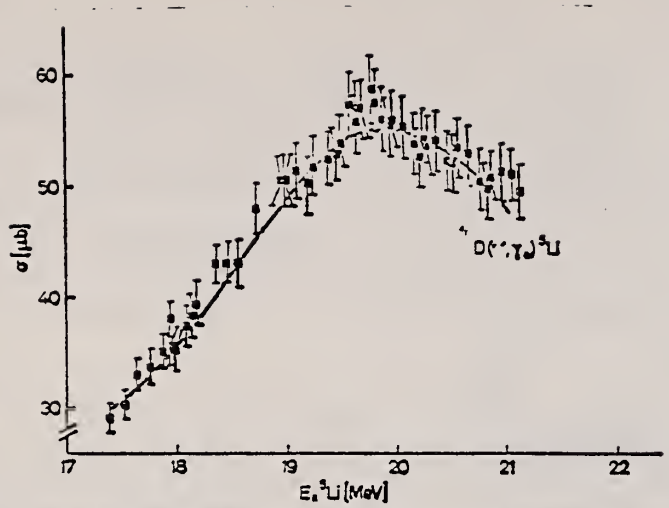

Fig. 4. Integrated cross section of the reaction $D(\pi, \gamma_0)^5Li$. The solid curve represents a fit with the "one-level-approximation with constant background"

REF.

H. T. King, W. E. Meyerhof and R. G. Hirko
Nucl. Phys. A178, 337 (1972)

ELEM. SYM.	A	Z
Li	5	3

METHOD

REF. NO. 72 Ki 2 egf

REACTION	RESULT	EXCITATION ENERGY	SOURCE		DETECTOR		ANGLE
			TYPE	RANGE	TYPE	RANGE	
HE,G	ABX	17-26	D	2-26	NAI-D		DST

HE=HE3

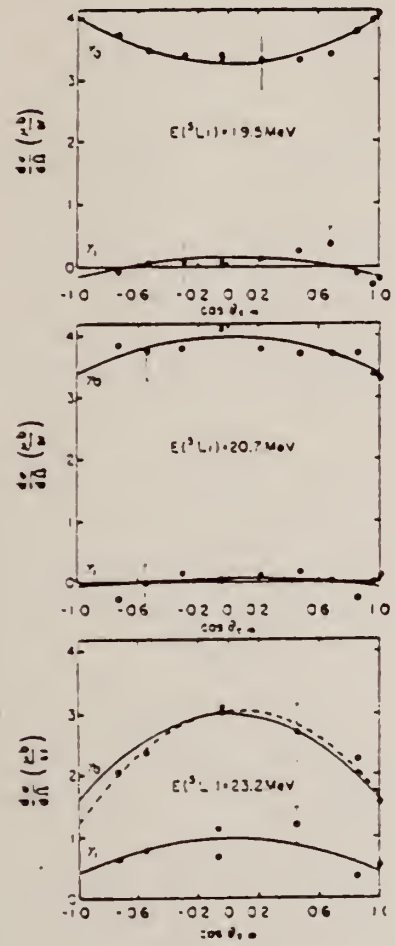

Fig. 9. Angular distributions at $E_x(^5Li) = 19.5$, 20.7 and 23.2 MeV, with even Legendre polynomial fits up to P_2. The broken line is a fit which included P_1 in addition to P_0 and P_2.

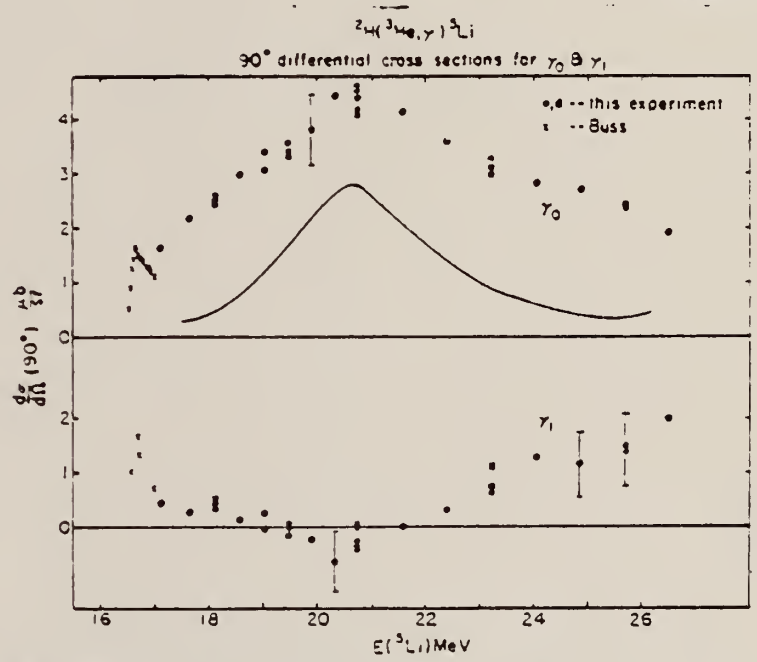

Fig. 8. Cross sections for $^2H(^3He, \gamma)^5Li$ at 90°, resolved into γ_0 and γ_1 contributions. Low-energy data are from ref. [13]). The solid line has been computed by ref. [9]).

[9] R. F. Wagner, C. Werntz, Phys. Rev. C4, 1 (1971).

[13] W. Buss, W. Del Bianco, H. Waffler and B. Ziegler, Nucl. Phys. A112, 47 (1968).

TABLE 1

Results of Legendre polynomial fits

$E(^5Li)$ (MeV)	γ_0			γ_1		
	even only	even and odd		even only	even and odd	
	A_2/A_0	A_2/A_0	A_1/A_0	A_2/A_0	A_2/A_0	A_1/A_0
18.1	0.03 ±0.10	0.03 ±0.13	0.01 ±0.11	−1.9 ±0.7	−1.4 ±0.8	−0.4 ±0.6
19.5	0.14 ±0.08	0.15 ±0.09	−0.02 ±0.09			
20.7	−0.10 ±0.07	−0.09 ±0.09	−0.02 ±0.08			
20.7	−0.13 ±0.06	−0.17 ±0.08	0.06 ±0.07			
23.2	−0.37 ±0.13	−0.43 ±0.16	0.09 ±0.14	−0.47 ±0.25	−0.54 ±0.31	0.10 ±0.26
25.7	−0.53 ±0.16	−0.66 ±0.19	0.22 ±0.16	−0.44 ±0.20	−0.45 ±0.23	0.01 ±0.19

Fits were performed using even polynomials only, as well as both even and odd. Around $E_x(^5Li) = 20$ MeV the γ_1 intensity is too small to be fitted meaningfully.

Li
A=6

Li
A=6

Li
A=6

Ref. R.D. Edge
Australian J. Phys. 9, 429 (1956)

Elem. Sym.	A	Z
Li	6	3

Method F(p,αγ) source; Sziland-Chalmers detector

Ref. No. 56 Ed 2 EGF

Reaction	E or ΔE	E_o	Γ	$\int \sigma dE$	Jπ	Notes
$Li^6(\gamma,n)$	6.2					$\sigma = (3\pm2)10^{-28}cm^2$ D(γ,n) used for σ calibrations.

Ref. L. Cohen, R.A. Tobin
Nuclear Phys. 14, 243 (1959)

Elem. Sym.	A	Z
Li	6	3

Method
Betatron; photon scattering; NaI

Ref. No. 59 Co 4 - JHH

Reaction	E or ΔE	E_o	Γ	$\int \sigma dE$	Jπ	Notes
$Li^6(\gamma,\gamma)$	6.5	3.56	$9.1^{+2.0}_{-1.5}$ eV		(0)	This value for Γ has been corrected for a Doppler width of 11.3 eV. The mean lifetime t= t/Γ is then: $(7.2^{+1.5}_{-1.3})\ 10^{-17}$ sec.

F. Däublin, F. Berthold and P. Jensen
Z. Naturforsch 14a, 208 (1959)

Li	6	3

METHOD

REF. NO. 59 Da 1 | EGF

REACTION	RESULT	EXCITATION ENERGY	SOURCE		DETECTOR		ANGLE
			TYPE	RANGE	TYPE	RANGE	
G.D	ABX	2.3	D	2.3	ION-D		4PI

2.20 MeV (RaC line) 7.3×10^{-31} cm^2 ± 75%
2.76 MeV (Na^{24}) 2.5×10^{-31} cm^2 ± 50%

Ref. T.A. Romanowski, V.H. Voelker
Phys. Rev. 113, 886 (1959)

Elem. Sym.	A	Z
Li	6	3

Method: Betatron; BF_3 counters

Ref. No.: 59 Ro 1 | JHH

Reaction	E or ΔE	E_o	Γ	$\int \sigma dE$	Jπ	Notes
$Li^6(\gamma, xn)$	Bremss. 4-20	12.5				σ_{max}(E = 12.5 MeV) = 2.8±0.53 mb.

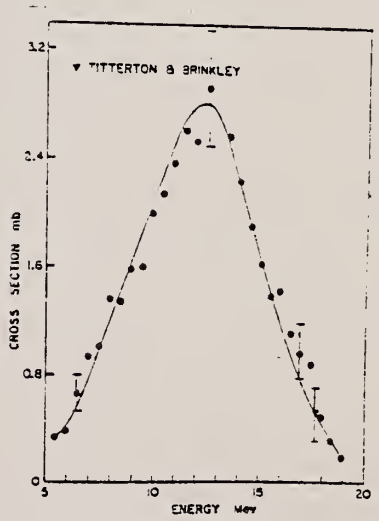

IG. 5. (γ,n) cross section for Li^6 as a function of γ-ray energy.

[19] E. W. Titterton and T. A. Brinkley, Proc. Roy Soc. (London.) A64, 212 (1951).

Ref. E.B. Bazhanov, L.A. Kul'chitskii
Zhur. Eksp. i Teoret. Fiz. 38, 1685 (1960)
Soviet Phys. JETP 11, 1215 (1960)

Elem. Sym.	A	Z
Li	6	3

Method: 100 MeV Synchrotron; Scint. telescopes; coinc.

Ref. No.: 60 Ba 3 JH

Reaction	E or ΔE	E_o	Γ	$\int \sigma dE$	Jπ	Notes
(γ,p) (γ,pn)	protons 35-87MeV					Yield curve for $\bar{E}_p$=16,20,25,30,35 MeV Yield curve and cross section all similar to figure 1 when energy scales are displaced. Figure 1 gives data for $\bar{E}_p$= 20 MeV at 57.5°. Figure 2 curve "a" direct shell model curve "c" quasi-deutron - both normalized at θ = 60°; curve "b" absolute theory for single particle (Shklyareoshii) n's in coincidence with p's at given angle are isotropic.

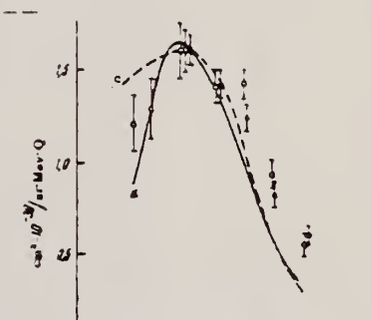

FIG. 2. Angular proton distribution for $\bar{E}_p$ = 25 Mev. The ordinate scale is given for the experimental points and for curve b. The errors are statistical.

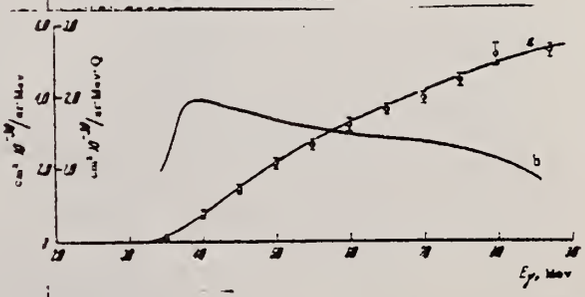

FORM NBS-418
(5-1-63)
USCOMM-OC 18556-P63

U.S. DEPARTMENT OF COMMERCE
NATIONAL BUREAU OF STANDARDS

Ref. W.C. Barber, F. Berthold, G. Fricke, F.E. Gudden
Phys. Rev. 120, 2081 (1960)

Elem. Sym.	A	Z
Li	6	3

Method Stanford Mark II linac; magnetic spectrometer; plastic scintellator counter telescope

Ref. No. 60 Ba 4 JHH

Reaction	E or ΔE	E_o	Γ	$\int \sigma dE$	$J\pi$	Notes
(e^-, e^-)	39.5	3.56	Γ_γ = 6.2±0.6eV	0.62±0.06 MeV-mb	0+	∫σdE is average of 0.613 and 0.634 MeV-mb measured at θ = 160° and 132° respectively. M 1 transition. Also observed small peaks (see Figures 5 and 6) due to 2.184 MeV E2 transition to 3+ state.

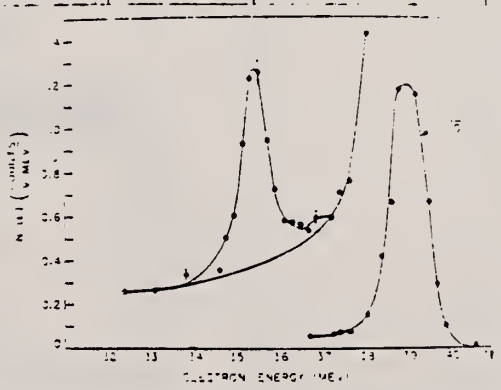

FIG. 5. Energy distribution of electrons, which were inelastically scattered from 39.5 Mev. after 160° scattering from a Li^6 target.

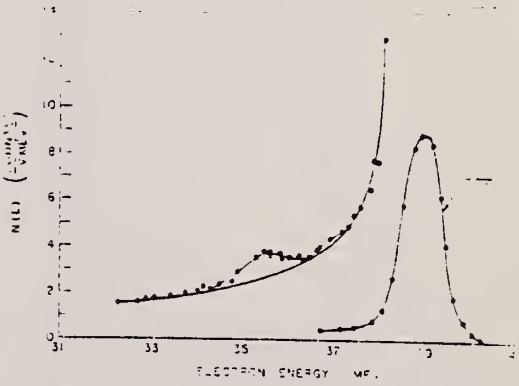

FIG. 6. Energy distribution of electrons, which were inelastically scattered from 39.5 Mev. after 132° scattering from a Li^6 target.

Ref. V.P. Chizhov
Zhur. Eksp. i Teoret. Fiz. 38, 809 (1960);
Soviet Phys. JETP 11, 587 (1960)

Elem. Sym.	A	Z
Li	6	3

Method: 90 MeV Bremsstrahlung; scintillator counter telescope

Ref. No.: 60 Ch 1 - JHH

Reaction	E or ΔE	E_o	Γ	$\int \sigma dE$	Jπ	Notes
$Li^6(\gamma,p)$						E_d - 15.5 - 31 MeV
$Li^6(\gamma,d)$						E_p - 15.5-30 MeV
$Li^6(\gamma,t)$						E_t - 17-30 MeV
						Angular distribution.
						Ratios: $\sigma(\gamma,d)/\sigma(\gamma,p)$ at $\theta = 80^\circ$
						$\sigma(\gamma,t)/\sigma(\gamma,d)$ summed over angles 35°-145°

TABLE I

Element	$100N_i/N_d$	Element	$100N_i/N_d$	Element	$100N_i/N_d$	Element	$100N_i/N_d$
Li^6	30±3	B	29±9	Ni	10±4	In	5±2.5
Li^7	22.5±2.5	Si	10±4	Co	2.5±2	Ta	10±4
Be	13±2.0	S	9±4	Cu	2.2±2	Au	3±3

TABLE II

	$\frac{\sigma_{\gamma p}\cdot 10^{26}}{Q\cdot sr}$, cm^2	$\frac{\sigma_{\gamma d}}{\sigma_{\gamma p}}\cdot 10^2$	$\frac{\sigma_{\gamma t}}{\sigma_{\gamma p}}\cdot 10^2$
Li^7	66.0±1.3	6.3±0.55	1.0±0.25
Li^6	62.5±1.3	2.10±0.25	0.70±0.20

YIELD DATA TABLE:

It should be noted that the yield of photoprotons of the energy considered rises smoothly with Z for the elements plotted in Fig. 3. and that starting already with Al, no direct proportionality to Z is observed on account of the effect of the Coulomb barrier. For illustration, we give the yields of photoprotons $Y(\gamma, p)$ per proton in the nucleus for several elements in relative units (the error in these measurements was estimated to be ±10%):

	Li^6	Li^7	Be	C	Al	Cu
$Y(\gamma,p)$ =	1.00	1.07	1.5	1.31	1.00	58

(for Figures see page 2) (continued)

Elem. Sym.	A	Z
Li	6	3

Method

Ref. No. 60 Ch 1

Reaction	E or ΔE	E_0	Γ	$\int \sigma dE$	Jπ	Notes

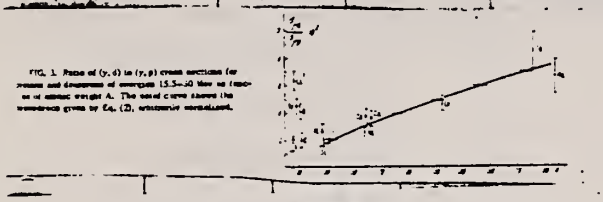

FIG. 1. Ratio of (γ, d) to (γ, p) cross sections for protons and deuterons of energies 15.5–30 Mev as function of atomic weight A. The solid curve shows the dependence given by Eq. (2), arbitrarily normalized.

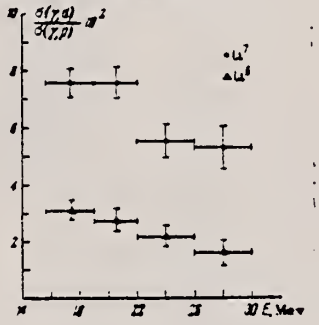

FIG. 4. Dependence of the ratio of (γ, d) to (γ, p) cross sections on the particle energy E for Li^6 and Li^7.

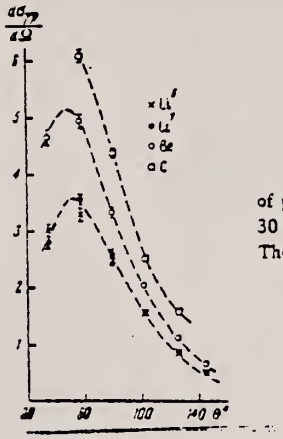

FIG. 6. Angular distributions of photoprotons of energies 15.5–30 Mev for Li^6, Li^7, Be, and C. The errors are statistical.

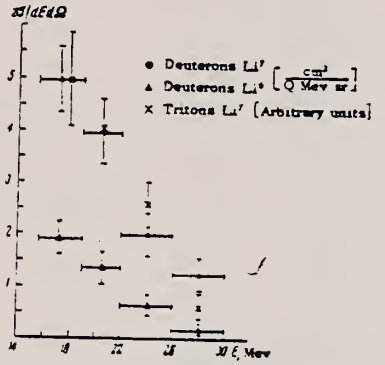

FIG. 5. Energy distributions of photodeuterons from Li^6 and Li^7 and phototritons from Li^7. The scale of the ordinate for phototritons is arbitrary.

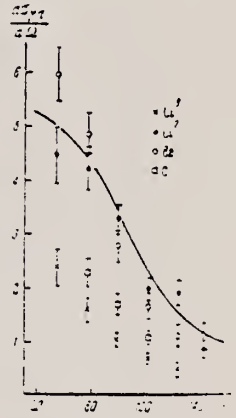

FIG. 7. Angular distributions of photodeuterons of energies 15.5–30 Mev for Li^6, Li^7, Be, and C. The errors are statistical. The solid curve gives the calculated results for photodeuterons from Be.

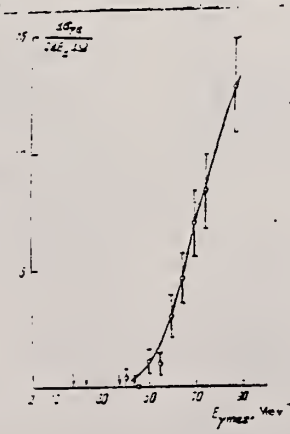

FIG. 10. Excitation function for photodeuterons of energies 15.6–22 Mev from Li^6.

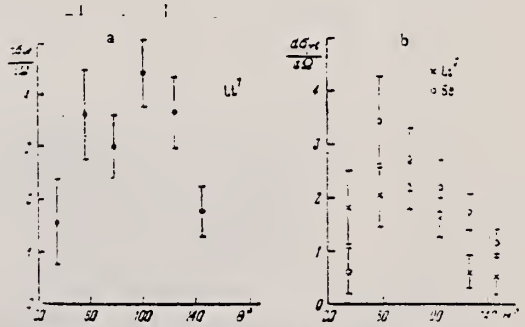

FIG. 9. Angular distributions of phototritons of energies 17–30 Mev for Li^7, Li^6, and Be. a – Li^7; b – Li^6 and Be. The scale is the same in a and b. The errors are statistical.

A.P. Komar, E.D. Makhnovskii
Dokl. Akad. Nauk SSSR 135, 52 (1960); Soviet Phys. Doklady 5, 1229 (1961)

Li	6	3

METHOD: Synchrotron; proton spectrum; nuclear emulsions

REF. NO.: 60 Ko 3 | NVB

REACTION	RESULT	EXCITATION ENERGY	SOURCE		DETECTOR		ANGLE
			TYPE	RANGE	TYPE	RANGE	
G,P	SPC	5-23	C	28	EMU-D	1-18	60

Sample 90% Li^6

SEP ISOTPS

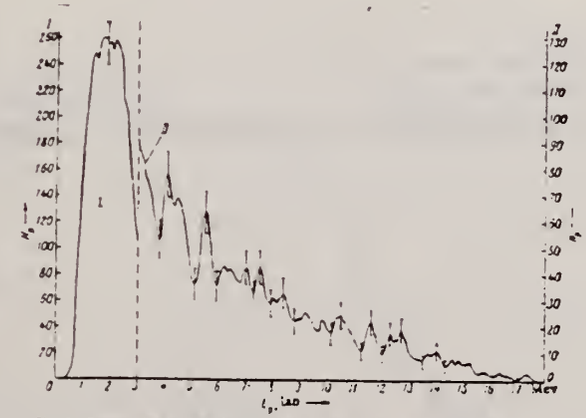

Fig. 1. Energy distribution of the protons during the photodisintegration of Li^6.

TABLE 1.

Location of maximum in E_p spectrum, Mev	Energy of level, Mev: established levels	Energy of level, Mev: proposed levels
4.1		9.5*
4.5		10.0**
5.5	11.2	
11.3	18.3	

* According to [5] there is a level of 9.3 ± 0.2 Mev.

** The works of E. A. Al'bits and others [4] indicate a level at 10 Mev.

4. Nuclear Reactions at Low and Medium Energies, Transactions of the All-Union Conference [in Russian] (Izd. AN SSSR, 1958) pp. 435, 33.

5. K. W. Allen, E. Almquist, and C. B. Bigham, Phys. Rev. 99, 631 (1955).

REF.

A. Komar
PICNS 494 (1960)

ELEM. SYM.	A	Z
Li	6	3

METHOD

Synchrotron

REF. NO.	
60 Ko 5	NVB

REACTION	RESULT	EXCITATION ENERGY	SOURCE		DETECTOR		ANGLE
			TYPE	RANGE	TYPE	RANGE	
G,P	SPC	6 - 28	C	28	EMU-D	1-20	60

Target 90% Li^6.

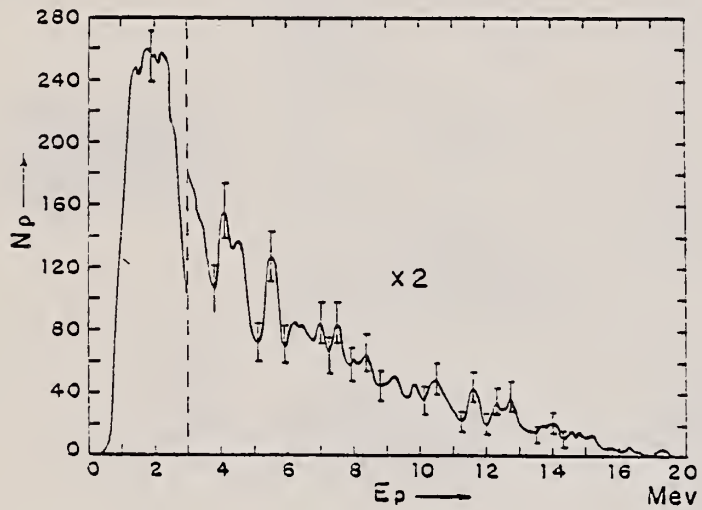

Fig. 1

TABLE I

Position of the Maximum in the spectrum in MeV.	Level energy (MeV) Established Levels	Assumed Levels	Notes
4,1		9,5	In accordance with ref. 5, there is a level at 9.3 ± 0.2 MeV.
4,5		10,0	In the work of Alveetska et al., ref. 4, a level is indicated at 10 Mev.
5,5	11,2		
11,6	18,3		

4) K.W. Allen, E. Almqvist and C.3. Bigham, Phys. Rev. 99, 631 (1955).

Ref. D.G. Proctor, W. H. Voelker
Phys. Rev. 118, 217 (1960)

Elem. Sym.	A	Z
Li	6	3

Method: Betatron; plastic scintillator proton counter; proton recoil neutron counter.

Ref. No.: 60 Pr 1 JH

Reaction	E or ΔE	E_0	Γ	$\int \sigma dE$	Jπ	Notes
$Li^6(\gamma,n)$	Bremss: 17.3			58% ± 11%		Independent-particle model indicated, in preference to deutron-alpha particle model.
$Li^6(\gamma,p)$				31% ± 11%		Large proton yield at E_p = 5.5 MeV is not explained; not due to correlated (n,p) pairs.
$Li^6(\gamma,np)$				< 2%		Figures given in $\int \sigma dE$ column are the per unit of the total neutron yield produced by each reaction.
						Measurements at 90°.

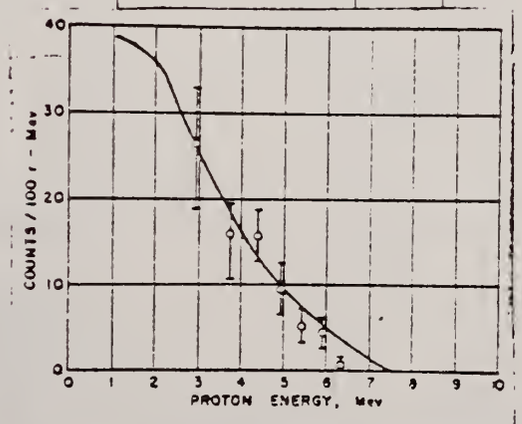

FIG. 3. $D(\gamma,p)p$ proton energy distribution after proton leaves target.

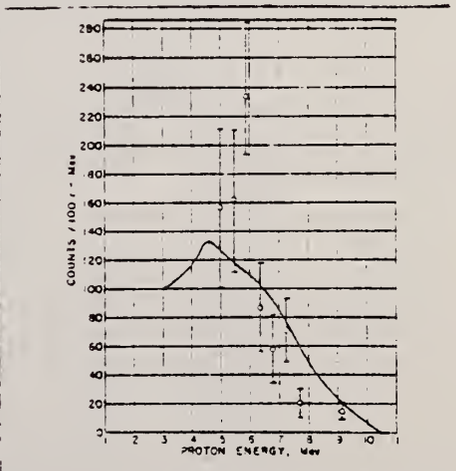

FIG. 4. $Li^6(\gamma,p)He^4$ proton energy distribution after proton leaves target. The point at 9.2 Mev is the surplus channel positioned and normalized to a channel from 7.9 Mev to 10.4 Mev.

Ref. E.C. Booth, K.A. Wright
Nuclear Phys. 35, 472 (1962)

Elem. Sym.	A	Z
Li	6	3

Method 4 MeV electron Van de Graaff; bremss.; nuclear resonance scattering, ring scatterer; NaI

Ref. No. 62 Bo 6 JHH

Reaction	E or ΔE	E_0	Γ	$\int \sigma dE$	Jπ	Notes
$Li^6(\gamma,\gamma)$	Bremss. 0 - 4					

TABLE 2

Comparison of mean lifetime measurements

Nucleus	Energy	%	Spins	J	T, T'	J' (g)	τ (10⁻¹⁴ sec) This work	τ (10⁻¹⁴ sec) Other
Li^6	3.56	7	$1^+ \to 0$	1	1)	1	0.012	0.012 ± 0.002 [10] 0.0105 ± 0.001 [11]
B^{11}	2.14	81	$\frac{1}{2}^- \to (\frac{1}{2})$	$\frac{1}{2}$	1	1	0.53	0.47 ± 0.06 [12]
Al^{27}	2.21	100	$\frac{1}{2}^+ \to \frac{1}{2}^-$	$\frac{1}{2}$	1)	1	3.2	2.7 ± 0.3 [13]
Al^{27}	1.01	100	$\frac{1}{2}^+ \to \frac{1}{2}^-$	$\frac{1}{2}$	0.96	1	320	170 ± 50 [14]
Si^{28}	1.78	92	$0^+ \to 2^+$	2	1	0.63	58	72 ± 12 [15]
Si^{28}	2.24	35	$0^+ \to 2^+$	2	1	0.63	24	≈16 [16]
Mg^{26}	1.37	79.6	$0^+ \to 2^+$	2	1	0.63	220	155 ± 40 [17]
Mg^{25}	1.61	25	$\frac{1}{2}^+ \to \frac{1}{2}$	$\frac{1}{2}$	(1)	1	3.6	2.5 ± 0.4 [18]
Cu^{65}	0.963	50	$\frac{1}{2}^- \to \frac{1}{2}$	$\frac{1}{2}$	1	0.92	230	72 ± 14 [19] 90 ± 15 [19]
Cu^{63}	0.67	69	$\frac{1}{2}^- \to \frac{1}{2}$	$\frac{1}{2}$	1	1	100	31 ± 3 [19]

The factor g equals $(2J-1)/(2J_0-1)$.

10) R. O. Haxby, Phys. Rev. 140 (1964) 1498
11) S. Vegors, L. Marsden and R. Heath, IDO-16370
12) Leslie Cohen and Ralph Taber, Nuclear Physics 14 (1960) 243
13) W. C. Barber, F. Berthold, G. Freier and P. E. Gedden, Phys. Rev. 120 (1960) 2128
14) F. R. Metzger, C. P. Swann and V. K. Rasmussen, Phys. Rev. 110 (1958) 906
15) F. R. Metzger, C. P. Swann and V. K. Rasmussen, Nuclear Physics 14 (1960) 563
16) S. Ofer and A. Schwarzschild, Phys. Rev Lett. 3 (1959) 384
17) V. K. Rasmussen, F. R. Metzger and C. P. Swann, Phys. Rev. 123 (1961) 1386
18) J. B. Cummings, A. Schwarzschild, A. W. Sunyar and N. T. Porile, Phys. Rev. 120 (1960) 2128
19) T. Rothem, F. R. Metzger and C. P. Swann, Nuclear Physics 23 (1961) 206

Ref. V.P. Chizhov, A.P, Komar, L.A. Kulchitsky, A.V. Kulikov, E.D. Makhnovsky, Yu.M. Volkov
Nuclear Phys. 34, 562 (1962)

Elem. Sym.	A	Z
Li	6	3

Method
90 MeV Synchrotron; magnetic spectrometer; emulsions; NaI counter telescope

Ref. No.
62 Ch 2

JHH

Reaction	E or ΔE	E_0	Γ	$\int \sigma dE$	Jπ	Notes
	Bremss.					
(γ,d)	30					
	43					
(γ,p)	90					

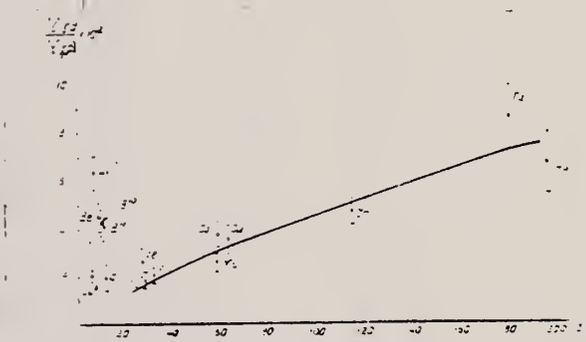

Fig. 4. The ratio of the yields of protons and neutrons with energies [illegible] MeV versus the mass number of nuclei A for E_{max} = [illegible] MeV. The solid line corresponds to [illegible]

Table 1

Experimental data

Elements	E_{max} MeV	Particle energy interval MeV	$\frac{N_n}{N_p}$	θ	Notes
Li^6	30	7.5 to 15	0.063 ± 0.006		
	43		0.087 ± 0.005	90°	[illegible]
	90		0.097 ± 0.014		
Li^7	25		0.020 ± 0.030		
	43	7.5 to 15	0.056 ± 0.006	90°	
	90		0.160 ± 0.054		
B^{10}	40	7.5 to 19	0.066 ± 0.002	90°	[illegible]
C^{12}	25	2.9 to 10	0.009 ± 0.007	30 – 150	[illegible]
C^{13}	35	3.7 to 10	0.038 ± 0.017	30° – 150°	[illegible]
O^{16}, nat	24	4.5 to 15	0.007 ± 0.003	90°	[illegible]
	34	7.5 to 15	0.007 ± 0.003	90°	[illegible]
	70	3 to 10	0.05 ± 0.01	20° – 150	[illegible]
	70	4 to 10	0.04 ± 0.01	20 – 150	[illegible]
	90	7 to 10	0.21 ± 0.05	90°	[illegible]

a Scintillation telescope method

b Method of detecting charged particles in magnetic field.

(continued)

Elem. Sym.	A	Z
Li	6	3

Method

Ref. No. 62 Ch 2 JHH

Reaction	E or ΔE	E_o	Γ	$\int \sigma dE$	Jπ	Notes

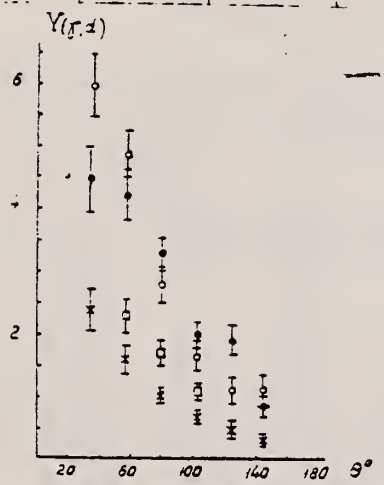

Fig. 7. Angular distributions of photodeuterons with the energies 15.5 to 30 MeV emitted in the photodisintegration by bremsstrahlung with $E_{\gamma max}$ = 90 MeV. Crosses denote Li^6, black circles Li^7, open circles Be, and open squares C. Particle yields are given in arbitrary units.

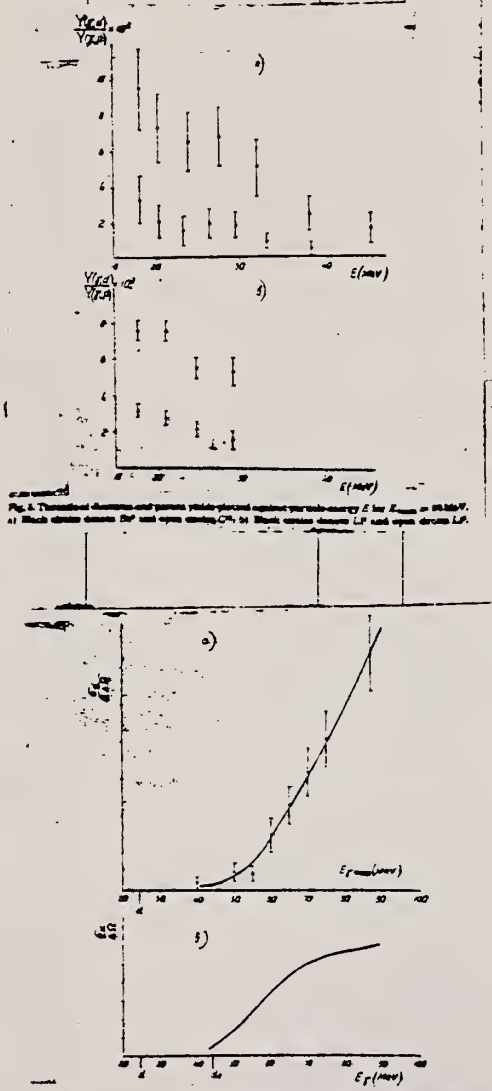

Fig. 9. Excitation functions for the reaction $Li^6(\gamma, d)$ for neutrons with energies 18.4 to 22 MeV. a) Cross sections are related for effective quantum. b) Cross sections are related for resultant quantum. The arrow A gives the threshold of the reaction $Li^6(\gamma, d)He^4$ for the minimum deuteron energy of 18.6 MeV, and A, the energy equal to the sum of the threshold energy d and the binding energy of the most weakly bound nucleon in the residual nucleus He^4.

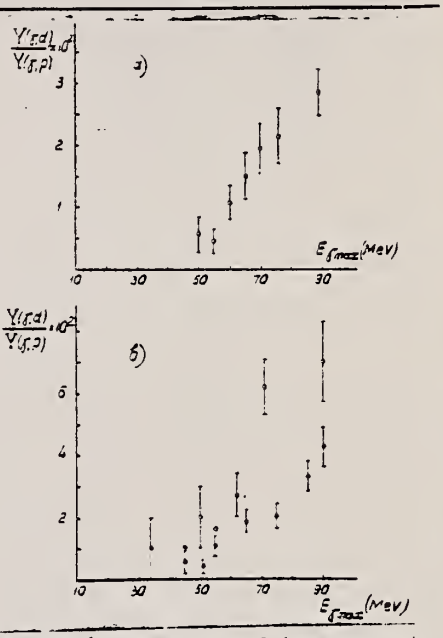

Figure 6: The ratio of deuteron and proton yields with E > 15 MeV plotted against $E_{\gamma max}$. a) Open circles denote Li^6. b) Open circles denote Be and black circles B.

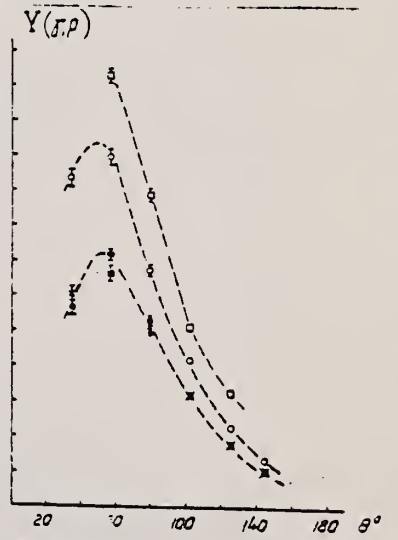

Fig. 8. Angular distributions of photo protons with the energies 15.5 to 30 MeV See caption fig. 7.

Ref. F.D. Seward
Phys. Rev. 125, 335 (1962)

Elem. Sym.	A	Z
Li	6	3

Method
Linac; NaI; detector at 90°.

Ref. No. 62 Se 1 JHH

Reaction	E or ΔE	E_o	Γ	$\int \sigma dE$	Jπ	Notes
$Li^6(\gamma,\gamma)$	Bremss; 17	3.56				According to Cohen and Tobin [Nuclear Phys. 14, 243 (1959)], this γ-ray is resonant-scattered from Li^6 second excited state.

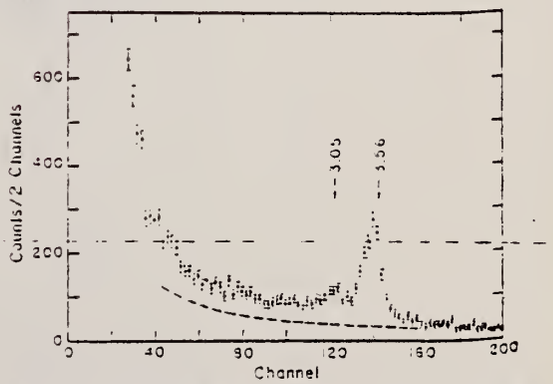

FIG. 2. Pulse-height spectrum for γ rays scattered from a Li^6H sample. The dashed line is the sample-out background. The rest of the counts are from resonant scattering from the 3.56-Mev level of Li^6 and from a sample-associated background. The horizontal energy scale was expanded compared to the other spectra to determine the spectrometer response to this γ ray.

Ref. Yu.M.Volkov, L.A.Kul'chitskii
Zhur.Eksptl. i Teoret.Fiz. 42, 108 (1962);
Soviet Phys.JETP 15, 77 (1962)

Elem. Sym.	A	Z
Li	6	3

Method
– Scintillation counter telescope

Ref. No. 62Vol BG

Reaction	E or ΔE	E_o	Γ	$\int \sigma dE$	Jπ	Notes
(γ,p)	$E_{\gamma max}$ =					Fig. 3: Particle energy interval 7.5-15 MeV, θ = 90°.
(γ.D)	30					Y(γ,D)/Y(γ,p) and Y(γ,T)Y(γ,p)
(γ,T)	43					given, relative yields of
	90					photodeuterons small for $E_{\gamma max}$ 30-40MeV and increases sharply with $E_{\gamma max}$.

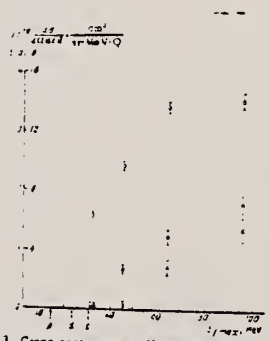

FIG. 3. Cross sections per effective quantum as a function of the energy $E_{\gamma max}$ for the reactions: o – $Li^6(\gamma,p)$; x – $Li^6(\gamma,D)$; and • – $Li^7(\gamma,t)$. The scale on the ordinate axis for cross sections of the $Li^6(\gamma,p)$ reaction is reduced fourfold; the arrows p, d, and t denote the thresholds for the reactions $Li^6(\gamma,p)He^6$, $Li^6(\gamma,d)He^4$, and $Li^7(\gamma,t)He^4$ for recording particles of energy 7.5 MeV.

Ref.	Elem. Sym.	A	Z
W.C.Barber, J.Goldemberg, G.A.Peterson, Y.Torizuka Nuclear Phys. 41, 461 (1963); erratum to be published (as of 9/5/63)	Li	6	3

Method	Ref. No.	
Linac (Stanford Mark II) - counter telescope	63Bal	BG

Reaction	E or ΔE	E_0	Γ	$\int \sigma dE$	Jπ	Notes
(e,e')	41.5		determined see Table II		see Table II	inelastic scattering cross section $(cm^2/sr)x10^{-32}$ at 180°
		3.56		0.42		4.0±20%
		5.7		0.03		0.15±50%
		9.3		0.20		0.6 ±30%
		14.0		0.14		0.25±50%
		15.8		0.17		0.25±50%

W. C. BARBER *et al.*

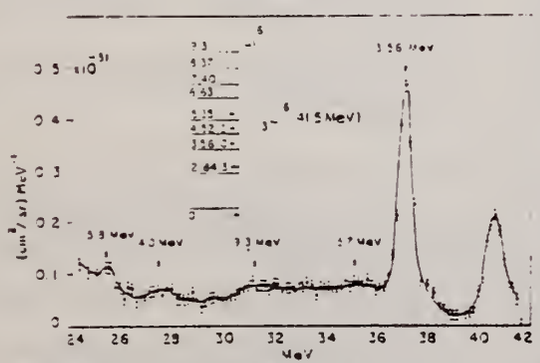

Fig. 4. Spectrum of 41.5 MeV electrons scattered from Li^6 at 180°.

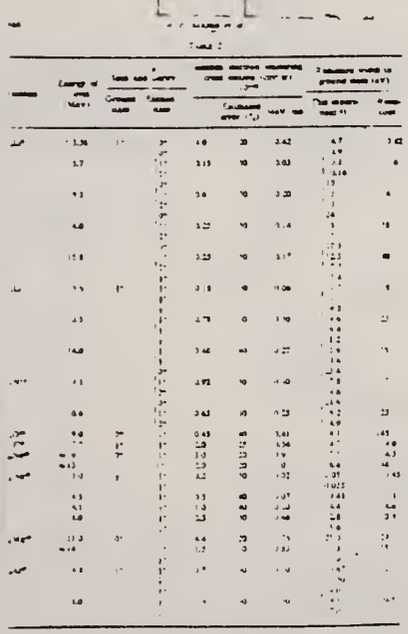

Ref. M. Bernheim, G.R. Bishop
Phys. Letters 5, 270 (1963)

Elem. Sym.	A	Z
Li	6	3

Method: Linac; inelastic scattering 101 MeV; magnetic spectrometer

Ref. No.: 63 Be 2 — BG

Reaction	E or ΔE	E_o	Γ	∫σdE	Jπ	Notes
$Li^6(e,e')$		2.184 3.560 4.52 5.35 6.63 7.40 8.37	9±2 eV			Pure E2 Pure M1 Program to establish validity of born approx. calculation of cross section.

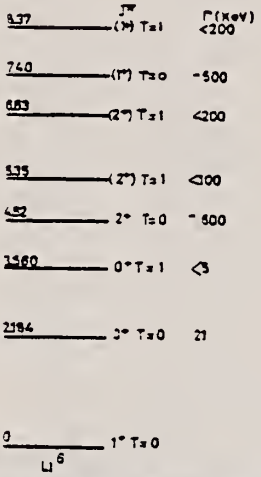

Fig. 1. The level scheme of Li^6. Spin and parity values indicated in brackets are not certain but are indicated by the calculated sequences of $T = 0$ and $T = 1$ levels which are found to be independent of assumptions about the two nucleon potential [6].

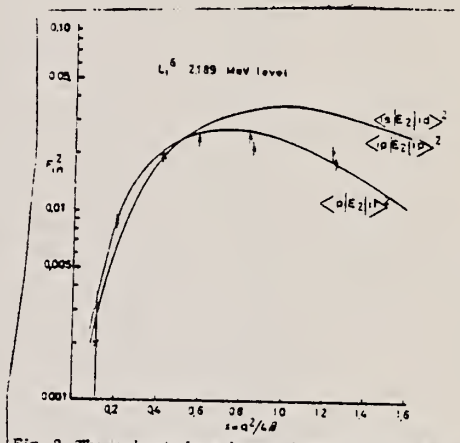

Fig. 2. The inelastic form factor of the level at 2.189 MeV in Li^6. That of the level at 4.52 MeV has a similar shape. Of the radial integrals $\langle 1p|J_2(qr)|1p\rangle^2$ and $\langle 1p|J_2(qr)|1f\rangle^2$, the latter seems to be preferred. The oscillator parameter $\beta^{-1} = 3.15$ fm as indicated by the elastic form factor.

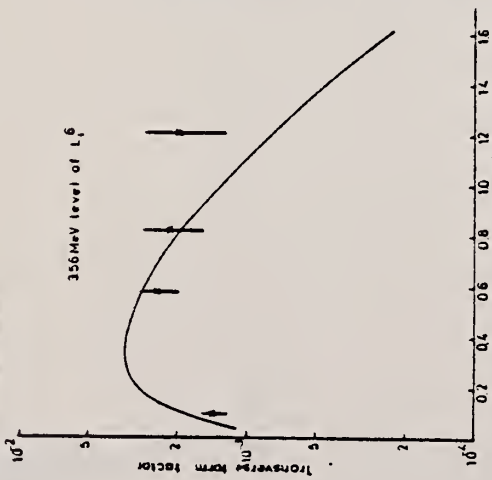

Fig. 3. The inelastic form factor of the level at 3.56 MeV in Li^6. The calculated curve is obtained as described in the text. The measured point at $x = 0.1$ is taken from the Stanford data [11].

Table 1
The reduced transition probabilities $B(E2\uparrow)$ for various transitions observed in Li^6. To calculate the radiative width these values must be multiplied by the statistical factor $3(2I_f + 1)^{-1}$.

Level energy (MeV)	2.189	4.52	5.35	7.40	8.37
Reduced transition probability $B(E2\uparrow) \times 10^{-52}$ cm⁴	30 ± 3	18 ± 1.3	7 ± 2	6 ± 2	4 ± 2

6) A. B. Clegg, Nuclear Phys. 33 (1962) 194.
7) F. Ajzenberg-Selove and T. Lauritsen, Revs. Modern Phys. 27 (1955) 77.
8) F. Ajzenberg-Selove and T. Lauritsen, Nuclear Phys. 11 (1959) 1.
9) P. Stoll and M. Wächter, Nuovo Cimento 10 (1953) 347; P. Stoll, Helv. Phys. Acta 27 (1954) 395; P. Erdos et al., Nuovo Cimento 12 (1954) 639.
10) M. E. Rose, Phys. Rev. 91 (1953) 610.
11) S. G. Nilsson, Dan. Mat. Fys. Medd., 29, no. 16 (1955).

FORM NBS-418 (9-1-63) USCOMM-OC 18556-P63
U.S. DEPARTMENT OF COMMERCE NATIONAL BUREAU OF STANDARDS

M. Bernheim, G.R. Bishop
J. de Physique 24, 970 (1963)

Li	6	3

METHOD: Linac; electron scattering; magnetic spectrometer; Faraday cup and SEM

REF. NO.: 63 Be 8 | NVB

REACTION	RESULT	EXCITATION ENERGY	SOURCE TYPE	SOURCE RANGE	DETECTOR TYPE	DETECTOR RANGE	ANGLE
E,E/	FMF	0-7	D	100-180	MAG-D		DST
		2.189					
		3.57					
		4.52					

J-PI, B(E2)

TABLEAU 2

Élément	Niveau	$B(E2) \times 10^{-48}$ cm^4
^{7}Li	4,61 MeV 7/2−	15,5 ± 0,8
	5,76 MeV 5/2−	4,1 ± 2
	6,80 MeV 5/2−	12,5 ± 1,2
^{6}Li	2,189 MeV 3+	32 ± 3
	4,52 MeV 2+	13,2 ± 1,5

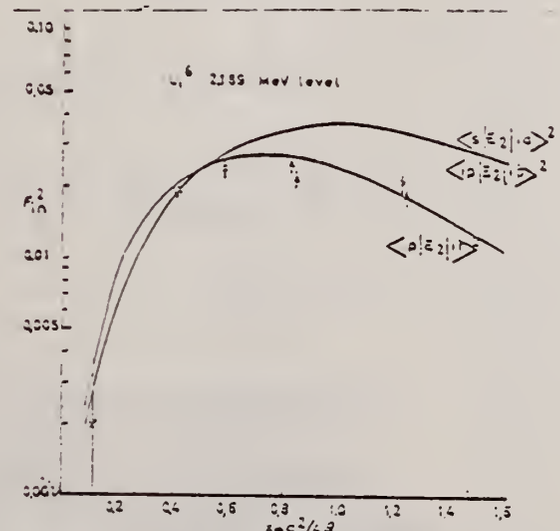

FIG. 2. — Le facteur de forme de la transition quadrupolaire électrique à l'état de 2,189 MeV 3+ de ^{6}Li. Les courbes théoriques sont les mêmes que pour la figure 1.

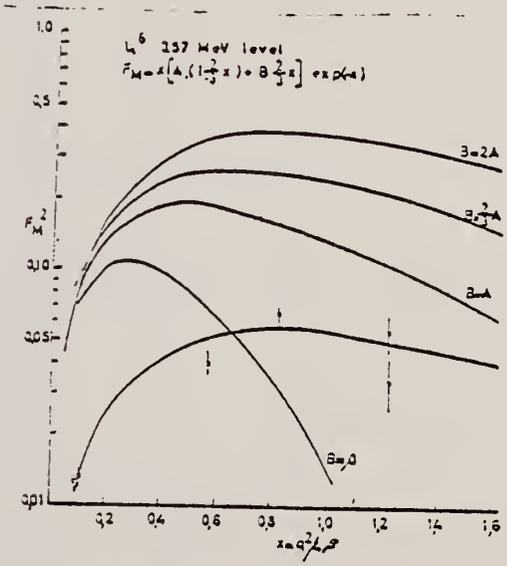

FIG. 3. — Le facteur de forme transversale de la transition dipolaire magnétique à l'état de 3,57 MeV 0V, $T = 1$ de ^{6}Li. Les courbes théoriques correspondent à l'expression

$$|A < 1p|J_0(qr)|1p > + B < 1p|J_2(qr)|1p >|$$

avec les valeurs de A et B indiquées.

Ref. G.R. Bishop, M. Bernheim
Phys. Letters 5, 140 (1963)

Elem. Sym.	A	Z
Li	6	3

Method: Linac; electron scattering; magnetic spectrometer

Ref. No.: 63 Bi 1 | BG

Reaction	E or ΔE	E_o	Γ	$\int \sigma dE$	Jπ	Notes
$Li^6(e,e')$	E incident: 101.4	7.5 8.4 (40)		cm^2/sterad		Values of $< r^2 >$ offer some confirmation of α + D model.
	E excitation:					
	9-17.5			$(9.2 \pm 0.5)10^{-31}$ | 9 17.5		
	17.5-32			$(2.37 \pm 0.09)10^{-30}$ | 17.5 32		

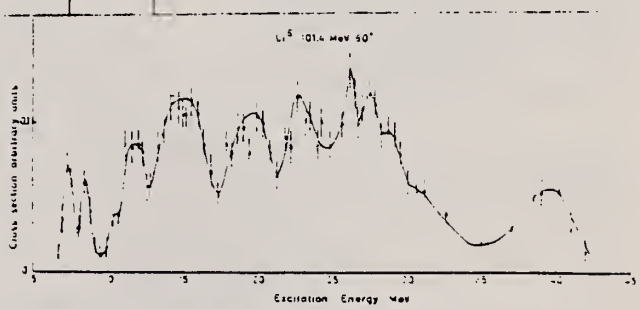

Fig. 2. The measured inelastic electron scattering spectrum from Li^6 at E = 101.4 MeV and θ = 50.0°. The absolute cross section is found by multiplying the ordinate scale by 1.36 × 10^{-30} cm² sterad. MeV

Table 1

The form factor effect is obtained by dividing the integrated electron cross section by the value obtained from virtual photon theory for a point scattering centre. The effect is 10 ± 3.5% for the α-particle region and 10 ± 4.3% for the deuteron region, leading to the given values of r^2.

Excitation energy	Integrated electron cross section	$\sigma_B = \int \sigma(k) k^{-1} dk$	$\frac{dN_T}{d\Omega} = \frac{dN_S}{d\Omega}$	Calculated electron cross section	$\langle r^2 \rangle$
9 - 17.5 MeV	$(9.2 \pm 0.5) \times 10^{-31}$ cm²·sterad	1.77 mbarns	8.51×10^{-4}	11.53×10^{-31} cm²·sterad	(4 ± 0.8) fm²
17.5 - 32 MeV	$(2.37 \pm 0.09) \times 10^{-30}$ cm²·sterad	3.6 mbarns	7.32×10^{-4}	2.64×10^{-30} cm²·sterad	(2.6 ± 1) fm²

Ref. S.Costa, S.Ferroni, V.Watachin, R.Malano

Phys.Letters 4, 308 (1963)

Elem. Sym.	A	Z
Li	6	3

Method
100 MeV Synchrotron

Ref. No.
63Col

BG

Reaction	E or ΔE	E_0	Γ	$\int \sigma dE$	Jπ	Notes
(γ, Tn)	0-30	11.5 26				A model in which Li^6 splits virtually into an and a D is considered.

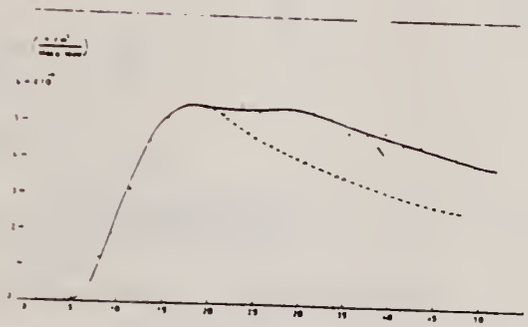

Fig. 1. Li^6 (γ, Tn) yield function.

Fig. 2. (γ, Tn) cross section in Li^6: the solid line is taken from ref. [3], the point ▼ from ref. [5].

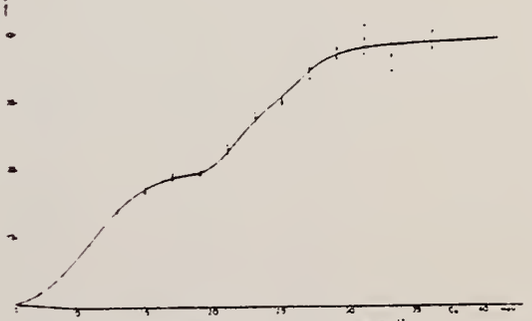

Fig. 3. (γ, Tn) integrated cross section in Li^6.

Ref. S.J. Skorka, R. Hübner, T.W. Retz-Schmidt, H. Wahl
Nuclear Phys. 47, 417 (1963)

Elem. Sym.	A	Z
Li	6	3

Method $Be^{9}(p,\alpha\gamma)Li^{6}$ source; photon scattering, self-absorption; NaI

Ref. No. 63 Sk 1 JHH

Reaction	E or ΔE	E_o	Γ	∫σdE	Jπ	Notes
$Li^{6}(\gamma,\gamma)$	3.56	3.56	+1.9 8.8-1.3eV			This Γ infers a mean life of $\tau_m = (7.5\pm1.3)\ 10^{-17}$ sec.

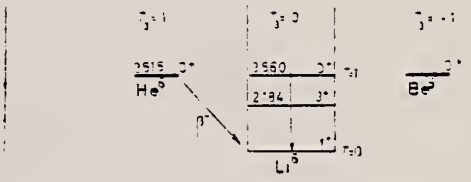

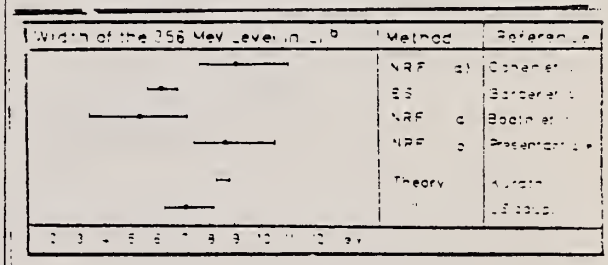

References

D. Kurath, Phys. Rev. 101, 216
D. Kurath, private communication quoted in ref. 1
N. Menkins, Nuclear Physics 35, 482
Cohen and R. K. Train, Nuclear Physics 14, 245
C. Barrett, I. Berlinod, O. Fiecke and F. E. Gudden, Phys. Rev. 120
Booth and K. V. Wright, Bull. Am. Phys. Soc.
C. Booth and K. V. Wright, Nuclear Physics 35, 472
Nuclear Data, F. E. Kirschmann, and D. V. Rubinstein, Nuclear Physics 23
R. Mc Donald, Nuclear Physics
Nuclear Physics
to be published

E.B. Bazhanov, A.P. Komar, A.V. Kulikov
Zhur. Eksp. i Teoret. Fiz. 46, 1497-1499 (1964)
Soviet Phys. JETP 19, 1014 (1964)

Li	6	3

METHOD
Synchrotron

REF. NO.
64 Ba 2

NVB

REACTION	RESULT	EXCITATION ENERGY	SOURCE		DETECTOR		ANGLE
			TYPE	RANGE	TYPE	RANGE	
G.XN	ABX	5-60	C	5-60	BF3-I		4PI

1058

$$\int_5^{60} \sigma(\gamma,xn)dE = (53.0 \pm 0.8)\text{MeV-mb}$$

$$\sigma_{-1} = \int \frac{\sigma(E_\gamma)}{E_\gamma} dE_\gamma = 4.2 \text{ mb}$$

rms radius of charge distribution = 1.9×10^{-13} cm.

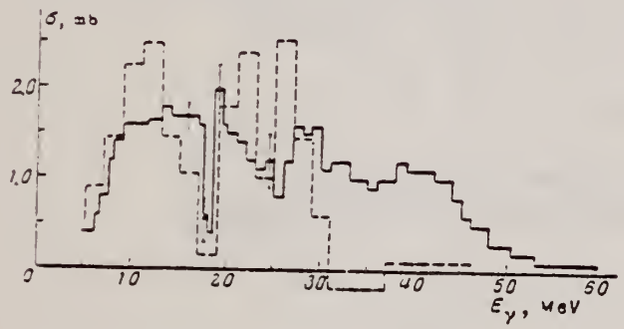

FIG. 1. Variation of photoneutron cross section with γ-ray energy for Li^6. The statistical errors are indicated.

REF.

K.W. Chen, J.R. Dunning,Jr., J.R. Rees, W. Shlaer, J.K. Walker and R. Wilson
Phys. Rev. 135, 4B B1030 (1964)

ELEM. SYM.	A	Z
Li	6	3

METHOD

REF. NO.	
64 Ch 1	JOC

REACTION	RESULT	EXCITATION ENERGY	SOURCE		DETECTOR		ANGLE
			TYPE	RANGE	TYPE	RANGE	
E,P	ABX		D	1 BEV	MAG-D	110-450	DST

TABLE I. Cross sections for production of protons by electron

Electron target	Energy angle (deg)	4 BeV proton energy (MeV)	$d^2\sigma/d\Omega dE$ 10^{-33} cm²/sr MeV
H	59.8	374	3.3[a]
Li_6	59.8	448	0.082
Li_6	59.8	368	0.175
Li_6	59.8	332	0.280
C	59.8	374	0.425
Al	59.8	374	1.19
H	63.1	291	7.5[a]
Li_6	63.1	355	0.146
Li_6	63.1	319	0.204
Li_6	63.1	290	0.313
C	63.1	291	1.01
Al	63.1	291	2.42
H	67.1	208	16[a]
Li_6	67.1	226	0.6
Li_6	67.1	206	0.92
C	67.1	209	2.37
Al	67.1	209	6.4
H	72.1	124	46[a]
Li_6	72.1	166	1.20
Li_6	72.1	144	1.53
Li_6	72.1	124	2.46
Li_6	72.1	119	2.80
Li_6	72.1	109	2.90
C	72.1	123	6.6
Al	72.1	124	16.9
Cu	72.1	124	42.3
H	44.8	291	2.9[a]
Li^6	44.8	337	0.16
Li^6	44.8	293	0.29
C	44.8	291	0.76
Al	44.8	291	1.58
H	52.3	208	8.5[a]
Li^6	52.3	200	0.91
C	52.3	208	2.13
Al	52.3	208	4.95
H	61.1	124	25[a]
C	61.1	145	3.95
C	61.1	124	5.75
C	61.1	115	6.43
Al	61.1	145	10.7
Al	61.1	124	16.0

[a] $d\sigma/d\Omega$ in mb/sr; inside a 5.5% momentum interval.

TABLE II. Cross section for $T_p = 145$ MeV, lithium target.

	θ	$d^2\sigma/d\Omega dE$ (cm²/sr MeV)
Bremsstrahlung energy, 335 MeV (cross section per Q)	72.1[a]	0.13×10^{-30}
	61.1[a]	0.20×10^{-30}
Electron energy, 335 MeV assuming $N_\gamma = 0.02$	72.1[a]	2.5×10^{-33}
	61.1[a]	4.0×10^{-33}
Electron energy, 1 BeV	61.1[b]	1.8×10^{-32}
Electron energy, 4 BeV	72.1	1.53×10^{-33}

[a] Extrapolated from C, Al data of Table I.
[b] Interpolated from data of Ref. 9.

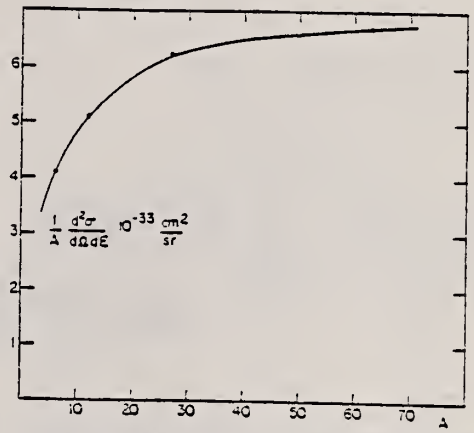

FIG. 4. Cross section, divided by A, as a function of A, for producing protons of 124 MeV from 4-BeV electrons at 72.1°.

REF. L. Green, D. J. Donahue
Phys. Rev. 135, B701 (1964)

ELEM. SYM.	A	Z
Li	6	3

METHOD
Reactor; neutron capture gamma rays

REF. NO. 64 Gr 2 NVB

REACTION	RESULT	EXCITATION ENERGY	SOURCE		DETECTOR		ANGLE
			TYPE	RANGE	TYPE	RANGE	
G,N	ABX	5-9	D	5-9	BF3-I		4PI

Enriched to 95.6% Li^6.

651

TABLE II. Summary of measured cross sections (millibarns).

Source	Energy[a] (MeV)	Targets Ta^{181}	Li^7	Li^6	C^{13}	B^{10}
Aluminum	7.72	4.1 ± 0.4	0.06 ±0.01	1.13±0.12	1.7 ±0.2	···
Copper	7.91	10 8±1.0	0.07 ±0.01	1.1 ±0.2	0.97±0.13	···
Chlorine	8.56	29 ± 6	0.17 ±0.12	···	···	···
Nickel	9.00	44 ± 6	0.16 ±0.06	1.6 ±0.3	0.6 ±0.1	0.11±0.01
Nitrogen	10.83	121 ±12	1.07 ±0.25	···	4 ±2	0.9 ±0.2
Chromium	9.72	84 ±25	0.55 ±0.25	···	···	0.23±0.05
Iron	7.64	0.0± 0.9	0.079±0.014	1.3 ±0.2	0.23±0.05	···
Iron	9.30	···	···	···	···	0.09±0.03
Lead	7.38	···	0.068±0.035	1.2 ±0.2	0.3 ±0.3	···
Sulphur	5.43	···	···	0.42±0.07		
Sodium	6.41	···	···	0.6 ±0.1		
Titanium	6.75	···	···	1.3 ±0.2	···	···
Titanium	6.61[b]	···	···	···	0.32±0.04	···
Manganese	7.16[c]	···	···	0.9 ±0.1	0.4 ±0.1	
Zinc	7.88	···	···	1.0 ±0.2	1.2 ±0.2	

[a] Energies taken from Refs. 4 and 5.
[b] Weighted average of 6.75-, 6.35-, and 6.41-MeV γ rays.
[c] Weighted average of 7.26-, 7.15-, and 7.05-MeV γ rays.

[4] G.A. Bartholomew and L.A. Higgs, Atomic Energy of Canada Ltd., Report No. 669 (unpublished).

[5] L. V. Groshev, V.N. Lutsenko, A.M. Demidov, and V.I. Pelekhov, Atlas of Gamma Ray Spectra from Radiative Capture of Thermal Neutrons Pergamon Press, Inc., New York, 1959).

[13] T.A. Romanowski and V.H. Voelker, Phys. Rev. 113, 886 (1959).

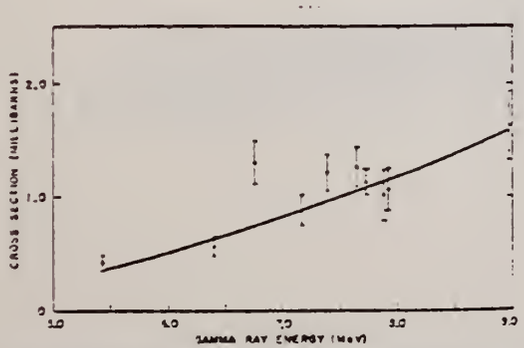

FIG. 4. Energy versus cross section, $Li^6(\gamma,n)$. Smooth curve from the data of Romanowski and Voelker (Ref. 13).

A.P. Komar, E.D. Makhnovskii
Dokl. Akad. Nauk.SSSR 156, 774-7 (1964);
Soviet Phys. Doklady 9, 463-65 (1964)

Li	6	3

METHOD: Quantometer

REF. NO.: 64 Ko 4 | NVB

	REACTION	RESULT	EXCITATION ENERGY	SOURCE TYPE	SOURCE RANGE	DETECTOR TYPE	DETECTOR RANGE	ANGLE
1)	G,T	SPC	THR-35	C	35	EMU-D	2-8	DST
2)	G,D	RLY	THR-35	C	35	EMU-D	1-5	DST

Target 90% Li^6, 10% Li^7

1) YLD REL TØ D
2) REL TØ T

Yield ratio $\frac{Y \text{ deuterons}}{Y \text{ tritons}} = 0.25^{+0.15}_{-0.06}$

for $1.2 < E < 4.8$ MeV

$$\int_{18.3}^{24.3} \sigma(\gamma,t)dE_\gamma \approx 29^{+9}_{-16} \text{ MeV - mb}$$

Deuterons have $1.2 < E < 4.8$ MeV, and $\bar{E}_d = 2.7$ MeV.

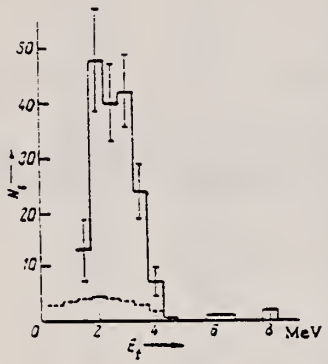

Fig. 2. Energy distribution of photo-tritons from Li^6. The broken line shows the calculated energy distribution of tritons due to $Li^6 + \gamma \rightarrow p + d + t$.

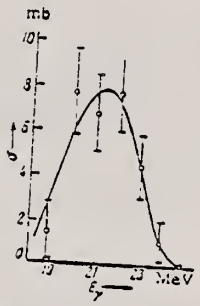

Fig. 3. Excitation function the $Li^6(\gamma, t)He^3$ reaction.

REF. E. D. Makhnovskii
J. Exptl. Theoret. Phys. (USSR) 46, 1136 (1964)
Soviet Phys. JETP 19, 769 (1964)

ELEM. SYM.	A	Z
Li	6	3

METHOD

REF. NO. 64 Ma 3 - EGF

REACTION	RESULT	EXCITATION ENERGY	SOURCE		DETECTOR		ANGLE
			TYPE	RANGE	TYPE	RANGE	
G,P		THR-20	C	20	EMU-D	0-12	DST

TARGET: 90% ^{6}Li; 10% ^{7}Li

For $E_p > 5.7$ MeV $N(\theta) = 41.0 + 43.6 \sin^2\theta(1 + 0.66 \cos\theta)^2$

Assuming $E_p > 5.7$ g.s. only $\int_{11.6}^{20} \sigma dE = (3.2 \pm 0.3)$ MeV-mb. Estimates $\int \sigma\gamma n$ and $\int \sigma\gamma, np$

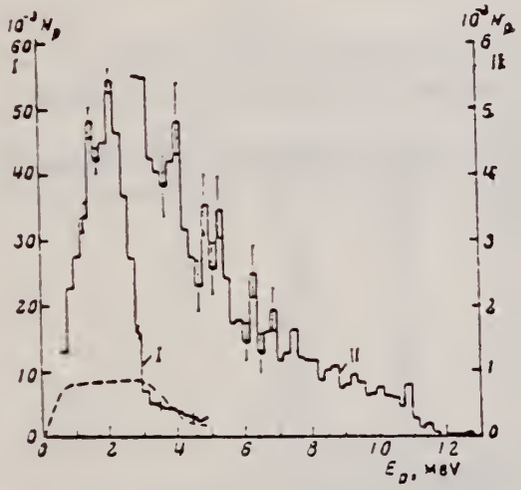

FIG. 1. Total energy distribution of photoprotons from Li^6. The dashed curve is the calculated total energy distribution of protons from the reactions $Li^6(\gamma,n)Li^5 \rightarrow p + He^4$ and $Li^6(\gamma,p)He^5 \rightarrow n + He^4$.

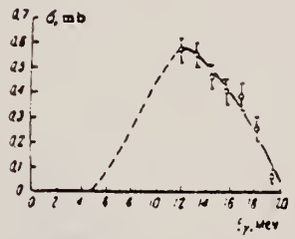

FIG. 2. Excitation function of the (γ,p) reaction for the case when the final He^5 nucleus is formed in the ground state. The dashed curve shows the extension of the excitation function to the low energy region with a form similar to the total cross section for reactions accompanied by neutron emission.

REF.

B.M.K. Nefkens and G. Moscati
Phys. Rev. 133, B17-19 (1964)

ELEM. SYM.	A	Z
Li	6	3

METHOD

Betatron

REF. NO. 64 Ne 1 NVB

REACTION	RESULT	EXCITATION ENERGY	SOURCE		DETECTOR		ANGLE
			TYPE	RANGE	TYPE	RANGE	
G, H4	ABY	24-250	C	250	ACT-I		4PI

NØ H4 FØUND

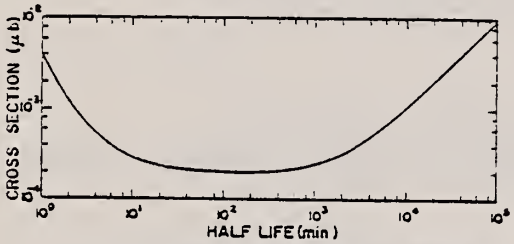

FIG. 2. Upper limit of the production cross section σ_γ versus half-life of H^4.

TABLE II. Production cross section for comparable reactions on light nuclei.

Reaction	E_γ (max)	σ_γ in μb	$-Q$ in MeV	Ref.
$He^4(\gamma,pn)d$	170	200	26	a
$He^4(\gamma,2pn)$	170	26	28	a
$Li^7(\gamma,2p)H^5$	320	1.8	31	a
$B^{11}(\gamma,2p)Li^9$	320	37	31	d
$N^{14}(\gamma,2p)$	170	250	25	a
$(\gamma,2pn)$	170	200	28	a
$O^{16}(\gamma,2p)$	170	500	22	a
$(\gamma,2pn)$	170	240	30	a
$Ne(\gamma,2p)$	170	590	21	a
$(\gamma,2pn)$	170	200	29	a
$F^{19}(\gamma,2p)N^{17}$	320	100	24	f
$F^{19}(\gamma,2pn)N^{16}$	303	100	24	g
$Li(\gamma,\ )H^4$	250	$<5\times10^{-1}$ [a] $<2\times10^{-1}$ [b]		This work

[a] Assuming that the half-life of H^4 is 1 year.
[b] Assuming that the half-life of H^4 is 1 h.
[a] A. N. Gorbunov and V. M. Spiridonov, Zh. Eksperim. i Teor. Fiz. 33, 21 (1957) [translation: Soviet Phys.—JETP 6, 16 (1958)].
[d] B. M. K. Nefkens, Phys. Rev. Letters 10, 243 (1963).
[e] A. N. Gorbunov, V. A. Dubrovina, V. A. Osipova, V. S. Silaeva, and P. A. Čerenkov, Zh. Eksperim. i Teor. Fiz. 42, 747 (1962) [translation: Soviet Phys.—JETP 15, 520 (1962)].
[f] G. W. Tautfest, Phys. Rev. 110, 708 (1958).
[g] R. A. Meyer (private communication).

REF.

A. Kh. Shardanov, V. G. Shevchenko and B. A. Yurev
Izv. Akad. Nauk SSR -Ser.Fiz. 28, 60 (1964) Jan.

ELEM. SYM.	A	Z
Li	6	3

METHOD

Betatron; proton cross section, spectrum, angular distribution; nuclear emulsions

REF. NO.: 64 Sh 2 NVB

REACTION	RESULT	EXCITATION ENERGY	SOURCE		DETECTOR		ANGLE
			TYPE	RANGE	TYPE	RANGE	
G,P	ABX	8 - 10	C 10		EMU-D	1-3	DST

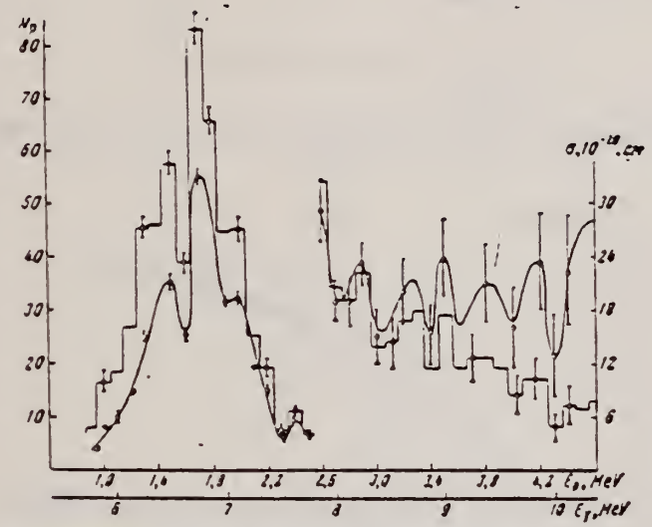

Рис. 1. Энергетическое распределение фотопротонов и сечение реакции Li^6 (т, p). Число протонов N_p и значения сечений в области $E_p < 2{,}8$ MeV уменьшены на рисунке в 10 раз

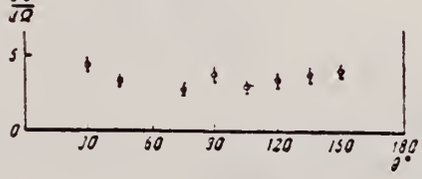

Рис. 2

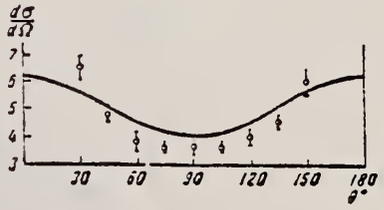

Рис. 3

Рис. 2. Угловое распределение фотопротонов (группы 1,3—1,5 MeV)

Рис. 3. Угловое распределение фотопротонов (группы 1,7—1,9 MeV) (сплошной линией проведена кривая, рассчитанная теоретически при $l = 1$)

REF.

E. B. Bazhanov, A. P. Komar, A. V. Kulikov and E. D. Makhnovsky
Nuclear Phys. 68, 191 (1965)

EL EM. SYM.	A	Z
Li	6	3

METHOD

REF. NO. 65 Ba 2 EGF

REACTION	RESULT	EXCITATION ENERGY	SOURCE		DETECTOR		ANGLE
			TYPE	RANGE	TYPE	RANGE	
G,XN	ABX	THR - 60	C	5-60	BF3-I		4PI
G,XP	RLY	THR - 30	C	20,28	EMU-D	1-18	DST
G,T	ABX	19 - 25	C	35	EMU-D	1-10	DST

660
677

Magnetic analysis used with emulsion for E_γ = 35 MeV.

$$\frac{Y_d}{Y_t} = 0.25^{+0.15}_{-0.05}$$

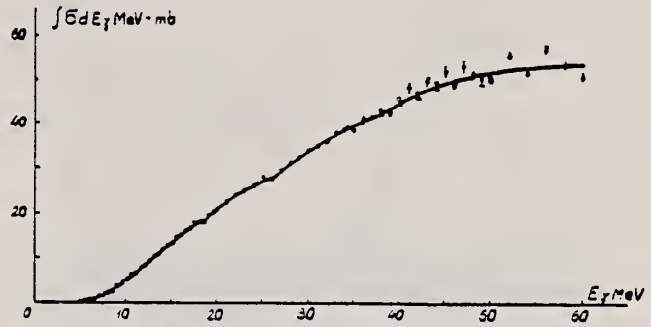

Fig. 3. Curve of the integral section of the whole complex of photoneutron on Li^6 reactions. The statistical errors are indicated.

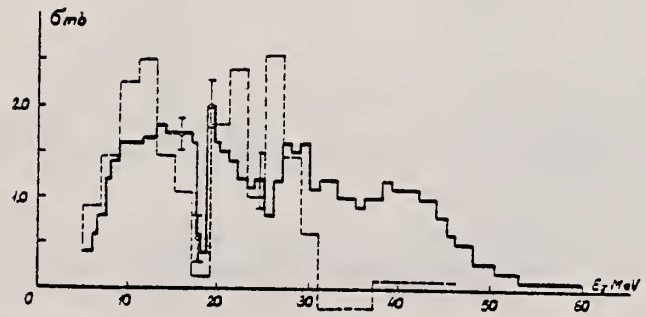

Fig. 4. Differential cross section of photoneutron reactions plotted against E_γ for the Li^6 nucleus. The statistical errors are indicated. The histogram represented by a dashed line corresponds to the results of ref. [3]).

(continued)

REACTION	RESULT	EXCITATION ENERGY	SOURCE TYPE	SOURCE RANGE	DETECTOR TYPE	DETECTOR RANGE	ANGLE

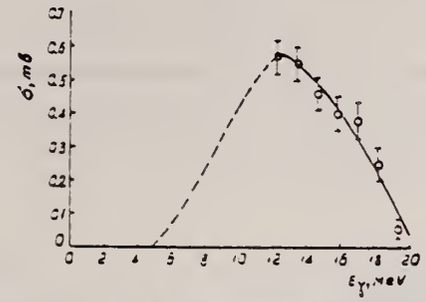

Fig. 6. Excitation function of the (γ, p) reaction when the He^3 nucleus is produced in the ground state.

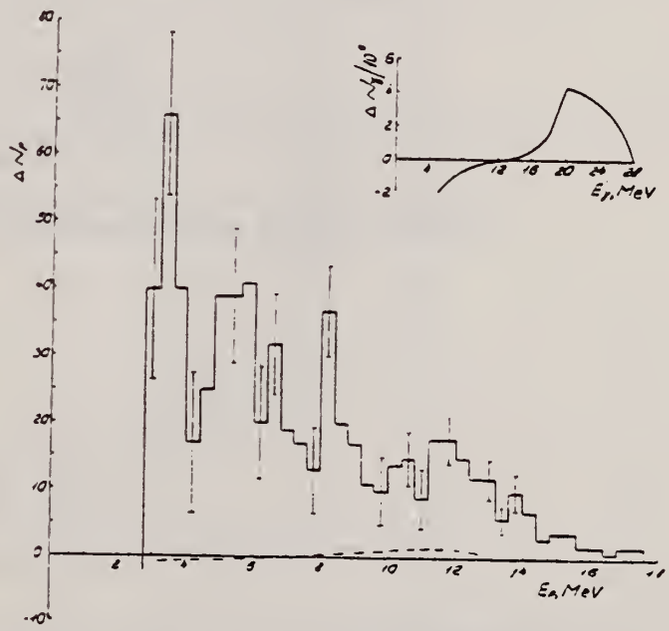

Fig. 8. Energy difference distribution of photoprotons from Li^6 $\Delta N_p = N_{p2s} - N_{p2p}$. The dashed curve shows the calculated difference spectrum of protons originating in the $Li^6(\gamma, p)He^5$ reaction when He^5 is produced in the ground state.

(continued)

REACTION	RESULT	EXCITATION ENERGY	SOURCE		DETECTOR		ANGLE
			TYPE	RANGE	TYPE	RANGE	

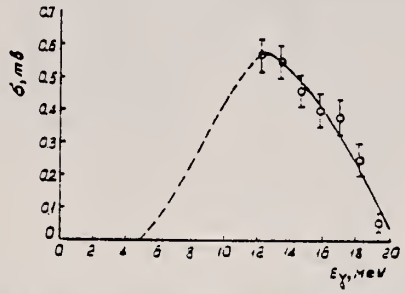

Fig. 6. Excitation function of the (γ, p) reaction when the He^3 nucleus is produced in the ground state.

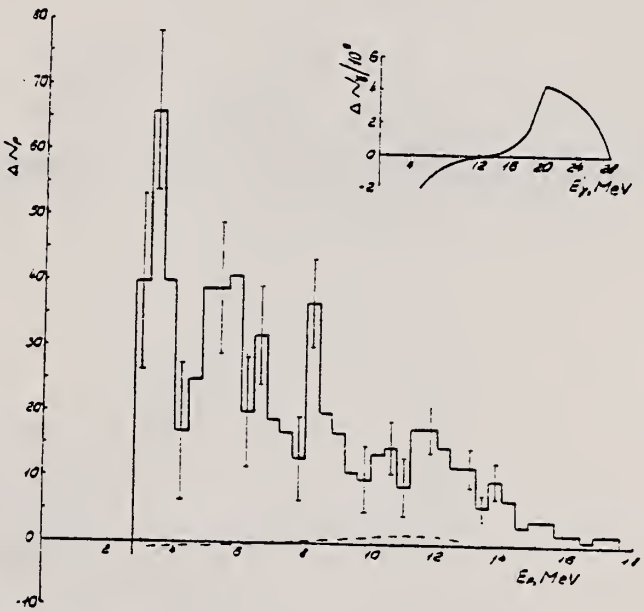

Fig. 8. Energy difference distribution of photoprotons from Li^6 $\Delta N_p = N_{p_{2s}} - N_{p_{2p}}$. The dashed curve shows the calculated difference spectrum of protons originating in the $Li^6(\gamma, p)He^5$ reaction when He^5 is produced in the ground state.

(continued)

REACTION	RESULT	EXCITATION ENERGY	SOURCE TYPE	SOURCE RANGE	DETECTOR TYPE	DETECTOR RANGE	ANGLE

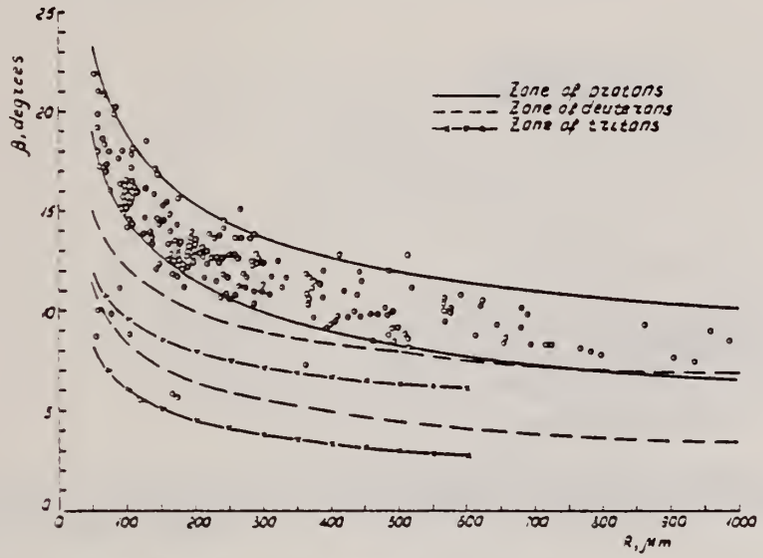

Fig. 10. Distribution of charged particles originating in the irradiation of Li^6 by bremsstrahlung with $E_{\gamma max} = 35$ MeV over magnetic deflection angles and ranges $R \geq 50$ μm in the emulsion.

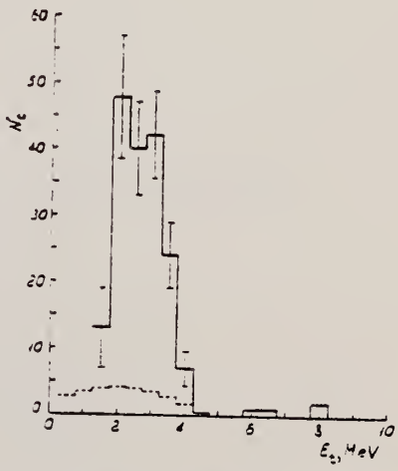

Fig. 11. Energy distribution of phototritons from Li^6 at $E_{\gamma max} = 35$ MeV. The dashed line shows the calculated energy distribution of tritons due to the $Li^6(\gamma, pd)H^3$ reaction.

(continued)

REACTION	RESULT	EXCITATION ENERGY	SOURCE		DETECTOR		ANGLE
			TYPE	RANGE	TYPE	RANGE	

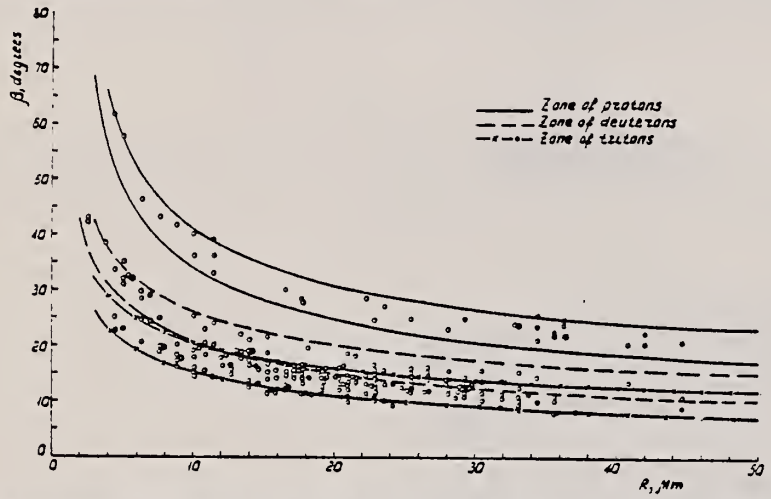

Fig. 9. Distribution of charged particles originating in the irradiation of Li^6 by bremsstrahlung with $E_{\gamma max} = 35$ MeV over magnetic deflection angles β and ranges $R \leq 50$ μm in the emulsion.

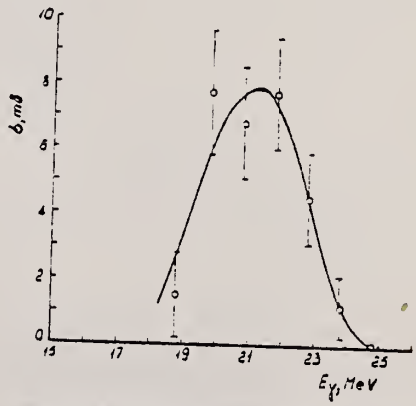

Fig. 12. Excitation function of the $Li^6(\gamma, t)He^3$ reaction. The statistical errors are indicated.

REF.

B.L. Berman, R.L. Bramblett, J.T. Caldwell, R.R. Harvey, and S.C. Fultz
Phys. Rev. Letters 15, 727 (1965)

ELEM.	A	Z
Li	6	3

METHOD

e^+ annihilahion in-flight gamma rays

REF. NO. 65 Be 1 JOC

REACTION	RESULT	EXCITATION ENERGY	SOURCE TYPE	SOURCE RANGE	DETECTOR TYPE	DETECTOR RANGE	ANGLE
G,XN	ABX	6 - 32	D	6-32	BF3 - I		4PI
		(5.7)		(5.7)			

Target 95% Li^6. #507 = (G,SN) $\sigma(\gamma,2n) < 0.1$ mb 507 & 508

$$\int_{5.55}^{\sim 32.05} \sigma dE\gamma = 27.4 \pm 2.0 \text{ MeV-mb}$$

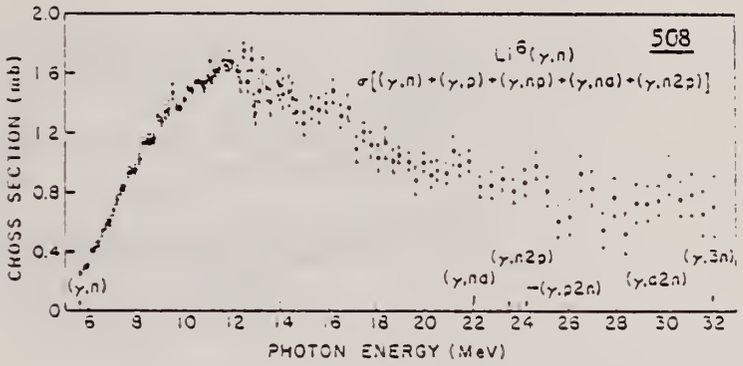

FIG. 1. Li^6 single-neutron-production cross section. This contains all partial cross sections except (a) those where all the emitted particles are charged, and (b) those where two or more neutrons are emitted. The errors given are statistical only.

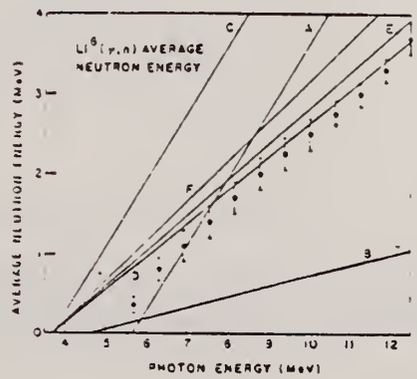

Curve B incorrect.

FIG. 2. Average neutron energy of photoneutrons from Li^6. The straight lines assume various reaction mechanisms, as follows: *A*, $Li^6(\gamma,n)Li^5 \rightarrow He^4 + p$; *B*, $Li^6(\gamma,p)He^6 \rightarrow He^4 + n$; *C*, $Li^6(\gamma,np)He^4$ and the neutron energy is the maximum possible; *D*, $Li^6(\gamma,np)He^4$ and the neutron energy is one-half the maximum possible; *E*, $Li^6(\gamma,np)He^4$ and the three omitted particles have equal center-of-mass momentum; *F*, $Li^6(\gamma,np)He^4$ and the neutron-proton pair are emitted back to back in the center-of-mass system (quasideuteron model).

P. J. Dallimore, K. S. Lam and H. H. Thies
Aust. J. Phys., 18, 389 (1965)

ELEM.	A	Z
Li	6	3

METHOD

REF. NO. 65 Da 1 JOC

REACTION	RESULT	EXCITATION ENERGY	SOURCE		DETECTOR		ANGLE
			TYPE	RANGE	TYPE	RANGE	
G,D	ABY	THR-4	C	4	SCD-D		90

$\bar{\sigma} < (6.70 \pm 1.00) \times 10^{-31}$ cm^2

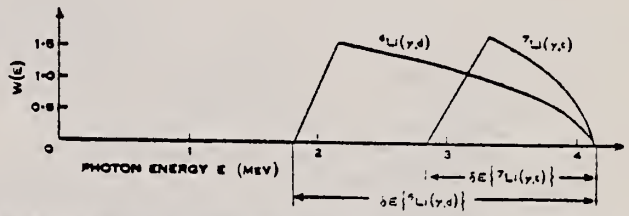

Fig. 2.—Weighting functions employed in the calculation of upper limits of the average reaction cross sections $\bar{\sigma}$, where

$$\bar{\sigma} = \frac{1}{\delta E} \int_{4{\cdot}1\ \mathrm{MeV} - \delta E}^{4{\cdot}1\ \mathrm{MeV}} W(E)\sigma(E)\,dE.$$

E. Hayward and T. Stovall
Nuclear Phys. 69, 241 (1965)

Li	6	3

METHOD

REF. NO. 65 Ha 1 EGF

REACTION	RESULT	EXCITATION ENERGY	SOURCE TYPE	SOURCE RANGE	DETECTOR TYPE	DETECTOR RANGE	ANGLE
G,XN	ABX	THR - 30	C	6-30	BF3-I		4PI

534

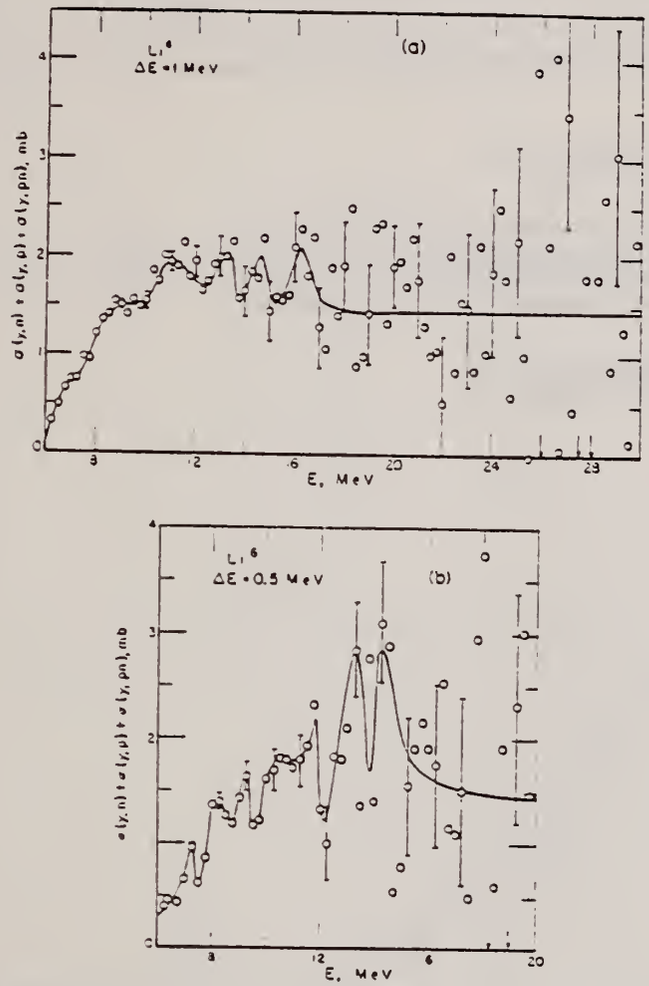

Fig. 3. The neutron production cross section for Li^6 where the analysis has been made using a 1 MeV grid (a) and a 0.5 MeV grid (b). The indicated errors are standard deviations based only on the number of counts. The arrows at the bottom represent negative points, and the horizontal line the average cross section above twenty MeV.

TABLE 3

Neutron emission cross sections integrated to 29 MeV

Target	$\int \sigma dE$ (MeV · mb)	$\int \sigma dE / (60NZ/A)$	$\int^{30} \sigma dE / (60NZ/A)$ [a]
Li^6	36.1	0.40 ± 0.03 [b]	0.42
Li^7	50.1	0.49 ± 0.04	0.64
B^{10}	66.7	0.44 ± 0.03	
B^{11}	68.6	0.42 ± 0.03	0.47 [c]
O^{16}	61.9	0.26 ± 0.02	0.30

[a]) Ref. [17]).
[b]) This value is for natural boron.
[c]) Estimated systematic errors.

FORM NBS-418
(REV. 7-1-64)
USCOMM-DC 26010-P64

G. Manuzio, R. Malvano, G. Ricco and M. Sanzone
Il Nuovo Cimento 40-B, 300 (1965)

ELEM.		
Li	6	3

METHOD

REF. NO. 65 Ma 5 JOC

REACTION	RESULT	EXCITATION ENERGY	SOURCE		DETECTOR		ANGLE
			TYPE	RANGE	TYPE	RANGE	
G,P	SPC	THR - 31	C	31	SCD-D	3-	90
G,D	SPC	THR - 31	C	31	SCD-D	3-	90
G,T	SPC	THR - 31	C	31	SCD-D	3-	90

Yields with 31 MeV bremsstrahlung

$$Y_p(E_p > 3 \text{ MeV}) = 2.7 \pm 0.4 \times 10^{-5} \ \frac{\text{proton} \cdot \text{cm}^2}{\text{mole} \cdot \text{MeV}}$$

$$Y_T(E_T > 3.6 \text{ MeV}) = (2.1 \pm .03) \times 10^{-6} \ \frac{\text{triton} \cdot \text{cm}^2}{\text{mole} \cdot \text{MeV}}$$

$$Y_p(E_d > 3 \text{ MeV}) = (4 \pm 0.6) \times 10^{-7} \ \frac{\text{deuterons} \cdot \text{cm}^2}{\text{mole} \cdot \text{MeV}}$$

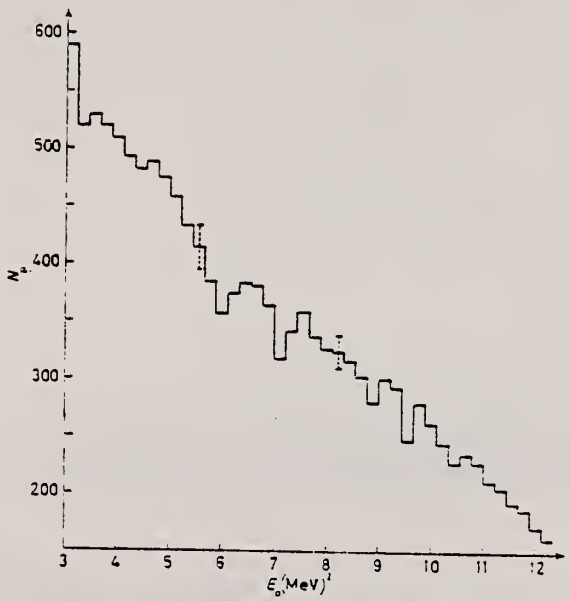

Fig. 3. – Spectrum of photoprotons from ^{6}Li produced by 31 MeV bremsstrahlung.

(continued)

Li	6	3

METHOD

REF. NO. 65 Ma 5 JOC

REACTION	RESULT	EXCITATION ENERGY	SOURCE TYPE	SOURCE RANGE	DETECTOR TYPE	DETECTOR RANGE	ANGLE

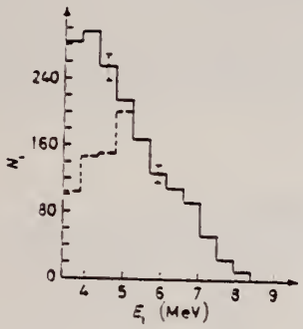

Fig. 4. – Spectrum of phototritons from ^{6}Li produced by 31 MeV bremsstrahlung (solid line). Same spectrum with the maximum estimated contribution of the three-body reaction subtracted (dashed line).

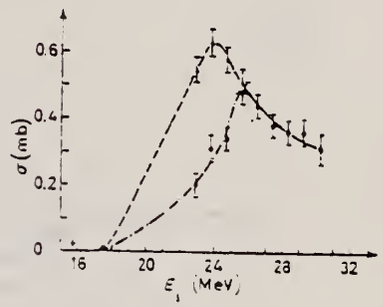

Fig. 5. – Maximum and minimum value of the cross-section for the ^{6}Li(γ, ^{3}He)^{3}H reaction: ▲ maximum cross-section; • minimum cross-section; ■ ref. ([12]).

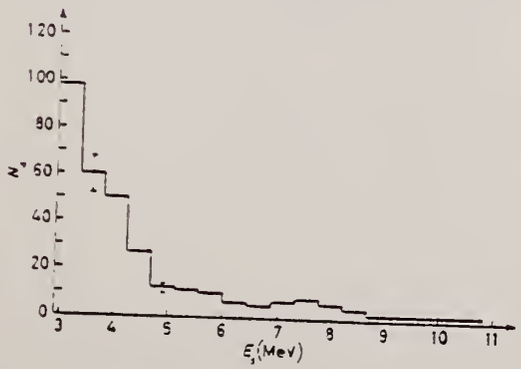

Fig. 6. – Spectrum of photodeuterons from ^{6}Li produced by 31 MeV bremsstrahlung.

REF. E. Allton, S. Ferroni, V. G. Gracco, B. Merkel and C. Schaerf
Nuovo Cimento 46A, 407 (1966)

ELEM. SYM.	A	Z
Li	6	3

METHOD	REF. NO.	
Linac	66 Al 1	JDM

REACTION	RESULT	EXCITATION ENERGY	SOURCE		DETECTOR		ANGLE
			TYPE	RANGE	TYPE	RANGE	
E,D	ABY	100-700	C	200-800	MAG-D		35

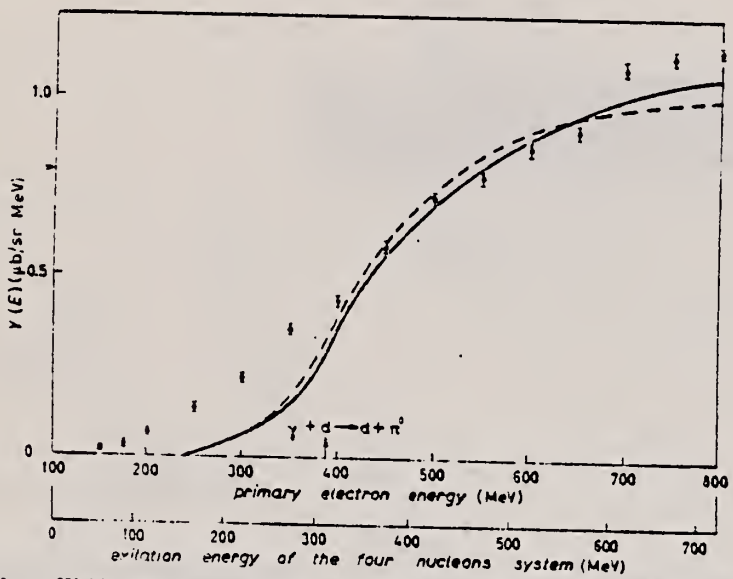

Fig. 1. – Yield curve measured in our experiment. Error bars indicate statistical fluctuations only. The solid line shows the result of our very crude model when no cut-off is introduced in the Li-d-α vertex. The broken line shows the result of the same calculations with a cut-off at 350 MeV/c. The two calculations have been indipendently normalized to compare with our experimental results. The arrow indicates the threshold for the reaction $\gamma+d\rightarrow d+\pi^0$ on a free deuteron.

REF. H. Artus, P. Brix, H. G. Clerc, F. Eigenbrod, A. Goldmann, F. Gudden, E. Spamer, P. Strehl, M. Stroetzel, O. Titze, and K. J. Wetzel
Proc. Gatlinburg Conference, 314 (1966)

ELEM. SYM.	A	Z
Li	6	3

METHOD

REF. NO. 66 Ar 2 hmg

REACTION	RESULT	EXCITATION ENERGY	SOURCE		DETECTOR		ANGLE
			TYPE	RANGE	TYPE	RANGE	
E,E/	LFT	2-4	D		MAG-D		
		(2.18.3.56)					

2=2.18. 4=3.56 MEV

TABLE 1

Summary of Experimental Results[a]

Nuclide	E_r(MeV)	Type	Γ_γ^0(eV)	Γ_γ^0/Γ_w	R_0 (F)
^{6}Li	2.18	E2	(3.9 ± 0.5) × 10^{-3}	14.4	3.77 ± 0.48
	3.56	M1	8.9 ± 0.4	9.4	2.96 ± 0.11
^{7}Li	11.28 ± 0.05	(M1) or	(1.3 ± 0.4)/g[b]	0.043/g	–
		(M2)	(0.025 ± 0.008)/g	2.6/g	–
^{9}Be	15.97 ± 0.03	M1	(3.7 ± 0.8)/g	0.043/g	–
^{11}B	4.46	E2 and	0.0173 ± 0.0021	8.2	3.44 ± 0.50
		M1	0.64 ± 0.08	0.34	2.60 ± 0.35
	5.04	M1	1.84 ± 0.14	0.69	2.60 ± 0.11
^{12}C	4.43	E2	0.0122 ± 0.0008	5.30	3.14 ± 0.30
^{16}O	6.92	E2	0.100 ± 0.015	3.28	3.32 ± 0.46
	11.52	E2	0.52 ± 0.13	1.31	–
^{24}Mg	9.85 ± 0.04	M1	7.95 ± 1.2	0.38	3.50 ± 0.49
	9.97 ± 0.03				
	10.35 ± 0.03	E2	0.24 ± 0.05	0.58	5.05 ± 0.50
	10.70 ± 0.03	M1	22.2 ± 2.4	0.36	3.50 ± 0.36
	10.93 ± 0.04	E2	0.26 ± 0.11	0.50	–
^{28}Si	4.97 ± 0.02	CO	(2.0 ± 0.5) < 10^{-5}[c]	–	6.90 ± 1.20
^{40}Ca	6.89 ± 0.05	E2	0.29 ± 0.04	2.85	4.50 ± 0.50

[a] The Born approximation has been used except for ^{16}O and ^{40}Ca.
[b] $g = (2I_f + 1)/(2I_i + 1)$.
[c] Γ_γ^0 equivalent to ME = (8.37 ± 1.00) F^2.

REF. S. Costa, F. Ferrero, C. Manfredotti, L. Pasqualini and L. Roasio
Nuovo Cimento 42B, 382 (1966)

ELEM. SYM.	A	Z
Li	6	3

METHOD

Betatron; Synchrotron

REF. NO. 66 Co 5 - JDM

REACTION	RESULT	EXCITATION ENERGY	SOURCE		DETECTOR		ANGLE
			TYPE	RANGE	TYPE	RANGE	
G,N	ABX	5 - 97	C	5 - 97	BF3-I		4PI

6.96

$$\int_{4.7}^{96} \sigma \, dE_\gamma = (130 \pm 20) \text{ mb. MeV}$$

$\sigma_{-1} = (3.2 \pm 0.3)$ mb

r.m.s. charge radius $\bar{R}_c = 1.2 \pm 0.1$ fermi

Compare peaks with other measurements.

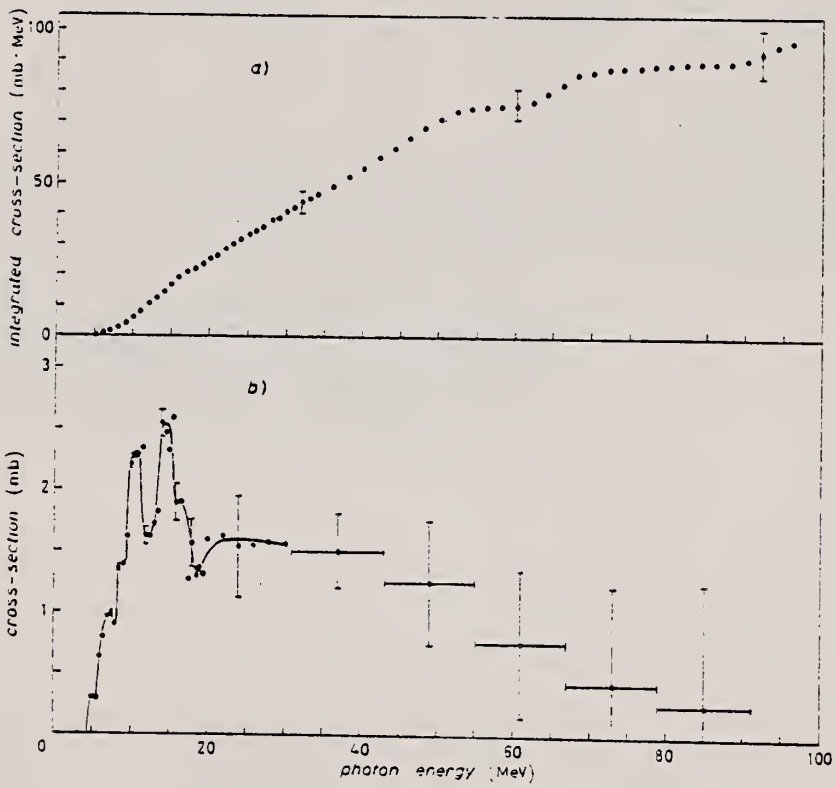

Fig. 1. – a) $\int_{4.7\,\text{MeV}}^{96\,\text{MeV}} \sigma(E)\,dE$; b) $\sigma(\gamma,\text{tn})$.

REF. J. L. Matthews, W. Bertozzi, S. Kowalski, C. P. Sargent, and W. Turchinetz
Proc. Gatlinburg Conference 386 (1966)

ELEM. SYM.	A	Z
Li	6	3

METHOD

REF. NO.	
66 Ma 4	hmg

REACTION	RESULT	EXCITATION ENERGY	SOURCE		DETECTOR		ANGLE
			TYPE	RANGE	TYPE	RANGE	
G,P	SPC	THR-102	C	95,102	TEL-D	45-86	DST

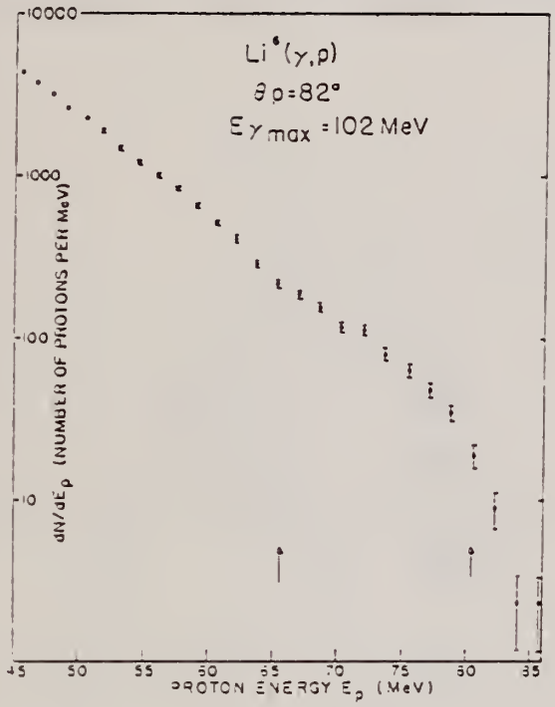

Fig. 1. Spectrum of photoprotons from ^6Li at $\theta_p = 82°$, with bremsstrahlung of maximum energy 102 MeV. The arrows indicate proton energies calculated from $^6Li(\gamma,p)^5He$ kinematics for $E_\gamma = 102$ MeV, and $E_x = 4.9$ and 22.7 MeV.

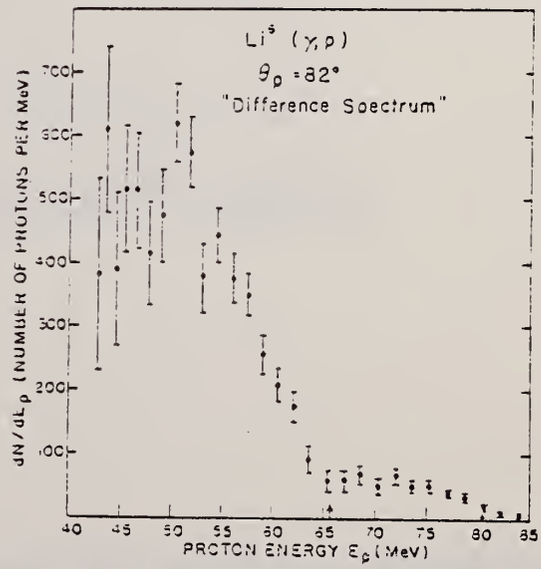

Fig. 2. "Difference spectrum": the photoproton spectrum measured with 95-MeV bremsstrahlung subtracted from that measured with 102-MeV bremsstrahlung, for ^6Li at $\theta_p = 82°$. The arrows indicate proton energies calculated from $^6Li(\gamma,p)^5He$ kinematics for $E_\gamma = 102$ MeV, and $E_x = 4.9$ and 22.7 MeV.

REF.

F. Nüsslin, H. Werner and J. Zimmerer
Z. Naturforschg. 21a, 1195 (1966)

EL EM. SYM.	A	Z
Li	6	3

METHOD

REF. NO.: 66 Nü 1 - egf

REACTION	RESULT	EXCITATION ENERGY	SOURCE		DETECTOR		ANGLE
			TYPE	RANGE	TYPE	RANGE	
HE,G	ABX	16-25	D	5-20	NAI-D	10-25	DST

$W(\Theta) = \sin^2\Theta + 0.07$ at 20 MeV

HE=HE3

667

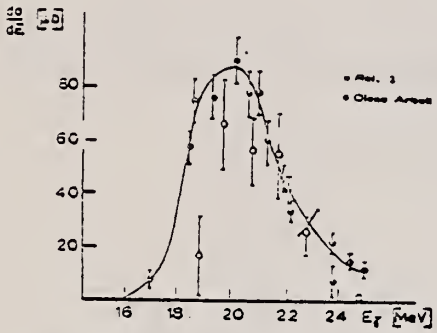

Abb. 1. Anregungsfunktion für $T(He^3,\gamma)Li^6$.

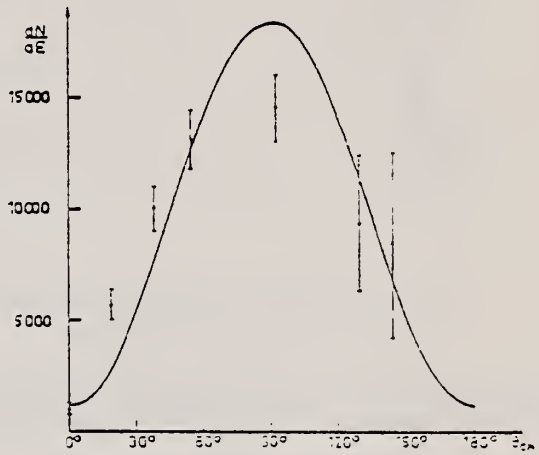

Abb. 2. Winkelverteilung der γ-Strahlung aus $T(He^3,\gamma)Li^6$.

REF.

G. Paoli, M. Scotto and A. Wataghin
Nuovo Cimento 43B, 189 (1966)

ELEM. SYM.	A	Z
Li	6	3

METHOD

Betatron

REF. NO. 66 Pa 1 JDM

REACTION	RESULT	EXCITATION ENERGY	SOURCE		DETECTOR		ANGLE
			TYPE	RANGE	TYPE	RANGE	
G,N	SPC	THR - 30	C	30	EMU-D	0 - 17	90

Table compares with peaks from other measurements.

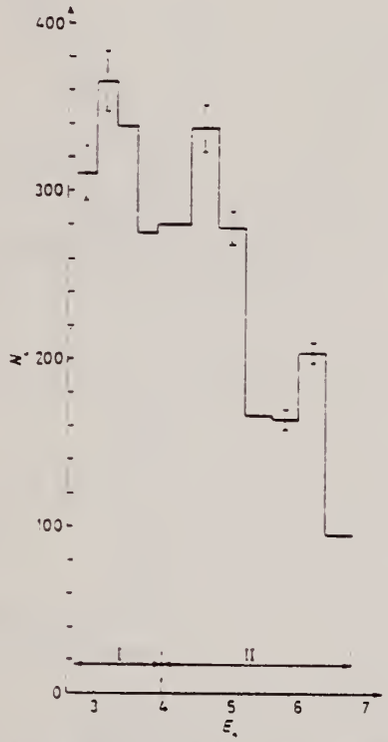

Fig. 1. – Neutron-corrected energy spectrum. The energy range is divided in two parts with different resolutions. N, in arbitrary units.

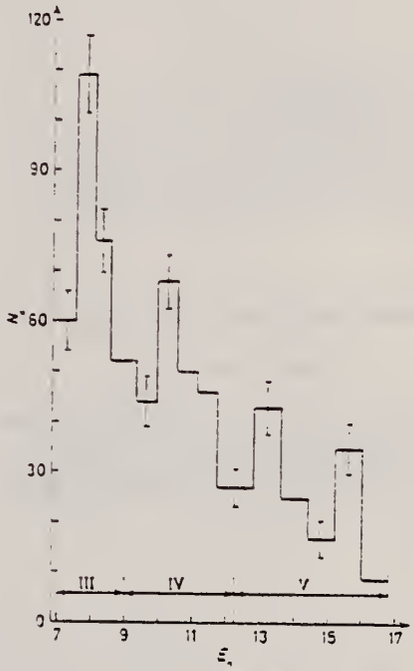

Fig. 2. – Neutron-corrected energy spectrum. The energy range is divided in three parts with different resolutions. N, in arbitrary units.

REF. N.K. Sherman, J.R. Stewart, and R.C. Morrison
Phys. Rev. Letters 17, 31 (1966)

ELEM. SYM.	A	Z
Li	6	3

METHOD: 40 MeV bremsstrahlung from Linac

REF. NO.: 66 Sh 1 JDM

REACTION	RESULT	EXCITATION ENERGY	SOURCE		DETECTOR		ANGLE
			TYPE	RANGE	TYPE	RANGE	
G,T	ABX	19 - 24	C	40	SCD-D	1 - 13	90

676

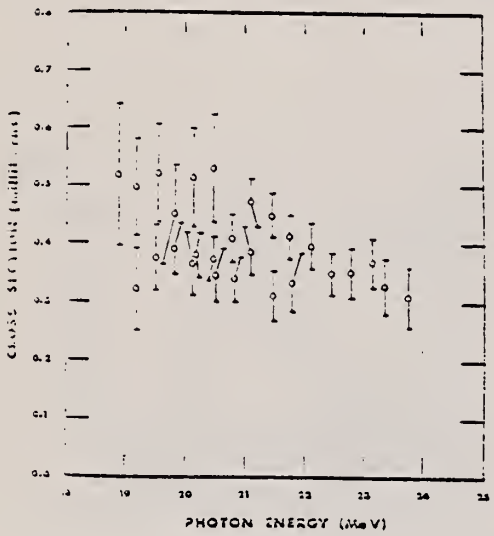

FIG. 2. Phototriton cross section obtained from data taken at three different magnet settings. The errors -- are greater than statistical, because of uncertainty in subtracting the proton transmission tail underlying the triton peak.

REF. V. P. Denisov, A. P. Komar, L. A. Kul'chitskii, and E. D. Makhnovskii
J. Nucl. Phys. (USSR) 5, 498 (1967)
Sov. J. Nucl. Phys. 5, 349 (1967)

ELEM. SYM.	A	Z
Li	6	3

METHOD

REF. NO. 67 De 2 HMG

REACTION	RESULT	EXCITATION ENERGY	SOURCE		DETECTOR		ANGLE
			TYPE	RANGE	TYPE	RANGE	
G,P	ABX	9-55	C	30-55	TEL-D	4-18	90
G,D	ABX	7-55	C	30-55	TEL-D	5-17	90
G,T	ABX	21-55	C	30-55	TEL-D	5-17	90

657, 661, 615

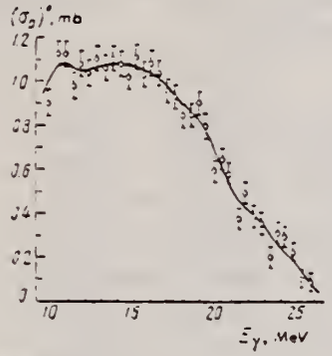

Fig. 1. Cross section for reactions with proton emission $(\sigma_p)^*$ for Li*, obtained from photoproton spectra for $E_{\gamma max}$ = 30 MeV.

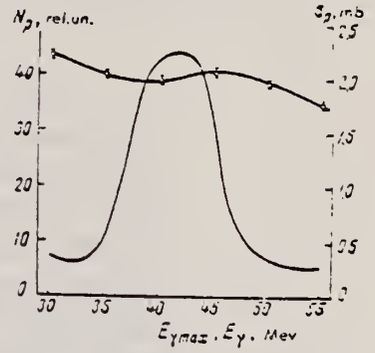

Fig. 2. Yield curve for photoprotons with energies 4.2–17.6 MeV (curve with experimental points) and cross section for reactions with proton emission (σ_p), obtained from the yield curve by the Penfold-Leiss method.

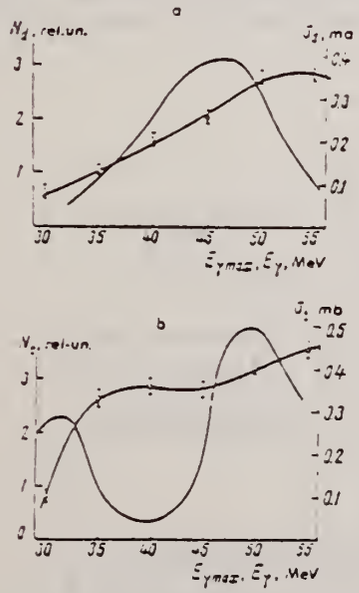

Fig. 3. Yield curves: *a* – photodeuterons and *b* – phototritons in the energy interval 5–17 MeV (curves with experimental points) and cross sections for production of deuterons (σ_d) and tritons (σ_t), obtained from the yield curves by the Penfold-Leiss method.

Y. Oda, H. Hirabayasi and K. Fujioka
PICNS-67 Contributions, International Conference on Nuclear Structure, Tokyo, Japan 1967 (Institute for Nuclear Study, University of Tokyo, Tanashi-shi, Tokyo, Japan) 10.10, p. 374

Li	6	3

METHOD

REF. NO. 67 Od 1 EGF

REACTION	RESULT	EXCITATION ENERGY	SOURCE		DETECTOR		ANGLE
			TYPE	RANGE	TYPE	RANGE	
G,XP	NOX	5-16	C	16	EMU-D	1-8	45
		(4.7-15.7)		(15.7)			

16= 15.7

On the Photo Nuclear Reactions of Li^6

T. ODA, H. HIRABAYASI,* and K. FUJIOKA

Faculty of Science, Tokyo Institute of Technology,

Megro Ookayama 1, Tokyo, Japan

The photo-nuclear reactions of Li^6 were studied at seven angles from 15^0 to 150^0 with respect to the incident Bremsstrahlung of the maximum energy $E_{\gamma m}$=15.7 MeV. In this energy region the $Li^6(\gamma,H^3)He^3$ reactions do not occur energetically. The foil of 5.5mg/cm^2 rolled from 99.8% Li^6 metal was used as the target. The product protons of energies larger than 800KeV were detected with the method of nuclear emulsion. As the proton energies are rather low, the effects of the target thickness to the energy spectrum were considered first analytically and were studied further by observing the elastic scattering on Al foil of 1.8 MeV protons accelerated by a Van de Graaff machine. Reasonable agreement with the analytical expectation was obtained.

The energy spectra of the protons emitted from Li^6 target show an eminent group at the proton energy E_p=1.85 MeV. This feature seems to be the same as the results shown by Bazhanov et al with Bremsstrahlung of $E_{\gamma m}$=25 MeV.(1) This proton group would be produced by one of the following two processes,

(1) $Li^6(\gamma,p)He^5$ (Q=-4.655 MeV) at E_x=6.38 MeV or

(2) $Li^6(\gamma,pn)He^4$ (Q=-3.697 MeV) at E_x=9.25 MeV.

Here E_x is the excitation energy in Li^6.
The former kind of interpretation was found in the literature.(2)

In the latter interpretation,(1)(3) the reaction would proceed following the scheme: $Li^6+\gamma \rightarrow He^4+H^2+\gamma \rightarrow He^4+p+n$(4).
In this case, some explanation must be, however, presented for the appearance of the eminent proton group. Further studies are now in progress both experimentally and theoretically.

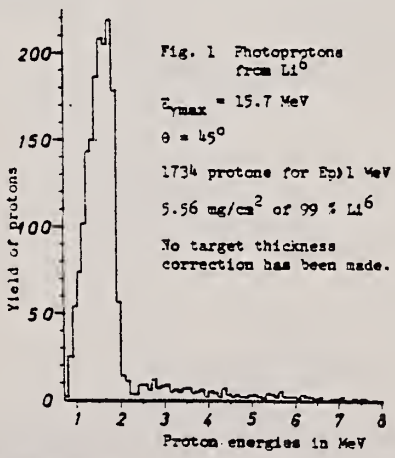

Fig. 1 Photoprotons from Li^6
$E_{\gamma max}$ = 15.7 MeV
θ = 45°
1734 protons for Ep>1 MeV
5.56 mg/cm^2 of 99 % Li^6
No target thickness correction has been made.

Reference: (1) E. B. Bazhanov et al. :Nucl.Phys.,60 (1965) 191.
(2) N.K.Sherman et al. :Bull.Am.Phys.Soc. 10 (1965) 541.
(3) E.Hayward and T.Stovall :Nucl.Phys. 69(1965) 241.
(4) S.Ferroni et al : Nucl.Phys. 76(1965) 58.

* Now at The Institute of Nuclear Study, Tokyo University, Tokyo, Japan.

REF. S. L. Blatt, A. M. Young, S. C. Ling, K. J. Moon and C. D. Porterfield
Phys. Rev. 176, 1147 (1968)

ELEM. SYM.	A	Z
Li	6	3

METHOD

REF. NO. 68 B1 1 egf

REACTION	RESULT	EXCITATION ENERGY	SOURCE		DETECTOR		ANGLE
			TYPE	RANGE	TYPE	RANGE	
HE,G	ABX	16-28	D	0-11	NAI-D	10-28	DST

HE = HE3

669

TABLE I. Measured 90° differential cross sections for the reactions $T(^3He,\gamma)^6Li$ leading to the ground and first two excited states of ^6Li.

$E_{lab}(^3He)$	$d\sigma/d\Omega\|_{90°}$ ($\mu b/sr$) γ_0	γ_1	γ_2
0.51	0.38±0.06	0.10±0.02	0.07±0.02
1.10	1.5 ±0.2	0.34±0.06	0.24±0.05
1.65	2.6 ±0.4	0.64±0.12	0.45±0.10
1.92	4.5 ±0.7	1.2 ±0.2	0.86±0.18
2.73	7.2 ±1.1	1.8 ±0.3	1.3 ±0.3
3.25	7.9 ±1.2	1.9 ±0.3	1.5 ±0.3
3.77	9.2 ±1.4	2.5 ±0.4	1.4 ±0.3
4.03	9.8 ±1.5	2.7 ±0.4	1.7 ±0.3
4.28	9.8 ±1.5	2.7 ±0.4	1.5 ±0.3
4.54	10.7 ±1.6	3.1 ±0.5	1.6 ±0.3
4.80	10.6 ±1.6	2.6 ±0.4	1.6 ±0.3
5.30	11.2 ±1.7	3.1 ±0.5	1.5 ±0.03
6.34	10.8 ±2.1		
7.36	10.4 ±2.1		
9.38	11.2 ±2.2		
11.0	12.6 ±2.5		

[9] A. E. Evans, R. Brown, and J. B. Marion, Rev. Sci. Instr. 37, 991 (1966).
[10] S. L. Blatt, J. Mahieux, and D. Kohler, Nucl. Instr. Methods 60, 221 (1968).

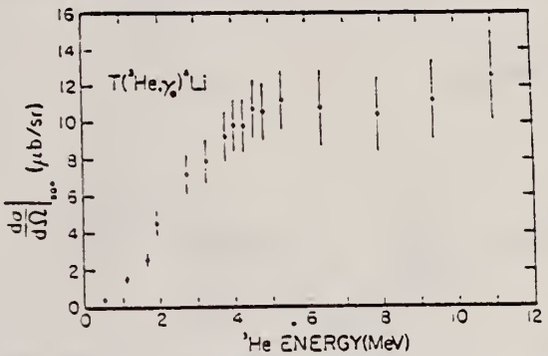

FIG. 3. Measured 90° differential cross section for ground-state capture in the reaction $T(^3He,\gamma)^6Li$.

TABLE III. Reported values for the integrated phototriton cross section in ^6Li up to $E_\gamma = 25$ MeV.

References	$\int \sigma(E_\gamma)dE_\gamma$ (MeV mb)	Reaction studied
Nüsslin *et al.*[a]	26±9[b]	capture
Sherman *et al.*[c]	<5	photo
Bazhanov *et al.*[d]	30^{+10}_{-15}	photo
Makhnovskii[e]	10–15	photo
Present work	9.3±1.4[f]	capture

[a] Reference 2.
[b] This value disagrees with the data from Ref. 2 converted to the inverse reaction using Eq. (1).
[c] Reference 4.
[d] Reference 3.
[e] References 17 and 18.
[f] Using data from Ref. 2 above 21 MeV.

[2] F. Nüsslin, H. Werner and J. Zimmerer, Z. Naturforsch. 21a, 1195 (1966).
[3] E. B. Bazhanov, M. P. Komar, A. V. Kulikov, and E. D. Mahknovskii, Nucl. Phys. 68, 191 (1965).
[4] N. K. Sherman, J. R. Stewart, and R. C. Morrison, Phys. Rev. Letters 17, 31 (1966).
[17] E. D. Mahknovskii (private communication).
[18] V. P. Denisov, A. P. Komar, L. A. Kal'shitskii, and E. D. Mahknovskii, Yad.Fiz. 5, 349 (1967); Sov. J. Nucl. Phys. 5, 493 (1967).

REF.

F. Eigenbrod
Z. Naturforsch. 23, 1671 (1968)

ELEM. SYM.	A	Z
Li	6	3

METHOD

REF. NO. 68 Ei 1 egf

REACTION	RESULT	EXCITATION ENERGY	SOURCE		DETECTOR		ANGLE
			TYPE	RANGE	TYPE	RANGE	
E,E/	LFT	2,4	D	30-58	MAG-D	26-58	DST

2=2.184. 4=3.562 MEV

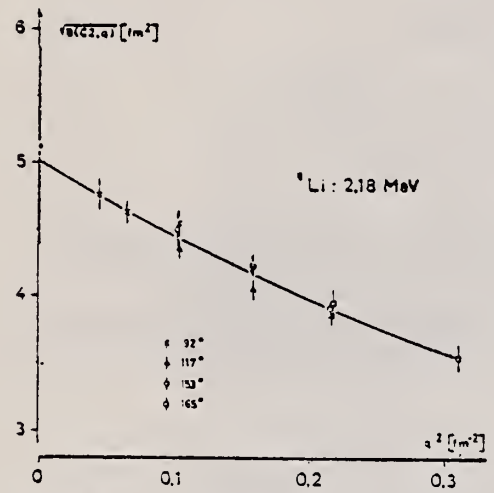

Fig. 2. Square roots of the reduced transition probabilities for the 2.18 MeV transition in ^{6}Li as a function of q^2. The curve fits the experimental points, obtained at different scattering angles, with arbitrary parameters $\Gamma_\gamma{}^0$, R_{tr} and $R_{tr}{}^*$. For comparison, the full point is the value taken from the ^{4}He(d,γ)^{6}Li experiment [9].

E_x (MeV)	2.184	3.562
$\Gamma_\gamma{}^0$ (eV)	$(4.31 \pm 0.34) \cdot 10^{-4}$ $(4.5 \pm 1.3) \cdot 10^{-4}$ a	8.35 ± 0.37 7.52 ± 0.43 c 8.4 calc. d
R_{tr} (fm)	4.10 ± 0.63	2.31 ± 0.18
R_{tr}^* (fm)	4.5 ± 1.4	2.3 ± 1.6
R_{tr}^*/R_{tr}	1.1 ± 0.4 1.06 calc. b	1.0 ± 0.6 1.12 calc. e

Table 1. Ground state radiative widths $\Gamma_\gamma{}^0$ and transition radii R_{tr} and $R_{tr}{}^*$ of the 2.18 and 3.56 MeV states of ^{6}Li. a) ref. [9]. b) ref. [10]. c) from Want et al. cit. in ref. [13]. d) ref. [14]. e) ref. [14].

REF. R. M. Hutcheon, T. E. Drake, V. W. Stobie, G. A. Beer and H. S. Caplan
Nucl. Phys. A107, 266 (1968)

ELEM. SYM.	A	Z
Li	6	3

METHOD

REF. NO. 68 Hu 1 — EGF

REACTION	RESULT	EXCITATION ENERGY	SOURCE		DETECTOR		ANGLE
			TYPE	RANGE	TYPE	RANGE	
E,E/	FMF	4	D	63-127	MAG-D	55-130	DST

b ≡ p-shell harmonic oscillator parameter of ground state

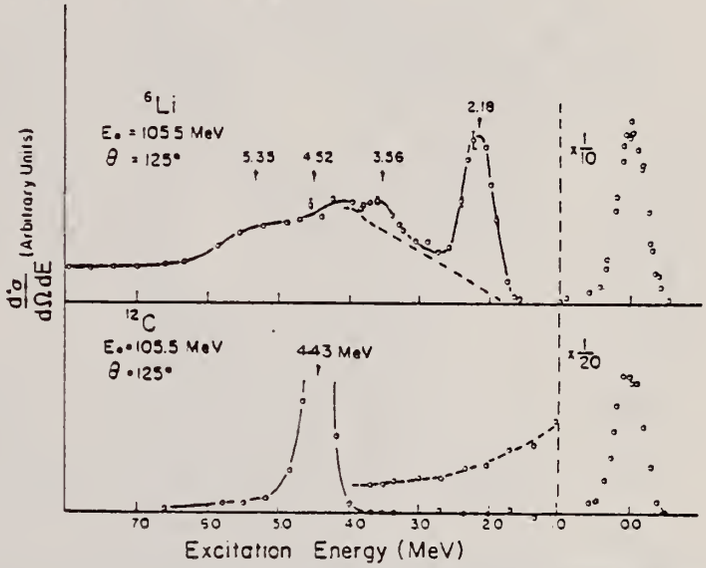

Fig. 1. Plot of the data with radiation tail subtracted for the 125° runs on ^{6}Li metal (99 % isotopic purity) and ^{12}C. The dotted line in the ^{6}Li spectrum shows the continuous cross section assumed under the first two excited states. The dotted line on the ^{12}C spectrum shows the actual size of the radiation tail which was subtracted.

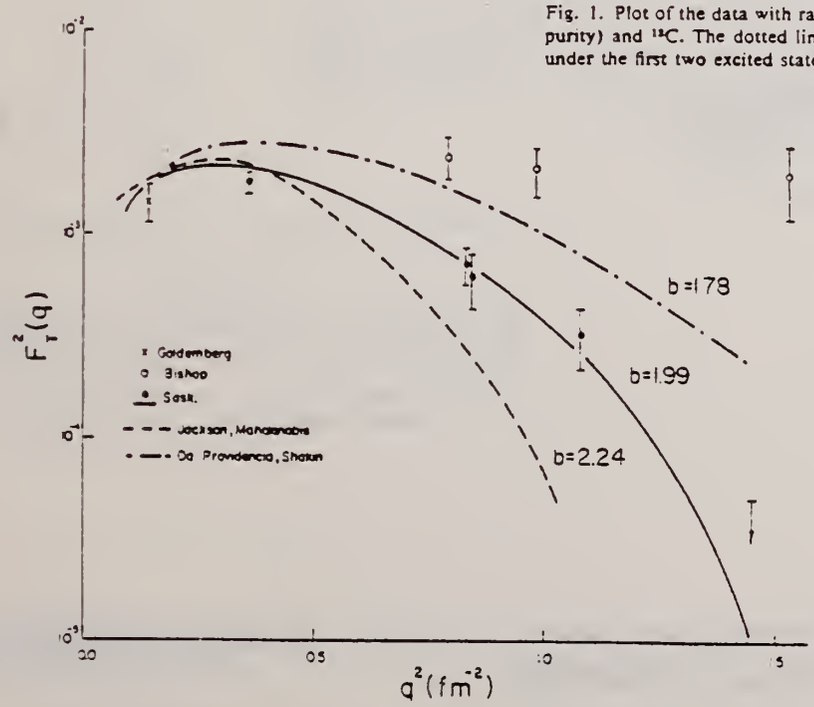

Fig. 3. Transverse form factor for electron excitation of the 3.56 MeV level in ^{6}Li.

REF.

J. L. Matthews, W. Bertozzi, S. Kowalski, C. P. Sargent and W. Turchinetz
Nucl. Phys. A112, 654 (1968)

ELEM. SYM.	A	Z
Li	6	3

METHOD

REF. NO. 68 Ma 1 - EGF

REACTION	RESULT	EXCITATION ENERGY	SOURCE		DETECTOR		ANGLE
			TYPE	RANGE	TYPE	RANGE	
G,P	ABX	100	C	95-102	TEL-D	40-95	DST

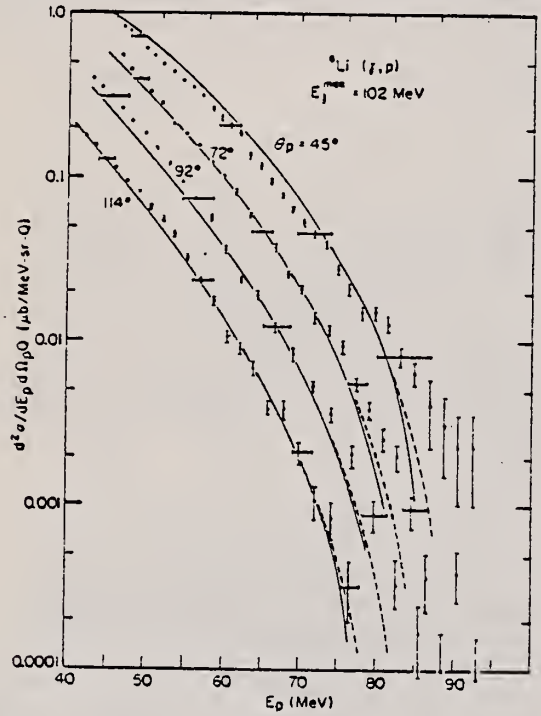

Fig. 11. Comparison of bremsstrahlung photoproton spectra from ^{6}Li at 45°, 72°, 92° and 114° with the prediction of a quasi-deuteron model. The parameters of the calculation (defined in the text) have the following values: $\alpha = 80$ MeV/c, $E_b = -10$ MeV, $E_{well} = 20$ MeV and $L = 4.5$. The dashed curves at the high-energy ends of the spectra represent the effect of the experimental resolution.

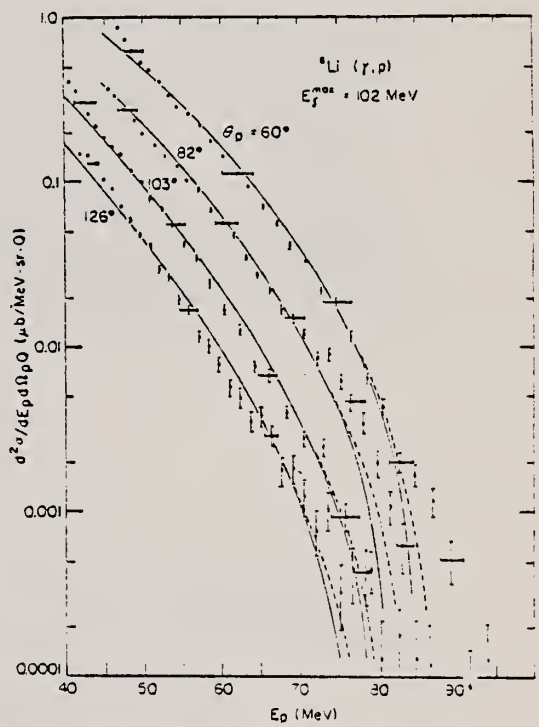

Fig. 12. Comparison of bremsstrahlung photoproton spectra from ^{6}Li at 60°, 82°, 103° and 126° with the prediction of a quasi-deuteron model. The parameters of the calculation (defined in the text) have the following values: $\alpha = 80$ MeV/c, $E_b = -10$ MeV, $E_{well} = 20$ MeV and $L = 4.5$. The dashed curves at the high-energy ends of the spectra represent the effect of the experimental resolution.

(continued)

REF.

J. L. Matthews, W. Bertozzi, S. Kowalski, C. P. Sargent and W. Turchinetz
Nucl. Phys. A112, 654 (1968)

ELEM. SYM.	A	Z
Li	6	3

METHOD

REF. NO. 68 Ma 1 EGF

REACTION	RESULT	EXCITATION ENERGY	SOURCE		DETECTOR		ANGLE
			TYPE	RANGE	TYPE	RANGE	

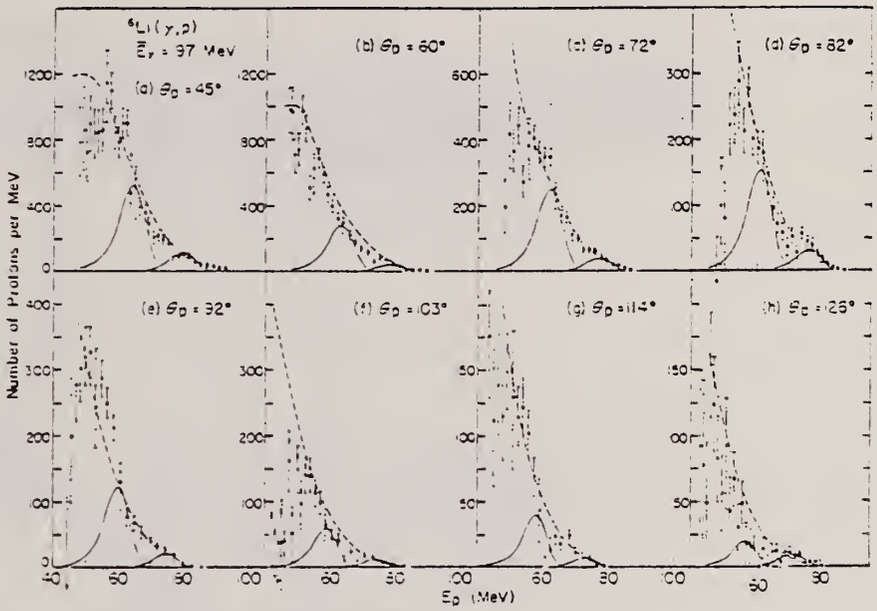

Fig. 14. The ^{6}Li photoproton spectra from "monochromatic" photons ($\bar{E}_\gamma$ = 97 MeV) formed by taking the difference of the 102 and the 95 MeV bremsstrahlung data. Multiplying the given numbers of counts per MeV by 1.80×10^{-3} converts the ordinate scales to μb/MeV · sr per photon of our assumed line width. The shape of the photon difference spectrum is similar to that of the solid curves, whose origin is explained in the text. The dashed curves represent the prediction of the quasi-deuteron model. The extended error bars and the crosses in fig. 14(f) refer to possible systematic uncertainties as discussed in the text.

REF.

A. Murakami
Nuovo Cimento 55B, 604 (1968)

ELEM. SYM.	A	Z
Li	6	3

METHOD

REF. NO.: 68 Mu 2 | HMG

REACTION	RESULT	EXCITATION ENERGY	SOURCE		DETECTOR		ANGLE
			TYPE	RANGE	TYPE	RANGE	
G,T	ABX	THR- 32	C	32	EMU-D		DST
G,PD	ABX	THR- 32	C	32	EMU-D		4PI

The absolute cross-section was obtained by measuring the $^{12}C(\gamma, 3\alpha)$ yield and by normalizing the observed $^{12}C(\gamma, 3\alpha)$ yield to that measured by MAIKOV (*). A bremsstrahlung spectrum $I(E_\gamma) \propto 1/E_\gamma$ was assumed in the cross-section calculation.

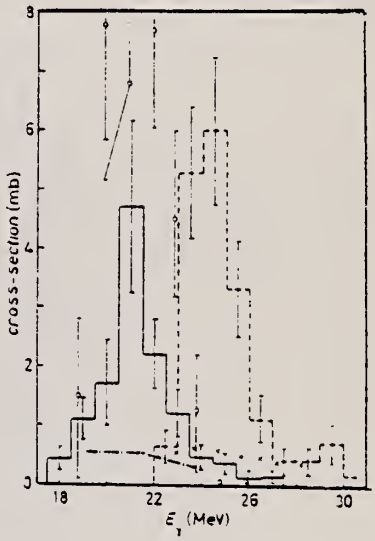

Fig. 2. – The cross-sections of the reactions $^6Li(\gamma,t)^3He$ and $^6Li(\gamma,pd)^4H$. – – – the $^6Li(\gamma,t)^3He$ cross-section obtained in the present work; the $^6Li(\gamma,pd)^4H$ cross-section obtained in the present work; o results of BAZHANOV *et al.* (†); —·—·— results of SUERMAN *et al.* (‡); × results of MANUZIO *et al.* (§).

(*) V. N. MAIKOV: *Sov. Phys. JETP*, 37, 973 (1958).

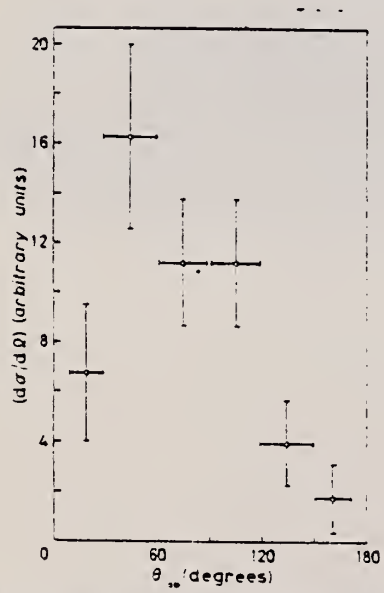

Fig. 3. – The angular distribution of phototritons in the reaction $^6Li(\gamma, t)^3He$ for 20 MeV $\leq E_\gamma \leq$ 22 MeV.

REF. N. K. Sherman, J. E. E. Baglin, R. O. Owens
Phys. Rev. 169, 771 (1968)

ELEM. SYM.	A	Z
Li	6	3

METHOD

REF. NO. 68 Sh 2 HMG

REACTION	RESULT	EXCITATION ENERGY	SOURCE		DETECTOR		ANGLE
			TYPE	RANGE	TYPE	RANGE	
G.T	ABX	24-35	C	40	MAG-D	8-19	90

422

The phototriton cross section of Li^6 has been measured between 24- and 35-MeV photon energy. This work complements an earlier experiment which established the production of the $Li^6(\gamma,t)$ reaction by giant-resonance photons and measured the cross section between 19 and 24 MeV. The phototriton cross section of Li^6 falls monotonically from 0.46±0.24 mb at 19 MeV to 0.11±0.06 mb at 35 MeV. The integrated (γ,t) cross section over this energy interval is 4.9±2.5 MeV mb. The measured bremsstrahlung-weighted cross section is 0.18±0.09 mb. Implications concerning the nuclear size are discussed.

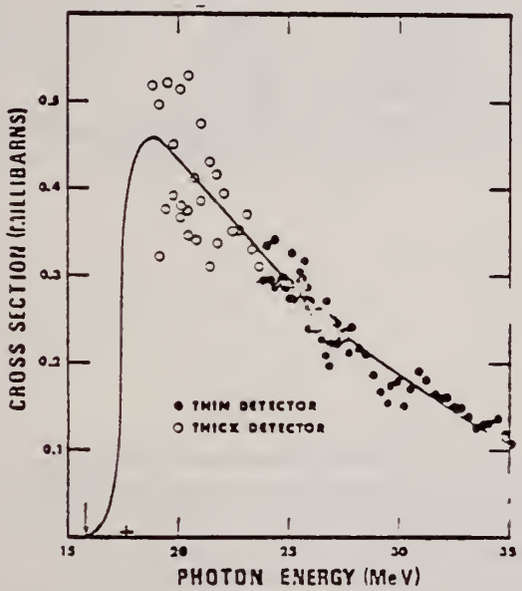

FIG. 5. Phototriton cross section of Li^6. The arrow indicates the reaction threshold. The cross represents the result of Ref. 1, the open circles that of Ref. 6, the solid circles that of the present work. The solid line, above 19 MeV, is an average of the experimental points.

	Li	6	3
METHOD	REF. NO.		
	69 Ei 2		egf

REACTION	RESULT	EXCITATION ENERGY	SOURCE		DETECTOR		ANGLE
			TYPE	RANGE	TYPE	RANGE	
E,E/	LFT	2-5	D	30-60	MAG-D		DST

∠ LEVELS 0 .2-.6

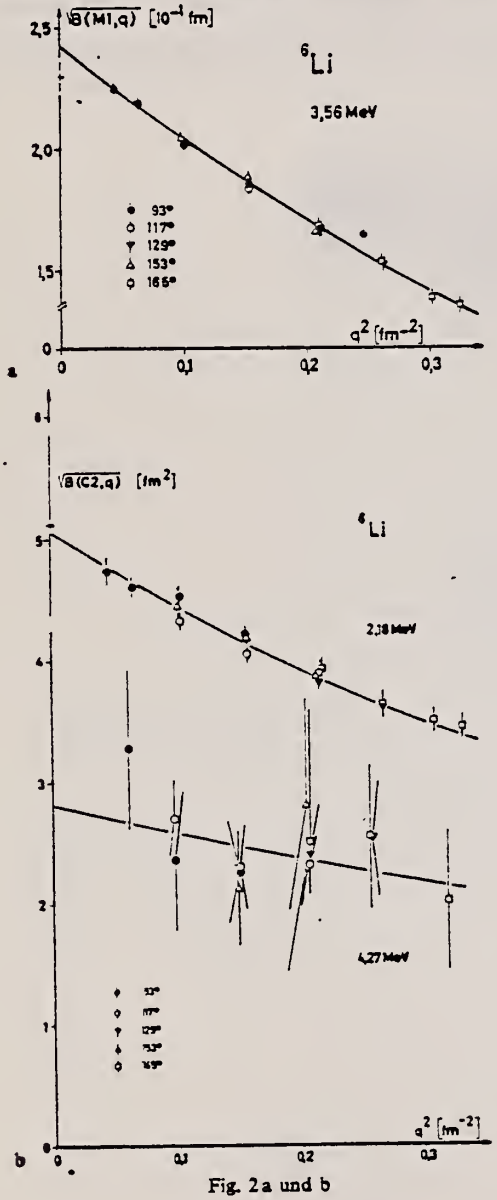

Fig. 2a und b

Tabelle 2. *Transversale (T_T) und longitudinale (T_L) Anteile der Wirkungsquerschnitte nach Gl. (5) aus Messungen von Winkelverteilungen bei konstantem Impulsübertrag q*

E_x [MeV]	q^2 [fm^{-2}]	T_T [a] [10^{-7}]	T_L [10^{-7}]	E_x [MeV]	q^2 [fm^{-2}]	T_T [10^{-7}]	T_L [10^{-7}]
2,18	0,269	0,009 ± 0,061	27,9 ± 1,2	3,56	0,262	9,12 ± 0,46	−0,75 ± 0,91
	0,217	0,023 ± 0,012	20,31 ± 0,24		0,211	8,57 ± 0,28	0,52 ± 0,58
	0,158	0,018 ± 0,052	12,67 ± 0,62		0,153	8,04 ± 0,21	−0,48 ± 0,29
	0,104	−0,011 ± 0,044	6,30 ± 0,38		0,100	6,08 ± 0,13	0,05 ± 0,44
4,27	0,258	0,00 ± 0,35	12,8 ± 4,0	5,37	0,253	0,79 ± 0,16	−0,95 ± 1,40
	0,208	0,03 ± 0,23	7,0 ± 1,0		0,203	0,51 ± 0,17	−0,80 ± 0,85
	0,151	−0,04 ± 0,13	3,7 ± 1,8		0,148	0,26 ± 0,07	−0,05 ± 0,39
	0,099	−0,07 ± 0,16	2,2 ± 1,1				

[a] Nach Abzug des durch Gl. (7) definierten transversal elektrischen Anteils.

Tabelle 3. *Zusammenstellung der Ergebnisse*

E_x = In der vorliegenden Arbeit gemessene Anregungsenergien. $X\lambda$ = Longitudinal elektrischer (C) oder magnetischer (M) Übergang der Multipolarität λ. $B(X\lambda, k)$ = Reduzierte Übergangswahrscheinlichkeit am Photonenpunkt $k = E_x/\hbar c$. $\Gamma_\gamma^0(X\lambda)$ = Grundzustandsstrahlungsbreite. Γ_W = Weisskopfeinheit nach [a]. Übergangsradius R_{tr} und R_{tr}^* gemäß Gl. (4). Für den 4,27 MeV-Übergang wurde $R_{tr} = R_{tr}^*$ angenommen.

E_x [MeV]	$X\lambda$	$B(X\lambda, k)$ [fm$^{2\lambda}$]	$\Gamma_\gamma^0(X\lambda)$ [eV]	Γ_γ^0/Γ_W	R_{tr} [fm]	R_{tr}^*/R_{tr}
2,183 ± 0,009	$C2$	25,6 ± 1,6	(4,40 ± 0,34) · 10^{-4} [b]	16,5	4,28 ± 0,39	1,09 ± 0,10
3,563 ± 0,010	$M1$	(5,86 ± 0,16) · 10^{-2}	8,31 ± 0,36 [b]	8,3	2,90 ± 0,10	1,06 ± 0,11
4,27 ± 0,04	$C2$	7,9 ± 2,5	(5,4 ± 2,8) · 10^{-3}	7,2	3,4 ± 1,2	

[a] Wilkinson, D. H., in: F. Ajzenberg-Selove, Nuclear spectroscopy, part B. New York and London: Academic Press 1960.

[b] Berechnet unter Benutzung der Anregungsenergien (2,184 ± 0,002) MeV bzw. (3,562 ± 0,004) MeV nach [35].

(continued)

Tabelle 1. *Gemessene Wirkungsquerschnittsverhältnisse* σ/σ_E

E_0 = Primärenergie. Θ = Streuwinkel. E_x = Anregungsenergie. $c = 100\,(1-f_c)$, wobei f_c der Korrekturfaktor der Gl. (6) ist. Die Fehler sind statistische Fehler.

E_0 [MeV]	Θ [Grad]	E_x [MeV] 2,18		3,56		4,27		5,37
		σ/σ_E [10^{-3}]	c	σ/σ_E [10^{-3}]	c	σ/σ_E [10^{-3}]	c	σ/σ_E [10^{-3}]
39,09	164,9	16,86 ± 2,5%	3,3	219,8 ± 0,6%	6,7	5,53 ± 18%	3,8	22,4 ± 5%
37,04	165,1	14,28 ± 2,5%	3,4	207,3 ± 1,3%	6,8			
33,13	164,9	10,72 ± 3,2%	3,9	198,4 ± 0,6%	6,8	5,01 ± 11%	4,5	15,9 ± 5%
39,20	129,0	10,40 ± 0,6%	3,5	16,83 ± 0,5%	6,5	4,77 ± 6%	4,1	1,05 ± 11%
33,04	164,9	7,59 ± 3,7%	4,5	172,3 ± 0,6%	7,0	2,92 ± 19%	4,7	11,5 ± 6%
37,91	165,1	7,32 ± 4,0%	4,4					
43,49	153,2	6,89 ± 1,2%	4,2	52,64 ± 0,3%	7,0	3,38 ± 15%	4,7	2,55 ± 7%
42,32	129,0	6,81 ± 0,9%	4,1	14,49 ± 0,3%	6,7	2,45 ± 5%	4,4	0,57 ± 11%
35,23	117,0	6,79 ± 0,9%	3,8	9,51 ± 0,6%	6,5	2,34 ± 4%	4,3	0,27 ± 16%
41,73	153,2	3,93 ± 1,3%	5,0	43,90 ± 0,3%	7,3	0,92 ± 18%	5,0	1,35 ± 8%
47,42	117,0	3,64 ± 1,2%	4,4	7,40 ± 1,1%	6,8	1,08 ± 15%	4,7	0,30 ± 26%
35,29	92,9	3,83 ± 1,0%	3,9	3,75 ± 0,9%	6,2	1,03 ± 6%	4,3	0,07 ± 61%
33,73	153,2	1,67 ± 2,0%	5,5	29,74 ± 0,5%	7,8	< 0,4%		0,98 ± 17%
33,58	117,0	1,61 ± 1,2%	5,0	5,20 ± 0,6%	7,2	0,57 ± 11%	5,0	
45,13	92,9	1,74 ± 1,3%	4,5	2,65 ± 0,7%	6,6	0,59 ± 7%	4,7	
34,02	92,9	0,665 ± 1,7%	5,0	1,78 ± 0,9%	7,0	0,30 ± 17%	5,0	
39,11	92,9	0,323 ± 2,6%	5,4	1,27 ± 0,6%	7,2			

REF.

R. M. Hutcheon and H. S. Caplan
Nucl. Phys. A127, 417 (1969)

ELEM. SYM.	A	Z
Li	6	3

METHOD

REF. NO. 69 Hu 1 egf

REACTION	RESULT	EXCITATION ENERGY	SOURCE		DETECTOR		ANGLE
			TYPE	RANGE	TYPE	RANGE	
E,E/	FMF	0-42	D	55-127	MAG-D		DST

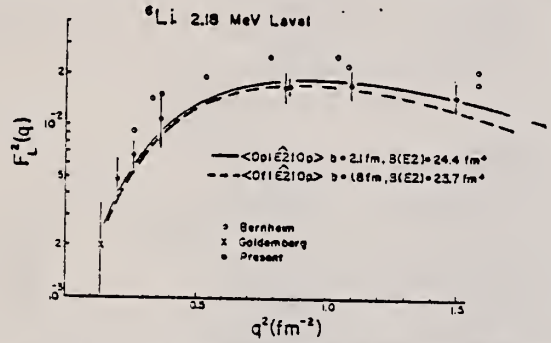

Fig. 2. The variation of the inelastic form factor with momentum transfer. The curves represent the normalised single-particle model predictions.

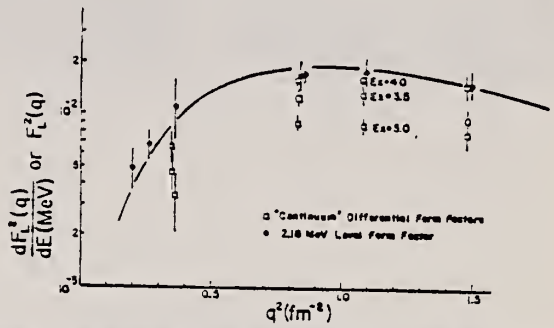

Fig. 4. The variation with momentum transfer of the longitudinal differential form factor. The data and curve in fig. 2 are reproduced here for comparison.

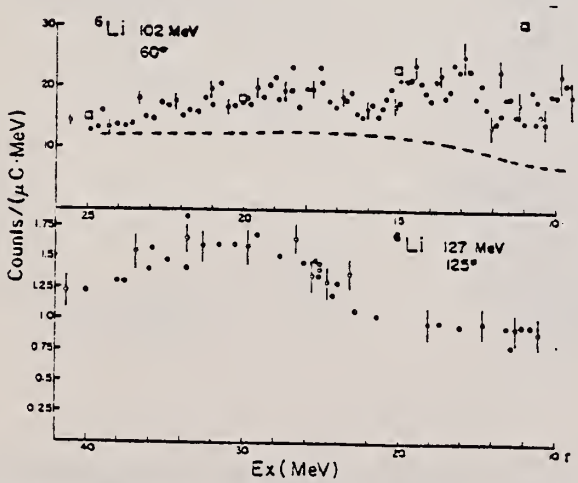

Fig. 5. Typical inelastic electron scattering spectra for higher excitation in ^{6}Li. On the upper spectra taken at low momentum transfer, the squares indicate the magnitude of the elastic radiation tail, which has already been subtracted.

Reiner Neuhausen
Z. Physik 220, 456 (1969)

Li	6	3

METHOD

REF. NO.: 69 Ne 1 | egf

REACTION	RESULT	EXCITATION ENERGY	SOURCE TYPE	SOURCE RANGE	DETECTOR TYPE	DETECTOR RANGE	ANGLE
E,E/	FMF	2,3	D	109-282	MAG-D	104-285	DST
		(2.184, 3.562)					

2=2.184; 3=3.562

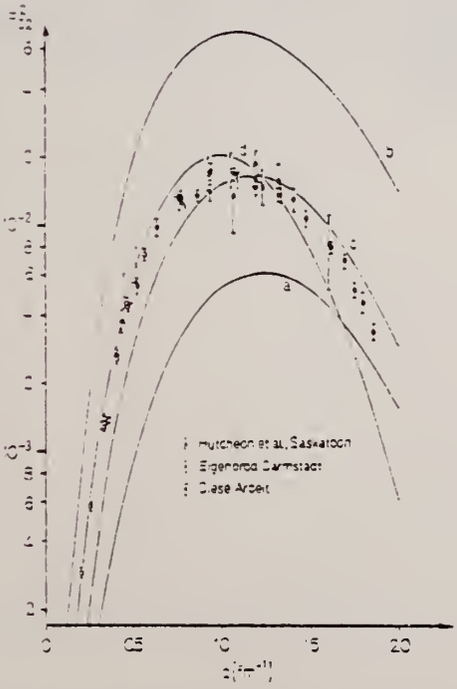

Fig. 2. Quadrat des Formfaktors für den $C2$-Übergang zum 2,184 MeV-Niveau in Li^6. a Schalenmodell[6], $b = 1.64$ fm; b Clustermodell[7]; c Hartree-Fock-Rechnung[8], $b = 1.60$ fm; d Schalenmodell angepaßt, $b = 2.10$ fm

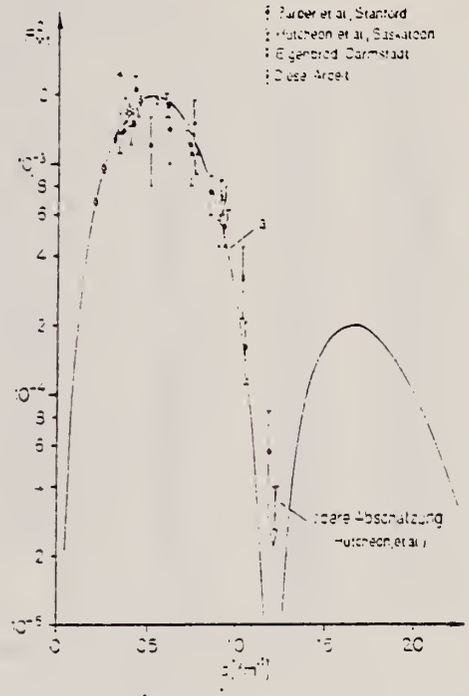

Fig. 3. Quadrat des Formfaktors für den $M1$-Übergang zum 3,562 MeV-Niveau in Li^6. a Schalenmodell, $b = 2.05$ fm

Tabelle. *Gemessene Verhältnisse der unelastischen Wirkungsquerschnitte zu den elastischen und Formfaktoren für die Übergänge zum 2,184 MeV- und 3,562 MeV-Niveau*

		2,184 MeV-Niveau			3,562 MeV-Niveau		
E_0 [MeV]	θ [°]	q [fm^{-1}]	$\left(\frac{d\sigma}{d\Omega}\right)_{I'} / \left(\frac{d\sigma}{d\Omega}\right)_E$	F^2_{C2}	q [fm^{-1}]	$\left(\frac{d\sigma}{d\Omega}\right)_{I'} / \left(\frac{d\sigma}{d\Omega}\right)_E$	F^2_{tr1}
122,9	158,63	1,188	$2{,}76 \cdot 10^{-1} \pm 13$ %	$1{,}88 \cdot 10^{-2}$	1,182	$2{,}4 \cdot 10^{-2} \pm 50$ %	$5{,}7 \cdot 10^{-5}$
152,2	139,40	1,403	$4{,}99 \cdot 10^{-1} \pm 11$ %	$1{,}31 \cdot 10^{-2}$	—	—	—
179,6	83,34	1,186	$2{,}11 \cdot 10^{-1} \pm 6{,}2$%	$1{,}46 \cdot 10^{-2}$	—	—	—
109,2	89,33	0,763	$4{,}28 \cdot 10^{-2} \pm 8{,}5$%	$1{,}31 \cdot 10^{-2}$	0,758	$7{,}4 \cdot 10^{-2} \pm 30$ %	$1{,}5 \cdot 10^{-3}$
109,0	119,42	0,931	$7{,}91 \cdot 10^{-2} \pm 8{,}5$%	$1{,}40 \cdot 10^{-2}$	0,925	$1{,}0 \cdot 10^{-2} \pm 20$ %	$5{,}3 \cdot 10^{-4}$
109,2	158,63	1,057	$1{,}17 \cdot 10^{-1} \pm 30$ %	$1{,}33 \cdot 10^{-2}$	1,050	$4{,}1 \cdot 10^{-2} \pm 30$ %	$1{,}6 \cdot 10^{-4}$
135,7	158,63	1,310	$3{,}84 \cdot 10^{-1} \pm 25$ %	$1{,}55 \cdot 10^{-2}$	1,303	—	$< 6 \cdot 10^{-5}$
166,9	158,63	1,606	$8{,}83 \cdot 10^{-1} \pm 35$ %	$8{,}23 \cdot 10^{-3}$	1,599	—	$< 1 \cdot 10^{-4}$
112,6	44,81	0,429	$5{,}58 \cdot 10^{-3} \pm 11$ %	$3{,}76 \cdot 10^{-3}$	0,427	$2{,}2 \cdot 10^{-3} \pm 25$ %	$2{,}2 \cdot 10^{-3}$
112,6	55,25	0,522	$9{,}60 \cdot 10^{-3} \pm 7{,}7$%	$5{,}40 \cdot 10^{-3}$	0,519	$1{,}7 \cdot 10^{-3} \pm 30$ %	$1{,}2 \cdot 10^{-3}$
112,6	67,89	0,627	$2{,}22 \cdot 10^{-2} \pm 7{,}8$%	$9{,}79 \cdot 10^{-3}$	0,623	$3{,}0 \cdot 10^{-3} \pm 30$ %	$1{,}4 \cdot 10^{-3}$
112,6	84,27	0,751	$3{,}97 \cdot 10^{-2} \pm 6{,}7$%	$1{,}25 \cdot 10^{-2}$	0,747	$4{,}8 \cdot 10^{-3} \pm 25$ %	$1{,}2 \cdot 10^{-3}$
112,5	84,17	0,750	$4{,}17 \cdot 10^{-2} \pm 5{,}9$%	$1{,}32 \cdot 10^{-2}$	0,745	$4{,}4 \cdot 10^{-3} \pm 25$ %	$1{,}1 \cdot 10^{-3}$
112,5	100,18	0,856	$5{,}84 \cdot 10^{-2} \pm 5{,}1$%	$1{,}34 \cdot 10^{-2}$	0,851	$6{,}4 \cdot 10^{-3} \pm 20$ %	$7{,}5 \cdot 10^{-4}$
230,8	54,76	1,062	$1{,}48 \cdot 10^{-1} \pm 6{,}1$%	$1{,}69 \cdot 10^{-2}$	—	—	—
230,8	62,10	1,188	$2{,}27 \cdot 10^{-1} \pm 5{,}2$%	$1{,}58 \cdot 10^{-2}$	—	—	—
230,8	69,82	1,315	$3{,}39 \cdot 10^{-1} \pm 6{,}4$%	$1{,}36 \cdot 10^{-2}$	—	—	—
230,8	80,00	1,472	$5{,}59 \cdot 10^{-1} \pm 7{,}1$%	$1{,}07 \cdot 10^{-2}$	—	—	—
230,8	90,00	1,613	$8{,}84 \cdot 10^{-1} \pm 6{,}4$%	$8{,}02 \cdot 10^{-3}$	—	—	—
230,8	100,01	1,742	$1{,}19 \pm 7{,}4$%	$5{,}18 \cdot 10^{-3}$	—	—	—
230,8	110,00	1,857	$1{,}59 \pm 7{,}8$%	$3{,}40 \cdot 10^{-3}$	—	—	—
281,7	80,00	1,791	$1{,}40 \pm 10$ %	$4{,}58 \cdot 10^{-3}$	—	—	—
281,7	74,08	1,683	$1{,}13 \pm 7{,}1$%	$7{,}03 \cdot 10^{-3}$	—	—	—

V. K. Rasmussen and C. P. Swann
Phys. Rev. 183, 918 (1969)

Li	6	3

METHOD

REF. NO. 69 Ra 3 hmg

REACTION	RESULT	EXCITATION ENERGY	SOURCE TYPE	SOURCE RANGE	DETECTOR TYPE	DETECTOR RANGE	ANGLE
G.G	LFT	3	C	3	NAI-D		DST
		(3.56)		(3.67)			(96,128)

$\bar{\Gamma}$ = 8.1 ± 0.5 eV

3 = 3.56 ME

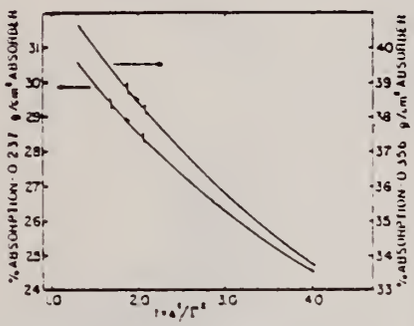

FIG. 3. Plot of the expected self-absorption versus Γ for the scatterer and absorbers used. The smooth curves connect calculated points (not shown) for Γ = 1.25, 1.50, 1.75, 2.00, 3.00 and 4.00. The experimental values and their statistical errors are shown.

REF. Yu. I. Sorokin, A. Kh. Shardanov, V. G. Shevchenko and B. A. Yur'ev
Izv. Akad. Nauk Fiz. 33, 721 (1969)
Bull. Acad. Sci. USSR-Phys. 33, 663 (1969)

ELEM. SYM.	A	Z
Li	6	3

METHOD

REF. NO. 69 So 3 egf

REACTION	RESULT	EXCITATION ENERGY	SOURCE		DETECTOR		ANGLE
			TYPE	RANGE	TYPE	RANGE	
G,P	ABX	5-12	C	12	EMU-D	2-6	4PI

Table 1

^{6}Li levels excited in (γ,p) and (γ,n) reactions, and dipole levels calculated with the many-particle shell model

(γ,p) reaction		(γ,n) reaction		Calculated (Ref. 1)	
The present work		Ref. 8			
E^*, MeV	$\sigma_{int}(\gamma p)$, MeV·mb	E^*, MeV	$\sigma_{int}(\gamma n)$, MeV·mb	E^*, MeV	σ_{int}^{γ}, MeV·mb
6,5*	1,0	—	—	—	—
6,7*	1,2	7,1	0,5	—	—
7,8	0,07	—	—	—	—
—	—	8,2	1,0	—	—
8,3	0,085	—	—	—	—
—	—	—	—	8,8	0,35
9,0	0,10	9,2	1,05	—	—
9,6	0,075	—	—	—	—
10,2	0,085	10,8	1,7	10,5	0,95
(10,7)	0,035	—	—	—	—
11,0	0,07	11	2,0	11,3	2,45
(11,4)	0,05	—	—	12,8	4,21

*From Ref. 4.

^{4}A.Kh.Shardanov, V.G.Shevchenko and B.A.Yur'ev, Izv. AN SSSR, Ser.Fiz.23,60 (1964).

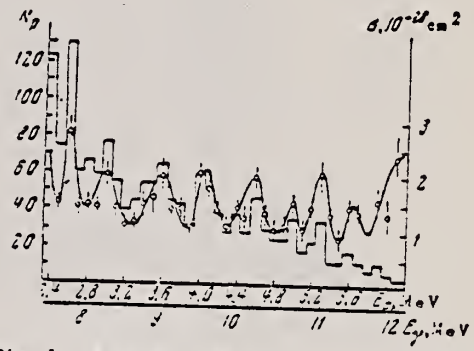

Fig.1. Energy distribution of photoprotons ejected from ^{6}Li by 12 MeV bremsstrahlung (histogram), and the ^{6}Li(γ,p) cross section (curve).

REF.

R. M. Hutcheon, R. Neuhausen, F. Eigenbrod
Z. Naturforsch. 25a, 973 (1970)

ELEM. SYM.	A	Z
Li	6	3

METHOD

REF. NO. 70 Hu 1 egf

REACTION	RESULT	EXCITATION ENERGY	SOURCE		DETECTOR		ANGLE
			TYPE	RANGE	TYPE	RANGE	
E,E/	FMF	5	D	50-160	MAG-D		DST

5.36 MEV LEVEL

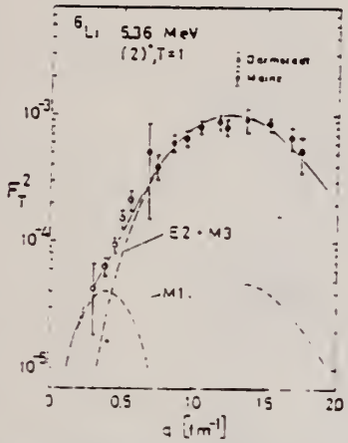

Fig. 2. Squared form factor for the excitation of the 5.36 MeV level. Measurements at equal momentum transfer [4] were combined to form single points. The solid line is the sum of the calculated M1, E2, M3 contributions to the form factor using the parameters of set I.

[4] T. Lauritsen and F. Ajzenberg-Selove, Nucl. Phys. 78, 1 [1966].
[5] C. L. Cocke, Nucl. Phys. A 110, 321 [1968].
[6] F. Eigenbrod, Z. Phys. 228, 337 [1969].
[7] R. M. Hutcheon and R. Neuhausen, to be published.
[8] L. R. Suelzle, M. R. Yearian, and H. Crannell, Phys. Rev. 162, 992 [1967].
[9] D. F. Jackson, Proc. Phys. Soc. London 76, 949 [1960].

A. Murakami
J. Phys. Soc. Japan 28, 1 (1970)

Li	6	3

METHOD

REF. NO. 70 Mu 1 egf

REACTION	RESULT	EXCITATION ENERGY	SOURCE TYPE	SOURCE RANGE	DETECTOR TYPE	DETECTOR RANGE	ANGLE
G,T	ABX	18-28	C	32	EMU-D		DST
G,PD	ABX	22-32	C	32	EMU-D		4PI

673
674

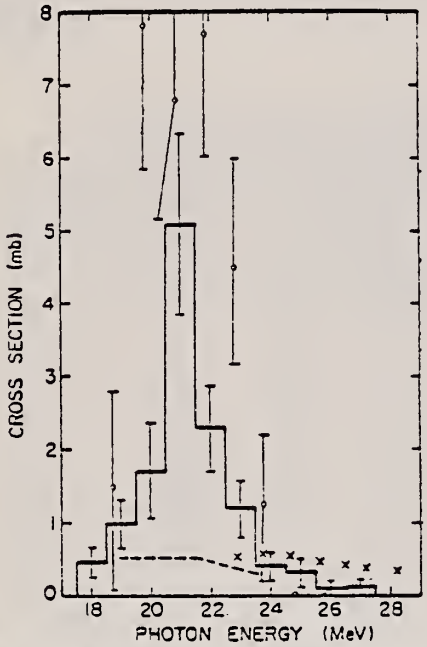

Fig. 5. The cross section for the reaction $^6Li(\gamma, t)^3He$.
—— results of the present work
⊼ results of Bazhanov *et al.*[7]
× results of Manuzio *et al.*[10]
—— results of Sherman *et al.*[11]
Only statistical errors are included.

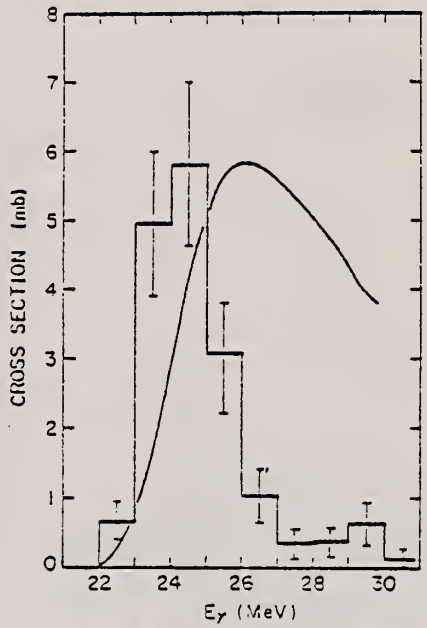

Fig. 7. The cross section obtained for the reaction $^6Li(\gamma, pd)^3H$. The theoretical cross section curve was calculated in terms of the $\alpha-d$ peripheral model. Only statistical errors are included.

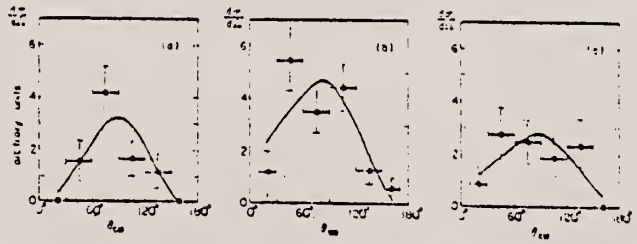

Fig. 6. The angular distributions of phototritons in the reaction $^6Li(\gamma, t)^3He$ are shown in the center of mass system. Figures (a), (b), (c) correspond to photon energies ranging from the threshold up to 20 MeV, from 20 MeV up to 22 MeV and from 22 MeV up to 28 MeV, respectively. Only statistical errors are included. The curves were obtained by a least squares fit of the data to $f(\theta)=a+b\cos\theta-c\cos^2\theta$.

REF. C. F. Wong, R. M. Hutcheon, Y. M. Shin, H. S. Caplan
Can. J. Phys. 48, 1917 (1970)

ELEM. SYM.	A	Z
Li	6	3

METHOD

REF. NO. 70 Wo 1 - egf

REACTION	RESULT	EXCITATION ENERGY	SOURCE		DETECTOR		ANGLE
			TYPE	RANGE	TYPE	RANGE	
G,T	ABX	20-52	C	90	MAG-D		90
G,HE3	ABX	20-52	C	90	MAG-D		90
G,XP	ABX	7-19	C	22,27	MAG-D		90

VIRT PHOT, SEE 79SK11

659
672
671

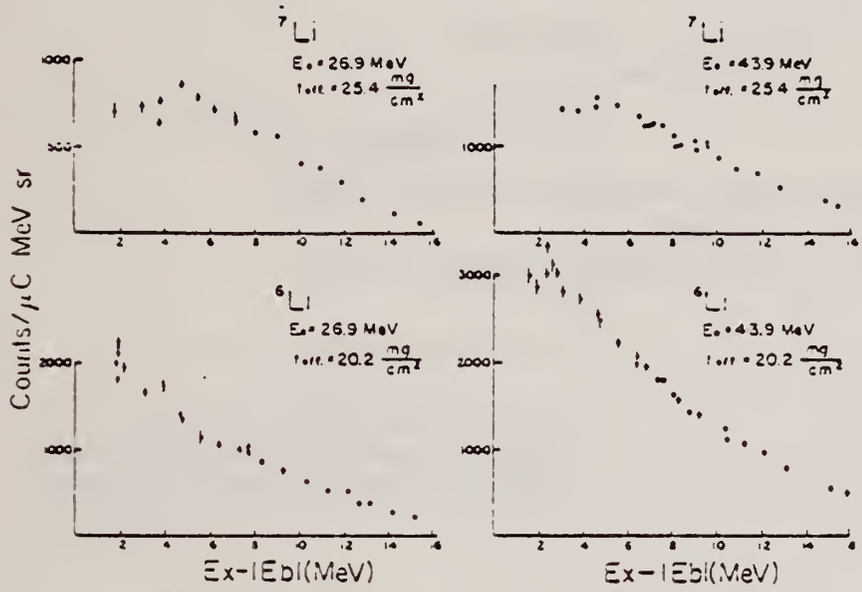

FIG. 4. Energy spectra of electro protons from ^{6}Li and ^{7}Li.

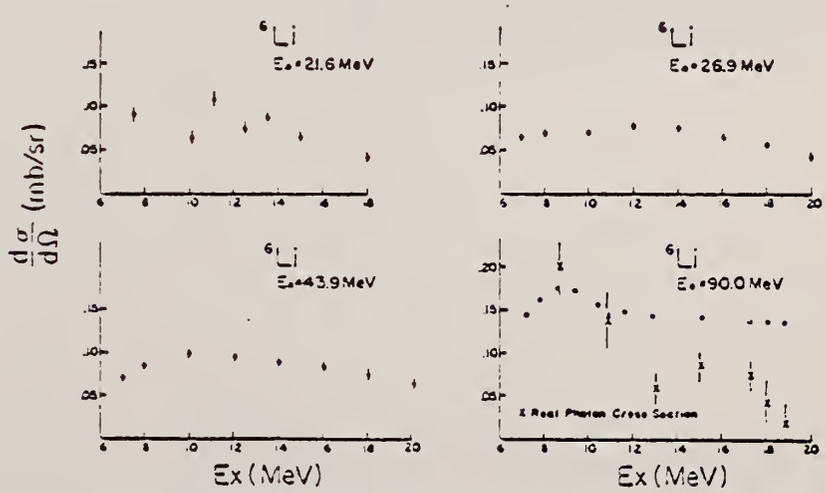

FIG. 5. The ^{6}Li photoproton cross sections obtained by unfolding the E1 virtual photon spectrum. The 90 MeV run also shows the real photon cross section.

(continued)

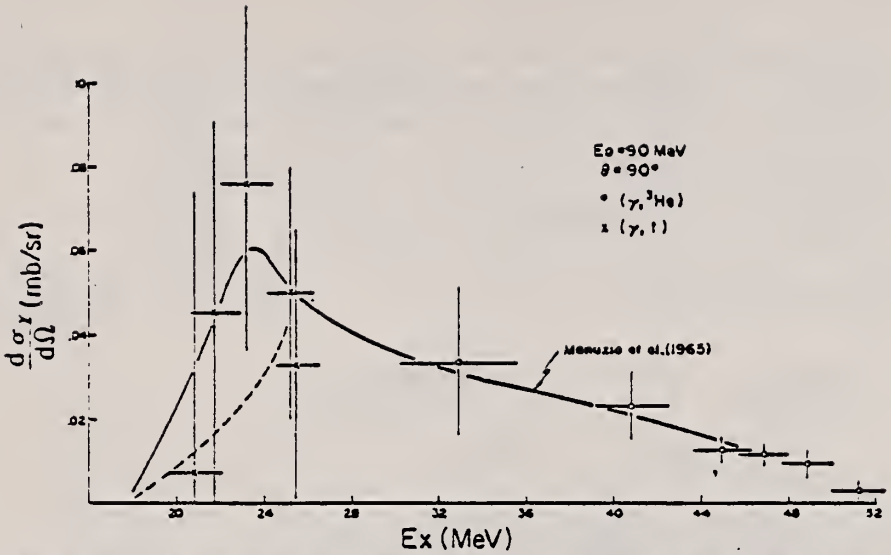

FIG. 8. Measured cross sections for the ^{6}Li(γ,^{3}He) and ^{6}Li(γ,t) reactions induced by real photons.

REF.

A.M. Young, S.L. Blatt, and R.G. Seyler
Phys. Rev. Letters 25, 1764 (1970)

ELEM. SYM.	A	Z
Li	6	3

METHOD

REF. NO.	
70 Yo 1	hmg

REACTION	RESULT	EXCITATION ENERGY	SOURCE		DETECTOR		ANGLE
			TYPE	RANGE	TYPE	RANGE	
HE,G	ABX	16-36	D	0-20	NAI-D		DST

HE=HE3, SEE 68BL1

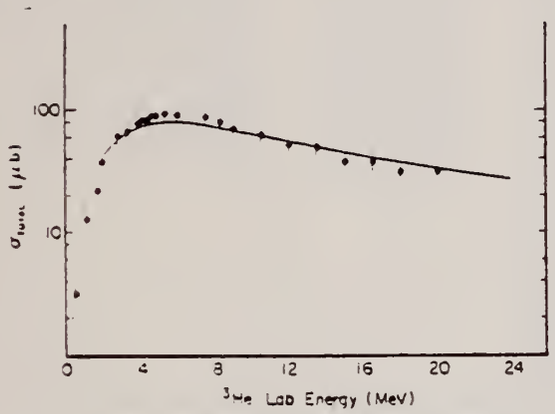

FIG. 1. Results of the direct-capture calculation for the energy dependence of the radiation to the ground state of ^{6}Li (solid curve). The theoretical cross section is normalized to the data of Ref. 4, yielding a value $\vartheta_0^2 = 0.69$.

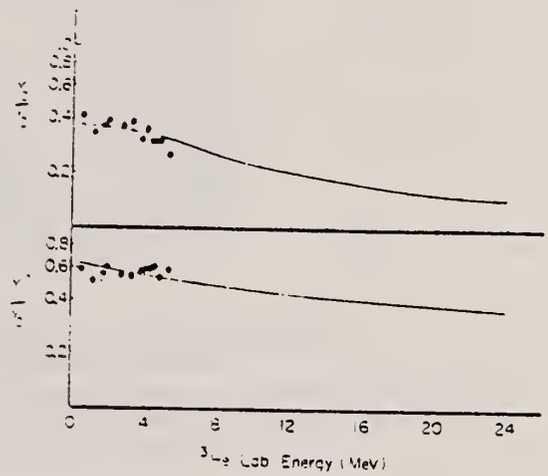

FIG. 2. The "reduced capture-cross-section ratio" defined in the text) for γ_1/γ_0 and γ_2/γ_0, as calculated solid curves). Comparisons are with data of Ref. 4.

^{4}T(^{3}He,γ)^{6}Li: S.L. Blatt, A.M. Young, S.C. Ling, K.J. Moon, and C.D. Porterfield, Phys. Rev. 176, 1147 (1968); A.M. Young, S.L. Blatt, J.F. Amann, and E.M. Diener, Bull. Amer. Phys. Soc. 15, 125 (1970).

REF. G. C. Li, I. Sick, R. R. Whitney and M. R. Yearian
Nucl. Phys. A162, 583 (1971)

ELEM. SYM.	A	Z
Li	6	3

METHOD

REF. NO. 71 Li 1 egf

REACTION	RESULT	EXCITATION ENERGY	SOURCE		DETECTOR		ANGLE
			TYPE	RANGE	TYPE	RANGE	
E,E/	FMF	2	D	200,500	MAG-D		DST

2 = 2.18

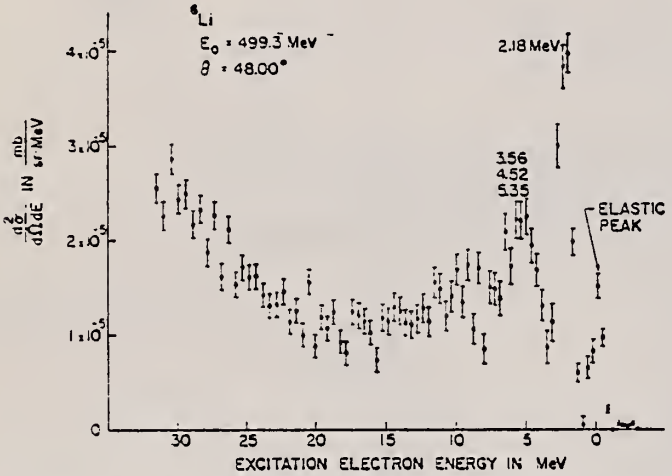

Fig. 1. Spectrum of scattered electrons for an incident energy of 499.3 MeV, a scattering angle of 48°, and target thickness of 745 mg/cm². The spectrum has been corrected for relative channel efficiencies and has been radiatively unfolded.

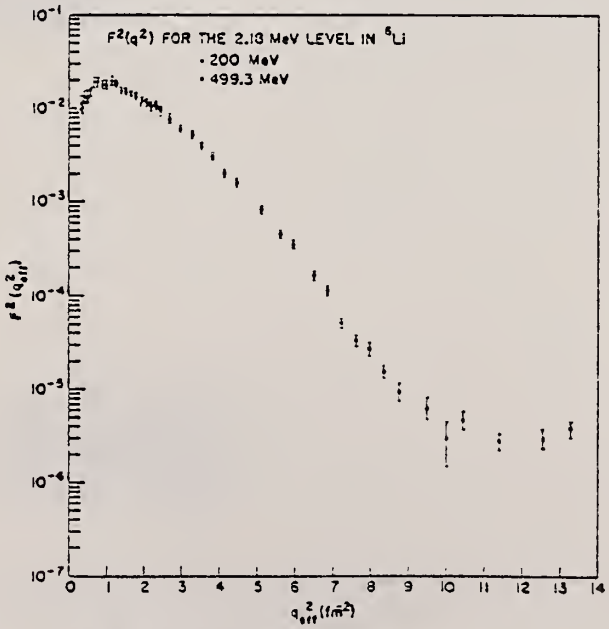

Fig. 3. Experimental form factor of the 2.18 MeV level in ^{6}Li.

(continued)

TABLE 1

Elastic and 2.18 MeV level cross sections for ^{6}Li(e, e)

E_e = 200.0 MeV			E_e = 499.3 MeV		
Angle (deg.)	Elastic cross section (mb/sr)	2.18 MeV level cross section(mb/sr)	Angle (deg.)	Elastic cross section (mb/sr)	2.18 MeV level cross section (mb/sr)
32.00	$(0.967 \pm 0.029)10^{-1}$	$(0.214 \pm 0.039)10^{-2}$	32.00	$(0.835 \pm 0.025)10^{-3}$	$(0.355 \pm 0.033)10^{-3}$
34.00	$(0.712 \pm 0.021)10^{-1}$	$(0.155 \pm 0.025)10^{-2}$	33.00	$(0.605 \pm 0.018)10^{-3}$	$(0.290 \pm 0.023)10^{-3}$
36.00	$(0.501 \pm 0.015)10^{-1}$	$(0.156 \pm 0.024)10^{-2}$	34.00	$(0.451 \pm 0.014)10^{-3}$	$(0.247 \pm 0.018)10^{-3}$
40.00	$(0.273 \pm 0.008)10^{-1}$	$(0.101 \pm 0.013)10^{-2}$	35.00	$(0.308 \pm 0.009)10^{-3}$	$(0.215 \pm 0.016)10^{-3}$
44.00	$(0.152 \pm 0.005)10^{-1}$	$(0.812 \pm 0.086)10^{-3}$	36.00	$(0.233 \pm 0.007)10^{-3}$	$(0.171 \pm 0.014)10^{-3}$
48.00	$(0.920 \pm 0.028)10^{-2}$	$(0.682 \pm 0.070)10^{-3}$	38.00	$(0.134 \pm 0.004)10^{-3}$	$(0.116 \pm 0.009)10^{-3}$
52.00	$(0.555 \pm 0.017)10^{-2}$	$(0.493 \pm 0.050)10^{-3}$	40.00	$(0.603 \pm 0.020)10^{-4}$	$(0.719 \pm 0.053)10^{-4}$
56.00	$(0.316 \pm 0.010)10^{-2}$	$(0.334 \pm 0.033)10^{-3}$	42.00	$(0.334 \pm 0.010)10^{-4}$	$(0.510 \pm 0.038)10^{-4}$
60.00	$(0.188 \pm 0.006)10^{-2}$	$(0.246 \pm 0.025)10^{-3}$	44.00	$(0.162 \pm 0.005)10^{-4}$	$(0.322 \pm 0.025)10^{-4}$
64.00	$(0.116 \pm 0.003)10^{-2}$	$(0.208 \pm 0.021)10^{-3}$	46.00	$(0.846 \pm 0.025)10^{-5}$	$(0.202 \pm 0.017)10^{-4}$
68.00	$(0.705 \pm 0.021)10^{-3}$	$(0.149 \pm 0.014)10^{-3}$	48.00	$(0.392 \pm 0.011)10^{-5}$	$(0.116 \pm 0.009)10^{-4}$
72.00	$(0.416 \pm 0.013)10^{-3}$	$(0.960 \pm 0.075)10^{-4}$	50.00	$(0.193 \pm 0.056)10^{-5}$	$(0.754 \pm 0.065)10^{-5}$
76.00	$(0.268 \pm 0.008)10^{-3}$	$(0.746 \pm 0.059)10^{-4}$	54.00	$(0.434 \pm 0.012)10^{-6}$	$(0.282 \pm 0.021)10^{-5}$
80.00	$(0.164 \pm 0.005)10^{-3}$	$(0.549 \pm 0.043)10^{-4}$	57.00	$(0.123 \pm 0.004)10^{-6}$	$(0.123 \pm 0.009)10^{-5}$
84.00	$(0.103 \pm 0.003)10^{-3}$	$(0.415 \pm 0.031)10^{-4}$	59.00	$(0.659 \pm 0.042)10^{-7}$	$(0.825 \pm 0.062)10^{-6}$
88.00	$(0.671 \pm 0.020)10^{-4}$	$(0.288 \pm 0.025)10^{-4}$	62.00	$(0.148 \pm 0.013)10^{-7}$	$(0.306 \pm 0.024)10^{-6}$
92.00	$(0.438 \pm 0.013)10^{-4}$	$(0.231 \pm 0.019)10^{-4}$	64.00	$(0.43 \pm 0.10)10^{-8}$	$(0.185 \pm 0.015)10^{-6}$
96.00	$(0.292 \pm 0.009)10^{-4}$	$(0.171 \pm 0.013)10^{-4}$	66.00		$(0.725 \pm 0.092)10^{-7}$
100.00	$(0.187 \pm 0.006)10^{-4}$	$(0.140 \pm 0.011)10^{-4}$	68.00		$(0.411 \pm 0.059)10^{-7}$
			70.00		$(0.296 \pm 0.049)10^{-7}$
			72.00		$(0.148 \pm 0.024)10^{-7}$
			74.00	$(0.115 \pm 0.038)10^{-8}$	$(0.80 \pm 0.15)10^{-8}$
			78.00	$(0.111 \pm 0.032)10^{-8}$	$(0.45 \pm 0.11)10^{-8}$
			81.00	$(0.92 \pm 0.22)10^{-9}$	$(0.17 \pm 0.09)10^{-8}$
			83.00	$(0.77 \pm 0.21)10^{-9}$	$(0.24 \pm 0.05)10^{-8}$
			88.00	$(0.56 \pm 0.23)10^{-9}$	$(0.11 \pm 0.02)10^{-8}$
			94.00	$(0.30 \pm 0.12)10^{-9}$	$(0.83 \pm 0.17)10^{-9}$
			98.00	$(0.26 \pm 0.08)10^{-9}$	$(0.88 \pm 0.16)10^{-9}$

REF.

E. J. Moniz, I. Sick, R. R. Whitney, J. R. Ficenec, R. D. Kephart and W. P. Trower

Phys. Rev. Letters 26, 445 (1971)

ELEM. SYM.	A	Z
Li	6	3

METHOD

REF. NO. 71 Mo 3 hmg

REACTION	RESULT	EXCITATION ENERGY	SOURCE		DETECTOR		ANGLE
			TYPE	RANGE	TYPE	RANGE	
E,E/	ABX	0-240	D	500	MAG-D		60

Table I. Nuclear Fermi momentum k_F and average nucleon interaction energy $\bar{\epsilon}$ determined by least-squares fit of theory to quasielastic peak.

Nucleus	k_F (MeV/c)[a]	$\bar{\epsilon}$ (MeV)[b]
$_3Li^6$	169	17
$_6C^{12}$	221	25
$_{12}Mg^{24}$	235	32
$_{20}Ca^{40}$	251	29
$_{28}Ni^{58.7}$	260	36
$_{39}Y^{89}$	254	39
$_{50}Sn^{118.7}$	260	42
$_{73}Ta^{181}$	265	42
$_{82}Pb^{208}$	265	44

[a]The fitting uncertainty in these numbers is approximately ± 5 MeV/c.

[b]The fitting uncertainty in these numbers is approximately ± 3 MeV. Simple estimates for $\bar{\epsilon}$ give numbers in reasonable agreement with those in the table.

REF.

R. Neuhausen and R. M. Hutcheon
Nucl. Phys. A164, 497 (1971)

ELEM. SYM.	A	Z
Li	6	3

METHOD

REF. NO. 71 Ne 1 egf

REACTION	RESULT	EXCITATION ENERGY	SOURCE		DETECTOR		ANGLE
			TYPE	RANGE	TYPE	RANGE	
E,E/	FMF	3.5	D	80-190	MAG-D		DST

3=3.56, 5=5.36

TABLE 1
Results of the backward angle spectra

		3.562 MeV level			5.36 MeV level		
E_0 (MeV)	θ (deg)	q (fm^{-1})	$\frac{(d\sigma/d\Omega)_{1a}}{(d\sigma/d\Omega)_{el}}$	$F^2_{c1}\times10^3$	q (fm^{-1})	$\frac{(d\sigma/d\Omega)_{1a}}{(d\sigma/d\Omega)_{el}}$	$F^2_{c1}\times10^3$
78.4	130.00	0.696	0.0209 ±0.0015	1.47 ±0.11	0.687	0.0048 ±0.0016	0.34 ±0.12
78.5	158.61	0.754	0.123 ±0.006	1.31 ±0.06	0.746	0.038 ±0.007	0.40 ±0.08
89.3	158.61	0.859	0.130 ±0.006	1.00 ±0.05	0.851	0.076 ±0.010	0.59 ±0.08
99.2	158.61	0.954	0.102 ±0.007	0.57 ±0.04	0.946	0.112 ±0.014	0.63 ±0.08
108.9	158.61	1.047	0.093 ±0.007	0.37 ±0.03	1.039	0.208 ±0.019	0.84 ±0.08
122.9	158.63	1.182	0.036 ±0.012	0.086 ±0.030	1.174	0.345 ±0.045	0.82 ±0.11
127.5	158.61	1.226	0.032 ±0.010	0.063 ±0.019	1.218	0.435 ±0.050	0.86 ±0.10
141.9	158.61	1.363		<0.018	1.355	0.82 ±0.13	0.88 ±0.14
159.0	158.61	1.525	0.070 ±0.023	0.034 ±0.012	1.518	1.82 ±0.14	0.88 ±0.07
175.5	158.61	1.680	0.43 ±0.07	0.088 ±0.018	1.673	3.1 ±0.4	0.64 ±0.09
182.6	158.61	1.747	0.64 ±0.16	0.090 ±0.022	1.740	3.8 ±0.7	0.53 ±0.10

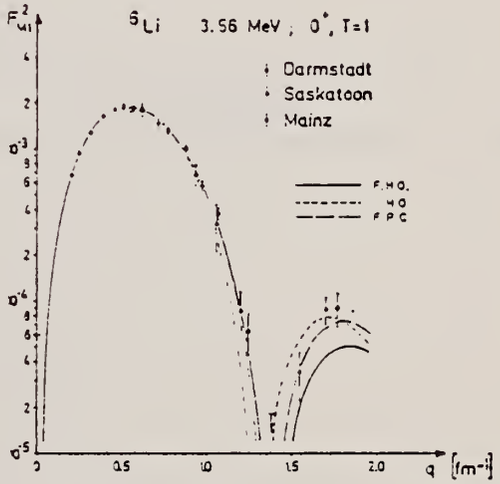

6. The form factors for the transition to the 3.56 MeV level.

TABLE 2
Results of the forward angle spectra

		Elastic data			2.184 MeV level		
E_0 (MeV)	θ (deg)	q (fm^{-1})	$\frac{(d\sigma/d\Omega)_{^6Li}}{(d\sigma/d\Omega)_{^{12}C}}$	F^2_{c0}	q (fm^{-1})	$\frac{(d\sigma/d\Omega)_{1a}}{(d\sigma/d\Omega)_{el}}$	$F_{c2}\times10^2$
99.2	60.00	0.500	0.237 ±0.014	0.573 ±0.035			
140.4	52.75				0.631	0.0231 ±0.0017	1.02 ±0.08
175.4	65.00	0.947	0.277 ±0.015	0.162 ±0.009	0.941	0.101 ±0.005	1.76 ±0.09
175.5	90.00	1.239	0.437 ±0.026	0.0528 ±0.0035	1.231	0.283 ±0.017	1.02 ±0.07

(continued)

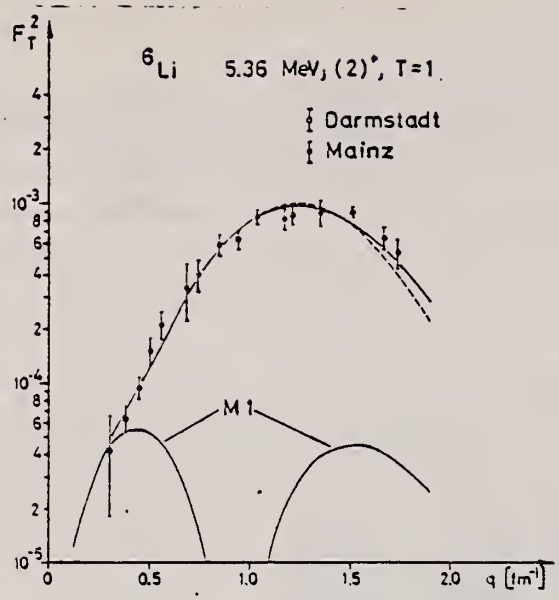

Fig. 7. The form factor for the transition to the 5.36 MeV level. The solid line represents both the f.h.o. and f.p.c. theoretical fits, the dotted line the h.o. fit.

REF.

E. Ventura, C. C. Chang and W. E. Meyerhof
Nucl. Phys. A173, 1 (1971)

ELEM. SYM.	A	Z
Li	6	3

METHOD

REF. NO. 71 Ve 1 egf

REACTION	RESULT	EXCITATION ENERGY	SOURCE		DETECTOR		ANGLE
			TYPE	RANGE	TYPE	RANGE	
HE,G	ABX	20-28	D	9-26	NAI-D		DST

HE3 BEAM 715

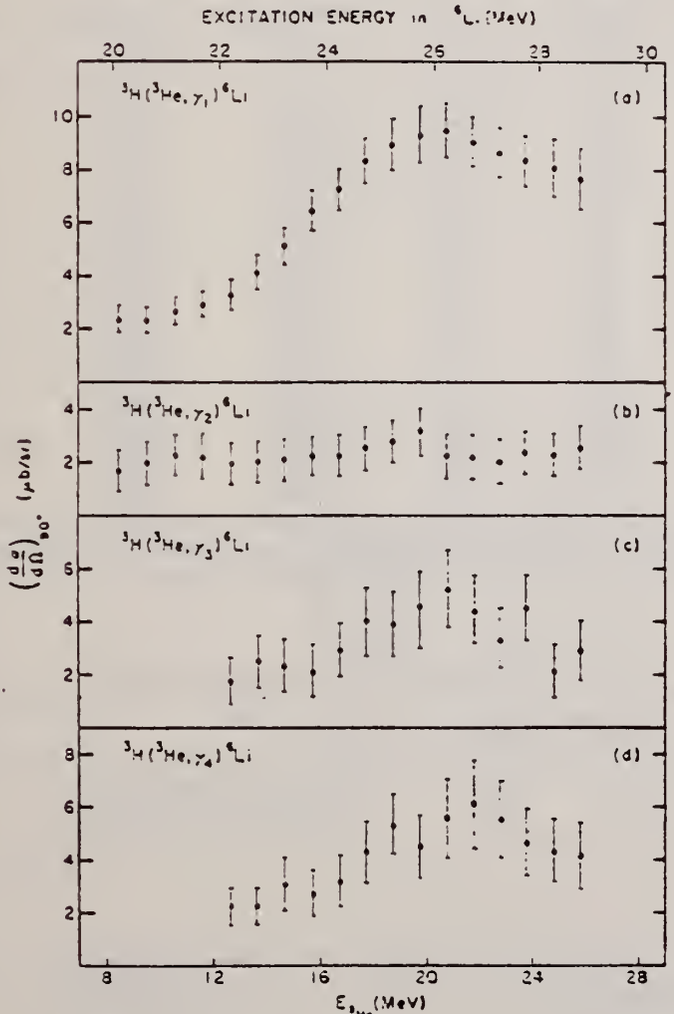

Fig. 5. Differential cross section as a function of $E_{^3He}$ for the transitions to the first four excited states in ^{6}Li at 90° lab.

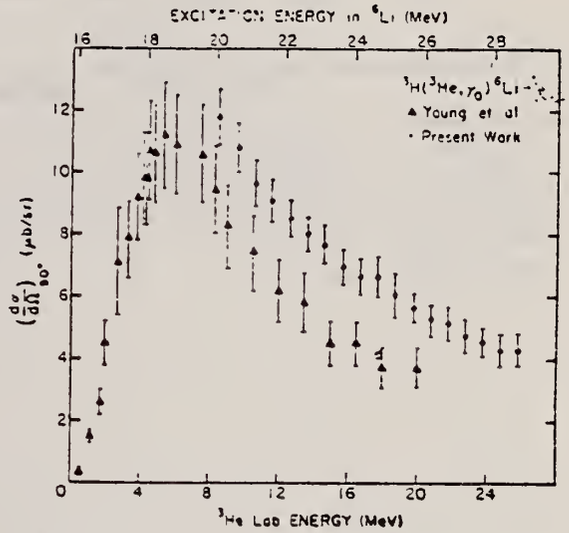

Fig. 3. Differential cross section as a function of $E_{^3He}$ for ^{3}H(^{3}He,γ_0)^{6}Li at 90° lab.

(continued)

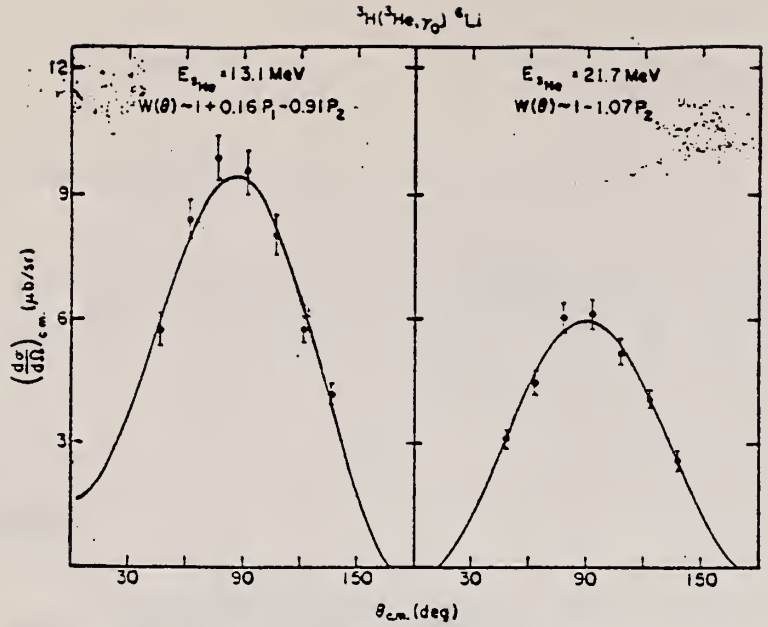

Fig. 4. Angular distributions of $^3H(^3He,\gamma_0)^6Li$. The curves are least-square fits of the expression $W(\theta) = A_0[1 + \Sigma_{k=1}^{2} a_k P_k(\cos\theta)]$.

TABLE 1

Experimental $^3H(^3He,\gamma)^6Li$ 90° differential cross sections [a])

$E_{^3He}$(lab) (MeV)	E_γ (MeV)	$\sigma_{^3He,\gamma_0}$(90° lab) (μb/sr)	$\sigma_{^3He,\gamma_0}$(90° lab) (μb/sr)
8.50	20.05	11.9±0.9	2.4±0.4
9.55	20.60	10.8±0.8	2.3±0.4
10.60	21.10	9.7±0.7	2.7±0.4
11.60	21.60	9.1±0.7	2.9±0.4
12.65	22.13	8.5±0.6	3.3±0.6
13.65	22.62	8.0±0.6	4.2±0.5
14.65	23.13	7.7±0.6	5.1±0.7
15.70	23.65	7.0±0.5	6.5±0.8
16.70	24.15	6.6±0.5	7.2±0.8
17.70	24.65	6.7±0.5	8.3±0.9
18.70	25.15	6.1±0.5	8.9±0.9
19.75	25.62	5.6±0.4	9.3±1.0
20.75	26.13	5.3±0.4	9.4±1.0
21.75	26.65	5.2±0.4	9.0±1.1
22.75	27.13	4.8±0.4	8.6±1.0
23.75	27.63	4.6±0.4	8.3±1.0
24.80	28.20	4.3±0.3	8.1±0.9
25.80	28.70	4.3±0.3	7.6±0.9

[a]) The errors shown include statistics, uncertainties in the least-square fitting, target thickness and non-uniformity, and the error of the $^3H(p,\gamma)^4He$ comparison cross section.

TABLE 2

$^3H(^3He,\gamma_0)^6Li$ angular distributions as determined from fig. 4

$E_{^3He}$ (MeV)	E_γ (MeV)	$W(\theta)$
13.1	22.3	$1+(0.16\pm0.03)P_1-(0.91\pm0.07)P_2$
21.7	26.6	$1-(0.01\pm0.03)P_1-(1.07\pm0.07)P_2$

REF. Yu. N. Antuf'ev, V. L. Agranovich, V. S. Kuz'menko, I. I. Miroshnichenko, and P. V. Sorokin
ZhETF Pis. Red. 16, 77 (1972)
JETP Letters (USSR) 16, 52 (1972)

EL EM. SYM.	A	Z
Li	6	3

METHOD

REF. NO. 72 An 11 hmg

REACTION	RESULT	EXCITATION ENERGY	SOURCE		DETECTOR		ANGLE
			TYPE	RANGE	TYPE	RANGE	
E,E/P	ABX	0* 20	D	999	MAG-D		20

proton angle is 68.3°
electron angle is 20°

* SEP E, 999=1.18 GEV

Shell	α MeV/c	$d^5\sigma_{theor} \cdot 10^{31}$ cm^2/sr^2MeV	$d^5\sigma_{exp} \cdot 10^{31}$ cm^2/sr^2MeV	$d^5\sigma_{exp}$ / $d^5\sigma_{theor}$
$1s$	110	2.02	1.06 ± 0.15	0.525 ± 0.074
$1p$	40	4.09	1.25 ± 0.18	0.306 ± 0.044

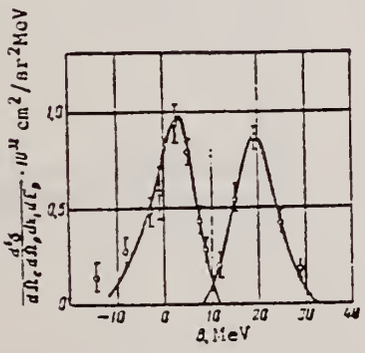

Cross section of the reaction $Li^6(e, e'p)He^5$.

REF. J. P. Genin, J. Julien, R. Letourneau, A. Mougeot, J. Rambaut and C. Samour
PICNS-72, p.439 Sendai

ELEM. SYM.	A	Z
Li	6	3

METHOD

REF. NO.	
72 Ge 4	- hvm

REACTION	RESULT	EXCITATION ENERGY	SOURCE		DETECTOR		ANGLE
			TYPE	RANGE	TYPE	RANGE	
E,E/D	ABX	-40* 40	D	515	MAG-D		DST
E,E/A	ABX	-50* 50	D	525	MAG-D		DST

*RECOIL P MEV/C

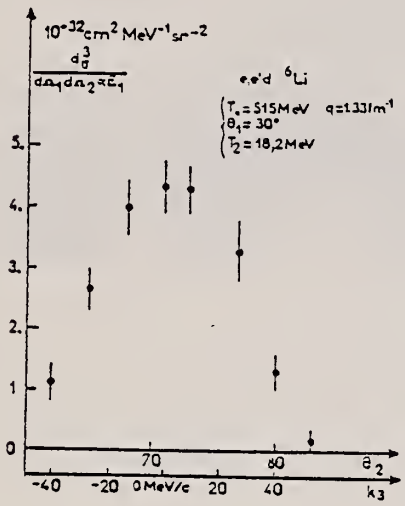

Fig.1

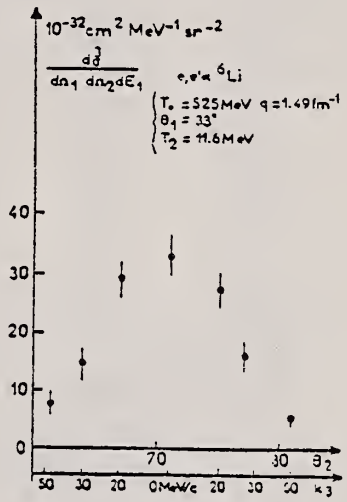

Fig.2

REF. S. Hiramatsu, T. Kamae, H. Muramatsu, K. Nakamura, N. Izutsu, and Y. Watase
PICNS-72, p.429 Sendai (see 73 Hi 5)

ELEM. SYM.	A	Z
Li	6	3

METHOD

REF. NO. 72 Hi 8 - hvm

REACTION	RESULT	EXCITATION ENERGY	SOURCE TYPE	SOURCE RANGE	DETECTOR TYPE	DETECTOR RANGE	ANGLE
E,E/P	NOX	0*30	D	700	MAG-D		DST

* SEP ENERGY RANGE

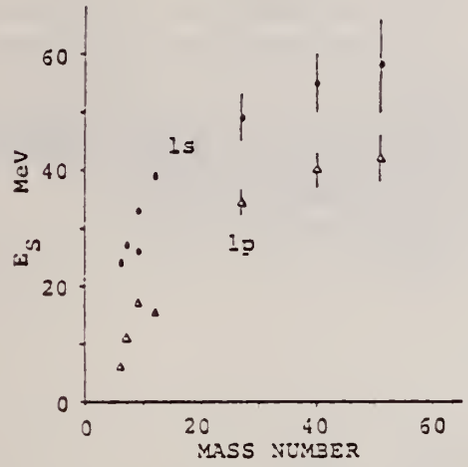

Fig. 6. The separation energy of 1s and 1p states as a function of the mass number.

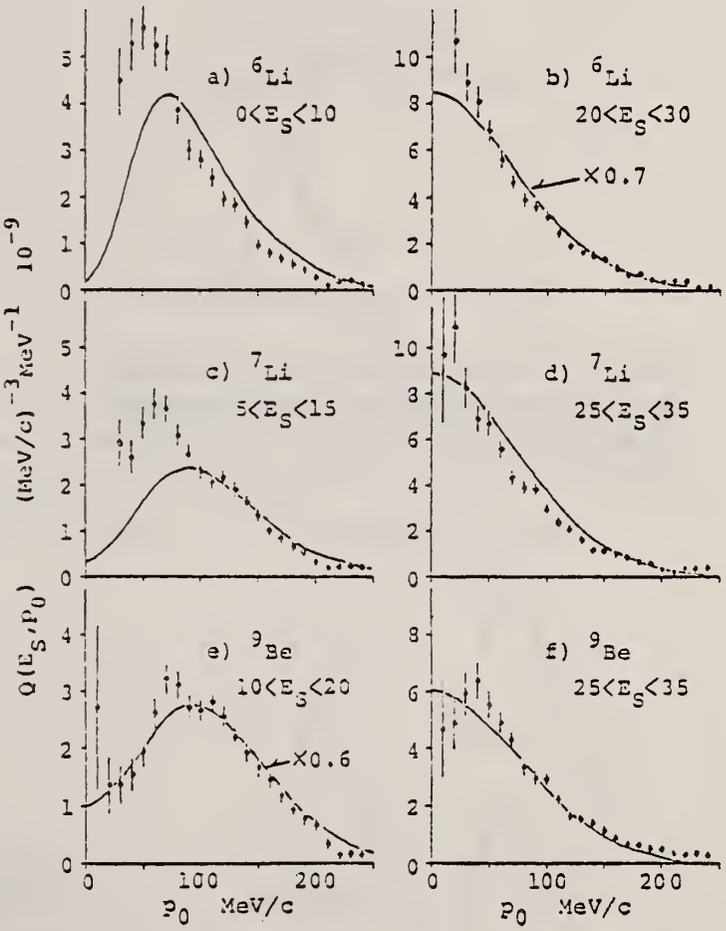

Fig. 4. Momentum distributions for ^{6}Li, ^{7}Li, and ^{9}Be the 1p state.

REF.

Yu. I. Titov and E.V. Stepula
Yad. Fiz. 15, 649 (1972)
Sov. J. Nucl. Phys. 15, 361 (1972)

ELEM. SYM.	A	Z
Li	6	3

METHOD

REF. NO.	
72 Ti 4	hmg

REACTION	RESULT	EXCITATION ENERGY	SOURCE		DETECTOR		ANGLE
			TYPE	RANGE	TYPE	RANGE	
E,E/	SPC	0-550	D	999	MAG-D		DST

999=1.18 GEV

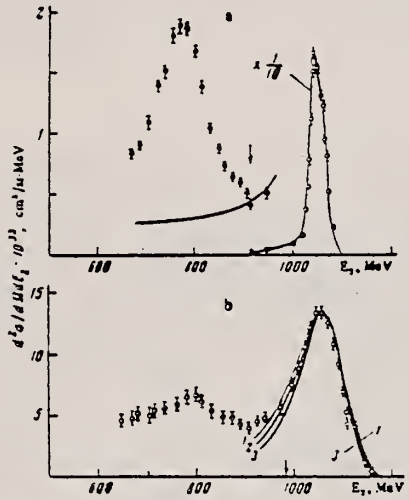

FIG. 1. Inelastic electron scattering spectra. b—in Li^6 for E_1 = 1180 MeV and θ = 24°40′. a—in protons for E_1 = 1170 MeV and θ = 24°40′. The solid line in Fig. a shows the radiation tail of the elastic scattering peak. Curves 1, 2, and 3 in Fig. a show the results of theoretical calculations according to the data of ref. 11 with α_0 = 150, 130, and 120 MeV/c.

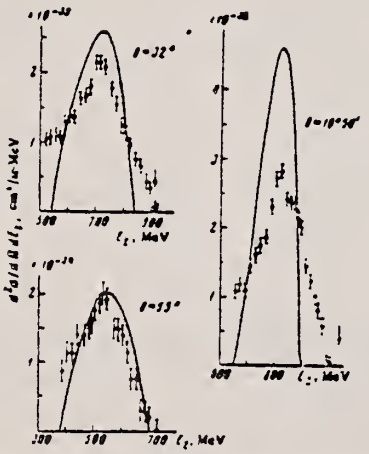

FIG. 2. Pion electroproduction spectra from Li^6 for scattering angles 16°50′, 32°, and 55° (the quasielastic scattering cross section has been subtracted) for E_1 = 1180 MeV. The arrows in the spectra show the Fermi threshold for pion production.

θ	Li^6 nucleus			Proton, $d\sigma/d\Omega$, cm²/sr	
	β	$(d\sigma/d\Omega)_{elast.}$, cm²/sr	$(d\sigma/d\Omega)_{qu.}$, cm²/sr	Present work	Theory [15]
16°50′	0.65±0.05	(6.45±0.71)·10⁻³⁰	(1.20±0.08)·10⁻³⁰	(1.04±0.12)·10⁻³⁰	0.99·10⁻³⁰
20°50′	0.66±0.06	(3.01±0.30)·10⁻³⁰	(4.09±0.30)·10⁻³⁰	(0.48±0.05)·10⁻³⁰	0.50·10⁻³⁰
24°40′	0.70±0.05	(1.39±0.15)·10⁻³⁰	(1.75±0.16)·10⁻³⁰	(0.29±0.03)·10⁻³⁰	0.28·10⁻³⁰
32°	0.72±0.05	(4.72±0.40)·10⁻³¹	(4.65±0.45)·10⁻³¹	(0.76±0.10)·10⁻³¹	1.02·10⁻³¹
40°	0.76±0.05	(1.71±0.15)·10⁻³¹	(1.39±0.15)·10⁻³¹	—	3.98·10⁻³²
47°	0.81±0.06	(8.61±0.80)·10⁻³²	(6.07±0.61)·10⁻³²	—	1.93·10⁻³²
55°	0.82±0.06	(3.80±0.30)·10⁻³²	(2.52±0.30)·10⁻³²	—	9.31·10⁻³³

Note. The initial electron energy is 1180 MeV.

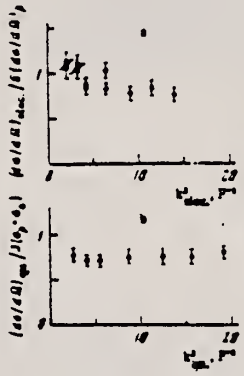

FIG. 3. Ratio of the integrated cross section in Li^6 to the corresponding sums of the cross sections in free nucleons of Li^6, b—in the region of the quasielastic peak, and a—in the region of the Δ_{1236} isobar. Points: ○—our measurements, ●—according to the data of ref. 13.

[11] A. G. Sitenko and V. N. Gur'ev, Zh. Eksp. Teor. Fiz. 39, 1760 (1960) [Sov. Phys.-JETP 12, 1228 (1961)].
[12] V. G. Vlasenko, N. G. Afanas'ev, V. A. Gol'dshtein, et al., Yad. Fiz. 13, 259 (1971) [Sov. J. Nucl. Phys. 13, 144 (1971)].
[13] F. W. Brasse, W. Fehrenbach, et al., DESY, 71/2, 1971.

REF.

V.P. Denisov, L.A. Kul'chitskii, and I.Ya. Chubukov
Izv. Akad. Nauk SSSR Ser. Fiz. 37, 107 (1973)
Bull. Acad. Sci. USSR Phys. Ser. 37, 94 (1973)

ELEM. SYM.	A	Z
Li	6	3

METHOD

REF. NO. 73 De 14 hmg

REACTION	RESULT	EXCITATION ENERGY	SOURCE		DETECTOR		ANGLE
			TYPE	RANGE	TYPE	RANGE	
G,PD	ABI	24-50	C	20- 57	TEL-D		90 (1)
G,PL	ABX	15-26	C	20- 57	TEL-D		90 (1)
G,T	ABX	25-51	C	20- 57	TEL-D		90
G,PD	ABI	21-50	C	20- 57	TEL-D		90
G,2PN	ABI	23-50	C	20- 57	TEL-D		90 (2)

(1) L=0,1,2

(2) INC G,P2N

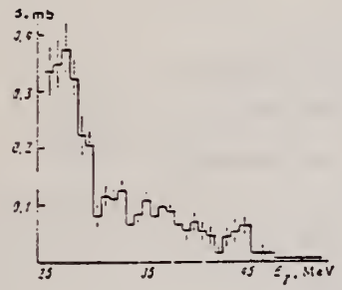

Fig. 5. The $^6Li(\gamma t)^3He$ cross section.

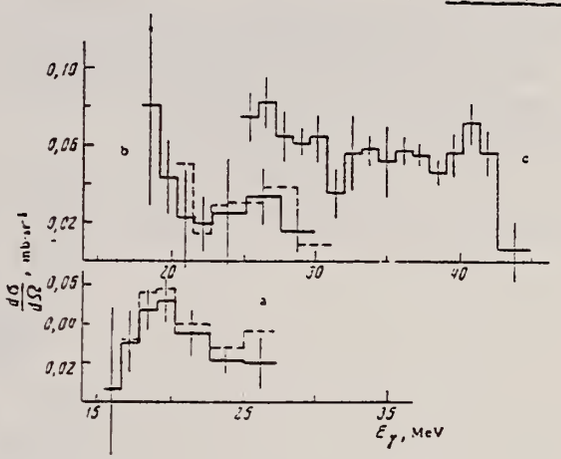

Fig. 2. Differential cross section for photoemission of protons at 90° to the photon beam in the following reactions: a) (γp_0) (^{5}He formed in its $I^\pi = 3/2^-$ ground state), b) (γp_1) (in the $1/2^-$ first excited state at 2.6 MeV), c) (γp_2) (in the $3/2^+$ second excited state at 16.7 MeV). The dashed histogram was drawn with allowance for the width of the first excited level.

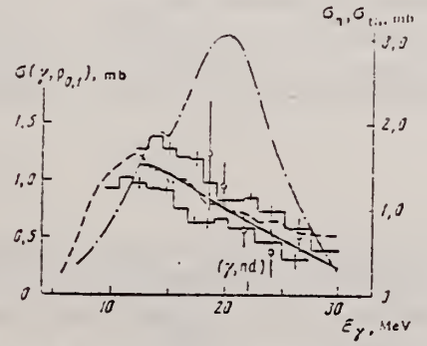

Fig. 3. Cross sections derived for protons from reactions with thresholds below the (γp_2) threshold. The lower (upper) histogram corresponds to the assumption that all the protons come from the (γp_0) ((γp_1)) reaction. The points represent the sum of the cross sections for these two reactions from the data of Fig. 2; the full curve is the average of the two histograms; the dashed curve gives the neutron photoproduction cross section σ_n [18]; and the dash-dot curve gives the theoretical value of the sum of the (γp_0), (γp_1), (γn_0), and (γn_1) cross sections [21].

(continued)

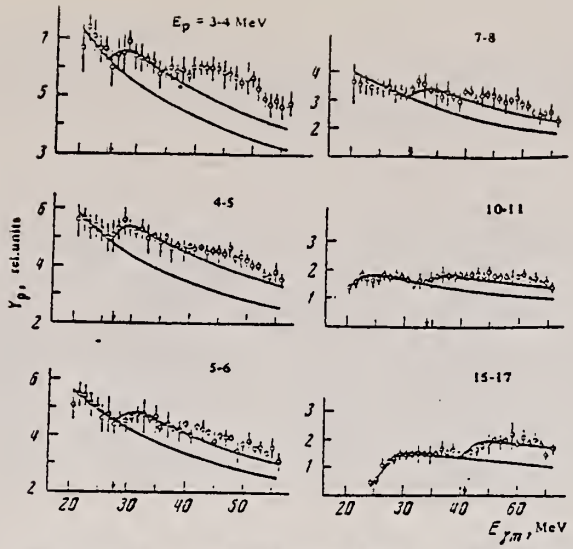

Fig. 1. The yields of protons in certain energy intervals as functions of $E_{\gamma m}$. The curves are isochromats for the (γp) reaction with the ^{5}He formed in its ground and first excited states (lower curves) and in its 16.7 MeV state (upper curves). The arrow marks the kinematic threshold for the (γp) reaction with the ^{5}He left in its 16.7 MeV state.

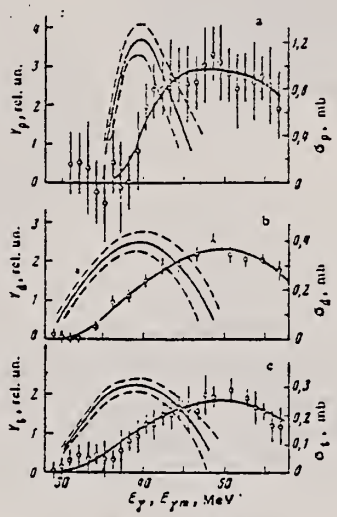

Fig. 4. $E_{\gamma m}$ dependence of particle yields from multiparticle photodisintegrations, and the corresponding cross sections: a) protons, $E_p \geq 3$ MeV; b) deuterons, $E_d \geq 4$ MeV; c) tritons, $E_t \geq 4$ MeV. The curve through the experimental points is an approximation to the yield curve derived from the measured cross section. The dashed curves mark the limits of statistical errors in the cross sections.

[17]A.M. Baldin, V.I. Gol'danskii, I.L. Rozental, Kinematics of Nuclear Reactions (in Russian) Fizmatgiz, Moscow, 1959.

[18]B.L. Berman, R.L. Bramblett, J.T. Caldwell, R.R. Harvey, and S.C. Fultz, Phys.Rev.Lett. 15, 727 (1965).

[21]I.V. Kurdyumov, S.Kh.El Samarai, Yu.F. Smirnov, and K.V. Shitikova, Izv. AN SSSR, Ser. Fiz. 30, 292 (1966)

REACTION	RESULT	EXCITATION ENERGY	SOURCE		DETECTOR		ANGLE
			TYPE	RANGE	TYPE	RANGE	

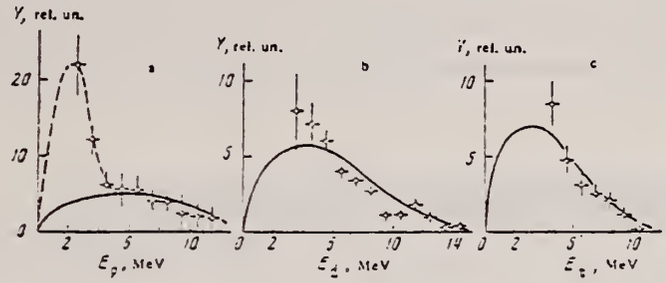

Fig. 7. Energy distributions of protons (a), deuterons (b), and tritons (c) from multiparticle photodisintegration of ^{6}Li. The curves are theoretical distributions from three-particle breakup [17] with allowance for the multiparticle photodisintegration cross-section curves (Fig. 4). The dashed curve is a rather arbitrary extrapolation of the part of the proton distribution that presumably contains a large contribution from disintegrations into more than three particles.

Table 2

^{6}Li Photodisintegration Channels

Reaction	E_γ interval, MeV	Integral cross section, MeV·mb	Contribution to the total absorption in the $E_\gamma \leq 50$ MeV interval, %
(γ, np) $(\gamma p_{0,1})^5$He$(3/2^-, 1/2^-)$ $\rightarrow n + {}^4$He $(\gamma n_{0,1})^5$Li$(3/2^-, 1/2^-)$ $(\gamma p_{0,1})^5$He$(3/2^-, 1/2^-)$	$E_\gamma \leq 30$	33,5 [3]	35
(γ, t)	$E_\gamma \leq 30$ $E_\gamma \leq 32$ $25 \leq E_\gamma \leq 50$ $E_\gamma \leq 50$	17,0±3.5 12,8±1,0 [8] 2,7±0,3 15±2	18 16
$(\gamma, p_2)^4$He(0^+) $\rightarrow p + d$	$25 \leq E_\gamma \leq 45$	9,0±1,0	
(γ, pdt)	$35 \leq E_\gamma \leq 50$	6±2	8
All disintegrations into $p + d + t$	$E_\gamma \leq 32$ $E_\gamma \leq 50$	18,2±2.0 [8] 34±4	35
$(\gamma n_2)^5$Li$(3/2^+)$ $\rightarrow d + {}^3$He	$30 \leq E_\gamma \leq 50$	9	9
$(\gamma, 2pnt)$ $(\gamma, p2n^3$He)	$35 \leq E_\gamma \leq 50$	~6	5
Total absorption	$E_\gamma \leq 50$	97±12	100

Note: All cross sections given without literature citations were determined in the present study.

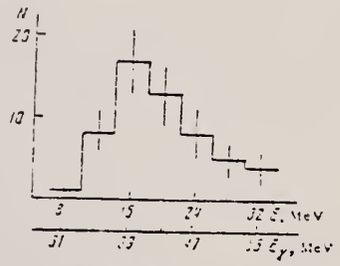

Fig. 6. Distribution of ^{6}Li(γ, pdt) events with respect to total particle energy. The E_γ scale shows the relation between the breakup and incident photon energies.

REF.

L.W. Fagg, W.L. Bendel, N. Ensslin, E.C. Jones, Jr.
Phys. Letters 44B, 163 (1973)

ELEM. SYM.	A	Z
Li	6	3

METHOD

REF. NO. 73 Fa 1 egf

REACTION	RESULT	EXCITATION ENERGY	SOURCE		DETECTOR		ANGLE
			TYPE	RANGE	TYPE	RANGE	
E,E/	SPC	11	D	50	MAG-D		180

The ^{6}Li analog of the 11.5 MeV, 0^{+} state in ^{6}Be proposed to explain the low flux of high-energy solar neutrinos has been searched for and not observed. An upper limit of 3 eV is placed on the M1 ground-state width of any such narrow 0^{+} state.

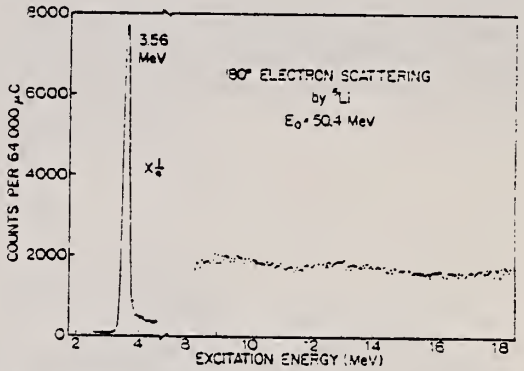

Fig. 1. Inelastic spectrum of 50.4 MeV electrons scattered at 180° by ^{6}Li. The regions of the spectrum from about 8.3 to 9.2 MeV and 17.5 to 18.4 MeV are based on 32 mC and scaled accordingly. The 3.56 MeV peak is based on 3 mC and scaled accordingly.

REF.

S.N. Gardiner, J.L. Matthews, R.O. Owens
Phys. Letters 46B, 186 (1973)

ELEM. STM.	A	Z
Li	6	3

METHOD

REF. NO. 73 Ga 3 egf

REACTION	RESULT	EXCITATION ENERGY	SOURCE		DETECTOR		ANGLE
			TYPE	RANGE	TYPE	RANGE	
G,P	ABX	60	D	60	MAG-D		45

Table 1
Measured ^{6,7}Li(γ, p) cross sections for E_γ = 60 MeV, ϑ_p = 45° and comparison with the calculations of Weise [3, 10]. The theoretical results include final-state distortions and those "with correlations" are obtained for a Gaussian momentum-exchange package of width Δq_c = 100 MeV/c centred at q_c = 300 MeV/c.

Nucleus	Hole state	Excitation energy range (MeV)	$\frac{d\sigma}{d\Omega}$ (expt.) (μb/sr)	$\frac{d\sigma}{d\Omega}$ (theory) (μb/sr)	
				No correlations	With correlations
^{6}Li	p	0 – 9	4.2 ± 0.4		
	s	11.5 – 26.5	9.4 ± 1.1		
^{7}Li	p	0 – 9	7.3 ± 0.5	2.1	5.5
	s	9 – 26	11.3 ± 1.3	0.28	2.5

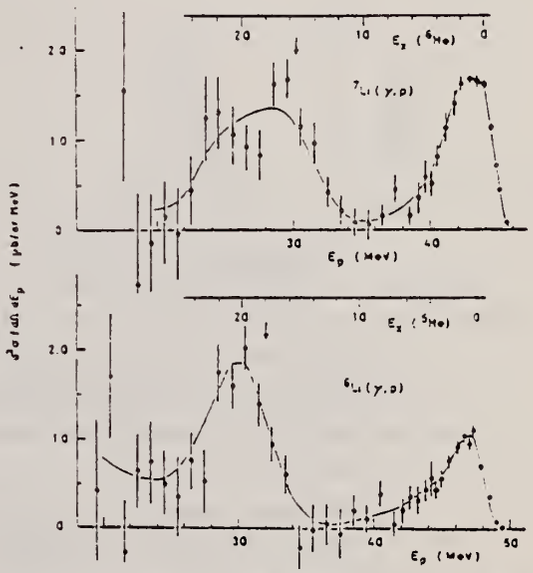

Fig. 2. Proton spectra from the ^{6}Li(γ, p) and ^{7}Li(γ, p) reactions for E_γ = 60 ± 1 MeV, ϑ_p(lab) = 45°. Excitation energies in the residual nuclei are also shown. The arrows in each spectrum indicate the location of the s-shell peak observed in the (p, 2p) reaction [8].

3
W. Weise, to be published.
8
G. Jacob and Th.A.J. Maris, Rev. Mod. Phys. 45, 6 (1973).
10
W. Weise, private communication.

REF. F.H. Heimlich, E. Roessle, M. Koebberling, J. Moritz, K.H. Schmidt, D. Wegener, D. Zeller, J.K. Bienlein, J. Bleckwenn, H. Dinter
PICNS-73, Vol.II, p.885 (1973) Asilomar

ELEM. SYM.	A	Z
Li	6	3

METHOD

REF. NO. 73 He 7 - egf

REACTION	RESULT	EXCITATION ENERGY	SOURCE TYPE	SOURCE RANGE	DETECTOR TYPE	DETECTOR RANGE	ANGLE
E,E/D	ABX	200	D	999	MAG-D		DST

999= 2.7 GEV

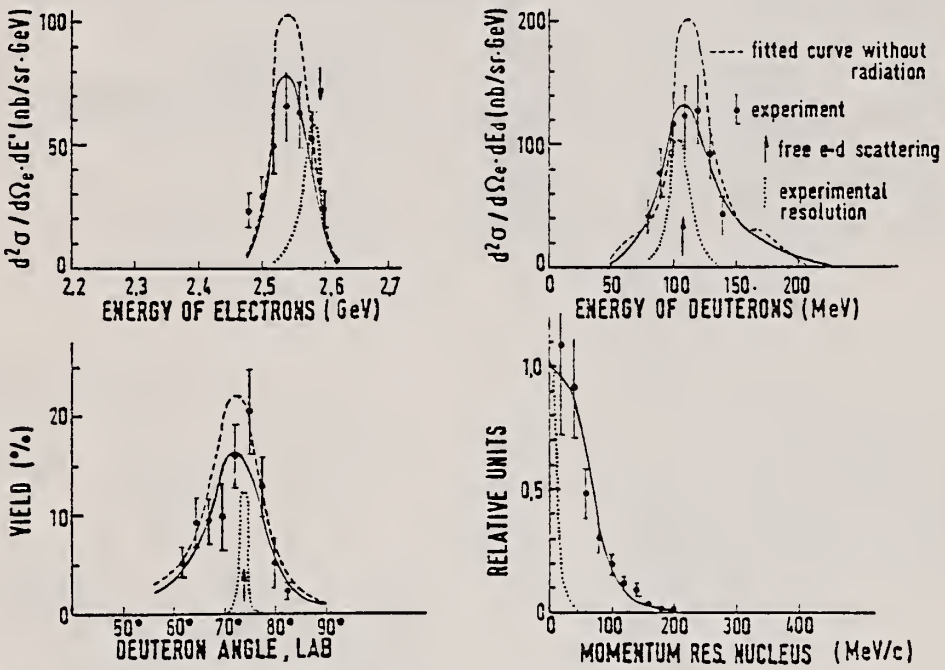

Fig.1 Deuteron coincidence data at E = 2.7 GeV, Θ_e = 13.8°

a) Double-differential cross section, depending on the energy of scattered electrons, integrated over deuteron energies and angles.

b) Double-differential cross section, depending on the deuteron energy, integrated over electron energies and deuteron angles.

c) Deuteron angular distribution, integrated over electron and deuteron energies. The area under the experimental points is normalized to 1.

d) Momentum distribution of the residual nucleus, computed using the data a) - c).

REF. H. Hiramatsu, T. Kamae, H. Muramatsu, K. Nakamura, N. Izutsu and Y. Watase
Phys. Letters 44B, 50 (1973)

ELEM. SYM.	A	Z
Li	6	3

METHOD

REF. NO. 73 Hi 5 - egf

REACTION	RESULT	EXCITATION ENERGY	SOURCE TYPE	SOURCE RANGE	DETECTOR TYPE	DETECTOR RANGE	ANGLE
E,E/P	SPC	0* 70	D	700	MAG-D		UKN

*SEP ENERGY RANGE

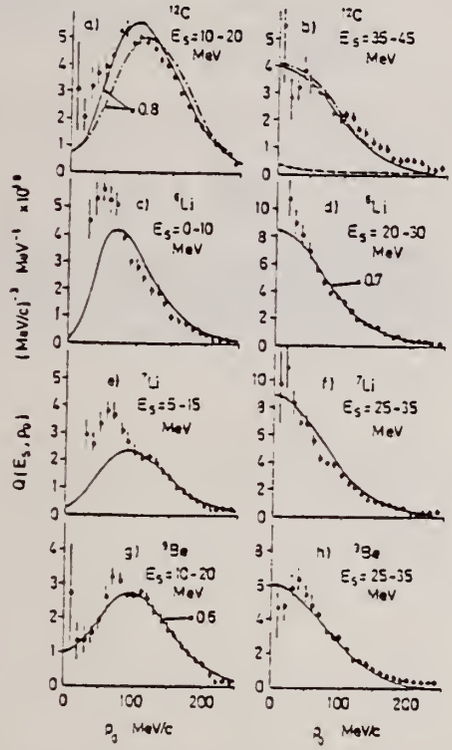

Fig. 2. Proton momentum distributions. See fig. 1 for the meaning of the curves in a) and b).

[5] C. Ciofi degli Atti, Nucl. Phys. A106 (1968) 215.

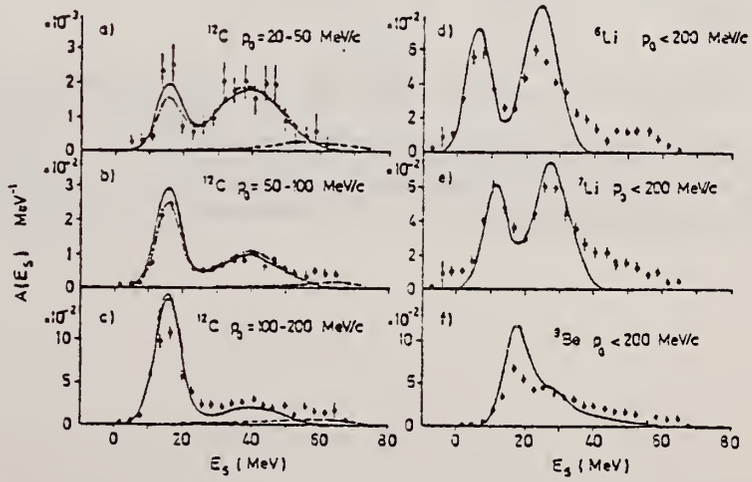

Fig. 1. Separation energy spectra. The solid curves show the DWIA results with the Woods-Saxon potentials. In a), b) and c) the dot-dashed curves represent the DWIA calculation with the harmonic oscillator potential given in ref. [5], and the dashed curves show the multiple collision background calculated by the Monte Carlo method.

REF. E.L. Kuplennikov, N.G. Afanas'ev, V.A. Gol'dshtein, V.I. Ogurtsov, and V.G. Vlasenko
Yad. Fiz. 18, 20 (1973)
Sov. J. Nucl. Phys. 18, 10 (1974)

ELEM. SYM.	A	Z
Li	6	3

METHOD

REF. NO.	
73 Ku 7	hmg

REACTION	RESULT	EXCITATION ENERGY	SOURCE		DETECTOR		ANGLE
			TYPE	RANGE	TYPE	RANGE	
E,E/	ABX	84-284	D	1*	MAG-D		DST

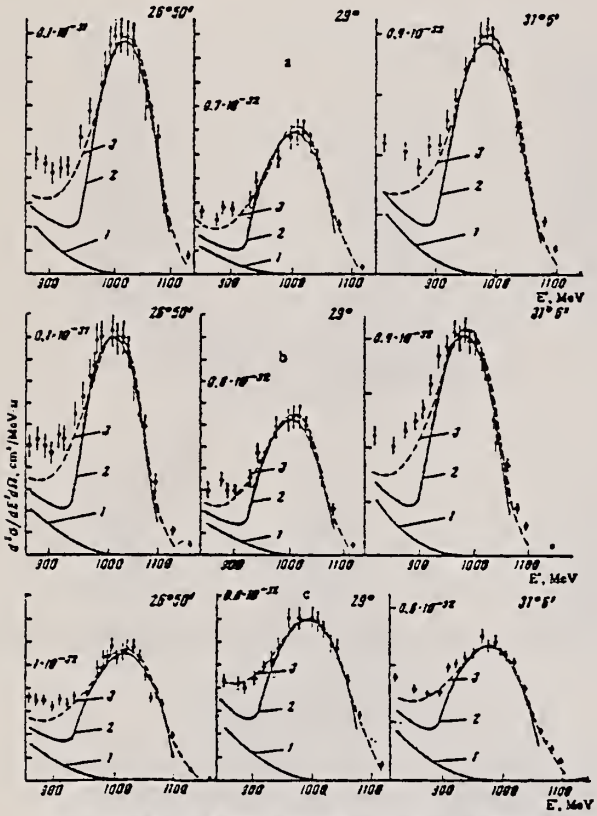

Cross sections for quasielastic scattering of 1184-MeV electrons on Li^6 (a), Li^7 (b), and Be^9 (c) vs energy E′ of electrons scattered at 26°50′, 29°, and 31°6′. The curves 1, 2, 3 represent calculations based, respectively, on allowance for the pion contribution, on the Fermi gas model, and on the single-particle shell model.

* 1=1.184 MEV

10 H. Überall, Electron Scattering fro Complex Nuclei, Academic Press, New York, 1971.

Nucleus	P_0, MeV/c	$\langle r^2\rangle^{1/2}_{qu.elast}$, F	$\langle r^2\rangle^{1/2}_{elast}$, F	P_F, MeV/c	$\bar{\varepsilon}$, MeV
Li^6	115±4	2.46±0.09	2.54±0.06	157±6	13±3
Li^7	116±4	2.43±0.09	2.37±0.03	160±6	14±3
Be^9	128±5	2.35±0.09	2.43±0.08	180±6	18±3

Remark. P is the oscillator parameter, $\langle r^2\rangle^{1/2}_{qu.elast}$ is the rms charge radius of the nucleus, P_F is the Fermi momentum, $\bar{\varepsilon}$ is the mean nucleon binding energy for $q \geq 400$ MeV/c; all these experimental values were obtained for quasielastic electron scattering on the light nuclei Li^6, Li^7, and Be^9; $\langle r^2\rangle^{1/2}_{elast}$ is the experiment rms radius derived from elastic electron scattering on the same nuclei. [10]

REF.

T. Saito
J. Phys. Soc. Japan 35, 1 (1973)

ELEM. SYM.	A	Z
Li	6	3

METHOD

REF. NO.	
73 Sa 14	egf

REACTION	RESULT	EXCITATION ENERGY	SOURCE		DETECTOR		ANGLE
			TYPE	RANGE	TYPE	RANGE	
G,G	LFT	3	C	5	NAI-D		120

Self-absorption measurements 3=3.56 MEV

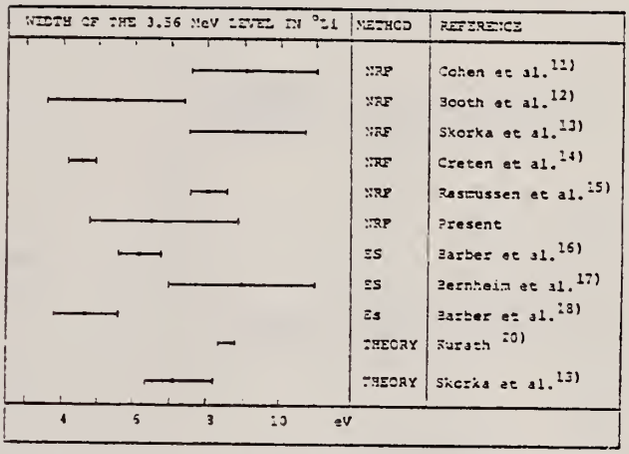

Fig. 4. Results of the width of the 3.56 MeV level in ^{6}Li measured by different authors. NRF denotes nuclear resonance fluorescence and ES denotes electron scattering. Lower two rows represent the theoretical results.

The bremsstrahlung beam from a 5 MeV electron linear accelerator was used to excite and study low-lying levels in ^{6}Li, ^{11}B and ^{27}Al. A self-absorption method was used to find the widths Γ of these levels. The following level widths are obtained: $\Gamma=(6.5^{+1.5}_{-1.2})$ eV for the 3.56 MeV level in ^{6}Li; $\Gamma=(0.23\pm0.09)$ eV for the 2.12 MeV level, and $\Gamma=(0.53\pm0.21)$ eV for the 4.44 MeV level in ^{11}B. For the 2.98 MeV level in ^{27}Al, the level width is found to be $\Gamma=(0.10\pm0.04)$ eV assuming that the lower energy member of the doublet at 3 MeV is excited.

REF. J. Deutsch, D. Favart, R. Prieels, B. Van Ostaeyen, G. Audit, N. de Botton, J.L. Faure, Cl. Schuhl, G. Tamas, and C. Tzara
Phys. Rev. Lett. 33, 316 (1974)

EL EM. SYM.	A	Z
Li	6	3

METHOD

REF. NO.	-
74 De 3	hmg

REACTION	RESULT	EXCITATION ENERGY	SOURCE		DETECTOR		ANGLE
			TYPE	RANGE	TYPE	RANGE	
G,PI+	ABX	145-155	C	145-154	ACT-I		4PI

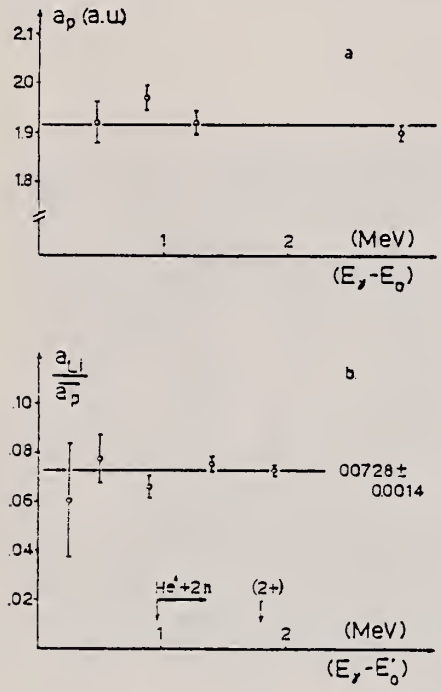

FIG. 1. (a) Coefficient a_p of the photoproduction on proton as a function of the lab photon energy above threshold. The line indicates the best-fit value $\overline{a_p}$. (b) Coefficient a_{Li} of the photoproduction on ^{6}Li normalized to the average a_p as a function of the lab photon energy above threshold. The position of the continuum and the 2^- level in ^{5}He are also shown.

TABLE I. Photoproduction yield as a function of the energy of the electron beam.

Target	Electron-beam energy (MeV)	Photoproduction yield (arbitrary units)
^{6}Li	145.68	1.38 ± 0.52
	145.93	8.4 ± 1.1
	146.33	26.0 ± 1.6
	146.83	76.3 ± 2.5
	147.33	140.1 ± 3.3
CH_2	151.90	215.6 ± 4.8
	152.30	681.4 ± 9.2
	152.70	1335 ± 17
	154.35	6175 ± 49

9 J.H. Koch and T.W. Donnelly, Nucl. Phys. B64, 478 (1973).

10 M.I. Adamovitch et al., Yad. Fiz. 9, 848 (1969); Sov. J. Nucl. Phys. 9, 496 (1969).

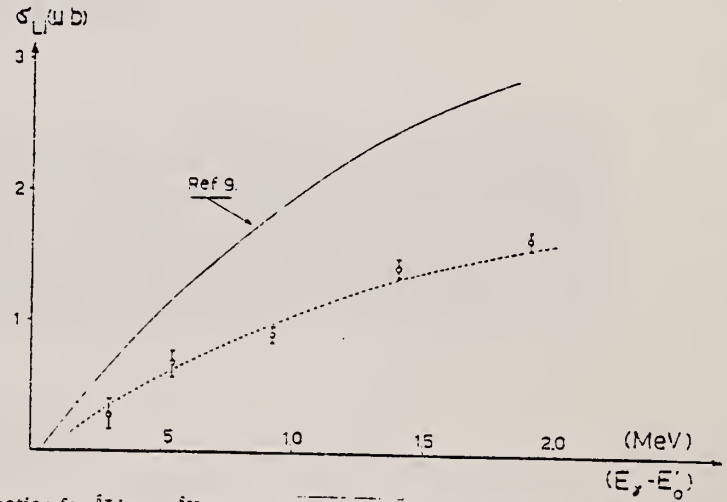

FIG. 2. Total photoproduction cross section for $^6Li + \gamma \rightarrow {}^5He_{g.s.} + \pi^+$ found in this experiment compared to the theoretical prediction, Ref. 9. The errors include the inaccuracy of σ_p, Ref. 10. The dashed curve is our best fit: it is 0.54 times the value from Ref. 9.

REF. J.P. Genin, J. Julien, M. Rambaut, C. Samour, A. Palmeri, and Vinciguerra
Phys. Lett. 52B, 46 (1974)

ELEM. SYM.	A	Z
Li	6	3

METHOD

REF. NO. 74 Ge 7 — egf

REACTION	RESULT	EXCITATION ENERGY	SOURCE TYPE	SOURCE RANGE	DETECTOR TYPE	DETECTOR RANGE	ANGLE
E,E/A	ABX	78*	D	520	MAG-D		DST
E,E/D	ABX	74*	D	520	MAG-D		DST

*MOM TRANS MEV/C

The reactions ^{6}Li(e,e'α) and ^{6}Li(e,e'd) have been studied at $T_0 \approx 520$ MeV and $q \approx 1.4$ fm^{-1}, by coincidence measurements. The angular dependence of the cross sections is interpreted in the plane wave impulse approximation to obtain the momentum distribution of α-particle and deuteron clusters in ^{6}Li. The amount of clustering of ^{6}Li is also discussed.

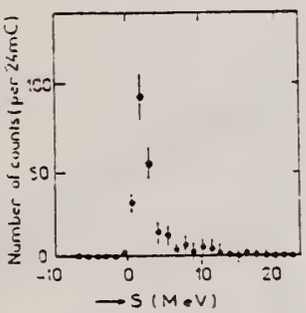

Fig. 1. Missing-energy spectrum for the (e,e'α) reaction on ^{6}Li at $k_3 = 0$ MeV/c, $T_0 = 525$ MeV, $\theta_1 = 33°$; $q = 1.79$ fm^{-1}, target thickness = 4.5 mg/cm^2 (the angle between target plane and incident beam is 50°). No corrections have been applied.

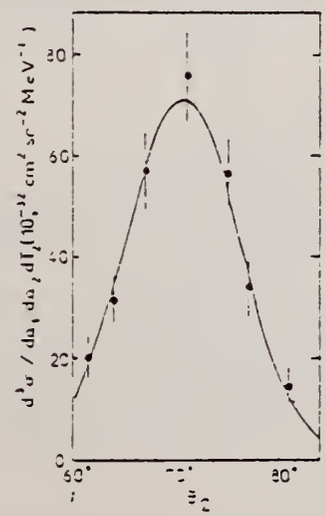

Fig. 2. The (e,e'α) coincidence cross section as a function of θ_2. The kinematical conditions are $T_0 = 525$ MeV, $\theta_1 = 33°$, $q = 1.49$ fm^{-1}, $T_2 = 11.5$ MeV. The curve is the best fit in PWIA for $Q_0 = 78.1$ MeV/c, $P_\alpha = 0.19$ and $\Delta\theta_2 = -0.21°$.

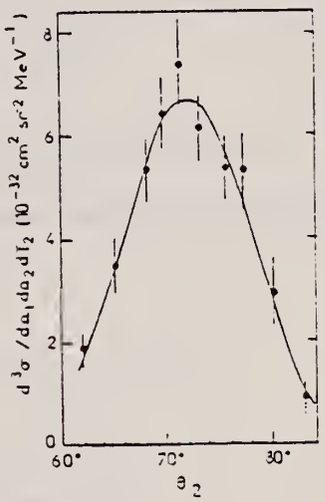

Fig. 3. The (e,e'd) coincidence cross section as a function of θ_2. The kinematical conditions are $T_0 = 515$ MeV, $\theta_1 = 30°$, $q = 1.33$ fm^{-1}, $T_2 = 18.2$ MeV. The curve is the best fit in PWIA for $Q_0 = 74$ MeV/c, $P_d = 0.073$ and $\Delta\theta_2 = -0.58°$.

REF. N.V. Goncharov, S.G. Tonapetyan, and V.M. Khvorostyan
Yad. Fiz. 19, 21 (1974)
Sov. J. Nucl. Phys. 19, 10 (1974)

ELEM. SYM.	A	Z
Li	6	3

METHOD

REF. NO.	-
74 Go 1	hmg

REACTION	RESULT	EXCITATION ENERGY	SOURCE		DETECTOR		ANGLE
			TYPE	RANGE	TYPE	RANGE	
G,PI+	ABY	150-400	C	400	BBL -D		90
G,PI-	ABY	150-400	C	400	BBL -D		90
G,P	ABY	4-400	C	400	BBL -D		90

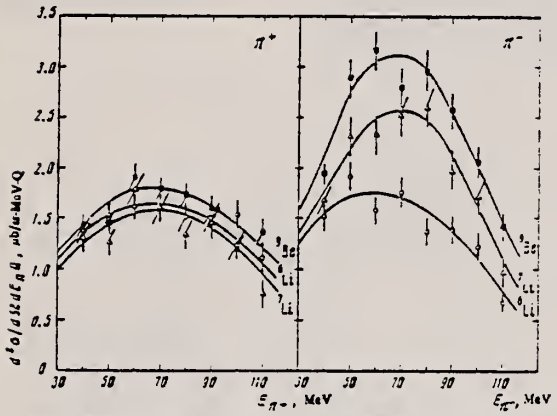

FIG. 1. Energy spectra of π^+ and π^- mesons. $E_\gamma^{max} = 400$ MeV, $\theta_{lab} = 90 \pm 7°$.

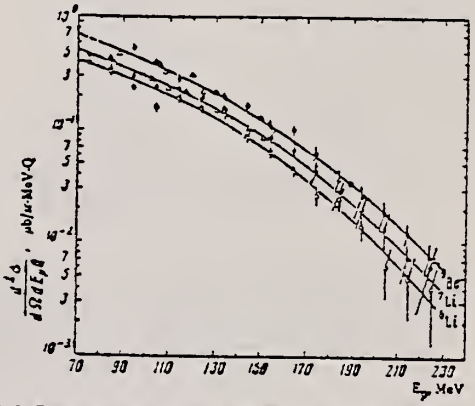

FIG. 2. Energy spectra of protons. $E_\gamma^{max} = 400$ MeV, $\theta_{lab} = 90 \pm 7°$. Points: circles—data of the present work, triangles—ref. 11.

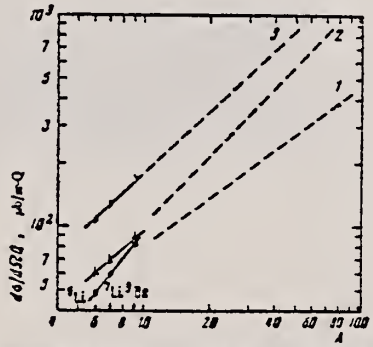

FIG. 3. Mass-number dependence of the yields of π mesons (points ▲, curve 1), protons (points ■, curve 2), and the sum of the π-meson and proton yields (points ●, curve 3). The dashed lines are the data from ref. 6.

[6] N.V. Goncharov et al., Yad.Fiz. 17, 242 (197 Sov. J. Nucl. Phys. 17, 125 (1973).

[11] P. Dougan and W. Stiefler, Preprint LUSU, 1002-1005, 1970.

REF. R.R. Whitney, I. Sick, J.R. Ficenec, R.D. Kephart, and W.P. Trower
Phys. Rev. C9, 2230 (1974)

EL EM. SYM.	A	Z
Li	6	3

METHOD

REF. NO.	
74 Wh 3	hmg

REACTION	RESULT	EXCITATION ENERGY	SOURCE		DETECTOR		ANGLE
			TYPE	RANGE	TYPE	RANGE	
E,E/	ABX	0-300	D	500	MAG-D		60

QUASIELASTIC SCAT

See further analysis of this data in reference 79Zil

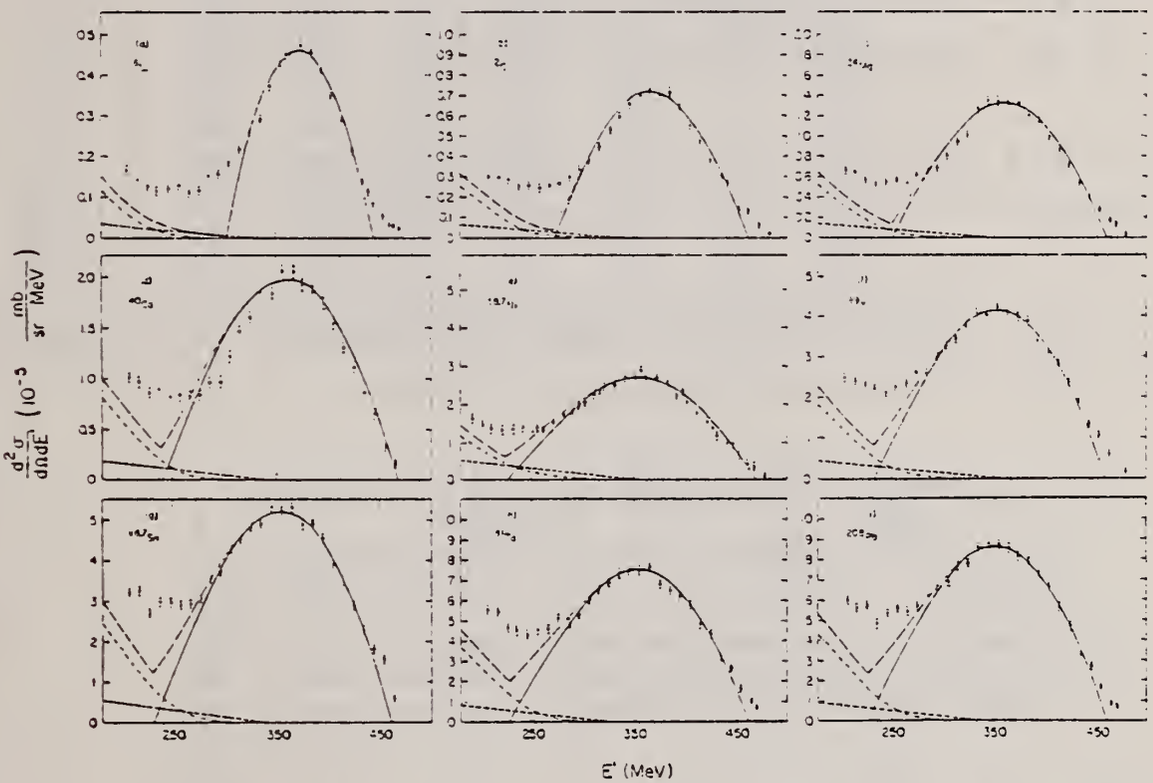

FIG. 1. The measured quasielastic peaks; the errors on the data points do not include an over-all 3% normalization uncertainty. The solid curve is a fit by the Fermi-gas model which yielded k_F (in MeV/c) and $\bar{\epsilon}$ (in MeV) as follows: (a) ^{6}Li (169, 17); (b) ^{12}C (221, 25); (c) ^{24}Mg (235, 32); (d) ^{40}Ca (249, 33); (e) ^{58,7}Ni (260, 36); (f) ^{89}Y (254, 39); (g) ^{118,124}Sn (260, 42); (h) ^{181}Ta (265, 42); (i) ^{208}Pb (265, 44). The fitting uncertainty in k_F is ±5 MeV/c and in $\bar{\epsilon}$ it is ±3 MeV. The small-amplitude dashed curve is the s-wave π-production contribution, the dot-dashed curve is the isobar excitation, and the large-amplitude dashed curve is the total result.

(continued)

TABLE I. Proton-normalized and radiative-corrected cross sections $d^2\sigma/d\Omega dE' = (N \pm \Delta N) \times 10^{-n}$ in mb/sr MeV, for $E = 500$ MeV and $\theta = 60°$.

E'	^{6}Li			^{12}C			^{24}Mg			^{40}Ca			^{58,7}Ni			^{89}Y			^{118,7}Sn			^{180,86}Ta			^{208}Pb		
(MeV)	N	ΔN	n	N	ΔN	n	N	ΔN	n	N	ΔN	n	N	ΔN	n	N	ΔN	n	N	ΔN	n	N	ΔN	n	N	ΔN	n
480.0	···			1.79	0.19	7	3.83	0.42	7	···			1.22	0.17	6	1.71	0.19	6	···			···			···		
474.0	···			1.02	0.13	7	···			···			···			···			···			···			···		
470.0	1.72	0.18	7	5.75	0.52	7	1.55	0.15	6	···			3.90	0.29	6	5.85	0.41	6	···			7.09	0.67	0	7.00	0.68	6
464.0	2.49	0.29	7	1.38	0.11	6	1.91	0.17	6	2.72	0.15	6	4.43	0.33	6	5.68	0.37	6	8.32	0.71	6	1.16	0.08	5	9.82	0.79	6
460.0	2.96	0.30	7	1.20	0.09	6	2.58	0.19	6	···			···			···			···			1.54	0.10	5	1.81	0.10	5
454.1	5.02	0.47	7	9.21	0.71	7	2.96	0.20	6	1.20	0.17	6	7.00	0.11	6	1.07	0.05	5	1.85	0.09	5	1.70	0.11	5	2.31	0.11	5
450.0	···			···			···			···			8.92	0.47	6	1.03	0.05	5	1.83	0.09	5	···			···		
444.3	8.68	0.58	7	1.26	0.07	6	1.11	0.25	6	6.67	0.27	6	1.02	0.05	5	1.33	0.05	5	···			2.77	0.14	5	2.74	0.12	5
440.0	1.11	0.06	6	2.59	0.13	6	5.23	0.26	6	···			···			···			···			3.43	0.16	5	3.24	0.13	5
434.2	1.32	0.06	6	2.99	0.14	6	5.60	0.26	6	8.74	0.35	6	1.19	0.05	5	1.90	0.07	5	2.27	0.09	5	3.14	0.15	5	3.34	0.14	5
430.0	···			···			···			···			1.40	0.07	5	2.11	0.08	5	2.77	0.11	5	···			···		
424.3	2.12	0.08	6	3.75	0.15	6	7.31	0.29	6	1.12	0.04	5	1.54	0.08	5	2.31	0.09	5	2.88	0.12	5	4.43	0.18	5	4.74	0.19	5
414.4	2.88	0.12	6	1.75	0.19	6	8.78	0.35	6	1.32	0.05	5	1.78	0.10	5	2.88	0.11	5	3.40	0.14	5	4.98	0.20	5	5.64	0.23	5
404.5	3.51	0.14	6	5.46	0.22	6	1.02	0.01	5	1.56	0.06	5	2.09	0.08	5	3.09	0.12	5	3.90	0.16	5	5.89	0.24	5	6.57	0.26	5
400.0	···			6.25	0.25	6	1.09	0.01	5	···			2.35	0.09	5	3.34	0.13	5	4.29	0.17	5	6.56	0.27	5	7.00	0.28	5
394.7	4.16	0.17	6	6.32	0.26	6	1.15	0.05	5	1.75	0.07	5	2.22	0.09	5	3.41	0.14	5	4.56	0.18	5	6.29	0.25	5	7.25	0.29	5
385.7	4.55	0.18	6	7.09	0.28	6	1.21	0.05	5	1.86	0.07	5	2.51	0.10	5	3.91	0.16	5	4.88	0.19	5	6.30	0.26	5	7.88	0.32	5
374.9	4.76	0.19	6	6.97	0.28	6	1.33	0.05	5	1.91	0.08	5	2.72	0.11	5	4.02	0.16	5	4.88	0.19	5	6.87	0.28	5	8.19	0.33	5
365.0	4.56	0.18	6	7.28	0.29	6	1.32	0.05	5	2.08	0.08	5	2.69	0.10	5	4.04	0.16	5	5.34	0.21	5	7.77	0.31	5	8.61	0.34	5
360.0	4.50	0.18	6	6.61	0.28	6	1.32	0.05	5	···			2.88	0.11	5	4.11	0.16	5	5.69	0.23	5	7.92	0.33	5	8.42	0.34	5
355.2	4.35	0.17	6	6.97	0.28	6	1.36	0.05	5	2.08	0.08	5	2.69	0.11	5	4.23	0.17	5	5.22	0.21	5	7.51	0.30	5	···		
345.3	3.68	0.15	6	6.54	0.26	6	1.35	0.05	5	1.85	0.07	5	2.72	0.11	5	4.02	0.16	5	5.37	0.21	5	7.59	0.30	5	8.83	0.35	5
335.4	2.90	0.12	6	5.91	0.24	6	1.29	0.05	5	1.87	0.08	5	2.48	0.10	6	4.08	0.16	5	4.92	0.19	5	7.44	0.29	5	8.68	0.35	5
325.5	2.59	0.10	6	5.23	0.21	6	1.05	0.04	5	1.01	0.07	5	2.48	0.11	5	3.78	0.15	5	4.83	0.19	5	6.93	0.28	5	7.81	0.31	5
320.0	···			···			···			···			2.35	0.09	5	3.34	0.14	5	4.53	0.18	5	···			···		
315.7	2.16	0.10	0	4.43	0.18	0	9.41	0.38	0	1.47	0.06	5	2.26	0.09	5	3.43	0.14	5	4.34	0.17	5	6.61	0.26	5	7.70	0.31	5
305.8	1.81	0.09	6	3.79	0.15	6	8.61	0.32	0	1.23	0.05	5	2.03	0.08	5	3.27	0.13	5	4.32	0.17	5	6.11	0.24	5	6.92	0.28	5
300.0	···			···			···			···			1.97	0.08	5	3.11	0.12	5	4.03	0.16	5	···			···		
295.9	1.55	0.09	6	3.38	0.14	6	6.77	0.29	0	9.97	0.40	0	1.80	0.07	5	3.02	0.12	5	3.74	0.15	5	5.38	0.22	5	6.73	0.27	5
285.9	1.50	0.09	6	2.96	0.11	0	6.64	0.31	6	9.73	0.39	0	1.72	0.07	5	2.60	0.13	5	3.55	0.15	5	4.92	0.23	5	6.30	0.29	5
276.2	1.14	0.08	6	2.64	0.13	6	6.03	0.32	6	8.35	0.41	6	1.60	0.07	5	2.64	0.13	5	3.10	0.15	5	5.22	0.24	5	5.73	0.30	5
266.3	1.08	0.08	6	2.61	0.14	6	5.32	0.31	6	8.57	0.43	0	1.31	0.08	5	2.37	0.14	5	2.72	0.16	5	4.62	0.26	5	5.51	0.31	5
260.0	···			···			···			···			1.39	0.08	5	1.95	0.13	5	2.94	0.18	5	···			···		
256.4	1.28	0.09	6	2.43	0.15	0	5.71	0.35	6	8.33	0.45	0	1.27	0.08	5	2.27	0.14	5	2.87	0.18	5	4.57	0.28	5	5.63	0.33	5
246.6	1.20	0.09	0	2.55	0.16	6	5.47	0.36	6	8.55	0.48	6	1.39	0.09	5	2.14	0.14	5	2.95	0.19	5	4.33	0.28	5	5.40	0.36	5
236.7	1.15	0.10	6	2.51	0.16	6	5.18	0.38	6	8.71	0.51	6	1.31	0.09	5	2.24	0.15	5	3.02	0.20	5	4.35	0.30	5	4.90	0.34	5
226.8	1.27	0.11	6	2.88	0.19	6	5.62	0.42	6	8.72	0.51	0	1.29	0.10	5	2.29	0.16	5	2.73	0.20	5	4.57	0.30	5	5.88	0.37	5
216.9	1.43	0.14	6	2.91	0.21	6	6.35	0.49	6	9.81	0.56	6	1.31	0.10	5	2.38	0.17	5	3.26	0.22	5	5.42	0.36	5	5.76	0.38	5
207.0	1.66	0.16	6	2.91	0.21	6	6.59	0.52	6	1.02	0.06	5	1.43	0.11	5	2.51	0.18	5	3.24	0.22	5	5.58	0.37	5	6.11	0.40	5
197.2	1.78	0.17	6	3.42	0.24	6	7.01	0.59	6	···			1.59	0.12	5	2.77	0.20	5	3.43	0.24	5	5.67	0.38	5	5.99	0.41	5

REF.	ELEM. SYM.	A	Z
R. Yen, L. S. Cardman, D. Kalinsky, J. R. Legg, C. K. Bockelman Nucl. Phys. A235, 135 (1974)	Li	6	3

METHOD	REF. NO.
	74 Ye 1 egf

REACTION	RESULT	EXCITATION ENERGY	SOURCE		DETECTOR		ANGLE
			TYPE	RANGE	TYPE	RANGE	
E,E/	FMF	2	D	30- 60	MAG-D		DST

2.18 MEV 3+

TABLE 3

Experimental data for the ^{6}Li 3^+ (2.18 MeV) state

E_0(MeV)	θ(deg)	q(fm^{-1})	$\lvert F_{stt}\rvert^2$	$10^2\times R_{1a}$	$10^2\times\lvert F_{1a1}\rvert^2$	$10^2\times\lvert F_{1a1}\rvert^2{}_N$	Error(%)	χ^2/n
59.81	150	0.569	0.561	1.351	0.758	0.758	6.3	11/38
59.81	150	0.569	0.561	1.298	0.729	0.729	6.2	17/38
59.91	130	0.535	0.600	1.050	0.630	0.630	6.7	10/38
59.91	130	0.535	0.600	0.938	0.562	0.562	7.2	9/38
59.91	110	0.485	0.661	0.599	0.396	0.396	5.2	11/38
59.91	110	0.485	0.661	0.711	0.470	0.470	7.6	5/38
59.91	110	0.485	0.661	0.686	0.453	0.453	7.9	16/38
59.91	90	0.419	0.740	0.390	0.289	0.306	12.6	11/28
60.02	70	0.341	0.843	0.185	0.156	0.156	20.8	23/28
59.95	70	0.341	0.845	0.213	0.180	0.180	19.6	11/28
59.95	70	0.341	0.845	0.194	0.164	0.164	20.4	12/28
59.95	70	0.341	0.845	0.167	0.141	0.141	23.6	7/28

Ground-state charge distribution parameters [22]: $a = 0.934\pm0.004$ fm, $b = 1.303\pm0.11$ fm, $c = 0.453\pm0.05$ fm.

TABLE 4

Results of the best-fits by allowing both $B(E2^\uparrow)$ and $R_{tr}^{(2)}$ as free parameters

	Assumptions							Results		
	Z	R_{eq}(fm)	a_{-1}	a_1	a_3	a_4	a_5	$B(E2^\uparrow)(e^2\cdot b^2)$	$R_{tr}^{(2)}$(fm^2)	χ^2/n
^{114}Cd	48	4.624	1.045	0.983	1.056	1.158	1.323	0.553 ± 0.018	38.1 ± 1.0	1.12
^{60}Ni	28	3.862	1.075	0.976	1.078	1.024	1.471	0.102 ± 0.004	31.9 ± 2.0	0.60
^{6}Li	3	2.540	1.208	0.941	1.189	1.572	2.290	$(0.218\pm0.008)\times10^{-2}$	17.6 ± 1.2	1.05

TABLE 7

Best fits of $R_{tr}^{(2)}$ with $B(E2^\uparrow)$ fixed

	$R_{tr}^{(2)}$(fm^2)	Statistical error (fm^2)	Systematic error (fm^2)	Total error (fm^2)	χ^2/n	$B(E2^\uparrow)(e^2\cdot b^2)$ assumed
^{114}Cd	35.7	±0.6	±0.3	±0.9	1.19	0.512 ± 0.05
^{60}Ni	27.5	±1.1	±0.2	±1.9	0.66	0.0926 ± 0.15

(continuec)

TABLE 8

Summary of $B(E2\uparrow)$ values for the ^{6}Li 3^+ (2.18 MeV) state

$10^2 \times B(E2\uparrow)(e^2 \cdot b^2)$	Type of experiment	Ref.
0.244	(e, e')	[43])
0.256±0.016	(e, e')	[44])
0.251±0.020	(e, e')	[47])
<0.082	(γ, γ')	[48])
0.262±0.076	^{4}He(d, γ)^{6}Li	[49])
0.30 ±0.03	(e, e')	[50])
0.32 ±0.03	(e, e')	[51])

22) L. R. Suelzle, M. R. Yearian and H. Crannell, Phys. Rev. 162 (1967) 992
45) R. M. Hutcheon and H. S. Caplan, Nucl. Phys. A127 (1969) 417
46) F. Eigenbrod, Z. Phys. 228 (1969) 337
47) F. Eigenbrod, Z. Naturf. 23A (1968) 1671
48) W. L. Creten, R. J. Jacobs and H. M. Ferdinande, Nucl. Phys. A120 (1968) 126
49) H. Wahl, thesis, Univ. of Hamburg, 1967 (unpublished)
50) M. Bernheim and G. R. Bishop, Phys. Lett. 5 (1963) 270
51) M. Bernheim and G. R. Bishop, J. de Phys. 24 (1963) 970

REF.

J. Barrette, W. Del Bianco, P. Depommier, S. Kundu,
N. Marquardt, A. Richter
Nucl. Phys. A238, 176 (1975)

ELEM. SYM.	A	Z
Li	6	3

METHOD

REF. NO.	
75 Ba 4	egf

REACTION	RESULT	EXCITATION ENERGY	SOURCE		DETECTOR		ANGLE
			TYPE	RANGE	TYPE	RANGE	
A,G	ABX	4	D	6- 8	NAI-D		90

4=3.562 LIMIT ON SIG

TABLE 1

Summary of experimental results for the heavy-particle width Γ'_{d_2} of the $E_x = 3.562$ MeV, $J^\pi = 0^+$, $T = 1$ state in ^{6}Li

Author	Year	Ref.	Γ'_{d_2} (eV)
Wilkinson	1958	[5])	$\leqq 0.2$
Wahl	1967	[6])	< 0.25
Rasmussen and Swann	1969	[7])	< 1.3
Artemov *et al.*	1972	[8])	< 0.2
Present experiment	1974		$\leqq 0.017$

REF.

J. C. Bergstrom, I. P. Auer, R. S. Hicks
Nucl. Phys. A251, 401 (1975)

ELEM. SYM.	A	Z
Li	6	3

METHOD

REF. NO.	
75 Be 5	egf

REACTION	RESULT	EXCITATION ENERGY	SOURCE		DETECTOR		ANGLE
			TYPE	RANGE	TYPE	RANGE	
E,E/	LFT	3	D	35-125	MAG-D		DST

Ground state radiation width = 8.16±0.19 eV.

3=3.562 MEV

TABLE 1

^{6}Li(e, e') kinematic parameters and experimental results for the 0$^+$ (3.562 MeV) $T = 1$ state

E_0 (MeV)	θ (deg)	q_{inel} (fm^{-1})	$\sigma_{inel}/\sigma_{el} \times 10^2$	$\lvert F(q)\rvert^2_{BA} \times 10^3$
124.90	140.7	1.153	1.47 ±0.11	0.144±0.011
119.26		1.101	2.09 ±0.09	0.246±0.011
107.60		0.994	2.81 ±0.11	0.478±0.019
97.14		0.897	3.38 ±0.09	0.789±0.020
86.58		0.799	3.73 ±0.07	1.18 ±0.02
76.62		0.706	3.56 ±0.09	1.46 ±0.04
70.26		0.647	3.56 ±0.07	1.70 ±0.04
65.54		0.603	3.38 ±0.07	1.80 ±0.04
54.58		0.500	2.69 ±0.05	1.80 ±0.03
48.84		0.446	2.32 ±0.04	1.73 ±0.03
43.75		0.398	1.98 ±0.04	1.60 ±0.03
38.99		0.353	1.62 ±0.03	1.41 ±0.03
72.35	99.9	0.544	0.694±0.019	1.86 ±0.05
62.68		0.470	0.578±0.011	1.81 ±0.04
53.65		0.400	0.443±0.011	1.57 ±0.04
46.76		0.348	0.361±0.007	1.39 ±0.03
40.90		0.303	0.297±0.007	1.21 ±0.03
35.04		0.257	0.219±0.010	0.943±0.043

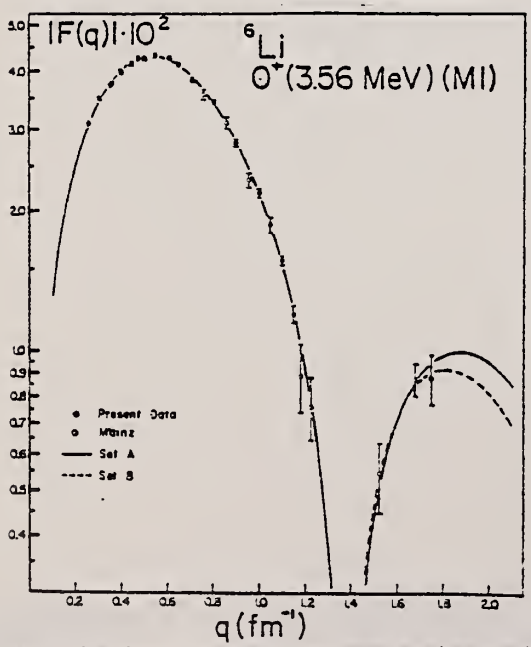

Fig. 2. The 3.562 MeV M1 form factor as measured in the present experiment combined with the high-q Mainz data. The lines represents fits based on the two sets of $T = 1$ configuration amplitudes.

REF. E. Bellotti, E. Fiorini, P. Negri, A. Pullia, L. Zanotti, and I. Filosofo
Nuovo Cimento 29A, 106 (1975)

ELEM. SYM.	A	Z
Li	6	3

METHOD

REF. NO. 75 Be 8 egf

REACTION	RESULT	EXCITATION ENERGY	SOURCE		DETECTOR		ANGLE
			TYPE	RANGE	TYPE	RANGE	
A,G	LFT	3	D	3	SCD-D		90

3=3.562,LIMIT ON LFT

Summary. — An experiment is reported on the parity-violating reaction $d(\alpha, \gamma)^6Li$, leading to the $J^P = 0^-$, $I = 1$, $E_x = 3.562$ MeV state, which, being a $\Delta I = 1$ transition, could be strongly enhanced by the presence of neutral currents in hadronic weak interactions in nuclei. The experiment has been carried out by exposing a deuterium target to a beam of α-particles reaching the resonant energy in the region in the middle of the tube containing the gas. Gamma-rays from this region are detected by a 90 cm^3 Ge(Li) counter connected to a 4096 channel analyser through an amplifying and analysing chain. The various sources of the background of spurious counting in the Ge(Li) and the procedure adopted to reduce their effect are discussed. We find no evidence for a nonzero parity-violating width of the 3.562 MeV state of ^6Li and can set an upper limit for this width of $8 \cdot 10^{-4}$ eV, which is an order of magnitude or more lower than that obtained in the previous experiments on this reaction.

REF. Y.M. Shin, D.M. Skopik and J.J. Murphy
Phys. Lett. 55B, 297 (1975)

ELEM. SYM.	A	Z
Li	6	3

METHOD

REF. NO.	
75 Sh 3	egf

REACTION	RESULT	EXCITATION ENERGY	SOURCE		DETECTOR		ANGLE
			TYPE	RANGE	TYPE	RANGE	
E,T	ABX	26- 68	D	UKN	MAG-D		DST

VIRTUAL PHOTON ANAL

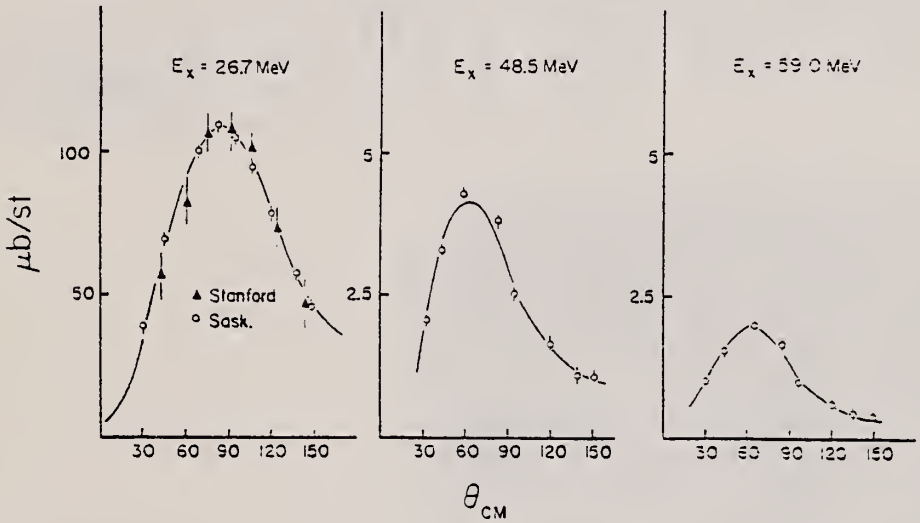

Fig. 2. Angular distribution for the (γ, t) reaction at $E_\chi = 26.7$ MeV and the $(\gamma, {}^3He)$ reaction at $E_\chi = 48.5$ and 59.0 MeV.

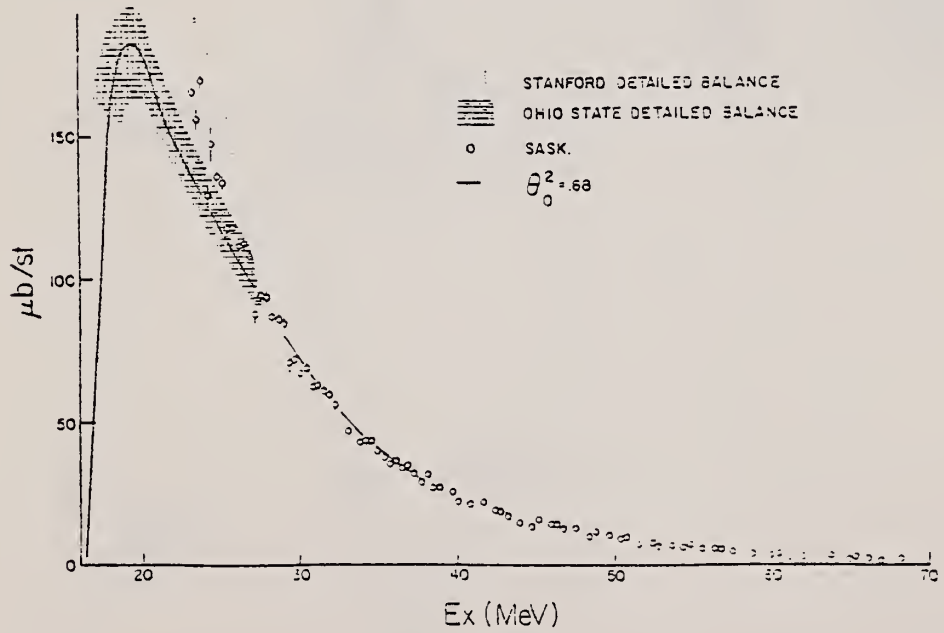

Fig. 1. The 90° differential cross section for the $^6Li(\gamma, t)$ reaction. For $E_\chi \gtrsim 30$ MeV the cross section is obtained by detecting the ^3He. The solid line is the calculated result using the wave function of ref. [7]. The shaded portions are the experimental result of the $^3H(^3He, \gamma)^6Li$ reaction [5, 6].

(continued)

Table 1
Dipole sum rules in ^{6}Li

	E_{max} = 32 MeV			E_{max} = 70 MeV		
	(γ, N)[a]	(γ, t)[b]	Total	(γ, N)[c]	(γ, t)[b]	Total[d]
σ_0 (mb/MeV)	27 ± 2	17 ± 1	44.5 ± 3	53 ± 1	21 ± 1	82
σ_{-1}(mb)	1.9 ± 0.1	0.77 ± 0.03	2.62 ± 0.13	4.2	0.78 ± 0.03	5
σ_{-2}(μb/MeV)	150 ± 10	36 ± 2	186 ± 12	270	38 ± 2	308

a) Ref. [1]. b) Present work. c) Ref. [2]. d) The result of ref. [2] is extrapolated to 70 MeV.

[1] B.L. Berman et al., Phys. Rev. Lett. 15 (1965) 727.

[2] E.B. Brazhanov et al., Nucl. Phys. 68 (1965) 191;
E.B. Brazhanov et al., JETP 19 (1964) 1014.

[5] S.L. Blatt et al., Phys. Rev. 176, 1147 (1968).

[6] E. Ventura, C.C. Chang and W.E. Meyerhof, Nucl. Phys. 173 (1971) 1.

[7] D.R. Thompson and Y.C. Tang, Nucl.Phys. A106 (1968) 591;
A.M. Young et al., Phys. Rev. Lett. 25 (1970) 1764).

REF.

J. C. Bergstrom, E. L. Tomusiak
Nucl. Phys. A262, 196 (1976)

ELEM. SYM.	A	Z
Li	6	3

METHOD

REF. NO. 76 Be 3 - egf

REACTION	RESULT	EXCITATION ENERGY	SOURCE		DETECTOR		ANGLE
			TYPE	RANGE	TYPE	RANGE	
E,E/	FMF	1- 8	D	41-125	MAG-D		DST

Abstract: The form factor for the alpha-deuteron continuum in ^{6}Li has been measured in the excitation region within 2 MeV of threshold, for momentum transfers $q < 1.2$ fm^{-1}. The results are interpreted in terms of an α-d cluster model. The monopole breakup appears to be predominant near threshold, but the influence of the $J = 2^+$ (4.31 MeV) quadrupole resonance becomes important a few MeV above threshold. The form factor for the C2 transition to the 3^- (2.185 MeV) state is also presented.

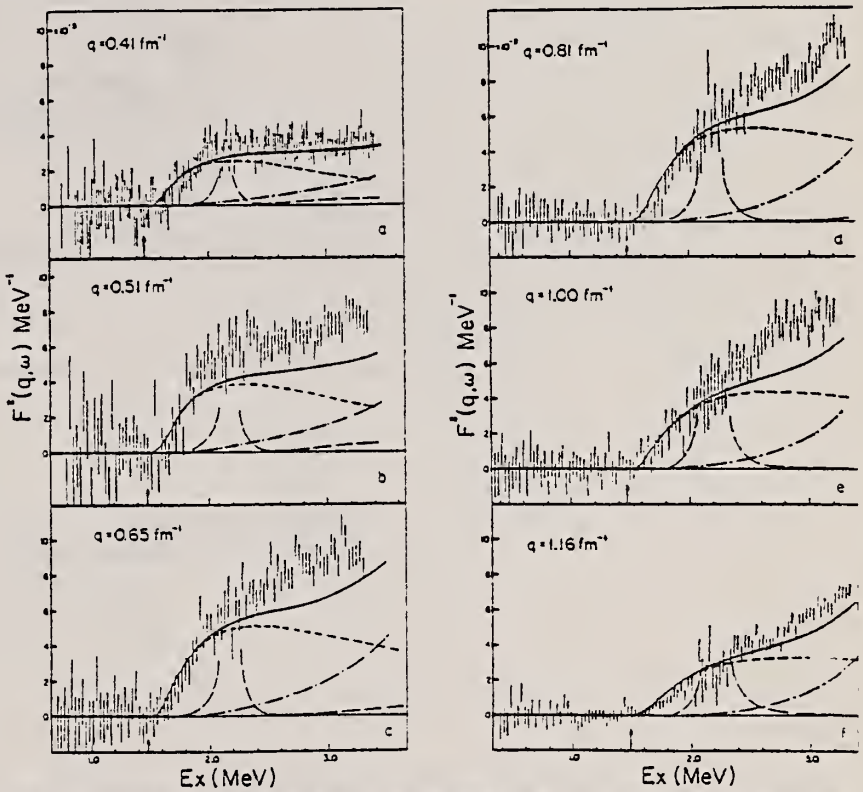

Fig. 2. Momentum transfer dependence of the continuum form factor near the α-d threshold. The theoretical monopole excitation is shown by the small dash curve, the $J = 3$ quadrupole by the large dash curve, and the tail of the $J = 2$ quadrupole resonance by the dot-dash curve. The main part of the 3^+ (2.185 MeV) resonance is not shown, as discussed in the text. The error bars are statistical and do not reflect the uncertainty in the elastic peak radiation tail.

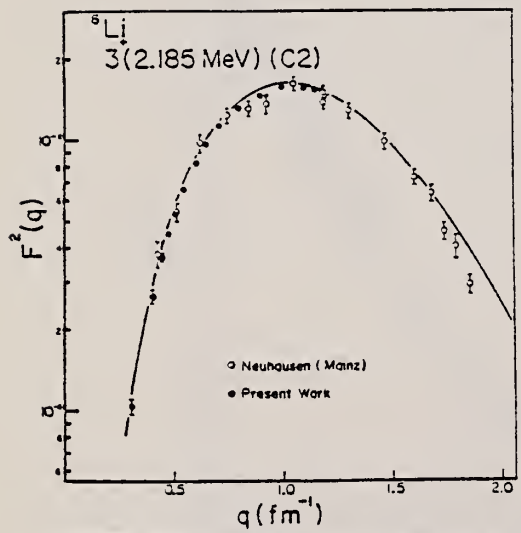

Fig. 3. Form factor of the $J = 3^+$ quadrupole excitation. The data from Mainz has been recalculated using the elastic parameters of Li *et al.*

(continued

[7] Li et al., Nucl. Phys. A162, 583 (1971).

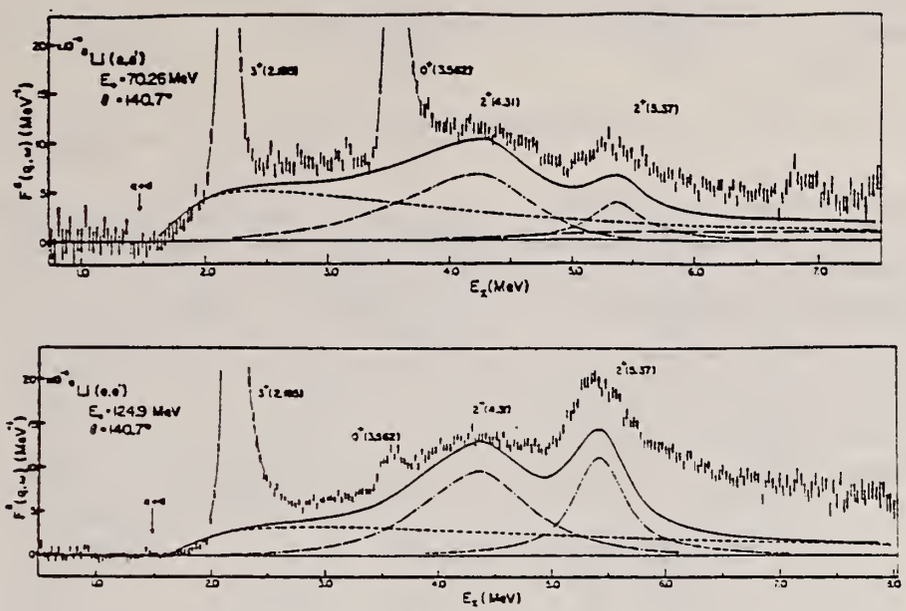

Fig. 4. Energy dependence of $F^2(q, \omega)$ for (a) $q \approx 0.65$ fm^{-1} and (b) $q \approx 1.15$ fm^{-1}. The calculated peak at $E_{ex} = 2.185$ MeV is not shown. The contribution from the 5.37 MeV level is obtained by a fitting procedure and is not a theoretical prediction.

REF. J. L. Matthews, D. J. S. Findlay, S. N. Gardiner, R. O. Owens
Nucl. Phys. A267, 51 (1976)

ELEM. SYM.	A	Z
Li	6	3

METHOD

REF. NO. 76 Ma 8 — egf

REACTION	RESULT	EXCITATION ENERGY	SOURCE		DETECTOR		ANGLE
			TYPE	RANGE	TYPE	RANGE	
G,P	ABX	60-100	D	60-100	MAG-D		DST

Cross Section Table given.

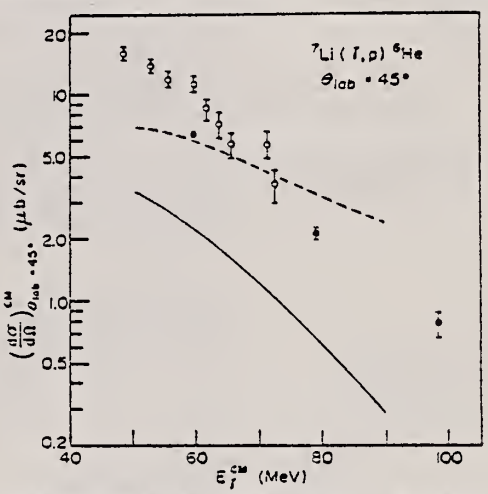

Fig. 12. The ^{7}Li(γ, p)^{6}He cross section at θ_p = 45° as a function of photon energy: solid circles, present measurement for ground +1.8 MeV states; open circles, results taken from ref. [14]). The latter data have been converted to c.m. cross sections and corrected by the factor dE_p/dE_γ which was apparently omitted from the published results [see ref. [14])]. The theoretical curves are discussed in sect. 6.

14 M. Sanzone et al., Nucl. Phys. A153 (1970) 401

TABLE 1

Cross sections for the ^{6}Li, ^{7}Li, ^{9}Be and ^{12}C(γ, p) reactions at E_γ(lab) = 60 MeV, θ_p(lab) = 45° populating the excitation energy regions E_x = 0–9 MeV and 9–26 MeV in the residual nuclei

Target nucleus	$(d\sigma/d\Omega)^{c.m.}$ (μb/sr)	
	residual nucleus excitation energy E_x	
	0–9 MeV	9–26 MeV
^{6}Li	5.5 ± 0.6	12.2 ± 2.0
^{7}Li	9.5 ± 0.8	14.7 ± 3.0
^{9}Be	31.8 ± 3.0	
^{12}C	36.4 ± 3.9	

Only statistical errors are tabulated: there is an additional common systematic error of ±22 %.

TABLE 5

Total cross sections at E_γ(lab) = 60, 80 and 100 MeV for the reactions ^{6}Li(γ, p)^{5}He (ground state +2.6 MeV state), ^{7}Li(γ, p)^{6}He (ground state +1.8 MeV state) and ^{12}C(γ, p)^{11}B (ground state, 2.1, 4.4, 5.0 and 6.7 MeV states in several combinations)

E_γ(lab) (MeV)	Total cross section (μb)				
	^{6}Li(γ, p_0+p_1)	^{7}Li(γ, p_0+p_1)	^{12}C(γ, p)		
			p_0	p_0+p_1	$p_0+p_1+\cdots p_4$
60	34.1 ± 1.6	43.8 ± 1.2	148.9 ± 4.6	182.7 ± 5.8	238.1 ± 11.7
80		11.39 ± 0.39	44.9 ± 2.1	48.4 ± 2.2	65.4 ± 3.9
100			17.2 ± 1.4	19.6 ± 1.1	

The errors shown are statistical. There is an additional common systematic error of ±22 %.

(continued)

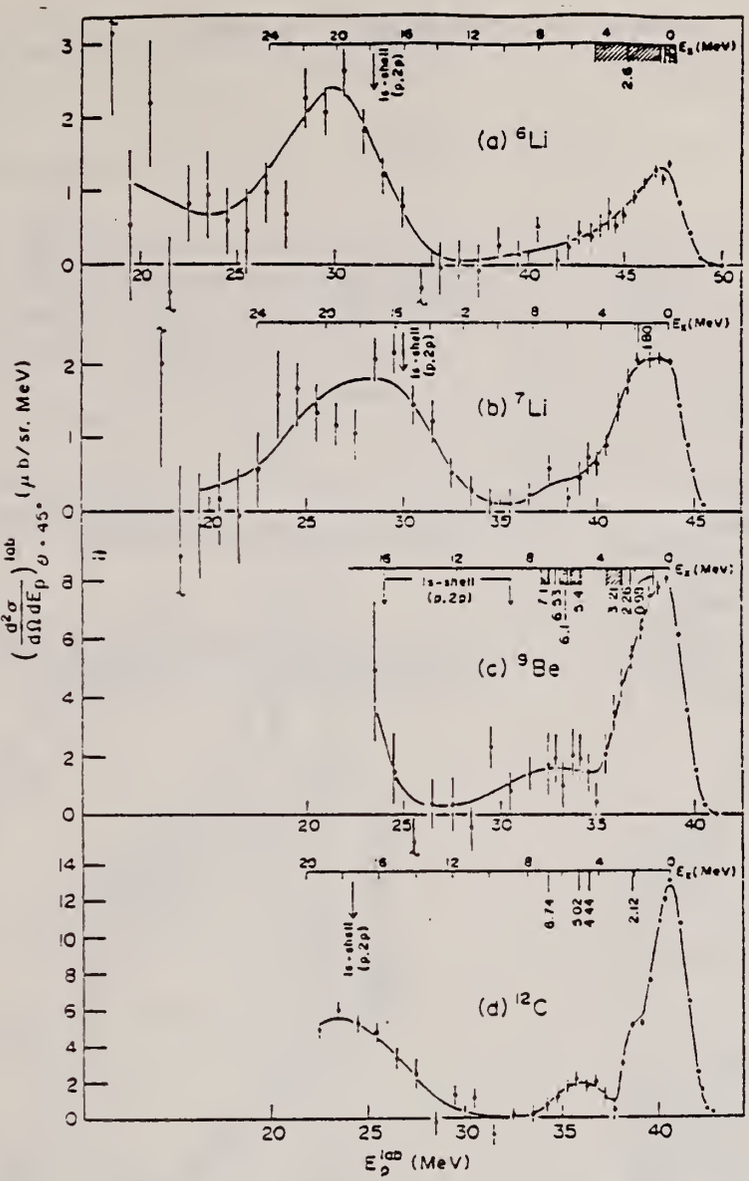

Fig. 8. Photoproton spectra for $E_\gamma = 60 \pm 1$ MeV, $\theta = 45°$ derived as described in the text from data such as those shown in fig. 7: (a) ^{6}Li(γ, p)^{5}He; (b) ^{7}Li(γ, p)^{6}He; (c) ^{9}Be(γ, p)^{8}Li; (d) ^{12}C(γ, p)^{11}B. The scale above each spectrum gives the excitation energy in the residual nucleus, with lines indicating the positions of known excited states. The location of the 1s shell peak observed in the (p, 2p) reaction is also marked.

REF. D. M. Skopik, E. L. Tomusiak, E. T. Dressler, Y. M. Shin, and J. J. Murphy, II
Phys. Rev. C14, 789 (1976)

ELEM. SYM.	A	Z
Li	6	3

METHOD

REF. NO.	
76 Sk 9	hmg

REACTION	RESULT	EXCITATION ENERGY	SOURCE		DETECTOR		ANGLE
			TYPE	RANGE	TYPE	RANGE	
E,D	ABX	10- 16	D	23	MAG-D		DST
				(23.8)			

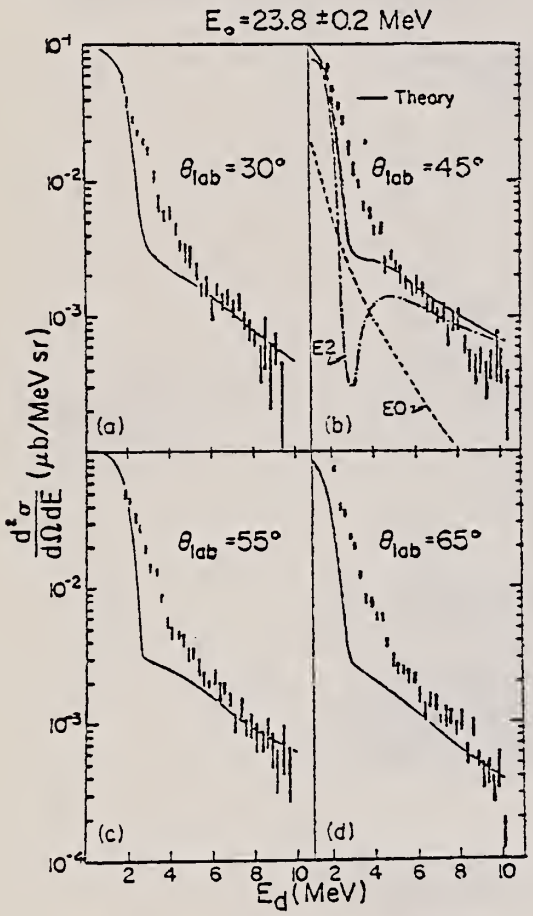

FIG. 2. Electrodisintegration theory and deuteron energy distributions at four laboratory angles for an incident electron energy of 23.8 MeV; (b) shows the $E2$ and $E0$ contributions to the differential cross sections.

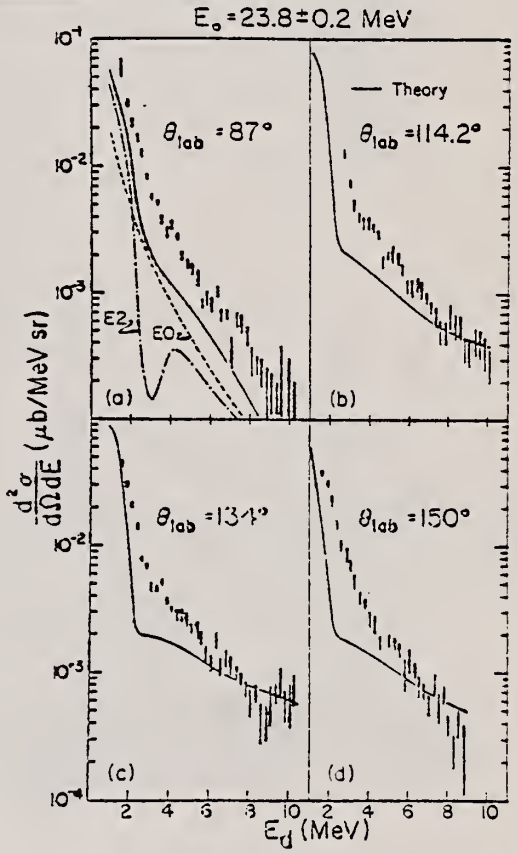

FIG. 3. Electrodisintegration theory and deuteron energy distributions at four laboratory angles for an incident electron energy of 23.8 MeV. (a) shows the $E2$ and $E0$ contribution to the differential cross section.

(continued)

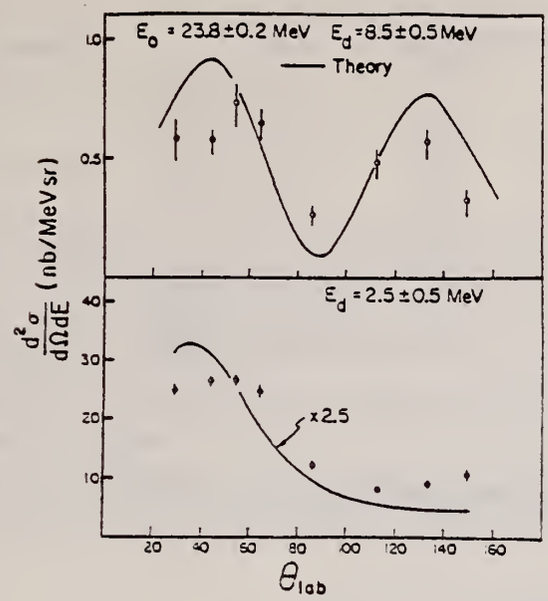

FIG. 4. Angular distribution of deuterons at $E_d = 8.5 \pm 0.5$ MeV and $E_d = 2.5 \pm 0.5$ MeV. The solid line is the electrodisintegration theory described in the text.

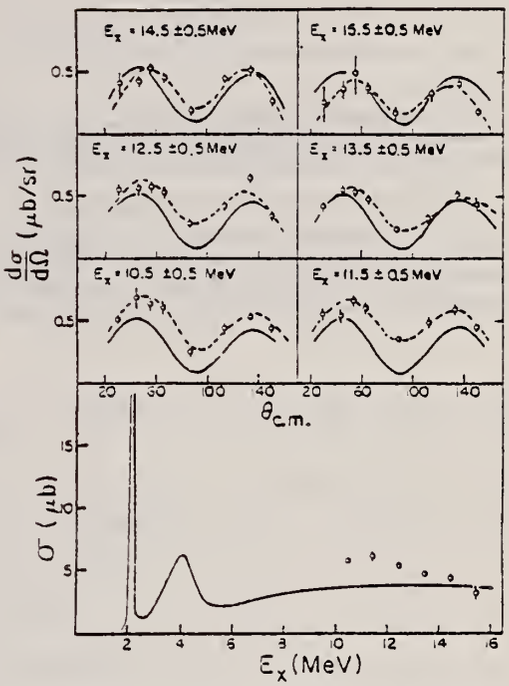

FIG. 5. Extracted photodisintegration cross sections for $E_x > 10$ MeV. The solid curves are the photodisintegration theory described in the text. The dashed lines in the angular distribution data are Legendre polynomial ($l_{max} = 5$) least square fits to the data. The resonance in the total cross section at $E_x = 2.185$ MeV reaches a peak value of 24 μb.

REF. G. Audit, A. Bloch, N. de Botton, C. Schuhl, G. Tamas, C. Tzara
Phys. Rev. C15, 1415 (1977)

ELEM. SYM.	A	Z
Li	6	3

METHOD

REF. NO. 77 Au 2 – hmg

REACTION	RESULT	EXCITATION ENERGY	SOURCE		DETECTOR		ANGLE
			TYPE	RANGE	TYPE	RANGE	
G,P+	RLX	150-157	C	147-158	ACT-I		90

We remeasured with improved techniques the positive-pion photoproduction yield on ^{6}Li near threshold and up to 7.2 MeV above it. If the total cross section of the reaction $\gamma+p\rightarrow\pi^++n$ is expressed as $\sigma_p=aq/k$, our result for the reaction $\gamma+{}^6\mathrm{Li}\rightarrow\pi^++{}^5\mathrm{He}_{g.s.}$ near threshold is

$$\sigma_{Li}=(0.098\pm0.004)(aq/k)\{(12.5/q)/[\exp(12.5/q)-1]\},$$

where q is the pion and k the photon c.m. momenta expressed in units of MeV/c. Deviations from this expression above threshold and the contribution of $\gamma+{}^5\mathrm{Li}\rightarrow\pi^-+{}^5\mathrm{He}$ (1.8 MeV) were also observed. The full understanding of this result requires further theoretical work and complementary experiments on the $A=6$ nuclear system.

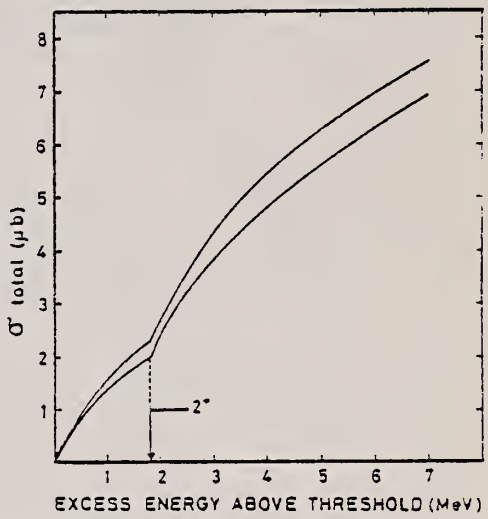

FIG. 10. Cross section of the (γ,π^+) reaction on ^{6}Li deduced from this experiment.

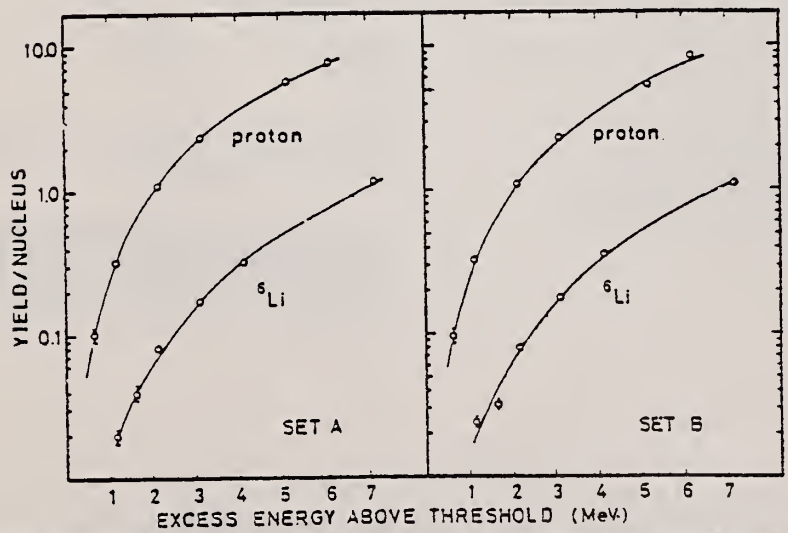

FIG. 9. Measured photoproduction yield per nucleus as a function of the excess energy above threshold for ^{6}Li and hydrogen. The curves indicate the best fit of Eq. (2) to our data.

(continued)

TABLE II. The theoretical predictions and our results.

Operator	Pion-wave distortion	Nuclear wave function: Configuration of ^{6}He(g.s.)	Nuclear wave function: Radial behavior	$\left(\frac{a(^6\mathrm{Li}\rightarrow{}^6\mathrm{He})}{a(p\rightarrow\pi)}\right)_{\mathrm{theor.}}$	Ref.
$\vec{\sigma}\cdot\vec{\epsilon}$	Mean optical potential (Krell-Ericson Ref. 21)	SASK A[a]	Phenomenological	0.091	12
		SASK B[a]		0.101	
$\vec{\sigma}\cdot\vec{\epsilon}$	Mean optical potential (Krell-Ericson Ref. 21)	STAN[b]	Harm. Oscil.	0.119	20
		STAN	Saxon-Wood	0.102	
		SASK A	Phenomenological	0.098	
		SASK B		0.109	
		Elementary particle treatment		0.106	
$\vec{\sigma}\cdot\vec{\epsilon}$	Optical potential adjusted to mesic x rays of light nuclei (Ref. 22)	SASK A	Phenomenological	0.097	18
		SASK B		0.109	
Momentum dependent terms included	Optical potential adjusted to mesic x rays of light nuclei (Ref. 22)	SASK A	Phenomenological	0.105	18
		SASK B		0.117	
This experiment ($0<\omega<2$ MeV)				$a(^6\mathrm{Li}\rightarrow{}^6\mathrm{He})/a(p\rightarrow\pi)=0.098\pm0.004$[c]	

[a] Strong $L=1$ admixture.

[b] Weak $L=1$ admixture.

[c] Comparing this result with the theoretical predictions, one should recall that it was deduced assuming $a(^6\mathrm{Li}\rightarrow{}^6\mathrm{He})/a(p\rightarrow\pi)=cte$ in the energy region of interest ($0<\omega<2$ MeV). As discussed in Sec. III C, this approximation has a negligible influence for reasonable variations of $a(^6\mathrm{Li}\rightarrow{}^3\mathrm{He})$ and $a(p\rightarrow\pi)$.

TABLE I. Photoproduction yield per nucleus, in arbitrary units, for different values of the nominal bremsstrahlung end-point energy both for the ^{6}Li and CH_2 targets.

E_e	Set A	Set B
	$A_p(E_e)$	
152.5	0.099 ± 0.011	0.095 ± 0.010
153	0.334 ± 0.011	0.331 ± 0.010
154	1.087 ± 0.023	1.123 ± 0.023
155	2.366 ± 0.066	2.264 ± 0.064
157	5.729 ± 0.141	5.417 ± 0.135
158	7.950 ± 0.198	8.415 ± 0.206
	$A_{^6\mathrm{Li}}(E_e)$	
147	0.020 ± 0.002	0.024 ± 0.002
147.5	0.040 ± 0.004	0.032 ± 0.003
148	0.082 ± 0.005	0.079 ± 0.005
149	0.168 ± 0.011	0.178 ± 0.012
150	0.322 ± 0.019	0.363 ± 0.021
153	1.194 ± 0.040	1.153 ± 0.036

[12] J.C. Bergstrom et al., Nucl. Phys. A251, 401 (1975).

[18] J. Delorme and A. Figureau (Private comm.)

[20] J. B. Cammarata et al., Nucl. Phys. A267, 365 (1976).

[21] M. Krell et al., Nucl. Phys. B11, 497 (1969).

[22] L. Tauscher et al., Z. Phys. 271, 409 (1974).

REF. A. Yu. Buki, N.G. Shevchenko, V.D. Efros, and I.I. Chkalov
Sov. J. Nucl. Phys. 25, 246 (1977)
Yad. Fiz. 25, 457 (1977)

ELEM. SYM.	A	Z
Li	6	3

METHOD

REF. NO. 77 Bu 13 hmg

REACTION	RESULT	EXCITATION ENERGY	SOURCE		DETECTOR		ANGLE
			TYPE	RANGE	TYPE	RANGE	
E,E/	FMF	UKN	D	82-292	MAG-D		DST

FIG. 1. The quantity $\sigma_1^{1a}(q^2)$: experimental values obtained with separation of the electron scattering cross section into longitudinal and transverse components (○); values of the same quantity obtained without separation (●); the solid line was drawn by eye through the experimental points. The dashed line is the ground-state form factor ^{6}Li $F_{01}^2(q)$ from Ref. 4. The dot-dash line is the square of the proton electric form factor multiplied by the atomic number of the nucleus, $3(G_E^2(q^2))^2$.

[4]G.C. Li et al., Nucl. Phys. A162, 583 (1971)

REF. L. W. Fagg, R. A. Lindgren, W. L. Bendel, E. C. Jones, Jr.
Phys. Rev. C15, 1181 (1977)

ELEM. SYM.	A	Z
Li	6	3

METHOD

REF. NO. 77 Fa 2 hmg

REACTION	RESULT	EXCITATION ENERGY	SOURCE		DETECTOR		ANGLE
			TYPE	RANGE	TYPE	RANGE	
E,E/	FMF	5	D	40,50	MAG-D		180
		(5.36)		(40.5,50.5)			

Using 180° electron scattering, two experimental points are determined for the form factor curve for the excitation of the 5.36 MeV transition in ^{6}Li at low momentum transfer. These results confirm earlier work at other laboratories.

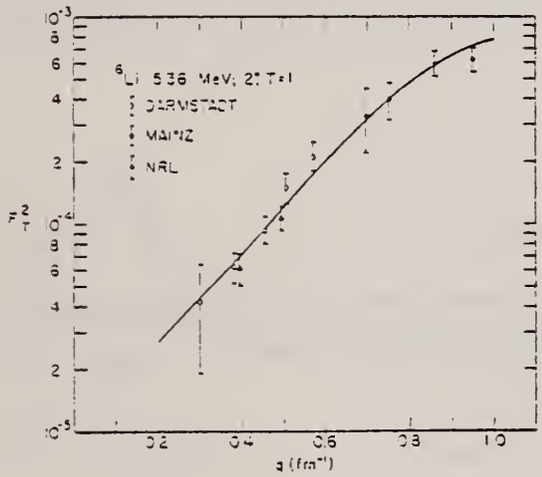

FIG. 2. Plot of values for the transverse form factor, F_T^2, as a function of momentum transfer q from Darmstadt (Ref. 2), Mainz (Refs. 3 and 4), and NRL data. See the text for the source of the curve through the experimental points. Except for the NRL values this figure was obtained from Ref. 4.

TABLE I. Values of cross sections for excitation of the 5.36 MeV transition at incident energies of 40.5 and 50.5 MeV.

Incident energy (MeV)	Cross section (nb/sr)
40.5	1.73 ± 0.31
50.5	1.94 ± 0.26

[2] F. Eigenbrod, Z. Phys. 228, 337 (1969).

[3] R. M. Hutcheon et al., Z. Naturforsch. 25a, 973 (1970).

[4] R. Neuhausen et al., Nucl. Phys. A164, 497 (1971).

REF. K. Nakamura, S. Hiramatsu, T. Kamae, H. Muramatsu, N. Izutsu, Y. Watase
Nucl. Phys. A296, 431 (1978)

ELEM. SYM.	A	Z
Li	6	3

METHOD

REF. NO.	
78 Na 3	hg

REACTION	RESULT	EXCITATION ENERGY	SOURCE		DETECTOR		ANGLE
			TYPE	RANGE	TYPE	RANGE	
E,E/P	SPC	0*60	D	700	MAG-D		53

Abstract: The proton spectral functions of ^{6}Li, ^{7}Li, ^{9}Be and ^{10}B obtained from the (e, e'p) reactions at 700 MeV are presented. The results were analyzed in the distorted-wave impulse approximation, using the shell-model single-particle wave functions consistent with the elastic electron scattering results. The observed 1p proton momentum distributions for the nuclei ^{6}Li, ^{7}Li and ^{9}Be show significant disagreement with the shell-model momentum distributions. The occupation probabilities of the proton single-particle states are around 0.7, with a few exceptions.

*SEPARATION ENERGY

E NUCLEAR REACTIONS ^{6,7}Li, ^{9}Be, ^{10}B(e, e'p), E = 700 MeV; measured $\sigma(E_p, \theta_p)$; deduced proton spectral functions. DWIA calculations. Enriched ^{6,7}Li, ^{10}B and natural ^{9}Be targets.

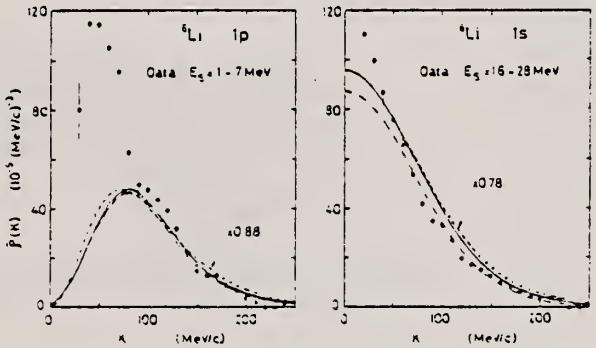

Fig. 5. The distorted momentum distributions corresponding to the optical potentials A (the solid curves) and B (the dot-dashed curves), and the undistorted momentum distributions (the dashed curves), calculated from the shell-model single-particle wave functions used in the DWIA analysis. (a) ^{6}Li, (b) ^{7}Li, (c) ^{9}Be and (d) ^{10}B. For comparison, data points in the appropriate separation energy ranges are shown. They are arbitrarily normalized to the calculated distorted momentum distributions.

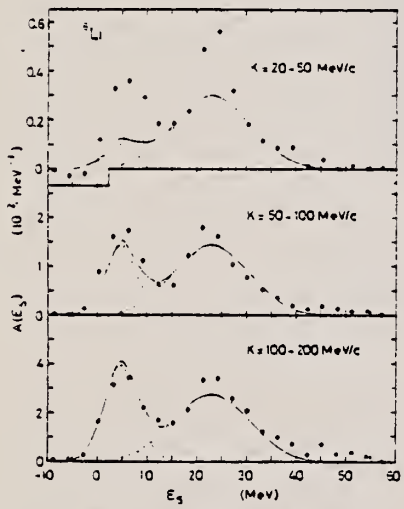

Fig. 1a. Proton separation energy spectra for ^{6}Li. The solid curves are the result of the DWIA fit using the shell-model momentum distributions. The contributions from the individual peaks are shown by the dashed curves. (The curves corresponding to the different optical potentials A and B are essentially indistinguishable.)

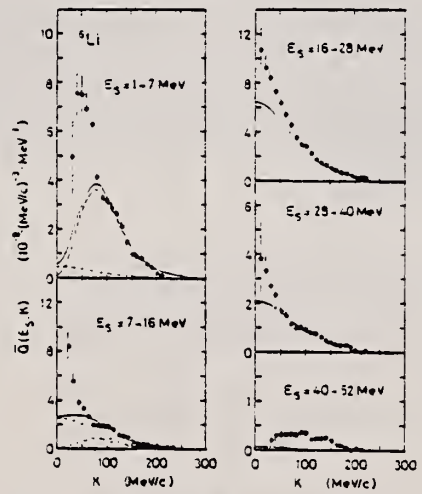

Fig. 1b. Recoil momentum distributions for ^{6}Li. The solid curves are the result of the DWIA fit using the shell-model momentum distributions. The contributions from the individual peaks in the separation energy spectra are shown by the dashed curves. (The curves corresponding to the different optical potentials A and B are essentially indistinguishable.)

REF. Yu.M. Volkov, G.A. Kolomenskii, E.F. Lakovichev, E.D. Makhnovskii, A.V. Nadtochii, V.V. Popov, V.P. Fominenko & V.P. Chizhov
Yad. Fiz. 27, 868 (1978)
Sov. J. Nucl. Phys. 27, 461 (1978)

ELEM. SYM.	A	Z
Li	6	3

METHOD

REF. NO. 78 Vo 4 — hmg

REACTION	RESULT	EXCITATION ENERGY	SOURCE		DETECTOR		ANGLE
			TYPE	RANGE	TYPE	RANGE	
G,T	ABX	16-55	C	29-55	TEL-D		90
G,TP	ABX	21-55	C	34-55	TEL-D		DST
G,TD	ABX	21-55	C	29-55	TEL-D		DST
G,T	ABX	16-55	C	38-55	TEL-D		DST

Results are presented of an experimental study of reactions of the type ^{6,7}Li (γ, ab)X with emission of charged particles a and b detected in coincidence. It is established that the major part of such reactions are reactions of the type ^{6,7}Li (γ,pt)X. The results of measurement of the correlations of the directions of emission and energy distributions of protons and tritons are explained on the basis of the assumption of photodisintegration of α clusters in the ground state of the nuclei ^{6,7}Li into a proton and triton and of formation of the residues X in the form of two $(d+n)$ particles in reactions ^{6}Li (γ, pt)X, and two $(d+n)$ particles and possibly three $(n+p+n)$ particles in reactions ^{7}Li (γ, pt)X. The value of the average differential cross section of the reaction ^{6}Li (γ, pt) ^{1}Hn in the γ-ray energy interval 35–55 MeV amounts to 0.7±0.2 of the value of the cross section for the reaction ^{4}He (γ, p) ^{3}H. It is shown that in addition, three-particle reactions of the type ^{6}Li (γ,td) ^{1}H and ^{7}Li (γ, π) ^{1}H occur, but with a kinematics differing from that of the photodisintegration of α clusters, and also two-particle reactions of the type ^{6}Li (γ, t) ^{3}He and ^{7}Li (γ, t) ^{4}He.

(G,T) ALL TRITONS
(G,TP) COINC: T WITH P
(G,TD) COINC: T WITH D
(G,T) 2 BODY BREAKUP ONLY

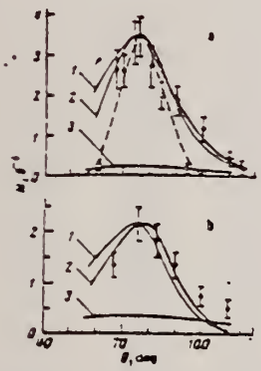

FIG. 3. Correlations of directions of emission of protons and tritons in the reactions: a—^{6}Li(γ, tp)X; b—^{7}Li(γ, tp)X. Points: ●—numbers of coincidences per unit dose, ○—experimental angular resolution of the apparatus; solid curves: 1—calculated angular correlation for the reactions ^{6,7}Li(γ, tp)^{1,2}Hn on the assumption of photodisintegration of α clusters; curve 2—the same, but for the reactions ^{6,7}Li(γ, tp)^{2,3}H; curve 3—calculation of the relative contribution of the three-particle reactions ^{6,7}Li(γ, tp)^{2}H on the assumption of phase-space kinematics; dashed curve—calculated angular resolution of the apparatus; curves 1 and 2 have been normalized to the experimental results at an arbitrary point.

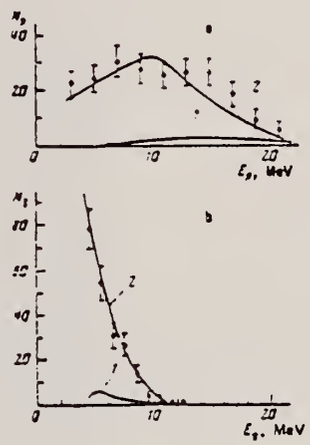

FIG. 4. Energy distributions of protons (a) and of tritons coincident with them (b) in the reaction ^{6}Li(γ, pt)X. Curves: 1—result of calculation on the assumption of photodisintegration of α clusters for the reaction ^{6}Li(γ, pt)^{2}H; 2—the same as curves 1, but for the reaction ^{6}Li(γ, pt)^{1}Hn. The curves in Fig. a have been normalized in such a way that the combined curve lies in the region of the ordinates of the experimental points.

(continued)

TABLE II. Differential cross sections of identified reactions.

Reaction	Average energy of γ rays $\bar{E}_\gamma$, MeV	$\frac{d\sigma(\theta=90°;\bar{E}_\gamma)}{d\Omega}$, μb/sr ($E_t \geq 4$ MeV, $E_p \geq 3$ MeV	Kinematic reaction threshold E_{th}, MeV	Reaction yield $\int_{E_{th}}^{55} E_\gamma \frac{dN_\gamma}{dE_\gamma} dE_\gamma$ at $\Delta E_\gamma = 1$ MeV, 10^{-30} MeV · sr · cm²	$\frac{d\sigma(\theta=90°;\bar{E}_\gamma)}{d\Omega}$, μb/sr ($E_t > 0$, $E_p > 3$)
$^6Li(\gamma,t)X$			29	7.9±1.5	
$^6Li(\gamma,tp(pt))pn$ *	48±6	9.8±1.5	34	3.3±0.5	68.7±11.5
$^6Li(\gamma,td)p$ **	43±10	0.9±0.4	29	0.5±0.2	2.0±0.9
$^6Li(\gamma,t)^3He$	45±7	6.0±0.9	38	3.1±0.5	
$^7Li(\gamma,t)X$			30	10.0±2.2	
$^7Li(\gamma,tp(pt))dn$ *	43±4	3.9±0.7	40	1.4±0.2	44.6±6.8
$^7Li(\gamma,td)p$ **	43±10	3.4±0.7	30	2.5±0.5	7.1±1.3
$^7Li(\gamma,t)^4He$	41±9	3.0±0.4	32	2.2±0.3	
$^4He(\gamma,t)p$ [7]	$\frac{d\sigma(\theta=90°;\bar{E}_\gamma=48\text{ MeV}}{d\Omega} = 93.0\pm9.5$ μb/sr				

Table II lists values of the differential cross sections of identified reactions $^{6,7}Li(\gamma,tp)X$ in which tritons with energy $E_t \geq 4$ MeV are emitted at an angle $\theta_t = 90°$ and protons with energy $E_p \geq 3$ MeV at all possible angles, and also values of the differential cross sections for the two-particle reactions $^{6,7}Li(\gamma,t)^{3,4}He$ and the correlations of particle-emission directions established after normalization of the theoretical results to the experimental data. Also in Table II we have given the energies of the γ-rays producing the reactions noted above. The

REF. J. C. Bergstrom, U. Deutschmann, R. Neuhausen
Nucl. Phys. A327, 439 (1979)

ELEM. SYM.	A	Z
Li	6	3

METHOD

REF. NO. 79Be6 hg

REACTION	RESULT	EXCITATION ENERGY	SOURCE		DETECTOR		ANGLE
			TYPE	RANGE	TYPE	RANGE	
E,E/	FMF	2-5	D	141-330	MAG-D		DST

Abstract: The form factor of the 3.56 MeV (0^+, $T = 1$) state of ^{6}Li has been measured for momentum transfers $q = 1.0$–3.0 fm^{-1}, and the 2.18 MeV (3^+, $T = 0$) and 5.37 MeV (2^+, $T = 1$) states have been measured up to $q = 2.5$ fm^{-1}. The 3.56 MeV form factor is analysed in terms of a phenomenological shell model with $l = 1$ valence nucleons. The radial wave functions are found to have a greater radial distribution than given by the harmonic oscillator, more closely resembling Woods-Saxon functions. The M1 form factor is found to decrease at high momentum transfer somewhat more slowly than the models predict. A technique for determining the M1 transition current density based on the Fourier-Bessel analysis is developed and applied to the M1 transition. The M1 transition current density is obtained within a moderate error band and compared with the harmonic oscillator and Woods-Saxon densities. The M1 radiative width is 8.18 ± 0.25 eV, in agreement with previous measurements.

E NUCLEAR REACTIONS ^{6}Li(e, e'), $E = 140$–330 MeV, $\sigma(E; E_x, \theta)$. ^{6}Li deduced form factors, transition current density and Γ_{γ_0}.

Q= 1-3 FM-1, 2+, 0+, 2+

TABLE I

Experimental form factors for the 3^+(2.18 MeV, C2), 0^+(3.56 MeV, M1) and 2^+(5.37 MeV, M1 + E2 − M3) levels of ^{6}Li

E_0 (MeV)	θ (deg)	q (fm^{-1})	$F_C^2 \times 10^3$ (3^+, 2.18 MeV)	$F_T^2 \times 10^4$ (0^+, 3.56 MeV)	$F_T^2 \times 10^4$ (2^+, 5.37 MeV)
140.5	87.6	0.96	14.9 ±0.7	5.62 ±0.24	8.4 ±2.4
140.5	96.0	1.03	14.1 ±0.7	3.59 ±0.17	9.8 ±2.3
140.5	104.0	1.09	14.2 ±0.4	2.78 ±0.19	10.5 ±1.4
140.5	119.9	1.20	13.5 ±0.4	0.90 ±0.11	11.6 ±1.2
140.5	127.9	1.24	13.4 ±0.3	0.532 ±0.087	11.1 ±0.8
140.5	135.3	1.28	12.7 ±0.3	0.167 ±0.062	11.0 ±0.6
154.5	125.0	1.35	11.8 ±0.2		12.7 ±2.0
154.5	131.0	1.38	10.7 ±0.2	< 0.06 *)	12.0 ±2.9
154.5	137.0	1.41	9.78 ±0.28		12.1 ±1.5
165.0	125.0	1.44	10.1 ±0.1		12.8 ±2.0
165.0	131.0	1.47	9.79 ±0.25	0.070 ±0.055	10.7 ±1.1
165.0	137.0	1.50	9.33 ±0.21	0.220 ±0.046	9.58 ±0.39
219.9	87.6	1.51	9.18 ±0.14		11.7 ±1.1
220.0	96.1	1.61	7.13 ±0.21	0.39 ±0.11	8.7 ±1.2
220.0	104.0	1.70	5.21 ±0.11	0.650 ±0.081	7.2 ±1.1
220.0	112.0	1.79	4.24 ±0.11	0.917 ±0.066	6.31 ±0.85
219.9	120.0	1.86	3.25 ±0.11	1.11 ±0.07	5.53 ±0.84
219.9	127.9	1.93	2.71 ±0.08	1.05 ±0.05	4.37 ±0.31
219.9	135.9	1.99	2.29 ±0.11	1.07 ±0.06	3.62 ±0.33
278.2	107.0	2.19	0.976 ±0.053	0.877 ±0.076	1.91 ±0.37
278.2	119.0	2.33	0.502 ±0.028	0.627 ±0.065	1.54 ±0.15
278.1	131.0	2.45	0.321 ±0.026	0.553 ±0.044	0.821 ±0.087
278.0	137.0	2.50	0.258 ±0.021	0.525 ±0.041	0.987 ±0.099
330.8	94.0	2.37		0.678 ±0.087	
330.4	96.0	2.40		0.563 ±0.053	
331.0	109.0	2.62		0.373 ±0.047	
330.6	119.0	2.76		0.250 ±0.063	
330.5	137.0	2.96		0.120 ±0.023	
330.7	137.0	2.96		0.113 ±0.028	

The 5.37 MeV results represent the strength within ±0.55 MeV of the peak centre (see text). The q-values are for the 3.56 MeV level.

*) The upper limit corresponds to two standard deviations of the measured counting rate at the expected location of the 3.56 MeV peak.

(continued

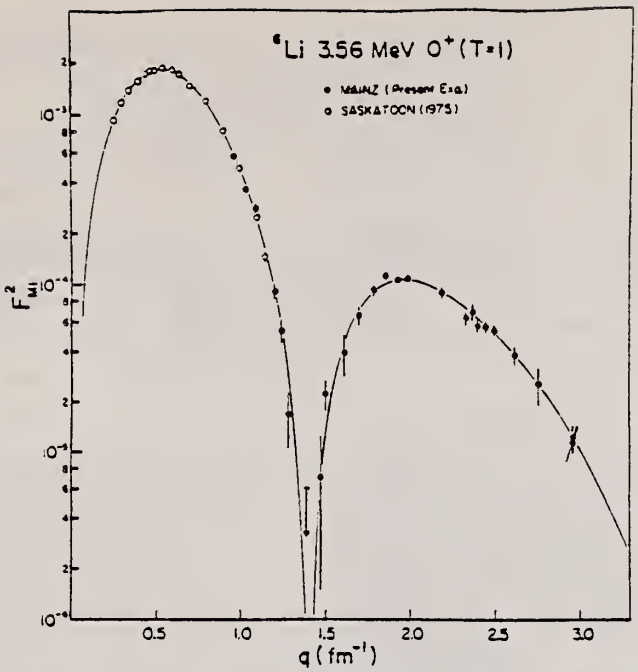

Fig. 2. The 3.56 MeV M1 form factor and the phenomenological shell model fit with the Sask-A amplitudes. The radial density is derived from the present analysis of the combined Mainz and Saskatoon [4]) data.

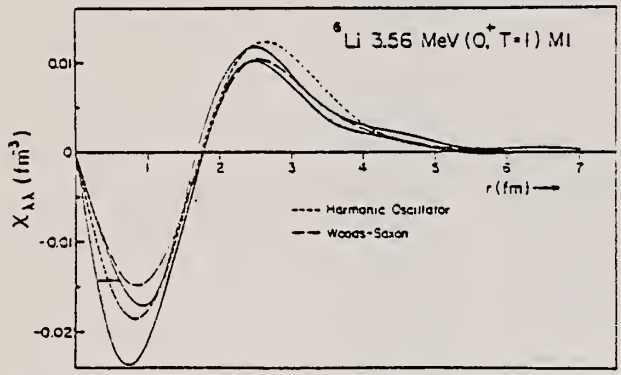

Fig. 5. The M1 transition current density for the 3.56 MeV level from the Fourier-Bessel analysis of the experimental form factor. The shaded region represents a ± 1 standard deviation error band and contains the statistical and model dependent errors. The wiggles at r = 4.5 and 6.5 fm are probably a consequence of the truncated series, although the rapid change in slope near r = 3.5 is believed genuine. The curves are predictions based on the harmonic oscillator and Woods-Saxon potentials with Sask-A amplitudes.

REF. V.N. Eponeshnikov, Yu.F. Krechetov
JETP Lett. 29, 401 (1979)

ELEM. SYM.	A	Z
Li	6	3

METHOD

REF. NO. 79 Ep 2 — hg

REACTION	RESULT	EXCITATION ENERGY	SOURCE		DETECTOR		ANGLE
			TYPE	RANGE	TYPE	RANGE	
G,PIOP	ABY	0*520	C	450	CKV-D		DST

*MOM, MEV/C, COIN

The cross sections of reaction $(\gamma,\pi^{\circ}p)$ on Li^{5} C^{12} nuclei were measured in the 0–600 MeV/c range of momentum transfer to the residual nucleus. For large values of momenta, cross section values disagree with calculations carried out within the framework of a shell model and a model of quasi-free meson photoproduction on nuclei.

PACS numbers: 25.20. + y

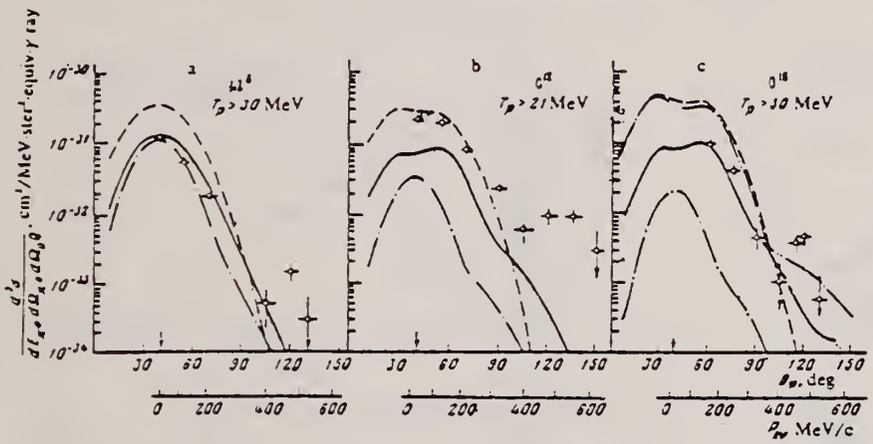

FIG. 1. Dependence of reaction cross section on the proton angle of emission: O—experiment, with total measurement errors;— —calculations using plane waves; —— final state interactions taken into account; ————effect of S-shell shown separately; ————calculations with momentum distribution from Ref. 3 with allowance for correlation by the Jastrow model. Oscillator parameters $\alpha_1 = \alpha_2 = 115$ MeV/sec for Li^6 nucleus,[12] 120 MeV/sec for C^{12} and 113 MeV/sec for O^{16}.[13] Arrow indicates angle of proton emission in the case of reaction $\gamma + p \rightarrow \pi^0 + p$.

REF. G. Junghans, K. Bangert
Z. Phys. A291, 353 (1979)

ELEM. SYM.	A	Z
Li	6	3

METHOD

REF. NO. 79 Ju 6 hg

REACTION	RESULT	EXCITATION ENERGY	SOURCE		DETECTOR		ANGLE
			TYPE	RANGE	TYPE	RANGE	
G,P	ABX	7-24	C	35	TEL-D		DST
G,D	ABX	4-14	C	35	TEL-D		90
G,T	ABX	19-36	C	30,35	TEL-D		DST
G,A	ABX	17-34	C	35	TEL-D		DST

The photodisintegration of the stable Lithium isotopes has been investigated by spectroscopy of the emitted charged particles using the Giessen bremsstrahlung facility. Protons, deuterons, tritons, ^{3}He and alpha particles were detected and identified up to 20 MeV particle energy. Angular distributions were measured using γ-ray energies up to $E_\gamma = 50$ MeV. They are compared with theoretical predictions and with other experiments. A remarkable low (γ, t)-cross section was found for both isotopes in disagreement to previous measurements using virtual photons. Coincidence measurements between the emitted particles were performed in order to study the manybody-breakups of ^{7}Li.

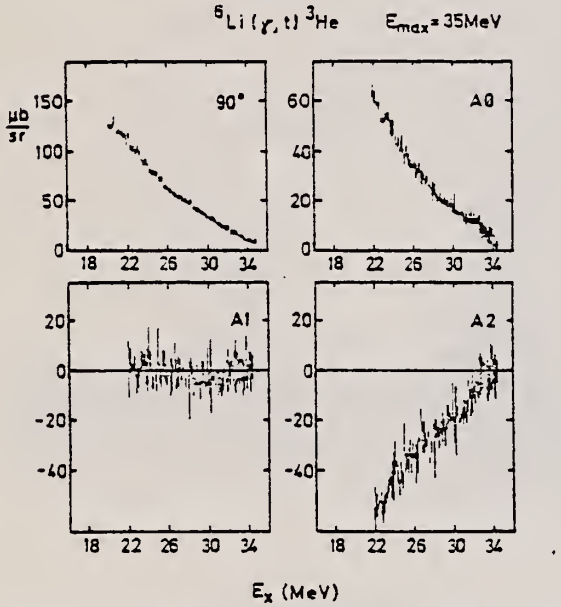

Fig. 2. ^{6}Li(γ, t) cross section and angular distribution, $E_{\gamma max} = 35$ MeV

$$\frac{d\sigma}{d\Omega}(\theta, E) = A_0(E)\left[1 + \sum_{i=1}^{n} a_i(E) P_i(\cos\theta)\right]$$

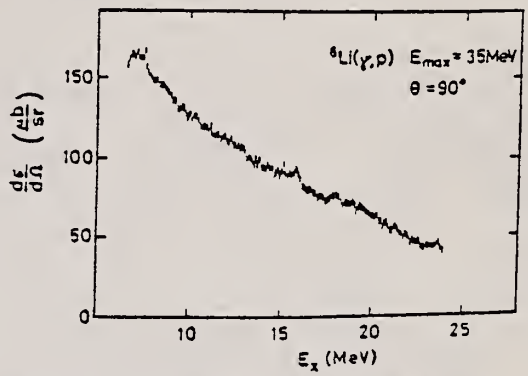

Fig. 5. The ^{6}Li(γ, p) cross section. $E_{\gamma max} = 35$ MeV, $\theta = 90°$

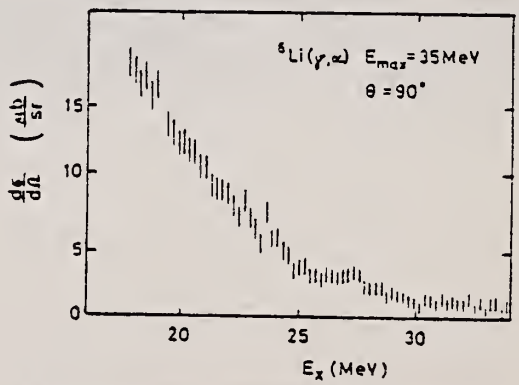

Fig. 9. ^{6}Li(γ, x) assumed cross section. $E_{\gamma max} = 35$ MeV, $\theta = 90°$

Not A-d break up. See discussion 4.4 in paper.

(continued)

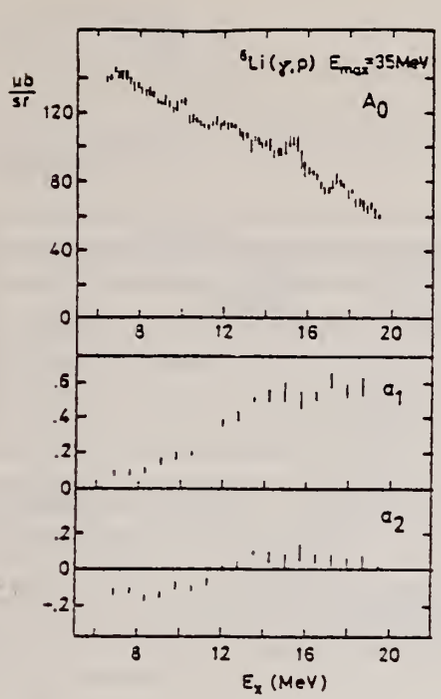

Fig. 6. Angular distribution of the ^{6}Li(γ, p) cross section: $E_{\gamma,max}$ = 35 MeV

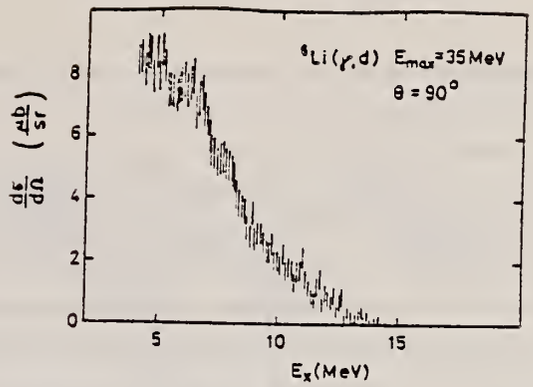

Fig. 8. ^{6}Li(γ, d) assumed cross section, $\theta = 90°$, $E_{\gamma,max} = 35$ MeV

Table 2. Dipol sum rules of ^{6}Li and ^{7}Li

	(γ, p)	(γ, n)	(γ, t)	Ref.
^{6}Li	23.4 ±3.8[a]			[34]
σ_{-1} MeVmb		27.4 ±2.0[a]		[28]
			17 ±1[b]	[3]
			4.9 ±2.5[c]	[3]
	16.3 ±2.5[c]		7.0 ±1.0[d]	this work
^{7}Li	21.6 ±3.5[a]			[34]
σ_{-1} MeVmb		20.1[i]		[21]
			8.0[e]	[11, 22]
	14.6 ±3.4[f]			[5]
	13.2 ±2.0[g]		4.4 ±0.7[h]	this work
^{6}Li	1.9 ±0.3[a]			[34]
σ_{-3} mb		1.85 ±0.1[a]		[28]
			0.77 ±0.03[b]	[8]
			0.18 ±0.09[c]	[3]
	1.4 ±0.2[c]		0.29 ±0.04[d]	this work
^{7}Li	1.17 ±0.19[a]			[34]
σ_{-3} mb		1.15[i]		[21]
			0.74[e]	[11, 22]
	0.8 ±0.1[g]		0.4 ±0.06[h]	this work

[a] 5.5–32 MeV [b] 22–32 MeV [c] 6.4–30 MeV
[d] 20–30 MeV [e] 5–15 MeV [11], 15–30 MeV [22]
[f] threshold to 34 MeV [g] 11–28 MeV [h] 5.5–28 MeV
[i] threshold to 30.5 MeV [k] 19–35 MeV

REF. D.M. Skopik, J.J. Murphy II, J Asai
Phys. Rev. C19, 1144 (1979)

ELEM. SYM.	A	Z
Li	6	3

METHOD

REF. NO. 79 Sk 11 egf

REACTION	RESULT	EXCITATION ENERGY	SOURCE		DETECTOR		ANGLE
			TYPE	RANGE	TYPE	RANGE	
G,XP	ABX	13-19	D	20 -35	MAG-D		DST

The 16 MeV level reported in the ^{6}Li(γ,p) cross section has been found to result from oxygen contamination.

VIR PHOT SEE 70 WO 1

[NUCLEAR REACTIONS ^{6}Li(e,p), E_x = 16 MeV, measured $\sigma(\theta, E)$. Deduced ^{6}Li(γ,p) $\sigma(\theta)$. No state at 16.1 MeV.]

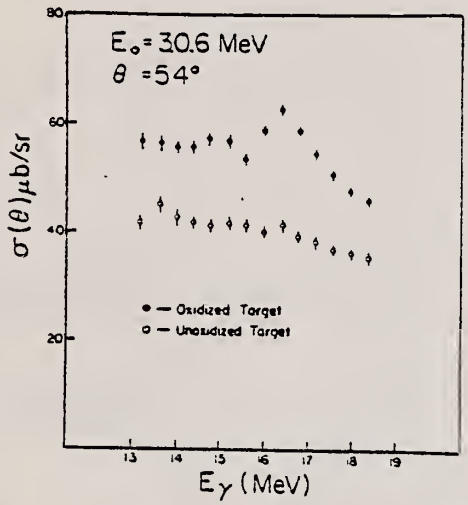

FIG. 1. Proton cross sections near 16 MeV excitation in ^{6}Li which show the effect of a small amount of surface oxygen contamination. The cross sections measured with the unoxidized target have been multiplied by 0.8 in order to visually separate the data points. The fact that the proton cross sections away from the peak region were statistically the same is taken as evidence for the oxide layer being a small fraction of the total target thickness.

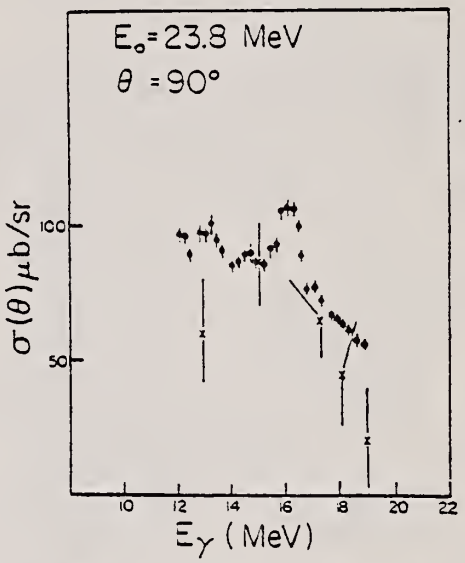

FIG. 2. 90° cross section data taken in 200 keV intervals. The X's are taken from Wong *et al.*[2] near the 16 MeV excitation region in ^{6}Li where evidence for a slight peaking was claimed.

REF. J.C. Bergstrom
Phys. Rev. C21, 2496 (1980)

ELEM. SYM.	A	Z
Li	6	3

METHOD

REF. NO. 80 Be 3 hg

REACTION	RESULT	EXCITATION ENERGY	SOURCE		DETECTOR		ANGLE
			TYPE	RANGE	TYPE	RANGE	
E,E/	FMF	6	D	76-141	MAG-D		DST
		(5.37)					

The transverse form factor for the 5.37 MeV(2^+,$T=1$) level of ^{6}Li is analyzed in terms of a phenomenological model to give the configuration amplitudes and transition density. Radiative pion capture rates for the 1s atomic orbital of ^{6}Li leading to the two lowest states of ^{6}He are estimated using the phenomenological functions. The radiative pion capture rate to ^{6}He(g.s.) agrees with experiment, but the rate to ^{6}He(2^+,1.8 MeV) is larger than the measured value. It is shown that if the longitudinal form factor is small at $q \simeq m_\pi$, the transverse 5.37 MeV form factor gives the radiative pion capture matrix elements directly. As part of this study, the C2 form factor was measured near $q = m_\pi$, and its implications on the wave functions are considered.

[NUCLEAR REACTIONS ^{6}Li(e,e'), E=76–141 MeV; $\sigma(E;E_{e'},\theta)$. ^{6}Li deduced form factors, wave functions, radiative capture.]

6=5.37 MEV

TABLE I. Summary of the present experimental results for the 5.37 MeV (2^+, $T=1$) state of ^{6}Li. Radiative corrections and the elastic form factor were calculated as in Ref. 3. The total form factor is defined within ±0.55 MeV of the peak center. Errors do not reflect uncertainties in the position and width of the state.

E_0 (MeV)	ϑ (deg)	$\sigma(5.37)/\sigma(\text{el})$ ($\times10^{-3}$)	$F_{el}^2(q)$ (calc.)	$F_{tot}^2(q,\vartheta)$ ($\times10^{-4}$)
140.9	59.0	1.12 ± 0.20	0.364	4.08 ± 0.71
99.3	90.0	1.80 ± 0.32	0.358	6.43 ± 1.14
75.6	140.0	8.83 ± 0.79	0.352	31.1 ± 2.8

$q = 0.687$ fm^{-1}
$F_L^2(q) = (9.7 \pm 9.5) \times 10^{-5}$
$F_T^2(q) = (3.73 \pm 0.40) \times 10^{-4}$

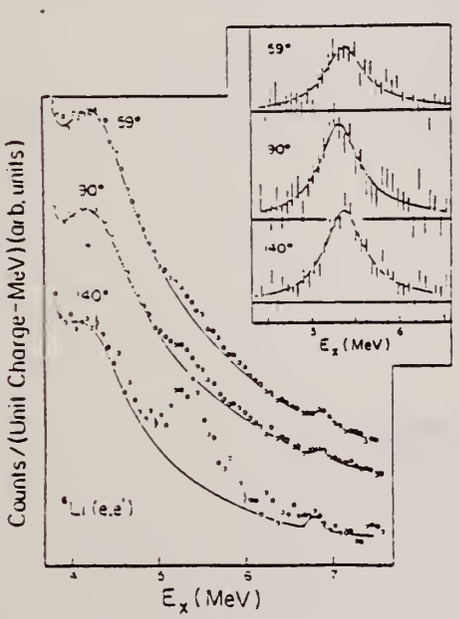

FIG. 1. Electron scattering spectra from ^{6}Li showing the 5.37 MeV peak on the flank of the broad 4.31 MeV (2^+) resonance. The three spectra do not have a common scale factor. The solid curve represents the total background under the 5.37 MeV resonance and the inset shows the background-subtracted spectra. The Breit-Wigner curves were fit simultaneously with the background by a least-squares procedure. The small peak near 7 MeV is the 7.66 MeV (0^+) state of ^{12}C, apparently introduced during target fabrication.

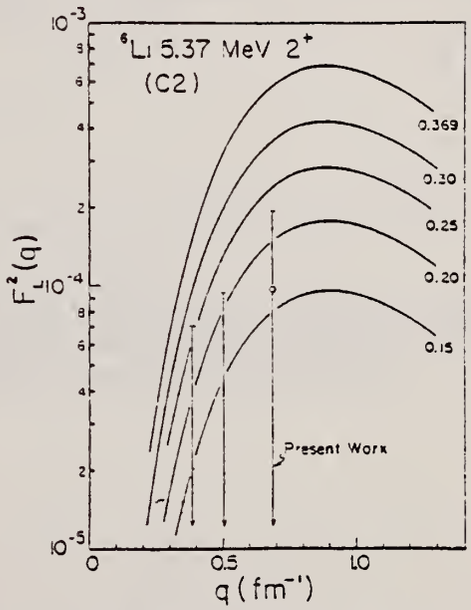

FIG. 2. Longitudinal form factors of the 5.37 MeV state based on the phenomenological densities and amplitudes determined from the experimental transverse form factor. The curves are labeled by β, the ground state $^1P_1$ amplitude. The experimental result at q=0.69 fm^{-1} is from the present work, the others are from Ref. 5.

REF. J.C. Bergstrom
Nucl. Phys. A341, 13 (1980)

ELEM. SYM.	A	Z
Li	6	3

METHOD

REF. NO. 80 Be 4 hg

REACTION	RESULT	EXCITATION ENERGY	SOURCE TYPE	SOURCE RANGE	DETECTOR TYPE	DETECTOR RANGE	ANGLE
E,E/	FMF	12-20	D	102,123 (101.8,122.7)	MAG-D		DST

Abstract: The form factor for excitation of the t-τ continuum in ^{6}Li has been measured within 4 MeV of threshold for momentum transfers q = 0.48 and 0.58 fm^{-1}. The results are in good agreement with the CI form factor calculated in the framework of a t-τ cluster model with a spectroscopic factor θ_0^2 = 0.67.

T, HE3 BREAK UP

E NUCLEAR REACTIONS ^{6}Li(e, e'), E = 102, 123 MeV; measured $\sigma(E; E_e, \theta)$. ^{6}Li deduced form factor. t-^{3}He cluster model.

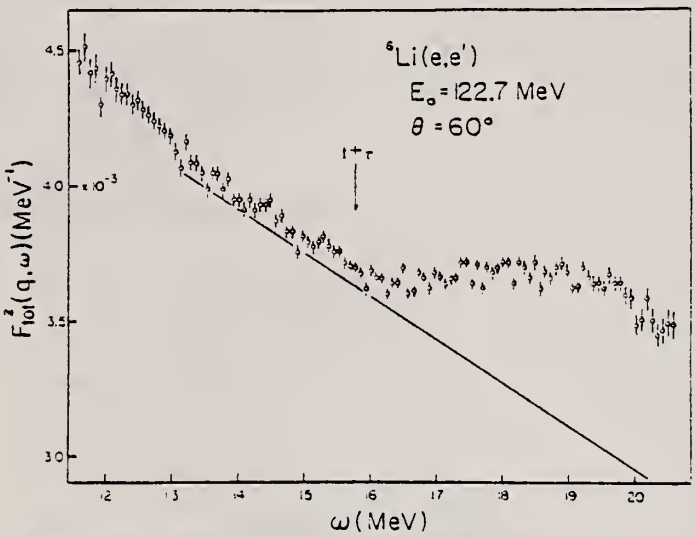

Fig. 1. Electron scattering spectrum for ^{6}Li in the excitation energy region ω = 12-20 MeV. The data are presented as a total differential form factor, defined by eq. (1). The scale is exaggerated to clearly display the t-τ continuum starting at 15.8 MeV, indicated by the arrow. The line represents the estimated total contribution from other processes, as discussed in the text.

(continued)

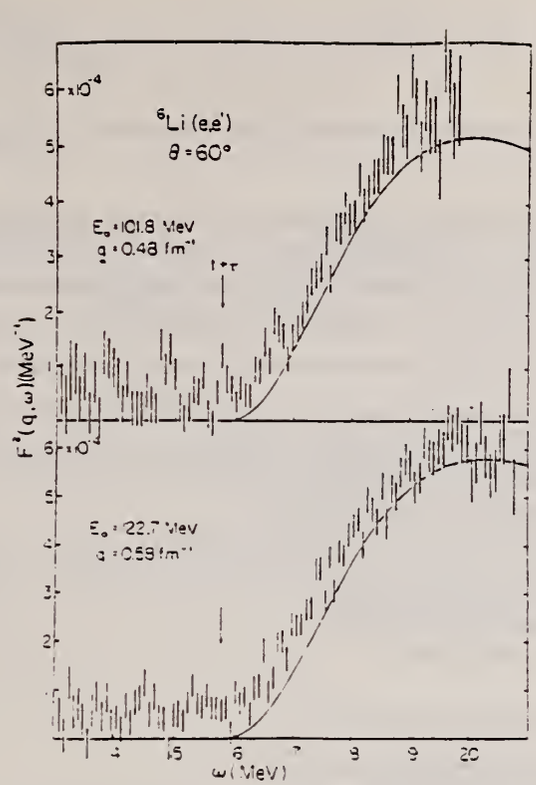

Fig. 2. Differential form factor for the t-r breakup of ^{6}Li. The excitation energies extend to about 4 MeV above threshold. The curves are the CI form factors predicted by the t-r cluster model with $\theta_S^2 = 0.67$.

REF. M. Kusuhara
Phys. Rev. C21, 1165 (1980)

ELEM. SYM.	A	Z
Li	6	3

METHOD

REF. NO. 80 Ku 1 - hg

REACTION	RESULT	EXCITATION ENERGY	SOURCE		DETECTOR		ANGLE
			TYPE	RANGE	TYPE	RANGE	
G,P	RCY	5-15	C	10,15	EMU-D		DST

Photoreaction mechanisms of ^{6}Li were studied using bremsstrahlung below the $(\gamma,^3H)$ threshold. It was confirmed by the present work that only the $^6Li(\gamma,p)^5He$ and $^6Li(\gamma,n)^5Li$ reactions actually occur in the energy range of incident γ ray lower than the $(\gamma,^3H)$ threshold, and the $^6Li(\gamma,np)^4He$ reaction in various types does not occur in practice although this reaction is energetically possible. The assignment of the reactions $^6Li(\gamma,p)^5He$ and $^6Li(\gamma,n)^5Li$ to the measured photoproton spectrum for 15.4 MeV irradiation is presented.

[NUCLEAR REACTIONS ^{6}Li, checked photoreaction mechanisms, bremsstrahlung E=15.4 and 10.2 MeV, measured proton spectra, peak energies and widths, $\sigma(\theta)$, confirmed only $^6Li(\gamma,p)^5He$ and $^6Li(\gamma,n)^5Li$ actually occur below the $^6Li(\gamma,^3H)^3He$ threshold.]

TABLE II. The peak energy and half-width for each peak of the first three peaks in the range $K \geq 2$ MeV of observed proton spectra of ^{6}Li.

15.4 MeV irradiation		10.2 MeV irradiation	
peak energy (MeV)	half-width (MeV)	peak energy (MeV)	half-width (MeV)
2.29 ± 0.19	0.691 ± 0.066	2.30 ± 0.20	0.693 ± 0.062
3.14 ± 0.18	0.606 ± 0.052	3.17 ± 0.17	0.601 ± 0.066
3.93 ± 0.18	0.605 ± 0.066	4.08 ± 0.16	0.600 ± 0.064

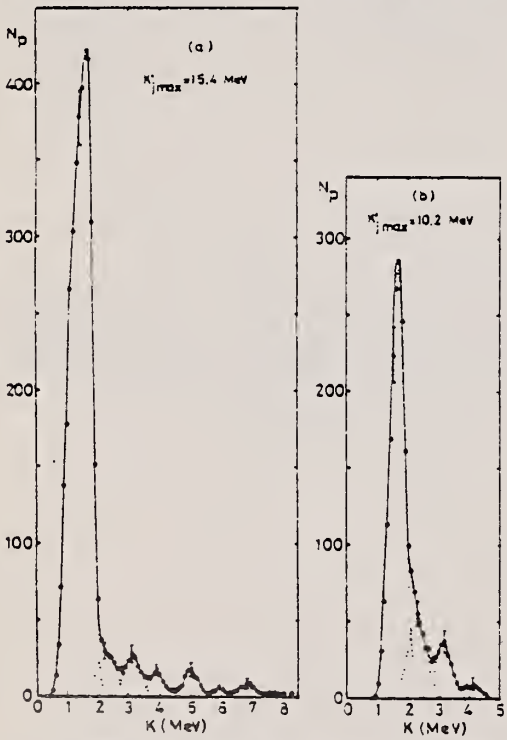

FIG. 2. Photoproton energy spectra of the ^{6}Li nucleus. The errors represent statistical errors.

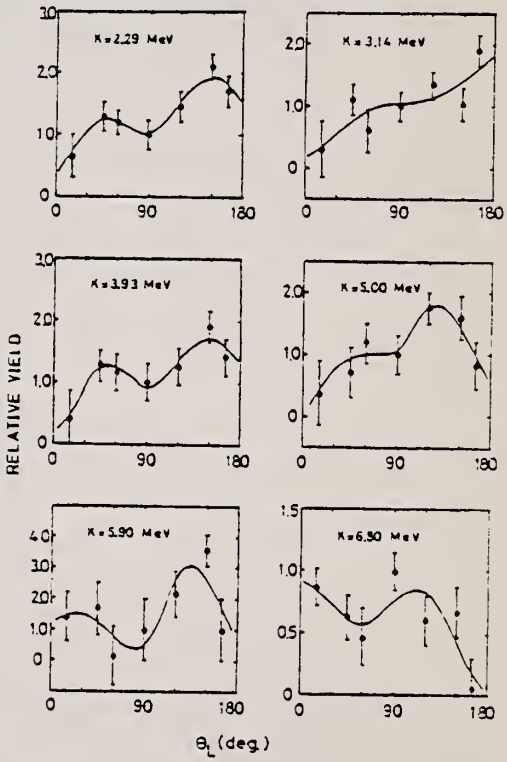

FIG. 3. Angular distributions for the proton groups in the 15.4 MeV irradiation. The errors represent $\pm[\sqrt{Y_p(\theta_L)}/Y_p(90°)]$ where $Y_p(\theta_L)$ is the proton yield for each group at θ_L. The solid curves are the least squares fit in terms of the Legendre polynomials up to order 4 for the groups of 2.29, 3.93, 5.00, and 5.90 MeV, and up to order 3 for the 3.14 and 6.80 MeV groups.

REF. R.G.H. Robertson, P. Dyer, R.A. Warner, R.C. Melin, T.J. Bowles, A.B. McDonald, G.C. Ball, W.G. Davies, E.D. Earle
Phys. Rev. Lett. 47, 1867 (1981)

ELEM. SYM.	A	Z
Li	6	3

METHOD

REF. NO.	
81 Ro 1	egf

REACTION	RESULT	EXCITATION ENERGY	SOURCE		DETECTOR		ANGLE
			TYPE	RANGE	TYPE	RANGE	
A,G	ABX	2-10	D	0-8	MAG-D		DST

detected recoil ^{6}Li in forward direction

The capture of α particles by deuterium has been observed by using a magnetic analysis technique to detect the recoiling ^{6}Li ions. Measurements of the cross section down to 1 MeV in the center-of-mass system can be interpreted accurately in terms of a direct-capture model, and it is found that production of ^{6}Li in the big bang is 3 times smaller than has been assumed

PACS numbers: 25.60.+t, 25.10.+s, 98.80.Ft

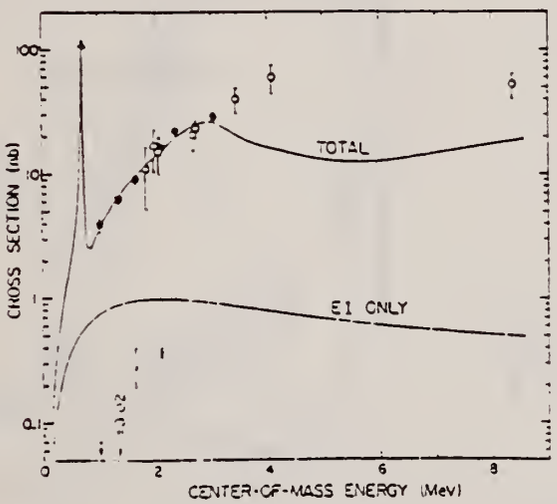

FIG. 1. Cross section for the reaction ^{2}H(α,γ)^{6}Li. Open circles, MSU data; closed circles, CRNL data; triangles, ^{6}Li($e,e'\alpha$) (Ref. 7); crosses, CRNL data for $E1$ component. The curves are a direct-capture calculation.

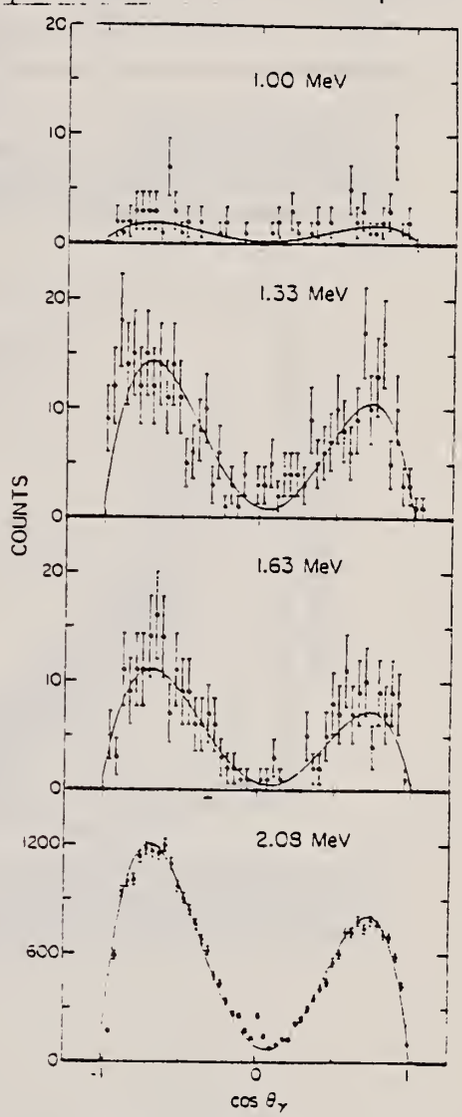

FIG. 2. Measured ^{6}Li momentum distributions for ^{2}H(α,γ)^{6}Li at four center-of-mass energies. The momentum varies linearly as the cosine of the angle between the incident beam and the outgoing photon, θ_γ. The curves are a direct-capture calculation in which the $E1$ operator has been renormalized. The small peak in the center of the lowest distribution is due to a weak ^{6}Li component in the beam, which was removed by means of a velocity filter in the other, more recent, data. The peak width is roughly the instrumental resolution.

REF. K. Shoda, O. Sasaki, T. Kohmura
Phys. Lett. 101B, 124 (1981)

ELEM. SYM.	A	Z
Li	6	3

METHOD

REF. NO. 81 Sh 3 hg

REACTION	RESULT	EXCITATION ENERGY.	SOURCE		DETECTOR		ANGLE
			TYPE	RANGE	TYPE	RANGE	
G,PI+	ABX	100*230	D	170-195	MAG-D		DST

*MEV/C G,PI FRM E,PI

Differential cross sections of ^{6}Li(γ, π^+)^{6}He leading to the ground and first excited residual states have been deduced in the range of momentum transfer $0.7\ m_\pi < q < 2\ m_\pi$ from the measured pion energy distributions of ^{6}Li(e, π^+)^{6}He. The results are compared with the shell-model estimates. In the case of the ground-state transition (M1), the experimental results show an enhancement in the region of $q > 1.6\ m_\pi$. It is not similar to the case of the first excited state transition (M1 + E2 + M3).

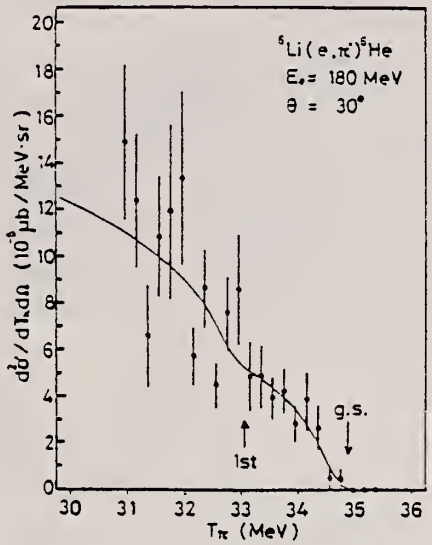

Fig. 1. An example of the energy distribution of pions emitted in the ^{6}Li(e, π^+)^{6}He reaction. Arrows show the end-point pion energies corresponding to the ground and first excited residual state. The best fitted curve is also shown.

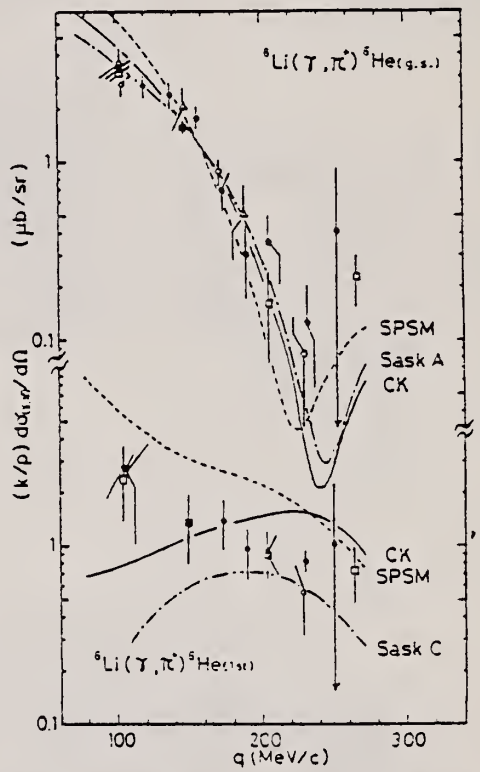

Fig. 2. Experimental results of $(k/p)\ d\sigma_{(\gamma,\pi^+)}/d\Omega$ leaving the ground and first excited residual state. Present results are given by open circles for E_e = 195 MeV (θ = 30°, 60°, 90°), open squares for E_e = 180 MeV (θ = 30°, 90°, 150°), open triangles for E_e = 170 MeV (θ = 30°, 60°, 90°). Closed circles are the previous results of angular distribution measurements (ref. [9]); closed squares are the previous results in the threshold region (ref. [8]). Theoretical curves with SPSM, CK (ref. [12]) and Sask A and C for E_e = 180 MeV are also given.

REF. G.W. Dodson, E.C. Booth, F.L. Milder, B.E. Parad, B.L. Roberts, D.R. Tieger, J. Comuzzi
Phys. Rev. C26, 2548 (1982)

ELEM. SYM.	A	Z
Li	6	3

METHOD

REF. NO. 82 Do 3 egf

REACTION	RESULT	EXCITATION ENERGY	SOURCE TYPE	SOURCE RANGE	DETECTOR TYPE	DETECTOR RANGE	ANGLE
G,PIØ	ABY	THR*20	C	140-155	CKV-I		1PI

Photoproduction of π^0 mesons off targets of ^{6}Li, ^{12}C, ^{28}Si, ^{40}Ca, natural Cd, and natural Pb was studied using a bremsstrahlung beam with endpoint energies of 140, 145, 150, and 155 MeV. Photoproduction from a liquid hydrogen target was employed as a normalization. The measured yields were found to be in disagreement with published theoretical cross sections for ^{6}Li$(\gamma,\pi^0)^6$Li and also in disagreement with a simple schematic model which assumed only coherent contributions from the M_{1+} multipole. The schematic model, however, did approximately predict the relative magnitudes of the yield curves for the energy range 14—20 MeV over threshold.

*MEV ABOVE THR

[NUCLEAR REACTIONS ^{6}Li, ^{12}C, ^{28}Si, ^{40}Ca, Cd, Pb, (γ,π^0); E_γ = 140—155 MeV; measured σ; test of reaction model.]

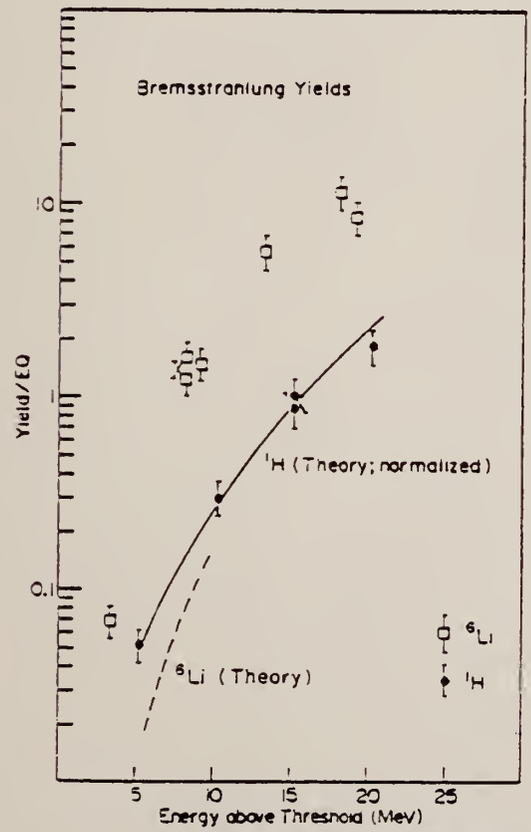

FIG. 5. The experimental and calculated yields for ^{6}Li(γ,π^0) and ^{1}H(γ,π^0). The calculated yield for ^{1}H(γ,π^0) was required to go through the data points at 15.33 MeV above threshold (see text).

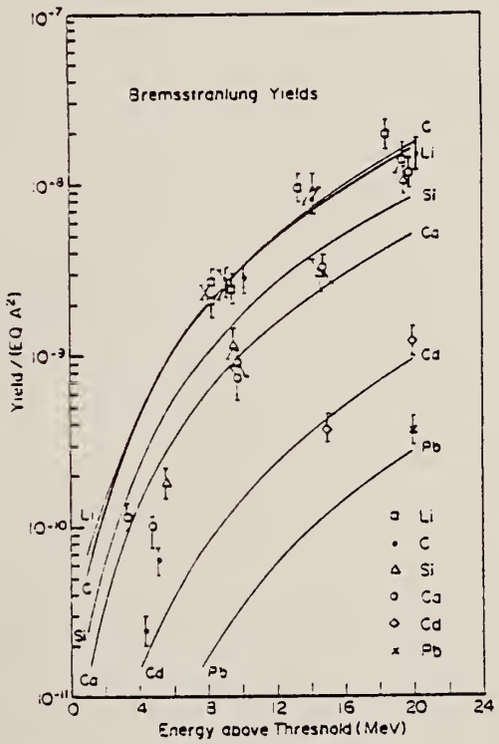

FIG. 6. The experimental and calculated yields for (γ,π^0) off a range of complex nuclei. The data were scaled so that the ^{12}C$(\gamma,\pi^0)^{12}$C experimental yield fit the calculated yield at 9.7 MeV over threshold (see text).

Li
A=7

Li
A=7

Mitsuo Miwa
J. Phys. Soc. Japan 10, 273 (1955)

Li	7	3

METHOD

REF. NO. 55 Mi 1 EGF

REACTION	RESULT	EXCITATION ENERGY	SOURCE		DETECTOR		ANGLE
			TYPE	RANGE	TYPE	RANGE	
G,T	ABX	6 - 19	C	10,20	EMU-D		4PI

r-chamber in lucite monitor.

287

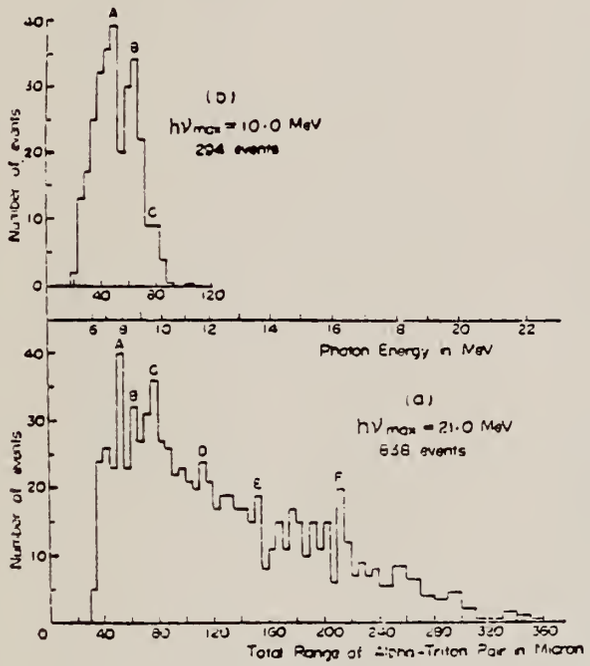

Fig. 2. Total range distribution.

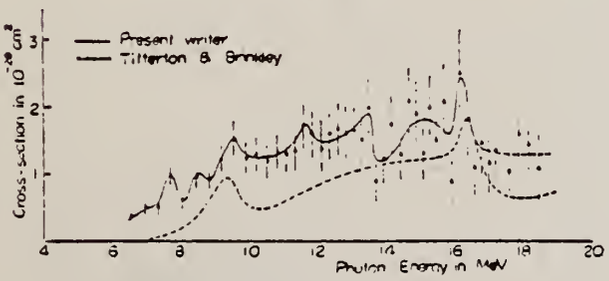

Fig. 3. Excitation function.

REF.

O. Beckman, R. Sandström
Nuclear Phys. 5, 595 (1958)

ELEM. SYM.	A	Z
Li	7	3

METHOD

Van de Graaff; NaI monitor; self-absorption

REF. NO.	
58 Be 3	NVB

REACTION	RESULT	EXCITATION ENERGY	SOURCE		DETECTOR		ANGLE
			TYPE	RANGE	TYPE	RANGE	
G,G	LFT	1	C	1	NAI-D		120
		(477 keV)					

WIDTH

$\tau = (1.1 \pm 0.3) \times 10^{-13}$ sec.

$\Gamma = 6.2 \times 10^{-13}$ eV

Ref. T.A. Romanowski, V.H. Voelker
Phys. Rev. 113, 886 (1959)

Elem. Sym.	A	Z
Li	7	3

Method: Betatron; BF_3 counters

Ref. No.: 59 Ro 1 - JHH

* 293

Reaction	E or ΔE	E_o	Γ	$\int \sigma dE$	Jπ	Notes
$Li^7(\gamma, xn)$	Bremss. 4-20	14				σ_{max}(E = 14 MeV) = 3±0.75 mb

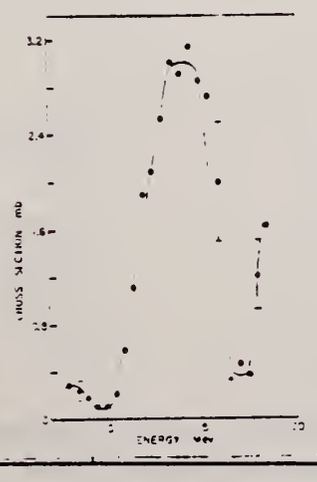

FIG. 6. (γ, n) cross section for Li^7 as a function of γ-ray energy.

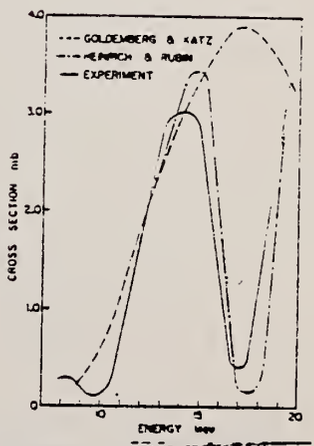

FIG. 7. Comparison of Li^7 cross sections.

[15] J. Goldemberg and L. Katz, Can. J. Phys. 32, 49 (1954).
[16] A. Heinrich and R. Rubin, Helv. Phys Acta 28, 185 (1955).

C.P. Swann, V.K. Rasmussen, F.R. Metzger
Phys. Rev. 114, 862 (1959)

ELEM. SYM.	A	Z
Li	7	3

METHOD
Photon scattering; absorption; NaI spectrometer

REF. NO.
59 Sw 1

NVB'

REACTION	RESULT	EXCITATION ENERGY	SOURCE		DETECTOR		ANGLE
			TYPE	RANGE	TYPE	RANGE	
G,G	LFT	0	D	0	NAI-D		
		(478 keV)		(478 keV)			

LIFETIME

Mean life:

$\tau = (1.15 \pm 0.14)\ 10^{-3}$ sec.

TABLE I. Summary of results for the self-absorption experiments.

Scatterer	Absorber	Resonance absorption (%)	T_{eff} (°K)	τ (10^{-13} sec)
¼ in. LiF	¼ in. LiF	26±4	389	$1.14_{-0.15}$
¼ in. LiF	¼ in. Li	28±2	366	$1.19_{-0.10}$
¼ in. LiF	½ in. Li	48±3	360	$1.21_{-0.10}$
2 in. Li	½ in. Li	52±4	330	$1.11_{-0.1}$

Ref. E.C. Booth
Nuclear Phys. 19, 426 (1960)

Elem. Sym.	A	Z
Li	7	3

Method Van de Graaff; electron bremss.; Ring scatterer; NaI

Ref. No. 60 Bo 3 — JHH

Reaction	E or ΔE	E_o	Γ	$\int \sigma dE$	Jπ	Notes
(γ,γ)	Bremss. 0.5-2.2	0.477			3/2	Mean lifetime t/g: $=(2.8)\times10^{-13}$ sec ±50% (absorption method) $=(2.0)\times10^{-13}$ sec ±50% (resonance scattering) where $g = (1+2I)/(1+2I_o)$.

Ref. V.P. Chizhov
Zhur. Eksp. i Teoret. Fiz. 38, 809 (1960);
Soviet Phys. JETP 11, 587 (1960)

Elem. Sym.	A	Z
Li	7	3

Method: 90 MeV Bremsstrahlung; scintillator counter telescope

Ref. No.: 60 Ch 1 — JHH

Reaction	E or ΔE	E_o	Γ	$\int \sigma dE$	Jπ	Notes
$Li^7(\gamma,p)$						E_d - 15.5 - 31 MeV
$Li^7(\gamma,d)$						E_p - 15.5-30 MeV
$Li^7(\gamma,t)$						E_t - 17-30 MeV
						Angular distribution.
						Ratios:
						$\sigma(\gamma,d)/\sigma(\gamma,p)$ at $\theta = 80^\circ$
						$\sigma(\gamma,t)/\sigma(\gamma,d)$ summed over angles 35°-145°

TABLE I

Element	$100N_t/N_d$	Element	$100N_t/N_d$	Element	$100N_t/N_d$	Element	$100N_t/N_d$
Li^6	30±3	B	39±8	Ni	10±4	In	5±2.5
Li^7	22.5±1.5	Si	10±4	Co	2.5±2	Ta	10±4
Be	13±2.6	S	9±4	Cu	2.2±2	Au	3±3

TABLE II

	$\frac{\sigma_{\gamma p}\cdot 10^{30}, \text{ cm}^2}{\Omega \cdot \text{sr}}$	$\frac{\sigma_{\gamma d}}{\sigma_{\gamma p}}\cdot 10^2$	$\frac{\sigma_{\gamma t}}{\sigma_{\gamma p}}\cdot 10^2$
Li^7	66.0±1.3	6.3±0.55	1.0±0.25
Li^6	82.5±1.3	2.10±0.25	0.70±0.20

YIELD DATA TABLE:

It should be noted that the yield of photoprotons of the energy considered rises smoothly with Z for the elements plotted in Fig. 3, and that starting already with Al, no direct proportionality to Z is observed on account of the effect of the Coulomb barrier. For illustration, we give the yields of photoprotons $Y(\gamma, p)$ per proton in the nucleus for several elements in relative units (the error in these measurements was estimated to be ± 10 %):

	Li^6	Li^7	Be	C	Al	Cu
$Y(\gamma,p) =$	1.49	1.37	1.3	1.31	1.00	0.56

(for Figures see page 2) (continued)

Elem. Sym.	A	Z
Li	7	3

Method

Ref. No. 60 Ch 1

Reaction	E or ΔE	E_0	Γ	$\int \sigma dE$	Jπ	Notes

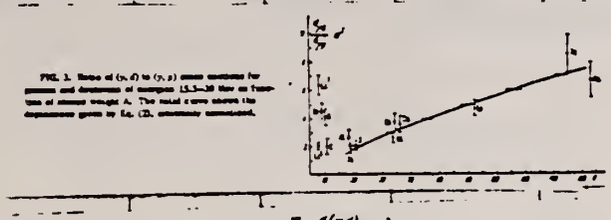

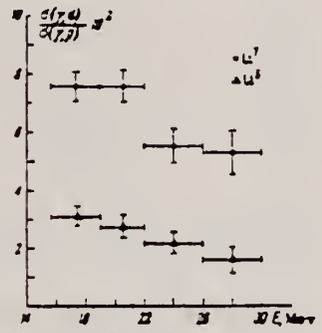

FIG. 4. Dependence of the ratio of (γ, d) to (γ, p) cross sections on the particle energy E for Li^6 and Li^7.

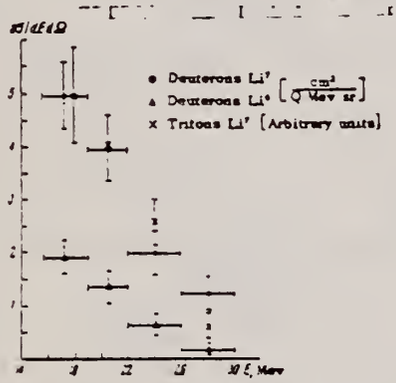

FIG. 5. Energy distributions of photodeuterons from Li^6 and Li^7 and phototritons from Li^7. The scale of the ordinate for phototritons is arbitrary.

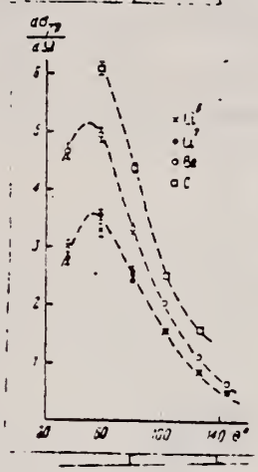

FIG. 6. Angular distributions of photoprotons of energies 15.5–30 Mev for Li^6, Li^7, Be, and C. The errors are statistical.

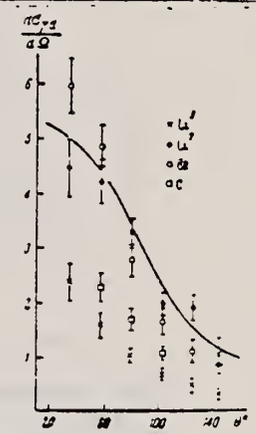

FIG. 7. Angular distributions of photodeuterons of energies 15.5–30 Mev for Li^6, Li^7, Be, and C. The errors are statistical. The solid curve gives the calculated results for photodeuterons from Be.

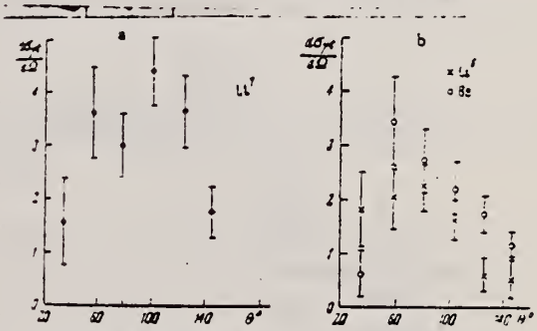

FIG. 9. Angular distributions of phototritons of energies 17–30 Mev for Li^7, Li^6, and Be. a – Li^7; b – Li^6 and Be. The scale is the same in a and b. The errors are statistical.

M. Miwa, M. Yamanouchi
J. Phys. Soc. Japan 15, 947 (1960)

Li	7	3

METHOD: Betatron; triton cross section; angular distribution; nuclear emulsion; r chamber

REF. NO.: 60 Mi 2 | NVB

REACTION	RESULT	EXCITATION ENERGY	SOURCE TYPE	SOURCE RANGE	DETECTOR TYPE	DETECTOR RANGE	ANGLE
G,T	ABX	6-15	C	11-20	EMU-D		DST
			(11,17,18,20)				

$J^{\pi} = 5/2^{+}$ for 8.9 MeV level

J-PI

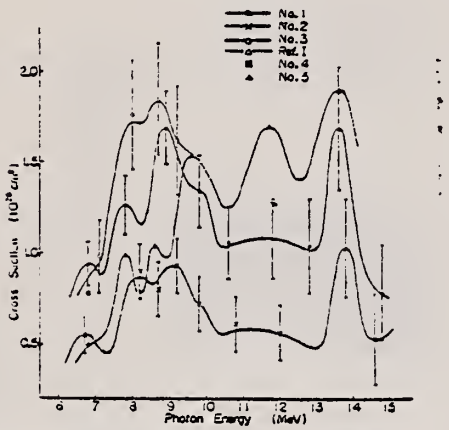

Fig. 2. Excitation function of the reaction ^{7}Li $(\gamma t)^{4}He$.

Table II.

Plate	Resonance Peaks (Mev)					
No. 1	6.8	7.8	8.9	(9.3)		13.5
2	6.7	(7.3)	9.0			(13.8)
3	(7.0)	(8.0)	8.8			
Ref. I		7.6	8.6	9.6	11.7	(13.5)
Ajzenberg and Lauritsen	6.54	7.47		9.6	10.8 12.4	14.0

References

1) M. Miwa: J. Phys. Soc. Japan 10 (1955) 173
2) J. Rotblat: Nature 165 (1950) 287.
3) M. Wächter: Diplomarbeit, E. T. H. (1954).
4) F. Ajzenberg-Selove and T. Lauritsen: Nucl. Phys. 11 (1959) 1.

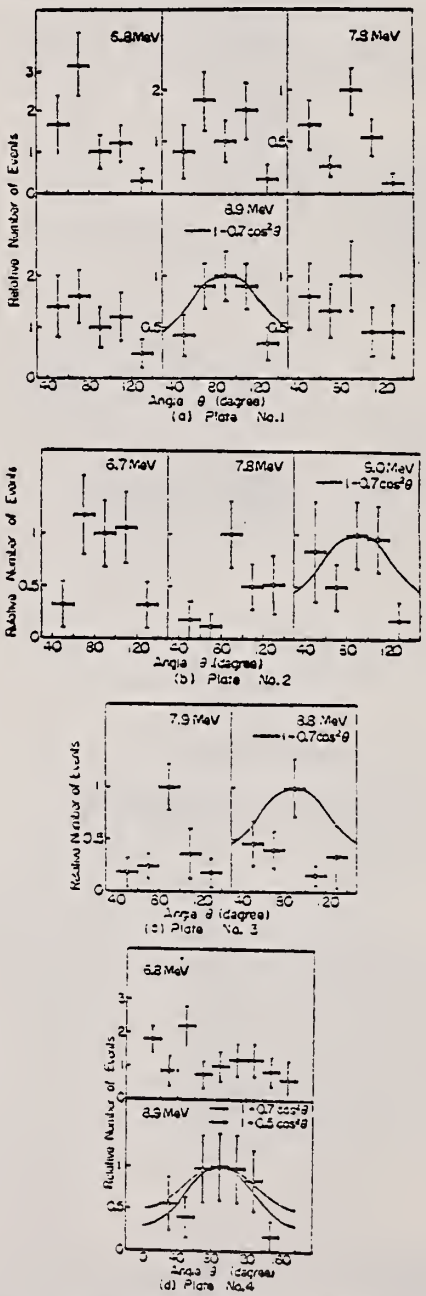

Fig. 3. Angular distribution in the center of mass system of tritons emitted by the reaction $^{7}Li(\gamma s)^{4}He$. Ordinates are in arbitrary units.

Ref. P.C. Stein, A.C. Odian, A. Wattenberg, R. Weinstein
Phys. Rev. 119, 348 (1960)

Elem. Sym.	A	Z
Li	7	3

Method: 320 MeV synchrotron; proton telescope; neutron counter

Ref. No.: 60 St 1 | JHH

Reaction	E or ΔE	E_o	Γ	$\int \sigma dE$	Jπ	Notes
$Li^7(\gamma, np)$	Bremss. 320					$(\sigma/\sigma_{H^2}) = 2.8 \pm 0.3$ ✓73 $[\sigma_{H^2} = 63\ \mu b]$ Mean photon energy - 262 MeV Proton counter at 76°

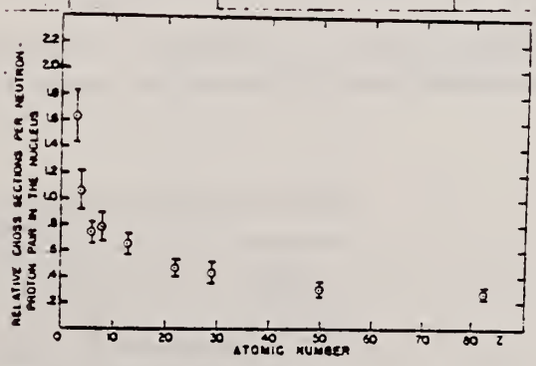

FIG. 2. Relative cross sections per neutron-proton pair in the nucleus versus atomic number. The cross section of the element of interest is divided by the cross section for deuterium and by the factor NZ/A.

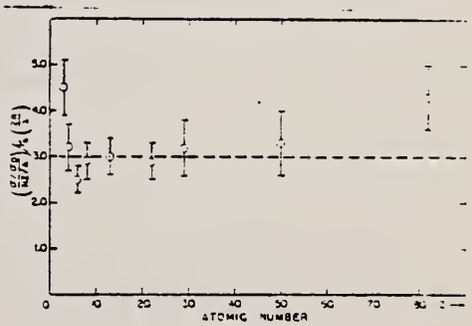

FIG. 3. The relative cross sections per neutron-proton pair corrected for the probability of escape is plotted against atomic number. The probability of escape factor is calculated for $r_0 = 1.30 \times 10^{-13}$ cm and $\lambda = 5.6 \times 10^{-13}$ cm. The probability of escape factor is given in expression (1). The data shown are those of Fig. 2 divided by $P(Z,R,\lambda)$.

REF.

V. G. Shevchenko and B. A. Yurev
Izv. Akad. Nauk SSSR 25, 1269 (1961)

ELEM. SYM.	A	Z
Li	7	3

METHOD

REF. NO. 61 Sh 6 EGF

REACTION	RESULT	EXCITATION ENERGY	SOURCE		DETECTOR		ANGLE
			TYPE	RANGE	TYPE	RANGE	
G,T	ABX	5 - 9	C	10	EMU-D	1 - 4	DST
				(9.5 MeV)			

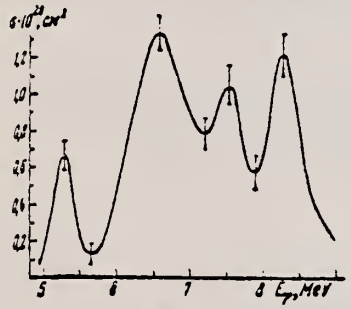

Рис. 3

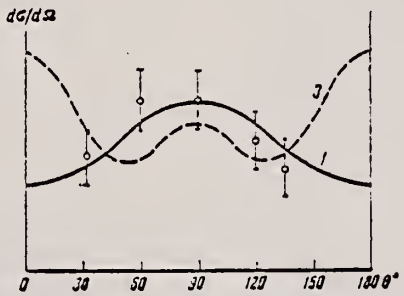

Рис. 4

Рис. 3. Зависимость сечения реакции $Li^7(\gamma, t)He^4$ от энергии γ-лучей

Рис. 4. Угловое распределение тритонов из возбужденного состояния 5,3 MeV Li^7. Сплошная и пунктирная линии, обозначенные цифрами, представляют расчетные угловые распределения, приведенные в табл. 1

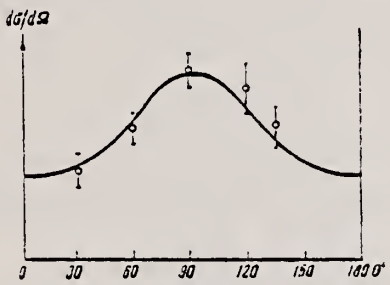

Рис. 5

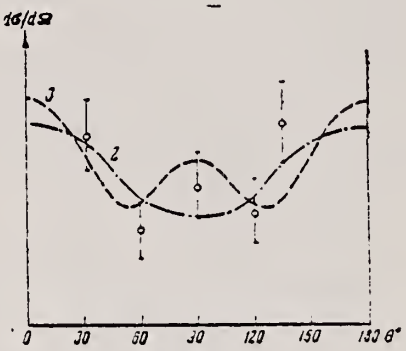

Рис. 6

Рис. 5. Угловое распределение тритонов из возбужденного состояния 6,6 MeV Li^7
(Сплошная линия — кривая 1 на табл. 1)

Рис. 6. Угловое распределение тритонов из возбужденного состояния 8,3 MeV Li^7

Таблица 2

Сравнение расчетных и экспериментальных радиационных ширин уровней Li^7

Энергия уровня, MeV	$\Gamma_{\gamma_{теор}}$, MeV			$\Gamma_{\gamma_{эксп}}$, MeV
	E1	M1	E2	
5,3	$2,2 \cdot 10^{-6}$	$4,2 \cdot 10^{-8}$	$1,1 \cdot 10^{-9}$	$(2,5 \pm 1,2) \cdot 10^{-6}$
6,6	$4,2 \cdot 10^{-6}$	$7,7 \cdot 10^{-8}$	$5,0 \cdot 10^{-9}$	$(0,9 \pm 0,4) \cdot 10^{-6}$
8,3	$1,68 \cdot 10^{-6}$	$0,8 \cdot 10^{-7}$	—	$(1,3 \pm 0,6) \cdot 10^{-7}$

(continued)

REACTION	RESULT	EXCITATION ENERGY	SOURCE		DETECTOR		ANGLE
			TYPE	RANGE	TYPE	RANGE	

Таблица 4

Энергии и квантовые характеристики уровней Li^7 по различным данным

[5]		[6]		Настоящая работа		[3]	
E, MeV	I^π	E, MeV	I^π	E, MeV	I^π	E, MeV	I^π
0	$^3/_2^-$	—	—	—	—	0	$^3/_2^-$
0,478	$^1/_2^-$	—	—	—	—	0,477	$^1/_2^-$
4,63	$^7/_2^-$	4,7	$^5/_2^-$	—	—	4,74	$^7/_2^-$
—	—	5,5	$^5/_2^-,^3/_2^-,^1/_2^-$,	5,3±0,2	$^5/_2^-$	5,50	$^5/_2^-$
6,54	($^1/_2^+$, $^3/_2^+$)	6,8	$^1/_2^+,^5/_2^-,^3/_2^-$, $^1/_2^-,^1/_2^+$	6,6±0,2	$^5/_2^+$	—	—
—	—	—	—	—	—	6,08	$^3/_2^-$
7,47	$^5/_2^-$	(7,4)	—	(7,5±0,25)	—	7,46	$^5/_2^-$
—	—	—	—	—	—	7,76	$^1/_2^-$
—	—	(8,3)	—	8,3±0,3	$^3/_2^-$	8,41	$^3/_2^-$
—	—	(9,0)	—	—	—	8,86	$^1/_2^-$

Литература

1. Inglis D. R., Rev. Mod. Phys., 25, 390 (1953).
2. Kurath D., Phys. Rev., 101, 216 (1956).
3. Бадагоп В. В., ЖЭТФ, 36, № 4, 1123 (1959); Диссертация. МГУ, 1958.
4. Meshkov S., Ufford C. W., Phys. Rev., 101, 734 (1956).
5. Ajzenberg-Selov F., Lauritzen T., Nucl. Phys., 11, N 1, 1 (1959).
6. Erdös P., Stoll P., Wächter M., Watagin V., Nuovo cimento, 12, N 5, 639 (1954).
7. Flowers B. H., Lawson I. D., Fossey E. B., Proc. Phys. Soc., 65B, 286 (1952).
8. Hamburger E. W., Cameron J. R., Phys. Rev., 117, 781 (1960).

Ref. V.P. Chizhov, A.P, Komar, L.A. Kulchitsky, A.V. Kulikov, E.D. Makhnovsky, Yu.M. Volkov
Nuclear Phys. 34, 562 (1962)

Elem. Sym.	A	Z
Li	7	3

Method
90 MeV Synchrotron; magnetic spectrometer; emulsions; NaI counter telescope

Ref. No.
62 Ch 2

JHH

Reaction	E or ΔE	E_0	Γ	$\int \sigma dE$
	Bremss.			
(γ,d)	25			
	43			
(γ,p)	90			

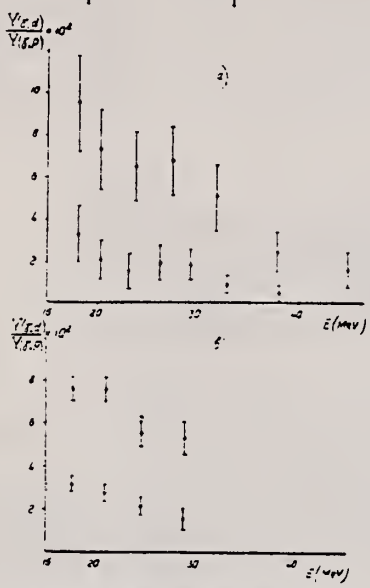

Fig. 5. The ratio of deuteron and proton yields plotted against particle energy [illegible] a) Black circles denote Be^9 and open circles C^{12}. b) Black circles denote Li^7 and open circles [illegible].

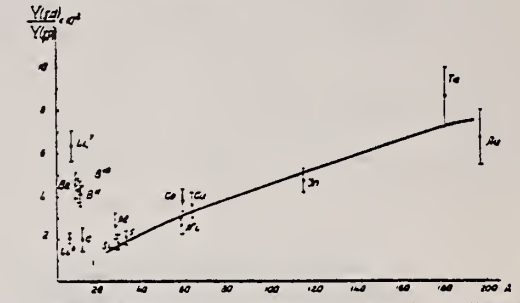

Fig. 6. The ratio of the yields of deuterons and protons with energies 15.5 to 30 MeV depending on the mass number of nuclei A for $E_{\gamma max}$ = 90 MeV. The solid line stands for the normalized dependence (5).

Table 1
Experimental data

Elements	$E_{\gamma max}$ (MeV)	Particle energy interval (MeV)	$\frac{Y(\gamma,d)}{Y(\gamma,p)}$	θ	Method
Li^6	30	7.5 to 15	0.003 ± 0.006	90°	I
	43		0.007 ± 0.003		
	90		0.097 ± 0.014		
Li^7	25	7.5 to 15	0.020 ± 0.030	90°	I
	43		0.038 ± 0.006		
	90		0.160 ± 0.034		
B^{11}	40	7.5 to 19	0.006 ± 0.002	90°	I
Al^{27}	35	2.9 to 10	0.009 ± 0.007	30° – 150°	II
Ca^{40}	35	3.7 to 10	0.038 ± 0.017	30° – 100°	II
$Cu^{63,65}$	34	4.5 to 15	0.007 ± 0.003	90°	I
	34	7.5 to 15	0.007 ± 0.002	90°	I
	70	3 to 10	0.03 ± 0.01	30° – 150°	II
	70	4 to 10	0.04 ± 0.01	30° – 150°	II
	90	7 to 19	0.021 ± 0.003	90°	I

I: Scintillation telescope method.
II. Method of deflecting charged particles in magnetic field.

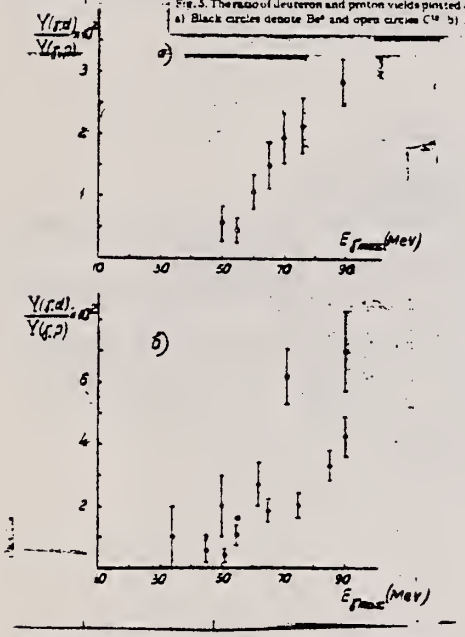

Figure 5: The ratio of deuteron and proton yields with E > 15 MeV plotted against $E_{\gamma max}$. a) Open circles denote Li^6. b) Open circles denote Be and black circles B.

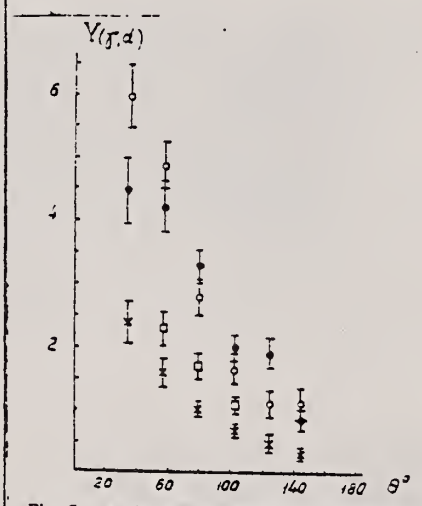

Fig. 7. Angular distributions of photodeuterons with the energies 15.5 to 30 MeV emitted in the photodisintegration by bremsstrahlung with $E_{\gamma max}$ = 90 MeV. Crosses denote Li^6, black circles Li^7, open circles Be, and open squares C. Particle yields are given in arbitrary units.

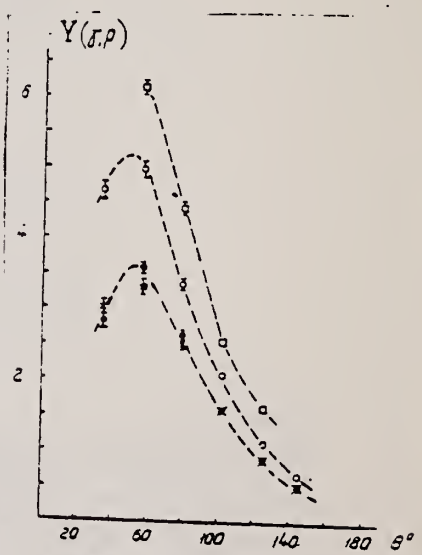

Fig. 8. Angular distributions of photo protons with the energies 15.5 to 30 MeV See caption fig. 7.

Ref. A.G. Gregory, T.R. Sherwood, E.W. Titterton
Nuclear Phys. 32, 543 (1962)

Elem. Sym.	A	Z
Li	7	3

Method 33 MeV electron synchrotron; activation; plastic scintillators for β^- from He^6.

Ref. No. 62 Gr 2 — JHH

Reaction	E or ΔE	E_0	Γ	$\int \sigma dE$	Jπ	Notes
$Li^7(\gamma,p)$	10-32			$\int_0^{34} = 14.6 \pm 3.4$ MeV-mb		291

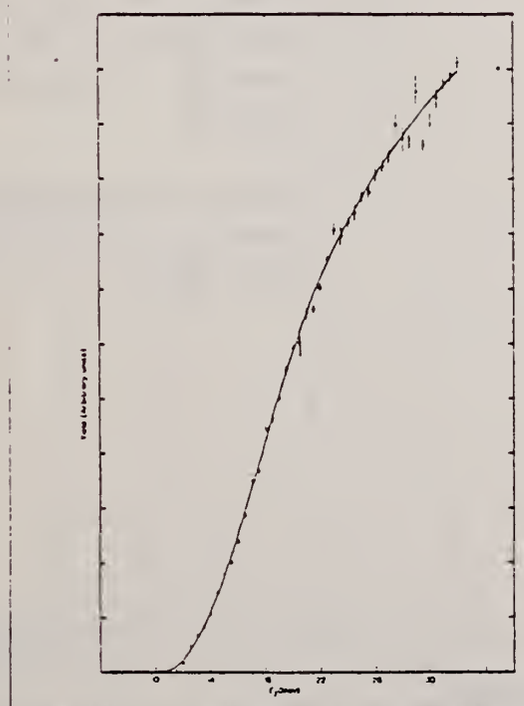

Fig. 6. Yield curve of the reaction $Li^7(\gamma, p)He^6$, as measured from the residual He^6 activity.

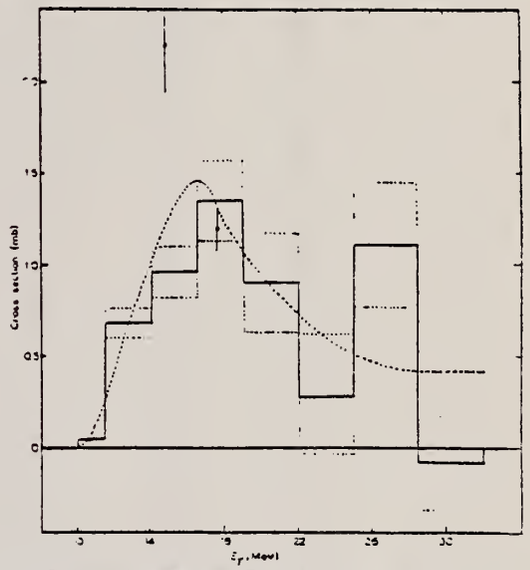

Fig. 6(a). The $Li^7(\gamma, p)He^6$ excitation curve. The dotted smooth curve was derived from the solid curve of fig. 5. The dotted portions of the histogram indicate the magnitudes of the standard deviations. The two points with error bars in (a) represent the results of Titterton and Brinkley [5] obtained for γ radiations of energy 14.8 and 17.8 MeV.

Ref 5: Titterton & Brinkley - Proc. Phys. Soc. 67, 469 (1954)

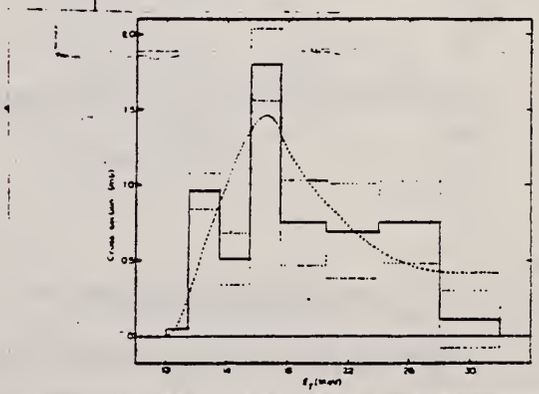

Fig. 6(b). The only difference with fig. 6(a) is that the histogram was obtained by averaging the cross-section over different ranges.

Ref. F.F.Liu, F.J.Loeffler, T.R.Palfrey, Y.S.Kim

Phys.Rev. 128, 2784 (1962)

Elem. Sym.	A	Z
Li	7	3

Method
Synch - defining counter telescope, proton counter telescope - C analyser

Ref. No. 62Lil

BG

Reaction	E or ΔE	E_o	Γ	$\int \sigma dE$	Jπ	Notes
(γ,p)	$E_{\gamma max}$ = 355					Polarization of high energy photo-protons is given in %. Mean proton production energy = 155 MeV. $\theta_p = 45^\circ$ +7.3±15 $\theta_p = 56^\circ$ -2.4±15 Postulates identical γ-absorption process for each kind of nucleus (quasi-deuteron). Fig. 2: Combined results of Li^7, Be^9, B^{11}, C^{12} at 3 angles of measurement. $\theta_p = 90^\circ$ only given for carbon data. Fig. 2: A: Only E1 transitions considered. C: M1 transitions from $^3S_1 - {}^1S_0$ also taken into account. Results consistent both with a zero value for the polarization and also with theory.

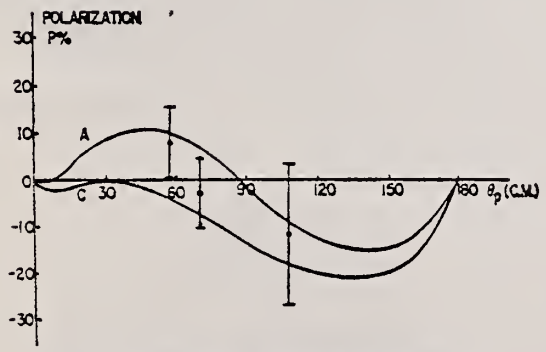

FIG. 2. Comparison of the experimental results with the predicted polarization.

he results for all four elements (by taking a weighted

Ref. W.L. Mouton, J.P.F. Sellschop, R.J. Keddy
Phys. Rev. 128, 2745 (1962)

Elem. Sym.	A	Z
Li	7	3

Method 1.4 MeV electron accelerator; NaI

Ref. No. 62 Mo 1 JHH

Reaction	E or ΔE	E_o	Γ	$\int \sigma dE$	Jπ	Notes
$Li^7(\gamma,\gamma)$	Bremss; 600 kev	480 kev	(5.28±0.27) X 10^{-3}ev			This Γ gives mean lifetime of $t = (1.25\pm0.06) \times 10^{-13}$ sec.

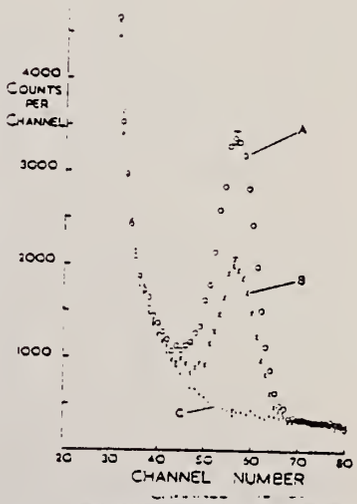

FIG. 2. Results for scattering from lithium. Curve A: lithium scatterer with carbon absorber. Curve B: lithium scatterer with lithium absorber. Curve C: carbon scatterer with lithium absorber.

Ref. A.Kh. Shardanov, V.G. Shevchenko
Zhur. Eksp. i Teoret. Fiz. 42, 1438 (1962);
Soviet Phys. JETP 15, 996 (1962)

Elem. Sym.	A	Z
Li	7	3

Method: 35 MeV betatron ; emulsions

Ref. No.: 62 Sh 1 — BG

Reaction	E or ΔE	E_0	Γ	∫σdE	Jπ	Notes
$Li^7(\gamma,p)$	16.5	12.5	1.3×10^{-5}			394 +
		13.5	4.6×10^{-7}			
		14.3	3.9×10^{-7}			

Table I. Comparison of the calculated and experimental radiation level widths of Li^7 and the results obtained

Level energy, MeV	Γ_γ, MeV				J, π
	Theory			Experiment	
	E1	M1	E2		
12.54	$13\cdot10^{-4}$	—	—	$9.9\cdot10^{-4}$	$3/2^-$
13.54	—	$5.8\cdot10^{-7}$	$8.20\cdot10^{-4}$	$4.65\cdot10^{-7}$	$1/2^-$
14.30	—	$6.75\cdot10^{-7}$	$10.60\cdot10^{-4}$	$3.9\cdot10^{-7}$	$1/2^-$

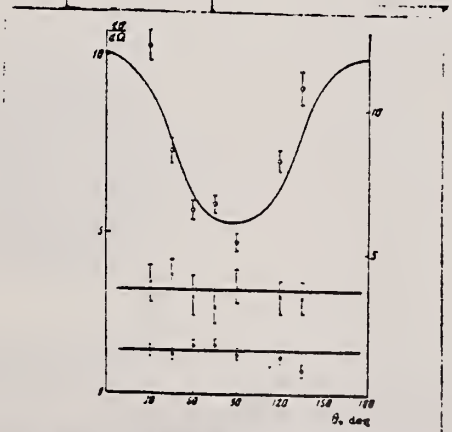

FIG. 2. Angular distributions of photoprotons corresponding to different excited states of the Li^7 nucleus: a — 12.5 MeV, b — 13.5 MeV, c — 14.3 MeV; left-hand ordinate scale corresponds to curve a, right hand — curves b and c.

Cross section curve and energy distribution (histogram) of photoprotons.

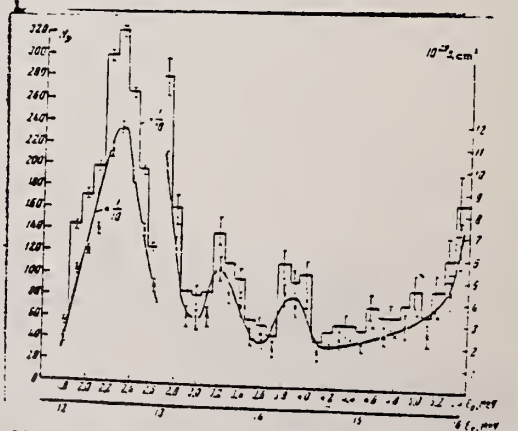

Ref. Yu.M.Volkov, L.A.Kul'chitskii

Zhur.Eksptl. i Teoret.Fiz. 42, 108 (1962)
Soviet Phys.JETP 15, 77 (1962)

Elem. Sym.	A	Z
Li	7	3

Method
- Scintillation counter telescope

Ref. No. 62Vol B G

Reaction	E or ΔE	E_0	Γ	$\int \sigma dE$	Jπ	Notes
	$E_{\gamma max}$ =					
(γ,p)	25					
(γ,d)	43					
(γ,t)	90					

Fig. 4a: Particle energy interval is 7.5 - 15 MeV. $\theta = 90^\circ$.

$Y(\gamma,d)/Y(\gamma,p)$ and $Y(\gamma,t)/Y(\gamma,p)$ are given.

Triton angular distribution has the form $A + B\sin^2\theta$.

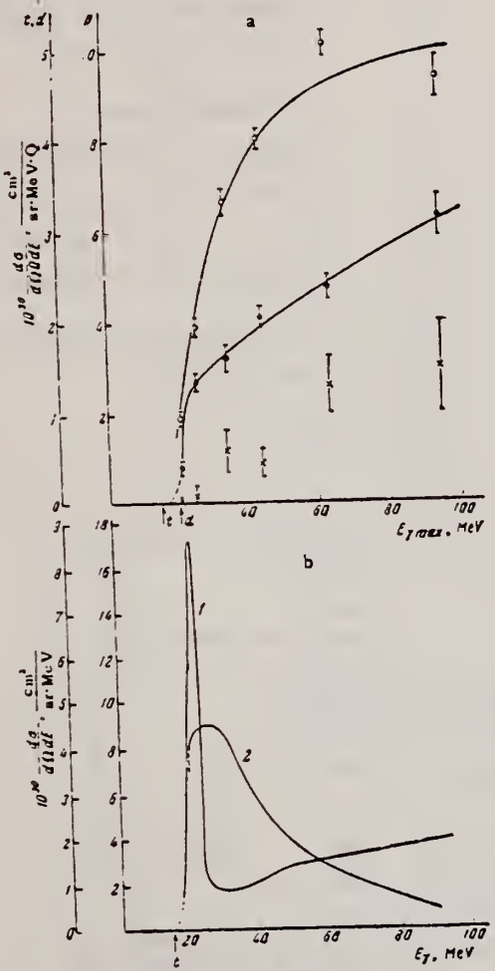

FIG. 4. a) Dependence of cross sections per effective quantum as a function of the energy: ○ – $Li^7(\gamma,p)$, × – $Li^7(\gamma d)$, and ● – $Li^7(\gamma,t)$. The scale along the ordinate axis for the $Li^7(\gamma,p)$ reaction is decreased in half. The arrows d and t denote the thresholds for the $Li^7(\gamma,d)He^5$ and $Li^7(\gamma,t)He^4$ reactions for recording particles of energy 7.5 MeV. b) Excitation function for the reactions $Li^7(\gamma,t)$ (curve 1) and $Li^7(\gamma,p)$ (curve 2).

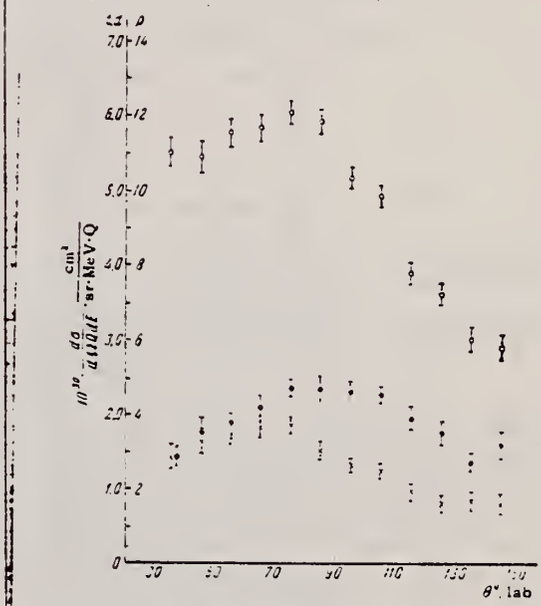

FIG. 5. Angular distribution of protons (○), deuterons (×), and tritons (●) of energy between 7.5 and 15 MeV emitted in the photodisintegration of Li^7 induced by bremsstrahlung with $E_{\gamma max}$ = 63 MeV. For protons the ordinate axis is shown in half scale.

W.C.Barber, J.Goldemberg, G.A.Peterson, Y.Torizuka

Nuclear Phys. 41, 461 (1963); erratum to be published (as of 9/5/63)

Elem. Syst.	A	Z
Li	7	3

Method
Linac (Stanford Mark II) - counter telescope

Ref. No. 63Bal

BG

Reaction	E or ΔE	E_o	Γ	$\int \sigma dE$	Jπ	Notes
(e,e')	41.5		determined see Table II		see Table II and erratum in notes.	inelastic scattering cross section at 180° $(cm^2/sr)x10^{-32}$
		6.9		0.06		0.18±50%
		10.5		0.30		0.78±30%
		14.0		0.27		0.48±40%
						There are known levels at 7.47, 19.8 and 14.0 MeV.
						Erratum: Table II
						line 14: 108 instead of 3.4
						line 15: 6.9 instead of 9.6; and 009 instead of 1.7
						line 16: 0.6 instead of 1.1
						In Fig.5 the label 9.6 MeV should be 6.9 MeV.

TABLE 2

Isotope	Energy of level (MeV)	Spin and parity: Ground state	Spin and parity: Excited state	Inelastic electron scattering cross section (cm^2/sr) x 10^{-33}: Estimated error (%)		Inelastic electron scattering cross section (cm^2/sr) x 10^{-33}: MeV·mb	Radiation width to ground state (eV): This experiment a)	Radiation width to ground state (eV): Weisskopf
$_3Li^6$	3.56	1+	0+	4.0	20	0.42	4.7	0.82
	5.7		0+	0.15	50	0.03	0.9	
			1+				0.3	1.6
			2+				0.16	
	9.3		0+	0.6	30	0.20	15	
			1+				5	16
			2+				3	
	14.0		0+	0.25	30	0.14	24	
			1+				8	38
			2+				5	
	15.8		0+	0.25	50	0.17	37.5	
			1+				12.5	88
			2+				7.5	
$_3Li^7$	9.6	3/2-	1/2-	0.18	50	0.06	3.4	
			3/2-				1.7	18
			1/2-				1.1	
	10.5		3/2-	0.78	30	0.30	19.2	
			1/2-				9.6	23
			3/2-				6.4	
	14.0		5/2-	0.48	40	0.27	31.2	
			3/2-				15.6	38
			1/2-				10.4	
$_7N^{14}$	9.3	1+	0+	0.92	30	0.30	23.4	
			1+				7.8	17
			2+				4.6	
	10.6		0+	0.65	30	0.25	24.6	
			1+				8.2	25
			2+				4.9	
$_8O^{16}$	19.0	0+	1-	0.45	40	0.41	14.1	145
$_9F^{19}$	7.7	1/2+	1/2-	2.0	25	0.54	4.7	9.8
$_{11}Na^{23}$	≈ 9	0+	1+	3.0	20	0.9	7.1	14.5
	≈13		1+	2.0	20	1.0	16.6	48
$_{11}Na^{24}$	3.0	1+	3+	0.2	50	0.02	0.05	0.43
			4+				0.035	
	4.6		3+	0.5	40	0.07	0.43	1.8
	6.1		3+	1.0	40	0.20	4.4	4.8
	8.0		1+	2.5	30	0.68	12.8	10.8
			3+				5.6	
$_{12}Mg^{26}$	11.0	0+	1-	4.4	20	1.76	21.0	29
	≈14		1-	1.5	30	0.83	13.5	58
$_{13}Al^{27}$	4.8	5/2+	3/2+	0.7	30	0.10	1.0	
			5/2+				0.67	2.1
			7/2+				0.50	
	8.0		1-	1.9	30	0.50	14.0	
			3-				9.3	10.8
			5-				7.0	

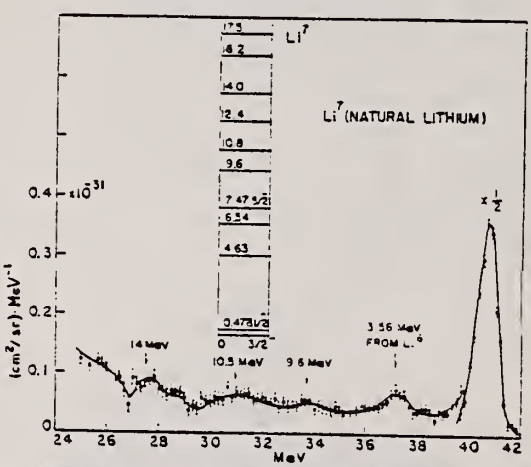

Fig. 5. Spectrum of 41.5 MeV electrons scattered from Li^7 at 180°.

Ref. M. Bernheim, G.R. Bishop
Phys. Letters 5, 294 (1963)

Elem. Sym.	A	Z
Li	7	3

Method Linac; electron scattering; magnetic spectrometer

Ref. No. 63 Be 3 — BG

Reaction	E or ΔE	E_o	Γ	$\int \sigma dE$	Jπ	Notes
$Li^7(e,e')$	100-180	4.63±0.05	93±8			Range of momentum transfer is chosen to given maximum sensitivity to quadrupole transitions.
		5.7±0.1	~ 500			
		6.8±0.1	~ 800		$5/2^-$	Energy resolution 0.3%.
		7.5±0.08	141±20		$5/2^-$	Angular distribution of 6.8 and 5.7 MeV level calculated and measured; comparisons made.
						B = reduced transition probability.
						Inelastic form factors given; compare with theory.

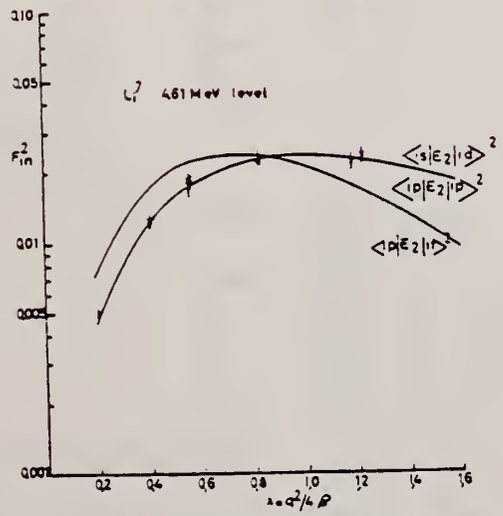

Fig. 2. The inelastic form factor of the transition to the 4.63 MeV level of Li^7. The electric character of the transition is demonstrated by the pairs of points for mixed momentum transfer and scattering angles of 90° and 120°. Comparison with the radial integrals $\langle 1p|J_2(qr)|1p\rangle^2$ and $\langle 1p|J_2(qr)|1f\rangle^2$ shows a preference for the former.

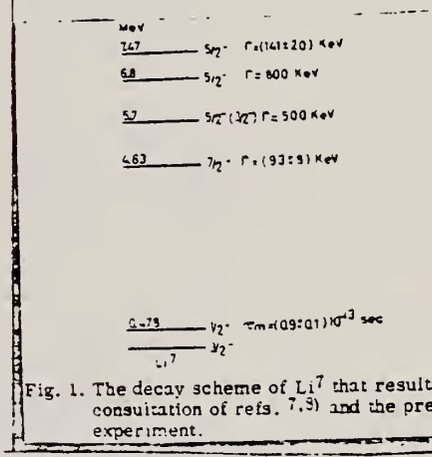

Fig. 1. The decay scheme of Li^7 that results from consultation of refs. [7,8] and the present experiment.

[7] R.S Willey, Nuclear Physics, to be published.
[8] H. Uberall, Phys. Rev. 116 (1959) 221.

Table 2

The values of $B(E2\uparrow)$ are determined by extrapolation to $q^2 = 0$ of a fit to the relation $\frac{3}{2}\langle 1p|J_2(qr)|1p\rangle^2 = \frac{3}{2}x^2 \exp(-2x)$, where $x \equiv \frac{1}{4}q^2a_o^2$ and the oscillator parameter $a_o^2 = 2.95$ fm^2, as determined from the elastic form factor of Li^7. The values of $B(M1\uparrow)$ are determined from the peak cross sections [9] of the reactions $Li^7(\gamma,t)He^4$.

Excitation energy (MeV)	Spin and parity	$B(E2\uparrow)$ (fm^4)	$B(M1\uparrow)$ fm^2	$\delta = \langle E2\rangle/\langle M1\rangle$
4.63 ± 0.05	$\frac{7}{2}^-$	17 ± 1.5	-	-
5.7 ± 0.1	$\frac{5}{2}^+$ or $\frac{3}{2}^+$	4.1 ± 1.5	13×10^{-3}	± 0.055
6.8 ± 0.1	$\frac{5}{2}^+$	12.5 ± 1.3	6.9×10^{-3}	± 0.254
7.5 ± 0.08	$\frac{5}{2}^-$	$2.5^{+0.5}_{-1.0}$	-	-

REF.

M. Bernheim, G.R. Bishop
J. de Physique 24, 970 (1963)

ELEM. SYM.	A	Z
Li	7	3

METHOD: Linac; electron scattering; magnetic spectrometer; Faraday cup and SEM

REF. NO.: 63 Be 8 NVB

REACTION	RESULT	EXCITATION ENERGY	SOURCE		DETECTOR		ANGLE
			TYPE	RANGE	TYPE	RANGE	
E,E/	FMF	0-7	D	100-180	MAG-D		DST
		0.478					
		4.61					
		5.76					
		6.8					

J-PI, B(E2)

Table I for 0.478 level

TABLEAU 1

Énergie incidente MeV	θ	$\frac{q}{f^{-1}}$	$F^2_{\text{inélastique}} \times 10^3$	$F^{2L-S}_{\text{calculé}} \times 10^2$	$F^{2s.p.}_{\text{calculé}} \times 10^2$
147,92	90°	1,060	8,07 ± 0,8	7,91	2,85
121,40	120°	1,066	12,9 ± 1,2	9,86	3,55
121,40	90°	0,870	3,3 ± 1,0	5,87	2,11
147,70	120°	1,297	15,7 ± 1,6	11,07	3,98
177,46	90°	1,272	8,4 ± 1,0	8,44	3,08
101,76	120°	0,893	11,2 ± 1,1	7,26	2,61
146,69	60°	0,743	4,6 ± 1,2	3,92	1,41

TABLEAU 2

Élément	Niveau	$B(E2) \times 10^{-52}$ cm^4
^{7}Li	4,61 MeV 7/2−	15,5 ± 0,8
	5,76 MeV 5/2−	4,1 ± 2
	6,80 MeV 5/2−	12,5 ± 1,2
^{6}Li	2,189 MeV 3+	32 ± 3
	4,52 MeV 2+	18,2 ± 1,5

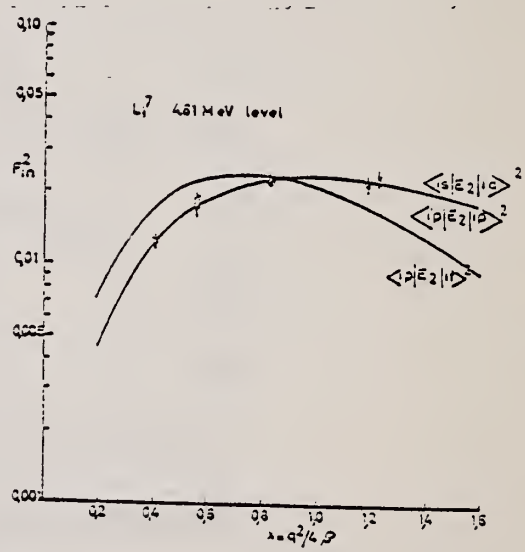

Fig. 1. — Le facteur de forme de la transition quadrupolaire électrique à l'état de 4,61 MeV 7/2− de ^{7}Li. Les courbes théoriques correspondant à

$$\langle 1p|J_2(qr)|1p\rangle^2 = \frac{4}{9}x^2 \exp(-2x) \text{ et à}$$

$$\langle 1p|J_2(qr)|1f\rangle^2 = \frac{5}{9}x^2\left(1-\frac{2}{7}x\right)^2 \exp(-2x).$$

Ref. L.A. Kul'chitskii, Yu. M. Volkov
Zhur. Eksp. i Teoret. Fiz. 44, 1153 (1963)
Soviet Phys. JETP 17, 780 (1963)

Elem. Sym.	A	Z
Li	7	3

Method: 30 MeV Synchrotron; Ar-methane proportional counter telescopes

Ref. No.: 63 Ku 1 JHH

Reaction	E or ΔE	E_o	Γ	$\int \sigma dE$	Jπ	Notes
(γ,p) (γ,Tr)	Bremss.: 20,25,30	E_γ for (γ,Tr) identified as: 14.1 16.2 18.0 19.6 21.5 23.5 25.3				Figure 1a and 1b: Sum of data taken at 54°, 72°, 90°, 108°, and 126°. $E_{\gamma max}$ = 30 MeV. (Figure 1b is smoothe version of Figure 1a). Figure 2: smoothed data θ = 90°. Figure 3: Triton spectrum $E_{\gamma max}$=30MeV

For Figures & Tables see next page.

Elem. Sym.	A	Z
Li	7	3

Method

Ref. No. 63 Ku 1 JHH

Reaction	E or ΔE	E_0	Γ	$\int \sigma dE$	Jπ	Notes

Table I

Proton energy interval, MeV	Proton angular distribution $a + b\sin^2\theta(1 + \gamma\cos\theta)^2$		Proton energy interval, MeV	Proton angular distribution $a + b\sin^2\theta(1 + \gamma\cos\theta)^2$	
	a/b	γ		a/b	γ
3.8—4.2	2.8±0.5	0.4±0.1	7.7—8.3	1.43±0.30	0.35±0.1
4.5—4.9	—5.0±0.7	—	8.6—9.2	0.28±0.04	0.08±0.1
5.2—5.7	3.2±0.7	0.25±0.1	9.4—10.0	1.35±0.25	0.24±0.1
5.8—6.4	0.57±0.07	0.135±0.1	10.2—10.8	1.28±0.25	0.23±0.1
6.6—7.2	0.61±0.08	0.20±0.1	11.0—12.1	0.89±0.15	0.0±0.1

Table II

Triton energy interval, MeV	Triton angular distribution $a + b\sin^2\theta(1 + \gamma\cos\theta)^2$	
	a/b	γ
6.7—7.2	—0.07±0.12	—0.05±0.05
7.4—8.4	0.15±0.13	—0.2±0.1
8.6—11.4	0.023±0.08	—0.05±0.05
11.8—12.8	0.50±0.15	—0.3±0.1
8.7—12.6	0.1±0.08	—0.12±0.1
7.5—15 [*]	0.4±0.07	—

Table III

Particle	$\frac{d\sigma}{d\Omega dE_\gamma Q} \cdot \frac{cm^2}{sr\text{-}MeV\text{-}Q}$		
	$E_{\gamma\,max}$ = 20 MeV	$E_{\gamma\,max}$ = 25 MeV	$E_{\gamma\,max}$ = 30 MeV
p	2.7±0.3	8.6±0.4	12.7±1.2
d	0.11±0.03	0.40±0.12	0.80±0.3
t	1.38±0.34	1.38±0.12	1.56±0.2

Table IV

E_t, MeV	E_γ, MeV	Energy level of Li^7 [*]	E_t, MeV	E_γ, MeV	Energy level of Li^7 [*]
6.6±0.2	14.1±0.3	14.0	10.0±0.2	(21.5±0.3)*	(21.5)
7.8±0.2	16.2±0.3	16.2	12.1±0.2	(23.5±0.3)	(23.5)
9.0±0.2	18.0±0.3	17.5	13.0±0.2	(25.3±0.3)	—
9.8±0.2	19.6±0.3	—			

*Less reliable values are given in parentheses.

Table V

Proton group energy, MeV	% of protons accompanying transitions to second and higher excited states of He^4		Proton group energy, MeV	% of protons accompanying transitions to second and higher excited states of He^4	
	$E_{\gamma max}$ = 25 MeV	$E_{\gamma max}$ = 30 MeV		$E_{\gamma max}$ = 25 MeV	$E_{\gamma max}$ = 30 MeV
3.8	50*	50*	6.80	28	40
4.6	90	90	7.70	30	50
5.25	75	85	8.60	45	85
5.85	34	60	10.20	0	45

*% of protons accompanying transitions to the third and higher excited states of He^4.

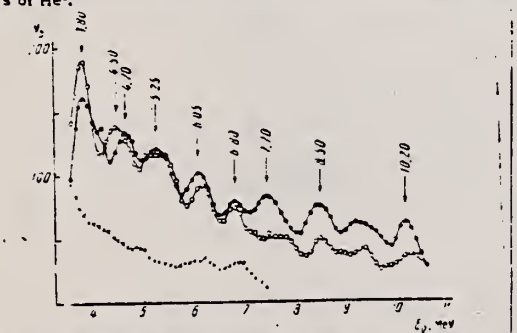

FIG. 2. Smoothed energy spectra of photoprotons from Li^7 for $E_{\gamma max}$ = 20 MeV (x), 25 MeV (o), and 30 MeV (•). Ordinates represent the proton yield (in arbitrary units) relative to an identical total γ-ray energy. The arrows indicate the spectral peaks.

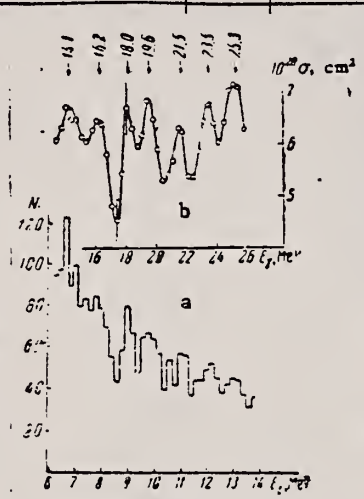

FIG. 3

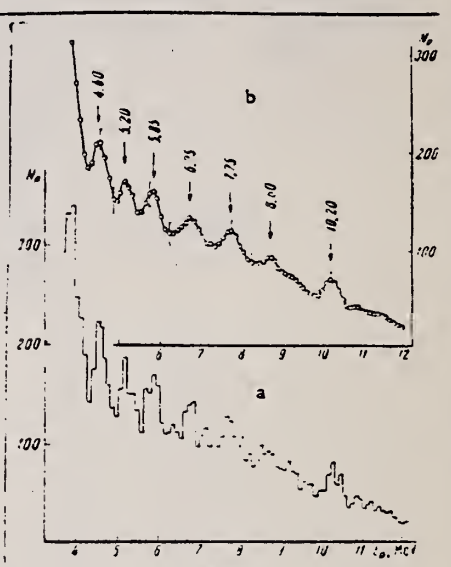

FIG. 1

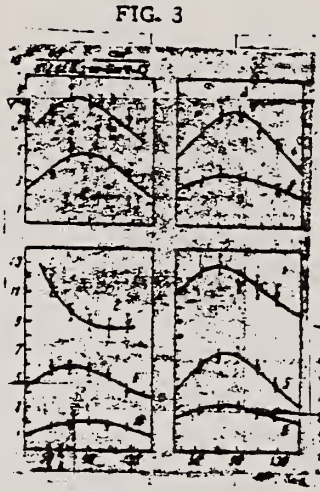

FIG. 5. Angular distributions of phototritons from $Li^7(\gamma, t)He^4$. Ordinates represent the reaction cross section in arbitrary units at $E_{\gamma max}$ = 30 MeV in different energy intervals: a – 6.7–7.2 MeV; b – 7.4–8.4 MeV; c – 8.6–11.4 MeV; d – 11.8–12.6 MeV. The continuous curves for the first energy interval were obtained using the formulas $\sin^2\theta$ and $1 + \sin^2\theta$; for the other intervals the curves were obtained by least squares from the formula $a + b\sin^2\theta(1 + \gamma\cos\theta)^2$.

FIG. 4. Angular distributions of protons from Li^7 photodisintegration at $E_{\gamma max}$ = 30 MeV for different energy intervals: 1 – 3.8–4.2 MeV; 2 – 4.5–4.9 MeV; 3 – 5.2–5.7 MeV; 4 – 5.8–6.4 MeV; 5 – 6.6–7.2 MeV; 6 – 7.7–8.3 MeV; 7 – 8.6–9.2 MeV; 8 – 9.4–10.0 MeV; 9 – 10.2–10.8 MeV; 10 – 11.0–12.1 MeV. The smooth curves were obtained by least squares using the formulas $a + b\sin^2\theta(1 + \gamma\cos\theta)^2$. Ordinates represent the differential cross section per effective quantum.

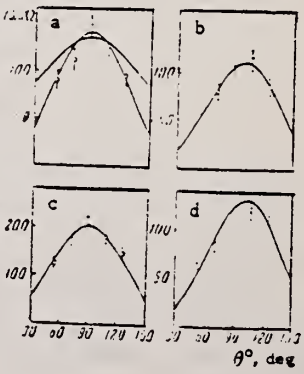

Ref. W.L. Mouton, J.P.F. Sellschop, G. Wiechers

Phys. Rev. 129, 361 (1963)

Elem. Sym.	A	Z
Li	7	3

Method
γrays from Co^{60} ; Compton scattering from Cu - NaI (Tl)

Ref. No. 63Mo1

BG

Reaction	E or ΔE	E_o	Γ	$\int \sigma dE$	$J\pi$	Notes
(γ,γ)	.21 -1.33	480KeV	4.42×10^{-3} eV(calculated)			Compton scattering to obtain variable and well defined energy from mono-energetic source discussed.

Ref. B.M.K. Nefkens
Phys. Rev. Letters 10, 55 (1963)

Elem. Sym.	A	Z
Li	7	3

Method: Synchrotron; β^- radioactivity of H^5

Ref. No.: 63 Ne 1 JHH

Reaction	E or ΔE	E_o	Γ	$\int \sigma dE$	Jπ	Notes
$Li^7(\gamma,2p)$	Bremss. 320					σ = 1.8±0.6μb (ABY) 1/2 life of H^5 = 110±30 m. sec.

REF.

G. R. Bishop and M. Bernheim
Phys. Letters 8, 48 (1964)

ELEM. SYM.	A	Z
Li	7	3

METHOD

Linac $Li^7(e,e')H^3 + He^4$

Page 1 of 2

REF. NO. 64 Bi 4 JOC

REACTION	RESULT	EXCITATION ENERGY	SOURCE		DETECTOR		ANGLE
			TYPE	RANGE	TYPE	RANGE	
E,E/	ABX	1 - 6	D	150	MAG-D		DST

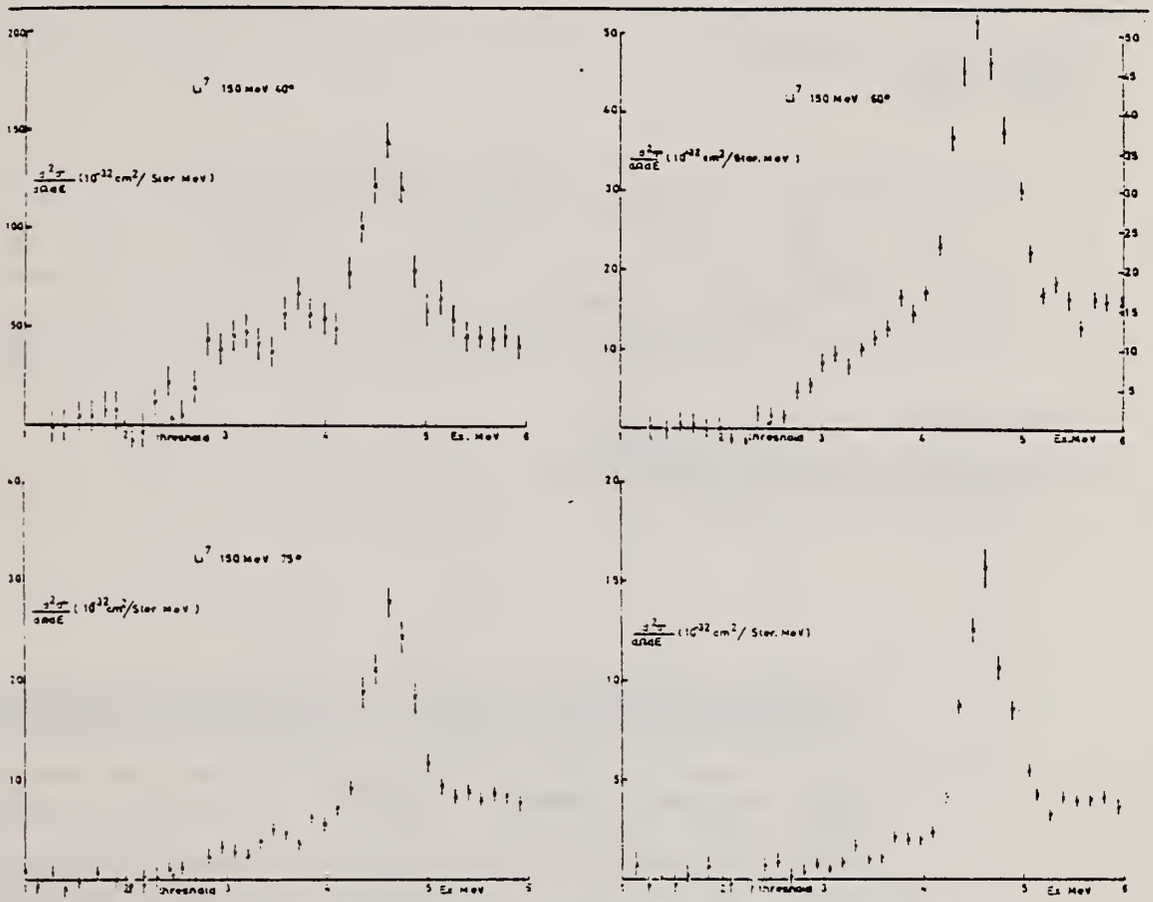

Fig. 1. The inelastic electron scattering spectra obtained for a nominal incident energy of 150 MeV on a target of Li^7 at angles of 40°, 60°, 75° and 90°. The exact incident energy is given in table 2. These curves are obtained after subtraction of the radiative tail of the elastic peak which is not shown.

(continued)

REACTION	RESULT	EXCITATION ENERGY	SOURCE		DETECTOR		ANGLE
			TYPE	RANGE	TYPE	RANGE	

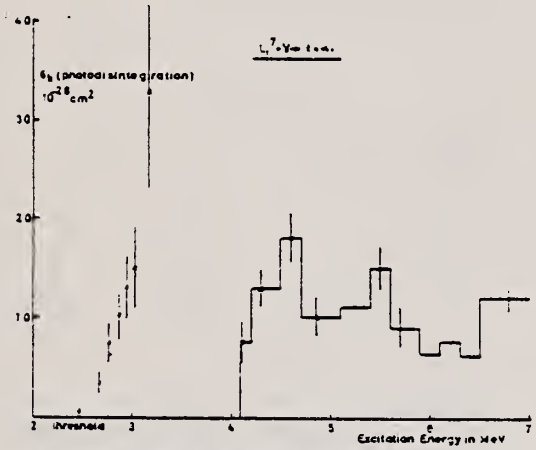

Fig. 2. The cross section of the photoreaction $Li^7(\gamma, \pi)t$ constructed as described in the text.

Table 2
The cross sections obtained from the spectra of fig. 1 for the peak at 4.63 MeV excitation energy, and the integrated cross section from threshold to the 4.63 MeV peak. The units of cross section are cm^2/steradian. The corresponding inelastic form factors are obtained after division by $\sigma_{point} = (Ze^2/2E)^2(\cos^2\frac{1}{2}\theta/\sin^4\frac{1}{2}\theta)$.

Incident energy (MeV)	Scattering angle θ^o	Integrated cross section 4.63 MeV level	Integrated cross section before 4.63 MeV level	F^2_{in} (4.63)	F^2_{in} (< 4.63)	$q^2 f^{-2}$
148.9	40°	9.71×10^{-31}	7.55×10^{-31}	7.15×10^{-3}	5.56×10^{-3}	0.266
149.2	60°	3.86×10^{-31}	1.66×10^{-31}	1.54×10^{-2}	6.59×10^{-3}	0.572
148.2	75°	1.78×10^{-31}	6.79×10^{-32}	1.83×10^{-2}	6.99×10^{-3}	0.838
147.9	90°	9.53×10^{-32}	2.36×10^{-32}	2.23×10^{-2}	5.53×10^{-3}	1.124

E. O. Booth, B. Chasan and K. A. Wright
Nucl. Phys. 57, 403-420 (1964)

Li	7	3

OD
Van de Graaff; resonance fluorescence

REF. NO. 64 Bo 1 | NVB

REACTION	RESULT	EXCITATION ENERGY	SOURCE TYPE	SOURCE RANGE	DETECTOR TYPE	DETECTOR RANGE	ANGLE
G.G	LFT	1-3	C	1 - 3	NAI-D		100
		(0.5 - 3.0)		(0.5 - 3.0)			

ABI

TABLE I
Cases of observed resonance fluorescence

Nucleus multipol.	State (MeV)	Spin	Γ_0/Γ	$\tau(\sigma w\Gamma_0^2/\Gamma^2)^{-1}$ (sec).	Mean lifetime τ BCW (sec)	Mean lifetime τ other (sec)	Ref.	Γ_0/Γ_W BCW
Li^7	0.00	$\frac{3}{2}^-$						
M1	0.48	$\frac{1}{2}^-$	1	absorption	$9.3\pm1.3\times10^{-14}$	$10.9\pm1\times10^{-14}$	7)	2.4

REF.	ELEM. SYM.	A	Z
L. Green, D. J. Donahue Phys. Rev. 135, B701-05 (1964)	Li	7	3

METHOD	REF. NO.	
Reactor; neutron capture gamma rays	64 Gr 2	NVB

REACTION	RESULT	EXCITATION ENERGY	SOURCE		DETECTOR		ANGLE
			TYPE	RANGE	TYPE	RANGE	
G,N	ABX	THR-11	D	THR-11	BF3-I		4PI

WIDTH 729

Enriched to 99.99% Li^7.
Ground-state radiative width of 7.47 MeV level,

$$\Gamma_\gamma^o = 0.9 \pm 0.4 \text{ eV}$$

TABLE II. Summary of measured cross sections (millibarns).

Source	Energy[a] (MeV)	Targets Ta^{181}	Li^7	Li^6	C^{13}	B^{10}
Aluminum	7.72	4.1± 0.4	0.06 ±0.01	1.13±0.12	1.7 ±0.2	···
Copper	7.91	10.8±1.0	0.07 ±0.01	1.1 ±0.2	0.97±0.13	···
Chlorine	8.56	29 ± 6	0.17 ±0.12	···	···	···
Nickel	9.00	44 ± 6	0.16 ±0.06	1.6 ±0.3	0.6 ±0.1	0.11±0.01
Nitrogen	10.83	121 ±12	1.07 ±0.25	···	4 ±2	0.9 ±0.2
Chromium	9.72	84 ±25	0.55 ±0.25	···	···	0.23±0.05
Iron	7.64	0.0± 0.9	0.079±0.014	1.3 ±0.2	0.23±0.05	···
Iron	9.30	···	···	···	···	0.09±0.03
Lead	7.38	···	0.068±0.035	1.2 ±0.2	0.3 ±0.3	···
Sulphur	5.43	···	···	0.42±0.07		
Sodium	6.41	···	···	0.6 ±0.1		
Titanium	6.75	···	···	1.3 ±0.2	···	···
Titanium	6.61[b]	···	···	···	0.32±0.04	···
Manganese	7.16[c]	···	···	0.9 ±0.1	0.4 ±0.1	
Zinc	7.88	···	···	1.0 ±0.2	1.2 ±0.2	

[a] Energies taken from Refs. 4 and 5.
[b] Weighted average of 6.75-, 6.55-, and 6.41-MeV γ rays.
[c] Weighted average of 7.26-, 7.15-, and 7.05-MeV γ rays.

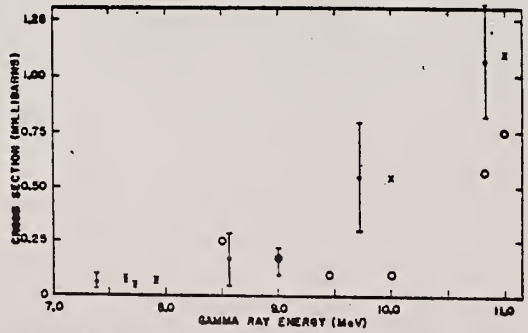

FIG. 3. Energy versus cross section, $Li^7(\gamma,n)$. Crosses are data of Goldemberg and Katz (Ref. 3), circles are data of Romanowski and Voelker (Ref. 12).

REF.

B.M.K. Nefkens and G. Moscati
Phys. Rev. 133, B17-19 (1964)

ELEM. SYM.	A	Z
Li	7	3

METHOD	REF. NO.	
Betatron	64 Ne 1	NVB

REACTION	RESULT	EXCITATION ENERGY	SOURCE		DETECTOR		ANGLE
			TYPE	RANGE	TYPE	RANGE	
G,H4	ABY	23 - 250	C	250	ACT-I		4PI

NØ H4 FOUND

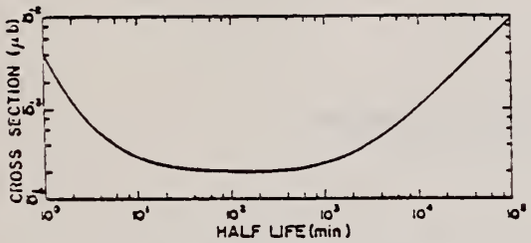

FIG. 2. Upper limit of the production cross section σ_γ versus half-life of H^4.

TABLE II. Production cross section for comparable reactions on light nuclei.

Reaction	E_γ (max)	σ_γ in μb	$-Q$ in MeV	Ref.
$He^4(\gamma,pn)d$	170	200	26	a
$He^4(\gamma,2pn)$	170	26	28	a
$Li^7(\gamma,2p)H^5$	320	1.8	31	b
$B^{11}(\gamma,2p)Li^9$	320	37	31	d
$N^{14}(\gamma,2p)$	170	250	25	e
$(\gamma,2pn)$	170	200	28	e
$O^{16}(\gamma,2p)$	170	500	22	e
$(\gamma,2pn)$	170	240	30	e
$Ne(\gamma,2p)$	170	590	21	e
$(\gamma,2pn)$	170	200	29	e
$F^{19}(\gamma,2p)N^{17}$	320	100	24	f
$F^{19}(\gamma,2pn)N^{16}$	303	100	24	g
$Li(\gamma,\ )H^4$	250	$<5\times10^{-3}$ a $<2\times10^{-1}$ b		This work

a Assuming that the half-life of H^4 is 1 year.
b Assuming that the half-life of H^4 is 1 h.
a A. N. Gorbunov and V. M. Spiridonov, Zh. Eksperim. i Teor. Fiz. 33, 21 (1957) [translation: Soviet Phys.—JETP 6, 16 (1958)].
b B. M. K. Nefkens, Phys. Rev. Letters 10, 243 (1963).
d A. N. Gorbunov, V. A. Dubrovina, V. A. Osipova, V. S. Silaeva, and P. A. Čerenkov, Zh. Eksperim. i Teor. Fiz. 42, 747 (1962) [translation: Soviet Phys.—JETP 15, 520 (1962)].
e G. W. Tautfest, Phys. Rev. 110, 708 (1958).
f R. A. Meyer (private communication).

N. K. Sherman and P. Barreau
Phys. Letters 9, 151 (1964)

ELEM. SYM.		
Li	7	3

METHOD

Linac β-activity from H^5

REF. NO.	
64 Sh 1	JOC

REACTION	RESULT	EXCITATION ENERGY	SOURCE		DETECTOR		ANGLE
			TYPE	RANGE	TYPE	RANGE	
G,2P	ABX	THR - 210	C	210	ACT-I		90

H^5 LIMIT

Limits

either $t(H^5) \gg 0.1$ sec,

or $t(H^5) \leq 3$ msec,

or $t(H^5) \sim 0.1$ sec and $\bar{\sigma}(H^5) \leq 0.2$ μb/equiv. quantum.

REF.

P. E. Argan, L. Meneghetti and S. Vitale
Il Nuovo Cimento 38, 1489 (1965)

ELEM. SYM.	A	Z
Li	7	3

METHOD

REF. NO. 65 Ar 2 JOC

REACTION	RESULT	EXCITATION ENERGY	SOURCE		DETECTOR		ANGLE
			TYPE	RANGE	TYPE	RANGE	
G,2P	ABY	THR-1BEV	D	1BEV	ACT-I		4PI

NO H^5 SEEN

σ for $H^5 < 1.3 \pm 0.4 \times 10^{-31}$ cm^2

REF.

B. T. Chertok and E. C. Booth
Nuclear Phys. 66, 230 (1965)

ELEM. SYM.	A	Z
Li	7	3

METHOD

REF. NO.	
65 Ch 1	EGF

REACTION	RESULT	EXCITATION ENERGY	SOURCE		DETECTOR		ANGLE
			TYPE	RANGE	TYPE	RANGE	
E,E'	ABX	.5	D	2 - 4	D MAG	2-3	162

ABX based on elastic peak and Mott scattering σ.

$\frac{d\sigma}{d\Omega}$ (3.0 MeV, 162°) = (3.0 ± 1.2) x 10^{-2} μb/sr, for 0.478 MeV state.

P. J. Dallimore, K. S. Lam and H. H. Thies
Aust. J. Phys. 18, 389 (1965)

ELEM. SYM.	A	Z
Li	7	3

METHOD

REF. NO.	
65 Da 1	JOC

REACTION	RESULT	EXCITATION ENERGY	SOURCE		DETECTOR		ANGLE
			TYPE	RANGE	TYPE	RANGE	
G,T	ABY	THR-4	C	4	SCD-D		90

$\bar{\sigma} < (1.55 \pm .20) \times 10^{-38}$ cm^2

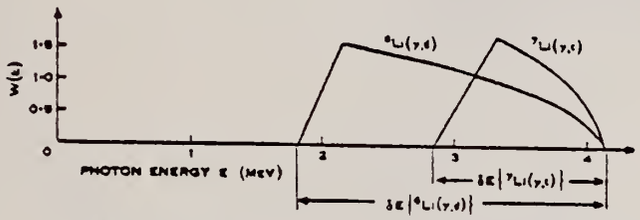

Fig. 2.—Weighting functions employed in the calculation of upper limits of the average reaction cross sections $\bar{\sigma}$, where

$$\bar{\sigma} = \frac{1}{\delta E} \int_{4{\cdot}1\ \mathrm{MeV} - \delta E}^{4{\cdot}1\ \mathrm{MeV}} W(E)\sigma(E)\,dE.$$

E. Hayward and T. Stovall
Nuclear Phys. 69, 241 (1965)

Li	7	3

METHOD

REF. NO. 65 Ha 1 EGF

REACTION	RESULT	EXCITATION ENERGY	SOURCE TYPE	SOURCE RANGE	DETECTOR TYPE	DETECTOR RANGE	ANGLE
G,XN	ABX	THR - 30	C	6-30	BF3-I		4PI

575

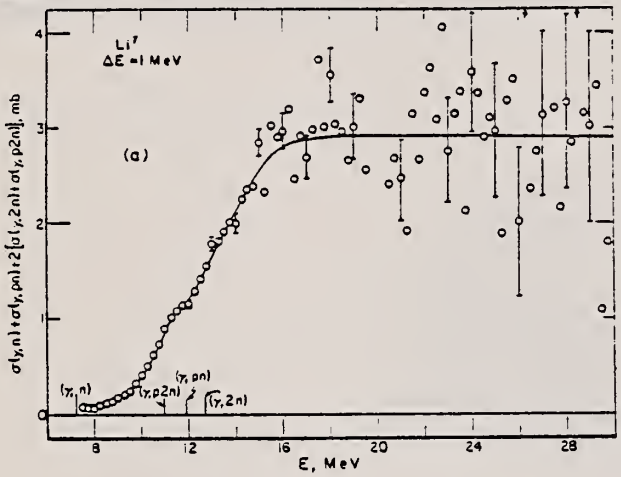

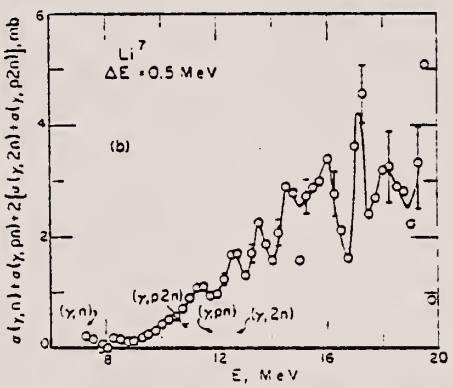

Fig. 4. The neutron production cross section for Li^7 where the analysis has been made using a 1 MeV grid (a) and a 0.5 MeV grid (b). Thresholds for the neutron producing cross sections are indicated by vertical lines at the bottom (a) and by dotted vertical lines at the bottom (b). The indicated errors are standard deviations based only on the number of counts. The arrows at the top represent points that exceed the dimensions of the graph, and the horizontal line is the average value of the cross section above 20 MeV.

TABLE 3

Neutron emission cross sections integrated to 29 MeV

Target	$\int \sigma dE$ (MeV · mb)	$\int \sigma dE/(60NZ/A)$	$\int^{30} \sigma dE/(60NZ/A)$ [a]
Li^6	36.1	0.40±0.03 [b]	0.42
Li^7	50.1	0.49±0.04	0.64
B^{10}	66.7	0.44±0.03	
B^{11}	68.6	0.42±0.03	0.47 [c]
O^{16}	61.9	0.26±0.02	0.30

[a]) Ref. [12]).
[b]) This value is for natural boron.
[c]) Estimated systematic errors.

216

FORM NBS-418
(REV. 7-14-64)
USCOMM-DC 28010-P64

FIERCE CARDS

A. Wataghin, M. Scotto and G. Paoli
Il Nuovo Cimento 40-B, 441 (1965

Li	7	3

METHOD

REF. NO. 65 Wa 1 JOC

REACTION	RESULT	EXCITATION ENERGY	SOURCE		DETECTOR		ANGLE
			TYPE	RANGE	TYPE	RANGE	
G,XN	SPC	THR-25	C	25	EMU	2 - 13	90

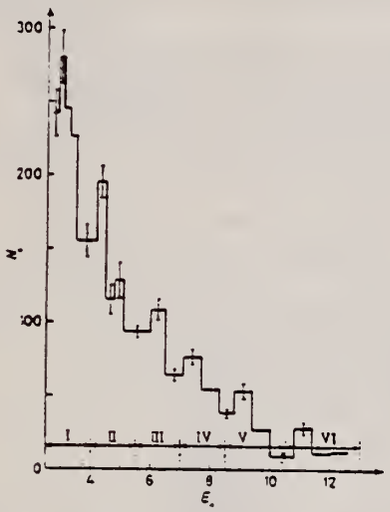

Fig. 1. – Neutron normalized energy spectra. The energy range is divided in six parts, and six corresponding spectra (with different resolutions) are given. N_n is in arbitrary units.

TABLE I.

Position of maximum in E_n spectrum (this work)	Energy levels of ^{7}Li, MeV			
	From our results (transitions to ground state)	From ref. (3)	From ref. (2)	From ref. (4)
3.0 ± 0.1	10.7 ± 0.1	10.8	—	—
4.35 ± 0.15	12.3 ± 0.2	12.4	12.3	—
6.25 ± 0.25	14.4 ± 0.3	14.0	14.3	—
7.5 ± 0.3	16.0 ± 0.35	16.2	16.2	16.3
9.1 ± 0.3	17.8 ± 0.35	17.5	(17.1) (18.1)	—
11.1 ± 0.3	20.1 ± 0.35	21.5	—	—

REF. H. Artus, P. Brix, H. G. Clerc, F. Eigenbrod, A. Goldmann, F. Gudden, E. Spamer, P. Strehl, M. Stroetzel, O. Titze, and K. J. Wetzel
Proc. Gatlinburg Conference, 314 (1966)

Li	7	3

METHOD

REF. NO. 66 Ar 2 hmg

REACTION	RESULT	EXCITATION ENERGY	SOURCE TYPE	SOURCE RANGE	DETECTOR TYPE	DETECTOR RANGE	ANGLE
E,E/	LFT	11	D	30-60	MAG-D		DST
		(11.28)					

11=11.28 MEV

TABLE I

Summary of Experimental Results[a]

Nuclide	E_r (MeV)	Type	Γ_γ^0(eV)	Γ_γ^0/Γ_w	R_w (F)
^{6}Li	2.18	E2	(3.9 ± 0.5) × 10^{-4}	14.4	3.77 ± 0.48
	3.56	M1	8.9 ± 0.4	9.4	2.96 ± 0.11
^{7}Li	11.28 ± 0.05	(M1) or	(1.3 ± 0.4)/g[b]	0.043/g	—
		(M2)	(0.026 ± 0.008)/g	2.6/g	—
^{9}Be	15.97 ± 0.03	M1	(3.7 ± 0.8)/g	0.043/g	—
^{11}B	4.46	E2 and	0.0173 ± 0.0021	8.2	3.44 ± 0.50
		M1	0.64 ± 0.08	0.34	2.60 ± 0.35
	5.04	M1	1.84 ± 0.14	0.69	2.60 ± 0.11
^{12}C	4.43	E2	0.0122 ± 0.0008	5.30	3.14 ± 0.30
^{16}O	6.92	E2	0.100 ± 0.015	3.28	3.82 ± 0.46
	11.52	E2	0.52 ± 0.13	1.31	—
^{24}Mg	9.85 ± 0.04	M1	7.95 ± 1.2	0.38	3.50 ± 0.49
	9.97 ± 0.03				
	10.35 ± 0.03	E2	0.24 ± 0.05	0.58	5.05 ± 0.50
	10.70 ± 0.03	M1	22.2 ± 2.4	0.86	3.60 ± 0.36
	10.93 ± 0.04	E2	0.26 ± 0.11	0.50	—
^{28}Si	4.97 ± 0.02	C0	(2.0 ± 0.5) × 10^{-5}[c]	—	6.30 ± 1.20
^{40}Ca	6.89 ± 0.05	E2	0.29 ± 0.04	2.85	4.60 ± 0.50

[a] The Born approximation has been used except for ^{16}O and ^{40}Ca.
[b] $g = (2I_f + 1)/(2I_i + 1)$.
[c] Γ_γ^0 equivalent to ME = (8.87 ± 1.00) F^2.

REF.

E. B. Bazhanov, A. P. Komar, and A. V. Kulikov
Dokl. Akad. Nauk SSSR 171, 549 (1966)
Soviet Phys. Doklady 11, 953 (1967)

ELEM. SYM.	A	Z
Li	7	3

METHOD

REF. NO.	
67 Ba 2	JDM

REACTION	RESULT	EXCITATION ENERGY	SOURCE		DETECTOR		ANGLE
			TYPE	RANGE	TYPE	RANGE	
G,XN	ABX	THR-50	C	7-50	BF3-I		4PI

323

TABLE 1. Energy of Excited States Discovered by Various Methods of Studying Photodisintegration of Li^7

Energies of maxima obtained from the analysis of yield curves					Energies of maxima obtained from the analysis of energy spectra				Energies of excited levels
photoneutrons				photoprotons	photoneutrons		photoprotons		
[1]	[4]	[5]	our data	[6]	[6]	[7]	[6]	[8]	[9]
	9.6							9.6	
	10.8	(11.3)	11.5±0.3	11.0±0.2		12.5		11.7	10.8
	12.4	12.8				13.5	14.1±0.2	13.5	14.0
13.6	14.0	13.5	13.5±0.3	14.0±0.2	14.4	14.3			
		14.5							
15.3			15.0±0.3						
16.5		(15.9)	16.3±0.3	16.0±0.2	16.1		16.2±0.2	16.2	16.2
		(17.1)							
	17.5	(18.0)	17.8±0.3	17.9±0.2	17.9		18.0±0.2		17.5
			19.5±0.5		19.6		19.6±0.2		
			22.0±0.5	21.4±0.3	21.5		21.5±0.2		21.5
			23.7±0.3		23.5		23.5±0.2		23.5
				24.5±0.3	25.3		25.3±0.3		
			26.0±0.3						
			28.3±0.3						
			30.3±0.3						
			33.0±0.5						
			34.7±0.5						
			41.0±1.5						
			46.5±1.5						

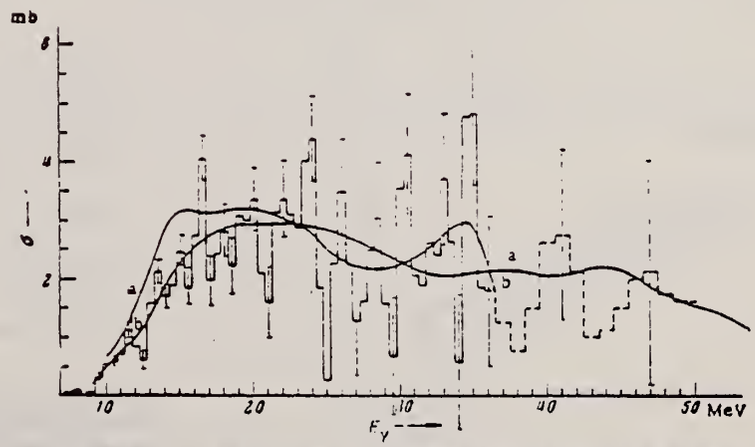

Fig. 1. Cross section of the photoneutron reaction on Li^7: a) data of [10]; b) the result of smoothing of the observed cross section.

REF. V. P. Denisov and L. A. Kul'chitskii
J. Nucl. Phys. (USSR) 5, 490 (1967)
Sov. J. Nucl. Phys. 5, 344 (1967)

ELEM. SYM.	A	Z
Li	7	3

METHOD

REF. NO. 67 De 1 - HMG

REACTION	RESULT	EXCITATION ENERGY	SOURCE TYPE	SOURCE RANGE	DETECTOR TYPE	DETECTOR RANGE	ANGLE
G,P 727	ABX	14-50	C	21-52	TEL-D	4-17	90
G,D	ABX	15-50	C	21-52	TEL-D	4-17	90
G,T 292	ABX	8-50	C	21-52	TEL-D	4-17	90

292-

Table II
Integrated cross sections

Reaction	σ_{int}, MeV-mb, Interval of energy E_γ, MeV: 0–23	23–33	33–52
(γ, p) *	14.0 ± 1.5	4.6 ± 0.5	Not determined
$(\gamma, p2n)$ *	13.3^{+3}_{-2}	12.0 ± 2.0	Not determined
(γ, pt) **	—	13.8 ± 2.5	22 ± 3
(γ, n) ***	$3.5^{+5}_{-3.5}$ $(2.5^{+5}_{-2.5})$	3^{+4}_{-3} (0^{+4}_{-3})	Not determined
(γ, nd) ***	—		33 ± 4 (32 ± 4)
(γ, nt) ***	Not determined		
(γ, nd) *	—	1.6 ± 0.4	4.2 ± 1
(γ, npd)	—		
$(\gamma, 2d)$	—		
(γ, t)	2.6 ± 0.3	1.2 ± 0.1	Not determined

*The cross section for the (γ, p) reaction was determined from curve 5, and for the $(\gamma, p2n)$ reaction from histogram 2 in Fig. 2; the cross sections for the (γ, nd), (γ, npd), and $(\gamma, 2d)$ reactions were determined from the curve for σ_4 in Fig. 5b.

**In the interval 23–33 from histogram 3, and in the interval 33–52 MeV from curve 4 in Fig. 2.

***The cross sections of the reactions indicated in the intervals 0–23 and 23–33 MeV were determined as $\sigma_n - 2\sigma(\gamma, p2n)$. The values without parentheses were computed from the data on σ_n from [1] and the values in parentheses were computed from [2]. In the interval 33–52 MeV the cross section was obtained on the assumption (see text) that $\sigma(\gamma, nt) \approx \sigma_n - \sigma_{4n}$.

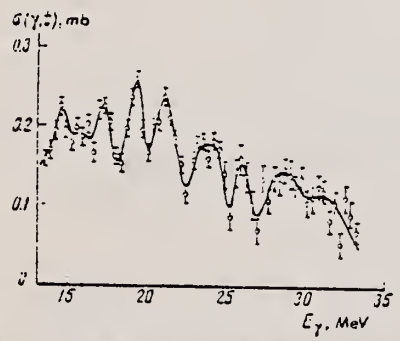

Fig. 4. Cross-section curve for the (γ, t) reaction.
From Brems spectrum

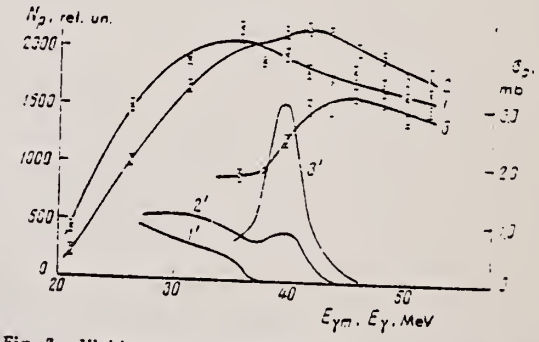

Fig. 3. Yield curves for protons (curves 1, 2, 3 with experimental points) and the corresponding curves 1', 2', 3' of the cross section for the following proton energy intervals: curve 1 – 4–7 MeV; curve 2 – 7–10.5 MeV; curve 3 – 10.5–17 MeV. The abscissa represents the value of $E_{\gamma m}$ for curves 1, 2, 3 and E_γ for curves 1', 2', 3'.

(continued)

REF. V. P. Denisov and L. A. Kul'chitskii
J. Nucl. Phys. (USSR) 5, 490 (1967)
Sov. J. Nucl. Phys. 5, 344 (1967)

ELEM. SYM.	A	Z
Li	7	3

REF. NO.

Page 2 of 2 67 De 1 HMG

DETECTOR		ANGLE
TYPE	RANGE	

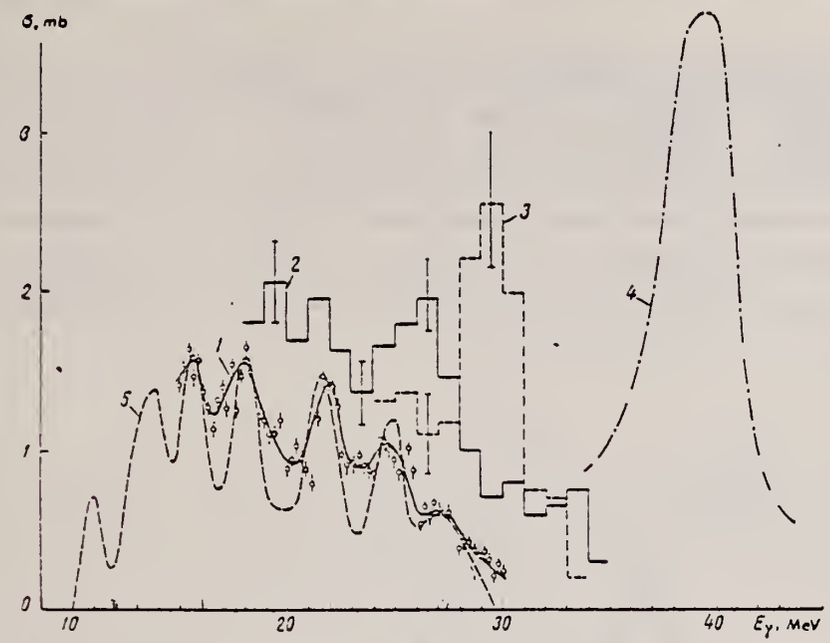

Fig. 2. Cross sections for reactions with proton emission. Curve *1*—cross section for transitions to the ground and first excited state (1.7 MeV) of He^3 ((γ, p) reaction); histogram 2—cross section for transitions to excited states of He^4 with energies of 3–7 MeV (reaction $(\gamma, p2n)$); histogram 3—cross section for transitions to excited states of He^4 with energies above 9 MeV (reaction $(\gamma, p\pi)$); curve *4*—cross section for emission of protons, σ_p, obtained from the yield curves in Fig. 3 (reaction $(\gamma, p\pi)$); curve *5*—cross section for (γ, p) reaction, obtained from activity of He^4 nuclei.[7]

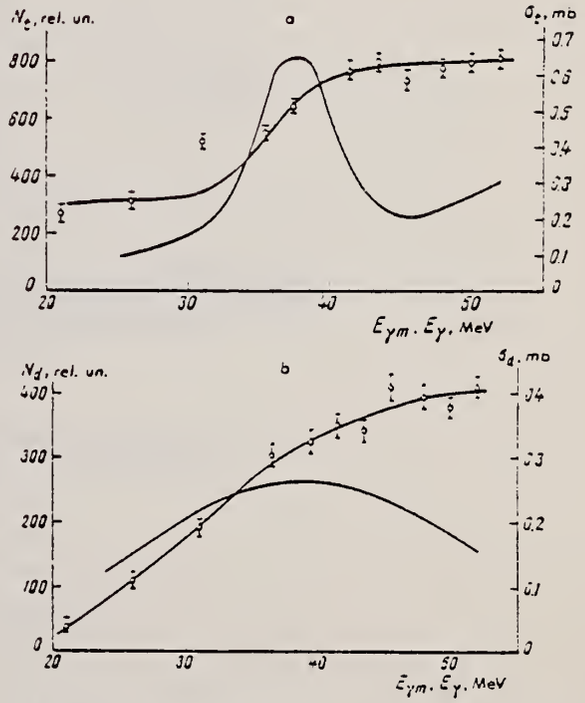

Fig. 5 Triton yield curve (curve with experimental points) and the corresponding curve for the triton emission cross section σ_t—*a*; deuteron yield curve (curve with experimental points) and the corresponding curve for the deuteron emission cross section σ_d—*b*.

REF. I. L. Smith, J. Garvey, J. G. Rutherglen, and G. R. Brookes
Nucl. Phys. B1, 483 (1967)

ELEM.		
Li	7	3

METHOD

REF. NO.	
67 Sm 1	JOC

REACTION	RESULT	EXCITATION ENERGY	SOURCE		DETECTOR		ANGLE
			TYPE	RANGE	TYPE	RANGE	
G,NP	ABX	150-250	C	250	TOF-D		DST

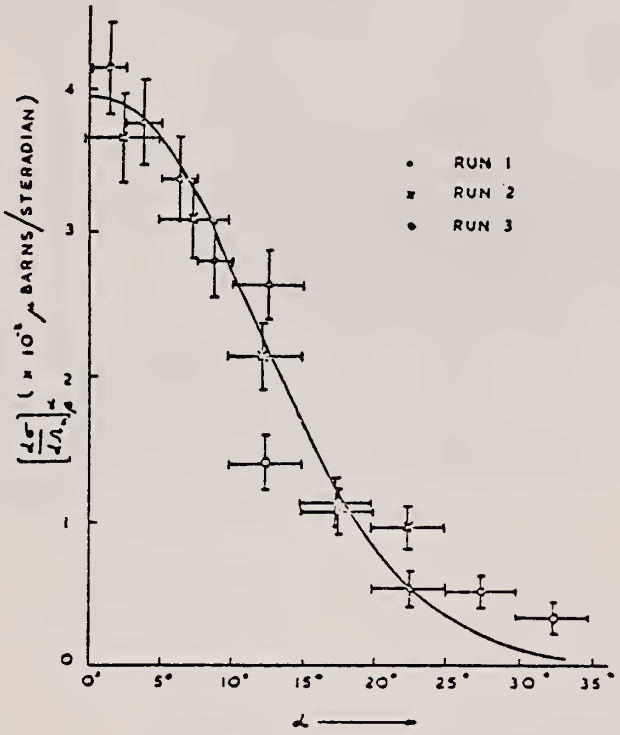

Fig. 5. Vertical angular distribution of coincident protons from lithium (the curve is explained in the text).

REF. J. L. Matthews, W. Bertozzi, S. Kowalski, C. P. Sargent and W. Turchinetz
Nucl. Phys. A112, 654 (1968)

ELEM. SYM.	A	Z
Li	7	3

METHOD

REF. NO. 68 Ma 1 _ EGF

REACTION	RESULT	EXCITATION ENERGY	SOURCE		DETECTOR		ANGLE
			TYPE	RANGE	TYPE	RANGE	
G,P	ABX	100	C	95-102	TEL-D	40-95	DST

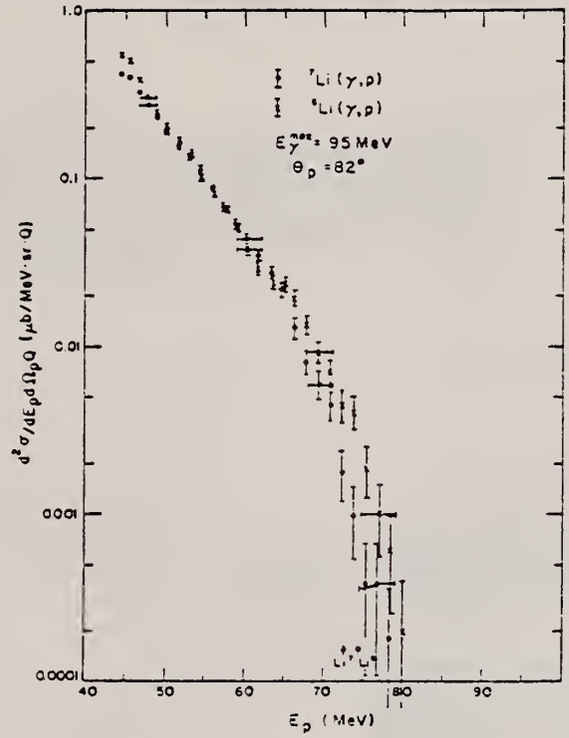

Fig. 9. Comparison of the ^{7}Li and ^{6}Li photoproton spectra at $\theta_p = 82°$, with 95 MeV bremsstrahlung. The arrows indicate the maximum proton energies allowed by the kinematics in each reaction.

V. S. Kuz'menko, I. I. Miroshnichenko, A. L. Rubashkin, P. V. Sorokin
Yad. Fiz. 9, 680 (1969)
Sov. J. Nucl. Phys. 9, 394 (1969)

Li	7	3

METHOD

REF. NO. 69 An 4 hmg

REACTION	RESULT	EXCITATION ENERGY	SOURCE		DETECTOR		ANGLE
			TYPE	RANGE	TYPE	RANGE	
$ G,P	RLY	320	D	320	MAG-D	68	33

Protons presumably associated with mesons produced from individual nucleons. Amorphous part is yield of 340 MeV protons.

COHERENT BREMS.

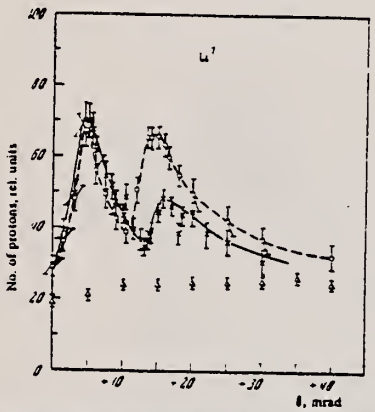

FIG. 3. Proton yield in the (γ, p) reaction in Li^7 as a function of crystal orientation angle θ for plane of polarization directions perpendicular (dashed curve and $O - N_\perp/N_0, \phi_1 = 90°$) and parallel (solid curve and $x - N_\parallel/N_0, \phi_1 = 0°$) to the plane of the reaction; Δ – amorphous part.

In Fig. 3 we have shown in relative units the experimentally measured proton yield from Li^7 for 68-MeV protons at an angle of 33°, as a function of the angle θ between the primary electron beam direction and the ⟨110⟩ axis. Here the ⟨001⟩ axis lies in the plane determined by the beam and the ⟨110⟩ axis of the crystal. The primary electron beam energy is 1120 MeV.

Yu. P. Antuf'ev, V. L. Agranovich, V. B. Ganenko, V. S. Kuzmenko,
I. I. Miroshnichenko, and P. V. Sorokin
Ukr. Fiz. Zh. 14, 248 (1969)

ELEM.		
Li	7	3

METHOD

REF. NO.	
69 An 6	egf

REACTION	RESULT	EXCITATION ENERGY	SOURCE		DETECTOR		ANGLE
			TYPE	RANGE	TYPE	RANGE	
G,P	ABY	107-999	C	700,999	TEL-D	97-230	DST
G,D	ABY	107-999	C	700,999	TEL-D	97-205	DST

999=1.2 GEV

Summary

The cross-sections of the (γ, p) (γ, d) reactions were investigated. Li^7, Be^9, C^{12}, Si^{28}, Cu^{63}, Mo^{94} and Ta^{181} targets were irradiated with the bremsstrahlung of 700 and 1200 MeV maximum energy from the Kharkov PhTI Ac. Sci. UkrSSR linear accelerator. The photoprotons and deuterons were detected by the scintillation telescope at 30°, 60°, and 120° with the beam. Possible mechanisms of the proton and deuteron photoproduction are discussed. The qualitative agreement of *A* dependence of the cross-sections is observed with a suggestion on the meson mechanism for these reactions.

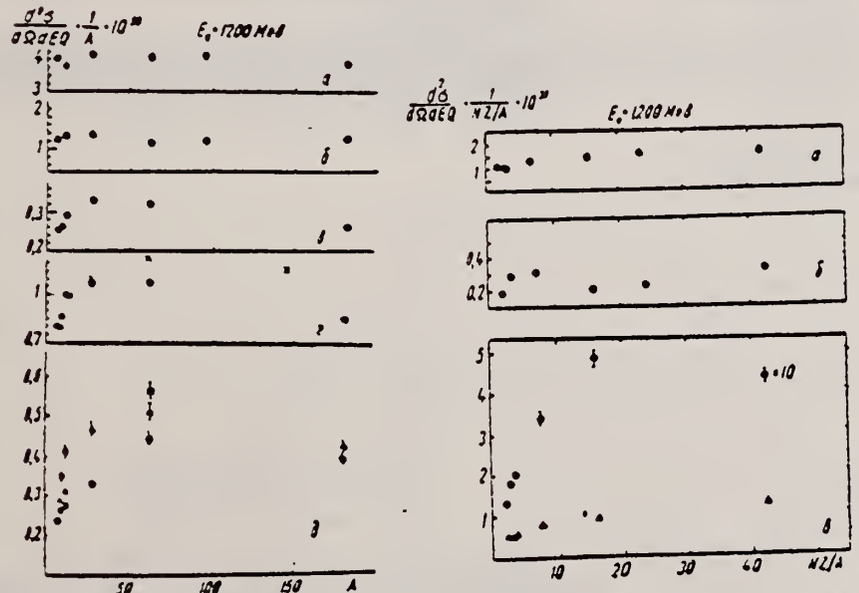

Рис. 1. Залежність перерізу (γ, p)-реакції від *A*: *а* — $\vartheta = 30°$, $E_\gamma = 97$ *Мев*; *б* — $E_\gamma = 205$ *Мев*; *в* — $\vartheta = 60°$, $E_\gamma = 230$ *Мев*; *г* — $E_\gamma = 157$ *Мев* (× — дані [3]); *д* — $\vartheta = 120°$, ○ — $E_\gamma = 120$ *Мев*, △ — $E_\gamma = 157$ *Мев*, ■ — $E_\gamma = 230$ *Мев*. Абсолютне значення перерізу наведено при енергії протонів $E_\gamma = 120$ *Мев*. Інші дані нормовані до перерізу для Li^7 при $E_\gamma = 120$ *Мев*.

Рис. 2. Залежність перерізу (γ, d)-реакції від *NZ/A*: *а* — $\vartheta = 30°$, $E_d = 97$ *Мев*; *б* — $\vartheta = 30°$, $E_d = 205$ *Мев*; *в*: △ — $\vartheta = 60°$, $E_d = 97$ *Мев*, ○ — $\vartheta = 120°$, $E_d = 97$ *Мев* (перерізи наведені в одиницях 10^{-32} *см²/стер · Мев · Q*).

REF. V.P. Denisov, A.P. Komar, L.A. Kul'chitskii, and I. Ya. Chubukov
Yad. Fiz. 10, 1116 (1969)
Sov. J. Nucl. Phys. 10, 635 (1970)

ELEM. SYM.	A	Z
Li	7	3

METHOD

REF. NO. 69 De 7 hmg

REACTION	RESULT	EXCITATION ENERGY	SOURCE		DETECTOR		ANGLE
			TYPE	RANGE	TYPE	RANGE	
G,G/T	ABX	23-32	C	18-32	TEL-D	3-10	90

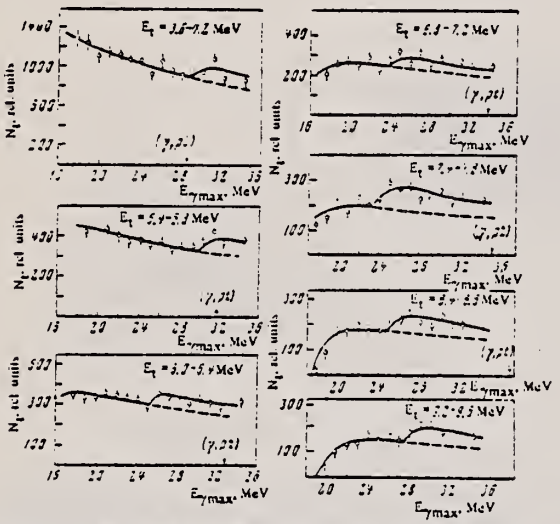

FIG. 1. Curves of phototritons in different energy intervals; the experimental points are approximated by isochromatic curves, with dashed segments beyond the approximation region. The kinematic thresholds of the (γ, pt) reaction are designated by arrows.

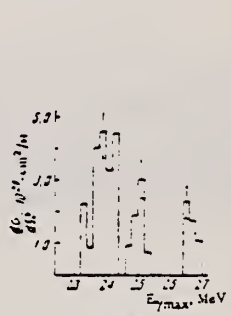

FIG. 2

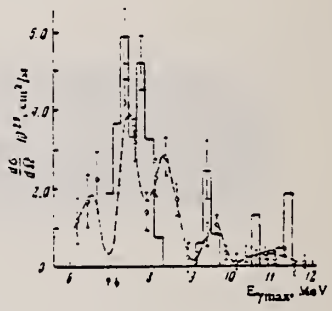

FIG. 3

FIG. 2. Dependence of the cross section for $Li^7(\gamma, \gamma' t)$ He^4 on the energy of scattered γ rays.

FIG. 3. The histogram represents the cross section for $Li^7(\gamma, \gamma' t)$ He^4 as a function of scattered γ – ray energy, as derived from the phototriton spectra. The dashed curve through the experimental points is the same function, as derived from the scattered γ – ray spectra.

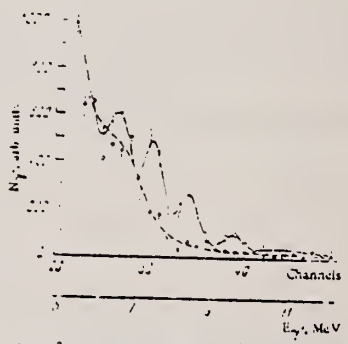

FIG. 4. Spectra of γ rays scattered in Li^7 and Li^6 targets for identical bremsstrahlung doses. For Li^7 – open circles and the solid curve; for Li^6 – filled circles and the dashed curve.

Inelastic scattering of γ rays, which is one of the inadequately investigated processes of nuclear physics, is studied in the reaction $Li^7(\gamma, \gamma')Li^{7*} \rightarrow He^4 + H^3$. When investigating phototritons from the Li^7 nucleus by analyzing triton yield curves for narrow energy intervals a triton group was found having its production threshold between the thresholds of the (γ, t) and (γ, pt) reactions (2.46 and 22.28 MeV, respectively). These tritons can be attributed only to a (γ, γ't) reaction. The integral cross section for the (γ, γ't) reaction was found to be 1.1 ± 0.3 MeV-mb for 3.5–10 MeV tritons. The (γ, γ') cross section was also investigated by direct registration of scattered γ rays. The spectrum of the scattered γ rays shows peaks at 7.5, 8.4, and 9.5 MeV.

REF.

R. Garfagnini, G. Piragino, A. Zanini
Nuovo Cimento 63B, 670 (1969)

ELEM. SYM.	A	Z
Li	7	3

METHOD

REF. NO.	
69 Ga 1	egf

REACTION	RESULT	EXCITATION ENERGY	SOURCE		DETECTOR		ANGLE
			TYPE	RANGE	TYPE	RANGE	
$ G,XN	SPC	2-85	C	85	CCH-D	1-14	DST

N POLARIZATION

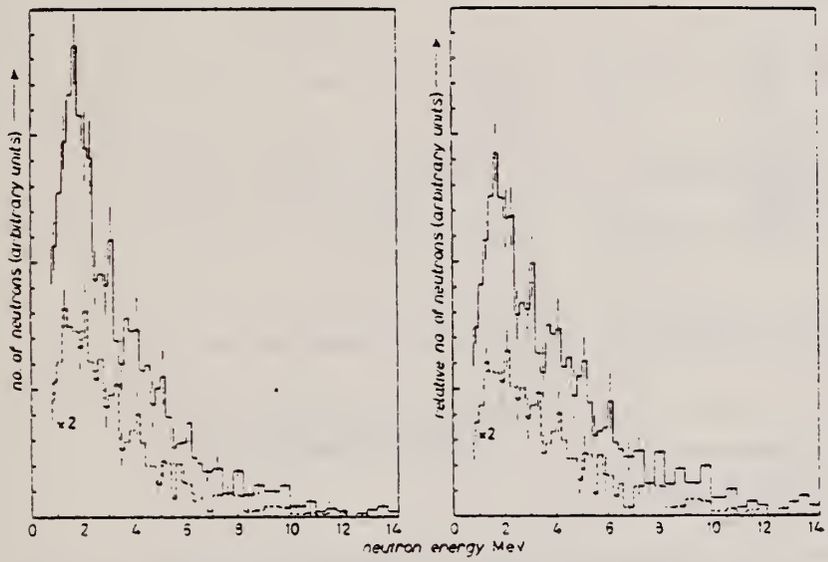

Fig. 2. – Energy spectrum of photoneutrons from ^{7}Li at 90° (full line) and at 135° (dashed line). On the right the spectra are normalized to the bremsstrahlung γ-ray spectrum with $E_{\gamma_{max}} = 85$ MeV.

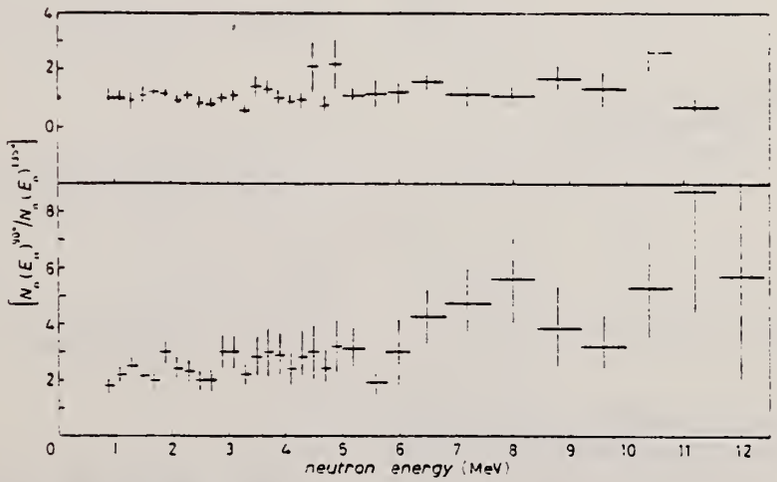

Fig. 4. – Ratio between the number of photoneutrons at 90° and that at 135° from ^{7}Li (upper part) and ^{9}Be (lower part) vs. photoneutron energy.

(continued)

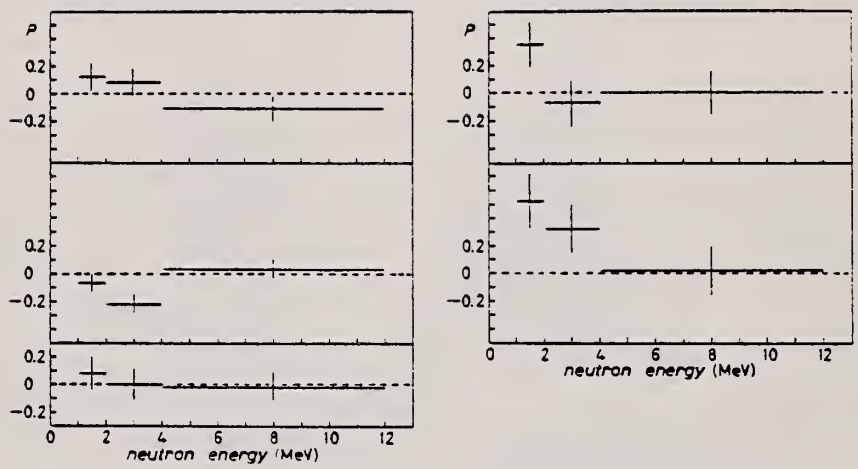

Fig. 5. – On the left is the photoneutron polarization of photoneutrons from ^{7}Li, ^{9}Be at 90° compared with the polarization of neutrons from a RaD-Be source. On the right is the polarization of photoneutrons at 135° previously measured ([7-10]). ^{7}Li, upper diagrams; ^{9}Be lower diagrams.

R. Garfagnini, G. Piragino & A. Zanini
Atti Accad. Naz. Lincei, Rend.
Cl. Sci. Fis. Mat. Natur. 47, 33 (1969)

Li	7	3

METHOD

REF. NO. 69 Ga 3 egf

REACTION	RESULT	EXCITATION ENERGY	SOURCE		DETECTOR		ANGLE
			TYPE	RANGE	TYPE	RANGE	
G,XN	SPC	8-85	C	85	CCH-D		DST

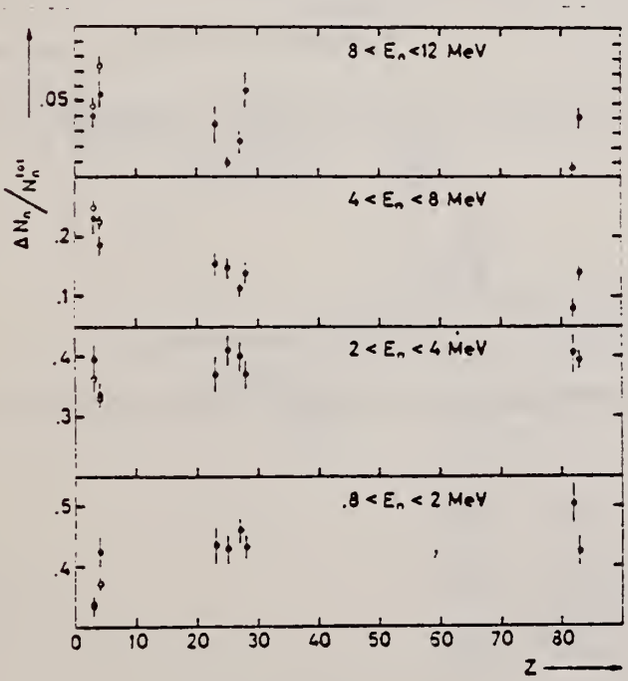

Fig. 1. – Percentage of the photoneutrons emitted at 135°, in the respective energy interval as a function of Z, by a γ-ray bremsstrahlung beam with $E_{\gamma max}$ = 85 MeV. The open circles represent the values obtained at 60° for ^{7}Li and ^{9}Be

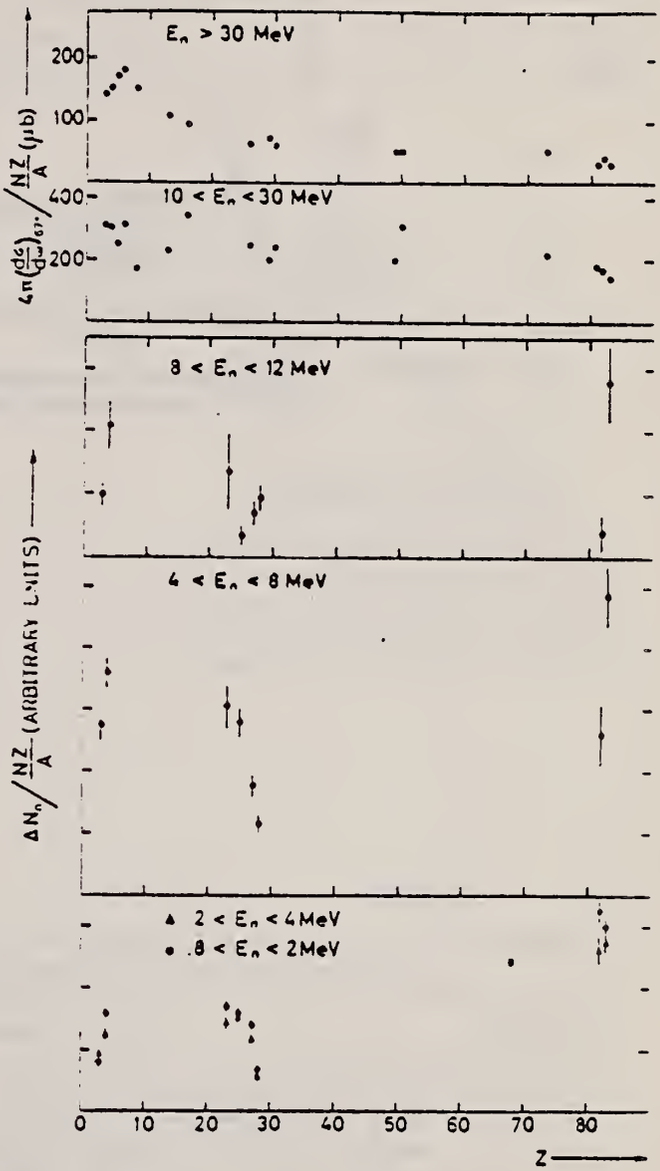

Fig. 2. Number of photoneutrons emitted at 135°, normalized to the sum rule factor NZ/A, as a function of Z. In the upper part is reported the effective cross section divided by NZ/A for photoproduction of fast neutron by 55–85 MeV bremsstrahlung photons as deduced by Kaushal *et al.* [1

[1] N.N. Kaushal et al., Phys. Rev. 175, 1330 (1968).

REF.

R. M. Hutcheon and H. S. Caplan
Nucl. Phys. A127, 417 (1969)

ELEM. SYM.	A	Z
Li	7	3

METHOD

REF. NO.	
69 Hu 1	egf

REACTION	RESULT	EXCITATION ENERGY	SOURCE		DETECTOR		ANGLE
			TYPE	RANGE	TYPE	RANGE	
E,E/	FMF	0-26	D	55-127	MAG-D		DST

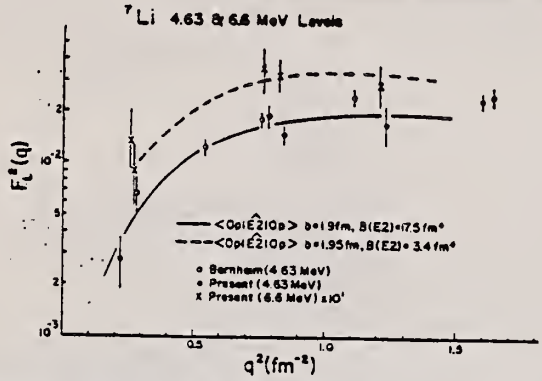

Fig. 7. The variation of the inelastic form factor with momentum transfer. The curves represent the normalized single-particle model predictions.

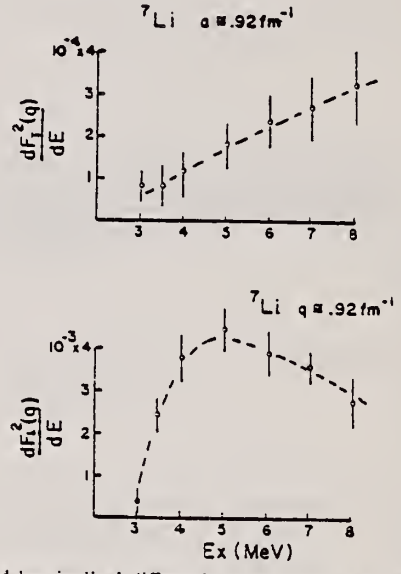

Fig. 8. The transverse and longitudinal differential form factors for the continuous cross section in ^{7}Li.

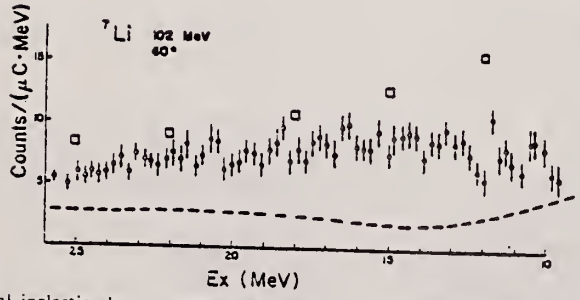

Fig. 9. A typical inelastic electron scattering spectrum for higher excitation in ^{7}Li. The squares indicate the magnitude of the elastic radiation tail, which has already been subtracted.

REF. Yu. I. Sorokin, A. Kh. Shardanov, V. G. Shevchenko and B. A. Yur'ev
Izv. Akad. Nauk Fiz. 33, 721 (1969)
Bull. Acad. Sci. USSR-Phys. 33, 663 (1969)

ELEM. SYM.	A	Z
Li	7	3

METHOD

REF. NO. 69 So 3 - egf

REACTION	RESULT	EXCITATION ENERGY	SOURCE		DETECTOR		ANGLE
			TYPE	RANGE	TYPE	RANGE	
G,T	ABX	5-11	C	12	EMU-D	1-5	4PI
							729

Table 1

^{6}Li levels excited in (γ,p) and (γ,n) reactions, and dipole levels calculated with the many-particle shell model

(γ,p) reaction		(γ,n) reaction		Calculated (Ref. 1)	
The present work		Ref. 8			
E^*, MeV	$\sigma_{int}(\gamma p)$, MeV·mb	E^*, MeV	$\sigma_{int}(\gamma n)$, MeV·mb	E^*, MeV	σ_{int}, MeV·mb
6,5*	1,0	—	—	—	—
6,7*	1,2	7,1	0,5	—	—
7,8	0,07	—	—	—	—
—	—	8,2	1,0	—	—
8,3	0,085	—	—	—	—
—	—	—	—	8,6	0,35
9,0	0,10	9,2	1,05	—	—
9,6	0,075	—	—	—	—
10,2	0,035	10,8	1,7	10,5	0,95
(10,7)	0,035	—	—	—	—
11,0	0,07	11	2,0	11,3	2,45
(11,4)	0,05	—	—	12,8	4,21

*From Ref. 4.

[4] A.Kh.Shardanov, V.G.Shevchenko and B.A.Yur'ev, Izv. AN SSSR, Ser.fiz.28, 60 (1964).

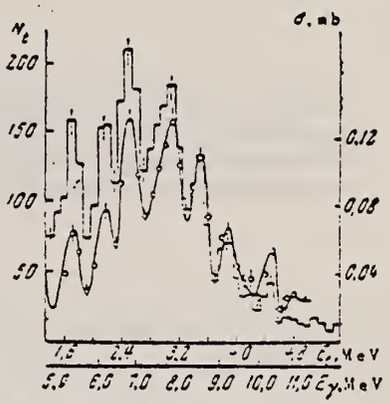

Fig.2. Energy distribution of the phototritons ejected from ^{7}Li by 12 MeV bremsstrahlung (histogram) and the ^{7}Li(γ,t)^{4}He cross section (smooth curve).

Table 2

Energy peaks, maximum and integral cross sections, and widths of resonances for the (γ,t) reaction on ^{7}Li

E_t,*MeV	E_γ, MeV	σ_{max}, mb	σ_{int}, MeV·mb	Γ_γ, eV (exp)			Γ_γ, eV (sing. part.)			Γ_γ, eV (int. coup.)	Many part. shell model calc. for E=1 absorp.	
				I=1/2	3/2	5/2	E1	M1	E2		E^*, MeV	σ_{int}
1,7±0,1	5,3±0,1	0,064	0,032	0,5	0,25	0,17	35	3	0,004	0,04—0,2	4,8	0,5
2,1±0,1	6,3±0,1	0,076	0,035	0,78	0,39	0,26	65	4,2	0,009	—	—	—
2,5±0,1	6,8±0,1	0,13	0,064	1,6	0,8	0,55	80	7	0,015	—	—	—
3,1±0,15	7,8±0,15	0,13	0,09	2,3	1,4	1,0	120	11	0,022	—	7,75	1,5
3,5±0,15	8,5±0,15	0,11	0,054	2,0	1,0	0,7	150	14	0,03	—	—	—
3,9±0,2	9,2±0,2	0,07	0,034	1,5	0,75	0,5	170	15	0,04	0,08—0,3	9,2 9,22	4,6 2,0
4,5±0,2	10,2±0,2	0,055	0,027	1,6	0,8	0,55	330	28	0,1	—	10,6	0,38

REF. Yu. P. Antuf'ev, V.L. Agranovich, V.B. Ganenko, V.S. Kuz'menko, I.I. Miroshnichenko, V.M. Sanin, P.V. Sorokin
Yad. Fiz. 11, 948 (1970)
Sov. J. Nucl. Phys. 11, 527 (1970)

ELEM. SYM.	A	Z
Li	7	3

METHOD

REF. NO.	
70 An 4	hmg

REACTION	RESULT	EXCITATION ENERGY	SOURCE		DETECTOR		ANGLE
			TYPE	RANGE	TYPE	RANGE	
G,XP	ABX	10-999	C	620,999	TEL-D	80-285	DST

999 = 1115 MEV

The angular distributions of photoprotons in the reaction $\gamma + Li^7 \rightarrow p + X$ have been measured for maximum γ-ray energies of 620 and 1115 MeV for proton energies of 80, 160, and 285 MeV in the angular range 25–140°. The experimental results agree satisfactorily with a calculation assuming two elementary processes: single meson production from free nucleons and disintegration of quasideuterons, in the region where the contribution of double meson photoproduction is small.

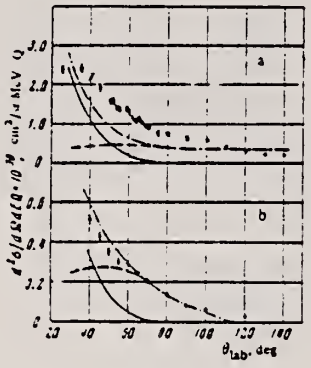

FIG. 1

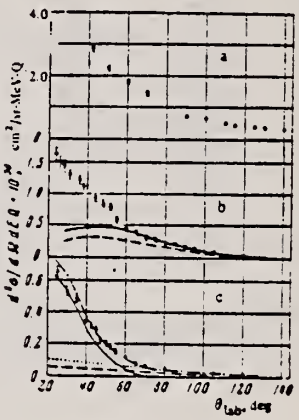

FIG. 2

FIG. 1. Angular distributions of protons from the nucleus Li^7 for a bremsstrahlung energy E_0 = 620 MeV: a–E = 80 MeV. Dashed line–calculation according to Levinger's quasideuteron model. [7] Solid line–calculation with inclusion of reactions (3) and (4) in the impulse approximation; dot-dash line–sum; b–the same for E = 160 MeV.

FIG. 2. Angular distribution of protons from the nucleus Li^7 for E_0 = 1115 MeV; a–E = 80 MeV, b–E - 106 MeV, c–E = 285 MeV. The designations are the same as in Fig. 1. The dotted curves indicates extrapolation of the quasideuteron yield to the small-angle region.

[7] J. S. Levinger, Phys. Rev. 84, 43 (1951).

REF. [illegible] Nucl. Phys. A153, 401 (1970)

ELEM. SYM.	A	Z
Li	7	3

METHOD

REF. NO. 70 Sa 2 egf

REACTION	RESULT	EXCITATION ENERGY	SOURCE		DETECTOR		ANGLE
			TYPE	RANGE	TYPE	RANGE	
G,P	ABX	50-84	D	50-84	TEL-D	37-50	45

TABLE 1

Parameters of the resonance cross section for $\Delta E_p = 2.5$ MeV

E_p (MeV)	E_R (MeV)	E_R (MeV)	$d\sigma_R/d\Omega$ ($\mu b \cdot MeV/sr^{-1}$)
35	49	8	47±3
37.5	53	8	41±3
40	56	7	35±3
42.5	60	8	33±3
45	62	6	25±3
47.5	64	7	21±3
50	66	6	17±2.5
52.5	72	7	17±2.5
55	73	6	11±2
all ±1.25	all ±1.5	all ±2.5	

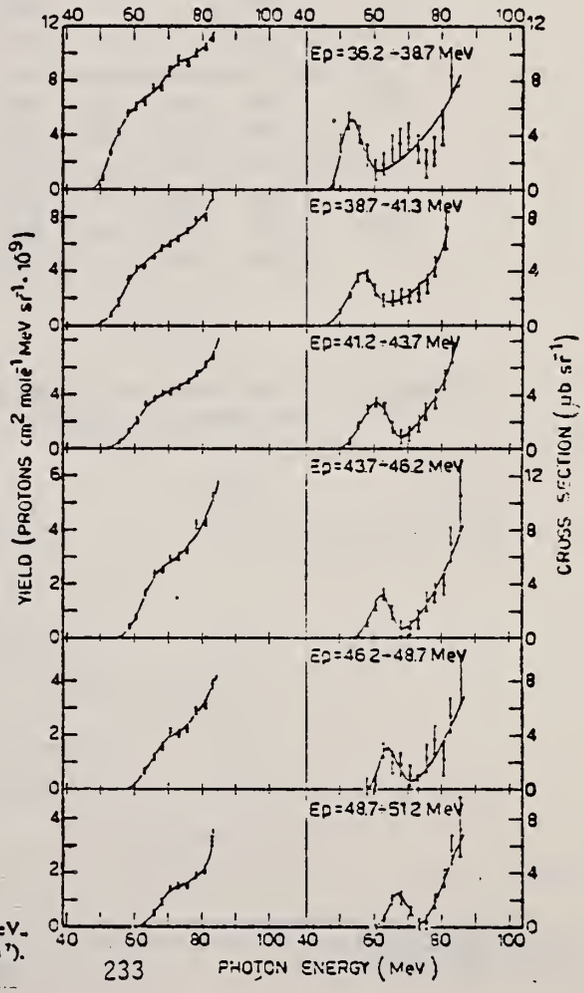

Fig. 2. Proton yields and cross sections at 45°, relative to the proton energy interval $\Delta E_p = 2.5$ MeV. The cross sections have been derived from the experimental data using Cook's least-squares analysis [7]).

REF.

S.G. Tonapetyan, O.G. Konovalov, A.I. Derebchinskii, A. A. Zybalov, V.M. Khvorostyan, N.V. Goncharov & V.A. Gol'dshtein
ZhETF Pis. Red. 11, 165 (1970)
JETP Letters 11, 101 (1970)

ELEM. SYM.	A	Z
Li	7	3

METHOD

REF. NO. 70 To 2 egf

REACTION	RESULT	EXCITATION ENERGY	SOURCE TYPE	SOURCE RANGE	DETECTOR TYPE	DETECTOR RANGE	ANGLE
$G,P	NOX	650-840	C	700,810	MAG-D		41

P-POLARIZATION

The table lists the preliminary results for the nuclei $_3Li^7$ and $_6C^{12}$.

Nucleus	$E_{\gamma max}$ MeV	$E_{\gamma eff}$ MeV	ΔE_γ MeV	P_γ MeV/c	ΔP_γ MeV/c	Polarization	Kinematic region
Li^7	700	-	-	755	23	-0.15± 0.19	I
	810			790	25	-0.15± 0.22	
C^{12}	700	-	-	755	23	+0. 05± 0.31	
	810			790	24	-0.05± 0.20	
	930			840	25	0.08 ± 0.43	
Li^7	700	650	33	618	18	-0.76 ±0.20	II
	810	715	38	655	20	-0.31± 0.19	
C^{12}	700	650	33	618	18	-0.71 ± 0.21	
	810	715	38	655	20	-0.35 ± 0.26	
	930	840	43	754	23	+0.48 ± 0.35	

Region I - no real mesons possible.
" II - real mesons possible.

REF. C. F. Wong, R. M. Hutcheon, Y. M. Shin, and H. S. Caplan
Can. J. Phys. 48, 1917 (1970)

ELEM. SYM.	A	Z
Li	7	3

METHOD

REF. NO.	
70 Wo 1	egf

REACTION	RESULT	EXCITATION ENERGY	SOURCE		DETECTOR		ANGLE
			TYPE	RANGE	TYPE	RANGE	
E,P	ABX	6-20	C	21-90	MAG-D		90
		(5.7-20)		(21.6-90)			
G,P	ABX	7-20	C	21-90	MAG-D		90
		(7.3-20)		(21.6-90)			

73C

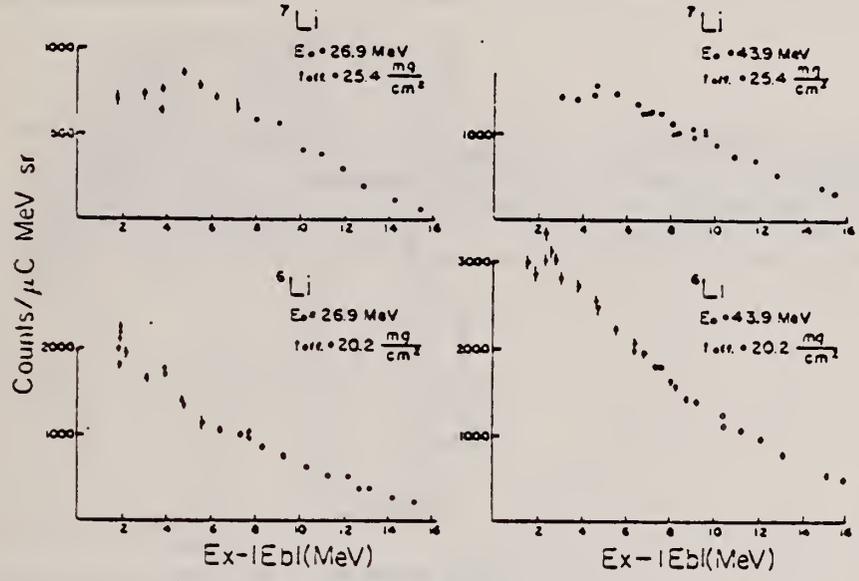

FIG. 4. Energy spectra of electro protons from ^{6}Li and ^{7}Li.

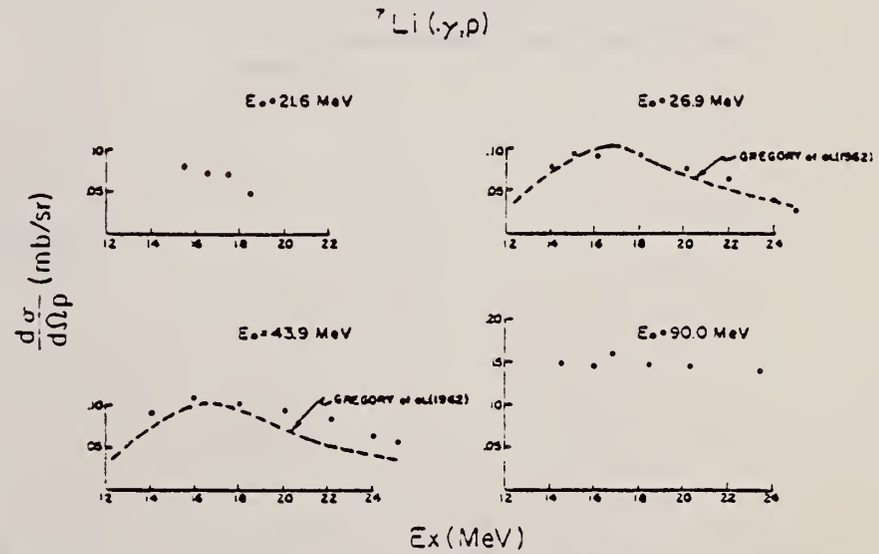

FIG. 6. The ^{7}Li photoproton cross sections obtained by unfolding the E1 virtual photon spectrum.

REF. Yu. P. Antuf ev, V.L. Agranovich, V.B. Ganenko, V.S. Kuz menko, I.I. Miroshnichenko, and P.V. Sorokin
Yad. Fiz. 14, 898 (1971)
Sov. J. Nucl. Phys. 14, 502 (1972)

ELEM. SYM.	A	Z
Li	7	3

METHOD

REF. NO.	
71 An 2	hmg

REACTION	RESULT	EXCITATION ENERGY	SOURCE		DETECTOR		ANGLE
			TYPE	RANGE	TYPE	RANGE	
G,XD	ABX	100-620	C	620	MAG-D		DST

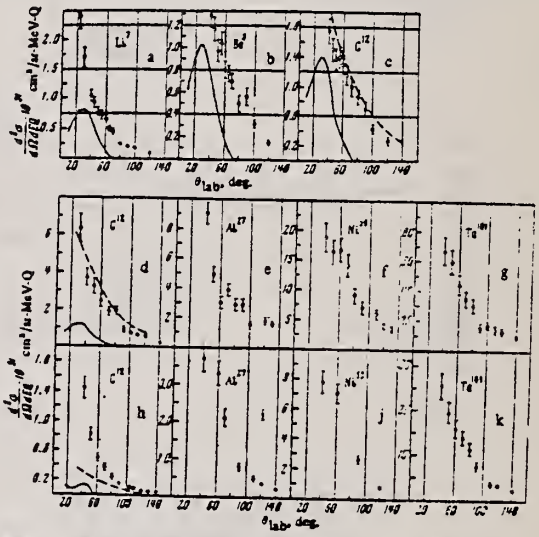

FIG. 1. Angular distributions of deuterons in (γ, d) reactions in nuclei for E_0 = 620 MeV (a–c) and E_0 = 1140 MeV (d–k). The statistical errors are shown. a–g–angular distributions of deuterons with energies of 90 MeV, h–k–with energy 160 MeV.

REF. N.V. Goncharov, A.I. Derebchinskii, O.P. Konovalov, S.G. Tonapetyan, and V.M. Khvorostyan
Yad. Fiz. 14, 31 (1971)
Sov. J. Nucl. Phys. 14, 18 (1972)

ELEM. SYM.	A	Z
Li	7	3

METHOD

REF. NO.	
71 Go 2	hmg

REACTION	RESULT	EXCITATION ENERGY	SOURCE		DETECTOR		ANGLE
			TYPE	RANGE	TYPE	RANGE	
G,PI+	RLY	150-500	C	500	CCH-D		DST

PI-/PI+ YIELD RATIO

Measurements are reported of the relative yield of π^+ mesons and the π^-/π^+ yield ratio for mesons with energy 40 ± 10 MeV emitted in the angular range θ_{lab} = 50—160° in photon-induced reactions with E_γ^{max} = 500 MeV with light and medium nuclei. The charged π-meson detector was a 34-cm Freon bubble chamber with a tube for the beam. The π^-/π^+ yield ratio for He^4, Li^7, C^{12}, Si^{28}, S^{32}, Ca^{40}, and Nb^{93} was found to be respectively 0.94 ± 0.14, 2.15 ± 0.31, 1.22 ± 0.21, 1.25 ± 0.15, 1.0 ± 0.13, 1.11 ± 0.13, and 1.53 ± 0.25. It was established that the π^+-meson yield follows a $ZA^{-1/3}$ law.

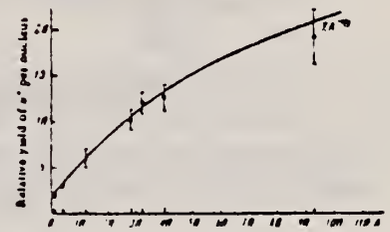

FIG. 2. Relative yield of π^+ mesons per nucleus as a function of mass number A.

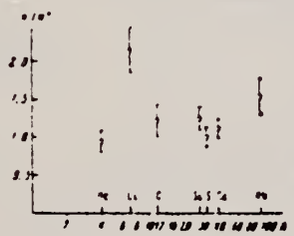

FIG. 3. π^-/π^+ yield ratio as a function of mass number A.

V. I. Noga, Yu. N. Ranyuk, P.V. Sorokin, V.A. Tkachenko
Ukr. Fiz. Zh. 16, 1850 (1971)

Li	7	3

METHOD

REF. NO. 71 No 1 egf

REACTION	RESULT	EXCITATION ENERGY	SOURCE		DETECTOR		ANGLE
			TYPE	RANGE	TYPE	RANGE	
G,BE7	ABY	THR-999	C	80-999	ACT-I		4PI
G,PI-	ABY	THR-999	C	140-999	ACT-I		4PI

999=1.2 GEV

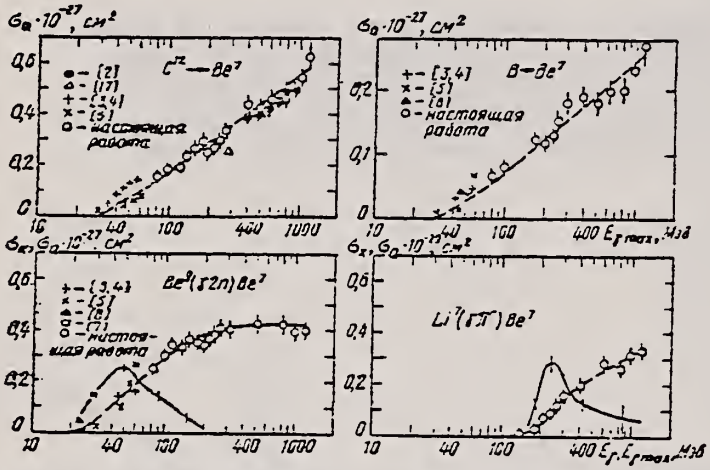

Рис. 3. Энергетическая зависимость сечений и выходов реакций: О — экспериментальные зависимости выхода от $E_{\gamma max}$; сплошная кривая — σ_A — функция возбуждения, вычисленная по способу наименьших квадратов по экспериментальным данным; пунктирная — σ_Q — выход, соответствующий функции возбуждения.

REF.

G.J.C. Van Niftrik, L. Lapikas, H. De Vries & G. Box
Nucl. Phys. A174, 173 (1971)

ELEM. SYM.	A	Z
Li	7	3

METHOD

REF. NO.	
71 Va 3	egf

REACTION	RESULT	EXCITATION ENERGY	SOURCE		DETECTOR		ANGLE
			TYPE	RANGE	TYPE	RANGE	
E,E/	LFT	1	D	25-90	MAG-D		DST

1 = 478 KEV

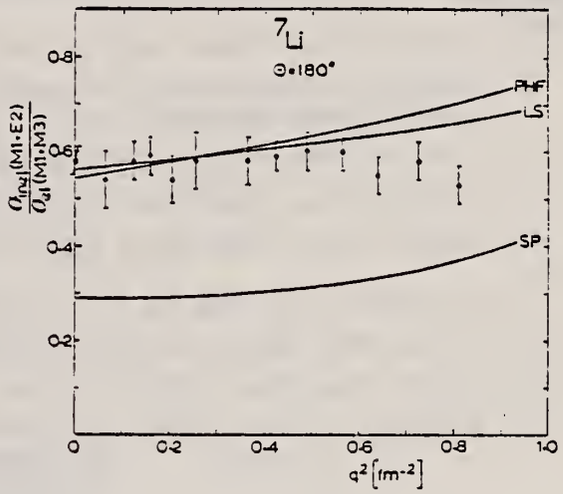

Fig. 3. Ratio of cross sections for transverse inelastic to transverse elastic scattering from the ground state doublet of ^{7}Li. The curves correspond to the PHF prediction (a = 1.60 fm) of ref. [20]), to the *LS* fit to our elastic scattering data (a = 1.90 fm) and to the SP model with a = 1.60 fm, respectively.

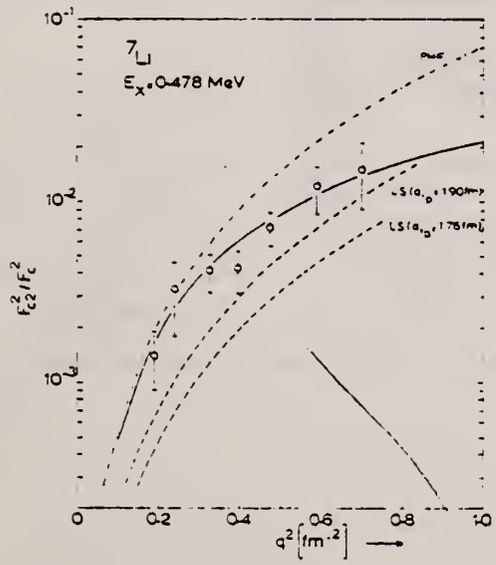

Fig. 6. Measured ratio of the longitudinal (C2) form factor for excitation of the 478 keV level to the elastic charge form factor as a function of momentum transfer squared. The theoretical dependence for a harmonic oscillator model with *LS* coupling is indicated by the dashed curves using a_{1p} = 1.90 fm and a_{1p} = 1.76 fm. The dot-dashed curve gives the projected Hartree-Fock prediction for a = 1.60 fm. A two-parameter fit, giving $B(C2, \uparrow; k)$ = 7.1 fm^4 and a_{1p} = 2.3 fm is indicated by the solid line.

(continued)

Results of longitudinal C2 excitation of the 478 keV state in ^{7}Li

Model/experiment	Ref.	$Q_{sp}/\langle r^2\rangle_{1p}$	$B(C2,\uparrow;k)$ [fm^4]	Q (fm^2]
$(1p_{\frac{3}{2}})^1$: single particle	[30]	$-\frac{2}{5}$	6.45	−3.60
$(1p_{\frac{3}{2}})^3$: jj coupling	[22,35]	$-\frac{22}{75}$	3.48	−2.64
$(1p)^3$: LS coupling	[22]	$-\frac{8}{33}$	2.33	−2.16
PHF prediction	[19,35]	−0.43	7.63	−3.91
Hyperfine structure				
molecular	[13-15]		(10.0)	−4.5±0.5
atomic	[16]		(4.5)	−3 ±2
atomic	[17]		(0.7)	−1.2±1.2
Coulomb excitation with				
heavy ions	[7-9 a)]		6.70±0.15	(±3.68)
electrons	[3,10,11]		6.8 ±1	(±3.7)
electrons	this work		7 ±4	(±3.7)

The size of the 1p shell used for the calculation of the predicted quadrupole moment is $\langle r^2\rangle_{1p} = 9$ fm^2. The reduced transition probability $B(C2,\uparrow;k)$ and the electric quadrupole moment Q are related through eq. (4) in sect. 5. The derived quantity is given in parentheses.
a) Weighted average.

[6] S.J. Skorka et al., Nucl. Data A, Vol. 2nr. 4 (1966).
[12] I. Lindgren, in Alpha-, beta- and gamma-ray spectroscopy, (North-Holland, Amsterdam, 1963).
[18] R.S. Willey, Nucl. Phys. 40 (1963) 529.
[19] M. Bouten et al., Nucl. Phys. A102 (1967) 322.
[20] J. Kruger et al., Nucl. Phys. A139 (1969) 418.
[35] B.H. Flowers, Phil. Mag. 43 (1952) 1330.
[36] A.M. Lane, Proc. Phys. Soc. 68 (1955) 189.
[37] D. Kurath, Phys. Rev. 101 (1956) 216.
[38] S. Cohen et al., Nucl. Phys. 73 (1965) 1.

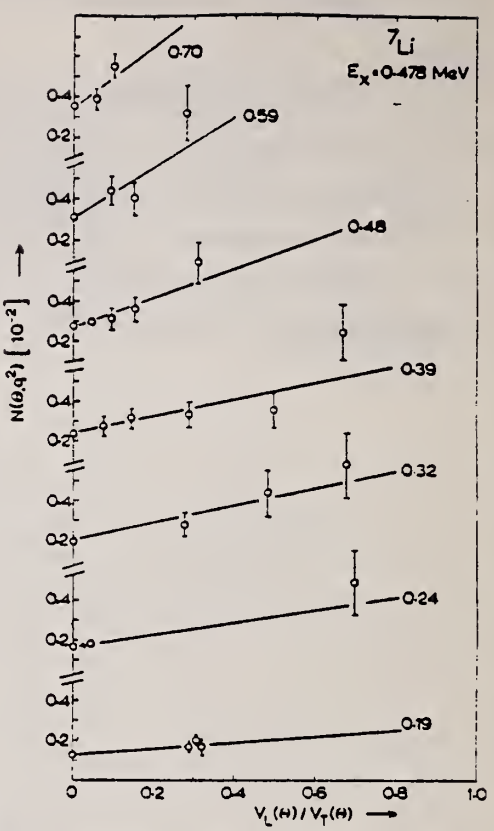

Fig. 5. Angular dependence of the cross section for excitation of the 478 keV level. The functions $N(\theta, q^2)$, $V_L(\theta)$ and $V_T(\theta)$ are explained in the appendix. The solid lines represent a straight line fit to the data at the constant momentum transfer squared indicated in the figure in units fm^{-2}.

TABLE 1

Theoretical and experimental values for magnetic properties of ^{7}Li

Quantity	Unit	SP	jj	Inter-mediate	LS	PHF	Experimental value	
							other experiments	this experiment
Magnetic dipole moment μ	[μ_N]	3.79 [a]	3.04 [b]	< 3.3 [b,c]	3.13 [b,c]	3.16 [d,e]	3.25628 [g]	3.2 ±0.4
$B(M1,\uparrow;k)$	[μ_N^2]	1.66 [f]	0.95 [f,b]	< 2.2 [c]	2.18 [c]	2.16 [c]	2.38±0.12 [h]	2.48±0.12

a) Ref. [35]). b) Ref. [36]). c) Refs. [37,38]). d) Ref. [19]). e) Ref. [20]). f) Ref. [18]).
g) Ref. [12]). h) Ref. [6]).

REF. D. Hiramatsu, T. Kamae, H. Muramatsu, K. Nakamura, N. Izutsu, and Y. Watase
PICNS-72, p.429 Sendai (see 73H15)

ELEM. SYM.	A	Z
Li	7	3

METHOD

REF. NO. 72 Hi 8 hvm

REACTION	RESULT	EXCITATION ENERGY	SOURCE TYPE	SOURCE RANGE	DETECTOR TYPE	DETECTOR RANGE	ANGLE
E,E/P	NOX	5*35	D	700	MAG-D		DST

* SEP ENERGY RANGE

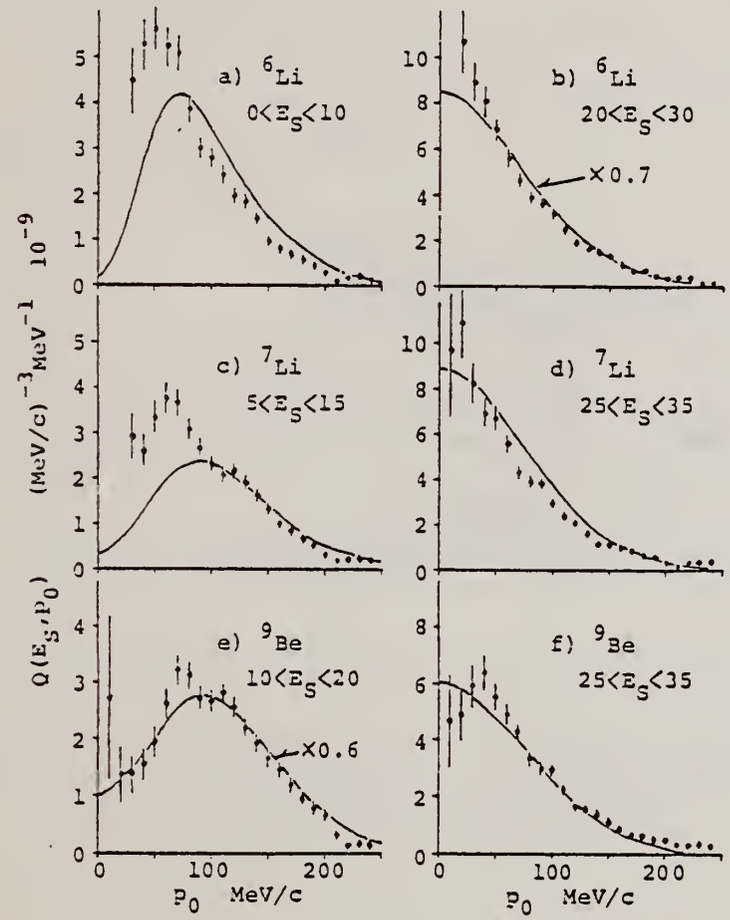

Fig. 4. Momentum distributions for ^{6}Li, ^{7}Li, and ^{9}Be

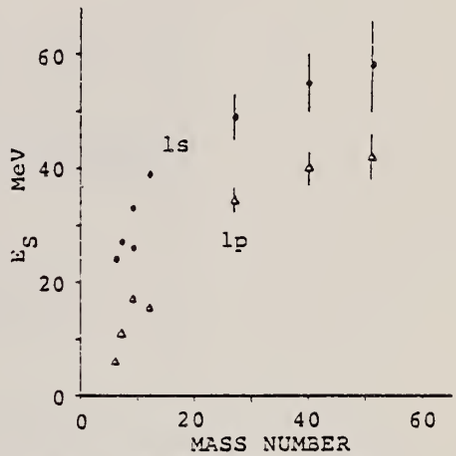

Fig. 6. The separation energy of 1s and 1p states as a function of the mass number.

the 1p state.

REF. J. Ahrens, H.B. Eppler, H. Gimm, H. Gundrum, M. Kroning, P. Riehn, G. SitaRam, A. Zieger, and B. Ziegler
PICNS-73, Vol.I, p.23 Asilomar

ELEM. SYM.	A	Z
Li	7	3

METHOD

REF. NO. 73 Ah 4 hmg

REACTION	RESULT	EXCITATION ENERGY	SOURCE		DETECTOR		ANGLE
			TYPE	RANGE	TYPE	RANGE	
G,MU-T	ABX	10-140	C	140	MGC-D		4PI

See figure on other side.

(continued)

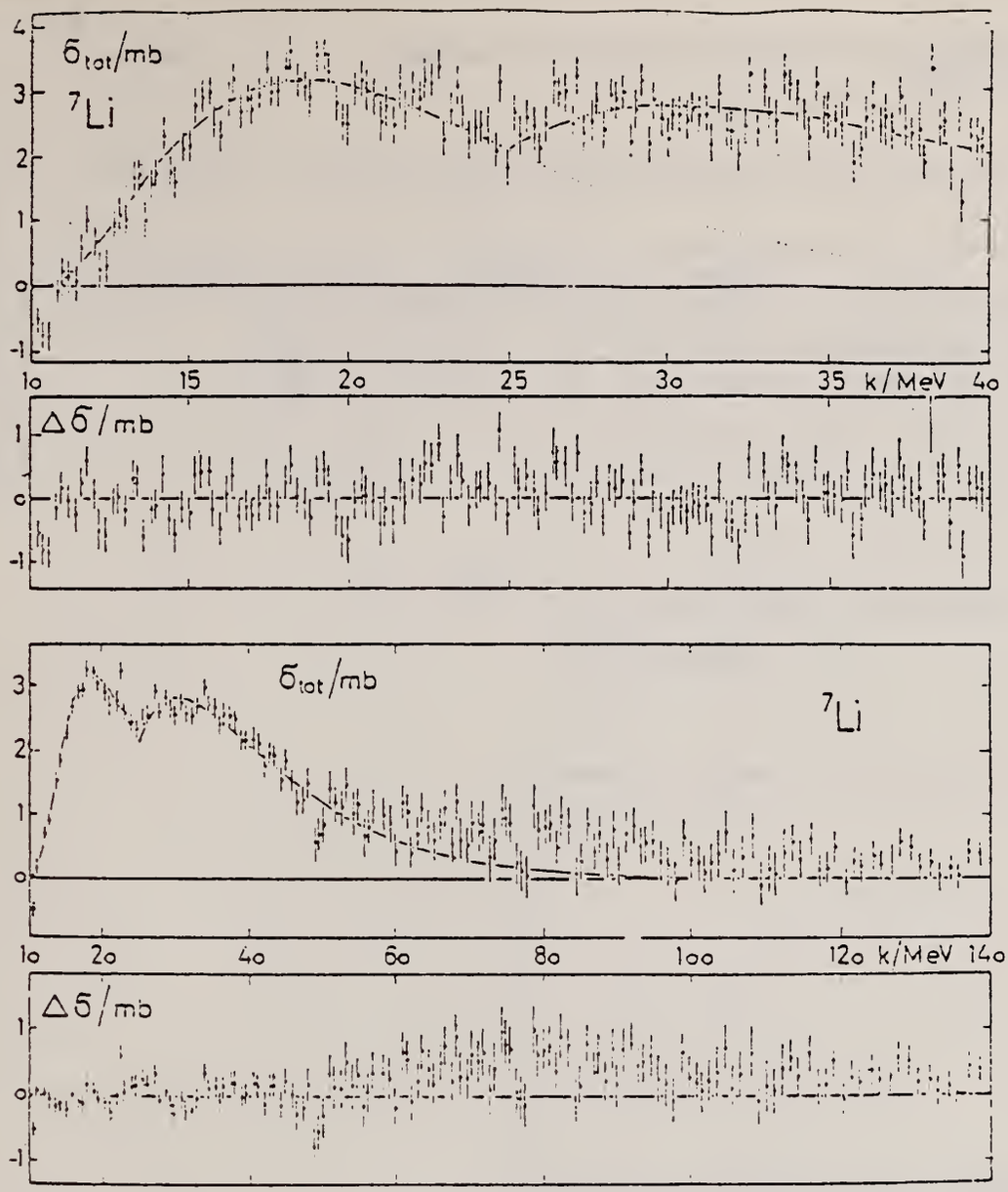

Fig. 2. Total photonuclear cross sections for Li. The dotted curves are the continuum functions given by Eq. (1), the sum of which is fitted to the points by eye. $\Delta\sigma$ is the difference cross section which remains after subtraction of the fitted curve from the measured points.

REF. R.L. Bramblett, B.L. Berman, M.A. Kelly, J.T. Caldwell, and S.C. Fultz
PICNS-73, Vol.I, p.175 Asilomar

ELEM. SYM.	A	Z
Li	7	3

METHOD

REF. NO. 73 Br 11 - hmg

REACTION	RESULT	EXCITATION ENERGY	SOURCE		DETECTOR		ANGLE
			TYPE	RANGE	TYPE	RANGE	
G,N	ABX	7- 31	D	7- 31	BF3-I		4PI
G,2N	ABX	11- 31	D	11- 31	BF3-I		4PI

510+

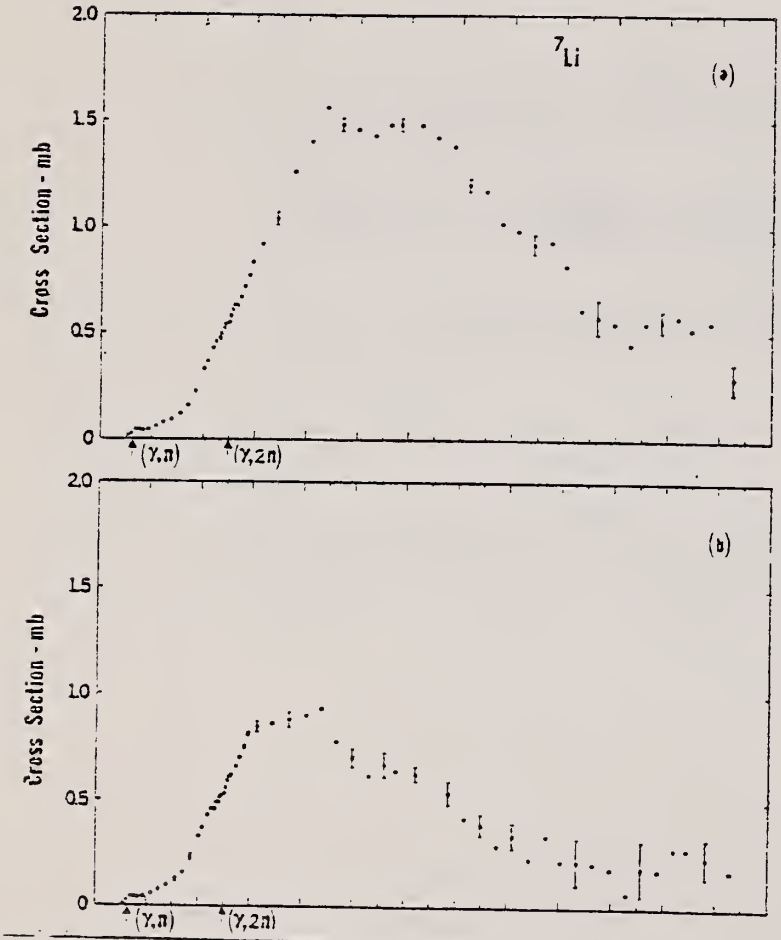

Figure 1. Photoneutron cross sections for ^{7}Li: (a) total photoneutron cross section $\sigma[(\gamma,n) + (\gamma,pn) + (\gamma,dn) + (\gamma,2n) + (\gamma,p2n)]$; (b) single photoneutron cross section $\sigma[(\gamma,n) + (\gamma,pn) + (\gamma,an)]$; (c) double photoneutron cross section $\sigma[(\gamma,2n) + (\gamma,p2n)]$.

(continued)

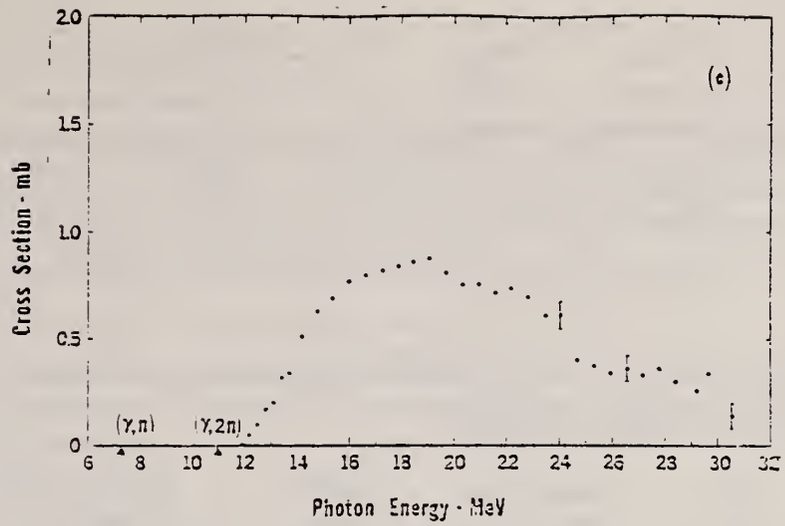
(c)
Cross Section - mb
2.0
1.5
1.0
0.5
0
(γ,n)
(γ,2n)
6
8
10
12
14
16
18
20
22
24
26
28
30
Photon Energy - MeV

REF.

S.N. Gardiner, J.L. Matthews, R.O. Owens
Phys. Letters 46B, 186 (1973)

Li	7	3

METHOD

REF. NO.

73 Ga 3 egf

REACTION	RESULT	EXCITATION ENERGY	SOURCE		DETECTOR		ANGLE
			TYPE	RANGE	TYPE	RANGE	
G,P	ABX	60	D	60	MAG-D		45

Table 1

Measured ^{6,7}Li(γ, p) cross sections for E_γ = 60 MeV, θ_p = 45° and comparison with the calculations of Weise [3, 10]. The theoretical results include final-state distortions and those "with correlations" are obtained for a Gaussian momentum-exchange package of width Δq_c = 100 MeV/c centred at q_c = 300 MeV/c.

Nucleus	Hole state	Excitation energy range (MeV)	$\frac{d\sigma}{d\Omega}$ (expt.) (μb/sr)	$\frac{d\sigma}{d\Omega}$ (theory) (μb/sr)	
				No correlations	With correlations
^{6}Li	p	0 – 9	4.2 ± 0.4		
	s	11.5 – 26.5	9.4 ± 1.1		
^{7}Li	p	0 – 9	7.3 ± 0.5	2.1	5.5
	s	9 – 26	11.3 ± 1.3	0.28	2.5

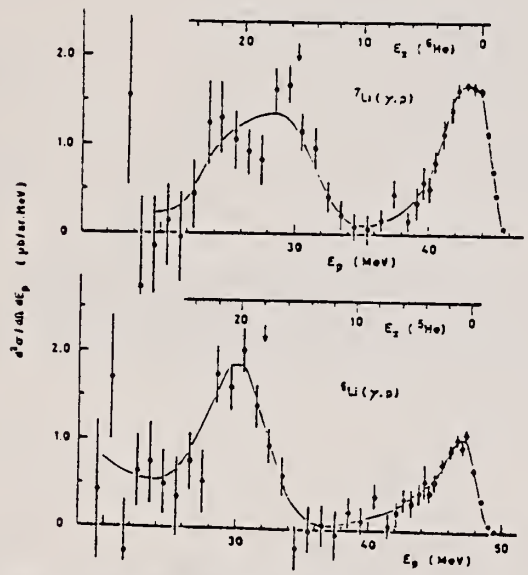

Fig. 2. Proton spectra from the ^{6}Li(γ, p) and ^{7}Li(γ, p) reactions for E_γ = 60 ± 1 MeV, θ_p(lab) = 45°. Excitation energies in the residual nuclei are also shown. The arrows in each spectrum indicate the location of the s-shell peak observed in the (p, 2p) reaction [8].

3
W. Weise, to be published.

8
G. Jacob and Th.A.J. Maris, Rev. Mod. Phys. 45, 6 (1973).

10
W. Weise, private communication.

REF. H. Hiramatsu, T. Kamae, H. Muramatsu, K. Nakamura, N. Izutsu, and Y. Watase
Phys. Letters 44B, 50 (1973)

ELEM. SYM.	A	Z
Li	7	3

METHOD

REF. NO. 73 Hi 5 egf

REACTION	RESULT	EXCITATION ENERGY	SOURCE TYPE	SOURCE RANGE	DETECTOR TYPE	DETECTOR RANGE	ANGLE
E,E/P	SPC	0*70	D	700	MAG-D		UKN

*SEP ENERGY RANGE

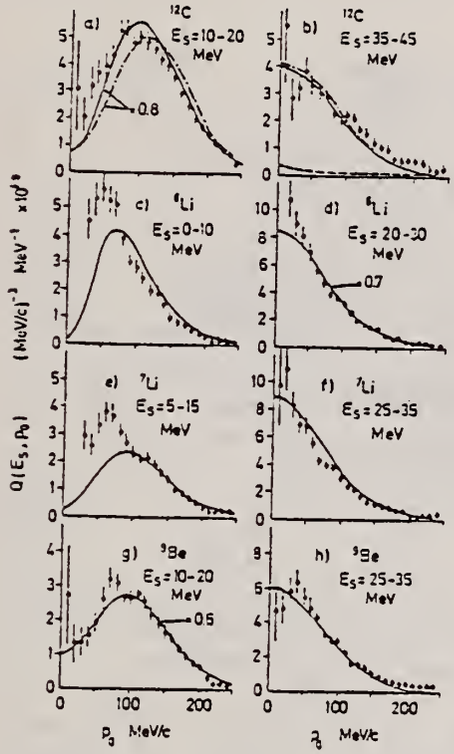

Fig. 2. Proton momentum distributions. See fig. 1 for the meaning of the curves in a) and b).

[5] C. Ciofi degli Atti, Nucl. Phys. A106 (1968) 215.

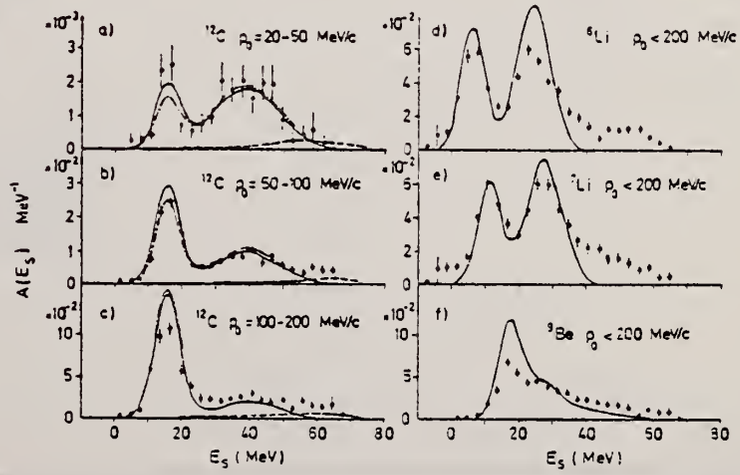

Fig. 1. Separation energy spectra. The solid curves show the DWIA results with the Woods-Saxon potentials. In a), b) and c) the dot-dashed curves represent the DWIA calculation with the harmonic oscillator potential given in ref. [5], and the dashed curves show the multiple collision background calculated by the Monte Carlo method.

REF. E.A. Kotikov and E.D. Makhnovskii
Yad. Fiz. 18, 245 (1973)
Sov. J. Nucl. Phys. 18, 125 (1974)

ELEM. SYM.	A	Z
Li	7	3

METHOD

REF. NO.	
73 Ko 6	- hmg

REACTION	RESULT	EXCITATION ENERGY	SOURCE		DETECTOR		ANGLE
			TYPE	RANGE	TYPE	RANGE	
G,PT	ABX	23- 27	C	27	EMU-D		90

$$\int_{23}^{27} \sigma dE = 1.0 \pm .1 \text{ MeV/mb.}$$

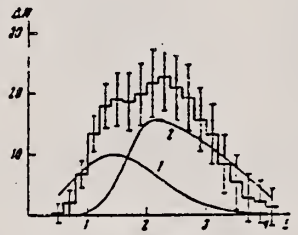

FIG. 2

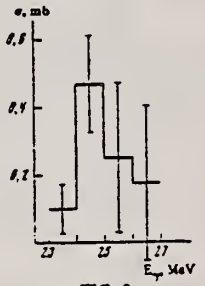

FIG. 3

FIG. 2. Difference distribution ΔN(B) (histogram). Curves: 1—contribution to the distribution of $Li^7(\gamma, pt)H^3$ reaction stars, 2—contribution of (3α) stars.

FIG. 3. Excitation function of the reaction $Li^7(\gamma, pt)H^3$.

REF. E.L. Kuplennikov, N.G. Afanas'ev, V.A. Gol'dshtein, V.I. Ogurtsov, and V.G. Vlasenko
Yad. Fiz. 18, 20 (1973)
Sov. J. Nucl. Phys. 18, 10 (1974)

ELEM. SYM.	A	Z
Li	7	3

METHOD

REF. NO.	
73 Ku 7	- hmg

REACTION	RESULT	EXCITATION ENERGY	SOURCE		DETECTOR		ANGLE
			TYPE	RANGE	TYPE	RANGE	
E,E/	ABX	84-284	D	1*	MAG-D		DST

* 1=1.184 MEV

10 ..

H. Uberall, Electron Scattering from Complex Nuclei, Academic Press, New York, 1971.

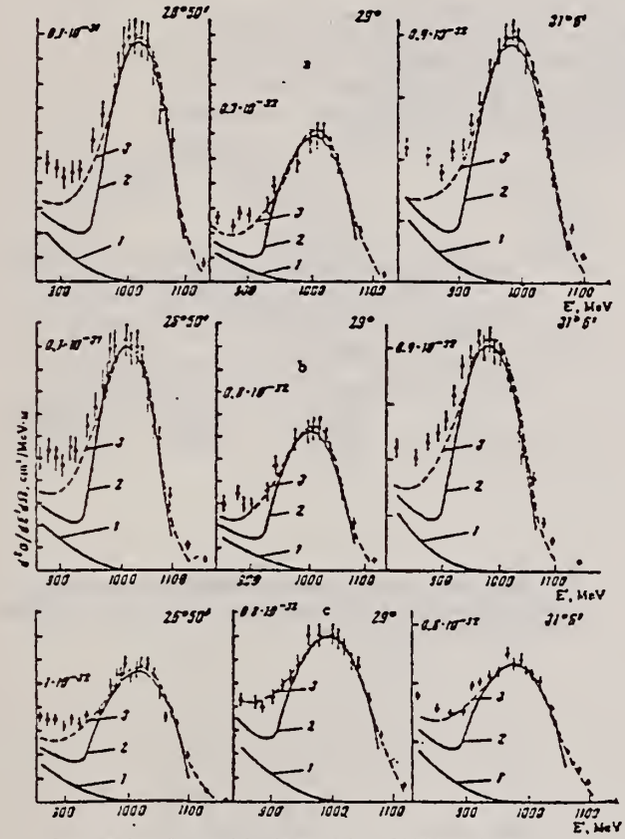

Cross sections for quasielastic scattering of 1184-MeV electrons on Li^6 (a), Li^7 (b), and Be^9 (c) vs energy E' of electrons scattered at 26°50', 29°, and 31°6'. The curves 1, 2, 3 represent calculations based, respectively, on allowance for the pion contribution, on the Fermi gas model, and on the single-particle shell model.

Nucleus	P_ϵ, MeV/c	$\langle r^2\rangle^{1/2}_{qu.elast}$, F	$\langle r^2\rangle^{1/2}_{elast}$, F	P_F, MeV/c	$\bar{\epsilon}$, MeV
Li^6	115±4	2.46±0.09	2.54±0.06	157±6	13±3
Li^7	116±4	2.43±0.09	2.37±0.03	160±6	14±3
Be^9	126±5	2.35±0.09	2.43±0.06	160±6	13±3

Remark. P is the oscillator parameter, $\langle r^2\rangle^{1/2}_{qu.elast}$ is the rms charge radius of the nucleus, P_F is the Fermi momentum, ϵ is the mean nucleon binding energy for $q \gtrsim 400$ MeV/c; all these experimental values were obtained for quasielastic electron scattering on the light nuclei Li^6, Li^7, and Be^9; $\langle r^2\rangle^{1/2}_{elast}$ is the experiment rms radius derived from elastic electron scattering on the same nuclei. [10]

REF. V. P. Denisov and I. Ya. Chubukov
Yad. Fiz. 20, 1106 (1974)
Sov. J. Nucl. Phys. 20, 579 (1975)

ELEM. SYM.	A	Z
Li	7	3

METHOD

REF. NO. 74 De 11 — hmg

REACTION	RESULT	EXCITATION ENERGY	SOURCE		DETECTOR		ANGLE
			TYPE	RANGE	TYPE	RANGE	
G,P	ABX	12- 40	C	15- 40	TEL-D		90

SEP ISOTOPES

2.4 MeV $\leq E_p \leq$ 23 MeV

The energy distributions of photoprotons from ^{7}Li have been measured for 40 values of the maximum bremsstrahlung energy $E_{\gamma m}$ ranging upwards from $E_{\gamma m} = 15.5$ MeV in $\Delta E_{\gamma m} \approx 1$ MeV steps. Analysis of these distributions shows that the ^{6}He final nucleus can be formed with excitations up to ~17 MeV. Transitions to the ^{6}He ground state and first excited state (1.8 MeV) were detected and indications were found of transitions to previously unknown levels (or groups of levels) at 2.5 and 8.5 MeV. Partial cross sections for the (γ, p) reaction with the formation of ^{6}He were found by the isochromat method.

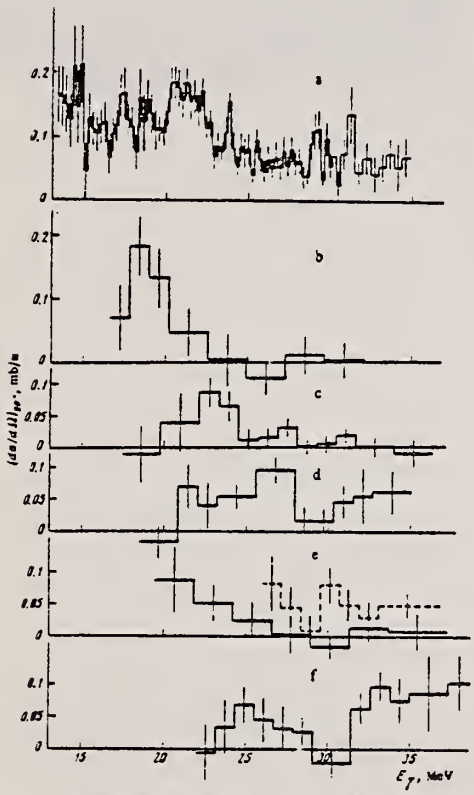

FIG. 3. Cross sections for individual ^{7}Li(γ, p) ^{6}He reaction channels corresponding to the formation of ^{6}He in the ground state (a), the first excited state at 1.8 MeV (b), and with excitation energies in the following intervals (MeV): 2.1–3.6 (c), 3.6–5.7 (d), 5.7–7.7 (e, full histogram), 7.7–11.0 (f), and 11.0–14.5 (e, dashed histogram).

TABLE II. Integral cross sections σ_{int} for individual channels of the ^{7}Li(γ, p)^{6}He reaction corresponding to the formation of ^{6}He with different excitation energies E(E_γ = 18–35 MeV)

E, MeV	σ_{int}, MeV·mb	E, MeV	σ_{int}, MeV·mb
0	14.4±0.6	5.7÷7.7	3.2±1.8
1.8	4.0±1.6	7.7÷11.0	5.3±1.7
2.1÷3.6	5.4±1.4	11.0÷14.5	6.2±1.5
3.6÷5.7	6.3±2.0	14.5÷17.5	5.3±1.5

[1]Translator's note: There is evidently a printer's error in the original Russian text, since there is no histogram g in Fig. 3; perhaps the dashed histogram on plot e is intended.

REF. N.V. Goncharov, S.G. Tonapetyan, and V.M. Khvorostyan
Yad. Fiz. 19, 21 (1974)
Sov. J. Nucl. Phys. 19, 10 (1974)

EL.EM. SYM.	A	Z
Li	7	3

METHOD

REF. NO.	
74 Go 1	hmg

REACTION	RESULT	EXCITATION ENERGY	SOURCE		DETECTOR		ANGLE
			TYPE	RANGE	TYPE	RANGE	
G,PI+	ABY	150-400	C	400	BBL -D		90
G,PI-	ABY	150-400	C	400	BBL -D		90
G,P	ABY	10-400	C	400	BBL -D		90

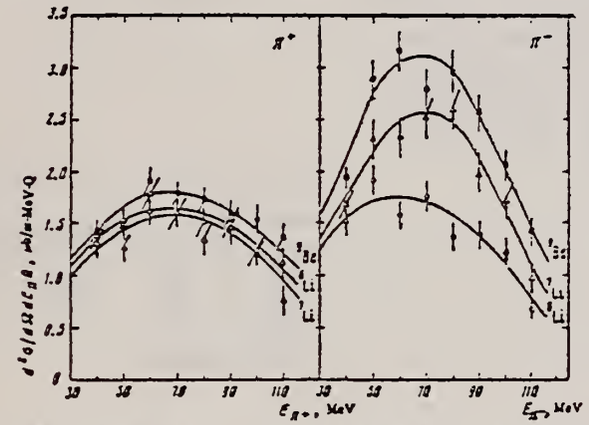

FIG. 1. Energy spectra of π^+ and π^- mesons. $E_\gamma^{max} = 400$ MeV, $\theta_{lab} = 90 \pm 7°$.

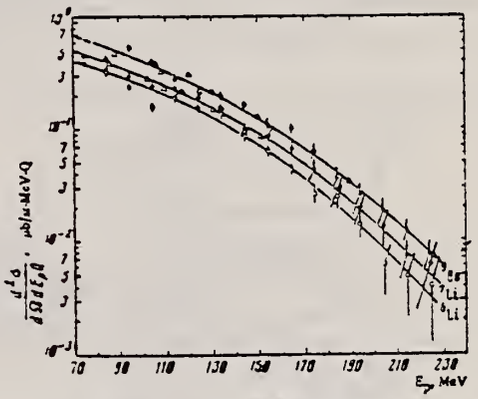

FIG. 2. Energy spectra of protons. $E_\gamma^{max} = 400$ MeV, $\theta_{lab} = 90 \pm 7°$. Points: circles—data of the present work, triangles—ref. 11.

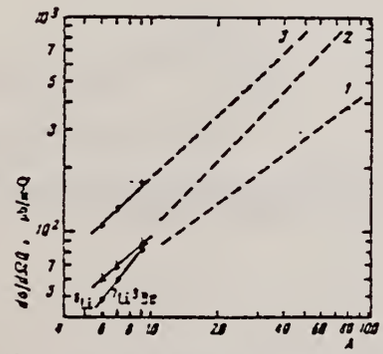

FIG. 3. Mass-number dependence of the yields of π mesons (points ▲, curve 1), protons (points ■, curve 2), and the sum of the π-meson and proton yields (points ●, curve 3). The dashed lines are the data from ref. 6.

[6] N.V. Goncharov et al., Yad. Fiz. 17, 242 (1973); Sov.J.Nucl.Phys. 17, 125 (1973).

[11] P. Dougan and W. Stiefler, Preprint LUSU, 1002-1005, 1970.

REF.

V. P. Denisov and I. Ya. Chubukov
Yad. Fiz. 22, 897 (1975)
Sov. J. Nucl. Phys. 22, 466 (1976)

ELEM. SYM.	A	Z
Li	7	3

METHOD

REF. NO. 75 De 7 hmg

REACTION	RESULT	EXCITATION ENERGY	SOURCE		DETECTOR		ANGLE
			TYPE	RANGE	TYPE	RANGE	
G,D	ABX	10- 51	C	15- 51	TEL-D		90
G,P *	ABI	10- 51	C	15- 51	TEL-D		90
G,T	ABI	2- 51	C	15- 51	TEL-D		90

*SEE ALSO 74DE11

Energy distributions of photodeuterons from ^{7}Li have been measured for various bremsstrahlung maximum energies. From difference spectra of the deuterons it has been established that in the region of the ^{7}Li giant resonance the (γ, d_0) reaction occurs intensely with formation of the ^{5}He nucleus in the ground state, and a group of deuterons has been observed which can be due to the reaction (γ, d_1) with formation of the final nucleus in the first excited state. The integrated cross sections of these reactions, on the assumption that the (γ, d_1) reaction actually occurs, are respectively 4.0±0.5 and 3.2±0.7 MeV-mb in the range $E_\gamma = 16.5$–30 MeV. In addition we have observed the emission of deuterons, which must be due to decay of ^{7}Li states with energies 25–30 MeV into $n + d + {}^4$He (5±2 MeV-mb), and also to some kind of complex disintegration of ^{7}Li (~5 MeV-mb) by γ rays with energy $E_\gamma = 37$–50 MeV.

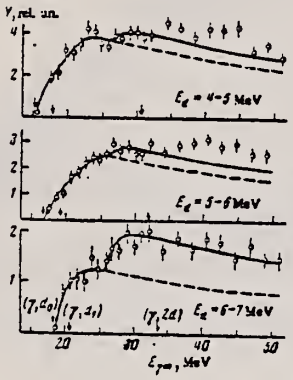

FIG. 3. Some deuteron yield curves and their approximation by isochromats. The arrows indicate the kinematic thresholds of the reactions shown.

Reaction	$E_{\gamma_1} \div E_{\gamma_2}$, MeV	σ^*_{int}, MeV-mb	$\frac{[\sigma(\gamma, d_0)]_{int}}{\sigma_{int}}$
(γ, p_0)	14–30	15.2±0.6	0.28
(γ, p)	16.5–30	44±4	0.16
(γ, t)	14–30	5.6±0.05	1.02
(γ, d_0)	14–30	5.7±0.23	1.0

*The errors are statistical.

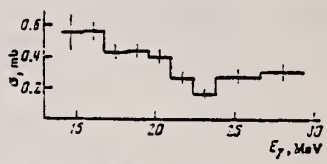

FIG. 4. Cross section for the reaction ^{7}Li$(\gamma, d_0)^5$He with formation of the final nucleus in the ground state.

REF.

J. L. Matthews, D. J. S. Findlay, S. N. Gardiner,
R. O. Owens
Nucl. Phys. A267, 51 (1976)

ELEM. SYM.	A	Z
Li	7	3

METHOD

REF. NO.	
76 Ma 8	egf

REACTION	RESULT	EXCITATION ENERGY	SOURCE		DETECTOR		ANGLE
			TYPE	RANGE	TYPE	RANGE	
G,P	ABX	60-100	D	60-100	MAG-D		DST

Cross Section Table given.

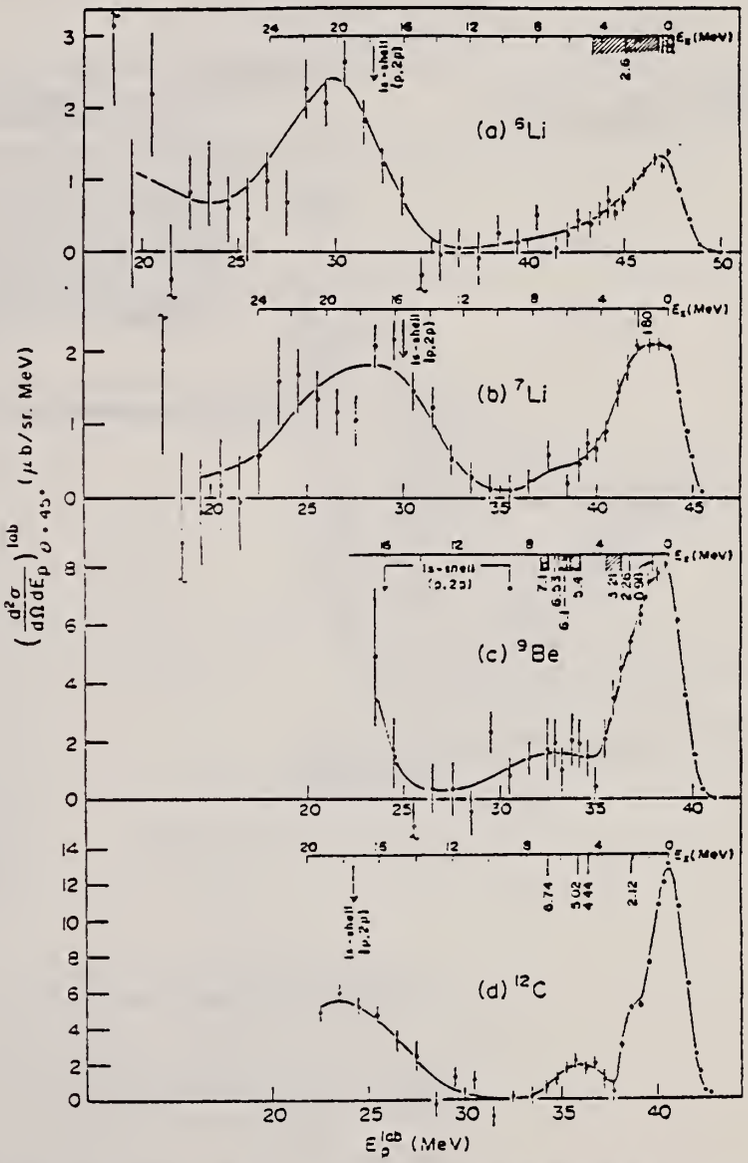

Fig. 8. Photoproton spectra for $E_\gamma = 60 \pm 1$ MeV, $\theta = 45°$ derived as described in the text from data such as those shown in fig. 7: (a) ^{6}Li(γ, p)^{5}He; (b) ^{7}Li(γ, p)^{6}He; (c) ^{9}Be(γ, p)^{8}Li; (d) ^{12}C(γ, p)^{11}B. The scale above each spectrum gives the excitation energy in the residual nucleus, with lines indicating the positions of known excited states. The location of the 1s shell peak observed in the (p, 2p) reaction is also marked.

(continued)

TABLE 1

Cross sections for the ^{6}Li, ^{7}Li, ^{9}Be and ^{12}C(γ, p) reactions at E_γ(lab) = 60 MeV, θ_p(lab) = 45° populating the excitation energy regions E_x = 0–9 MeV and 9–26 MeV in the residual nuclei

Target nucleus	$(d\sigma/d\Omega)^{\theta=45°}$ (μb/sr)	
	residual nucleus excitation energy E_x	
	0–9 MeV	9–26 MeV
^{6}Li	5.5 ± 0.6	12.2 ± 2.0
^{7}Li	9.5 ± 0.8	14.7 ± 3.0
^{9}Be	31.8 ± 3.0	
^{12}C	36.4 ± 3.9	

Only statistical errors are tabulated; there is an additional common systematic error of ± 22 %.

TABLE 5

Total cross sections at E_γ(lab) = 60, 80 and 100 MeV for the reactions ^{6}Li(γ, p)^{5}He (ground state + 2.6 MeV state), ^{7}Li(γ, p)^{6}He (ground state + 1.8 MeV state) and ^{12}C(γ, p)^{11}B (ground state, 2.1, 4.4, 5.0 and 6.7 MeV states in several combinations)

E_γ(lab) (MeV)	Total cross section (μb)				
	^{6}Li(γ, p_0+p_1)	^{7}Li(γ, p_0+p_1)	^{12}C(γ, p)		
			p_0	p_0+p_1	$p_0+p_1+\cdots p_4$
60	34.1 ± 1.6	43.8 ± 1.2	148.9 ± 4.6	182.7 ± 5.8	238.1 ± 11.7
80		11.39 ± 0.39	44.9 ± 2.1	48.4 ± 2.2	65.4 ± 3.9
100			17.2 ± 1.4	19.6 ± 1.1	

The errors shown are statistical. There is an additional common systematic error of ± 22 %.

REF. H. Ferdinande, N.K. Sherman, K.H. Lokan, C.K. Ross
Can. J. Phys. 55, 428 (1977)

ELEM. SYM.	A	Z
Li	7	3

METHOD

REF. NO. 77 Fe 1 hmg

REACTION	RESULT	EXCITATION ENERGY	SOURCE		DETECTOR		ANGLE
			TYPE	RANGE	TYPE	RANGE	
G,N	ABX	8- 23	C	13- 25	TOF-D		90

Photoneutron energy spectra from ^{7}Li have been measured by time-of-flight methods, for bremsstrahlung end-point energies increasing in 2 MeV steps from 13 to 25 MeV. The ground-state and approximate first-excited-state differential cross sections at 90° have been obtained from 8.5 to 23 MeV. No pronounced fine structure has been observed. The measured branching ratio to the first excited state falls from an average value of 0.70 between 10.3 and 14.5 MeV to an average of 0.29 between 14.5 and 18 MeV, and rises again to an average of 0.38 between 18 and 23 MeV. This behaviour can be explained by a crude theoretical model in which $1p \rightarrow 2s$ and $1p \rightarrow 1d$ single particle transitions dominate below 18 MeV. The calculation predicts a branching ratio of 0.50 near threshold, falling to 0.23 at higher energies, in reasonable agreement with the experiment. The integrated value of the ground-state cross section up to 23 MeV is about (38.7 ± 3.9) MeV mb, while that for the first excited state is about (17.2 ± 3.4) MeV mb. Together they account for 39% of the exchange-augmented dipole sum of ^{7}Li.

GND, 1ST EXCT STATE
OPEN SQUARES (G,NO) 1060

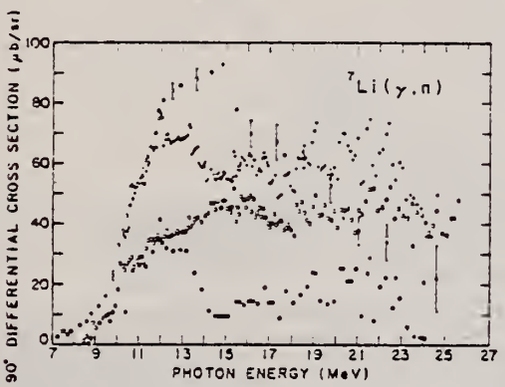

FIG. 4. The 90° differential photoneutron cross section for the reaction ^{7}Li(γ,n$_0$)^{6}Li (open squares), for the reaction ^{7}Li(γ,n$_1$)^{6}Li* (solid squares), and for the sum of both (solid circles), compared with the single-neutron cross section ^{7}Li(γ,n)^{6}Li of Bramblett *et al.* (1973) (open circles).

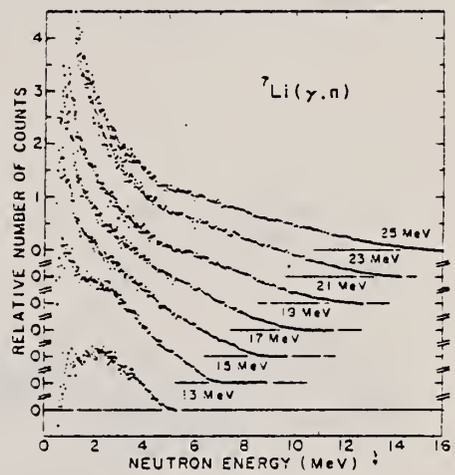

FIG. 2. Photoneutron energy distributions from ^{7}Li for bremsstrahlung end points increasing in 2 MeV steps from 13 to 25 MeV.

Bramblett et al., 1973. Proc. Int. Conf. Photonucl. React. Appl., ed. by B. L. Berman (Lawrence Livermore Laboratory, Univ. of California, Livermore, Calif.), p.175.

TABLE 1. The measured differential cross sections at 90°, $d\sigma_0/d\Omega$ for the ground state and $d\sigma_1/d\Omega$ for the first excited state, are given, integrated over intervals of photon energy k. The measured 90° branching ratio σ_1/σ_0 to the first excited state is compared to the calculated value for emitted neutrons having angular momentum $l = 0$ and the calculated value when $l = 0$ and $l = 2$

Photon energy (MeV)	$\int \left(\frac{d\sigma_0}{d\Omega}\right) dk$ (MeV mb sr^{-1})	$\int \left(\frac{d\sigma_1}{d\Omega}\right) dk$ (MeV mb sr^{-1})	σ_1/σ_0		
			Measured	$l = 0$	$l = 0, 2$
8.5 to 10.3	0.12 ± 0.04	0	0	—	—
10.3 to 14.5	1.08 ± 0.36	0.76 ± 0.15	0.70	0.50	—
14.5 to 18	1.07 ± 0.36	0.33 ± 0.07	0.29	—	0.23
18 to 23	1.58 ± 0.53	0.62 ± 0.12	0.38	—	—

REF. V.P. Denisov, I.Ya. Chubukov
Yad. Fiz. 27, 882 (1978)
Sov. J. Nucl. Phys. 27, 469 (1978)

ELEM. SYM.	A	Z
Li	7	3

METHOD

REF. NO. 78 De 7 hg

REACTION	RESULT	EXCITATION ENERGY	SOURCE		DETECTOR		ANGLE
			TYPE	RANGE	TYPE	RANGE	
G,NG	ABI	7-55	C	58	SCD-D		125

Assumed photon ang. dist. was isotopic. 6LI 3.56 MEV GAMMA

$\int_{30}^{55} \sigma d\epsilon$ = 7±3 MEV mb but affected by a strong background.

A Ge(Li) detector has been used to measure the spectra of photons emitted by residual nuclei from the reaction ^{7}Li (γ, n) ^{6}Li*, formed in the state with energy 3.56 MeV. The integrated cross section for the reaction up to $E_\gamma = 30$ MeV turned out to be 4±1 MeV-mb, and in the interval up to $E_\gamma = 55$ MeV it amounted to 11±3 MeV-mb.

PACS numbers: 25.20.+y, 27.20.+n

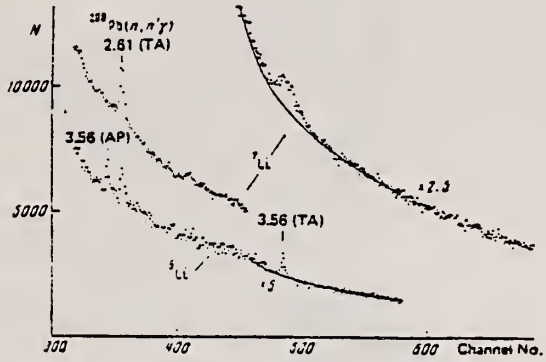

FIG. 1. Pulse-height spectra for targets of ^{7}Li and ^{6}Li. The smooth curves are the background level. TA and AP designate respectively the total-absorption peak and the peak with emission of two annihilation photons.

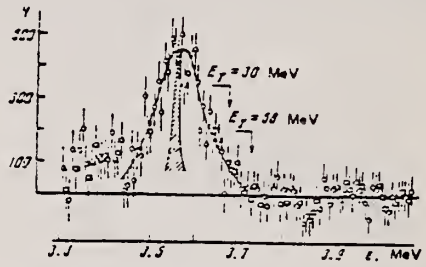

FIG. 2. Energy distribution of photons from the ^{7}Li target after background subtraction. The arrows indicate the Doppler broadening in absorption of γ rays of these energies. The errors do not include the inaccuracy in inclusion of the background. The crosshatched region is the distribution of photons from the ^{6}Li target (in arbitrary units) in the vicinity of the 3.56-MeV total-absorption peak.

REF. K. Nakamura, S. Hiramatsu, T. Kamae, H. Muramatsu, N. Izutsu, Y. Watase
Nucl. Phys. A296, 431 (1978)

ELEM. SYM.	A	Z
Li	7	3

METHOD

REF. NO.	
78 Na 3	- hg

REACTION	RESULT	EXCITATION ENERGY	SOURCE TYPE	SOURCE RANGE	DETECTOR TYPE	DETECTOR RANGE	ANGLE
E,E/P	SPC	0*60	D	700	MAG-D		53

Abstract: The proton spectral functions of ^{6}Li, ^{7}Li, ^{9}Be and ^{10}B obtained from the (e, e'p) reactions at 700 MeV are presented. The results were analyzed in the distorted-wave impulse approximation, using the shell-model single-particle wave functions consistent with the elastic electron scattering results. The observed 1p proton momentum distributions for the nuclei ^{6}Li, ^{7}Li and ^{9}Be show significant disagreement with the shell-model momentum distributions. The occupation probabilities of the proton single-particle states are around 0.7, with a few exceptions.

*SEPARATION ENERGY

E NUCLEAR REACTIONS ^{6,7}Li, ^{9}Be, ^{10}B(e, e'p), E = 700 MeV; measured $\sigma(E_p, \theta_p)$; deduced proton spectral functions. DWIA calculations. Enriched ^{6,7}Li, ^{10}B and natural ^{9}Be targets.

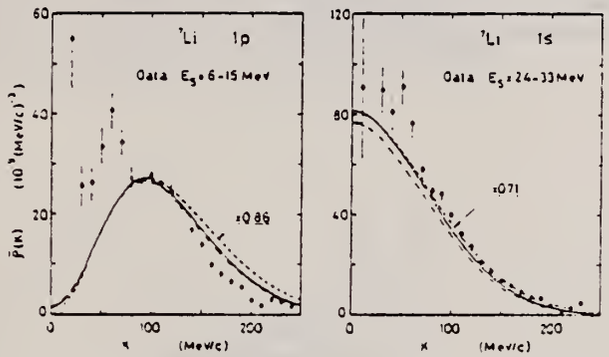

Fig. 5 The distorted momentum distributions corresponding to the optical potentials A (the solid curves) and B (the dot-dashed curves), and the undistorted momentum distributions (the dashed curves), calculated from the shell-model single-particle wave functions used in the DWIA analysis. (a) ^{6}Li, (b) ^{7}Li, (c) ^{9}Be and (d) ^{10}B. For comparison, data points in the appropriate separation energy ranges are shown. They are arbitrarily normalized to the calculated distorted momentum distributions.

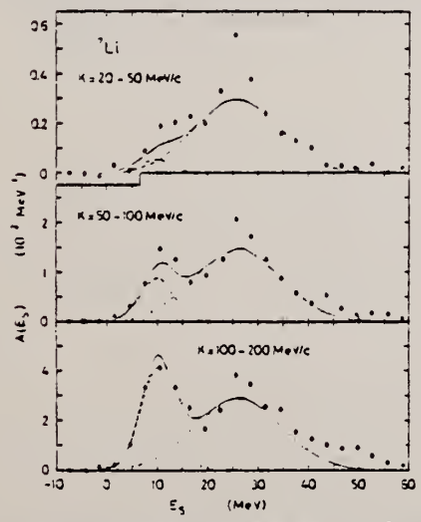

Fig. 2a. Proton separation energy spectra for ^{7}Li. The curves are as in fig. 1a.

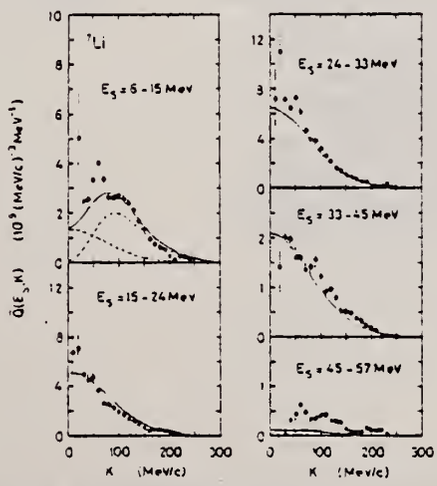

Fig. 2b Recoil momentum distributions for ^{7}Li. The curves are as in fig. 1b.

REF. Yu.M. Volkov, G.A. Kolomenskii, E.F. Lakovichev, E.D. Makhnovskii, A.V. Nadtochii, V.V. Popov, V.P. Fominenko & V.P. Chizhov
Yad. Fiz. 27, 868 (1978)
Sov. J. Nucl. Phys. 27, 461 (1978)

ELEM. SYM.	A	Z
Li	7	3

METHOD

REF. NO. 78 Vo 4 hmg

REACTION	RESULT	EXCITATION ENERGY	SOURCE		DETECTOR		ANGLE
			TYPE	RANGE	TYPE	RANGE	
G,T	ABX	3-55	C	30-55	TEL-D		90
G,TP	ABX	21-55	C	40-55	TEL-D		DST
G,TT	ABX	21-55	C	30-55	TEL-D		DST
G,T	ABX	3-55	C	32-55	TEL-D		DST

Results are presented of an experimental study of reactions of the type ^{6,7}Li (γ, ab)X with emission of charged particles a and b detected in coincidence. It is established that the major part of such reactions are reactions of the type ^{6,7}Li (γ,pt)X. The results of measurement of the correlations of the directions of emission and energy distributions of protons and tritons are explained on the basis of the assumption of photodisintegration of α clusters in the ground state of the nuclei ^{6,7}Li into a proton and triton and of formation of the residues X in the form of two ($d+n$) particles in reactions ^{6}Li (γ, pt)X, and two ($d+n$) particles and possibly three ($n+p+n$) particles in reactions ^{7}Li (γ, pt)X. The value of the average differential cross section of the reaction ^{6}Li (γ, pt) ^{1}Hn in the γ-ray energy interval 35–55 MeV amounts to 0.7±0.2 of the value of the cross section for the reaction ^{4}He (γ, p) ^{3}H. It is shown that in addition, three-particle reactions of the type ^{6}Li (γ,td) ^{1}H and ^{7}Li (γ, π) ^{1}H occur, but with a kinematics differing from that of the photodisintegration of α clusters, and also two-particle reactions of the type ^{6}Li (γ, t) ^{3}He and ^{7}Li (γ, t) ^{4}He.

(G,T) ALL TRITONS
(G,TP) COINC. T WITH P
(G,TT) COINC. T WITH T
(G,T) 2 BODY BREAKUP ONLY

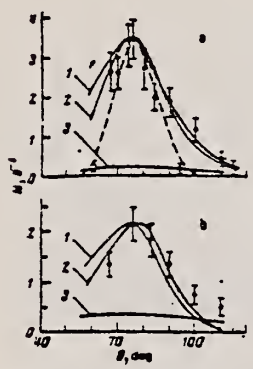

FIG. 3. Correlations of directions of emission of protons and tritons in the reactions: a—^{6}Li(γ, tp)X; b—^{7}Li(γ, tp)X. Points: ●—numbers of coincidences per unit dose, O—experimental angular resolution of the apparatus; solid curves: 1—calculated angular correlation for the reactions ^{6,7}Li(γ, tp)^{1,2}Hn on the assumption of photodisintegration of α clusters; curve 2—the same, but for the reactions ^{6,7}Li(γ, tp)^{2,3}H; curve 3—calculation of the relative contribution of the three-particle reactions ^{6,7}Li(γ, tp)^{2,3}H on the assumption of phase-space kinematics; dashed curve—calculated angular resolution of the apparatus; curves 1 and 2 have been normalized to the experimental results at an arbitrary point.

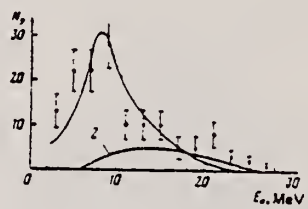

FIG. 5. Energy distribution of protons coincident with tritons in the reaction ^{7}Li(γ, pt)X. Curves: 1—result of calculation on the assumption of photodisintegration of α clusters for the reaction ^{7}Li(γ, pt)^{2}Hn; 2—the same as curve 1, but for the reaction ^{7}Li(γ, pt)^{3}H. The normalization is the same as in Fig. 4a.

TABLE II. Differential cross sections of identified reactions.

Reaction	Average energy of γ rays $\bar{E}_\gamma$, MeV	$\frac{d\sigma(\theta=90°;\bar{E}_\gamma)}{d\Omega}$, μb/sr ($E_t \geq 4$ MeV, $E_p \geq 3$ MeV	Kinematic reaction threshold E_{th}, MeV	Reaction yield $\int_{E_{th}}^{55} E_\gamma \frac{dN_\gamma}{dE_\gamma} dE_\gamma$, 1 MeV · 10^{-30} / MeV · sr · atom/cm²	$\frac{d\sigma(\theta=90°;\bar{E}_\gamma)}{d\Omega}$, μb/sr ($E_t > 0$, $E_p > 0$)
$^6Li(\gamma, t)X$			23	7.9±1.5	
$^6Li(\gamma, tp(pt))pn$ *	48±6	9.8±1.5	34	3.3±0.5	66.7±11.5
$^6Li(\gamma, td)p$ **	43±10	0.9±0.4	23	0.3±0.2	2.0±0.9
$^6Li(\gamma, t)^4He$	45±7	6.0±0.9	28	3.1±0.5	
$^7Li(\gamma, t)X$			30	10.0±2.2	
$^7Li(\gamma, tp(pt))dn$ *	49±4	3.9±0.7	40	1.4±0.2	44.8±6.8
$^7Li(\gamma, td)p$ **	43±10	3.4±0.7	30	2.5±0.5	7.1±1.3
$^7Li(\gamma, t)^4He$	41±9	3.0±0.4	31	2.2±0.3	
$^{12}C(\gamma, t)p$ [7]	$\frac{d\sigma(\theta=90°;\bar{E}_\gamma=34\ \text{MeV}}{d\Omega} = 93.0 \pm 9.5\ \mu b/sr$				

Table II lists values of the differential cross sections of identified reactions $^{6,7}Li(\gamma, tp)X$ in which tritons with energy $E_t \geq 4$ MeV are emitted at an angle $\vartheta_t = 90°$ and protons with energy $E_p \geq 3$ MeV at all possible angles, and also values of the differential cross sections for the two-particle reactions $^{6,7}Li(\gamma, t)^{3,4}He$ and the correlations of particle-emission directions established after normalization of the theoretical results to the experimental data. Also in Table II we have given the energies of the γ-rays producing the reactions noted above. The

REF. P.E. Bosted, K.I. Blomqvist, A.M. Bernstein
Phys. Rev. Lett. 43, 1473 (1979)

ELEM. SYM.	A	Z
Li	7	3

METHOD

REF. NO. 79 Bo 3 hg

REACTION	RESULT	EXCITATION ENERGY	SOURCE TYPE	SOURCE RANGE	DETECTOR TYPE	DETECTOR RANGE	ANGLE
G,PI-	ABX	150-360	C	150-360	ACT-I		90
E,PI-	RLX	200-360	D	150-360	ACT-I		90

Total cross sections for $^{12}C(\gamma,\pi^-)^{12}N$ and $^7Li(\gamma,\pi^-)^7Be$ have been measured from threshold to 360 MeV photon energy by detecting the radioactivity of the residual nuclei, thereby singling out the ground state of ^{12}N and the ground and first excited states of ^7Be. The cross sections are found to peak at about 40 MeV pion energy and then to fall gradually. In contrast to pion charge exchange and other photopion experiments, these results are well reproduced both in shape and in magnitude by distorted-wave impulse-approximation calculations.

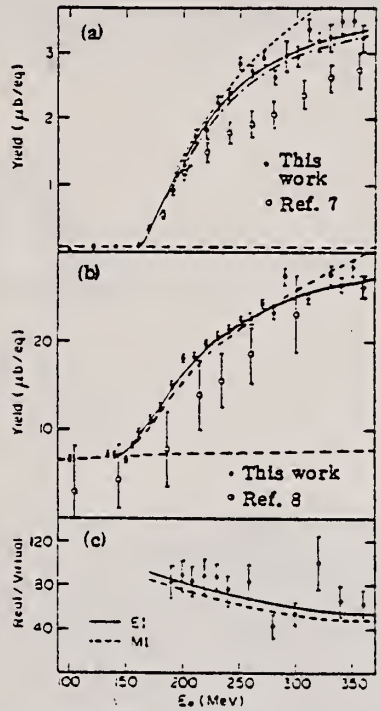

FIG. 2. Yields for (a) ^{12}C and (b) ^7Li as a function of incident electron energy. The theoretical curves are those calculated from the corresponding cross sections shown in Fig. 3 with the two-step background added back in. (c) Real-to-virual ratios per equivalent quantum (i.e., photoproduction-to-electroproduction ratios) for ^{12}C vs endpoint energy compared with Dalitz-Yennie predictions.

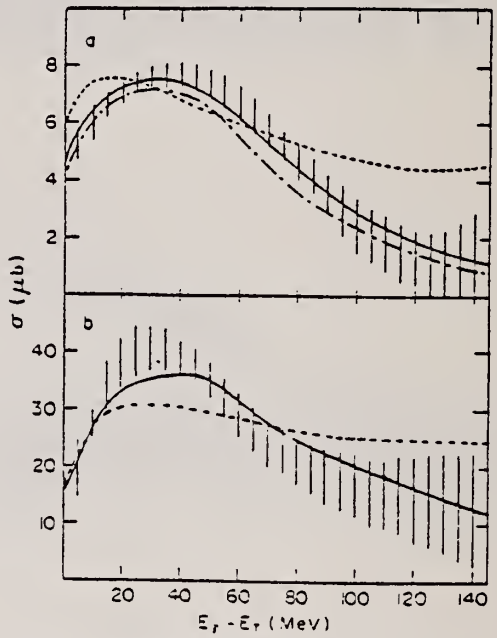

FIG. 3. Extracted cross sections for (a) ^{12}C and (b) ^7Li vs photon energy above threshold (shaded regions). Calculation of EST (see Ref. 13) shown as solid lines (full interaction) and dotted line (Coulomb only). Calculation of NU (see Ref. 15) shown as dash-dotted line.

REF. G. Junghans, K. Bangert
Z. Phys. A291, 353 (1979)

ELEM. SYM.	A	Z
Li	7	3

METHOD

REF. NO. 79 Ju 6 hg

REACTION	RESULT	EXCITATION ENERGY	SOURCE		DETECTOR		ANGLE
			TYPE	RANGE	TYPE	RANGE	
G,P	ABX	11-27	C	28,50	TEL-D		DST
G,D	ABX	5-22	C	28,50	TEL-D		DST
G,T	ABX	6-28	C	28,50	TEL-D		DST
G,He3	RLY	6-11	C	50	TEL-D		DST
G,A	ABX	16-27	C	28	TEL-D		DST

The photodisintegration of the stable Lithium isotopes has been investigated by spectroscopy of the emitted charged particles using the Giessen bremsstrahlung facility. Protons, deuterons, tritons, ^{3}He and alpha particles were detected and identified up to 20 MeV particle energy. Angular distributions were measured using γ-ray energies up to $E_\gamma = 50$ MeV. They are compared with theoretical predictions and with other experiments. A remarkable low (γ, t)-cross section was found for both isotopes in disagreement to previous measurements using virtual photons. Coincidence measurements between the emitted particles were performed in order to study the manybody-breakups of ^{7}Li.

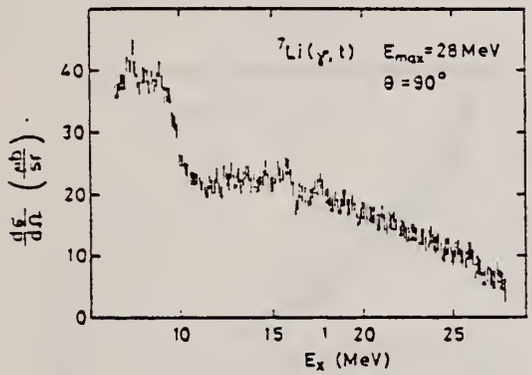

Fig. 3. Phototriton cross section of ^{7}Li. $E_{\gamma,max}$=28 MeV, θ=90°

Table 2. Dipol sum rules of ^{6}Li and ^{7}Li

	(γ, p)	(γ, n)	(γ, t)	Ref.
^{6}Li	23.4 ±3.8[b]			[34]
σ_{-1} MeVmb		27.4 ±2.0[a]		[28]
			17 ±1[b]	[8]
			4.9 ±2.5[k]	[3]
	16.3 ±2.5[c]		7.0 ±1.0[d]	this work
^{7}Li	21.6 ±3.5[a]			[34]
σ_{-1} MeVmb		20.1[i]		[21]
			8.0[e]	[11, 22]
	14.6 ±3.4[f]			[5]
	13.2 ±2.0[g]		4.4 ±0.7[h]	this work
^{6}Li	1.9 ±0.3[b]			[34]
σ_{-1}/mb		1.85±0.1[a]		[28]
			0.77±0.03[b]	[8]
			0.18±0.09[k]	[3]
	1.4 ±0.2[c]		0.29±0.04[d]	this work
^{7}Li	1.17±0.19[a]			[34]
σ_{-1}/mb		1.15[i]		[21]
			0.74[e]	[11, 22]
	0.8 ±0.1[g]		0.4 ±0.06[h]	this work

[a] 5.5–32 MeV [b] 22–32 MeV [c] 6.4–30 MeV
[d] 20–30 MeV [e] 5–15 MeV [11], 15–30 MeV [22]
[f] threshold to 34 MeV [g] 11–28 MeV [h] 5.5–28 MeV
[i] threshold to 30.5 MeV [k] 19–35 MeV

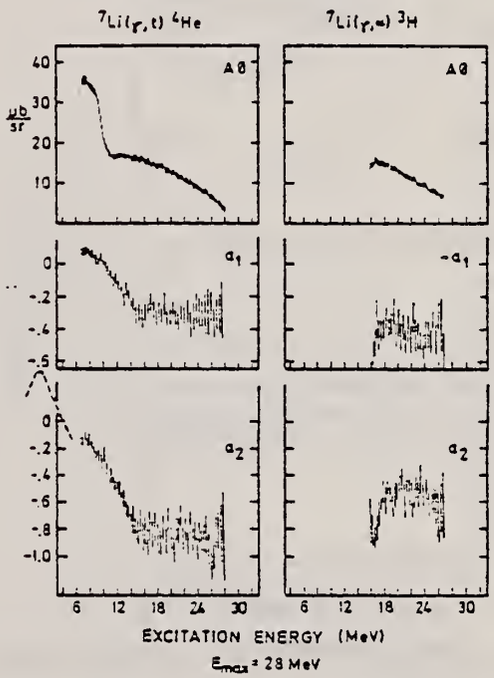

Fig. 4. Angular distribution of the ^{7}Li(γ, t) and ^{7}Li(γ, α) cross section; $E_{\gamma,max}$=28 MeV

$$\frac{d\sigma}{d\Omega}(\alpha, E) = A_0(E)\left[1 + \sum_{i=1}^{n} a_i(E) P_i(\cos\theta)\right]$$

(continued)

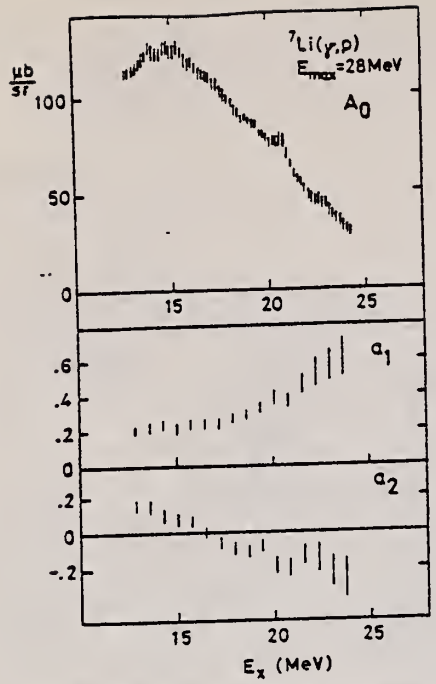

Fig. 10. Angular distribution of the ^{7}Li photoproton cross section; $E_{\gamma max} = 28$ MeV

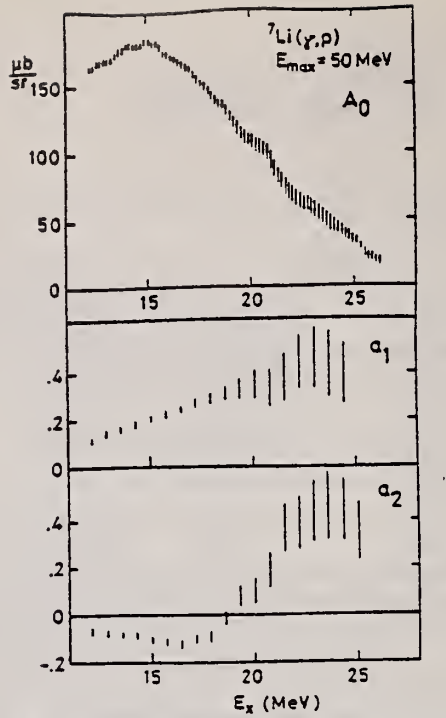

Fig. 11. Angular distribution of the ^{7}Li photoproton cross section; $E_{\gamma max} = 50$ MeV

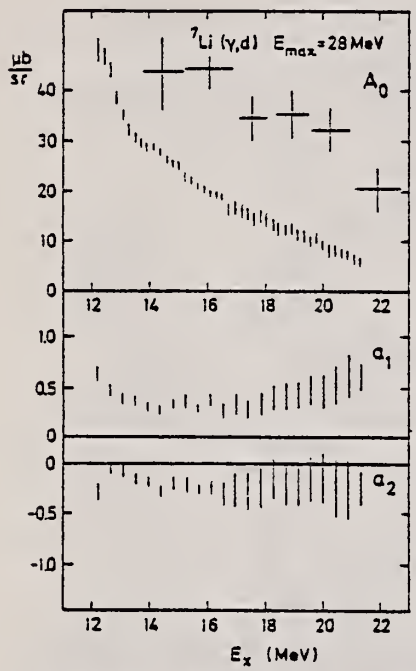

Fig. 12. Angular distribution of the ^{7}Li photodeuteron cross section; $E_{\gamma max} = 28$ MeV

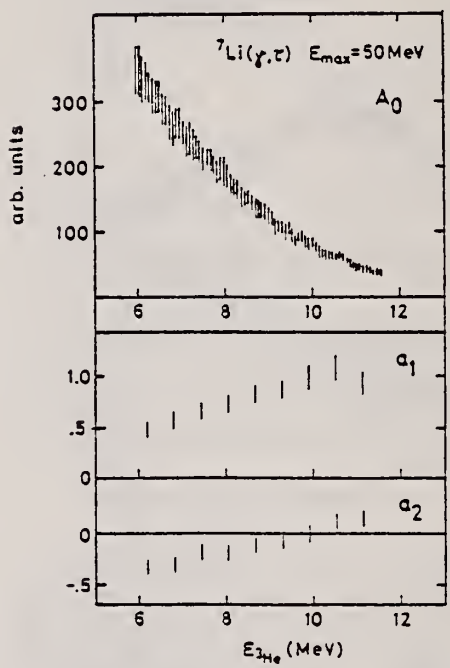

Fig. 13. Angular distribution of the ^{7}Li(γ, τ) yield. $E_{\gamma max} = 50$ MeV

REF. J. Asai, J.J. Murphy II, D.M. Skopik
Phys. Rev. C21 (1980)

ELEM. SYM.	A	Z
Li	7	3

METHOD

REF. NO. 80 As 3 hg

REACTION	RESULT	EXCITATION ENERGY	SOURCE		DETECTOR		ANGLE
			TYPE	RANGE	TYPE	RANGE	
E,HE6	ABX	80-110	D	108-198	MAG-D		DST
E,LI6	ABX	80-163	D	163	MAG-D		DST

The reactions ^{7}Li(e,^{6}He)pe' and ^{7}Li(e,^{6}Li)ne' have been studied at intermediate excitation energies. Angular distributions as well as energy distributions are presented. The experimental cross sections are compared to the results obtained from a simple model.

2 BODY, VIR PHOT ANAL

[NUCLEAR REACTIONS ^{7}Li(e,^{6}He), ^{7}Li(e,^{6}Li), E=108, 163, 198 MeV; measured $\sigma(E,\theta)$. Natural targets.]

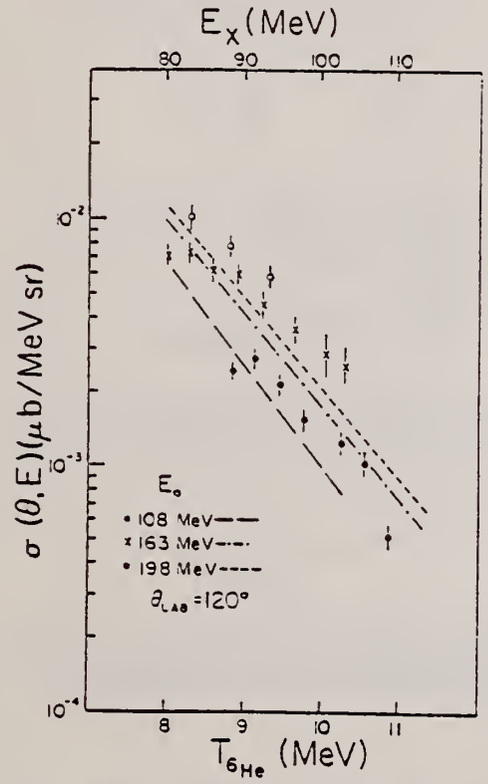

FIG. 2. Electrodisintegration cross sections at 120° in the laboratory for the reaction ^{7}Li(e,^{6}He)pe'. The curves are the cross sections calculated from the simple model described in the text. Cross sections for incident electron energies of 108, 163, and 198 MeV are shown.

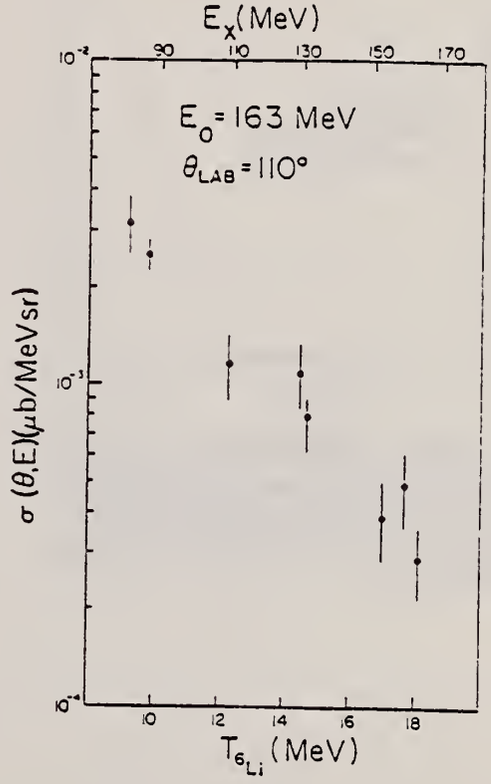

FIG. 3. Electrodisintegration cross sections at 110° in the laboratory for the reaction ^{7}Li(e,^{6}Li)ne'. No theoretical curve is shown because it is several orders of magnitude smaller than the experimental results. The data shown are for an incident electron energy of 163 MeV.

(continued)

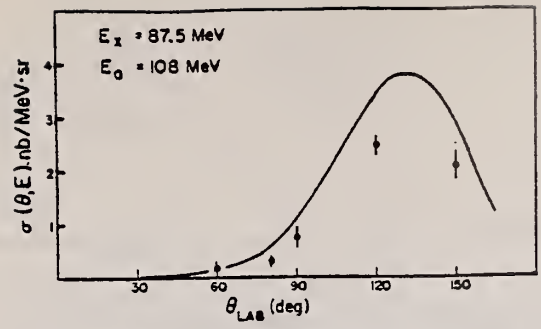

FIG. 4. The ^{7}Li(e,^{6}He)pe' angular distribution for an excitation energy of 87.5 MeV and an incident electron energy of 108 MeV. The curve is calculated from the model described in the text.

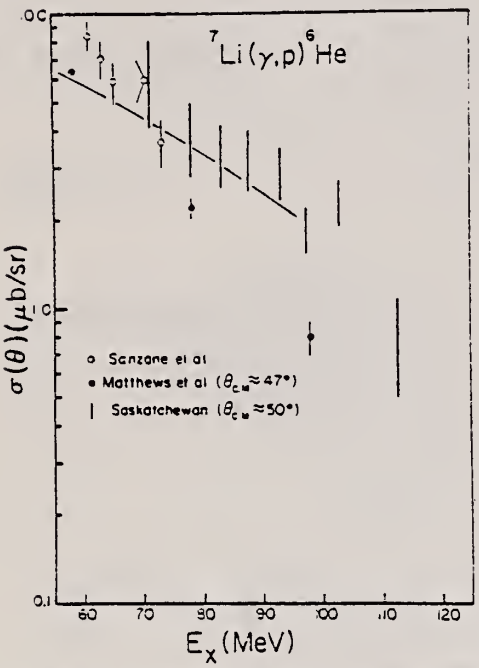

FIG. 6. Equivalent photodisintegration cross sections for the reaction ^{7}Li(γ,p)^{6}He. The errors reflect statistical and systematic effects associated with using the $E1$ and $E2$ virtual photon spectra, respectively, in the analysis. The data from other laboratories are taken from Ref. 2. The solid line is the calculation of Weise and Huber (Ref. 6).

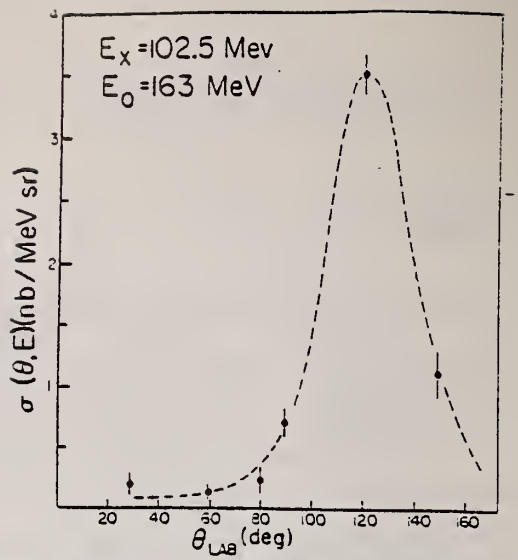

FIG. 5. The ^{7}Li(e,^{6}Li)ne' angular distribution for an excitation energy of 102.5 MeV and an incident electron energy of 163 MeV. No theoretical curve is shown because it is several orders of magnitude smaller than the experimental results and shows peaking at the forward angles. The dashed line is only meant to guide the eye.

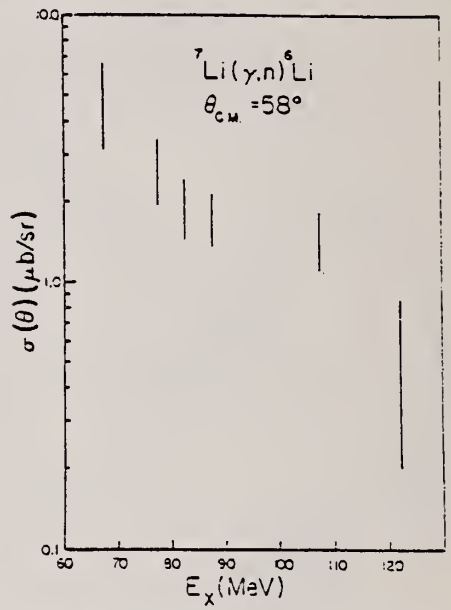

FIG. 7. Equivalent photodisintegration cross sections for the reaction ^{7}Li(γ,n)^{6}Li. The same comment concerning the errors made for Fig. 6 applies here.

REF. Yu.I. Titov, A.S. Esaulov, R.V. Akhmerov, N.G. Afanas'ev, A.S. Omelaenko, E.M. Smelov
Sov. J. Nucl. Phys. 31, 724 (1980)
Yad. Fiz. 31, 1396 (1980)

EL EM. SYM.	A	Z
Li	7	3

METHOD

REF. NO.	
80 Ti 4	- hg

REACTION	RESULT	EXCITATION ENERGY	SOURCE		DETECTOR		ANGLE
			TYPE	RANGE	TYPE	RANGE	
E,E/	ABX	100-400	D	450*999	MAG-D		DST

Measurements have been made for the first time of the contributions of the longitudinal and transverse components to the cross section for inelastic scattering of electrons by the ^{7}Li nucleus in the region of the pion-production threshold and the (33) resonance. The violation of the impulse approximation in the region of the minimum between the quasielastic scattering peak and the (33) resonance peak is associated with the contribution of meson-exchange currents.

*999=1096 MEV

PACS numbers: 25.30.Cg, 27.20. + n

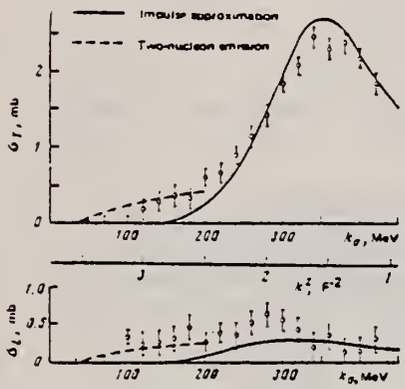

FIG. 1. Longitudinal and transverse components of inelastic scattering of electrons by ^{7}Li. The contribution of quasielastic scattering was subtracted before separation of σ_T and σ_L.

REF. B.S. Ishkhanov, Yu.A. Novikov, I.M. Piskarev
Sov. J. Nucl. Phys. 33, 15 (1981)
Yad. Fiz. 33, 28 (1981)
Sov. J. Nucl. Phys. 33, 15 (1981)

ELEM. SYM.	A	Z
Li	7	3

METHOD

REF. NO. 81 Is 7 egf

REACTION	RESULT	EXCITATION ENERGY	SOURCE TYPE	SOURCE RANGE	DETECTOR TYPE	DETECTOR RANGE	ANGLE
G,G/	ABI	2-8	C	27,31	SCD-D		135

The photon spectra from the reaction ^{7}Li(γ,γ') have been studied in bremsstrahlung beams with maximum energies 27 and 31 MeV. It is shown that the peak at 8.5 MeV is due to formation of the ^{3}H nucleus during the reaction.

PACS numbers: 25.20. + y, 27.20. + n

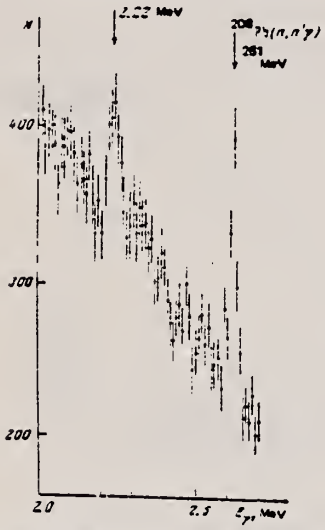

FIG. 1. Portion of the energy spectrum of photons from the reaction ^{7}Li(γ,γ') at E_{max} 31 MeV. The energy scale was established on the basis of the total-absorption peak.

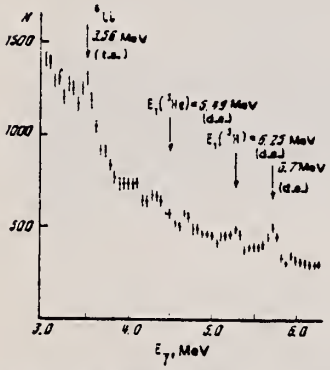

FIG. 2. The same as Fig. 1. t. a. —total absorption peak, d. e. —double-escape peak (E_γ = 1.02 MeV).

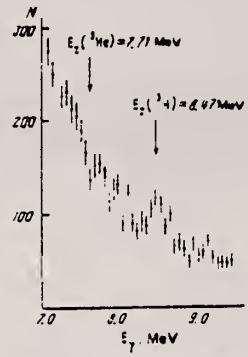

FIG. 3. The same as Fig. 1. The energy scale corresponds to the double-escape peak.

TABLE I. Characteristics of peaks observed in the energy spectra of photons from the reaction ^{7}Li(γ,γ').

Energy of peak, MeV	Integrated cross section, MeV · mb		
	Present work		
	E_{max} = 31 MeV	E_{max} = 27 MeV	Data from (γ,γ') reaction
2.22±0.01	1.5±0.4	1.1±0.3	1.6±0.5 *
3.55±0.05	3±1	2.5±1	4±1 **
3.49	<1	<1	–
6.25±0.1	1.5±0.5 ***	1.4±0.5 ***	–
6.32	–	–	–
6.7±0.15	2.5±1	<0.5	22 ****
7.71	<0.5	<0.5	–
8.5±0.1	1±0.5	0.8±0.4	–

*From Ref. 1, E_{max} = 32 MeV.
**From Ref. 8, E_{max} = 30 MeV.
***Obtained on the assumption that the peak is due to the reaction ^{7}Li($\gamma,^3$H).
****From Ref. 7, E_{max} = 30 MeV.

REF. V.P. Denisov, I.Ya. Chubukov
Yad. Fiz. 35, 11 (1982)
Sov. J. Nucl. Phys. 35, 6 (1982)

ELEM. SYM.	A	Z
Li	7	3

METHOD

REF. NO.	
82 De 2	egf

REACTION	RESULT	EXCITATION ENERGY	SOURCE		DETECTOR		ANGLE
			TYPE	RANGE	TYPE	RANGE	
G,T	ABX	10-17	C	25,37	TEL-D		DST

The α-t interaction potential model, which takes into account forbidden states in ^{7}Li, was used to calculate cross sections for the ^{7}Li(γ, t)^{4}He reaction. In addition, the energy and angular dependence of the reaction cross section was also measured. Comparison of experiment and calculation shows that the model describes $E1$ absorption well. However, there are discrepancies in the coefficients which determine the contribution of $E2$ absorption to the angular distribution.

PACS numbers: 25.20. + y, 27.20. + n, 21.60.Gx

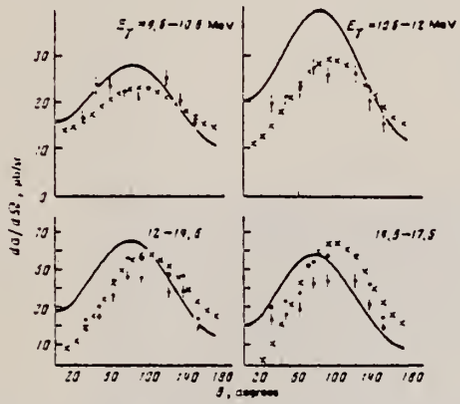

FIG. 2. Triton angular distributions: full curve—calculation, points with experimental errors—present work, crosses—Ref. 7, and solid points—present data normalized to the data in Ref. 6.

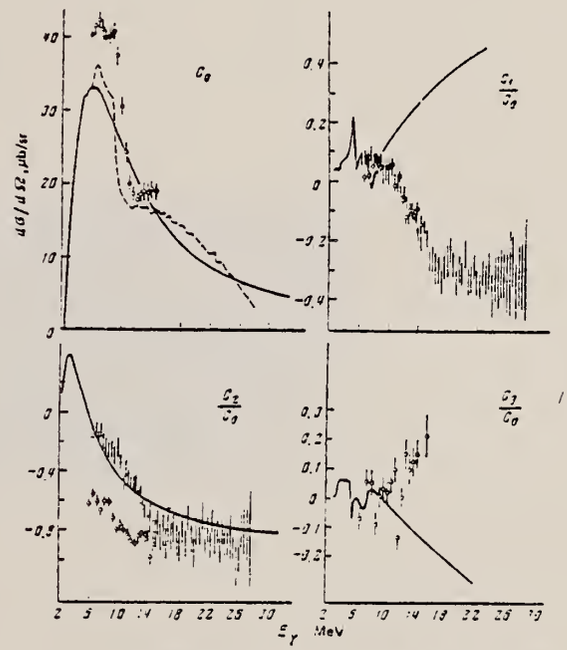

FIG. 3. Coefficients for Legendre polynomials: full curve—calculation, vertical lines and dashed curve—Ref. 6, and, open points—Ref. 7.

79 Ju 6 [6]G. Junghans *et al.*, Z. Phys. A291, 353 (1979).
[7]D. M. Skopik *et al.*, Phys. Rev. C 20, 2025 (1979).

BERYLLIUM
Z=4

Berylia (beryllium oxide) was first isolated in 1797 by L. N. Vauquelin from beryl, a silicate of beryllium and aluminum, from which came the name beryllium. The word has its origin from the German word Brille "eye glasses" for the reason that Nero had a kind of monocle made from optically clear polished beryl. The alternate name, glucinum, reluctantly adopted by Vauquelin, was suggested by the editors of Annales de Chimie, publishers of Vauquelin's article, because of the pronounced sweetish taste of its salts.

BE
A=6

BE
A=6

REF. E. Ventura, J.R. Calarco, C.C. Chang, E.M. Diener, and W.E. Meyerhof
PICNS-73, Vol.II, p.925 (1973) Asilomar

ELEM. SYM.	A	Z
Be	6	4

METHOD

REF. NO. 73 Ve 4 - egf

REACTION	RESULT	EXCITATION ENERGY	SOURCE		DETECTOR		ANGLE
			TYPE	RANGE	TYPE	RANGE	
HE,G	ABX	13- 25	D	1- 28	NAI-D		DST

HE=HE-3

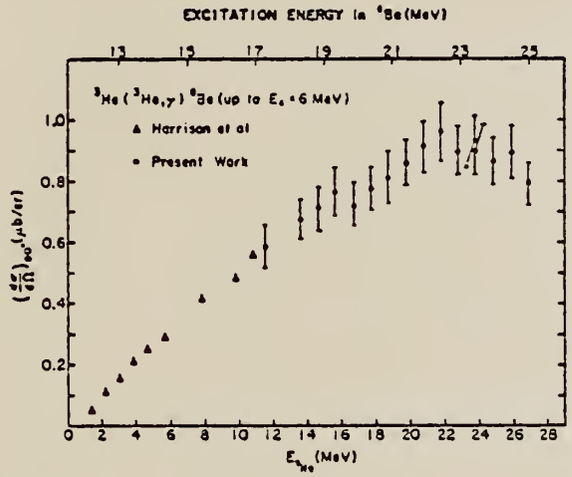

Fig. 1. Excitation function.

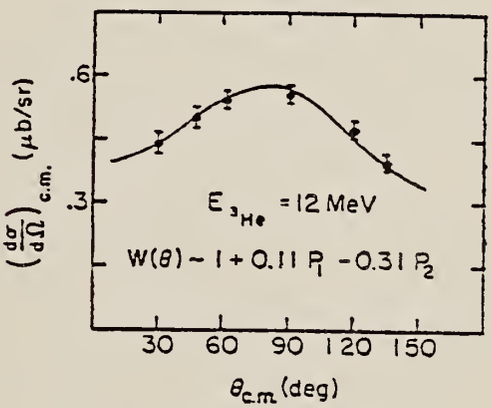

Fig. 2. Angular distribution.

BE
A=7

BE
A=7

H. Langevin-Joliot, C. Stephan, G. Johnson and J. Vernotte
Phys. Letters 14, 208 (1965)

Be	7	4

METHOD

Cherenkov detector for photons, semiconductor detector for recoils

REF. NO. 65 La 1 EGF

REACTION	RESULT	EXCITATION ENERGY	SOURCE		DETECTOR		ANGLE
			TYPE	RANGE	TYPE	RANGE	
P,G	ABX	160	D	155	SCD	0-30	DST

Note measured G and recoil in coincidence.

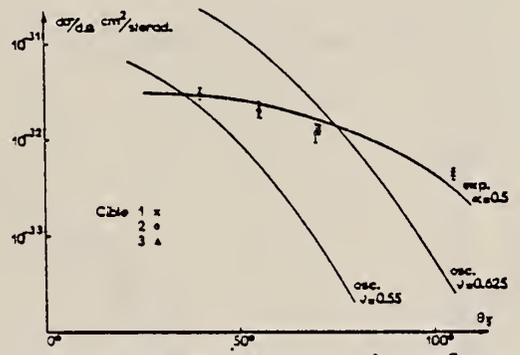

Fig. 2. Distribution angulaire de la réaction $Li^6(p,\gamma)Be^7$ à 155 MeV.

REF.

K. Nagatani, M. R. Dwarakanath and D. Ashery
Nucl. Phys. A128, 325 (1969)

ELEM. SYM.	A	Z
Be	7	4

METHOD

REF. NO.: 69 Na 2 egf

REACTION	RESULT	EXCITATION ENERGY	SOURCE		DETECTOR		ANGLE
			TYPE	RANGE	TYPE	RANGE	
A,G	ABX	1-2	D	0-1	NAI-D	1-2	90
				(.164-.245)			

SOURCE 164-245 KEV

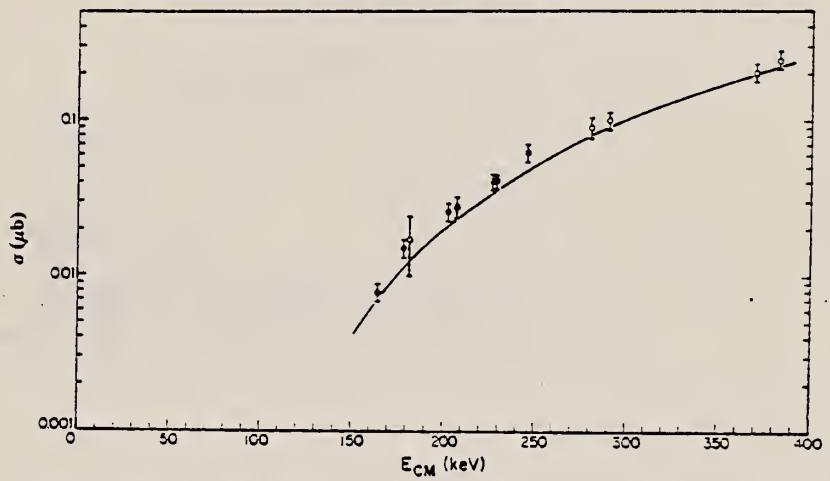

Fig. 2. The cross sections $\sigma(E)$: The solid points are the present results while the open circles are those of Parker's corrected values [12]). The solid curve indicates the theoretical prediction of ref. [3]).

Be
A=8

Be
A=8

Ref. D.S. Gemmell, A.H. Morton, E.W. Titterton
Nuclear Phys. 10, 33 (1959)

Elem. Sym.	A	Z
Be	8	4

Method Cyclotron; gamma-ray yield; NaI(Tℓ) detector

Ref. No. 59 Ge 1 EH

Reaction	E or ΔE	E_o	Γ	$\int \sigma dE$	Jπ	Notes
$Li^7(p,\gamma)$		22.3				Yield curve includes transitions to the ground state but mostly to the 2.9 MeV state. Yield curve indicates a peak in the $Be^8(\gamma,p)Li^7$ cross section of $(1.4\pm0.4) \times 10^{-28} cm^2$ at 22.3 MeV. Proton energy range 4 - 7.7 MeV. Yield at 90°

Ref. B. Mainsbridge
Nuclear Phys. 21, 1 (1960)

Elem. Sym.	A	Z
Be	8	4

Method
1.2 MeV Cockcroft-Walton accelerator; NaI

Ref. No. 60 Ma 2 — JHH

Reaction	E or ΔE	E_o	Γ	$\int \sigma dE$	$J\pi$	Notes
(p,γ)	200-1100 kev	441 kev 1030 kev			1^+	$E_{\gamma o}$ = 17.6 MeV observed, also 14.8 Me γ to 2.90 MeV level. Angular distribution parameters for $W(\theta_\gamma) = A_o + A_1 \cos\theta + A_2 \cos^2\theta$ in Table I. Parameters for $W(\theta_\gamma)=A_o(1+a_1\cos\theta+a_2\cos^2\theta)$ in Figures 10 and 12.

TABLE I

Values of the coefficients of the angular distributions in figs. 7 and 8

Proton energy (keV)	$W(\theta)_{14.8+17.6}$		$W(\theta)_{17.6}$	
	A_1/A_o	A_2/A_o	A_1/A_o	A_2/A_o
1100	0.52	0.35	1.15	0.4
1070	0.41	0.36	0.90	0.39
1050	0.46	0.36	0.87	0.43
1030	0.31	0.26	0.56	0.23
786	0.18	0.2	0.20	0.17
581	0.33	0.14	0.49	0.10
471	0.17	0.08	0.20	0.07
440	0.056	0.008	0.064	0.015
428	−0.057	−0.029	−0.070	0.004
396	−0.27	−0.02	−0.41	0.04
321	−0.22	0.01	−0.56	0.00

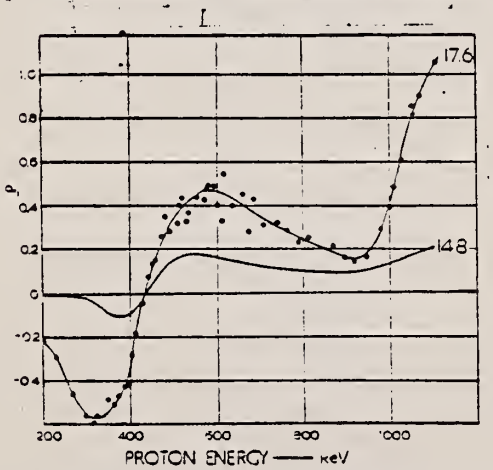

Fig. 10. Variation of a_1 in $W(\theta)_{17.6}$ and $W(\theta)_{14.8}$.

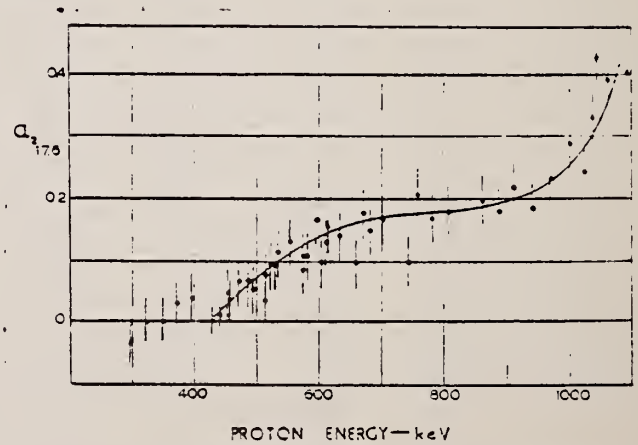

Fig. 12 Variation of a_2 in $W(\theta)_{17.6}$.

Ref. V. Meyer, H. Muller, H.H. Stanb, R. Zhurmuhle
Nuclear Phys. 27, 284 (1961)

Elem. Sym.	A	Z
Be	8	4

Method 2 MeV Van de Graaff; NaI

Ref. No. 61 Me 1 JHH

Reaction	E or ΔE	E_o	Γ	$\int \sigma dE$	Jπ	Notes
(p,γ)	441.3kev	441.3kev	$\Gamma_{\gamma 17.6}$ = 16.7ev		1^+ M 1	E_{γ_o} = 17.6 MeV $W(\theta_{\gamma_o}) = 1 + (0.067 \pm 0.025)\cos^2\theta$

Ref. S. Cavallaro, R. Potenza, A. Rubbino
Nuclear Phys. 36, 597 (1962)

Elem. Sym.	A	Z
Be	8	4

Method: 2 - MeV Van de Graaff; NaI

Ref. No.: 62 Ca 3 - JHH

Reaction	E or ΔE	E_o	Γ	$\int \sigma dE$	$J\pi$	Notes
$Li^7(p,\gamma)$	0.4-2.2					

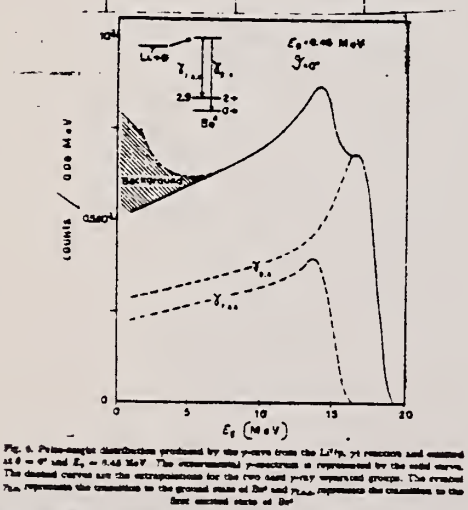

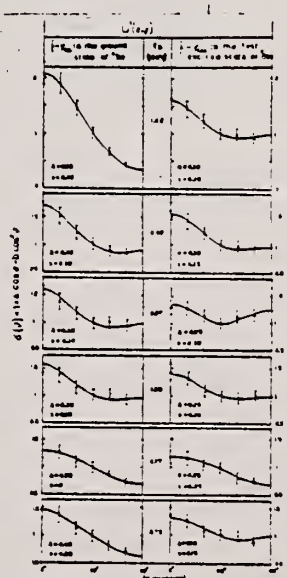

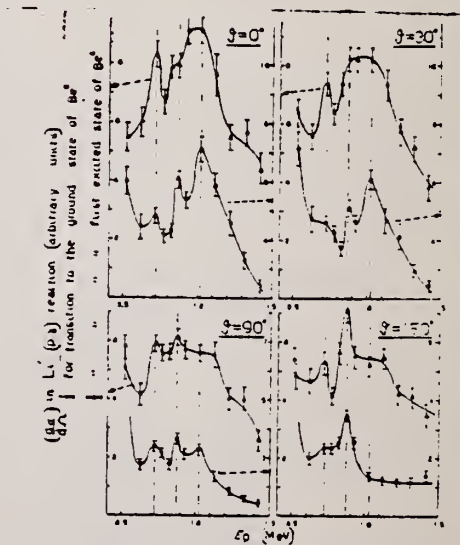

FORM NBS-418
(8-1-63)
USCOMM-OC 18656-P63

U.S. DEPARTMENT OF COMMERCE
NATIONAL BUREAU OF STANDARDS

Ref. I.V.Mitchell, R.B.Taylor

Nuclear Physics 44, 664 (1963)

Elem. Sym.	A	Z
Be	8	4

Method
Tandem accelerator - 2 NaI spectrometers

Ref. No. 63Mil BG

Reaction	E or ΔE	E_o	Γ	∫σdE	Jπ	Notes
$Li^7(p,\gamma)Be^8$	E_p= 2.5-9	E_p=				Angular distribution fitted by $w(\theta) = \sum_{n=0}^{2} A_n P_n(\cos\theta)$
(p,γ_0)		~ 5	~ 5			γ_0 from ground state transitions
(p,γ_1)		~ 6 7.3	~ 8			γ_1 transitions to 2.9 MeV broad excited state. The two broad resonances seen in $\gamma_0 + \gamma_1$ excitation functions at 21.6 and 23.6 MeV can be interpreted as corresponding to inverse resonant E1 absorption by the ground and first excited states.

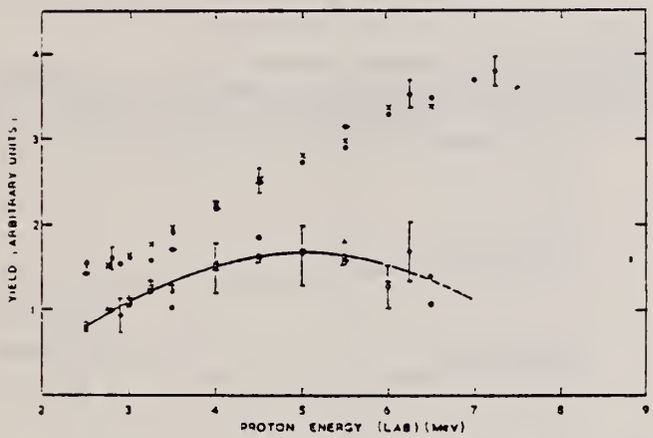

Fig. 3. The excitation functions for the $Li^7(p,\gamma_0)Be^8$ (lower curve) and $Li^7(p,\gamma_1)Be^{8*}$ (upper curve) reactions. Errors shown are of the order of 20 % for γ_0 and 8 % for γ_1, (see text). Normalized results from various measurements are distinguished by different symbols. The ordinate scale is arbitrary for both yield curves and therefore does not indicate the relative intensities of the two γ-ray components.

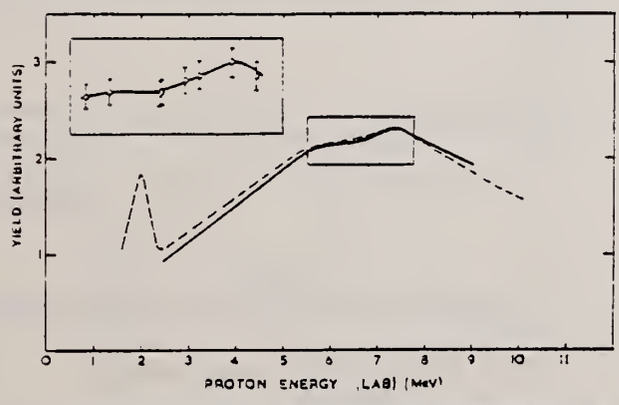

Fig. 4. The $(\gamma_0+\gamma_1)$ yield curve (unbroken line) determined by the present experiment, and the yield curve of Perry *et al.* (broken line) normalized at E_p = 7.3 MeV. The suggested structure was established by careful experiment and a typical measurement is displayed in the inset (magnification × 2)

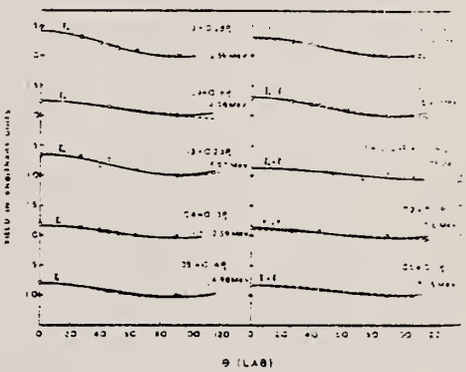

Fig. 5. Angular distributions for separated and combined γ-rays. The broken and unbroken lines are obtained for polynomial analyses with and without the inclusion of P_3 terms, respectively. Errors on the experimental points are estimated to be 10 %, for γ_0, 5 %, for γ_1, and 8 %, for the sum. The results of Perry *et al.* at E_p = 7.3 MeV are displayed for comparison.

Ref. R. R. Perry, B. Mainsbridge, J. Richards
Nuclear Phys. 45, 586 (1963)

Elem. Sym.	A	Z
Be	8	4

Method: Tandem Van de Graaff; γ-ray yield, spectra, angular distribution; NaI

Ref. No.: 63 Pe 1 JHH

Reaction	E or ΔE	E_0	Γ
$Li^7(p,\gamma)$	1.5-11		
			$\Gamma_{(p,\gamma)}$:
	7.3	23.6	~ 6 MeV
	(6.0)	(22.5)	

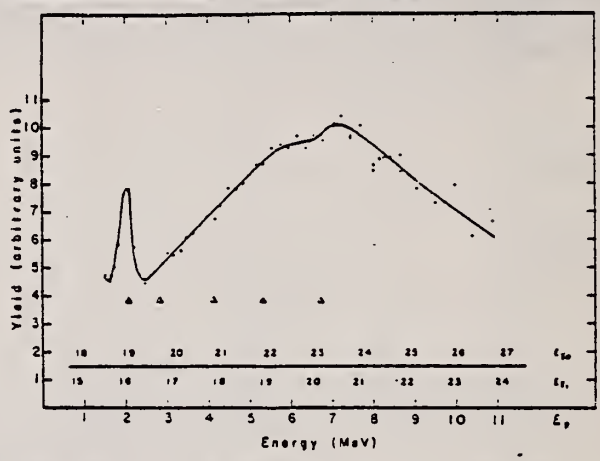

Fig. 2. The 90° excitation curve showing a resonance at 2.1 MeV and the asymmetric giant resonance at 7.3 MeV. Additional scales give the gamma ray energies for transitions to the ground (γ_0) and first excited (γ_1) states. The triangles indicate where angular distributions were measured.

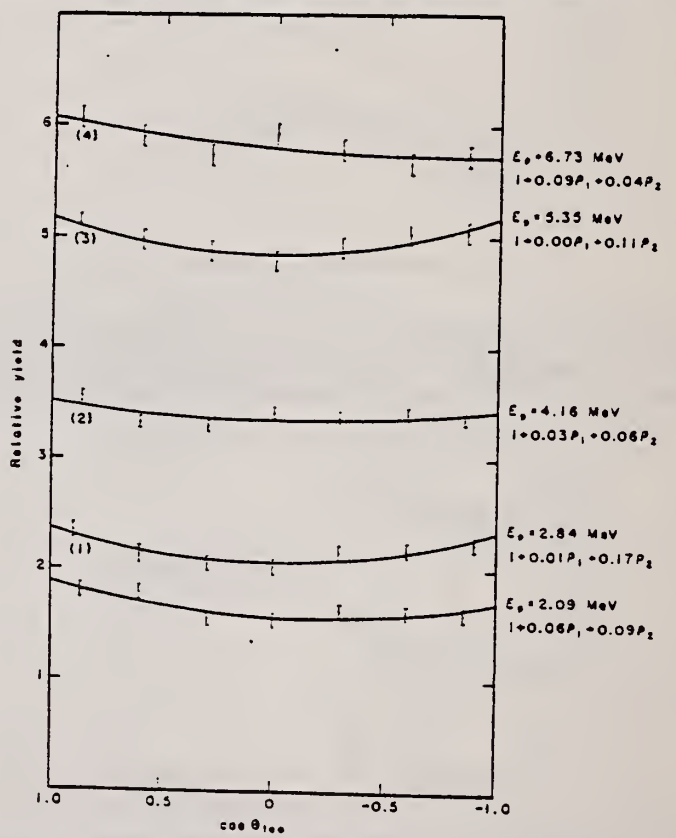

Fig. 3. Angular distributions of both gamma rays at 2.09, 2.84, 4.16, 5.35 and 6.73 MeV bombarding energy. To obtain the relative yields of various distributions subtract the number in parenthesis from the ordinate. The curves are least-square Legendre polynomial fits; the corresponding coefficients are shown at the right.

Ref. N.W.Reay, N.M.Hintz, L.L.Lee,Jr.

Nuclear Phys. 44, 338 (1963)

Elem. Sym.	A	Z
Be	8	4

Method: 26 MeV Linac - NaI(Tl)

Ref. No.: 63Rel | BG

Reaction	E or ΔE	E_o	Γ	$\int \sigma dE$	Jπ	Notes
	E_p=4.3-8					
$Li^7(p,\gamma_0)Be^8$				0.37±0.15		
$Be^8(\gamma,p_o)Li^7$				22±4		obtained using reciprocity

Fig. * Ground and first excited state transitions for the reaction $Li^7(p,\gamma)Be^8$. The circles represent the present data, the crosses the data of ref. [*]) · 0.8, the triangles represent the data of ref. [*]), normalized to fit the data of ref. [*]) at lower energies.

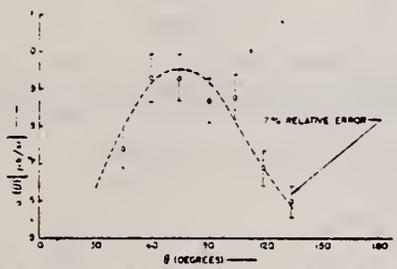

Fig. 8. Angular distribution for the reaction $Li^7(p,\gamma)Be^8$ at E_p = 8.0 MeV (cm.), ground and first excited state transitions summed. Least-squares fit to trigonometric series is shown by dashed line.

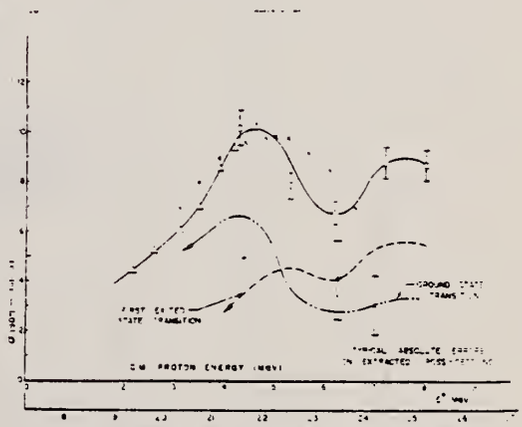

Fig. * Ground and first excited state transitions for the reaction $Li^7(p,\gamma)Be^8$. The circles represent the present data, the crosses the data of ref. [*]), the triangles represent the data of ref. [*]), normalized to fit the data of ref. [*]) at lower energies.

Ref. V. Riech
Phys. Letters 6, 267 (1963)

Elem. Sym.	A	Z
Be	8	4

Method: Van de Graaff; photon spectrum; NaI

Ref. No.: 63 Ri 1 - JHH

Reaction	E or ΔE	E_o	Γ	∫σdE	Jπ	Notes
$Li^7(p,\gamma)$	E_p= 0.88-3.06					Yield 90°
	E_{Po}= 1.03±0.01	$E_{\gamma o}$= 18.16	190±20 keV			

D. J. Schlueter, R. W. Krone and F. W. Prosser, Jr.
Nucl. Phys. 58, 254-272 (1964)

Be	8	4

METHOD: $Li^7(p,\gamma_0)Be^8$ Van de Graaff

REF. NO.: 64 Sc 2 JOC

REACTION	RESULT	EXCITATION ENERGY	SOURCE TYPE	SOURCE RANGE	DETECTOR TYPE	DETECTOR RANGE	ANGLE
P,G	RLX	17-19	D	0-2	NAI-D		DST
				(0.2 - 1.7)			

Levels at E_p = 441 keV and 1030 keV J-PI

J-PI = 1^+ J-PI = 1^+

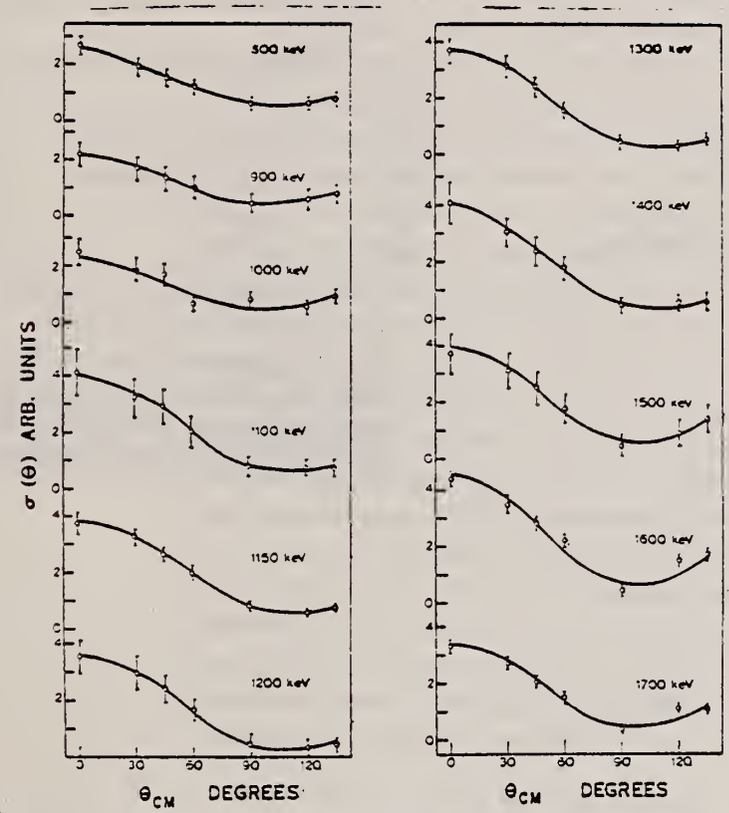

Fig. 2. Angular distributions for $Li^7(p,\gamma)Be^8$ transitions to the Be^8 ground state for various proton energies. The ordinate is in arbitrary units and not necessarily the same for all the curves. These curves should, therefore, not be used to compare the cross sections at the different proton energies.

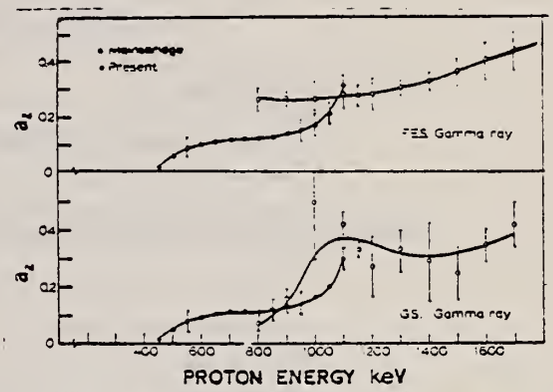

Fig. 5. Values of the $a_2(E)$ coefficients as a function of proton energy. The graph shows the results obtained by Mainsbridge and the extension of his work to higher proton energy.

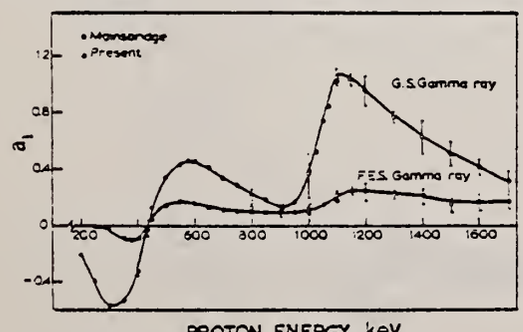

Fig. 4. Values of the $a_1(E)$ coefficients as a function of proton energy. The graph shows the results obtained by Mainsbridge and the extension of his work to higher proton energy.

REF.

N. W. Tanner, G. C. Thomas and E. D. Earle
Nucl. Phys. 52, 29-44 (1964)

ELEM. SYM.	A	Z
Be	8	4

METHOD

$Li^7(p,\gamma)Be^8$ Tandem

REF. NO. 64 Ta 1 JOC

REACTION	RESULT	EXCITATION ENERGY	SOURCE		DETECTOR		ANGLE
			TYPE	RANGE	TYPE	RANGE	
P,G	ABX	21-25	D	4-9	NAI-D		90

At E_p = 5.4 MeV $\left.\frac{d\sigma\gamma_0}{d\Omega}\right|_{90}$ = 45 μb/4πsr

From detailed balance:

$$\int_{19.6}^{25.0} \sigma(\gamma,Po)dE_\gamma = 20 \text{ MeV - mb}$$

Comparison with several other (p,γ) results

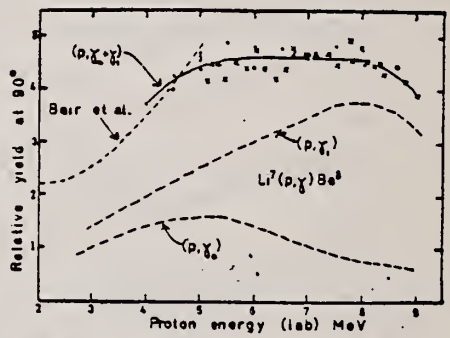

Fig. 3. The excitation function at 90° of $Li^7(p,\gamma)Be^8$. The data were normalized to those of ref. [5]) at 4.5 MeV. The two symbols represent two runs with different targets. The separation into curves for γ_0 and γ_1 individually was done with the data shown in table 1.

REF.
J.L. Black, F. Riess, P. Paul, W. J. O'Connell, G.A. Fisher, S. S. Hanna PICNS-67 Contributions, International Conference on Nuclear Structure, Tokyo, Japan 1967 (Institute for Nuclear Study, University of Tokyo, Tanashi shi, Tokyo, Japan) 10.11, p. 375

EL EM. SYM.	A	Z
Be	8	4

METHOD

REF. NO.
67 B1 2 EGF

REACTION	RESULT	EXCITATION ENERGY	SOURCE		DETECTOR		ANGLE
			TYPE	RANGE	TYPE	RANGE	
P.G	RLX	17-34	D	1-18	NAI-D	17-33	90

Giant Dipole Resonances in p-Shell Nuclei.*

J. L. Black, F. Riess, P. Paul,# W. J. O'Connell, G. A. Fisher, and S. S. Hanna

Department of Physics, Stanford University, Stanford, California, U.S.A.

The giant dipole resonances in p-shell nuclei have been studied by means of the (p,γ) capture reaction. The capture gamma rays are detected with good resolution with a 24 x 24 cm NaI detector encased in an anticoincidence plastic shield and employing pulse pile up suppression. The region of the giant resonance can be covered with good energy resolution with protons from an FN tandem accelerator up to proton energies of 18 MeV. Fine structure and gamma ray angular distributions for giant resonances observed in ^{8}Be, ^{14}N, and ^{16}O have been studied. For ^{8}Be and ^{14}N the giant resonances based on the first excited state can also be studied. The resonances observed in $^{7}Li(p,\gamma)^{8}Be$ are shown in Fig. 1. The γ_0 giant resonance shows little structure. The γ_1 resonance exhibits some structure at E_x = 22 MeV. The center of the γ_1 resonance lies about 2.5 MeV above the center of the γ_0 resonance. Thus, the excitation energy for both resonances is about the same, 21.5 MeV. The dipole strengths of the resonances are about equal i.e., the integrated yields are roughly proportional to 2J + 1, where J is the spin of the final state. In ^{14}N the first excited state has T = 1, so that resonances based on a T = 1 level are observed. Previous measurements[1] on $^{15}N(p,\gamma_0)^{16}O$ have been extended to E_p = 17.5 MeV. Above E_x = 25.5 MeV, no pronounced structure was revealed. In addition, the main peak of the giant resonance at E_x = 22.2 MeV has been studied in detail with high resolution to search for possible fine structure. Results at θ = 45°, shown in Fig. 2, indicate the existence of structure in this peak. A measurement at θ = 90° displays similar structure. The results are compared with recent $^{16}O(\gamma,p)^{15}N$ data.[2]

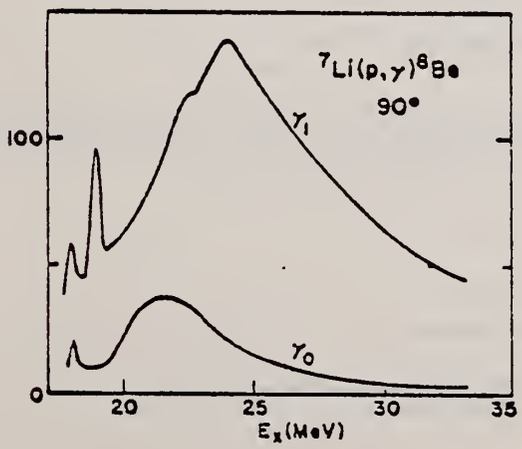

Fig. 1

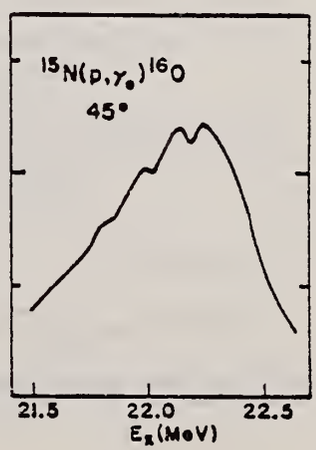

Fig. 2

* Supported in part by the National Science Foundation.
# Present address: State University of New York, Stony Brook, New York.
1 N. W. Tanner, G. C. Thomas, and E. D. Earle, Nucl. Phys. 52, 45 (1964).
2 J. Baglin, private communication.

REF. L. Nilsson and I. Bergqvist
Arkiv Fysik 35, 411 (1967)

ELEM. SYM.	A	Z
Be	8	4

METHOD

REF. NO. 67 Ni 1 egf

REACTION	RESULT	EXCITATION ENERGY	SOURCE		DETECTOR		ANGLE
			TYPE	RANGE	TYPE	RANGE	
P,G	RLY	18-19	D	1-3	NAI-D	7-20	DST

$$W(\theta) = A_0[1 + \sum_{i=1} a_i P_i(\cos\theta)]$$

Table 1. Values of angular distribution coefficients for gamma-ray transitions to the ground state and the first excited state in the $^7Li(p,\gamma)^8Be$ reaction in terms of Eq. (2).

Proton energy (MeV)	Transitions to: Ground state a_1	Ground state a_2	First excited state a_1	First excited state a_2
1.40	0.62 ± 0.04	0.42 ± 0.04	0.13 ± 0.03	0.36 ± 0.04
1.60	0.43 ± 0.05	0.41 ± 0.07	0.06 ± 0.04	0.37 ± 0.05
1.80	0.31 ± 0.05	0.48 ± 0.06	0.09 ± 0.05	0.30 ± 0.06
2.00	0.41 ± 0.09	0.40 ± 0.11	0.10 ± 0.06	0.12 ± 0.07
2.10	0.14 ± 0.09	0.43 ± 0.12	0.02 ± 0.04	0.14 ± 0.05
2.20	0.10 ± 0.07	0.38 ± 0.09	0.01 ± 0.04	0.12 ± 0.0.
2.40	−0.10 ± 0.10	0.45 ± 0.13	−0.06 ± 0.06	0.42 ± 0.0:

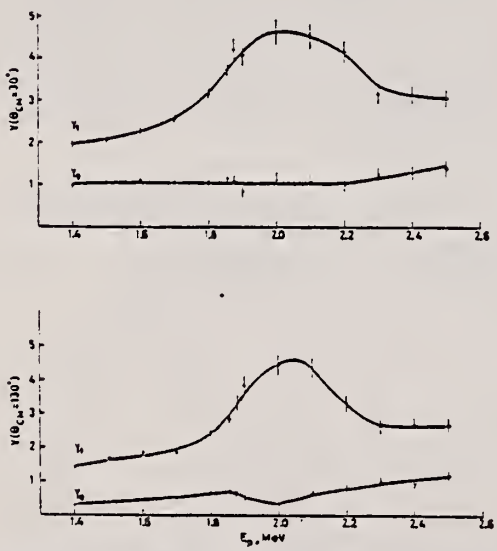

Fig. 3. Yield of the gamma-ray transitions to the ground state (γ_0) and the first excited state (γ_1) at 30° and 130°. Curves are drawn to guide the eye.

(continued)

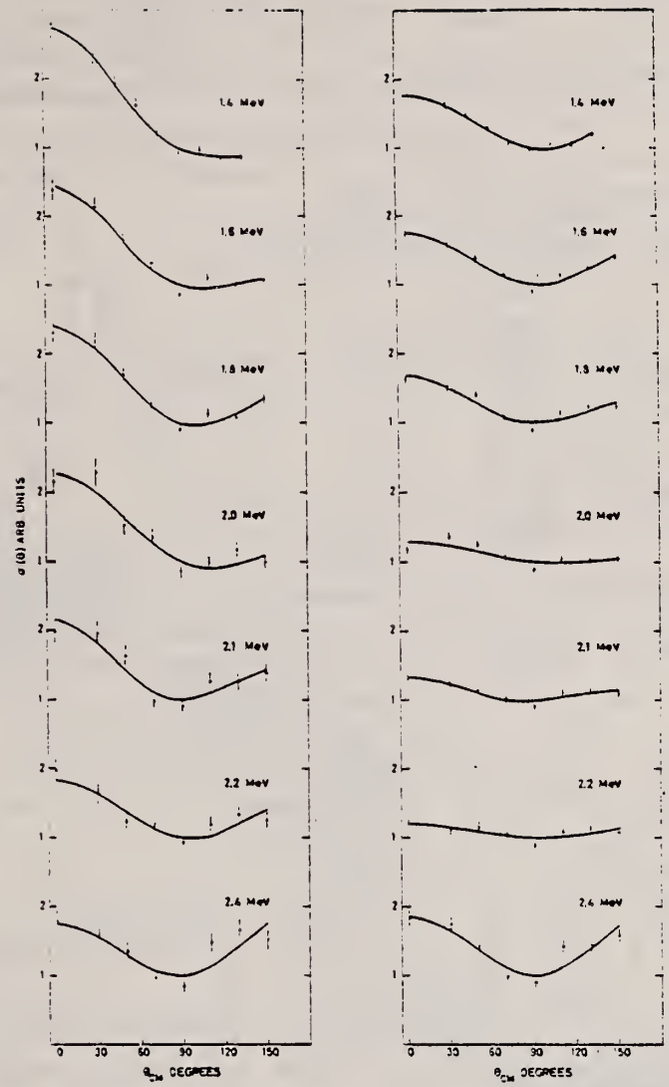

Fig. 5. Angular distributions of ^{7}Li$(p,\gamma)^8$Be transitions to the ground state (left column) and to the first excited state (right column) for various proton energies. Crosses represent experimental values and solid curves are Legendre polynomial fits of the form $W(\theta) = A_0[1 + a_1 P_1(\cos\theta) + a_2 P_2(\cos\theta)]$. The curves are normalized to unity at 90°.

REF.

G.A. Fisher, P. Paul, F. Riess, and S.S. Hanna
Phys. Rev. C14, 28 (1976)

ELEM. SYM.	A	Z
Be	8	4

METHOD

REF. NO. 76 Fi 3 hmg

REACTION	RESULT	EXCITATION ENERGY	SOURCE TYPE	SOURCE RANGE	DETECTOR TYPE	DETECTOR RANGE	ANGLE
P,G	ABX	17- 33	D	0- 18	NAI-D		DST

$$W(\theta) = A_o \left[1 + \sum_{n=1}^{N} a_n P_n\right] \quad \text{(Legendre polynomial used)}$$

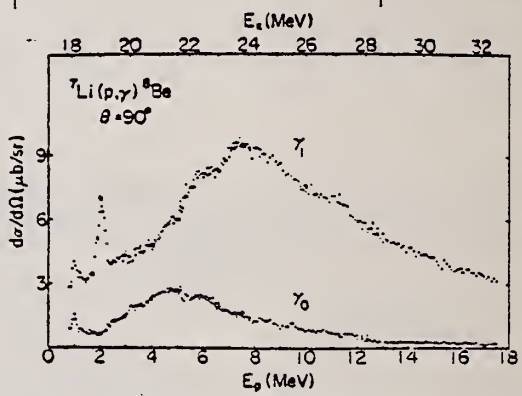

FIG. 3. The yield functions for the γ_0 and γ_1 transitions obtained at 90°, which show the broad giant resonances built on the ground state and the first excited state of ^{8}Be.

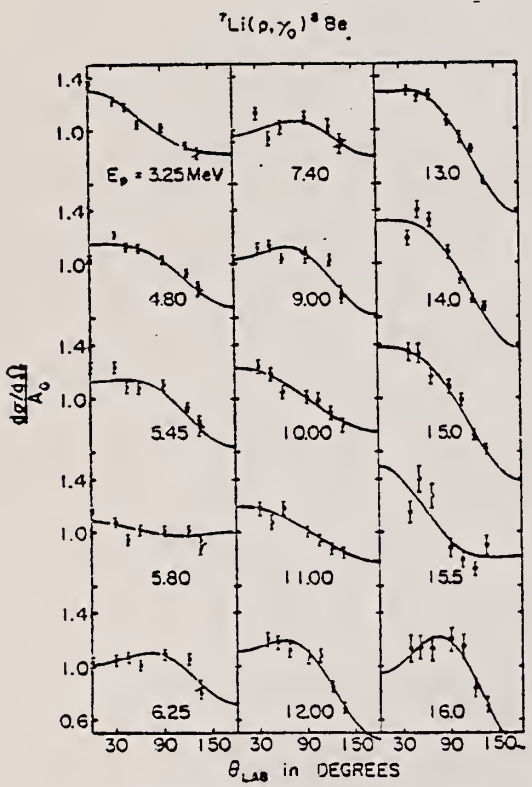

FIG. 4. Angular distributions obtained from the reaction ^{7}Li(p,γ_0)^{8}Be over the energy range of the giant dipole resonance. The least-squares fits were computed with a series of Legendre polynomials up to N = 2.

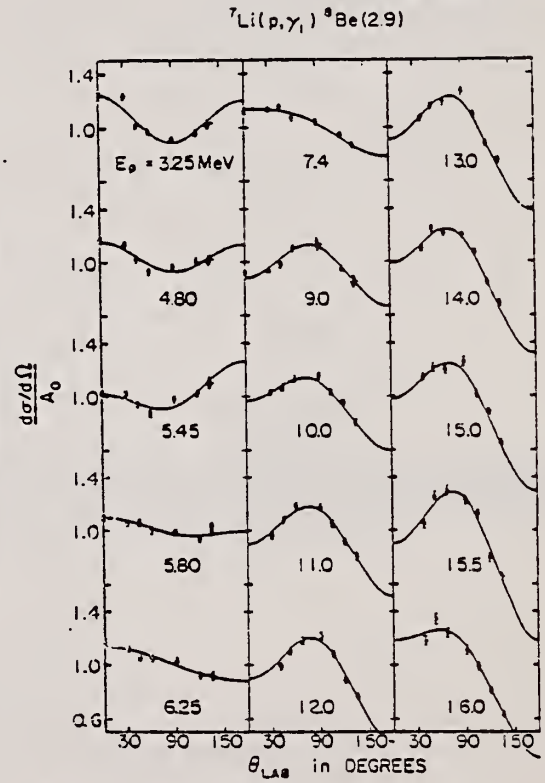

FIG. 5. Angular distributions obtained from the reaction ^{7}Li(p,γ_1)^{8}Be over the energy range of the giant dipole resonance. The least-squares fits were computed with a series of Legendre polynomials up to N = 2.

(continued)

TABLE II. Properties of GDR in light 4N nuclei.

	Values on peak of GDR						$\int_{E_1}^{E_2}\sigma(\gamma,p_0)dE$[a]	
	E_p (MeV)	E_γ (MeV)	$\sigma(p,\gamma_0)$ (ub)	$\sigma(\gamma,p_0)$ (mb)	Γ_{cm} (MeV)	$\langle a_2\rangle$	(mb MeV)	(% S.R.)
^{6}He[b]	10.0	27.3	68	1.92	20	-0.98	21^{13}_{10}	35
^{8}Be[c]	5.0	21.6	33	2.05	5.3	-0.05	13^{23}_{10}	11
^{12}C[d]	7.3	22.6	137	12.2	3.5	-0.55	56^{29}_{10}	31
^{16}O[e]	10.8	22.2	177	12.7	4.2	-0.51	43^{29}_{12}	18

[a] E_1 and E_2 are shown as subscripts and superscripts, respectively.

[b] References 20 and 21.

[c] Present work.

[d] References 2 and 21.

[e] Reference 22.

TABLE I. Gamma decay properties of states in ^{8}Be at 18.15 and 19.05 MeV.

	Γ_γ(eV)			$A(M1)/(2J+1)$[a]		
Transition	This exp.[b]	Other exps.	W.u.[c]	This exp.	Theor.[d]	Theor.[e]
18.15 → 0.0	3.0	1.8[f]	115	0.19	0.03	0.05
18.15 → 2.9	3.8	3.6[f]	70	0.07	0.004	0.09
19.06 → 2.9	10.5	17.0[g]	80	0.11		

[a] A(M1) is the reduced M1 width; J is the final-state spin.

[b] $\Gamma_p = \Gamma$ is assumed.

[c] W. u. is Weisskopf estimate for an M1 transition.

[d] Reference 15.

[e] With 5% mixture from a possible $(1^+,1)$ state at 19.4 MeV, see text.

[f] Reference 12.

[g] Reference 13.

2 R.G. Allas et al., Nucl. Phys. 58, 122 (1964); W.A. Lockstet et al., Phys. Rev. 141, 1002 (1966).

20 W.E. Meyerhof et al., Nucl. Phys. A148, 211 (1970).

21 S.S. Hanna, in Proc.Int.Conf. on Photonuclear Reactions & Applications, Asilomar, 1973.

22 W.J. O'Connell, Stanford Univ. Ph.D. Thesis, 1969.

12 A.A. Kraus, Phys. Rev. 93, 1308 (1954); B. Mainsbridge, Aust. J. Phys. 13, 204 (1960)

13 L. Nilsson et al., Ark.Fysik 35, 411 (1967).

15 S. Cohen et al., Nucl. Phys. 73, 29 (1965).

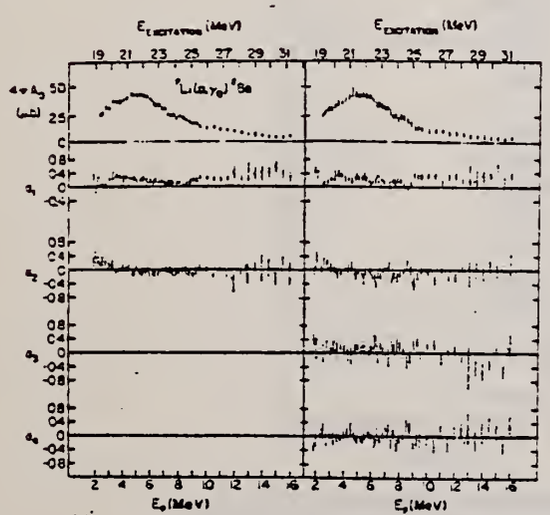

FIG. 6. Plot of the total cross section $4\pi A_0$ and the Legendre coefficients a_1 and a_2 (left side) and a_1 through a_4 (right side), obtained from the angular distribution fits, as a function of bombarding energy for the γ_0 transition.

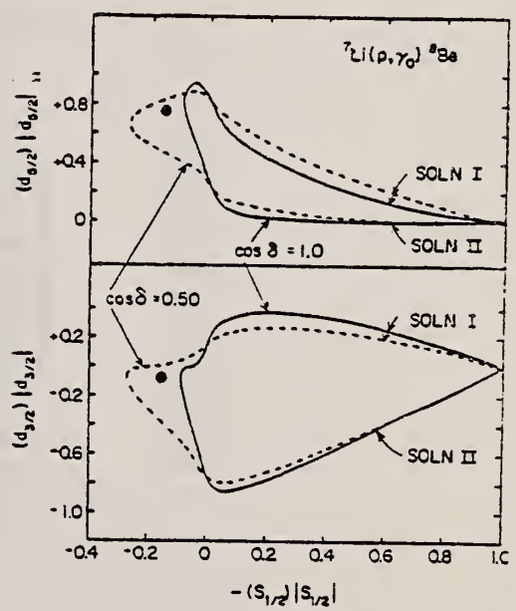

FIG. 8. Contour diagram of the relative $d^2_{5/2}$, $d^2_{3/2}$ and $s^2_{1/2}$ intensities in the proton capture reaction ^{7}Li(p,γ_0) which yield the observed a_2 coefficient (a_2 = 0.05). Curves are given for the two extreme relative phases δ between s and d waves and for the two branches corresponding to the two possible solutions. The configurations predicted by the schematic model (see text) are shown by the dots.

REF. J. Ulbricht, W. Arnold, H. Berg, E. Huttel, H. H. Krause and G. Clausnitzer
Nucl. Phys. A287, 220 (1977)

ELEM. SYM.	A	Z
Be	8	4

METHOD

REF. NO. 77 U1 1 egf

REACTION	RESULT	EXCITATION ENERGY	SOURCE TYPE	SOURCE RANGE	DETECTOR TYPE	DETECTOR RANGE	ANGLE
$ P,G	ABX	17- 18	D	380*960	SCD-D		DST

* ENERGY KEV, POL G

Abstract: The polarized proton capture in ^{7}Li was used to study the reaction mechanism and to obtain spectroscopic information on the ^{8}Be nucleus. Gamma-ray angular distributions of the analyzing power were measured as a function of proton energy from E_p = 330–960 keV with three Ge(Li) detectors simultaneously. The excitation functions of the cross section and the analyzing power are strongly energy dependent. The data were analyzed unambiguously and represented by three R-matrix elements, two M1 and one E1. The energy dependence of the two M1 matrix elements agrees with the well-known two 1^+ resonances at E_x = 17.642 and 18.157 MeV. The energy dependence of the E1 matrix element shows a smooth background presumably caused by a direct-capture mechanism, and furthermore, a resonant contribution, which is a significant suggestion of a new 1^- state in the ^{8}Be system at E_x = 17.70 MeV with a width of Γ_p = 180 keV.

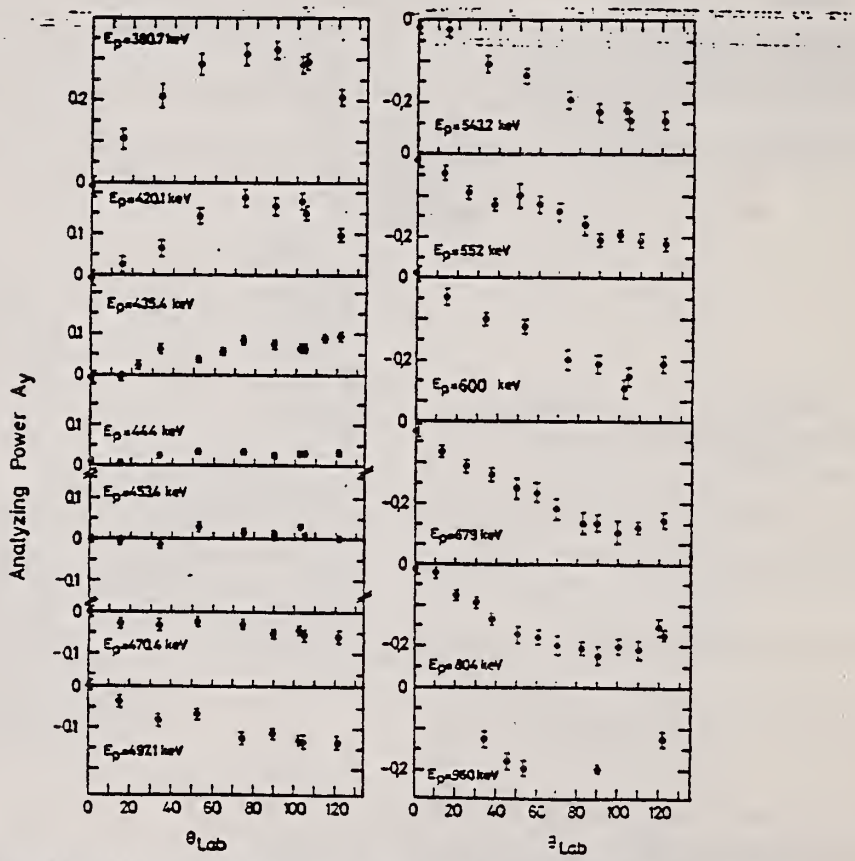

Fig. 4. Analyzing power angular distributions $A_y(E, \theta)$ of the ^{7}Li(p, γ)^{8}Be reaction for proton energies between 380 and 960 keV. All proton energies refer to the center of the target. Error bars are from statistics only.

(continued)

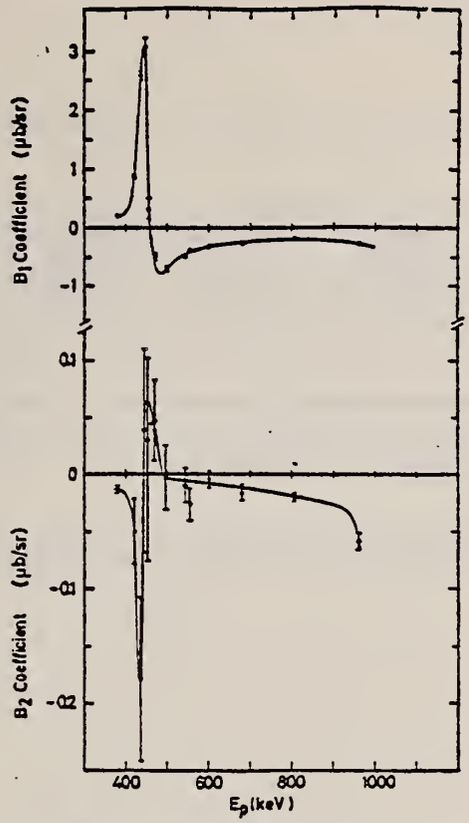

Fig. 6. The B_1 and B_2 coefficients obtained from the fits (eq. (3)) of the data. The solid lines are only to guide the eye. The assigned errors result from the fitting procedure of the complete angular distribution.

TABLE 1

Coefficients of Legendre functions from the best fit to the experimental results

E_p (keV)	B_1	ΔB_1	B_2	ΔB_2
380.7	0.193	0.004	−0.0133	0.0029
420.1	0.877	0.039	−0.0501	0.0304
435.4	2.606	0.072	−0.1804	0.0809
444.0	3.064	0.158	0.0387	0.1403
453.4	0.279	0.125	0.0193	0.1113
470.4	−0.487	0.050	0.0473	0.0498
497.1	−0.702	0.036	−0.0036	0.0315
543.2	−0.490	0.014	−0.0097	0.0147
552	−0.405	0.021	−0.0272	0.0165
600	−0.319	0.011	−0.0046	0.0100
679	−0.272	0.011	−0.0172	0.0079
804	−0.204	0.004	−0.0211	0.0032
960	−0.290	0.011	−0.0591	0.0075

$w(E, \theta)A(E, \theta) = B_1 P_1{}^1(\cos\theta) + B_2 P_2{}^1(\cos\theta)$, where $w(E, \theta)$ is in μb/sr.

$$A_y(E,\theta) = \frac{1}{P}\,\frac{N\uparrow - N\downarrow}{N\uparrow + N\downarrow}$$

$N\uparrow \equiv \gamma$'s counted when beam with polarization P pointed up with respect to scattering plane interacts with ^{7}Li target

REF. C. Wiezorek, H. Krawinkel, R. Santo, L. Wallek
Z. Phys. A282, 121 (1977)

ELEM. SYM.	A	Z
Be	8	4

METHOD

REF. NO. 77 Wi 3 hg

REACTION	RESULT	EXCITATION ENERGY	SOURCE		DETECTOR		ANGLE
			TYPE	RANGE	TYPE	RANGE	
P,G	ABX	452*	D	360*	ACT-I		4PI

Measured delayed alpha-particles from ^{8}Be*

*ENERGY, KEV

The cross section of the ^{7}Be$(p,\gamma)^{8}$B reaction has been determined at $E_p = 360$ keV to $\sigma_{360} = 0.17 \pm 0.04$ μb.

BE
A=9

BE
A=9

P. S. Baranov, V. I. Goldanskii
Zhur. Eksp. i.Teoret. Fiz.28, 746 (1955)
Soviet Phys. JETP 1, 613 (1955)

Be	9	4

METHOD: Synchrotron; ion chamber monitor; $^{12}C(n,2n)$ threshold detector

REF. NO.: 55 Ba 5 EGF

REACTION	RESULT	EXCITATION ENERGY	SOURCE		DETECTOR		ANGLE
			TYPE	RANGE	TYPE	RANGE	
G,XN	ABY	30-200	C	150-250	THR	30-	DST

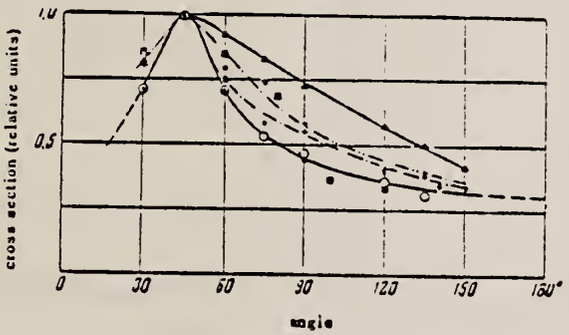

FIG. 2. Angular distribution of photoneutrons with energies higher than 30 mev. ● – C_{250}; + – C_{200}; ▲ – Be_{250}; O – Al_{250}; * – Pb_{250}; ■ – data of work[5].

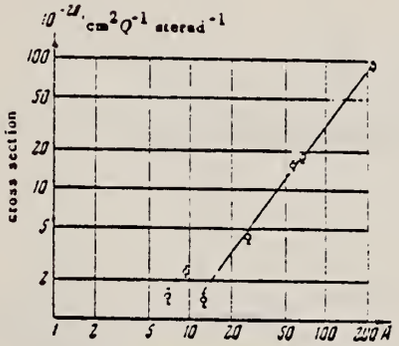

FIG. 4. The dependence of the yield of photoneutrons with energies higher than 30 mev at an angle of 90° (in units 10^{-28}cm^2 per eff. quant steradian on the mass number A).

Ref. W.R. Dixon
Can. J. Phys. 33, 785 (1955)

Elem. Sym.	A	Z
Be	9	4

Method: Synchrotron; neutron angular distribution; scintillator; ion chamber

Ref. No.: 55 Di 1 d S — NVB

Reaction	E or ΔE	E_0	Γ	$\int \sigma dE$	Jπ	Notes
Be(γ,xn)	70					Curves fitted to a + b $\sin^2\theta$ Anisotropy suggests direct effects in light nuclei.

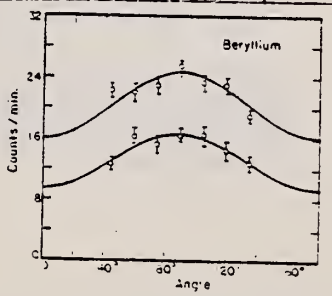

Fig. 3. The angular distribution of neutrons [illegible] in the gas-filled-counter spectrometer. The [illegible]

TABLE II

EXPERIMENTAL VALUES FOR $\bar{b}\,\alpha$

Target	Correction factor for self-scattering	Corrected $\bar{b}\,\alpha$
Lead	1.10	−0.08±0.08
Tin	1.08	0.12±0.17
Copper	1.48	0.23±0.15
Iron	1.35	0.09±0.25
Aluminum	1.17	0.36±0.29
Carbon	1.8	1.6 ±0.8
Beryllium (1)	2.6	1.2 ±0.4
Beryllium (2)	1.35	

Sven A. E. Johansson
Phys. Rev. 97, 434-43 (1955)

Be	9	4

METHOD

Synchroton; ZnS counter; ion chamber

REF. NO. 55 Jo 1 NVB

REACTION	RESULT	EXCITATION ENERGY	SOURCE		DETECTOR		ANGLE
			TYPE	RANGE	TYPE	RANGE	
G,N	RLY	12 - 65	C 65		SCI-D	10 - +	DST

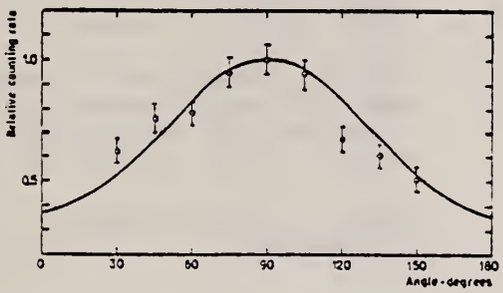

FIG. 6. The angular distribution of the neutrons from beryllium. Counter threshold at 10 Mev.

Curve of form $a + b \sin^2\theta$

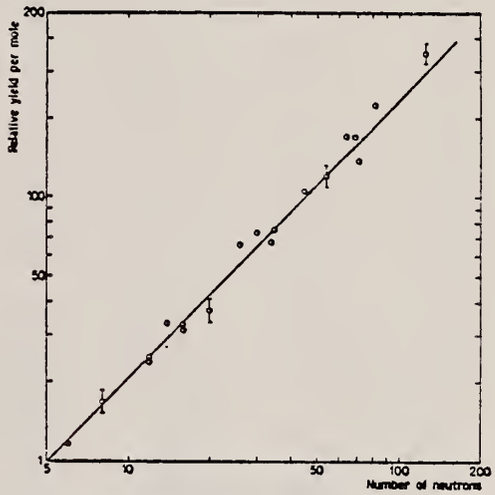

FIG. 11. The relative yield per mole for neutrons above 7.5 Mev as a function of the neutron number.

Ref. L. Cohen, A.K. Mann, B.J. Patton, K. Reibel, W.E. Stephens, E.J. Winhold
Phys. Rev. 104, 108 (1956)

Elem. Sym.	A	Z
Be	9	4

Method: 90° plates; 25 MeV Bremss.

Ref. No.: 56 Co 1 EGF

Reaction	E or ΔE	E_o	Γ	$\int \sigma dE$	Jπ	Notes
(γ,p)	Bremss. 23.5			~ 32 MeV-mb		E_{th} = 16.68 MeV. Proton yeild at 23.5 MeV; Bremss. was about (5.8±3)X10^4 p/mole r. Find few transitions to ground state and first excited states of Li^8; (γ,pn) or (γ,d) may also be included since the (γ,d) = 16.87 MeV. Target 5.8 mg/cm^2; Losses in target are uncertain.

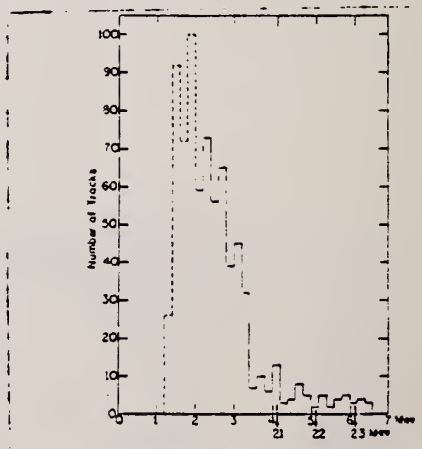

FIG. 3. Corrected energy distribution of photoprotons from beryllium. The upper energy scale is the disintegration energy. The lower scale is the photon energy if the recoil nucleus were left in its ground state.

Ref. R.D. Edge
Nuclear Phys. 2, 485 (1956)

Elem. Sym.	A	Z
Be	9	4

Method Photons from (p,γ) reactions in light nuclei; Szilard-Chalmers neutron detector

Ref. No. 56 Ed 1 JOC

Reaction	E or ΔE	E_o	Γ	$\int \sigma dE$	Jπ	Notes
$Be^9(\gamma,n)$		2.61				$\sigma = 3.9\pm0.2 \times 10^{-28}$ cm^2 556
		4.4				$\sigma = 1.86\pm3.6 \times 10^{-28}$cm^2
		6.2				$\sigma = 11.4\pm1.0 \times 10^{-28}$cm^2
		8.1				$\sigma = 13.8\pm1.6 \times 10^{-28}$cm^2

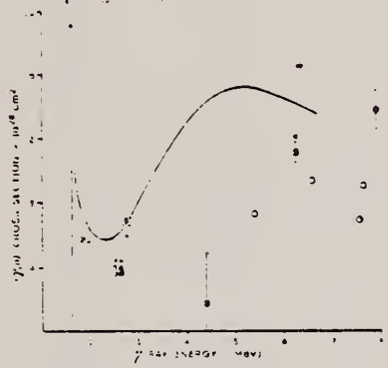

Fig. 2 Experimental and theoretical results at low and intermediate energies for the photoneutron cross section for Be^9. The curve follows the theory of Guth and Mullin. The points have been obtained experimentally as follows: (1) Watten[illegible]

Source	Energy of gamma ray MeV	$Be^9(\gamma,n)$ Cross section x (10^{-28} cm^2	Reference
Ra(B C)	Mixture	2.0	41
		19.75±3.0	42
		19.6	43
		10.8±2.2	44
		3.09	45
		4.83	
		2.43	
Th C'	2.61		46
		9.0±2.3	42
		3.0	35
		4.4	46
		4.0	3
		4.1	36
Na^{24}	2.76	7.0	3
		6.6	35
		6.74	35
Mn^{56}	2.06±1.77	3.9	2
Sb^{124}	1.67	19.0	2
		10.0	1
La^{140}	2.50	4.5	1
Pr^{144}	2.185	3.9	47
Ga^{72} ??	2.51		2
In^{116m} ??	1.8, 2.1		2

† Yield ratio Ra/Th = 1.15 [illegible].
†† Ratio Be:D yield = 0.36 [illegible].
††† Yield per curie = 0.82 x $10^{[illegible]}$.

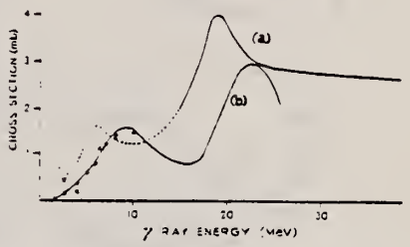

Fig. 3. A comparison of bremsstrahlung results with the results of this experiment. Curve a) follows the results obtained by Jones and Terwilliger [38]. b) follows the results obtained by Nathans and Halpern [37]. X Author. ○ Nathans and Halpern [37].

References

1) A. H. Snell, E. C. Barker and R. L. Sternberg, Phys. Rev. 80 [illegible]
2) A. Wattenberg, R. Russell, D. Sachs and R. Fields, Phys. Rev. 73 [illegible]
35) E. Guth and C. J. Mullin, Phys. Rev. 76 (1949) 234
36) C. J. Mullin and E. Guth, Phys. Rev. 76 (1949) 462
37) R. Nathans and J. Halpern, Phys. Rev. 92 (1953) 940
38) L. W. Jones and K. M. Terwilliger, Phys. Rev. 91 (1953) 699
39) D. Arakatsu, M. Sonada, Y. Uemura, S. Yasumi and Y. Saji, Jrnl. Phys. Soc. Jap. 66 (1951) 66
40) V. D. Eriksen and C. P. Zaleski, Jrnl. Phys. Rad. 15 (1954) 492
41) W. Gentner, C. R. 200 (1935) 310
42) L. I. Rusinov, Phys. Zeits. Zowjetunion 10 (1936) 203, 219
43) D. H. Frisch, H. Halban and J. Koch, Dan. Mat. Fys. Medd. 15 (1938) nr. 10
44) Z. Ollano, Nuovo Cimento 15 (1938) 604
45) F. G. Houtermans and I. Bartz, Phys. Zeit. 44 (1943) 167
46) D. L. Allan and M. J. Poole, Nature 162 (1950) 873
47) B. Hamermesh and C. Ruhoff, Phys. Rev. 90 (1953) [illegible]

REF. S.L. Blatt, M. Suffert, A. Degre and M. Schaeffer
PICNS-73, Vol.II, p.927 (1973) Asilomar)

ELEM. SYM.	A	Z
Be	10	4

METHOD

REF. NO. 73 B1 5 - egf

REACTION	RESULT	EXCITATION ENERGY	SOURCE		DETECTOR		ANGLE
			TYPE	RANGE	TYPE	RANGE	
T,G	RLX	17- 20	D	0- 3	NAI-D		90

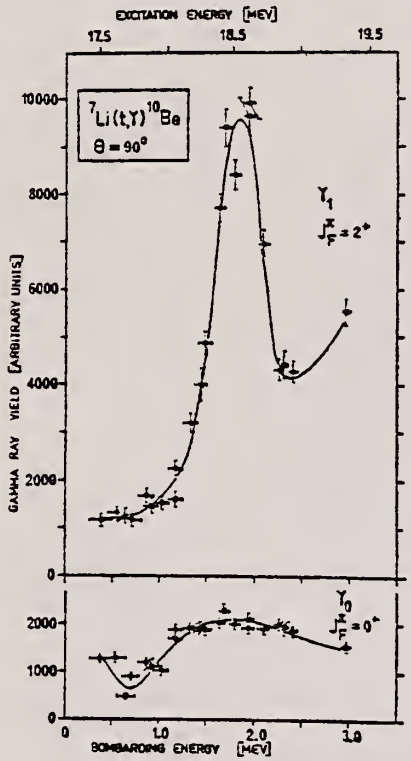

Fig.2 : Excitations curves for γ_0 and γ_1 transitions. The dots and crosses represent two independent sets of runs. The solid curves are artist's conceptions, not analytical fits to the data.

Ref. B.P. Fabricand, B.A. Allison, J. Halpern
Phys. Rev. 103, 1755(1956)

Elem. Sym.	A	Z
Be	9	4

Method ZnS paraffin; 18 MeV Bremss.

Ref. No. 56 Fa 1 EGF

Reaction	E or ΔE	E_o	Γ	$\int \sigma dE$	Jπ	Notes
(γ,n)	Bremss. 18					Angular distribution measured $60^\circ \longrightarrow 160^\circ$. $\sigma(\theta) = (1.25 \pm 0.11) + \sin^2\theta$; about same as found by Hamermish, Hamermish and Wattenberg [Phys. Rev. 76, 611 (1949)] at 2.76 MeV.

I. V. Chuvilo, and V. G. Shevchenko
J. Exptl. Theoret. Phys. (USSR) 32, 1335 (1957)
Soviet Phys. JETP 5, 1090 (1957)

Be	9	4

METHOD

REF. NO. 57 Ch 1

EGF

REACTION	RESULT	EXCITATION ENERGY	SOURCE		DETECTOR		ANGLE
			TYPE	RANGE	TYPE	RANGE	
G,XP	SPC	THR - 84	C	68,84	EMU-D	20-50	DST

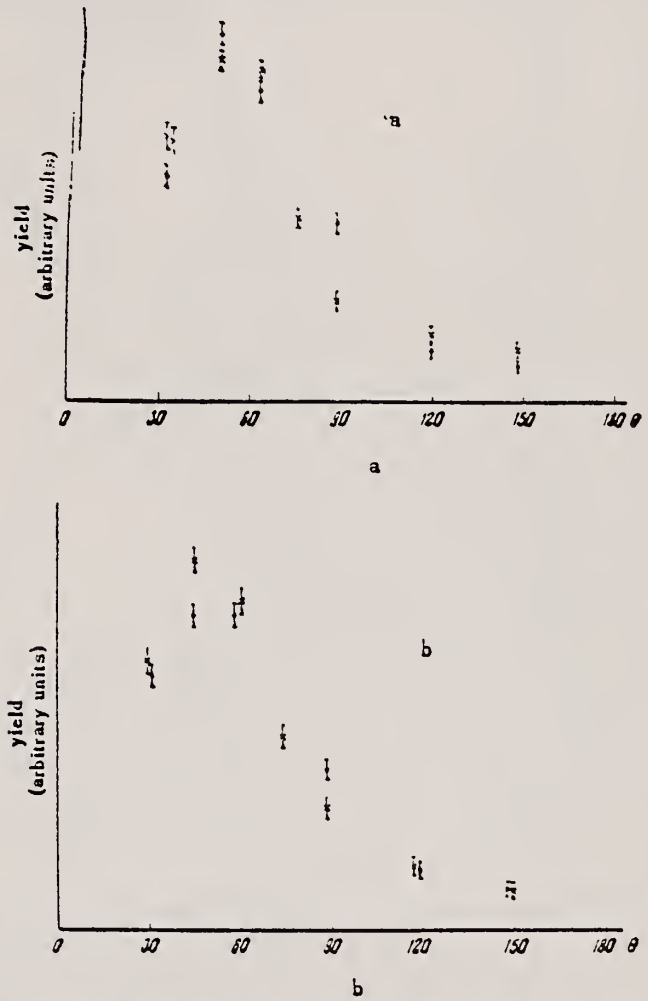

FIG. 2. Angular distributions of the photoprotons. *a*) Be^9: dots — $E_p > 20$ Mev, $E_{\gamma max} = 68$ Mev; crosses — $E_p > 32$ Mev, $E_{\gamma max} = 84$ Mev; *b*) C^{12}: dots — $E_p > 18$ Mev, $E_{\gamma max} = 64$ Mev; crosses — $E_p > 26$ Mev, $E_{\gamma max} = 84$ Mev.

(continued)

Ref. I. V. Chuvilo, and V. G. Shevchenko
J. Exptl. Theoret. Phys. (USSR) 32, 1335 (1957)
Soviet Phys. JETP 5, 1090 (1957)

Elem. Sym.	A	Z
Be	9	4

Method

Ref. No.	
57 Ch 1	EGF

Reaction	Result	Excitation Energy	Source Type	Source Range	Detector Type	Detector Range	Angle

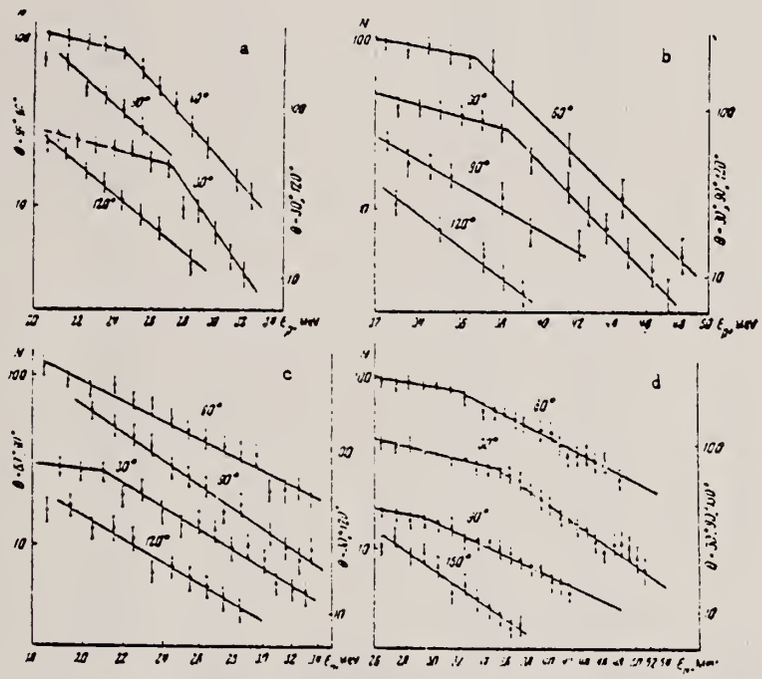

FIG. 3. Energy distribution of photoprotons (yield given in relative units): a – Be^9, $E_{\gamma max}$ = 68 Mev; b – Be^9, $E_{\gamma max}$ = 84 Mev; c – C^{13}, $E_{\gamma max}$ = 64 Mev; d – C^{13}, $E_{\gamma max}$ = 84 Mev.

Ref. K.H. Lokan
Proc. Phys. Soc. A, 70, 836 (1957)

Elem. Sym.	A	Z
Be	9	4

Method: 30 MeV Canberra synchrotron; NaI(Tℓ) scintillation counter

Ref. No.: 57 Lo 1 JHH

Reaction	E or ΔE	E_o	Γ	$\int \sigma dE$	Jπ	Notes
$Be^9(\gamma,2n)$	Bremss. 30			$\int_{20.56}^{30} = 1.2\pm0.2$ MeV-mb		E_{th} = 20.56 MeV $\int \sigma dE$ based on: Yield curve normalized to Ta(γ,n This ion in turn normalized to $Cu^{63}(\gamma,n)Cu^{62}$. Take Berman and Brow [Phys. Rev. 96, 83 (1954)] for absolute $Cu^{63}(\gamma,n)$. Measured yield to 30 MeV only. To get $\int \sigma dE$, assume shape like $He^4(\gamma,n)$ [symmetrical peak centered at ~ 25 MeV]; results not t sensitive to this.

Ref. T. Asada, M. Masuda, M. Okumura, J. Okuma
J. Phys. Soc. Japan 13, 1 (1958)

Elem. Sym.	A	Z
Be	9	4

Method: Betatron; angular distribution; scintillator; ionization chamber

Ref. No.: 58 As 1 — EH

Reaction	E or ΔE	E_o	Γ	$\int \sigma dE$	Jπ	Notes
$Be^9(\gamma,n)$	Bremss. 17					Angular distribution has form $(a + b \sin^2 \theta)$, where b/a = 1.29±0.53.

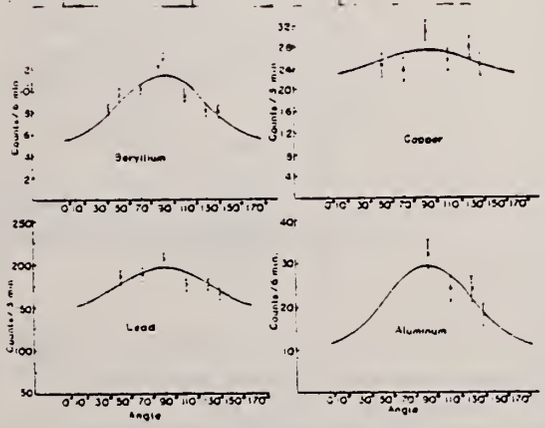

Fig. 6. The angular distributions of photo-neutrons as measured with Emmerich button type scintillation detector.

Table I. The values of b/a.

Energy	Target nucleus Al	Cu	Pb	Be	Detector
Present (17 Mev)	1.9±0.8	0.17±0.06	0.20±0.11	1.29±0.53	Emmerich
Dixon (20 Mev)	0.36±0.29	0.23±0.15	uniform	1.2±0.4	Hornyak
Halpern (20 Mev)				1.26±0.11	Emmerich
Price (22 Mev)		0.33	0.84	uniform	Al [a], [b]
Johanson (65 Mev)	1		0.8	1.5 *	Hornyak

a) A scintillation detector with a ZnS paraffin-Lucite light guide.
b) A scintillation detector with a ZnS-Lucite
c) A fast neutron detector by measuring the beta activity of $Al^{27}(n, p)Mg^{27}$ reaction

References

1) E. D. Courant: Phys. Rev. **82** (1951) 703.
2) S. A. E. Johanson: Phys. Rev. **97** (1955) 434.
3) W. R. Dixon: Can. J. Phys. **33** (1956) 785.
4) G. A. Price: Phys. Rev. **93** (1954) 1269

FORM NBS-418
(8-1-63)
USCOMM-DC 18556-P63

U.S. DEPARTMENT OF COMMERCE
NATIONAL BUREAU OF STANDARDS

Ref. W.C. Barber
Phys. Rev. 111, 1642 (1958)

Elem. Sym.	A	Z
Be	9	4

Method
Neutron counting

Ref. No.
58 Ba 2 EH

Reaction	E or ΔE	E_o	Γ	$\int \sigma dE$	Jπ	Notes
$Be^9(\gamma,n)$						Ratio of (γ,n) to (e,e'n) in Figure 2 for Be^9 agrees with electric dipole assumption.

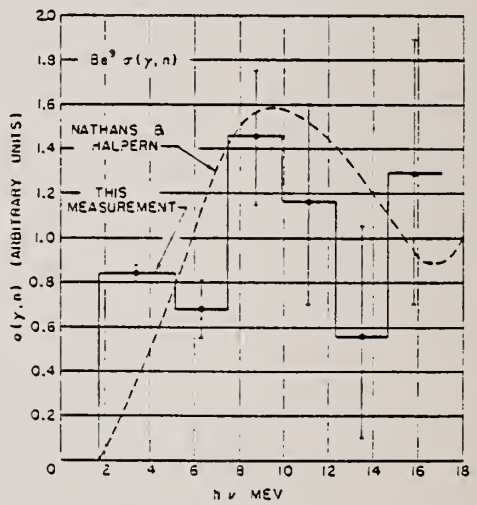

FIG. 2. Cross-section curves for the reaction $Be^9(\gamma,n)$. The histogram is the cross section derived by photon difference analysis of the photon activation curve shown in Fig. 1. The dashed curve is the cross section as determined by Nathans and Halpern.[12]

Ref. 12: Nathans and Halpern, Phys. Rev. 92, 940 (1953).

Ref. I.V. Chuvilo, V.G. Shevchenko
Zhur. Eksp. i Teoret. Fiz. 34, 593 (1958)
Soviet Phys. JETP 7, 410 (1958)

Elem. Sym.	A	Z
Be	9	4

Method emulsions; 44 MeV Bremss.

Ref. No. 58 Ch 1 EH

Reaction	E or ΔE	E_o	Γ	$\int \sigma dE$	Jπ	Notes
(γ,p)	44					Angular distribution for proton energy groups 4-5, 5-6, 6-9, 9-12, 12-15, and ≥ 15 MeV; calculated for ground state transitions (2^+ state of Li^8).

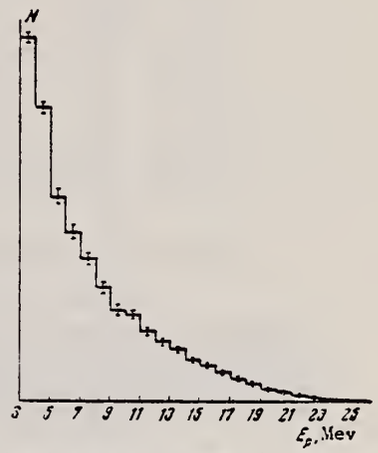

Fig. 3. Complete energy spectrum of protons from photodisintegration of Be^9; $E_{\gamma max}$ = 44 Mev.

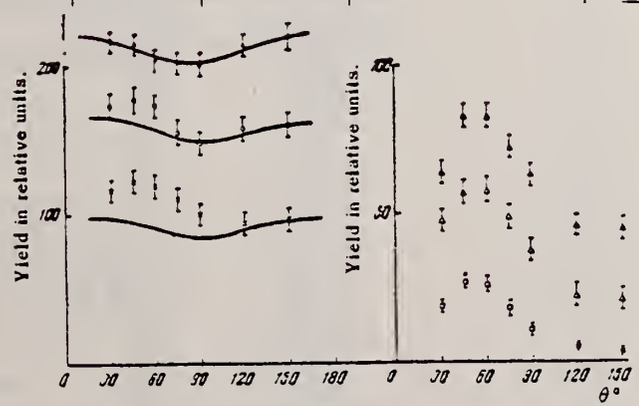

Fig. 1. Angular distributions of proton groups from photodisintegration of Be^9 by γ quanta with $E_{\gamma max}$ = 44 Mev. The solid curves show the angular distributions calculated from the intermediate nucleus model, with transition to the ground 2^+ state of Li^8. • – E_p = 4–5 Mev, ○ – E_p = 5–6 Mev, × – E_p = 6–9 Mev, ▲ – E_p = 9–12 Mev, △ – E_p = 12–15 Mev, □ – $E_p \geq 15$ Mev.

Ref. C. Whitehead, W.R. McMurray, M.J. Aitken, N. Middlemas, C.H. Collie
Phys. Rev. 110, 941 (1958)

Elem. Sym.	A	Z
Be	9	4

Method
counter telescope; Bremss.

Ref. No.
58 Wh 2

EH

Reaction	E or ΔE	E_o	Γ	$\int \sigma dE$	Jπ	Notes
$Be^9(\gamma,p)$	Bremss.					
	37					
	96					

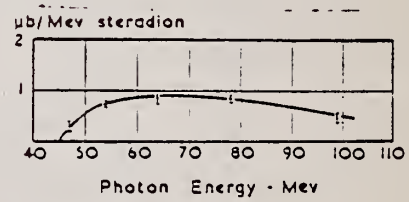

FIG. 11. Cross sections for the production of 37-Mev photoprotons from beryllium ($\theta_{lab}=90°$).

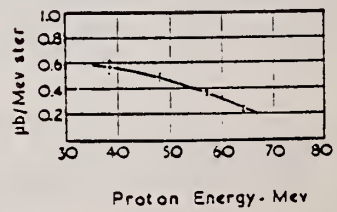

FIG. 12. Energy spectrum of photoprotons emitted from beryllium at 90° by 96-Mev photons.

W. C. Barber and W. D. George
Phys. Rev. 116, 1551 (1959)

Be	9	4

METHOD

REF. NO. 59 Ba 3 EGF

REACTION	RESULT	EXCITATION ENERGY	SOURCE TYPE	SOURCE RANGE	DETECTOR TYPE	DETECTOR RANGE	ANGLE
E,N	ABY	THR - 36	D	10 - 36	BF3-I		4PI

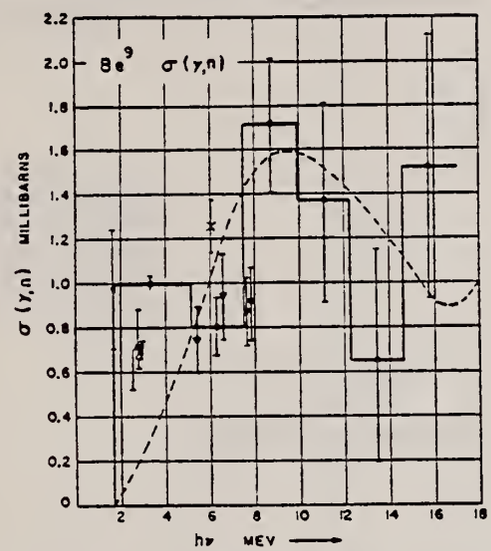

FIG. 3. Cross section for the $Be^9(\gamma,n)$ reaction as determined from a number of experiments: circles, present measurements; dashed curve, Nathans and Halpern (reference 18); cross, Carver, Kondaiah, and McDaniel [Phil. Mag. 45, 948 (1954)]; squares, Russel, Sacks, Wattenberg, and Fields [Phys. Rev. 73, 545 (1948)]; triangle, Snell, Barber, and Sternberg [Phys. Rev. 80, 637 (1950)]; inverted triangles, V. O. Eriksen and C. P. Zaleski [J. phys. radium 15, 492 (1954)].

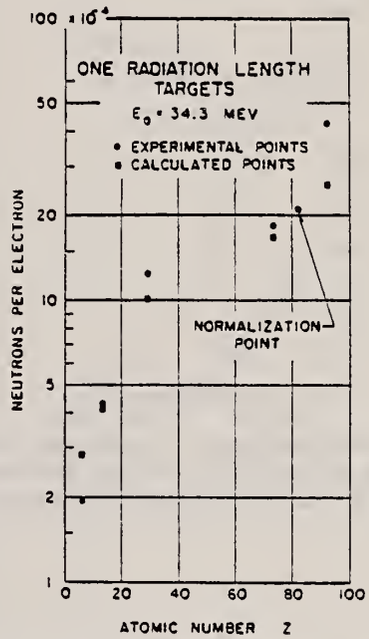

FIG. 14. Experimental and expected yields of neutrons per incident electron for 1-radiation-length targets at 34.3 Mev, as a function of atomic number Z. The experimental yields were obtained by dividing the measured yields from the targets labeled I by the actual target thicknesses listed in Table I. The expected yields were calculated from expression (8).

TABLE I. Thicknesses of the targets used in the experiment. with the exception of heavy water, all targets contained isotopes in their naturally-occurring proportions.

Target	Thickness (g/cm²)	Thickness (radiation lengths)
Heavy water	0.698	"thin"
Be	0.589	0.00867
C-I	38.91	0.88
Al-I	24.19	1.00
Cu-A	1.372	0.108
Cu-I	13.26	1.04
Cu-II	26.56	2.08
Cu-III	39.86	3.13
Cu-IV	53.13	4.17
Ta-I	6.21	0.98
Pb-I	5.88	1.01
Pb-II	11.42	1.97
Pb-III	17.30	2.98
Pb-IV	22.89	3.94
Pb-VI	34.42	5.93
U-I	6.17	1.14
U-II	12.42	2.30
U-III	18.61	3.46
Concrete	28.5	1.19

V. P. Chizhov and L. A. Kul'Chitskii
J. Exptl. Theoret. Phys. (USSR) 36, 345 (1959)
Soviet Phys. JETP 36(9) 239 (1959)

	Be	9	4
METHOD	REF. NO.		
	59 Ch 1		EGF

REACTION	RESULT	EXCITATION ENERGY	SOURCE		DETECTOR		ANGLE
			TYPE	RANGE	TYPE	RANGE	
G,XP	RLY	THR - 80	C	90	TEL-D	15 - 60	DST
G,XD	RLY	THR - 80	C	90	TEL-D	15 - 60	DST

REL D TO P YLD

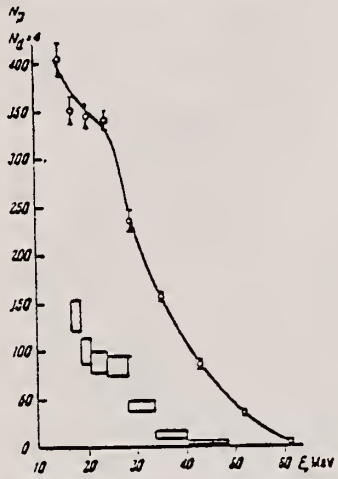

FIG. 2. Energy distributions; o — photoprotons and □ — photodeuterons from Be^9 with $E_{\gamma max}$ = 90 Mev. The scale of the ordinate axis for deuterons is enlarged by a factor of 4.

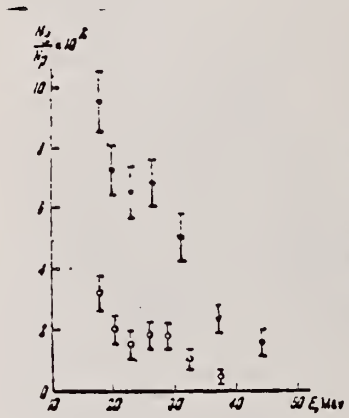

FIG. 4. Ratio of the number of photodeuterons to the number of photoprotons with the same energy, as a function of energy: o — for C^{13} and • — for Be^9.

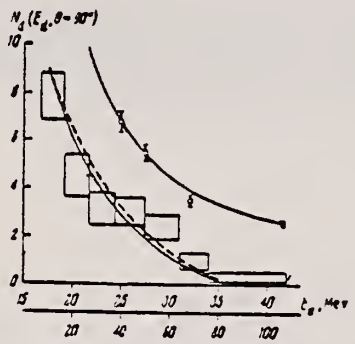

FIG. 6. Experimental and calculated energy distributions of photodeuterons from C^{13}: o — experimental values for $E_{\gamma max}$ = 300 Mev (lower abscissas), rectangles — for $E_{\gamma max}$ = 80 Mev (upper abscissas); the heights of the rectangles represent the statistical errors and the widths represent the energy intervals.

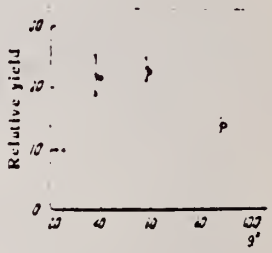

FIG. 5. Angular distributions of photodeuterons (solid circles) and of photoprotons (open circles) from Be^9.

Ref. J.H. Gibbons, R.L. Macklin, J.B. Marion, H.W. Schmitt
Phys. Rev. 114, 1319 (1959)

Elem. Sym.	A	Z
Be	9	4

Method: Radioactive sources; BF_3 4π neutron counters

Ref. No.: 59 Gi 1 — JHH

Reaction	E or ΔE	E_o	Γ	$\int \sigma dE$	Jπ	Notes
$Be^9(\gamma,n)$	1.69					$\sigma_{(\gamma,n)} = (12.62\pm0.69)\ 10^{-28}\ cm^2$
	1.85					$= (6.54\pm0.31)\ 10^{-28}\ cm^2$
						Sources: Sb^{124} (1.69 MeV) Y^{88} (1.85 MeV)

Ref. L.A. Kul'chitskii, V. Presperin
Zhur. Eksp. i Teoret. Fiz. 37, 1524 (1959);
Soviet Phys., JETP 10, 1082 (1960).

Elem. Sym.	A	Z
Be	9	4

Method
88 MeV Synchr.; proton recoil counter telescopes

Ref. No. 59Kul JH

Reaction	E or ΔE	E_o	Γ	$\int \sigma dE$	Jπ	Notes
(γ,n)	Bremss: $E_{\gamma max}$=88Mev; $E_n \geq 10$ Mev.					Angular distribution; results consistent with quasi-deutron model, but some direct resonance abs. may be present.

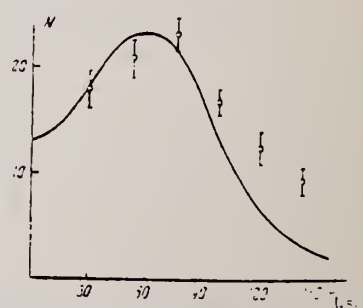

FIG. 5. Angular distribution of photoneutrons from Be⁹. Solid curve – data calculated in reference 14.

Ref. H.H. Thies, B.M. Spicer, J.E.E. Baglin
Australian J. Phys. 12, 21 (1959)

Elem. Sym.	A	Z
Be	9	4

Method: 18 MeV Melbourne synchrotron; γ - ray; ionization chamber; BF_3 counters

Ref. No.: 59 Th 1 EH

Reaction	E or ΔE	E_o	Γ	$\int \sigma dE$	$J\pi$	Notes
$Be^9(\gamma,n)$	Bremss. 6.5-18			$\int_{6.5}^{18}$ = 22 MeV-mb		σ = 3 mb.
		11.25	}	$\int$ = ~ 4 MeV-mb		
		13.25				

553

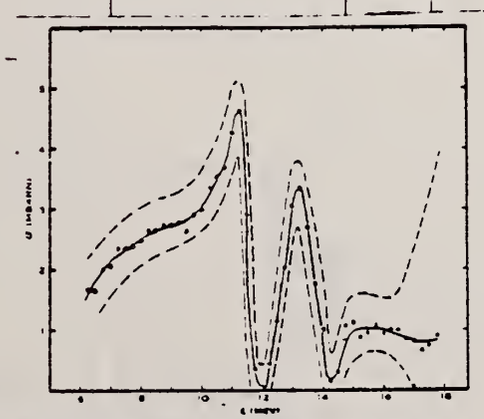

Fig. 1.—The cross section for production of photoneutrons from beryllium. The dashed lines represent the extremes of the area of statistical variation, which is to be interpreted as indicated in the text.

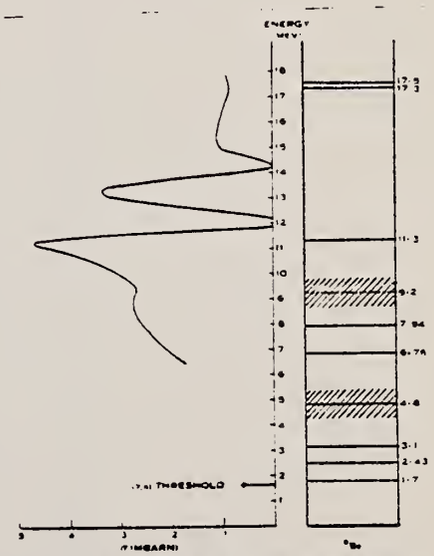

Fig. 4.—The cross section for nuclear absorption of photons in beryllium plotted beside a diagram of previously observed energy levels of ^9Be.

Ref. W.C. Barber, F. Berthold, G. Fricke, F.E. Gudden
Phys. Rev. 120, 2081 (1960)

Elem. Sym.	A	Z
Be	9	4

Method Stanford Mark II Linac; magnetic spectrometer; plastic scintillator counter telescope

Ref. No. 60 Ba 4 JHH

Reaction	E or ΔE	E_o	Γ	$\int \sigma dE$	Jπ	Notes
$(e^-,e^{-\prime})$	42.5	2.43	Γ_γ = 0.13±0.03 eV	0.13 ± 0.03 MeV-mb	$5/2^-$	$\int \sigma dE$ is average of 0.118 and 0.165 MeV-mb measured at $\theta = 160^\circ$ and 132° respectively. M1 transition. Data at 160° indicate 50% possibility of 4.2 MeV level. Peak observed at 16.9 ± 0.4 MeV, but insufficient data for multipolarity assignment.

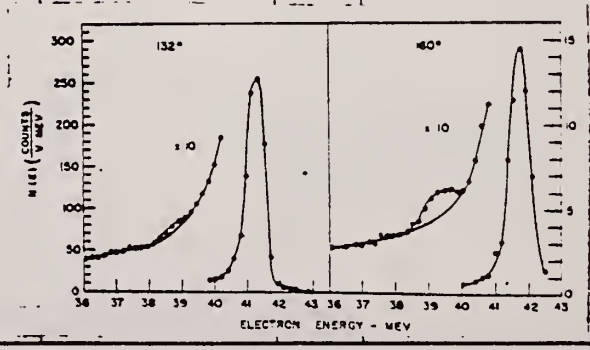

FIG. 7. Energy distributions of electrons scattered from Be at scattering angles of 132° and 160°. The primary electron energy was 42.5 Mev in both experiments, but in the 132 scattering the target angle was such that the electrons entered one side and left from the opposite side. This caused an increase in the energy loss in the target over that observed in the 160° experiment.

W. Bertozzi, P.T. Demos, S. Kowalski, F. Paolini, C.P. Sargent, PICNS 746 (1960) (Proceedings of the International Conference on Nuclear Structure, University of Toronto Press, 1960)

Be	9	4

METHOD: Neutron cross section; time-of-flight

REF. NO.: 60 Be 1 NVB

REACTION	RESULT	EXCITATION ENERGY	SOURCE TYPE	SOURCE RANGE	DETECTOR TYPE	DETECTOR RANGE	ANGLE
G,N	ABX	2 - 17	C	5 - 17	TΦF-D		DST
		(1.7 - 17)					

557

For transitions leaving Be^8 in ground state:

σ_{peak} at 3.0 MeV excitation energy

$\int\sigma_{peak}$ = 0.2 MeV-mb

Γ_{peak} = 180 keV

$W(\theta)$ = isotropic

σ smooth and flat at 6-7 MeV, has minimum at 13 MeV.

For transitions leaving Be^8 in 2.9 MeV excited state:

$\sigma_{peak} \simeq$ 1 mb at 6-7 MeV.

σ has minimum at 13 MeV.

Ref. V.P. Chizhov
Zhur. Eksp. i Teoret. Fiz. 38, 809 (1960);
Soviet Phys. JETP 11, 587 (1960)

Elem. Sym.	A	Z
Be	9	4

Method 90 MeV Bremsstrahlung; scintillator counter telescope ...

Ref. No. 60 Ch 1 JHH

Reaction	E or ΔE	E_o	Γ	$\int \sigma dE$	Jπ	Notes
$Be^9(\gamma,p)$						E_d - 15.5 - 31 MeV
$Be^9(\gamma,d)$						E_p - 15.5-30 MeV
$Be^9(\gamma,t)$						E_t - 17-30 MeV
						Angular distribution.
						Ratios:
						$\sigma(\gamma,d)/\sigma(\gamma,p)$ at $\theta = 80^\circ$
						$\sigma(\gamma,t)/\sigma(\gamma,d)$ summed over angles 35°-145°

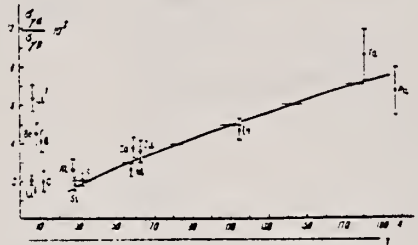

FIG. 3. Ratio of (γ, d) to (γ, p) cross sections for protons and deuterons of energies 15.5–30 Mev as function of atomic weight A. The solid curve shows the dependence given by Eq. (2), arbitrarily normalized.

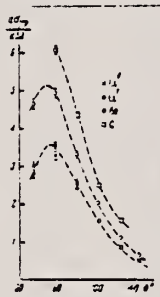

FIG. 6. Angular distributions of photoprotons of energies 15.5–30 Mev for Li^6, Li^7, Be, and C. The errors are statistical.

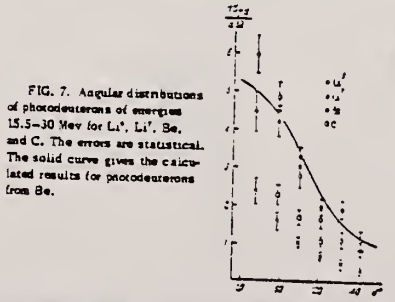

FIG. 7. Angular distributions of photodeuterons of energies 15.5–30 Mev for Li^6, Li^7, Be, and C. The errors are statistical. The solid curve gives the calculated results for photodeuterons from Be.

YIELD DATA TABLE:

It should be noted that the yield of photoprotons of the energy considered rises smoothly with Z for the elements plotted in Fig. 3, and that starting already with Al, no direct proportionality to Z is observed on account of the effect of the Coulomb barrier. For illustration, we give the yields of photoprotons $Y(\gamma, p)$ per proton in the nucleus for several elements in relative units (the error in these measurements was estimated to be ±10%):

	Li^6	Li^7	Be	C	Al	Cu
$Y(\gamma,p)$ =	1.10	1.07	1.0	1.01	1.00	0.56

TABLE I

Element		Element		Element		Element	
Li^6	30±3	B	20±6	Ni	10±4	Sn	5±2.5
Li^7	13.5±2.5	Si	10±4	Cu	2.5±1	Ta	10±4
Be	13±2.5	S	4±1	Ge	2.5±1	Au	2±1

Ref. L.A. Kul'chitskii, V. Presperin
Zhur. Eksp i Teoret. Fiz. 39, 1001 (1960);
Soviet Phys. JETP 12, 696 (1960)

Elem. Sym.	A	Z
Be	9	4

Method
90 MeV Synchr.; proton recoil counter telescopes

Ref. No. 60 Ku 2 JH

Reaction	E or ΔE	E_o	Γ	$\int \sigma dE$	Jπ	Notes
$Be^9(\gamma,n)$	Bremss.; $E_{\gamma max}$=90MeV					Relative yields in table are per nuclear neutron.

Element	Relative neutron yield	Element	Relative neutron yield
Li	1.00±0.05	Cu	0.37±0.02
Be	1.22±0.09	Cd	0.35±0.02
O	0.74±0.05	I	0.30±0.02
Al	0.49±0.03	Bi	0.41±0.03
Ca	0.33±0.02		

Ref. P.C. Stein, A.C. Odian, A. Wattenberg, R. Weinstein
Phys. Rev. 119, 348 (1960)

Elem. Sym.	A	Z
Be	9	4

Method: 320 MeV synchrotron; proton telescope; neutron counter

Ref. No.: 60 St 1 JHH

Reaction	E or ΔE	E_0	Γ	$\int \sigma dE$	Jπ	Notes
$Be^9(\gamma, np)$	Bremss. 320					$(\sigma/\sigma_{H^2}) = 2.3 \pm 0.3$ $[\sigma_{H^2} = 63\ \mu b]$ Mean photon energy - 262 MeV Proton counter at 76°

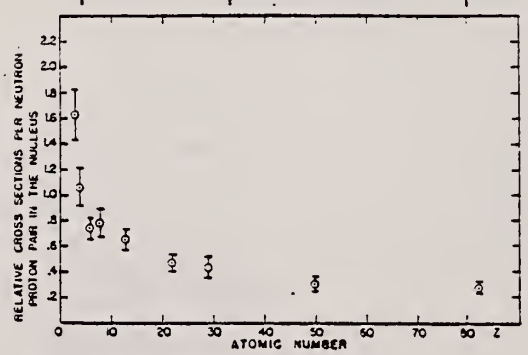

FIG. 2. Relative cross sections per neutron-proton pair in the nucleus versus atomic number. The cross section of the element of interest is divided by the cross section for deuterium and by the factor NZ/A.

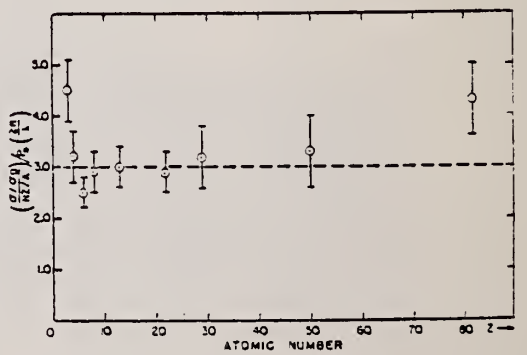

FIG. 3. The relative cross sections per neutron-proton pair corrected for the probability of escape is plotted against atomic number. The probability of escape factor is calculated using $r_0 = 1.30 \times 10^{-13}$ cm and $\lambda = 3.6 \times 10^{-13}$ cm. The probability of escape factor is given in expression (1). The data shown are those of Fig. 2 divided by $P(2R/\lambda)$.

Ref. M.J. Jakobson
Phys. Rev. 123, 229 (1961)

Elem. Sym.	A	Z
Be	9	4

Method: Bremss; BF_3 counter; photon difference method

Ref. No.: 61 Ja 1 JHH

Reaction	E or ΔE	E_o	Γ	$\int \sigma dE$	Jπ	Notes
(γ,n)		1.70				$\sigma_{max}(\gamma,n)$ = 1.15 ± 0.15 mb
		2.40				= 0.55 ± 0.1 mb
		2.95				" = 1.2 ± 0.2 mb
		4.6				" = 1.0 ± 0.3 mb
						σ(θ)(1.70 MeV) = sph. symm.
						σ(θ)(2.4 MeV) = almost isotropic; slightly higher at θ = 90°.
						σ(θ)(2.95 MeV) = a + b $\sin^2\theta$, where a/b = 1.0 ± 0.2.
						σ(θ)(4.6 MeV) = sph. symm.

539

A bremsstrahlung-photon difference method measurement of the $Be^9(\gamma,n)$ cross section indicates maxima in the cross section of 1.15±0.15, 0.55±0.1, 1.2±0.2, and 1.0±0.3 mb at energies of 1.70, 2.40, 2.95, and 4.6 Mev, respectively. The angular distribution of the neutrons corresponding to the 1.70- and 4.6-Mev peaks is spherically symmetric; $d\sigma/d\Omega = a + b \sin^2\theta (a/b = 1.0 \pm 0.2)$ for the 2.95-Mev peak.

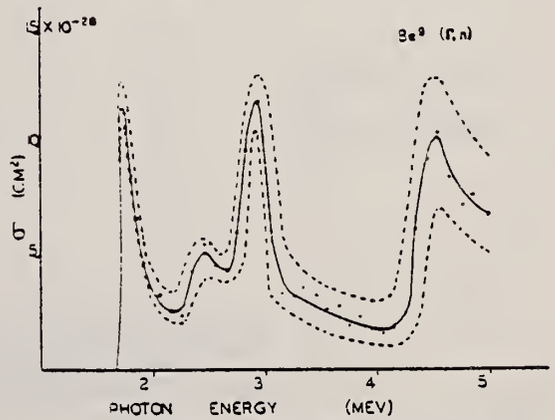

FIG. 1. Plot of the photoneutron cross section of Be^9 resulting from measurements described in this article. The errors indicated by the dashed lines represent standard deviations associated with reproducibility.

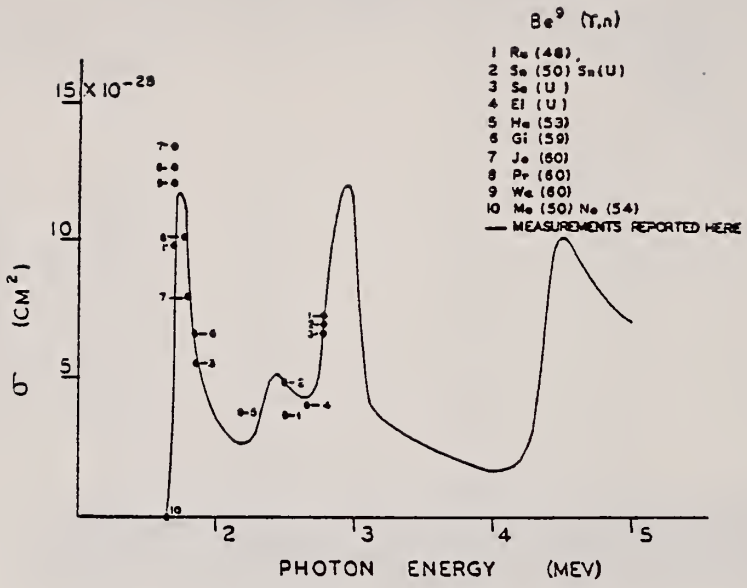

FIG. 2. Previously published measurements for the $Be^9(\gamma,n)$ cross section are indicated so that they can be compared with the results presented in Fig. 1.

Ref. V.V. Balashov, V.N. Fetisov
Izv. Akad. Nauk SSSR, Ser. Fiz. 26, 1188 (1962)

Elem. Sym.	A	Z
Be	9	4

Method: counted neutrons from Li^7 decay

Ref. No.: 62 Ba 1 JHH

Reaction	E or ΔE	E_o	Γ	$\int \sigma dE$	Jπ	Notes
(γ,nd)	45 - 62					cross section about 2 order of mag. lower then (γ,p).

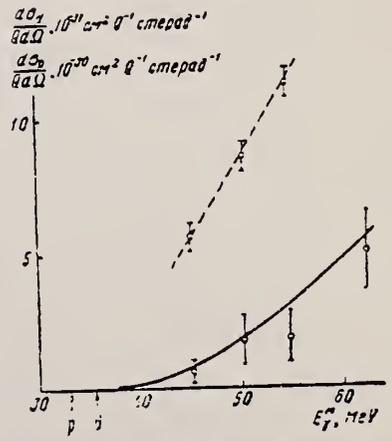

Сплошная линия — рассчитанное нормированное сечение $Be^9(\gamma, d)Li^7$. Точки — экспериментальные данные работы [1]. Для сравнения пунктиром показан ход сечения $Be^9(\gamma, p)$ [1]. $\theta_{лаб} = 90°$

Ref. R. Bösch, J. Lang, R. Muller, W. Wolfli
Phys. Letters 1, 114 (1962)

Elem. Sym.	A	Z
Be	9	4

Method: Radioactive source (Na^{24}); long counter

Ref. No.: 62 Bo 4 JHH

Reaction	E or ΔE	E_o	Γ	$\int \sigma dE$	Jπ	Notes
$Be^9(\gamma,n)$	2.753					

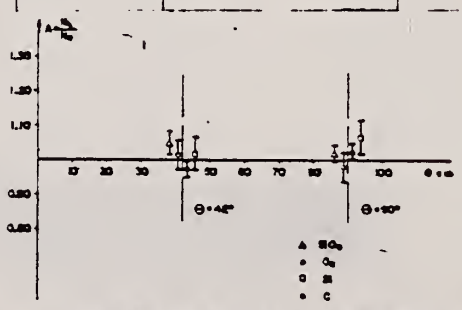

Fig. 1. Gemessene Asymmetrien: Die O_2-Resultate setzen sich aus Messungen mit flüssigem Sauerstoff und aus Differenzmessungen SiO_2–Si zusammen. Zur Kontrolle wurden auch die SiO_2- und Si-Messungen aufgetragen.

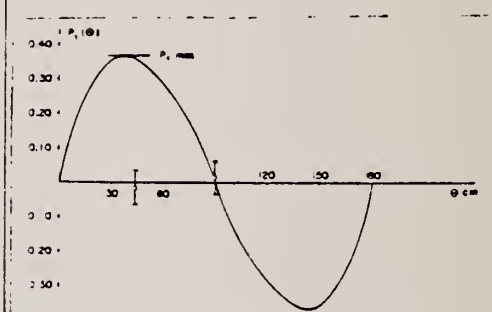

Fig. 2. Polarisation der Photoneutronen vom Be^9 in Abhängigkeit des Gamma-Neutronenemissionswinkel für E_γ = 2.753 MeV. Die ausgezogene Kurve wurde nach der Theorie von Czyz und Sawicki [1] auf Grund des Modells von Guth und Mullin [7] berechnet.

1) W. Czyz und J. Sawicki, Nuovo Cimento 3 (1956) 864.
2) L. N. Rosentsveig, J. Expt. Theor. Phys. 4 (1957) 230.
3) W. Czyz und J. Sawicki, Nuovo Cimento 5 (1957) 45; Phys. Rev. 110 (1958) 900.
4) J. J. de Swart, W. Czyz und J. Sawicki, Phys. Rev. Letters 2 (1959) 51.
5) M. L. Rustgi, W. Zernik, G. Breit und D. J. Andrews, Phys. Rev. 120 (1960) 1881.
6) J. J. de Swart, Physica 25 (1959) 233.
7) E. Guth und C. J. Mullin, Phys. Rev. 76 (1949) 234.

Ref. R. Bosch, J. Lang, R. Muller, W. Wolfli
Helv. Phys. Acta 35, 288 (1962)

Elem. Sym.	A	Z
Be	9	4

Method Reactor (n,γ); neutron angular distribution; sctintillator

Ref. No. 62 Bo 7 NVB

Reaction	E or ΔE	E_o	Γ	$\int \sigma dE$	Jπ	Notes
$Be^9(\gamma,n)$	5.4 6.5 7.6 9.0					Angular distribution: $a + b \sin^2\theta$ $E_{\gamma(MeV)}$ a/b 5.4 3.80 6.5 5.00 7.6 4.40 9.0 4.10

Ref. V.P. Chizhov, A.P, Komar, L.A. Kulchitsky, A.V. Kulikov, E.D. Makhrovsky, Yu.M. Volkov
Nuclear Phys. 34, 562 (1962)

Elem. Sym.	A	Z
Be	9	4

Method: 90 MeV Synchrotron; magnetic spectrometer; emulsions; NaI counter telescope

Ref. No.: 62 Ch 2 JHH

Reaction	E or ΔE	E_0	Γ	$\int \sigma dE$	Jπ	Notes
(γ,d)	Bremss. 90					
(γ,p)						

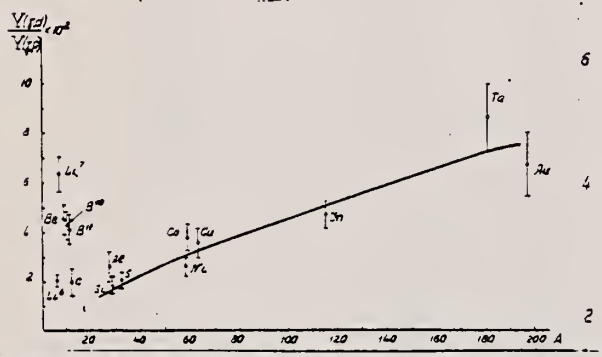

Fig. 4. The ratio of the yields of deuterons and protons with energies 15.5 to 30 MeV depending on the mass number of nuclei A for $E_{\gamma max}$ = 90 MeV. The solid line stands for the normalized dependence (5).

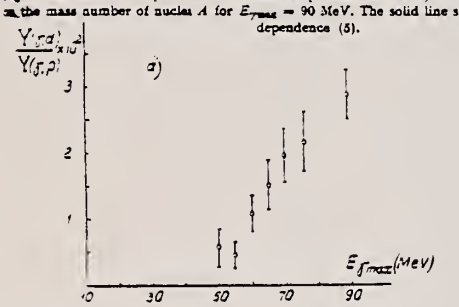

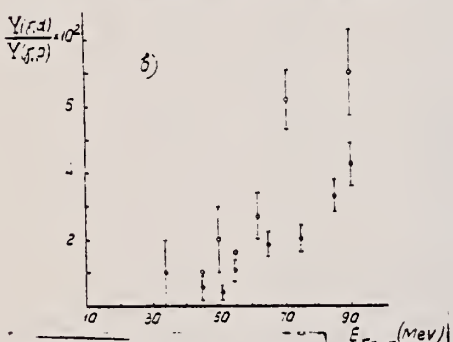

Figure 6: The ratio of deuteron and proton yields with E > 15 MeV plotted against $E_{\gamma max}$. a) Open circles denote Li^6. b) Open circles denote Be and black circles B.

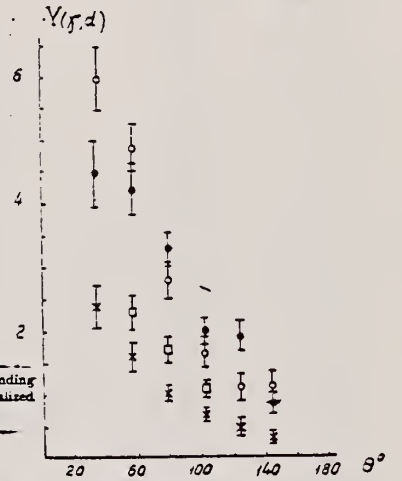

Fig. 7. Angular distributions of photodeuterons with the energies 15.5 to 30 MeV emitted in the photodisintegration by bremsstrahlung with $E_{\gamma max}$ = 90 MeV. Crosses denote Li^6, black circles Li^7, open circles Be, and open squares C. Particle yields are given in arbitrary units.

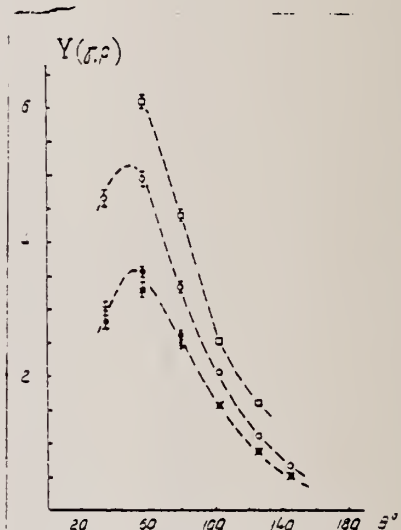

Fig. 8. Angular distributions of photoprotons with the energies 15.5 to 30 MeV See caption fig. 7.

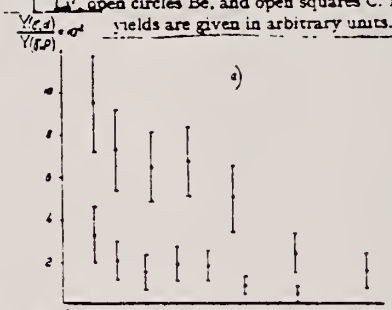

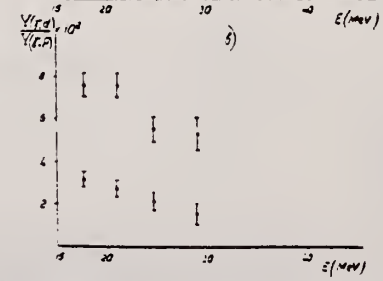

Fig. 5. The ratio of deuteron and proton yields plotted against particle energy E for $E_{\gamma max}$ = 90 MeV. a) Black circles denote Be^9 and open circles C^{12}. b) Black circles denote Li^7 and open circles Li^6.

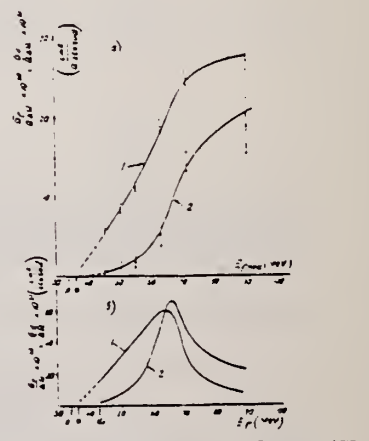

Ref. F.M. Clikeman, A.J. Bureau, M.G. Stewart
Phys. Rev. 126, 1822 (1962)

Elem. Sym.	A	Z
Be	9	4

Method 65 MeV synchrotron; proton yield; activity; NBS chamber

Ref. No. 62 Cl 1 | BG

Reaction	E or ΔE	E_0	Γ	$\int \sigma dE$	Jπ	Notes
$Be^9(\gamma,p)$	up to 57	23		$\int_{16.89}^{57} = 41.4 \pm 4.6$		Peak value of giant resonance cross section: 2.64±0.30 mb.

331

1044

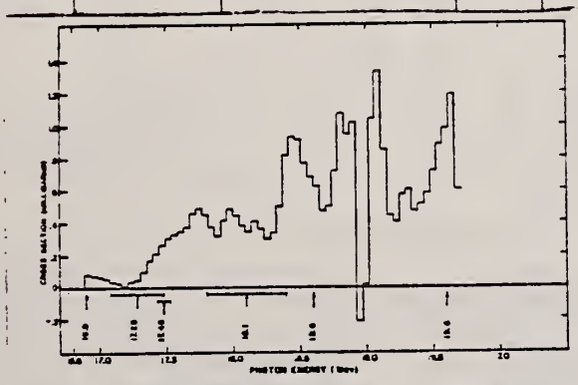

FIG. 3. Smoothed cross section for the $Be^9(\gamma,p)Li^8$ reaction for the energy interval 16 Mev to 20 Mev. The smoothing applied is discussed in the text. The known levels in Be^9 are shown by the arrows with the horizontal bars indicating their widths.

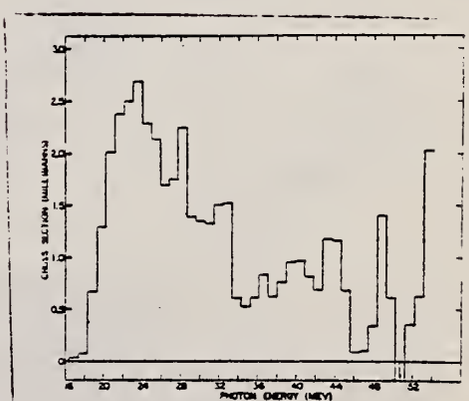

FIG. 7. Smoothed cross section for the $Be^9(\gamma,p)Li^8$ reaction. The smoothing applied is discussed in the text.

Ref. B. Cujec
Nuclear Phys. 37, 396 (1962)

Elem. Sym.	A	Z
Be	9	4

Method: 32 MeV bremss.; emulsions

Ref. No.: 62 Cu 1 JHH

Reaction	E or ΔE	E_o	Γ	$\int \sigma dE$	Jπ	Notes
$Be^9(\gamma,n)$	Bremss.					
$Be^9(\gamma,p)$	32					

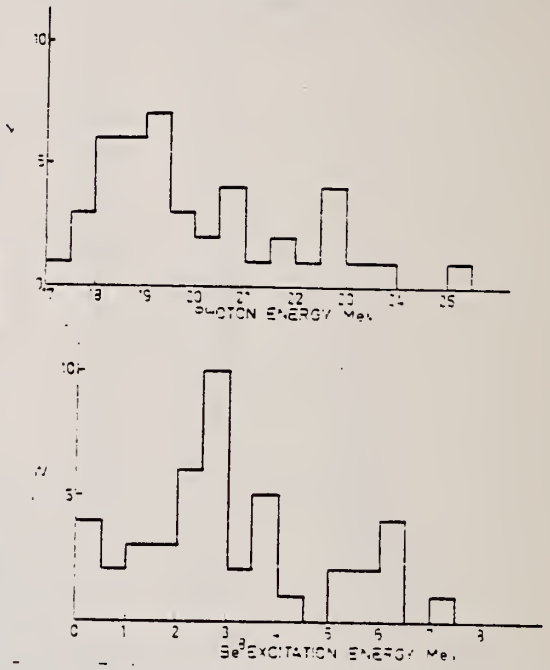

Fig. 2. The distribution of proton, [illegible] and Be^8 excitation energy in the reaction $Be^9 + \gamma \rightarrow Li^8 + Be^8$. In determining the photon energy it was assumed that Li^8 was left in its ground state.

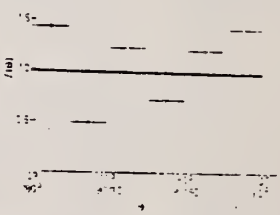

Fig. 3. Angular distribution of protons in the reaction $Be^9 + \gamma \rightarrow Li^8 + Be^8$. The quantity [illegible] actually the sum [illegible].

Fig. 4. Total cross section for the reactions $Be^9 + \gamma \rightarrow Li^8 + n$ and $Be^9 + \gamma \rightarrow Be^8 + p$ as a function of photon energy. The errors are statistical.

TABLE 4

Experimental and theoretical cross sections of particular states of Be^8 and Li^8

State	Theory	Experiment	Ratio
Be^8, $^3P_1(31)$, 16.0 Mev	0.34	0.11	3.1
Be^8, $^3P_1(31)$, 16.8 Mev	0.51	0.26	1.9
Be^8, $^3P_1(31)$, 17.6 Mev	[illegible]	[illegible]	[illegible]
Li^8, $^3P_1(31)$, 2.5	[illegible]	[illegible]	[illegible]
Li^8, $^3P_1(21)$, 0.98 Mev	[illegible]	[illegible]	[illegible]

Elem. Sym.	A	Z
Be	9	4

Method

Ref. No. 62 Cu 1 — JHH

Reaction	E or ΔE	E_0	Γ	$\int \sigma dE$	Jπ	Notes
						Emulsion soaked in $BeSo_4$

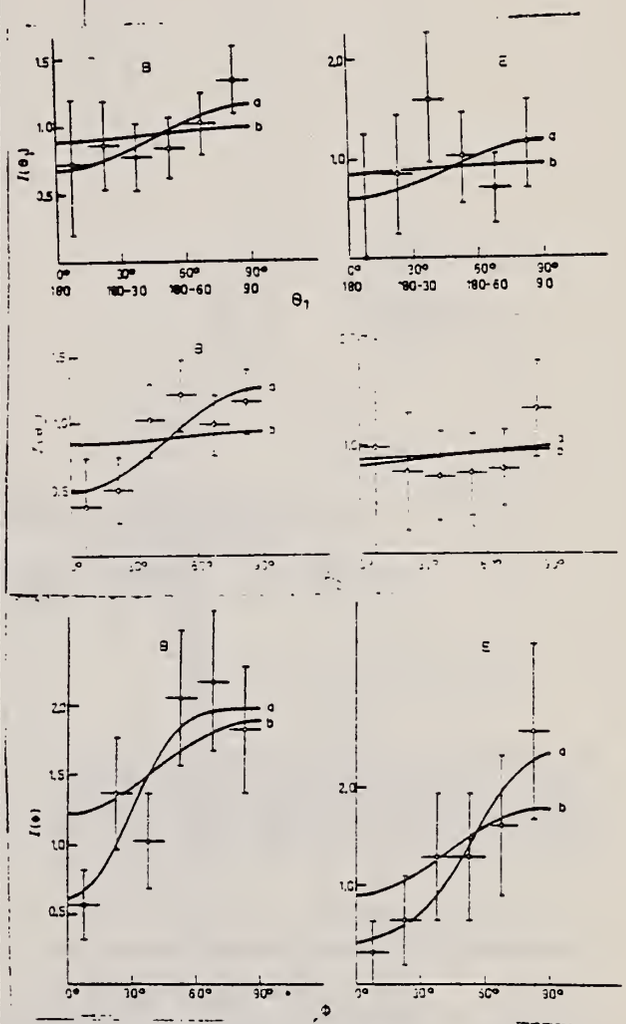

Fig. 7. Angular distributions for the angle θ_1 between neutron and neutron, and the angle Φ between photon and disintegration of Be^9 in C. M. S. and for the dihedral angle Φ between the planes of θ_1 and θ_2 in the reaction $Be^9(\gamma, n)Be^8$ with Be^8 in the 2.9 MeV state (group B) and in the 16.6, 17.6 and 18 MeV states (group E). Indicated errors are statistical. Curves a give the best least square fit to experimental points. Curves b represent results of further theoretical calculations [8] with the intermediate Be^8 nucleus. They were obtained on the assumptions of all particles being excited states of Be^8 proper weighted for transitions to the ground and [illegible]

TABLE 3

Experimental and theoretical cross sections of the $Be^9(\gamma, n)Be^8$ reaction

Reaction		$\int \frac{\sigma(E)dE}{E}$ (mb)			
$Be^9(\gamma, n)Be^8$		Experiment			Theory
Group	$E^*_{Be^8}$ (MeV)	$E < 16$ MeV	$16 < E < 32$ MeV	$0 < E < 32$ MeV	$0 < E$ [illegible]
A	0 -1.5	0.14 0.57 a)	0.06	0.63 a)	0.64
B	1.5-4.5	0.46 0.56 a)	0.25	0.81 a)	0.71
C	4.5-11	0.27 0.39 a, c)	0.32	0.71 a)	1s → 1p
D	11 -15	0.03	0.18	0.21	1 ≈ 1.0
E	15 -18		0.37	0.37	0.85
F	18 -23		0.06	0.06	0.36
$Be^9(\gamma, p)Li^8 \rightarrow Be^8$			0.58 0.66 a)	0.58	1.06

a) Ref. [5].
b) With E_γ < 16 MeV the value of ref. [5] has been taken into account.
c) The reaction mechanism suggested is $Be^9(\gamma, \alpha)He^5$.
d) Ref. [5] with scale calibration according to ref. [6].

References

1) E. W. Titterton, Nature 165 (1950) 721
2) F. Ajzenberg-Selove and T. Lauritsen, Nuclear Physics 11 (1951) 1
3) K. H. Lokan, Proc. Phys. Soc. 70 (1957) 836
4) U. Miklavčič, N. Bezić, D. Jamnik, G. Kernel, Z. Milavec and J. Scayder, to be published
5) B. Čujec, Bull. Am. Phys. Soc. 7 (1962) 59
6) F. L. Hereček and B. Dobovišek, Phys. Rev. 109 (1955) 1355
7) U. Miklavčič and C. Zupančič, Reports J. Stefan Inst. 5 (1958) 3
8) W. Bertozzi, P. T. Demos, C. P. Sargent, W. Turchinetz, D. McConnell and S. [illegible], Karlsruhe Photonuclear Conference 1960
9) R. N. H. Haslam, L. Katz, E. H. Crosby, R. G. Summers-Gill and A. G. W. Cameron, Can. J. Phys. 31 (1953) 210
10) L. Cohen, A. K. Mann, B. J. Patton, K. Reibel, W. E. Stephens and E. J. Winhold, Phys. Rev. 104 (1956) 108
11) V. P. Chizhov, L. A. Kul'chitskii, JETP 36 (1959) 345, JETP (Soviet Physics) 9 (1959) 239
12) V. P. Chizhov, JETP 38 (1960) 809, JETP (Soviet Physics) 11 (1960) 587
13) M. G. Stewart, Ames Lab. Research and Development Report IS-191 (August 1960)

Ref. R.D. Edge, G.A. Peterson
Phys. Rev. 128, 2750 (1962)

Elem. Sym.	A	Z
Be	9	4

Method: Linac; counter telescope

Ref. No.: 62 Ed 1 - BG

Reaction	E or ΔE	E_0	Γ_γ(eV)	$\int \sigma dE$(MeV-mb)	Jπ	Notes
Be^9 (e,e')	41.5	2.43	0.12	0.12±0.08		Nuclear states excited by 180° electron scattering; M1 transitions assumed.
		14.7	36	0.3±0.15		Inelastic electron scattering cross sections obtained by comparing inelastic peaks to e-p eleastic scattering peak.
						Γ_γ from virtual photon theory.
						Limits not given for cross sections.

TABLE I. Parameters of nuclear states excited by 180° electron scattering, assuming transitions are M1.

Isotope	Excitation energy, a MeV)	Spin and parity: Ground state I_0	Spin and parity: Excited state I_x	Inelastic cross section $d\sigma/d\Omega$ (10^{-28} cm² sr⁻¹)	$\int \sigma dk$ (MeV-mb)	Percentage experimental error	Ground state radiation widths, Γ_γ (eV): This experiment	Weisskopf units	Other experiments
Be^9	2.4	3/2⁻	5/2⁻	1.3	0.12	15	0.12	0.50	0.13[a]
	14.7	3/2⁻	1/2⁻	0.042	0.3	50	36	67	
			3/2⁻				18		
			5/2⁻				12		
B^{10}	7.9	3⁺	1⁺		1.9	0.75	30	17	10	9.5[a]
			3⁺				12		
			4⁺				10		
	11.8	3⁺	1⁺		1.2	0.75	50	34	34	
			3⁺				25		
			4⁺				22		
	14.0	3⁺	1⁺		0.6	0.5	50	34	58	
			3⁺				24		
			4⁺				15		
B^{11}	2.1	3/2⁻	1/2⁻		0.72	0.72	35	0.17	0.21	0.15[a]
	4.4	3/2⁻	5/2⁻		1.5	0.34	40	1.1	1.8	0.602[a]
	4.9	3/2⁻	3/2⁻		2.4	0.59	45	3.7	2.5	
	7.3	3/2⁻	5/2⁻		0.4	0.12	50	1.0	8.1	
	9.1[a]	3/2⁻	7/2⁻		1.9	0.0097	20	0.10	4×10^{-4}	0.1[a]
	12.9	3/2⁻	1/2⁻		1.4	1.0	30	20	45	
			3/2⁻				16		
			5/2⁻				24		
C^{12}	15.1	0⁺	1⁻		1.82	1.95	10	39	73	40[a], 54.5[b], 59.2[c]
N^{14}	9.2	1⁺	0⁻		1.3	0.65	50	43	17	
			1⁻				14			
			2⁻				9			
	10.5	1⁺	2⁻		1.9	1.2	30	100	24	
			1⁻				34			
			2⁻				20			
O^{16}	No resonances detected below 16 MeV.									
S^{32}	11.6	0⁺	1⁻		1.5	2.8	40	33	33	47[a], 68[b]

[a] W. C. Barber, F. Bertrand, G. Fricke, and F. E. Gudden, Phys. Rev. 128, 2081 (1962).
[b] G. Fricke (private communication).
[c] F. R. Metzger, C. P. Swann, and V. K. Rasmussen, Phys. Rev. 118, 909 (1960).
[d] This transition is assumed to be M1.
[e] L. Meyer-Schützmeister and S. S. Hanna, Bull. Am. Phys. Soc. 5, 166 (1956).
[f] E. Hayward and E. Feller, Phys. Rev. 104, 861 (1957).
[g] R. L. Garwin, Phys. Rev. 114, 133 (1959).
[h] A. B. De Neuve, thesis, University of Paris, Orsay Center, 1962 (unpublished).

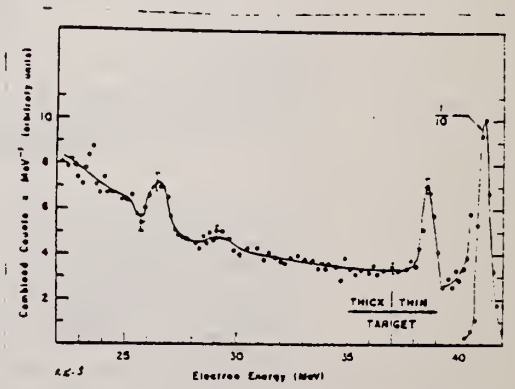

FIG. 1. Energy distribution of electrons, which were initially 41.5 MeV, after scattering through 180° from a Be^9 target

Ref. W. John, J.M. Prosser
Phys. Rev. 127, 231 (1962)

Elem. Sym.	A	Z
Be	9	4

Method: Reaction (γ's from Sb^{124}, Bi^{206}, Al^{28}) - $MnSO_4$ bath

Ref. No.: 62 Jo 2 BG

Reaction	E or ΔE	E_o	Γ	$\int \sigma dE$	Jπ	Notes
(γ,n)	1.692 1.720 1.78					Measured cross sections given in Table II.

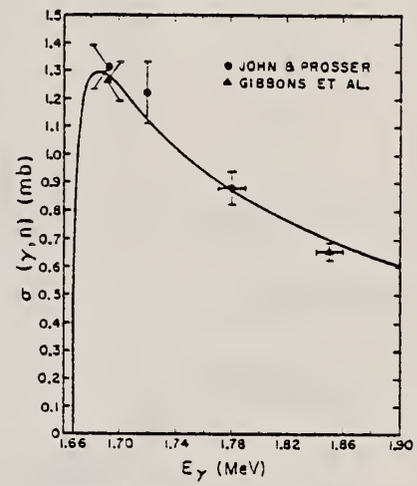

FIG. 3. Total cross section for the reaction $Be^9(\gamma,n)$ near threshold. The curve is the theoretical *S*-wave photoneutron cross section derived by Francis *et al.* for a final-state diffuseness parameter of 0.6 F. The theoretical values have been multiplied by a reduction factor of 0.56. As discussed in the text, Blair has calculated a reduction factor of 0.60 by introducing coupling to the Be^8 core.

TABLE II. Measured cross sections for $Be^9(\gamma,n)$.

Gamma-ray source	E_γ (MeV)	$\sigma(\gamma,n)/\sigma_{1.692}(\gamma,n)$	$\sigma(\gamma,n)$ (mb)
Sb^{124}	1.692	...	1.31±0.08
Bi^{206}	1.720	0.93±0.05	1.22±0.11
Al^{28}	1.78	0.67±0.03	0.88±0.06

Ref. F.F.Liu, F.J.Loeffler, T.R.Palfrey, Y.S.Kim

Phys.Rev. 128, 2784 (1962)

Elem. Sym.	A	Z
Be	9	4

Method
Synch-defining counter telescope, proton counter telescope - C analyser

Ref. No. 62Lil

BG

Reaction	E or ΔE	E_o	Γ	$\int \sigma dE$	Jπ	Notes
(γ,p)	$E_{\gamma max}$= 355					Polarization of high energy photo-protons given in %. Mean proton production energy = 175 MeV θ_p =45° -12.9±15 θ_p =56° -5.7±15 Postulates identical γ absorption process for each kind of nucleus (quasi-deuteron). Fig.2: combined results of Li^7, Be^9, B^{11}, C^{12} at 3 angles of measurement. θ_{plab}= 90° only for Carbon data. Fig. 2. A: Only E1 transitions considered. C-M1 transitions from $^3S_1$ - $^1S_0$ also taken into account. Results are consistent both with a zero value for the polorization and also with theory.

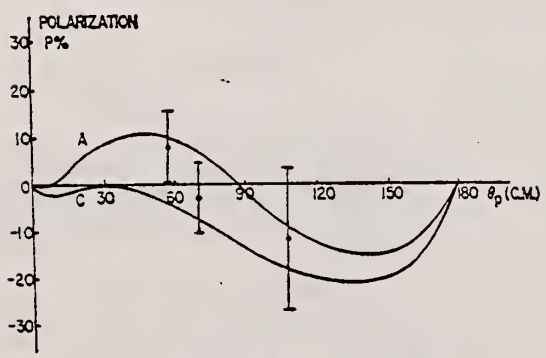

FIG. 2. Comparison of the experimental results with the predicted polarization.

he results for all four elements (by taking a weighted

Ref. U. Miklavžič, N. Bezič, D. Jamnik, G. Kernel, Z. Milavc, J. Snajder
Nuclear Phys. 31, 570 (1962)

Elem. Sym.	A	Z
Be	9	4

Method: 31 MeV betatron; totalabsorption; magnetic compton spectrometer

Ref. No.: 62 Mi 4 - JHH

Reaction	E or ΔE	E_o	Γ	$\int \sigma dE$	Jπ	Notes
Be (μ_t)	15-27					938

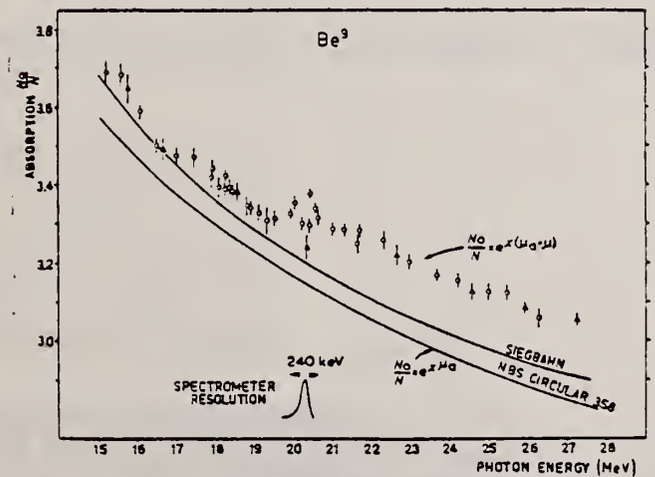

Fig. 2. The measured total absorption $N_0/N = \exp x(\mu_0+\mu)$ and atomic absorption $N_0/N = \exp(x\mu_0)$ are plotted versus photon energy, where $x = 95.93$ g/cm², while μ_0 and μ are atomic and photonuclear absorption coefficients, respectively. Two different values for μ_0 are taken from Siegbahn [3]) and NBS circular [4]).

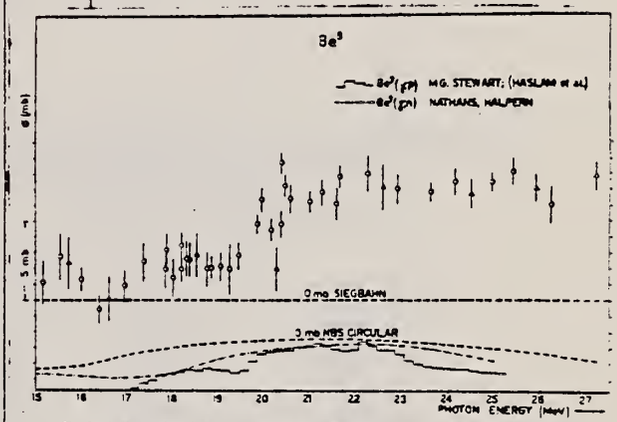

Fig. 3. Absolute value of the photonuclear cross section is plotted as a function of energy and compared with measured partial cross sections for reactions (γ, p) from refs. [7, 8]) and (γ, n) from ref. [9]). Two dashed lines indicate different zero values for the two differing atomic absorption coefficients [3, 4]).

References

1) J. Dubar *et al.*, Nuclear Physics 14 (1959) 131
2) M. V. Mihailović *et al.*, Phys. Rev. 114 (1959) 1621
3) U. Miklavčič and Č. Zupančič, Rep. J. Stefan Inst. 5 (1958) 3
4) J. S. Pruitt and S. R. Domen, supersedes NBS Report no. 6218 (1958)
5) K. Siegbahn, Beta and gamma-ray spectroscopy (Interscience Publ. Inc., New York, 1955)
6) G. W. Grodzens, NBS circular 584 (1957)
7) M. G. Stewart, Ames Lab. Research and Development Report IS-191 (August 1959)
8) R. N. H. Haslam, L. Katz and E. H. Crosby, Can. J. Phys. 31 (1953) 210
9) R. Nathans and J. Halpern, Phys. Rev. 92 (1953) 940

Ref. Yu.M. Volkov, A.V. Kulikov, V. P. Chizov
Zhur. Eksp. i Teoret. Fiz. 42, 61 (1962);
Soviet Phys. JETP 15, 42 (1962)

Elem. Sym.	A	Z
Be	9	4

Method
Synchrotron; scintillator counter telescope

Ref. No.
62 Vo 2

Reaction	E or ΔE	E_o	Γ	$\int \sigma dE$	Jπ	Notes
(γ,d) (γ,p)	Bremss. 90					E_d, E_p > 15 MeV

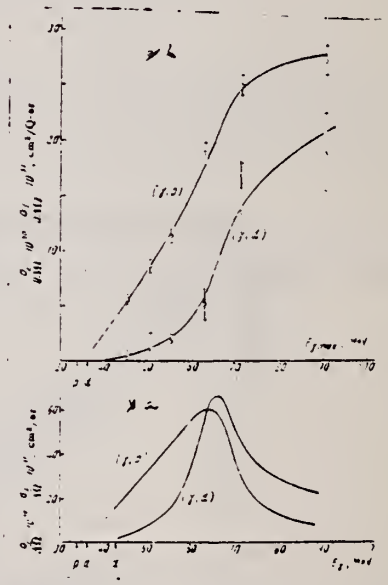

Figure 3: (b) excitation functions of reactions, $Be^9(\gamma,d)$ and $Be^9(\gamma,p)$, for particles of energies > 15 MeV; (a) cross section of the same reactions normalized per effective photon.

R. Bosch, J. Lang, R. Muller, W. Wolfli
Helva. Phys. Acta 36, 657 (1963)

Be	9	4

METHOD: Radioactive source; neutron cross sectinn; angular distribution; scintillator

REF. NO.: 63 Bo 4 NVB

REACTION	RESULT	EXCITATION ENERGY	SOURCE TYPE	SOURCE RANGE	DETECTOR TYPE	DETECTOR RANGE	ANGLE
$G,N	ABX	3-9	D	5-9	SCI-D		DST
		(2.75-9.0)		(5.4-9.0)			

In Table I, $W(\theta) = a + b \sin^2\theta$

N POL

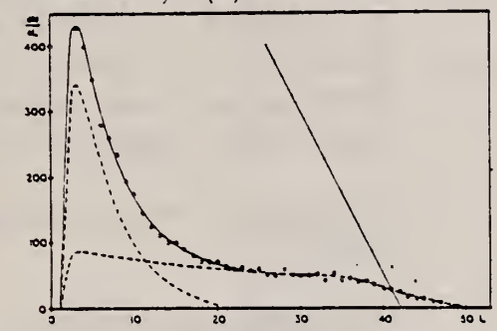

Figur 7

Zerlegung des Impulsspektrums der Photoneutronen von Be^9 (Untergrund abgezogen.) Gammaspektrum wie in Figur 6. Energie der energetisch höher liegenden Neutronengruppe $E_n = 4.2$ MeV.

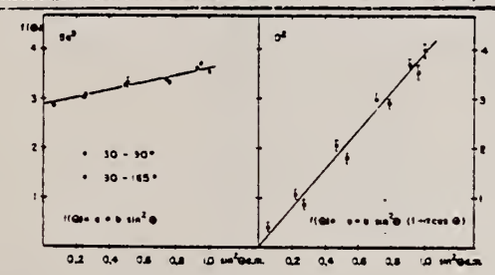

Figur 8

Winkelverteilung der Photoneutronen von Be^9 und H^3 bei einer Gammaenergie von 9.0 MeV.

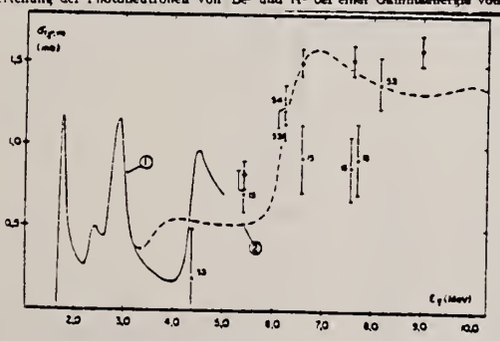

Figur 11

Vergleich der experimentell bestimmten Wirkungsquerschnitte bei Be^9: ○ nach Jakobson[12], □ nach Bertozzi *et al.*[12], ● Vorliegende Arbeit; ◇ Übrige Messungen mit monoenergetischen Gammaquellen über 2,75 MeV. Die Ziffern verweisen auf die entsprechenden Literaturangaben.

Eine Zusammenstellung der Resultate für Energien kleiner als 2.75 MeV findet man in [15].

Tabelle I

Resultate $Be^9(\gamma, n)$

$\bar{E}_\gamma$ (MeV)	a/b	$\frac{\sigma\, Be^9(\gamma,n)\, Be^8}{\sigma_{tot}(\gamma,n)}$
5.5	3.68 ± 0.39	0.50
6.5	5.05 ± 0.14	0.30
7.2	4.40 ± 0.13	0.32
8.5	4.00 ± 0.12	0.35

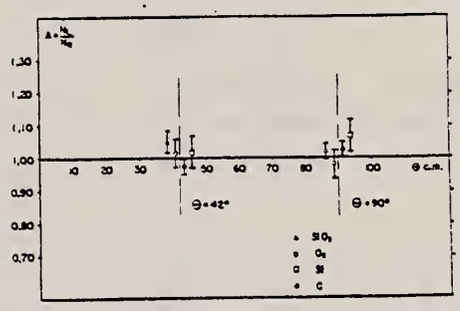

Figur 14

Gemessene Asymmetrie der Photoneutronen bei Be^9 mit den verschiedenen Analysatoren.

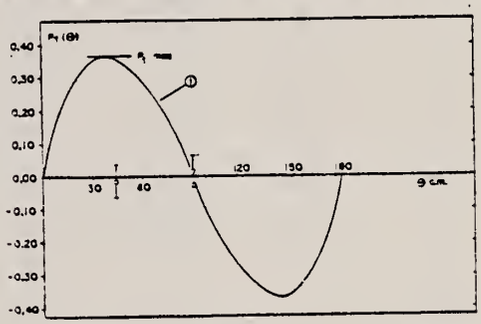

Figur 15

Vergleich der experimentellen und theoretischen Polarisationswerte der Photoneutronen bei Be^9. Der theoretische Verlauf wurde mit der Theorie von Czyż und Sawicki[14] unter Verwendung der Daten aus dem Modell von Guth und Mullin[11] berechnet.

Tabelle II

Vergleich der Winkelverteilungsmessungen bei Be^9

E_γ (MeV)	Winkelverteilung	
1.70*	isotrop	Jakobson[12]
2.75	$1 + 0.82 \sin^2\theta$	Hammermesh *et al.*[13]
2.95*	$1 + 1.00 \sin^2\theta$	Jakobson
	isotrop	Bertozzi *et al.*[12]
4.0	$1 + 0.30 \sin^2\theta$	Bertozzi
4.6*	isotrop	Jakobson
5.0	isotrop	Bertozzi
5.6	$1 + 0.27 \sin^2\theta$	vorliegende Arbeit
6.0	$1 + 0.50 \sin^2\theta$	Bertozzi
6.6	$1 + 0.20 \sin^2\theta$	vorliegende Arbeit
7.2	$1 + 0.25 \sin^2\theta$	vorliegende Arbeit
8.5	$1 + 0.22 \sin^2\theta$	vorliegende Arbeit

* Resonanzenergie

[11] E. Guth und C. J. Mullin, Phys. Rev. *76*, 234 (1949).
[12] M. J. Jakobson, Phys. Rev. *123*, 229 (1961).
[13] W. Bertozzi, P. T. Demos, C. P. Sargent, W. Tuchineta, D. M. Connell und S. Kowalski, Karlsruhe Photonuclear Conference 1960, R 15/1 (unveröffentlicht).
[14] L. Jarczyk, H. Knöpfel, J. Lang, R. Müller und W. Wölfli, Nucl. Instr. Meth. *13*, 287 (1961).
[15] V. O. Erikson und C. P. Zalseki, J. Phys. Rad. *15*, 492 (1954).
[33] B. Hammermesh, M. Hammermesh und A. Wattenberg, Phys. Rev. *76*, 611 (1949).
[34] H. R. Striebel, S. E. Darden und W. Haeberli, Nucl. Phys. *6*, 188 (1958).

Z. und J. Sawicki, Nuovo cim. *5*, 864 (1956).

Ref. Y.S.Kim, F.F.Liu, F.J.Loeffler, T.R.Palfrey,Jr.

Phys.Rev. 129, 1362 (1963)

Elem. Sym.	A	Z
Be	9	4

Method
335 MeV Synch-scintillation counter telescope

Ref. No. 63Ki1 BG

Reaction	E or ΔE	E_o	Γ	$\int \sigma dE$	Jπ	Notes
(γ,p)	$E_{\gamma max}$= 335					Data corrected for: nuclear absorption , γ attenuation, multiple scattering in counter,target pion contamination. Photoproton cross section was found proportional to NZ/A (NZ is probability of having np pair) over angular and energy region examined. (Z=3,4,5,6). Differential cross section data given. T_p = proton energy (Fig.4)

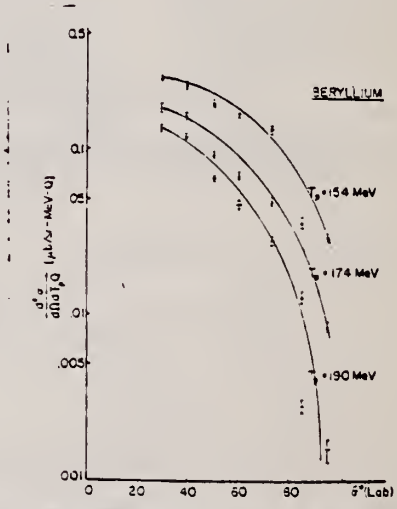

FIG. 4. Differential cross sections for photoproton production from boron.

Ref. H. Nguyen Ngoc, M. Hors, J. Perez y Jorba

Nuclear Phys. 42, 62 (1963)

Elem. Sym.	A	Z
Be	9	4

Method

Linac - double focusing spectrometer

Ref. No. 63Ng1 BG

Reaction	E or ΔE	E_o	Γ	∫σdE	Jπ	Notes
			eV			
(e,e')	60-250	1.6±0.2	4.5±0.6			El most probable transition - $\frac{1}{2}^+$ from other experiments
		2.47±0.02	(2.6±0.1) x10^{-3}		-	E2 transition. Established spin value 5/2.
		6.4 ±0.1	0.109±0.005		$7/2^-$	E2 transition. Assignment of spin 7/2 excludes M1 transition to ground state.
		no other levels seen up to 17				2.4 and 6.4 MeV levels are members of a rotational band with K= $\frac{3}{2}^-$ based on the ground state.

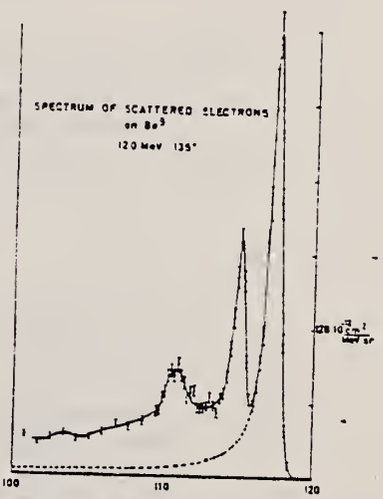

Fig. 1. Measured spectrum of electrons scattered from Be^9 at a backward angle of 135° with 120 MeV incident energy. The 3 peaks correspond to elastic scattering and inelastic excitation of the 2.47 MeV and 6.4 MeV excited states.

H. Nguyen Ngoc, J. Perez y Jorba
J. de Physique 24, 965 (1963)

ELEM.		
Be	9	4

METHOD: Linac; electron scattering; magnetic spectrometer; Faraday cup and SEM

REF. NO.: 63 Ng 2 — NVB

REACTION	RESULT	EXCITATION ENERGY	SOURCE		DETECTOR		ANGLE
			TYPE	RANGE	TYPE	RANGE	
E,E/	FMF	4 - 47	D	100-180	MAG - D		135

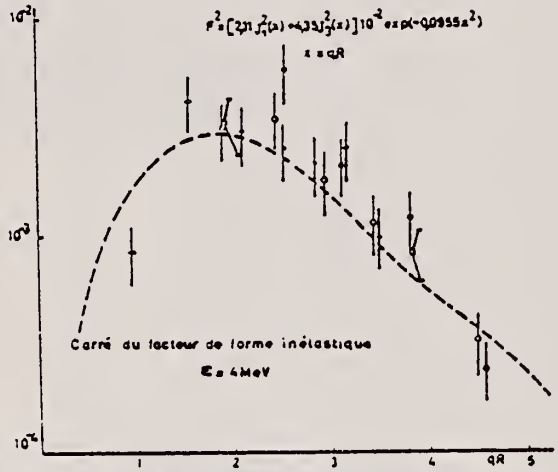

FIG. 2. — Facteur de forme du continuum à $\varepsilon = 4$ MeV (compte non tenu des niveaux discrets).

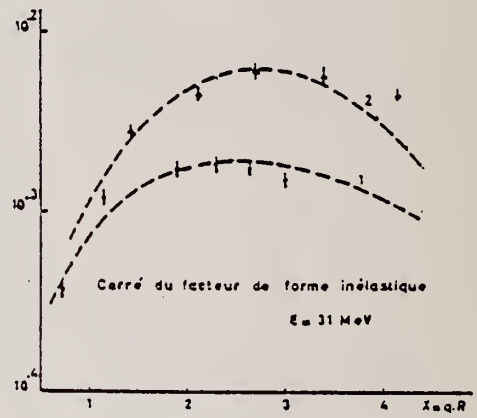

FIG. 3. — Facteur de forme du continuum à $\varepsilon = 31$ MeV.
Courbe 1 : l'angle de diffusion à 60°.
Courbe 2 : l'angle de diffusion à 135°.

TABLEAU I

ÉLECTRODÉSINTÉGRATION DU ^{8}Be

ε MeV	λ_1	λ_2	λ_3
4	(2,11 ± 0,22) 10^{-8}	0 ±	0,043 ± 0,006
8	(1,86 ± 0,22) 10^{-8}	0	0,106 ± 0,014
12	(1,34 ± 0,17) 10^{-8}	0	0,131 ± 0,015
16	(1,04 ± 0,14) 10^{-8}	0	0,109 ± 0,013
19	(0,925 ± 0,09) 10^{-8}	(0,85 ± 0,06) 10^{-8}	0,063 ± 0,008
23	(0,856 ± 0,09) 10^{-8}	(1,48 ± 0,11) 10^{-8}	0,065 ± 0,009
27	(0,87 ± 0,09) 10^{-8}	(1,81 ± 0,13) 10^{-8}	0,077 ± 0,010
31	(0,83 ± 0,09) 10^{-8}	(2,61 ± 0,16) 10^{-8}	0,078 ± 0,010
35	(0,75 ± 0,08) 10^{-8}	(2,26 ± 0,16) 10^{-8}	0,093 ± 0,012
39	(0,69 ± 0,08) 10^{-8}	(2,56 ± 0,19) 10^{-8}	0,081 ± 0,010
43	(0,82 ± 0,10) 10^{-8}	(2,43 ± 0,20) 10^{-8}	0,071 ± 0,010
47	(0,72 ± 0,10) 10^{-8}	(1,73 ± 0,16) 10^{-8}	0,089 ± 0,014

$$\frac{d^2\sigma}{d\Omega\, dE} = \left(A + B\, tg^2\frac{\theta}{2}\right)\cdot\frac{d\sigma}{d\Omega}\,\text{Mott}$$

$$A - \frac{B}{2} = (\lambda_1 j_1^2(x) + \lambda_3 j_3^2(x))\, e^{-q^2\sigma^2}$$

$$B = \lambda_3 j_3^2(x)\, e^{-q^2\sigma^2}$$

$$x = qR \quad R = 2{,}75\, f \quad g = 0{,}85\, f$$

F.R. Allum, T.W. Quirk, and B.M. Spicer
Nucl. Phys. 53, 545 (1964)

Be	9	4

METHOD

REF. NO. 64 A1 5 JOC

REACTION	RESULT	EXCITATION ENERGY	SOURCE		DETECTOR		ANGLE
			TYPE	RANGE	TYPE	RANGE	
G,XN	NØX	THR-34	C	34	THR-I	6-	DST

TABLE I

Summary of present experimental data at 34 MeV bremsstrahlung

Element		$-\frac{a_2}{a_0}$	$\frac{a_1}{a_0}$
$_{4}$Be		0.43±0.02	0.05±0.01
$_{6}$C		0.61±0.04	0.09±0.02
$_{13}$Al		0.39±0.03	0.05±0.01
$_{22}$Ti		0.34±0.02	0.06±0.01
$_{24}$Cr	34 MeV	0.33±0.02	0.02±0.01
	22 MeV	0.13±0.07	−0.02±0.01
$_{29}$Cu		0.36±0.02	0.10±0.01
$_{50}$Sn		0.38±0.02	0.11±0.01
$_{56}$Ba		0.39±0.03	0.11±0.02
$_{73}$Ta	Before installation of iron shielding	0.26±0.04	0.13±0.02
	After installation of iron shielding	0.27±0.02	0.12±0.01
$_{82}$Pb	target diameter 3.0 cm	0.39±0.03	0.15±0.02
	target diameter 1.5 cm	0.40±0.03	0.19±0.02
$_{83}$Bi		0.42±0.03	0.17±0.02

$$Y = a_0 + a_1 \cos\theta + a_2 \cos^2\theta$$

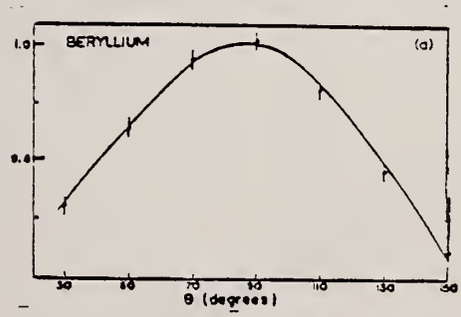

H. Artus, G. Fricke, D.E. von Stein
Z. Physik 178, 109-12 (1964)

Be	9	4

METHOD
Linac

REF. NO.
64 Ar 2

NVB

REACTION	RESULT	EXCITATION ENERGY	SOURCE		DETECTOR		ANGLE
			TYPE	RANGE	TYPE	RANGE	
G,2N	RLY	21-57	C	44,57	ACT-I		4PI

REL TØ C12 (G,N)

Tabelle. *Ausbeuten an Be^7*

Isotop	Be^7-Ausbeute relativ zu $C^{12}(\gamma, n)C^{11}$ in Prozent			Niedrigste Schwellenenergie
	Foster und Voigt	Diese Arbeit		
	$E_0 = 45$ MeV	$E_0 = 44$ MeV	$E_0 = 56{,}5$ MeV	
Be^9	8 ± 2	$7{,}6^{+0{,}5}_{-1{,}0}$	$8{,}2^{+0{,}5}_{-1{,}3}$	20,6 MeV
B^{10}	–	$7{,}1^{+0{,}5}_{-0{,}9}$	$8{,}3^{+0{,}6}_{-1{,}4}$	18,7 MeV
B^{11}	–	$0{,}54^{+0{,}13}_{-0{,}17}$	$0{,}84^{+0{,}17}_{-0{,}25}$	30,1 MeV
C^{12}	12 ± 4	$4{,}5^{+0{,}3}_{-0{,}4}$	$5{,}8 \pm 0{,}3$	26,3 MeV
Natürlich . . .	$2 \pm 0{,}6$	$1{,}8^{+0{,}2}_{-0{,}3}$	$2{,}3^{+0{,}2}_{-0{,}4}$	–
Angereichert . .	–	$6{,}9^{+0{,}5}_{-0{,}9}$	$8{,}0^{+0{,}5}_{-1{,}3}$	–

REF.
C. Becchi, L. Meneghetti, M. Sanzone and S. Vitale
Nucl. Phys. 59, 375-84 (1964)

ELEM. SYM.	A	Z
Be	9	4

METHOD
Betatron

Page 1 of 2

REF. NO.
64 Be 1 JOC

REACTION	RESULT	EXCITATION ENERGY	SOURCE		DETECTOR		ANGLE
			TYPE	RANGE	TYPE	RANGE	
G,2A	SPC	THR - 34	C	18-34	SCD-D	3-	90
				(18-33.5)			
G A	SPC	THR - 34	C	34	SCD-D	3-	DST

J-PI

At least 80% of $Be^9(\gamma,n)2\alpha$ yield in range 18-25 MeV goes through Be^8 16.6 MeV level.

Fig. 3. Sum energy spectrum of α pairs produced in the reaction $Be^9 + \gamma = n + 2\alpha$ at $E_{\gamma max} = 33.5$ MeV. Corrections are made for α–p and α–d coincidences.

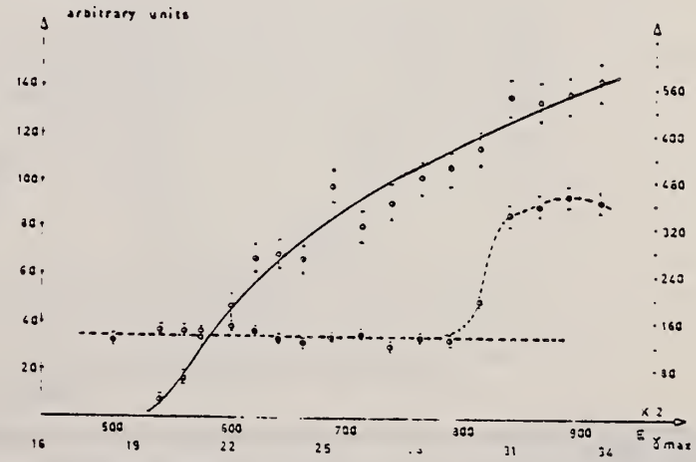

Fig. 4. Excitation curves. Full line, the production of Be^8 in the ... MeV state; dashed line, the production of pairs of charged particles with sum energy lower than 15 MeV.

(continued)

REACTION	RESULT	EXCITATION ENERGY	SOURCE TYPE	SOURCE RANGE	DETECTOR TYPE	DETECTOR RANGE	ANGLE

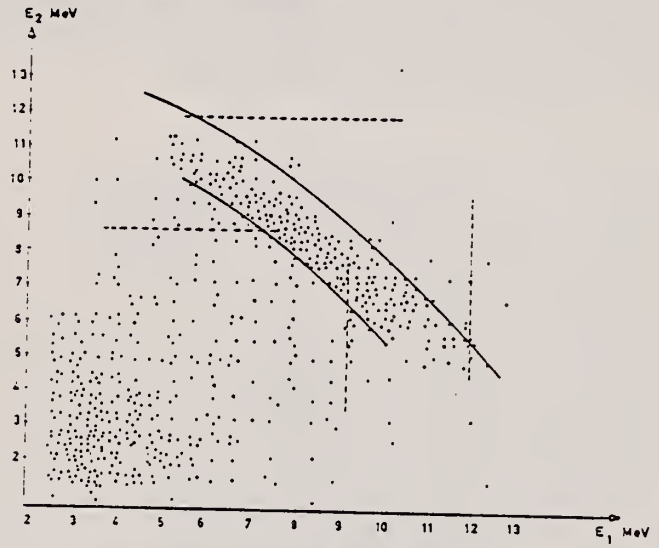

Fig. 5. Energy distribution between correlated α-particles. These results were obtained by the photographic method of sect. 2. The events due to the reaction $Be^9(\gamma, \alpha)He^5$ should correspond to points placed between the dashed lines. The points corresponding to events due to the reaction $Be^9(\gamma, n)Be^{4*}$ are expected to be distributed between the solid lines. $E_{\gamma max} = 33.5$ MeV.

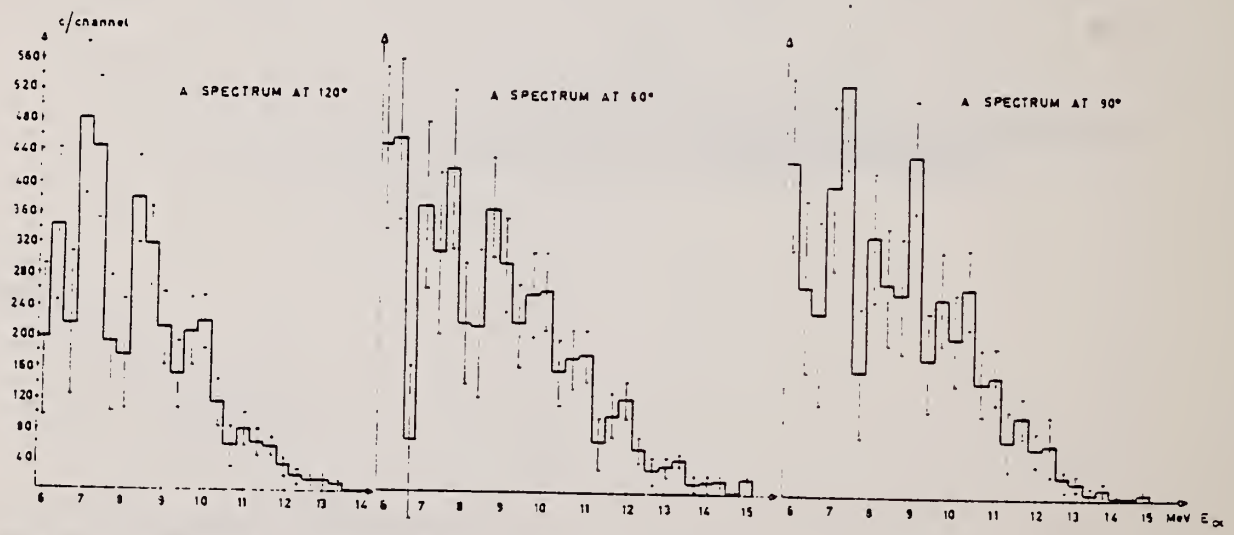

Fig. 8. Spectra of photoproduced α-particles from Be^9 at 60°±20°(A), 90°±20°(B) and 120°±20°(C). These spectra were corrected for target self-absorption. $E_{\gamma max} = 33.5$ MeV.

E. G. Corman, R. W. Jewell, W. John, J. E. Sherwood and D. White
Phys. Letters 10, 116 (1964)

Be	9	4

METHOD: Na^{24} gamma rays

REF. NO.: 64 Co 1 JOC

REACTION	RESULT	EXCITATION ENERGY	SOURCE TYPE	SOURCE RANGE	DETECTOR TYPE	DETECTOR RANGE	ANGLE
$ G,N	NØX	3	D	3			DST
		(2.753)		(2.753)			

POL OF NEUTS

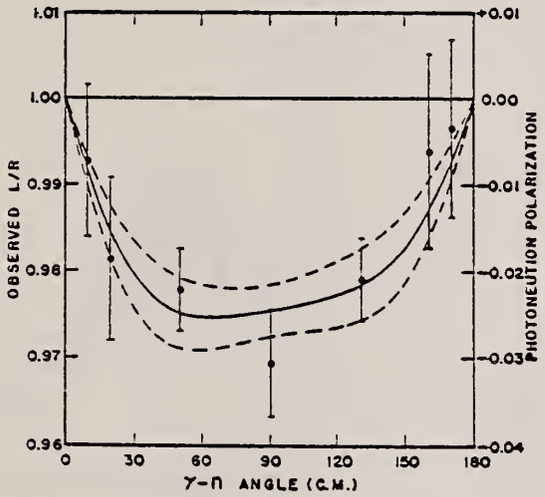

Fig. 1. Plot of the polarization of photoneutrons from $Be^9(\gamma,n)$. The abscissa is the γ-n angle, the left ordinate the observed left-right ratio of the neutrons scattered from a helium analyzer. The right ordinate is the polarization of the neutrons calculated from the data (Basel sign convention). The errors on the measured points are statistical only. The solid curve is a least-squares fit of eq. (1) to the data, the dotted curves being one standard deviation from the best fit.

A. P. Komar and Eu. D. Makhnovsky
Nuclear Phys. 65, 662 (1964)

Be	9	4

METHOD

Nuclear Emulsion

REF. NO. 64 Ko 5

EGF

REACTION	RESULT	EXCITATION ENERGY	SOURCE		DETECTOR		ANGLE
			TYPE	RANGE	TYPE	RANGE	
G,P 9.37	ABX	15 - 32	C	35	D MAG	1-15	DST
G,N	RLY	15 - 32	C	35	D MAG	4-20	DST
G,D	RLY	21 - 35	C	35	D	4-14	DST

$Y_d/Y_p = 0.2 \pm 0.1$

$$\int_{18}^{26} \sigma_{\gamma,p}\, dE_\gamma = 11.9 \pm 1.8 \text{ mb - MeV}$$

$$\int_{18}^{31} \sigma_{\gamma,p}\, dE_\gamma = 15.6 \pm 2.5 \text{ mb - MeV}$$

$$\int_{18}^{31} \frac{\sigma_{\gamma,p}(E_\gamma)}{E_\gamma}\, dE_\gamma = 0.67 \pm 0.09 \text{ mb}$$

$$\int_{21.4}^{35} \frac{\sigma_{\gamma d}}{E_\gamma}\, dE_\gamma = 0.10 \pm 0.07 \text{ mb}$$

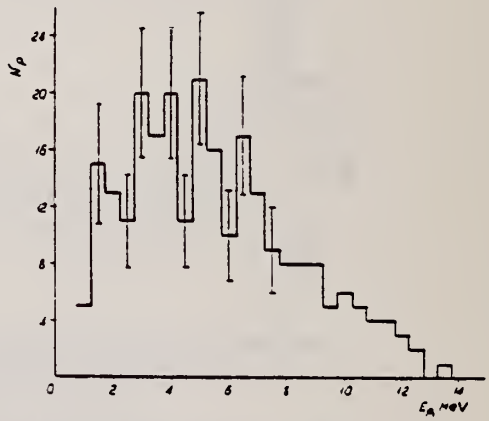

Fig. 2. Energy distribution of Be^9 photoprotons.

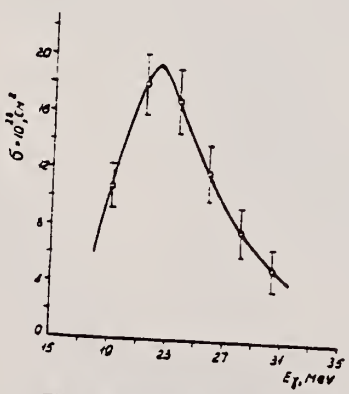

Fig. 3. Excitation function of the $Be^9(\gamma, p)Li^8$ reaction.

(continued)

REACTION	RESULT	EXCITATION ENERGY	SOURCE		DETECTOR		ANGLE
			TYPE	RANGE	TYPE	RANGE	

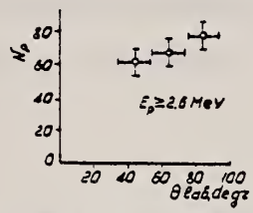

Fig. 4. Angular distribution of Be^9 photoprotons.

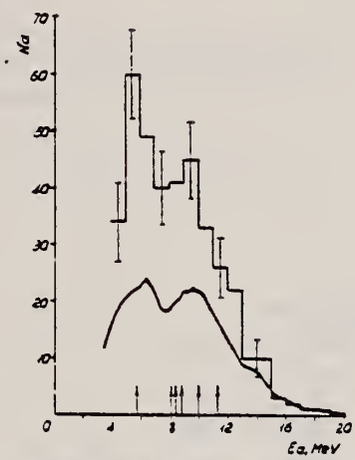

Fig. 5. Energy spectrum of α-particles originating in the photodisintegration of Be^9. The histogram represents the overall spectrum for the two photoplates. The smooth curve shows the spectrum for the photoplate with $\varphi_0 = 35°$. Arrows indicate the energies of α-particles due to the decay of the Be^8 nucleus in the known excited states.

REF.

J. M. Loiseaux, M. Langevin and J. M. Maison
Proc. Paris Conf. 1048 (1964)

ELEM. SYM.	A	Z
Be	9	4

METHOD

Betatron

REF. NO.

64 Lo 3

JDM

REACTION	RESULT	EXCITATION ENERGY	SOURCE		DETECTOR		ANGLE
			TYPE	RANGE	TYPE	RANGE	
G,G	ABX	10-30	C	10-30	NAI-D		140

The effective differential scattering cross section remains quite constant from 20-30 MeV.

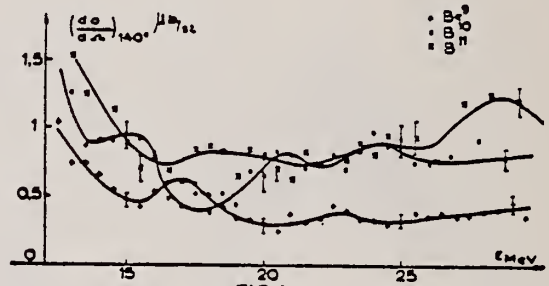

FIG.1.

G. Tessler, W.E. Stephens
Phys. Rev. 135, B129-36 (1964)

Be	9	4

METHOD: Tandem, $T^3(p,\gamma)$

REF. NO.: 64 Te 1 NVB

REACTION	RESULT	EXCITATION ENERGY	SOURCE TYPE	SOURCE RANGE	DETECTOR TYPE	DETECTOR RANGE	ANGLE
G,MU-T	ABX	20-21	D	20-21	NAI-I		96

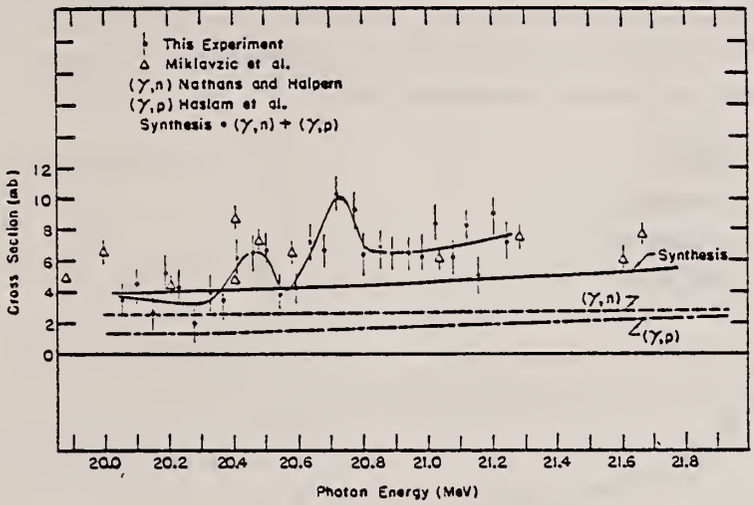

FIG. 8. Nuclear absorption cross section in Be^9 as a function of photon energy. The results of this experiment are plotted as dots. Other results are shown for comparison.

TABLE IV. Structure observed in the nuclear absorption cross section curves.

Element	E_{peak} (MeV)	σ_{peak} (mb)	Half-width (MeV)	$\int_{peak} \sigma dE$ (MeV-mb)
Be^9	20.47	6.8	0.13	0.45
	20.73	10.1	0.15	0.9
O^{16}	20.62	21.5	0.19	3.9
	21.02 {20.86 / 21.05}	23.5	~0.40	10.4
	>22			
F^{19}	20.09	21.9	0.16	3.5

REF. U. Amaldi, Jr., G. Campos Venuti, G. Cortellessa, G. Fronterotta, A. Reale, P. Salvadori
Rend. Acc. Naz. Lincei 38, 499 (1965)

ELEM. SYM.	A	Z
Be	9	4

METHOD

REF. NO. 65 Am 3 egf

REACTION	RESULT	EXCITATION ENERGY	SOURCE		DETECTOR		ANGLE
			TYPE	RANGE	TYPE	RANGE	
E,E/P	RLY	8-80	D	510-590	MAG-D	407	51

100 MEV P COINC

Table gives parameters of Maxwellian distribution used to fit data.

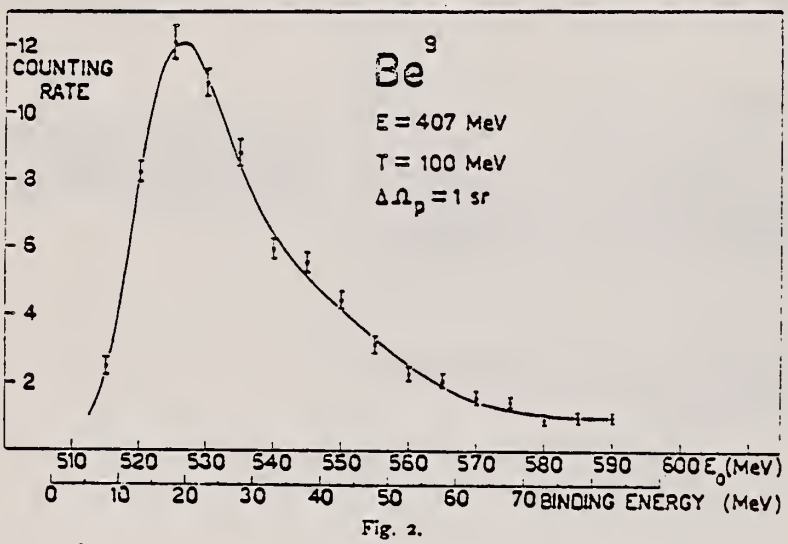

Fig. 2.

TABLE I.

h (counting rate)	σ(MeV)	x_0(MeV)
9.0 ± 0.9	13.2 ± 1.0	524.9 ± 0.7
4.3 ± 1.6	26.2 ± 2.7	539.4 ± 1.9

REF. S. Costa, B. Minetti, C. Molino, L. Pasqualini and G. Piragino
Atti Cl. di Sci.Fis. 99, 1157 (1965)

ELEM. SYM.	A	Z
Be	9	4

METHOD
31 MeV Betatron and 100 MeV Synchrotron

REF. NO.
65 Co 2 JDM

REACTION	RESULT	EXCITATION ENERGY	SOURCE TYPE	SOURCE RANGE	DETECTOR TYPE	DETECTOR RANGE	ANGLE
G,XN	ABX	6 - 80	C	6 - 80	BF3-I		4PI

55%

$\int_0^{50} (\gamma,Tn)\,dE\gamma = 133 \pm 9$ MeV-mb

$\int_0^{50} \sigma(\gamma,p)\,dE\gamma \cong 39$ MeV.mb

If $\int_0^{50} \sigma abs\,dE\gamma \cong 172$ MeV-mb

$\int_0^{\infty} \sigma abs\,dE\gamma = 187$ MeV-mb

$\int_0^{80} \sigma abs\,dE\gamma \cong 186$ MeV mb

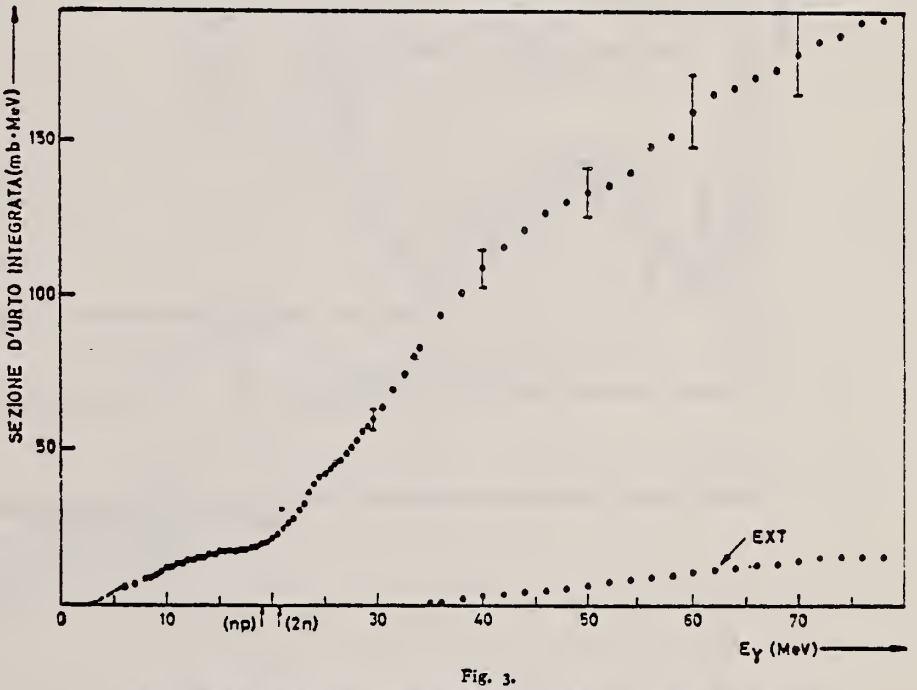

Fig. 3.
Sezione d'urto integrata della reazione $Be^9(\gamma, Tn)$. È anche rappresentato il contributo dei contatori EXT. La parte tratteggiata è stata ricavata dai dati di Jakobson [6].

(continued)

ELEM. SYM.	A	Z
Be	9	4

METHOD

REF. NO. 65 Co 2 JDM

REACTION	RESULT	EXCITATION ENERGY	SOURCE		DETECTOR		ANGLE
			TYPE	RANGE	TYPE	RANGE	

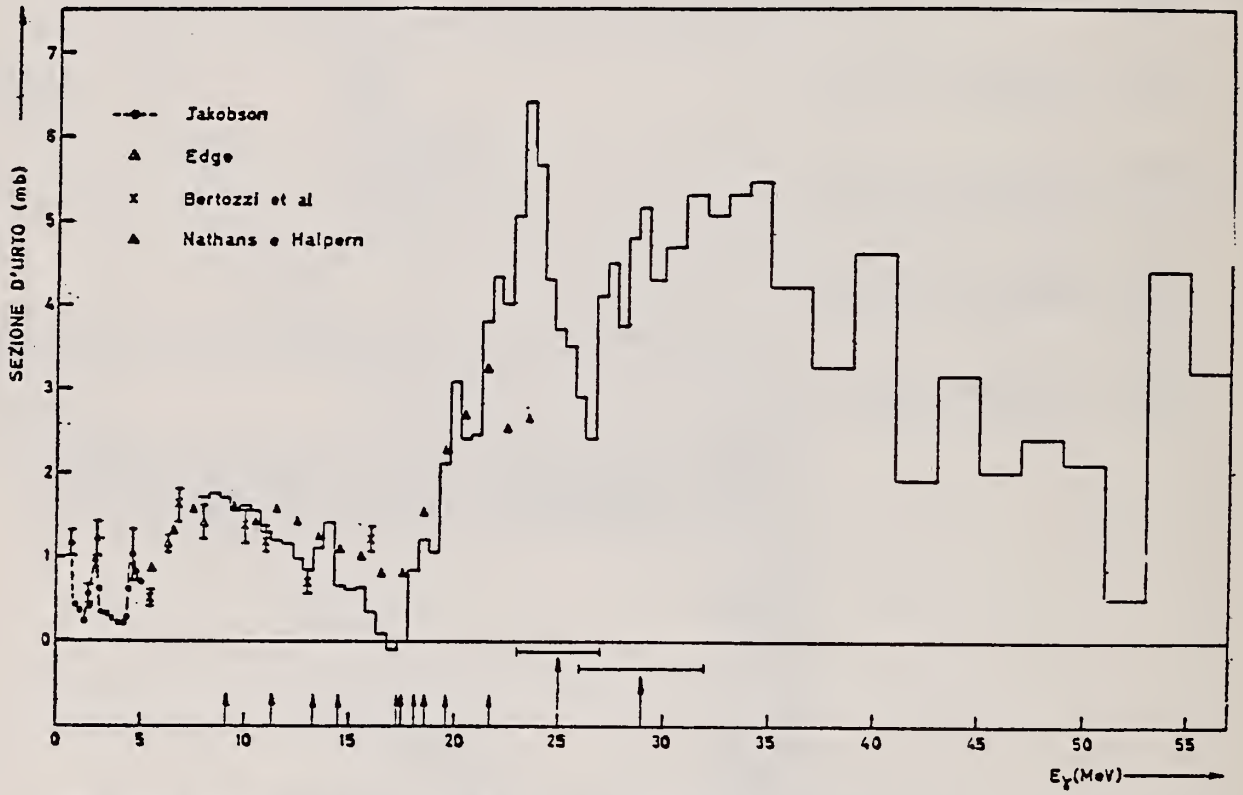

Fig. 2.

Sezione d'urto di fotoproduzione di neutroni da Be^9. L'istogramma rappresenta i valori ottenuti nel presente lavoro. Sono pure indicati i risultati ottenuti da altri autori.

REF. A. P. Komar and E. D. Makhnovskii
Dokl. Akad. Nauk SSSR 160, 1300 (1965)
Sov. Phys. Dokl. 10, 150 (1965)

ELEM. SYM.	A	Z
Be	9	4

METHOD

REF. NO. 65 Ko 2 HMG

REACTION	RESULT	EXCITATION ENERGY	SOURCE		DETECTOR		ANGLE
			TYPE	RANGE	TYPE	RANGE	
G,P	ABX	18-31	C	35	EMU-D	1-20	DST
							(35,65)

Note: Magnetic spectrometer used.

(1) $\int_{18}^{26} \sigma_{\gamma p}(E_\gamma)\,dE_\gamma = (12 \pm 1.8)$ MeV-mb.

(2) $\int_{18.9}^{35} \sigma_{\gamma p}(E_\gamma)$

(3) $\frac{\gamma D}{\gamma P} = 0.20 \pm 0.10$

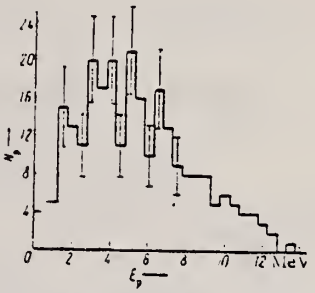

Fig. 2. Energy distribution of photoprotons from Be^9.

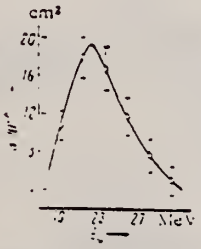

Fig. 3. Excitation function for the $Be^9(\gamma, p)Li^8$ reaction.

Caption: Assumes all identified protons resulted from $Be^9(\gamma,p)Li^8$, that the angular distribution was isotropic, and that the recoil nucleus was produced in the ground state in every case.

REF. H. Nguyen Ngoc
Ann. Phys. 10, 315 (1965)

EL EM. SYM.	A	Z
Be	9	4

METHOD

REF. NO. 65 Ng 1 egf

REACTION	RESULT	EXCITATION ENERGY	SOURCE TYPE	SOURCE RANGE	DETECTOR TYPE	DETECTOR RANGE	ANGLE
E,E/	FMF	2-47	D	50-250	MAG-D	20-250	DST

Tabular Data

2.47.6.4 MEV,CONT

$$F_{iA} = \sqrt{\beta(I_i, I_f, \lambda)} j_\lambda(qR) \exp(-q^2 g^2/2). \quad (IV\text{-}7$$

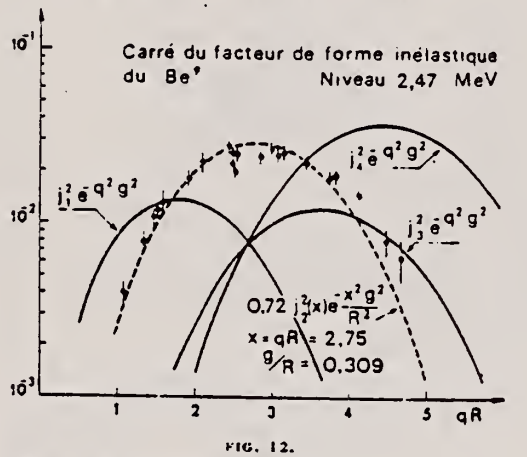

FIG. 12.

c) Facteurs de forme inélastiques comparés avec la prédiction du modèle de Helm. Niveau 2,47 MeV.

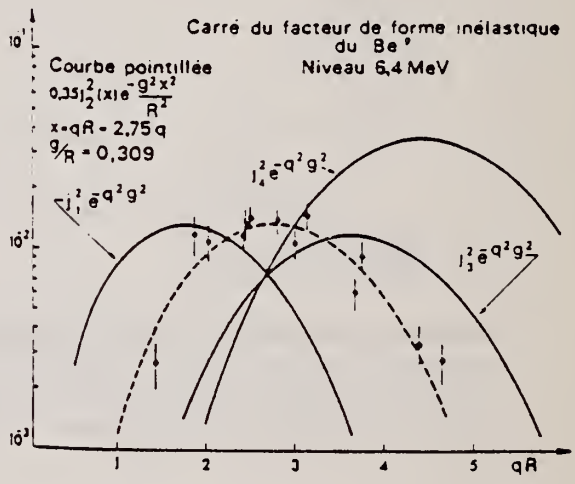

FIG. 12.

d) Facteurs de forme inélastiques comparés avec la prédiction du modèle de Helm. Niveau 6,4 MeV.

(continued

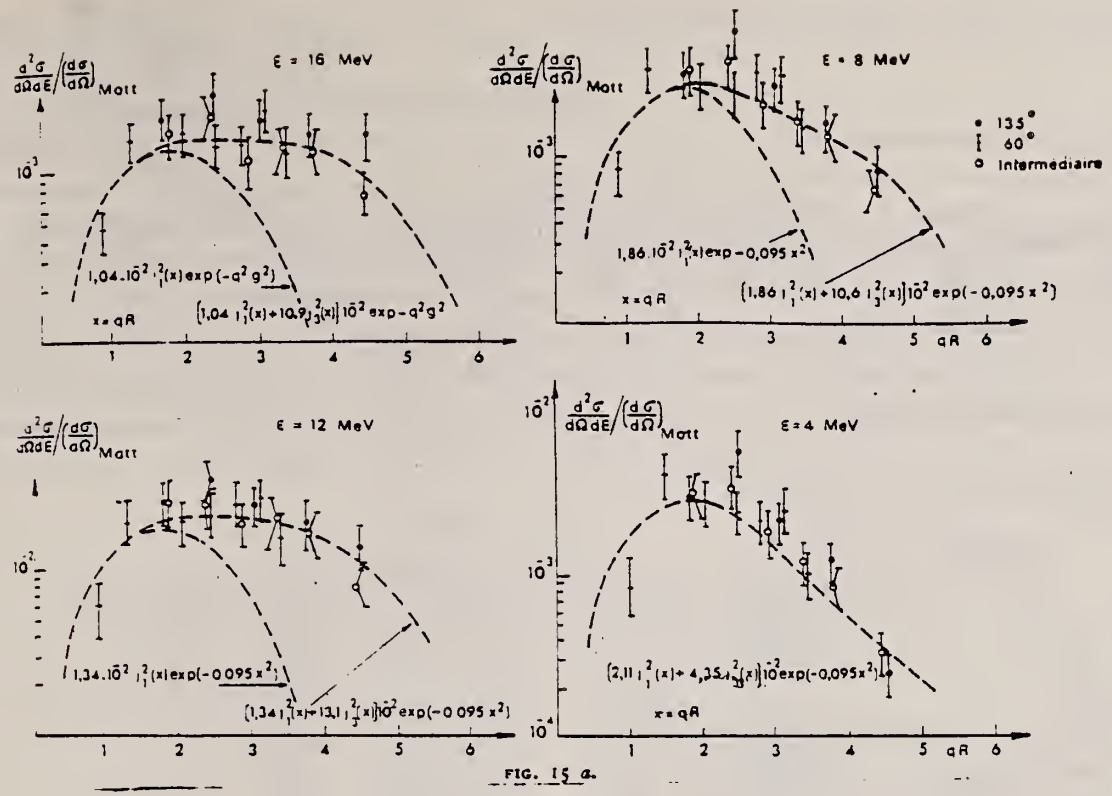

FIG. 15 a.

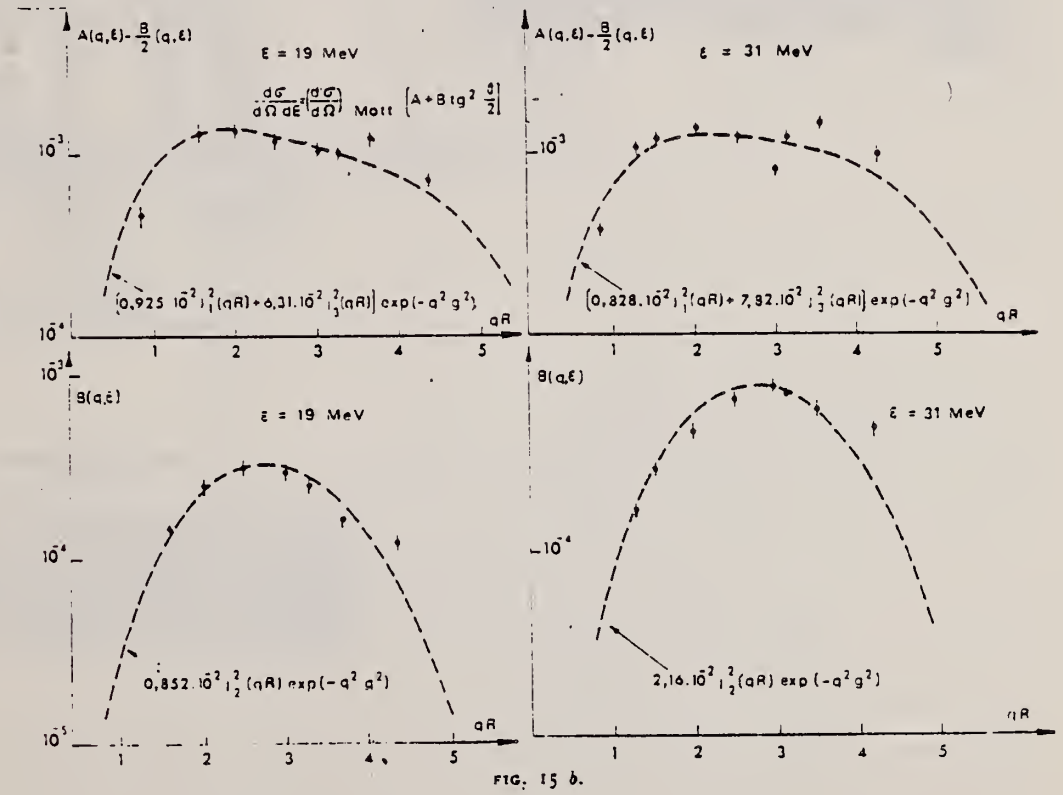

FIG. 15 b.

REF.

J.M. Wyckoff, B. Ziegler, H.W. Koch, and R. Uhlig
Phys. Rev. 137, B576-94 (1965)

Be	9	4

METHOD

Synchrotron; ion chamber monitor

REF. NO. 65 Wy 1 NVB

REACTION	RESULT	EXCITATION ENERGY	SOURCE		DETECTOR		ANGLE
			TYPE	RANGE	TYPE	RANGE	
G,MU-T	ABX	10 - 35	C	90	SCI-D		

5-1

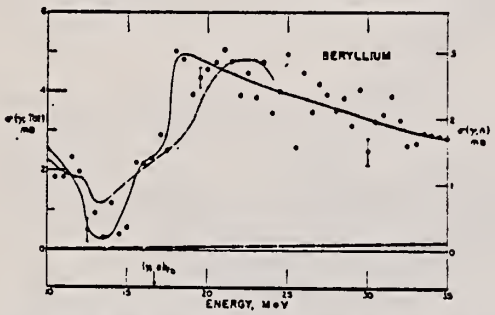

FIG. 4. Beryllium total photonuclear cross sections. The solid line is drawn as the best approximation to the experimental points using the left hand scale. The (γ,n) cross section obtained by Bertozzi *et al.* (Ref. 22) combined with that obtained by Nathan and Halpern (Ref. 23) is shown as a dashed line using the right-hand scale.

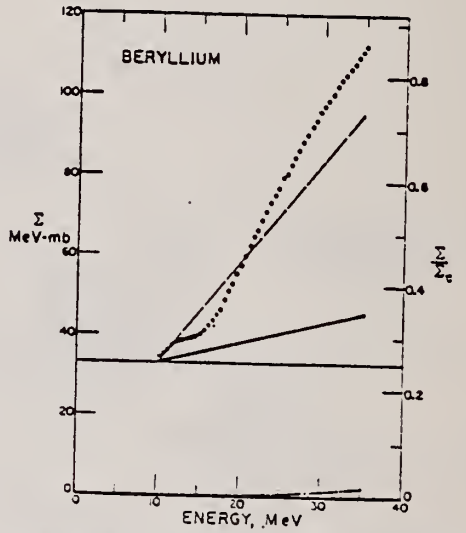

FIG. 5. Beryllium total photonuclear cross section integrated over energy. The points represent the experimental data. The solid line is the uncertainty in the baseline introduced by statistical considerations. The dashed line is the magnitude of baseline correction applied to bring the cross section to values measured by Bertozzi at 10 MeV. The dot-dashed line is the corrected baseline when the radiative correction is applied to the electronic cross section.

REF. H. Artus, P. Brix, H. G. Clerc, F. Eigenbrod, A. Goldmann, F. Gudden, E. Spamer, P. Strehl, M. Stroetzel, O. Titze, and K. J. Wetzel
Proc. Gatlinburg Conference, 314 (1966)

ELEM. SYM.	A	Z
Be	9	4

METHOD

REF. NO. 66 Ar 2 hmg

REACTION	RESULT	EXCITATION ENERGY	SOURCE TYPE	SOURCE RANGE	DETECTOR TYPE	DETECTOR RANGE	ANGLE
E,E/	LFT	16	D		MAG-D		
		(15.97)					

16=15.97 MEV

TABLE 1

Summary of Experimental Results[a]

Nuclide	E_x (MeV)	Type	Γ_γ^0 (eV)	Γ_γ^0/Γ_w	R_σ (F)
^{6}Li	2.18	E2	$(3.9 \pm 0.5) \times 10^{-4}$	14.4	3.77 ± 0.48
	3.56	M1	8.9 ± 0.4	9.4	2.96 ± 0.11
^{7}Li	11.28 ± 0.05	(M1) or	$(1.3 \pm 0.4)/g^2$	0.043/g	—
		(M2)	$(0.026 \pm 0.008)/g$	2.6/g	—
^{9}Be	15.97 ± 0.03	M1	$(3.7 \pm 0.8)/g$	0.043/g	—
^{11}B	4.46	E2 and	0.0173 ± 0.0021	8.2	3.44 ± 0.50
		M1	0.64 ± 0.08	0.34	2.60 ± 0.35
	5.04	M1	1.84 ± 0.14	0.69	2.60 ± 0.11
^{12}C	4.43	E2	0.0122 ± 0.0008	5.30	3.14 ± 0.30
^{16}O	6.92	E2	0.100 ± 0.015	3.28	3.82 ± 0.46
	11.52	E2	0.52 ± 0.13	1.31	—
^{24}Mg	9.85 ± 0.04	M1	7.95 ± 1.2	0.38	3.50 ± 0.49
	9.97 ± 0.03				
	10.35 ± 0.03	E2	0.24 ± 0.05	0.58	5.05 ± 0.50
	10.70 ± 0.03	M1	22.2 ± 2.4	0.86	3.60 ± 0.36
	10.93 ± 0.04	E2	0.26 ± 0.11	0.50	—
^{28}Si	4.97 ± 0.02	C0	$(2.0 \pm 0.5) \times 10^{-5}$ [c]	—	6.90 ± 1.20
^{40}Ca	6.89 ± 0.05	E2	0.29 ± 0.04	2.85	4.60 ± 0.50

[a] The Born approximation has been used except for ^{16}O and ^{40}Ca.
[b] $g = (2I_f + 1)/(2I_i + 1)$.
[c] Γ_γ = equivalent to ME = (8.87 ± 1.00) F^2.

H. G. Clerc, K. J. Wetzel and E. Spamer
Phys. Letters 20, 667 (1966)

Be	9	4

METHOD

REF. NO. 66 C1 1 EGF

REACTION	RESULT	EXCITATION ENERGY	SOURCE TYPE	SOURCE RANGE	DETECTOR TYPE	DETECTOR RANGE	ANGLE
E,E/	LFT	14 - 17	D	40 - 60	MAG-D	36 - 40	DST

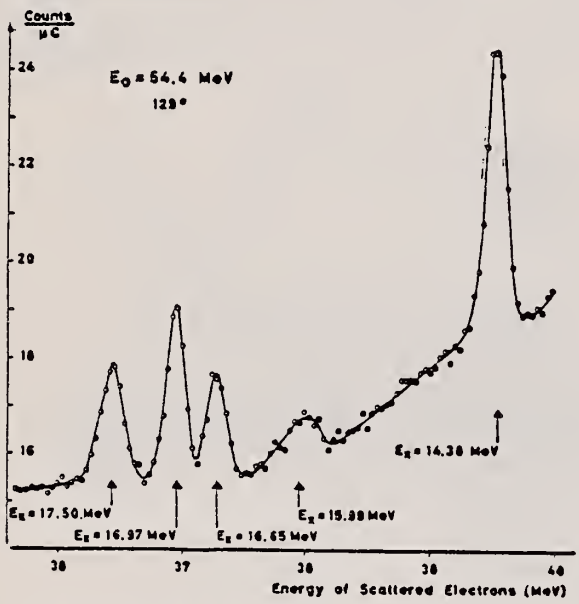

Fig. 1. Spectrum of inelastically scattered electrons from ^{9}Be. Note the suppressed zero of the ordinate scale.

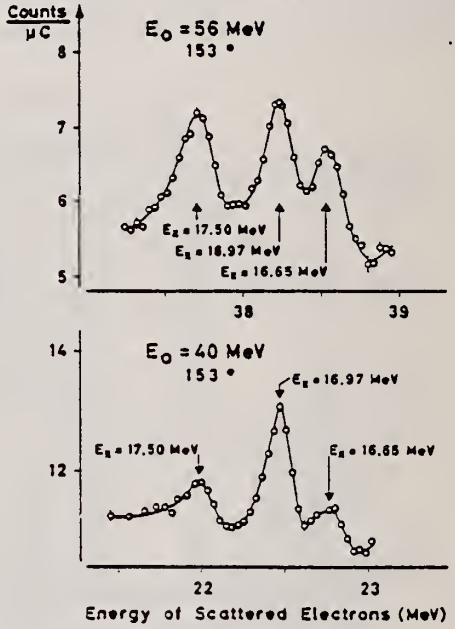

Fig. 2. Spectrum of inelastically scattered electrons from ^{9}Be. The inelastic momentum transfer if q = 0.467 fm^{-1} in the upper and q = 0.310 fm^{-1} in the lower part of the figure. Note the suppressed zero of the ordinate scales.

Table 1: Summary of experimental results
The first and second columns give the excitation energies in ^{9}Be and the multipolarities as determined in this experiment. For the type of transition indicated in column 2, the ground state radiation widths Γ_γ^0 and the transition strengths in Weisskopf units Γ_W are given in column 3 and 4. respectively; the statistical factor g is defined by $g = (2I_f + 1)/(2I_i + 1)$ with $I_i = \frac{3}{2}$. The last column lists the transition radii R_{tr} as defined in refs. 15 or 14.

E_x (MeV)		$g\Gamma_\gamma^0$ (eV)	$g\Gamma_\gamma^0/\Gamma_W$	R_{tr} (fm)
14.38 ± 0.03	M1	10.5 ± 1.5	0.17	2.4 ± 0.4
15.99 ± 0.06				
16.65 ± 0.03	(M2)	0.30 ± 0.08	3.6	3.6 ± 0.5
16.97 ± 0.03	M1	9.4 ± 1.3	0.09	2.2 ± 0.4
17.50 ± 0.03	(M2)	0.7 ± 0.2	6.6	4.3 ± 0.6

REF. S. Costa, L. Pasqualini, G. Piragino and L. Roasio
Nuovo Cimento 42B, 306 (1966)

Page 1 of 2

ELEM. SYM.	A	Z
Be	9	4

METHOD

31 MeV Betatron, 1000 MeV Betatron; NBS Ionization Chamber

REF. NO.	
66 Co 4	JDM

REACTION	RESULT	EXCITATION ENERGY	SOURCE		DETECTOR		ANGLE
			TYPE	RANGE	TYPE	RANGE	
G,XN	ABX	6 - 80	C	6 - 80	BF3-I		4PI

342

$$\sigma_o = \int_o^{70} \sigma_{abs}(E)dE = (220\pm26)\text{ mb MeV}$$

$\sigma_{-1} = (7.75\pm0.6)$ mb

r.m.s. radius of ^{9}Be charge distribution using $R_p = 0.77$ fermi is $R_c = (2.2\pm0.2)$ fermi.

$\sigma_{-2} = 680\ \mu\text{b MeV}^{-1}$

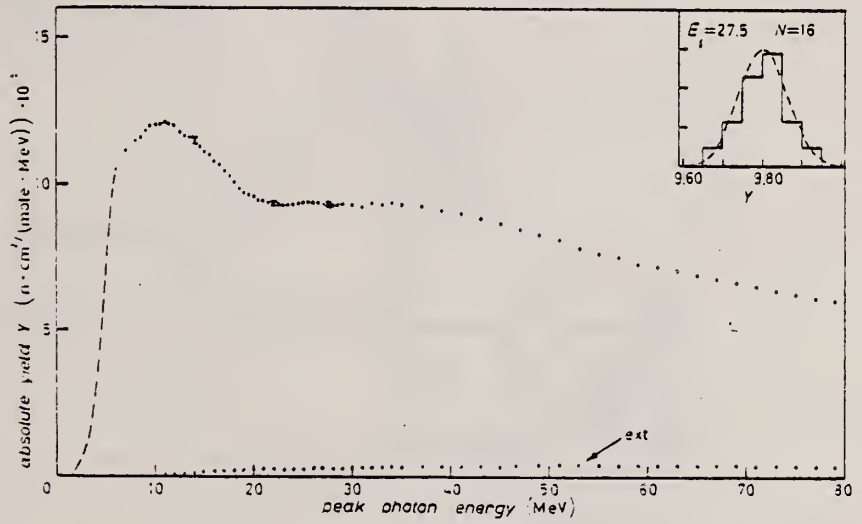

Fig. 1. – Absolute yield for the ^{9}Be(γ, Tn) reaction. The points labelled EXT represent the contribution from the external BF_3 counters (see text). Up to 6 MeV the yield curve has been deduced from Jakobson's data ([4]). The insert reproduces the frequency distribution of the sixteen experimental measurements at 27.5 MeV.

(continued)

ELEM. SYM.	A	Z
Be	9	4

METHOD

31 MeV Betatron, 1000 MeV Betatron; NBS Ionization Chamber

REF. NO.

66 Co 4 JDM

REACTION	RESULT	EXCITATION ENERGY	SOURCE		DETECTOR		ANGLE
			TYPE	RANGE	TYPE	RANGE	

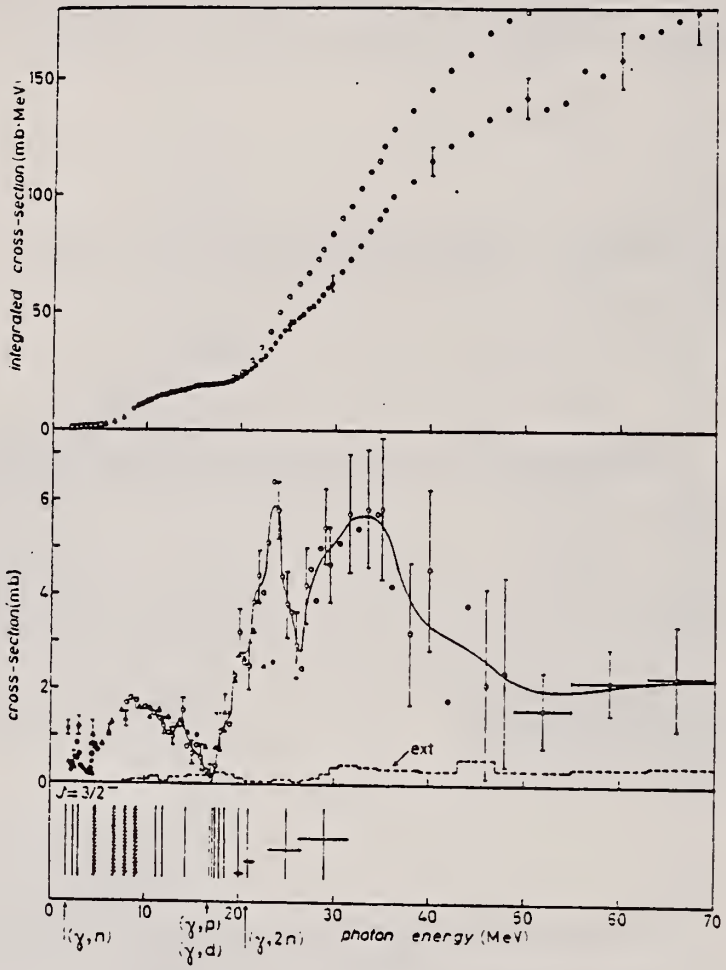

Fig. 2. – Upper part: the integrated cross-section of process ^{9}Be(γ, Tn) is shown (points). The open circles represent the sum of the (γ, Tn) and (γ, p) integrated cross-sections; ▫ $\int\sigma(\gamma, \mathrm{Tn})$, JAKOBSON; ▲ $\int\sigma(\gamma, \mathrm{Tn})$, NATHANS and HALPERN. Middle part: cross-section of the process ^{9}Be(γ, Tn). An average curve (solid line) is drawn through the experimental values (open circles). In the high-energy tail these values have been averaged over the indicated intervals. Previous measurements up to 23 MeV are also reported: • JAKOBSON; ▲ EDGE; ▲ NATHANS and HALPERN. The dashed histogram shows the contribution to the (γ, Tn) cross-section arising from the EXTernal counters. Lower part: energy-level diagram of ^{9}Be [ref. (10)]. Vertical lines with horizontal arrows indicate the levels at (20 ± 0.5), (21 ± 0.6), (25 ± 2) and (29 ± 3) MeV suggested in ref. (4).

REF.

A. De Marco, R. Garfagnini and G. Piragino
Nuovo Cimento, 42B, 355 (1966)

ELEM. SYM.	A	Z
Be	9	4

METHOD

Synchrotron

REF. NO. 66 De 3 JDM

REACTION	RESULT	EXCITATION ENERGY	SOURCE		DETECTOR		ANGLE
			TYPE	RANGE	TYPE	RANGE	
G,N	SPC	THR-85	C	85	CCH-D	C-15	135

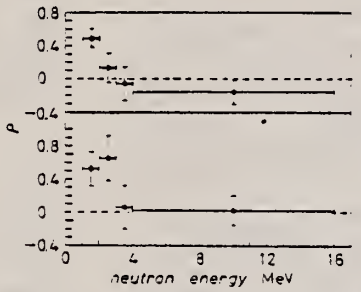

Fig. 2. – Upper part: polarization of photoneutrons from ^{9}Be. Lower part: difference between the polarization value of photoneutrons from ^{9}Be and the value measured for neutrons from a Ra D-Be source.

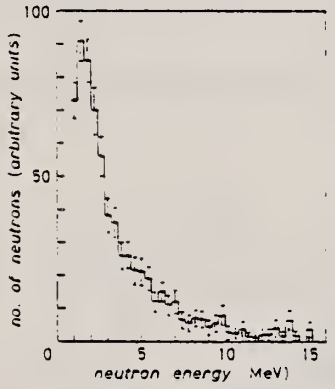

Fig. 3. – Energy distribution of photoneutrons from ^{9}Be.

REF.
V.P. Denisov and L.A. Kul'chitskii
J. Nucl. Phys. (USSR) 3, 268-276 (1966)
Sov. J. Nucl. Phys. 3, 192 (1966)

ELEM. SYM.	A	Z
Be	9	4

METHOD

[Page 1 of 3]

REF. NO.	
66 De 6	JDM

REACTION	RESULT	EXCITATION ENERGY	SOURCE		DETECTOR		ANGLE
			TYPE	RANGE	TYPE	RANGE	
G,P 940	ABX	THR - 50	C	20 - 50	ACT-I		4PI
G,D	ABX	THR - 50	C	20 - 50	TEL-D	4 - 10	90
G,T	ABX	THR - 50	C	20 - 50	TEL-D	4 - 11	90
G,P	ABX	THR - 50	C	20 - 50	TEL-D	3 - 11	90

$$\int_{17}^{40} [\sigma(\gamma,p) + \sigma(\gamma,pn) + \sigma(\gamma,d) + \sigma(\gamma,t)]dE$$

$$= 14.7 + 10.1 + 4.7 + 3.5 = (33\pm3) \text{ MeV-mb.}$$

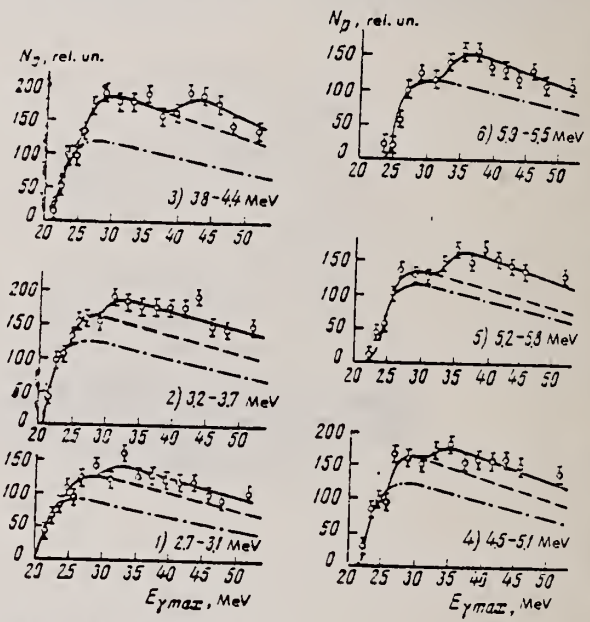

Fig. 2. Proton yield curves for individual sections of the proton spectra, as a function of $E_{\gamma max}$. The points denote the experimental values. The solid curve is a superposition of bremsstrahlung isochromats normalized to the total energy, chosen so as to best approximate the experimental points; the dot-dash curves are isochromats of transitions to the ground and first excited states; the dashed curves are with the isochromats of transitions to the second and third excited states added to the first. N_p is the relative number of protons.

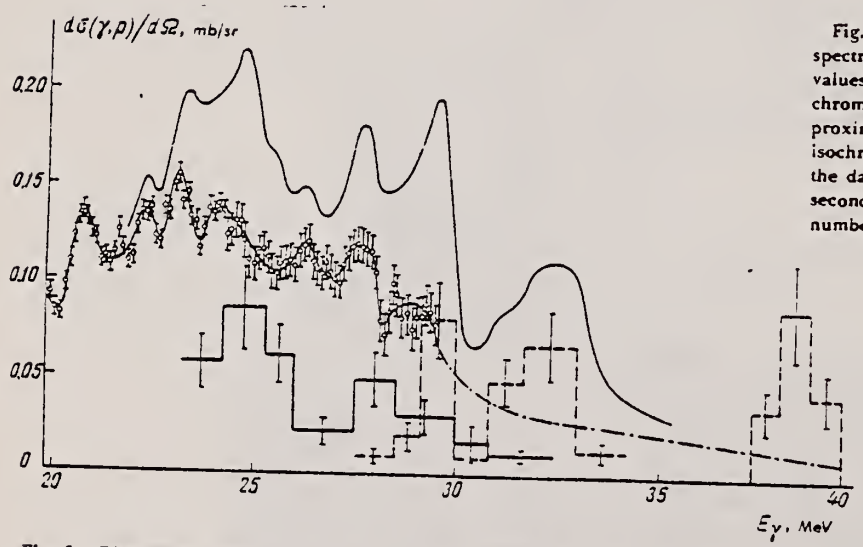

Fig. 3. Differential cross-section curves for the reaction $Be^9(\gamma,p)Li^8$, obtained from photoproton spectra for an angle of 90°. The curve with the experimental points is the sum of the cross sections for transitions to the ground state and first excited state (0.98 MeV); its extension (the dot-dash curve) is the cross section obtained from the proton spectra of Chuvilo and Shevchenko[13] on the assumption of transitions only to the ground state, normalized to our data; the solid histogram is the sum of cross sections for transitions to the second and third excited states; the dashed histograms are the cross sections for transitions to the states ~9 MeV and ~17 MeV; the solid curve represents the smoothed combined cross sections for the reaction, $d\sigma/d\Omega$.

REF.

V.P. Denisov and L.A. Kul'chitskii
J. Nucl. Phys. (USSR) 3, 268-276 (1966)
Sov. J. Nucl. Phys. 3, 192 (1966)

ELEM. SYM.	A	Z
Be	9	4

METHOD

REF. NO. 66 De 6 JDM

REACTION	RESULT	EXCITATION ENERGY	SOURCE		DETECTOR		ANGLE
			TYPE	RANGE	TYPE	RANGE	

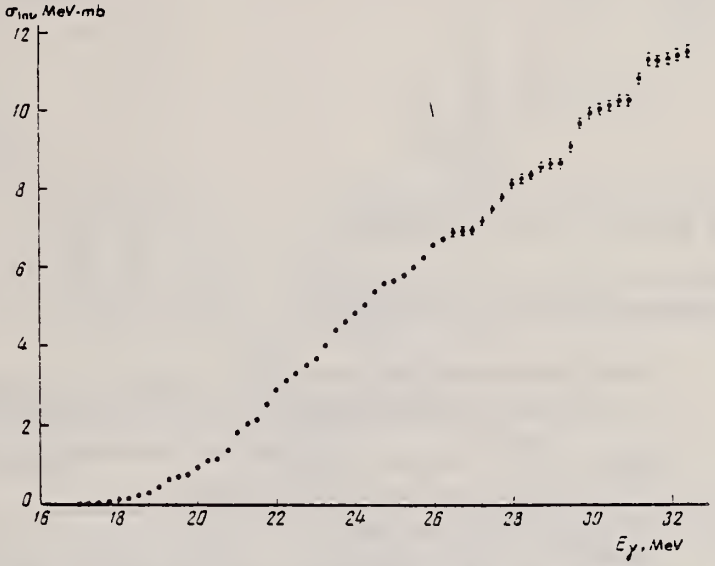

Fig. 4. Integrated cross section for the reaction $Be^9(\gamma, p)Li^8$, obtained by the method of Penfold and Leiss[111] from the yield curve of the Li^8 activity.

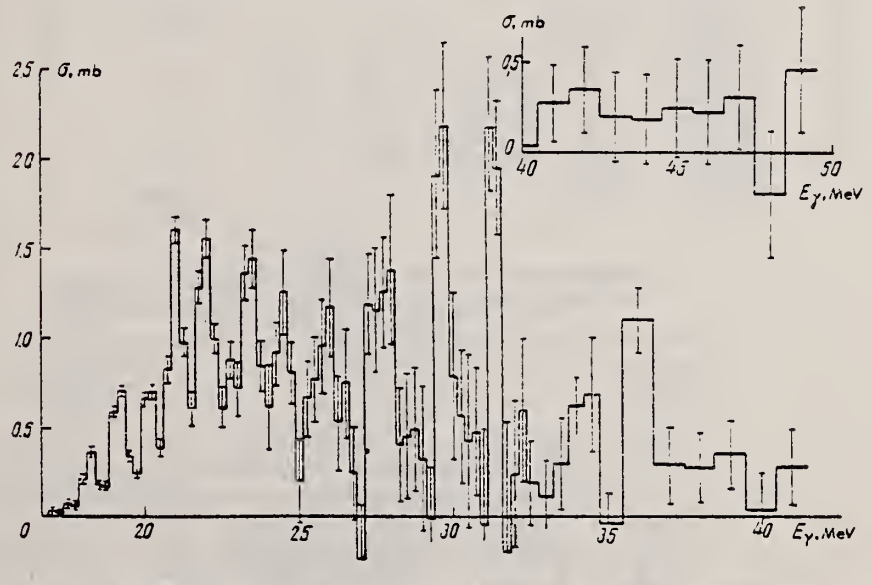

Fig. 5. Differential cross section for the reaction $Be^9(\gamma, p)Li^8$, obtained by the method of Penfold and Leiss[111] from the Li^8 activity yield curve.

REF.

V.P. Denisov and L.A. Kul'chitskii
J. Nucl. Phys. (USSR) 3, 268-276 (1966)
Sov. J. Nucl. Phys. 3, 192 (1966)

EL EM. SYM.	A	Z
Be	9	4

METHOD

REF. NO.	
66 De 6	JDM

REACTION	RESULT	EXCITATION ENERGY	SOURCE TYPE	SOURCE RANGE	DETECTOR TYPE	DETECTOR RANGE	ANGLE

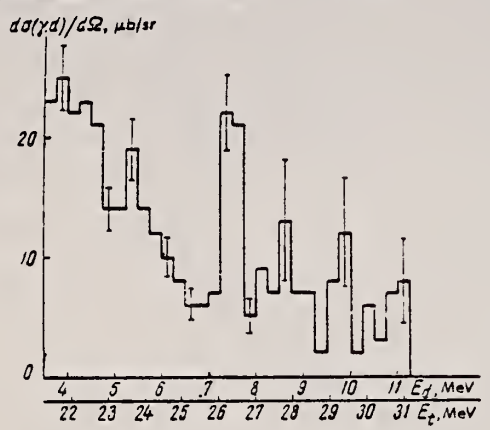

Fig. 6. Differential eross section for the (γ,d) reaction for transitions to the ground state of the final nucleus for an angle of 90°.

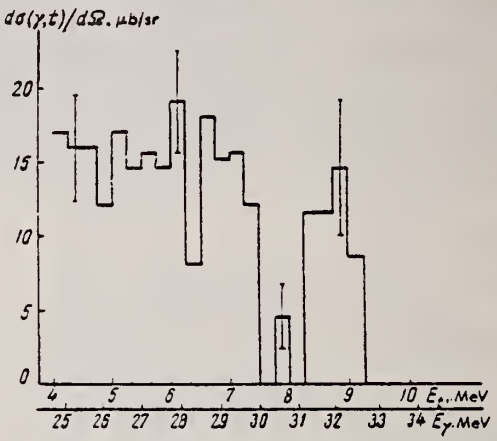

Fig. 7. Differential cross section for the (γ, t) reaction for transitions to the ground state of the final nucleus for an angle of 90°.

Table I

Energy E_i and integrated cross section of resonances obtained in different experiments of the present work, and comparison with the results of other investigations

E_i, MeV	$\int\sigma_i dE_i$, MeV-mb	E_i, MeV	$4\pi\int\frac{d\sigma}{d\Omega}dE_i$, MeV-mb	E_i, MeV			
From Li^8 activity		From photoproton spectra (gnd. + 0.98 MeV)		[6], from spectra, (γ,p)	[4], from Li^8 activity	[3], from reaction $Be^9(\gamma,n)Be^{8*} \rightarrow 2\alpha$	Ref. [12]
—	—	—	—	—	17.5; 18.5	—	18.1
18.2±0.2	0.19	—	—	—	18.8; 19.1	18.7	—
19.2±0.2	0.50	—	—	—	19.7	20.0	19.6
21.0±0.2	1.47	20.7±0.2	1.60	20.8	—	20.9	—
22.0±0.2	1.12	22.1±0.2	1.65	22.5	~22	—	21.7
23.4±0.2	1.32	23.2±0.2	1.90	—	—	—	—
24.5±0.2	1.02	24.4±0.2	1.80	24.3	~25	25	—
26.0±0.2	1.31	26.1±0.2	1.65	—	—	—	—
27.7±0.3	1.20	27.7±0.2	1.90	—	~27.5	—	—
28.7±0.3	0.49	28.6±0.2	1.0	—	—	—	—
29.7±0.3	1.38	—	—	—	~30	29	—
32.2±0.3	1.32	—	—	—	~31.5	—	—

Table II

Integrated cross sections for the (γ,p) reaction, obtained in different experiments of the present work, in comparison with the results of other investigations

Limits of integration of $\int\sigma(\gamma,p)dE$, MeV	$\int\sigma(\gamma,p)dE$, MeV-mb, from the data of the present work			$\int\sigma(\gamma,p)dE$, MeV-mb, from the data of	
	From Li^8 activity	From proton spectra		[4], from Li^8 activity	[6], from proton spectra
		Gnd. + 0.98	Combined		
17—26	6.6±1.0	8.4±1.5	12.8±1.5	15.3	11.9±1.8
17—31	11.0±1.6	12.5±2.0	21.1±2.2	~20	15.6±2.5
17—40	13.9±2.0	14.7±2.2	24.8±2.5	~27	—
17—50	16.0±2.3	—	—	—	
17—57	—	—	—	41.4±4.6	

REF.

M. N. Thompson and J. M. Taylor
Nuclear Physics 76, 377 (1966)

ELEM. SYM.	A	Z
Be	9	4

METHOD

Betatron, measured knock-on-protons

REF. NO.	
66 Th 1	JDM

REACTION	RESULT	EXCITATION ENERGY	SOURCE		DETECTOR		ANGLE
			TYPE	RANGE	TYPE	RANGE	
G,N	SPC	THR-17	C	17	SCI-D	2-12	90

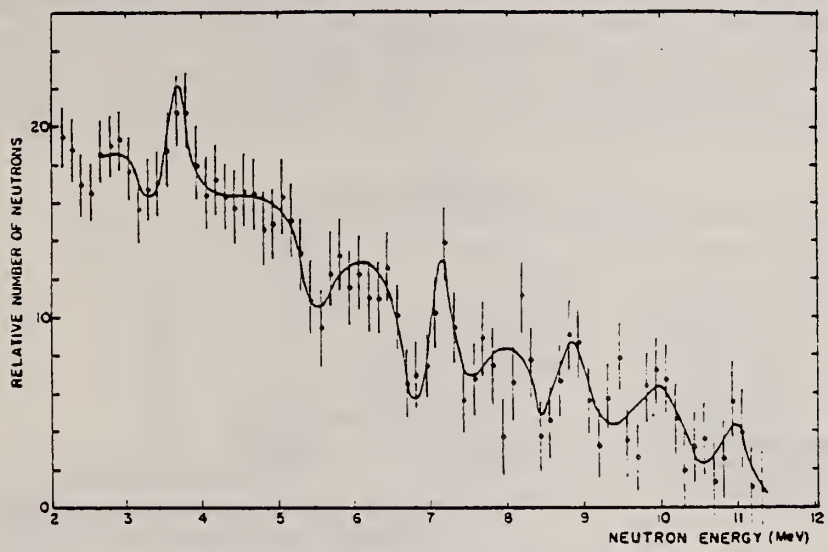

Fig. 3. The spectrum of photoneutrons from ^{9}Be.

TABLE 1

Energies of states in ^{9}Be (MeV) giving rise to the neutron groups observed, assuming decay to g.s. and first excited state of ^{9}Be respectively

Neutron energy	Emission to g.s.	Emission to 2.90 MeV state
10.9	14.0	16.9
9.9	12.7	15.6
8.75	11.4	14.4
8.0	10.6	13.5
7.0	9.6	12.5
6.0	8.4	11.3
4.7	7.1	9.9
3.6	5.7	8.6

TABLE 2
Levels in ^{9}Be

Levels assigned energies in MeV error ±200 keV	Decay	Other reports	
		Ref.	Energies
14.0	g.s.	[14]	14.4
12.7	g.s.	[15]	12.0–12.5
11.4	g.s. + first	[16,18,19,20]	11.3
9.6	g.s.		
9.1	first	[21]	9.2

In addition, the following four levels are consistent with the observed spectrum but it is not possible to decide on the present information which of each pair of states is the correct one:

Levels assigned energies in MeV error ±200 keV	Decay	Other reports	
		Ref.	Energies
13.4	first	[13,14]	13.3
or 10.6	g.s.		
8.6	first		
or 5.7	g.s.		

REF.

Yu. M. Volkov, A.P. Komar and V.P. Chizhov
J. Nucl. Phys. (USSR) 3, 277 (1966)
Sov. J. Nucl. Phys. 3, 198 (1966)

ELEM. SYM.	A	Z
Be	9	4

METHOD

REF. NO. 66 Vo 1 JDM

REACTION		RESULT	EXCITATION ENERGY	SOURCE TYPE	SOURCE RANGE	DETECTOR TYPE	DETECTOR RANGE	ANGLE
G,P		ABX	THR - 81	C	21 - 81	TEL-D	3 - 5	90
G,D	843	ABX	THR - 81	C	21 - 81	TEL-D	3 - 6	90
G,T	844	ABX	THR - 81	C	21 - 81	TEL-D	4 - 7	90

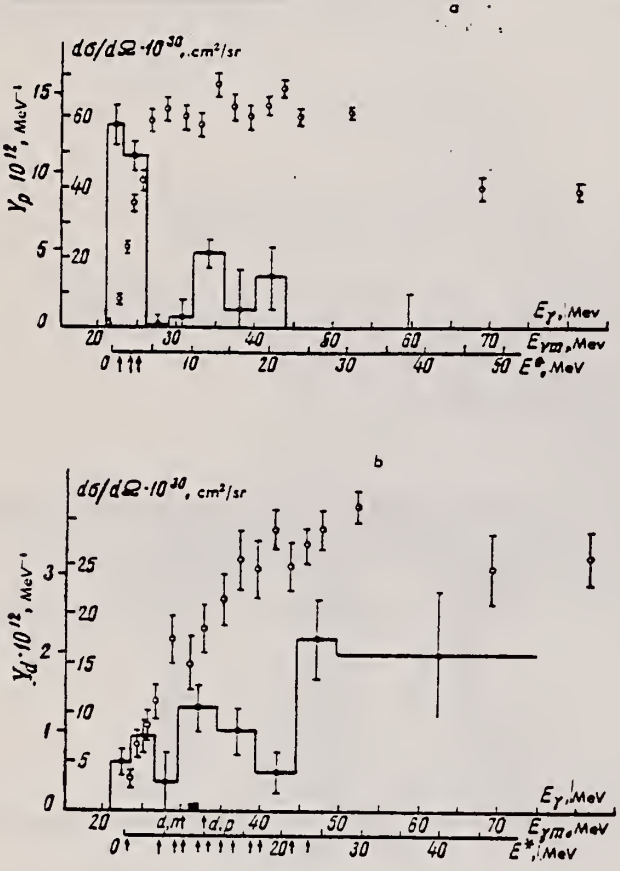

Fig. 2. Yields of photoprotons, photodeuterons, and phototritons as a function of $E_{\gamma m}$ – hollow circles; differential cross sections for the reactions as a function of γ-ray energy E_γ – solid circles; the arrows indicate the positions of known levels E^* of the residual nuclei. *a* – reaction $Be^9(\gamma, p)$; *b* – reaction $Be^9(\gamma, d)$, the heavy black bar denoting the theoretical result of Madsen and Henley,[8] and the arrows (d, n) and (d, p) denoting the energy thresholds of the reactions $Be^9(\gamma, dn)Li^8$ and $Be^9(\gamma, dp)He^8$; *c* – the reaction $Be^9(\gamma, t)$.

Table I

	$\bar{E}$, MeV	$\int_{E_{thr}}^{75} B\,dE_\gamma$, μb-MeV/sr	E'_γ, MeV	$\int_{E_{thr}}^{E'_\gamma} B\,dE_\gamma$, μb-MeV/sr	$\int_{E'_\gamma}^{75} B\,dE_\gamma$, μb-MeV/sr	$\int_{E'_\gamma}^{75} B\,dE_\gamma \Big/ \int_{E_{thr}}^{75} B\,dE_\gamma$
1	2	3	4	5	6	7
(γ, p)	4.4	435±32	26	264±8	171±26	0.65
(γ, d)	4.8	645±63	29.5	45±20	600±43	13.3
(γ, t)	5.4	329±36	30.5	56±10	273±26	4.9

Note. The function B under the integral sign is $B = d\sigma(\bar{E}, E_\gamma)/d\Omega$.

REF.

M. Bernheim, T. Stovall and D. Vinciguerra
Nucl. Phys. A97, 488 (1967)

ELEM. SYM.	A	Z
Be	9	4

METHOD

REF. NO. 67 Be 1 JOC

REACTION	RESULT	EXCITATION ENERGY	SOURCE		DETECTOR		ANGLE
			TYPE	RANGE	TYPE	RANGE	
E,E/	FMF	2	D	340	MAG-D		DST
		(2.43 MeV)					

TABLE 1
Measured elastic and inelastic form factors

E_0 (MeV)	θ (deg)	$F^2_{elastic}$	$F^2_{inelastic}$
338.6	40	$(4.49 \pm 0.45) 10^{-3}$	$(1.90 \pm 0.30) 10^{-2}$
338.6	50	$(1.38 \pm 0.14) 10^{-3}$	$(1.66 \pm 0.24) 10^{-2}$
339.1	60	$(2.74 \pm 0.35) 10^{-3}$	$(4.8 \pm 0.7)\ 10^{-3}$
339.7	70	$(8.3 \pm 2.0)\ 10^{-4}$	$(1.3 \pm 0.7)\ 10^{-3}$
336.3	80	$(3.9 \pm 1.0)\ 10^{-4}$	$(1.0 \pm 0.3)\ 10^{-3}$
338.6	90	$(1.8 \pm 0.6)\ 10^{-4}$	$(2.3 \pm 1.1)\ 10^{-4}$
337.3	100	$(1.4 \pm 0.7)\ 10^{-4}$	$(8.8 \pm 4.5)\ 10^{-5}$

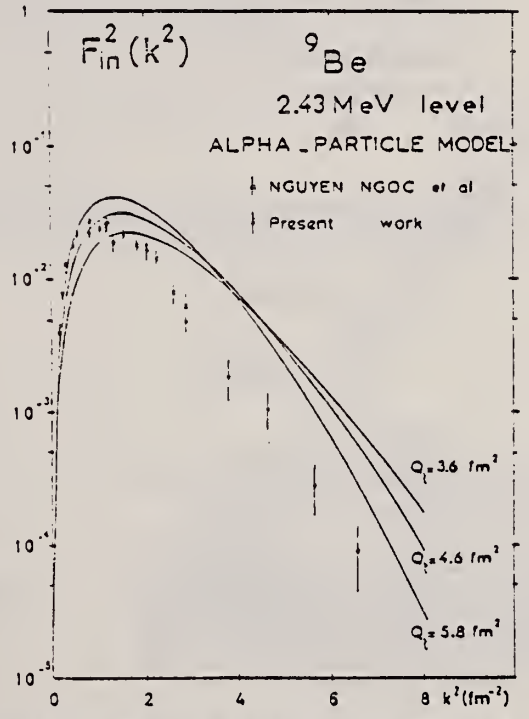

Fig. 11. Same as fig. 8 for alpha-particle model. Best fit is obtained with $\xi = 1.7$ fm and $Q_t = 4.6$ fm^2. Form factors calculated with $Q_t = 3.6$ fm^2 and $Q_t = 5.8$ fm^2 are also reported.

TABLE 2
Root mean square charge radius a and spectroscopic quadrupole moment Q

Reference	r.m.s. charge radius a(fm)	quadrupole moment Q(fm²)
this work (Harmonic-well model)	2.50	3.8
this work (Nilsson model)	2.45	2.34
this work (Alpha-particle model)	2.48	5.8
this work (Deformed-oscillator model)	2.45	8.4
Ref. [1])		2.0
Ref. [3])		2.9
Ref. [22])		6.9
Refs. [25, 28])		3.2
Ref. [27])		5.17

E	DETECTOR TYPE	DETECTOR RANGE	ANGLE

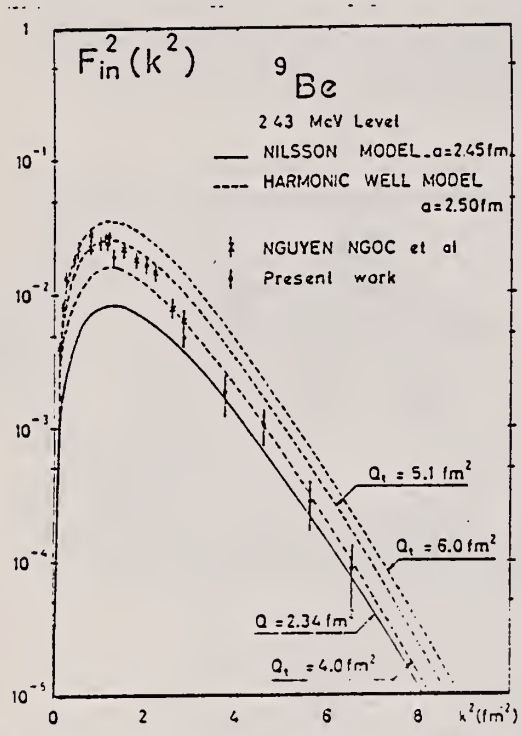

Fig. 8. The quantity $F^2_{in}(q^2)$ which is the ratio of the differential scattering cross section to the Mott cross section is reported for the 2.43 MeV level. Best fit is shown in the harmonic-well model for $a = 2.5$ fm and $Q_t = 5.1$ fm² and the curves for $Q_t = 4.0$ fm² and $Q_t = 6.0$ fm² are also reported. The best fit in the Nilsson model is also shown for $a = 2.45$ fm and $Q = 2.34$ fm².

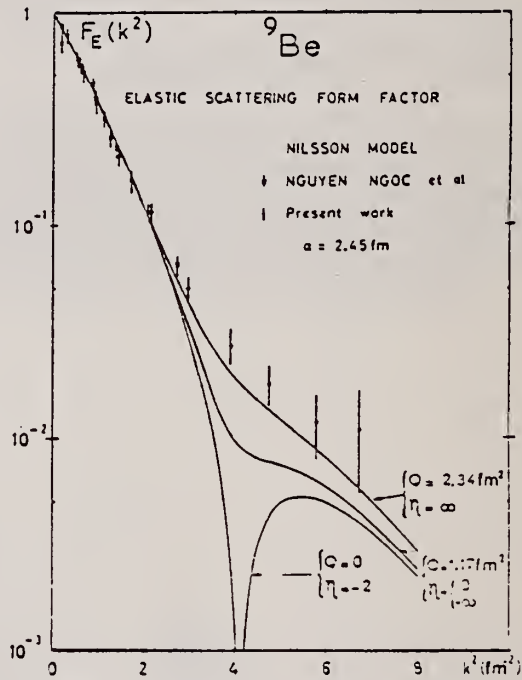

Fig. 7. The ^{9}Be elastic form factor, calculated in the Nilsson model for a r.m.s. radius $a = 2.45$ fm and different values of the deformation parameter η.

REF. B. L. Berman, K. G. Van Nemert and C. D. Bowman
Phys. Rev. 163, 958 (1967)

ELEM. SYM.	A	Z
Be	9	4

METHOD

REF. NO. 67 Be 6 HMG

REACTION	RESULT	EXCITATION ENERGY	SOURCE		DETECTOR		ANGLE
			TYPE	RANGE	TYPE	RANGE	
G,N	ABX	2-4	C	2-4	TOF-D	0-1	135
		(1.665 - 3.5)				(450 eV - 33 keV)	

Cross section data cannot be fitted satisfactorily by a function of the Breit-Wigner form.

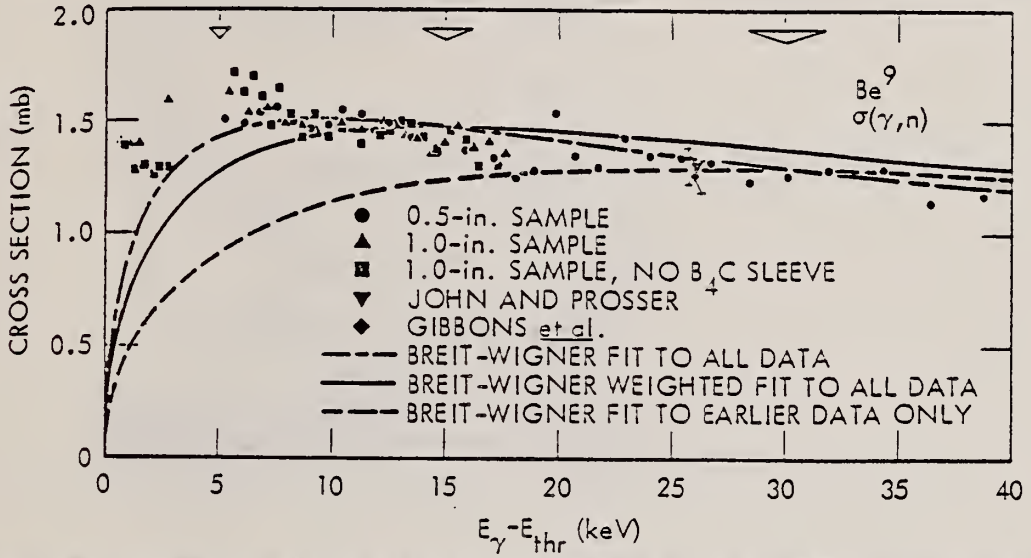

FIG. 3. Threshold photoneutron cross section for Be^9. The data have been normalized to the average of the gamma-ray source measurements of Gibbons *et al.* (Ref. 7) and John and Prosser (Ref. 8) at $E_\gamma - E_{thr} = 26$ keV. Data from three independent runs are shown as well as three different Breit-Wigner curves fitted to various sets of data points (see text). The energy resolution is indicated by the open triangles along the top of the figure.

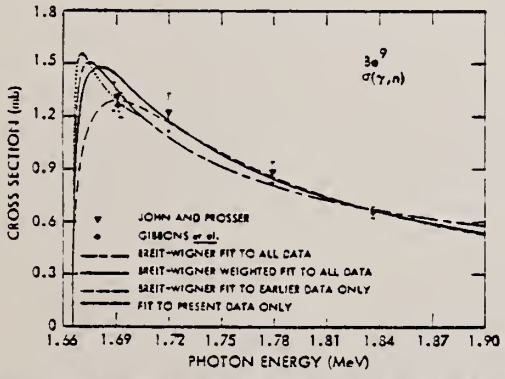

FIG. 5. The same three Breit-Wigner curves as shown in Fig. 3, together with the data points of Refs. 7 and 8. The dotted line is a fourth curve fitted to the present data only (see text).

TABLE II. Breit-Wigner parameters for Be^9.

Case	$E_R - Q$ (MeV)	G_n (MeV)	G_γ (eV)	Γ_γ (eV)
(a) Old data only	−0.087	0.5	0.44	1.8
(b) All data	−0.078	2.1	0.37	1.5
(c) All data, weighted	−0.115	0.9	0.31	1.2

REF.
O. L. Garzon and G. G. Rocco
J. Inorg. Nucl. Chem. 29, 1 (1967)

ELEM. SYM.	A	Z
Be	9	4

METHOD

REF. NO.	
67 Ga 1	JOC

REACTION	RESULT	EXCITATION ENERGY	SOURCE		DETECTOR		ANGLE
			TYPE	RANGE	TYPE	RANGE	
G,2N	ABY	THR-23	C	23	ACT-I		4PI

Estimated $\int_0^{23} \sigma dE = 0.47 \pm 0.09$ MeV-mb.

REF.

J. M. Loiseaux, J. M. Maison and M. Langevin
J. de Physique 28, 11 (1967)

ELEM. SYM.	A	Z
Be	9	4

METHOD

REF. NO.	
67 Lo 1	JOC

REACTION	RESULT	EXCITATION ENERGY	SOURCE		DETECTOR		ANGLE
			TYPE	RANGE	TYPE	RANGE	
G,G/	ABX	12-30	C	34	NAI-D		DST

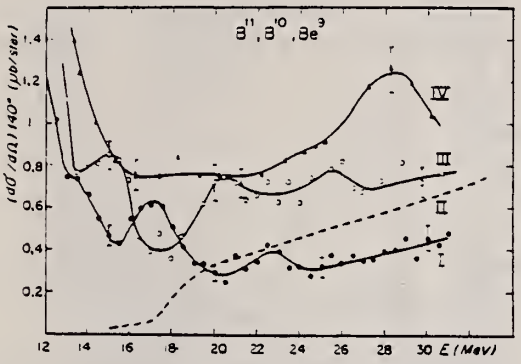

FIG. 5.

Sections efficaces différentielles de diffusion à 140° pour ^{9}Be (I), ^{10}B (III) et ^{11}B (IV).
Section efficace prévue par la relation de dispersion pour ^{9}Be (courbe II).

Jan-Olof Adler and Bengt Forkman
Arkiv Fysik 38, 389 (1968)

Be	9	4

METHOD

REF. NO. 68 Ad 1 egf

REACTION	RESULT	EXCITATION ENERGY	SOURCE		DETECTOR		ANGLE
			TYPE	RANGE	TYPE	RANGE	
G,P	RLY	17-28	C	28	MAG-D	1-11	4PI
G,D	RLY	17-28	C	28	MAG-D	2	4PI
G,T	RLY	18-28	C	28	MAG-D	2	4PI
G,A	RLY	3-28	C	28	MAG-D	2-16	4PI

FORWARD YIELDS

$\frac{Y_d}{Y_p} = 0.10 \pm 0.04$ $E_d \geq 2.5$ MeV $E_p \geq 1.5$ MeV

$\frac{Y_t}{Y_p} < 0.1$

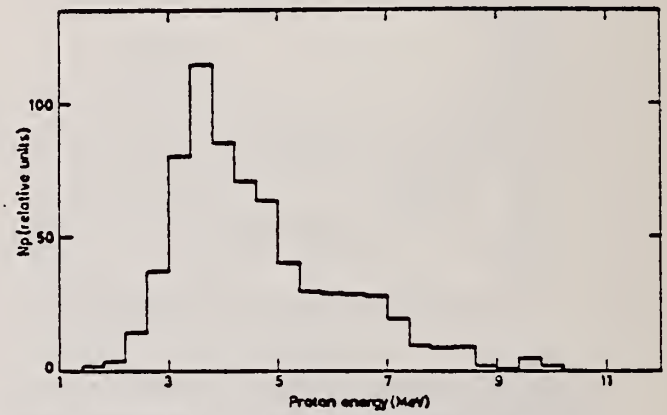

Fig. 5. Energy distribution of the photoproton tracks in the area—$12.0 \leq x_p \leq -9.0$ and $-3.0 \leq x_p \leq 3.0$. Corrections have been made for the energy dependence of the detection efficiency and for self-absorption in the target.

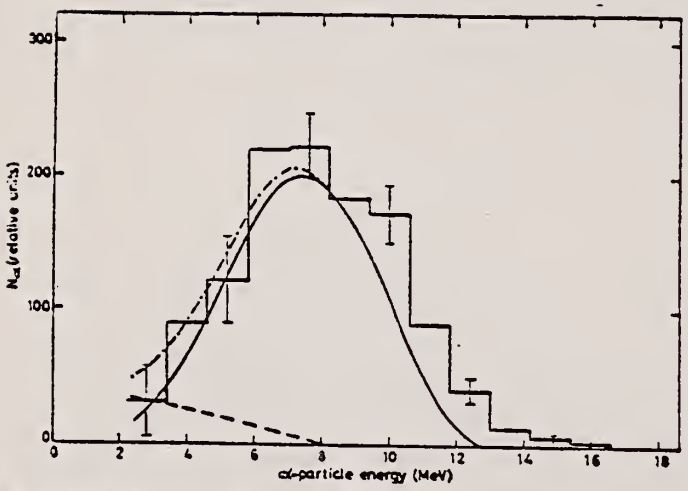

Fig. 13. Experimental alpha-particle-energy distribution (histogram). The statistical errors are shown. No correction for the target self-absorption has been introduced. The solid curve gives the expected alpha spectrum from a level around 17 MeV in ^{8}Be and the dashed curve the alpha spectrum expected from the ^{9}Be$(\gamma,\alpha)^5$He reaction (see text). The dot-and-dash curve shows the sum of the two calculated curves.

REF. V. F. Borzhkovskii, A. S. Cherkasov, N. G. Afanas'ev, I. A. Grishaev, and I. I. Zalyubovskii
Yad. Fiz. 7, 261 (1968)
Sov. J. Nucl. Phys. 7, 181 (1968)

ELEM. SYM.	A	Z
Be	9	4

METHOD

REF. NO. 68 Bo 2 hmg

REACTION	RESULT	EXCITATION ENERGY	SOURCE		DETECTOR		ANGLE
			TYPE	RANGE	TYPE	RANGE	
E,XXX	RLY	THR-119	D	119	MAG-D		76

XXX=MASS SPECTRU

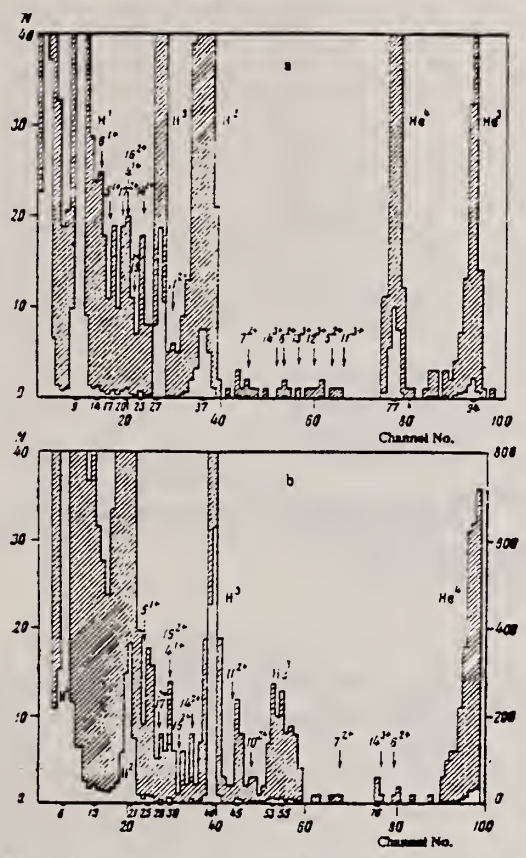

FIG. 1. Pulse spectrum in AI-100 analyzer at $\theta = 76°$. Target – Be^9 (~70 mg/cm²). Electron energy 119 MeV. The magnetic field of the spectrometer corresponds to the following proton energies: a – 12.3 MeV, counter bias voltage 60 V; b – 18.3 MeV, counter bias voltage 50 V.

REF.

H. G. Clerc, K. J. Wetzel, E. Spamer
Nucl. Phys. A120, 441 (1968)

ELEM. SYM.	A	Z
Be	9	4

METHOD

REF. NO. 68 Cl 2 - egf

REACTION	RESULT	EXCITATION ENERGY	SOURCE TYPE	SOURCE RANGE	DETECTOR TYPE	DETECTOR RANGE	ANGLE
E,E/	LFT	1- 7	D	25- 58	MAG-D		DST

5 LEVELS

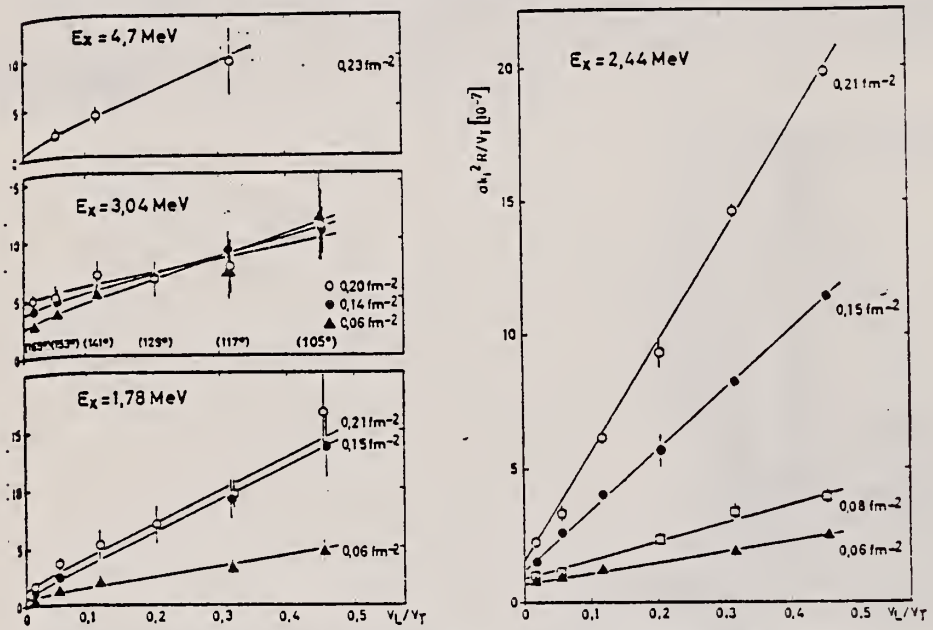

Fig. 3. Angular dependence of cross sections (see eq. 2) at different momentum transfers (q^2 as indicated) for the transitions at 1.78, 2.44, 3.04 and 4.7 MeV. The straight lines are least squares fits (see table 2).

TABLE 3
Experimental results

E_x (MeV)	Γ (keV)	$X\lambda$	R_{tr} (fm)	$B(k, \uparrow)$ [a])	Γ_γ^0 (eV)	Γ_γ^0/Γ_W
1.78±0.03	150± 50	C1	(2.46)	$2.5 \cdot 10^{-2}$	0.3±40 %	0.18
2.44±0.02	< 30	M1	2.7±0.5	$8.9 \cdot 10^{-3}$	$89 \cdot 10^{-3}$±11 %	0.30
		C2	3.1±0.4	41.6	$1.89 \cdot 10^{-3}$±7 %	24.4
3.04±0.03 [b])	450±150	C1	(2.46)	$1.5 \cdot 10^{-2}$	0.45/g±83 %	0.054/g
		M1	2.9±0.9	$3.0 \cdot 10^{-2}$	$3.8 \cdot 10^{-2}$/g±51 %	0.15/g
4.7 ±0.2	700±300	C(1)	(2.46)	$2.3 \cdot 10^{-2}$	2.4/g±47 %	0.079/g
6.4 ±0.2	1100±300	(C2)	(3.1)	15	$8.2 \cdot 10^{-2}$±42 %	8.3

Column 3 gives the character and multipolarity of the transitions as determined in this experiment; Cλ denotes a longitudinal electric, Mλ a magnetic transition of multipolarity λ. Values in parenthesis have been used but not determined by this experiment; the M1 assignment for E_x = 3.04 MeV is tentative. The M1 and C2 reduced photon transition probabilities and ground state widths Γ_γ^0 have been decreased by 4 % to account for the error of the Born approximation. To calculate Γ_γ^0 the excitation energies given in column 1 were used (without errors); only for the 2.44 MeV level was the value 2.429 MeV from ref. [1]) used. The statistical factor is $g = (2I+1)/4$, with I the spin of the excited state. For the spins of the levels at 1.78, 2.44 and 6.4 MeV, $I = \frac{1}{2}, \frac{4}{2}$ and $\frac{7}{2}$, respectively, were assumed. The last column gives the transition strengths in Weisskopf units Γ_W defined in ref. [47]).

[a]) Units are fm² for C1 and M1, and fm⁴ for C2; $k = E_x/\hbar c$.

[b]) Energy of the centre of the peak.

[1] T. Lauritsen et al., Nucl. Phys. 78, 1 (1966).

[47] D.H. Wilkinson, in Ajzenberg-Selov Nuclear Spectroscopy, Part B (Acad. Press, N.Y. 1960).

REF. N. N. Kaushal, E. J. Winhold, P. F. Yergin, H. A. Medicus and R. H. Augustson
Phys. Rev. 175, 1330 (1968)

ELEM. SYM.	A	Z
Be	9	4

METHOD

[Page 1 of 2]

REF. NO. 68 Ka 1 HMG

REACTION	RESULT	EXCITATION ENERGY	SOURCE		DETECTOR		ANGLE
			TYPE	RANGE	TYPE	RANGE	
G,N	ABX	50-85	C	55,85	TOF-D	10-85	67
							(67,5)

NEUT ENGY SPEC

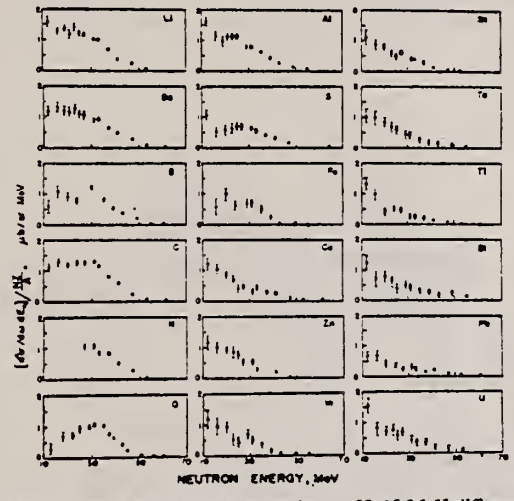

FIG. 6. Observed neutron spectra due to 55–85-MeV difference photon spectra. The effective cross sections have been divided by NZ/A.

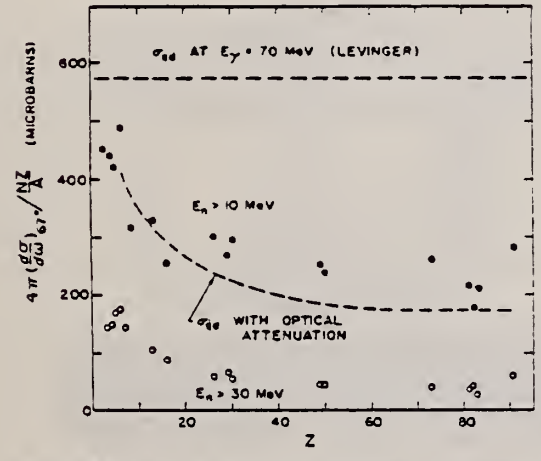

FIG. 7. Effective cross sections for production of fast neutrons with energies greater than 10 MeV (solid circles) and 30 MeV (open circles) by the 55–85-MeV photon difference spectrum. The dashed curves are modified quasideuteron model predictions as discussed in the text.

TABLE I. Comparison of present cross-section values in mb for production of high-energy photoneutrons by 55–85-MeV photons with measured cross sections $\sigma(\gamma,Tn)$, also in mb, for total photoneutron production. The present cross-section values are uncertain by 8 to 10% because of counting statistics and normalization errors; in addition all values depend on an absolute normalization in terms of the deuteron photodisintegration cross section, which is known to about 10% at these energies.

Target	$4\pi(d\sigma/d\omega)_{E1}$ ($E_n > 10$ MeV) [Present experiment]	$\sigma(\gamma,Tn)$ Jones and Terwilliger[a]	$\sigma(\gamma,Tn)$ Costa *et al.*[b]	Other results
Li	0.75		1.0	
Be	1.0	2.7	2.3	2.3[c]
B	1.0		1.4	
C	1.5	1.3	1.4	2.4[d]
O	1.3		1.6	
Al	2.8	5.5	4.6	8[d]
S	2.1		4.4	6.5[d]
Fe	4.2	16	12	
Cu	4.3	20	19	
Zn	4.4		15	
In	7.4			
Sn	7.0			
Ta	10.7	95		
Tl	10.7			
Pb	8.3	100		
Bi	13			
U	16	65		

[a] Average cross sections between 55 and 85 MeV, as read from Figs. 4 and 5 of Ref. 4.
[b] $\int_{\pi}^{85}\sigma dE - \int_{\pi}^{55}\sigma dE/50$, as taken from Fig. 4 of Ref. 5 and Table I of Ref. 6.
[c] S. Costa, L. Pasqualini, G. Piragino, and L. Roasio, Nuovo Cimento 42, 306 (1966).
[d] G. Bishop, S. Costa, S. Ferroni, R. Malvano, and G. Ricco, Nuovo Cimento 42, 148 (1966).

REF. N. N. Kaushal, E. J. Winhold, P. F. Yergin, H. A. Medicus and R. H. Augustson
Phys. Rev. 175, 1330 (1968)

ELEM. SYM.	A	Z
Be	9	4

METHOD

REF. NO.	
68 Ka 1	HMG

REACTION	RESULT	EXCITATION ENERGY	SOURCE		DETECTOR		ANGLE
			TYPE	RANGE	TYPE	RANGE	

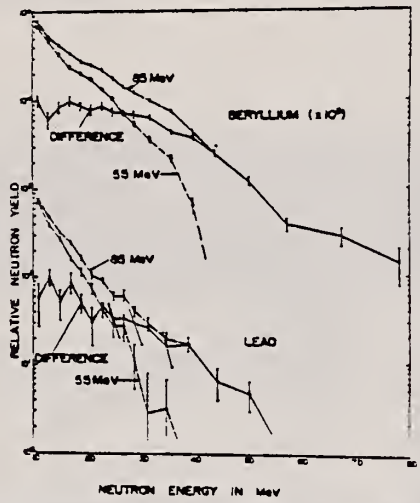

FIG. 5. Neutron energy spectra for beryllium and lead due to 55- and 85-MeV bremsstrahlung, together with the corresponding difference neutron spectra. Error bars indicate statistical errors only.

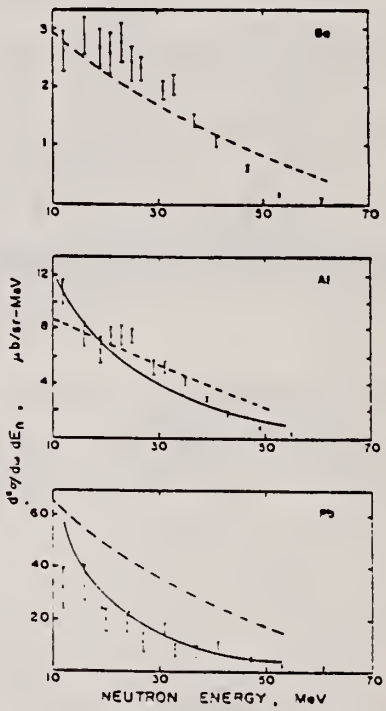

FIG. 8. Neutron energy spectra for beryllium, aluminum, and lead. The dashed curves are Dedrick's quasideuteron model calculations of the primary neutron spectra, arbitrarily multiplied by 1.15. For aluminum and lead these have been modified by estimates of the effects of secondary interactions on the outgoing neutrons, as discussed in the text, to produce the solid curves.

REF. G. J. Vanpraet and W. C. Barber
Z. Physik 211, 213 (1968)

ELEM. SYM.	A	Z
Be	9	4

METHOD

REF. NO. 68 Va 1 egf

REACTION	RESULT	EXCITATION ENERGY	SOURCE		DETECTOR		ANGLE
			TYPE	RANGE	TYPE	RANGE	
E,E/	ABX	0-26	D	42-68	MAG-D	30-70	180

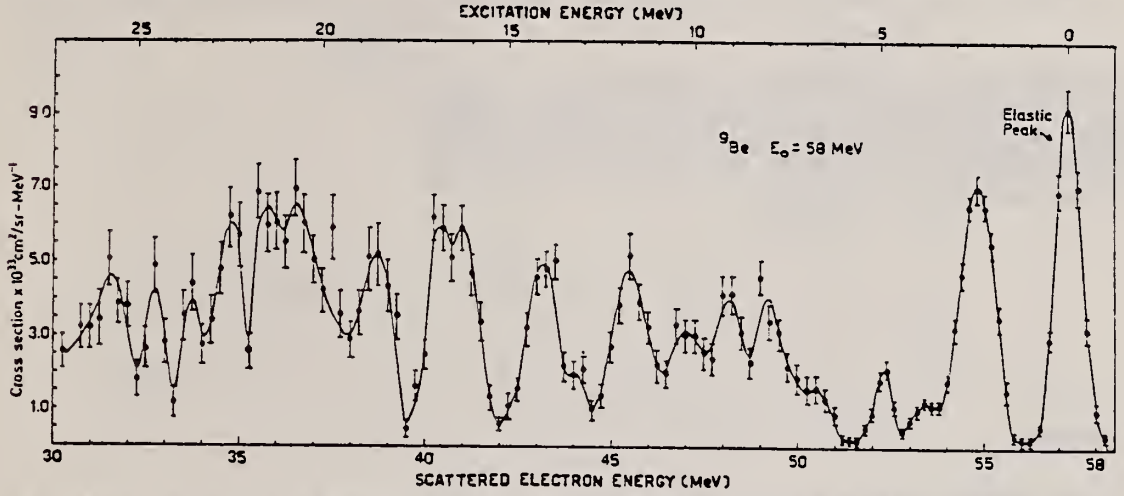

Fig. 1. Energy spectrum of 58 MeV electrons scattered at 180° from a Be^9 target. Top scale gives the excitation energy (MeV)

Table 2. *Data on the 2.4 MeV transition*

(MeV/c)	cross section (10^{-33} cm²/sr)	(form factor)² × 10^4 theory[15]	experiment
82.5	12.5 ± 1.3	1/2 3.0 5/2 0.45	3.1 ± 0.3
113.5	8.2 ± 0.8	1/2 3.6 5/2 0.6	4.3 ± 0.4
133.5	4.1 ± 0.4	1/2 3.3 5/2 0.5	3.0 ± 0.3

Table 1. *Excited States from* $Be^9(e, e')$ *at 180°,* $E_0 = 58$ *MeV*

Levels (MeV) (± 0.2 MeV)	Inelastic cross section (10^{-33} cm²/sr)	$g\Gamma_\gamma^0$ (eV)	$g\Gamma_\gamma^0/\Gamma_w$	Percentage experimental error
2.4	8.2	0.19	0.63	10
8.0	3.2	3.5	0.31	30
9.1	3.5	5.8	0.37	25
10.2	2.3	5.4	0.24	25
11.2	5.6	17.6	0.51	20
14.3	4.8	26	0.42	25
16.3, 16.9	9.2	78	0.75	25
18.5	5.5	74	0.56	25
20.8, 21.6	11.2	196	1	30
22.5	5.2	110	0.45	25
24.4	2.6	78	0.2	30
25.7	4.5	162	0.45	35

Yu. P. Antuf'ev, V. L. Agranovich, V. B. Ganenko, V. S. Kuzmenko,
I. I. Miroshnichenko, and P. V. Sorokin
Ukr. Fiz. Zh. 14, 248 (1969)

Be	9	4

METHOD

REF. NO. 69 An 6 egf

REACTION	RESULT	EXCITATION ENERGY	SOURCE		DETECTOR		ANGLE
			TYPE	RANGE	TYPE	RANGE	
G,P	ABY	114-999	C	700,999	TEL-D	97-230	DST
G,D	ABY	114-999	C	700,999	TEL-D	97-205	DST

999 = 1.2 GEV

Summary

The cross-sections of the (γ, p) (γ, d) reactions were investigated. Li^7, Be^9, C^{12}, Si^{28}, Cu^{63}, Mo^{96} and Ta^{181} targets were irradiated with the bremsstrahlung of 700 and 1200 MeV maximum energy from the Kharkov PhTI Ac. Sci. UkrSSR linear accelerator. The photoprotons and deuterons were detected by the scintillation telescope at 30°, 60°, and 120° with the beam. Possible mechanisms of the proton and deuteron photoproduction are discussed. The qualitative agreement of A dependence of the cross-sections is observed with a suggestion on the meson mechanism for these reactions.

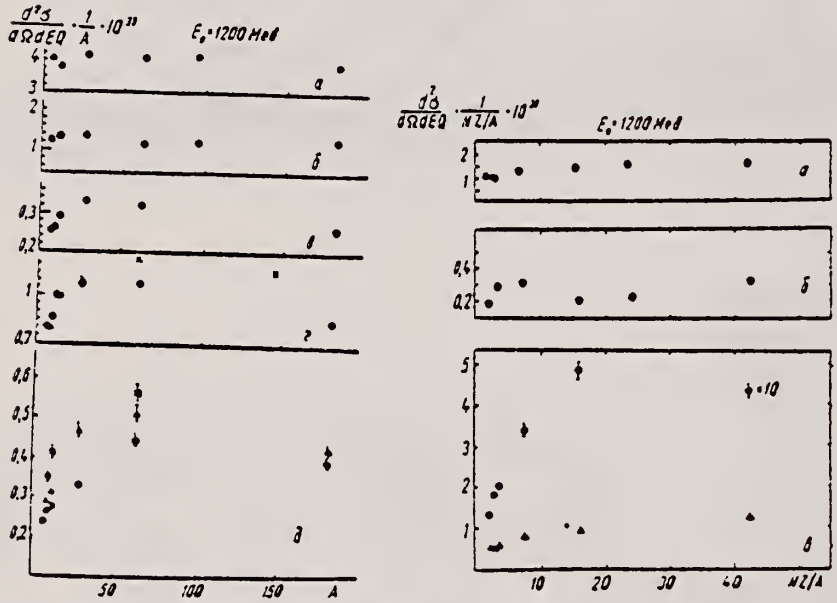

Рис. 1. Залежність перерізу (γ, p)-реакції від A: а — θ=30°, E_p=97 *Мев*; б — E_p=205 *Мев*; в — θ=60°, E_p=230 *Мев*; г — E_p=157 *Мев* (× — дані [3]); д — θ=120°, ○ — E_p=120 *Мев*, △ — E_p=157 *Мев*, □ — E_p=230 *Мев*. Абсолютне значення перерізу наведено при енергії протонів E_p=120 *Мев*. Інші дані нормовані до перерізу для Li^7 при E_p=120 *Мев*.

Рис. 2. Залежність перерізу (γ, d)-реакції від *NZ/A*: а — θ=30°, E_d=97 *Мев*; б — θ=30°, E_d=205 *Мев*; в: △ — θ=60°, E_d=97 *Мев*, ○ — θ=120°, E_d=97 *Мев* (перерізи наведені в одиницях 10^{-33} *см²/стер · Мев · Q*).

B. S. Dolbilkin, A. I. Isakov, V. I. Korin, L. E. Lazareva, N. V. Lin'kova, and F. A. Nikolaev
Yad. Fiz. 9, 914 (1969)
Sov. J. Nucl. Phys. 9, 534 (1969)

Be	9	4

METHOD

REF. NO. 69 Do 3 egf

REACTION	RESULT	EXCITATION ENERGY	SOURCE TYPE	SOURCE RANGE	DETECTOR TYPE	DETECTOR RANGE	ANGLE
G.MUT	ABX	10-30	C	250	MGP-D	10-30	4PI

Table I. Resonances in the photodisintegration cross section of Be^9

Theory		(γ, Tot)			(γ, n)								(γ, p), (γ, d), (γ, t)					
[7]	[8]	Present work	[9]	[10]	[10]	[5]	[6]	[10]	[6]	[10]	[7]	[5]	[10]	[8]	[10]	[11] (γ, p0,1)	[11] (γ, p1,2)	[11] (γ, d, t)
1.67					1.7	1.7												
2.43					2.43													
3.03					2.9	3.0												
4.07					4.6													
5.6	7.8						9.2											
	8.3	11.8				9.0	11.3		10.0	11	11.5	9						
		(13 5)					13.25			13.0								
										13.8		13.5						
	14.0																	
	15.0	14.8																
	15.5		15.5															
														17.5				
	16.2													18.1				
														18.5		18.2		
		(17.3)												18.8				
	18.2		18.0					18.7				(19)		19.1		19.2		
	19.2	(19.5)																
	20.1		20.0	20.47				20.0										
	21.2	21.0	20.5	20.73				20.9				(21)	22	22		21		
	22.0															22.0		
		(23)	23.5						22.0			23.5			23	23.4		
																24.5		
																	25	
	23.8—25.6	(25)	26					25						25		26.0		
	29							29		27				28.5		27.7		
																28.8	28	
	32.3											33		32	33 (p, d, t)	29.7		32
														47				

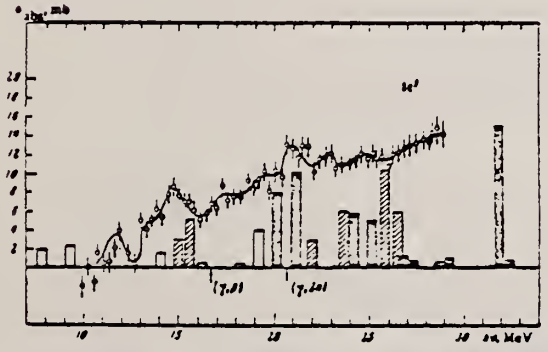

FIG. 1. Cross section for the absorption of γ quanta by Be^9 nuclei. The columns show the results of the calculation in [10].

Table II. Integral section of the photodisintegration of Be^9

Source	Reaction	E, MeV	σ_{int}, mb·MeV	Remarks	Thresholds, MeV
[5]	(γ, n)	≤25	37		(γ, n) — 1.67
[6]	(γ, n)	6.5—18	22		(γ, np) — 18.9
[8]	(γ, Tn)	1.6—57	143		(γ, 2n) — 20.56
[7]	(γ, Tn)	1.6—70	179±26		
[17]	(γ, 2n)	≤30	1.2±0.2		
[16]	(γ, 2n)	≤45	5±2		
[10]	(γ, 2n)	≤275	10		
[37]	(γ, p)	17—25	13		(γ, p) — 16.88
[34]	(γ, p)	16.9—57	41.4±4.6		(γ, d) — 16.59
[35]	(γ, p)	16.9—30	25±4		(γ, t) — 16.69
[11]	(γ, p)	17—40	14.7	From photoprotons from activity of Li^8 (Li^8)* in 2 + 3 excitations	(γ, α) — 2.53
	(γ, pn)	17—40	10.1		
	(γ, p0,1)	17—33	13.7±2.5		
	(γ, p1,2)	17—33	11.6±1.8		
	(γ, pn)	17—33	5.1±2		
	(γ, d0,1)	17—33	1.0±0.3		
	(γ, d)	17—40	4.7		
	(γ, t)	17—40	3.5		
	(γ, p) + + (γ, d) + + (γ, t)	17—40	33±3		
[18]	(γ, Tot)	20.04—21.0	1.35	γ rays from T(p, γ)	
[17]	(γ, Tot)	10—35	112±10		
[11]	(γ, Tot)	15—27	60±15		
Our data	(γ, Tot)	10—29	160±16		
Bethe-Levinger theory	(γ, Tot)	≤Threshold (γ, α)	187	with exchange-forces (racah $x = 0.5$	
[20]			276		
[21, 22]			292		

REF.

R. Garfagnini, G. Piragino, A. Zanini
Nuovo Cimento 63B, 670 (1969)

ELEM. SYM.	A	Z
Be	9	4

METHOD

REF. NO. 69 Ga 1 egf

REACTION	RESULT	EXCITATION ENERGY	SOURCE		DETECTOR		ANGLE
			TYPE	RANGE	TYPE	RANGE	
$ G,XN	SPC	2-85	C	85	CCH-D	1-14	DST

N POLARIZATION

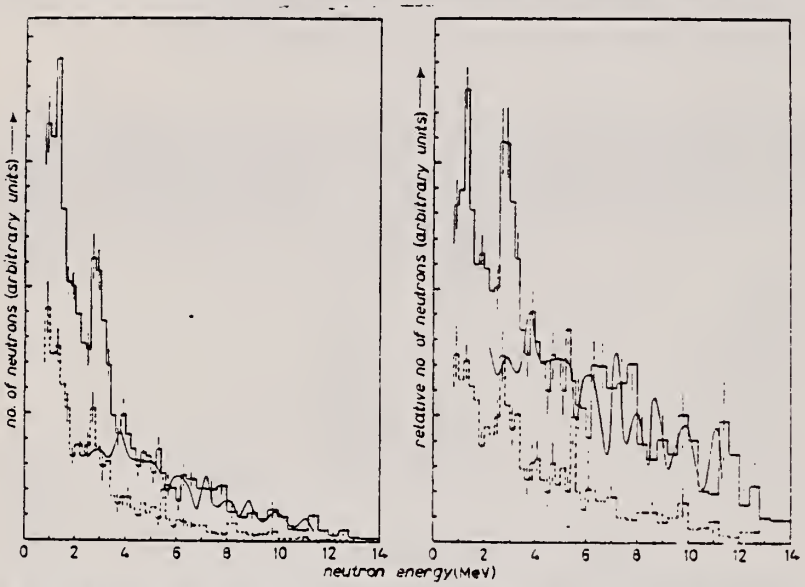

Fig. 3. – Energy spectrum of photoneutrons from ^{9}Be at 90° (full-line histogram) and at 135° (dashed-line histogram). The full-curve line represents the spectrum at 90) deduced in ref. ([11]) for $E_{\gamma_{max}} = 17$ MeV. On the right the photoneutron spectra are normalized to the respective bremsstrahlung spectra.

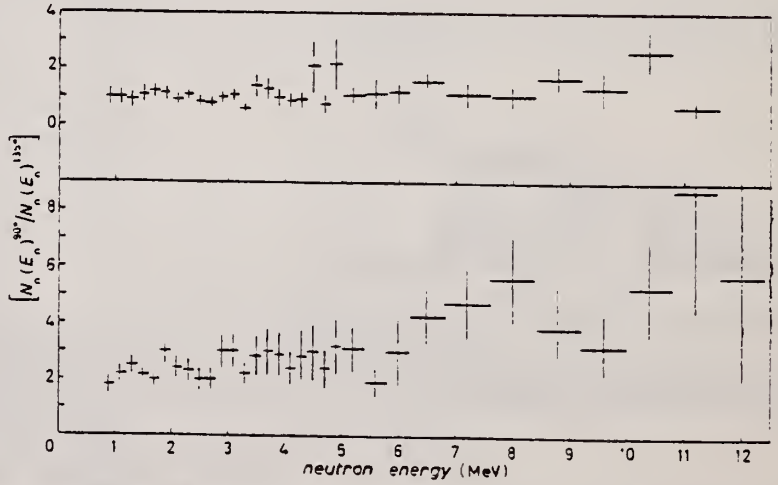

Fig. 4. – Ratio between the number of photoneutrons at 90° and that at 135° from ^{7}Li (upper part) and ^{9}Be (lower part) vs. photoneutron energy.

over

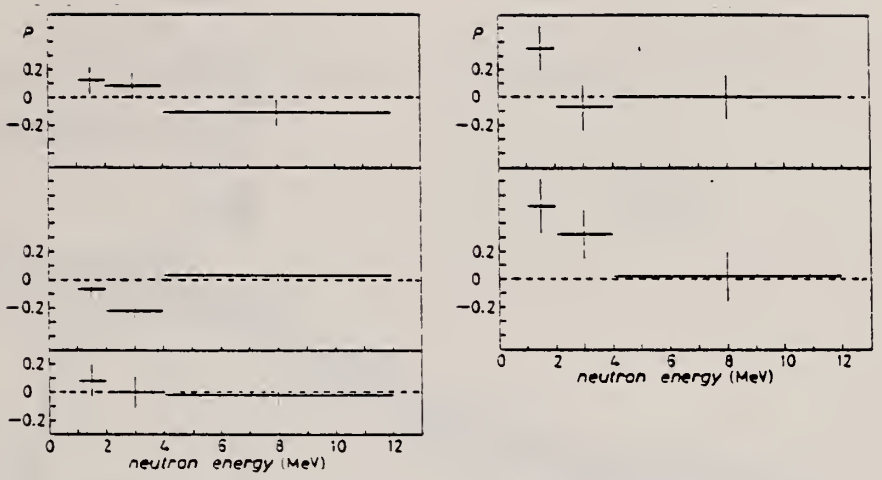

Fig. 5. – On the left is the photoneutron polarization of photoneutrons from ^{7}Li, ^{9}Be at 90° compared with the polarization of neutrons from a RaD-Be source. On the right is the polarization of photoneutrons at 135° previously measured ([7,10]). ^{7}Li, upper diagrams; ^{9}Be lower diagrams.

REF.

R. Garfagnini, G. Piragino & A. Zanini
Atti Accad. Naz. Lincei, Rend.
Cl. Sci. Fis. Mat. Natur. 47, 33 (1969)

Be	9	4

METHOD

REF. NO. 69 Ga 3 egf

REACTION	RESULT	EXCITATION ENERGY	SOURCE		DETECTOR		ANGLE
			TYPE	RANGE	TYPE	RANGE	
G,XN	SPC	3-85	C	85	CCH-D		DST

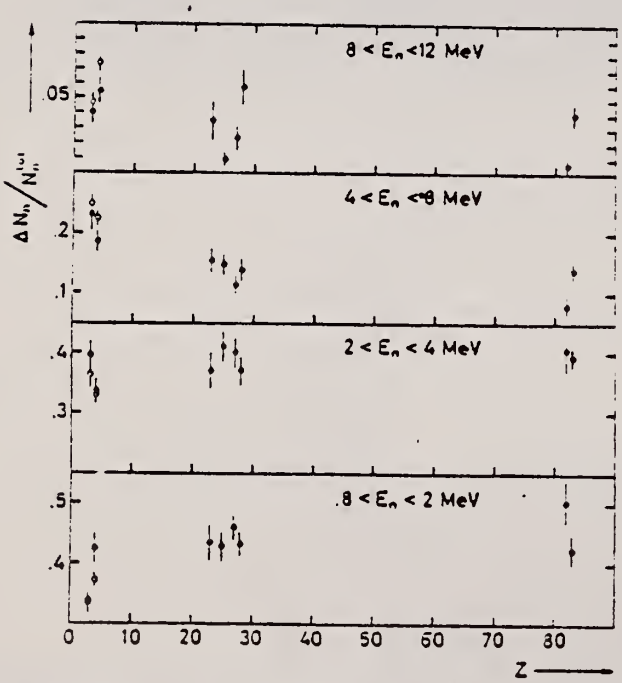

Fig. 1. – Percentage of the photoneutrons emitted at 135°, in the respective energy interval as a function of Z, by a γ-ray bremsstrahlung beam with $E_{\gamma max}$ = 85 MeV. The open circles represent the values obtained at 60° for ^{7}Li and ^{9}Be.

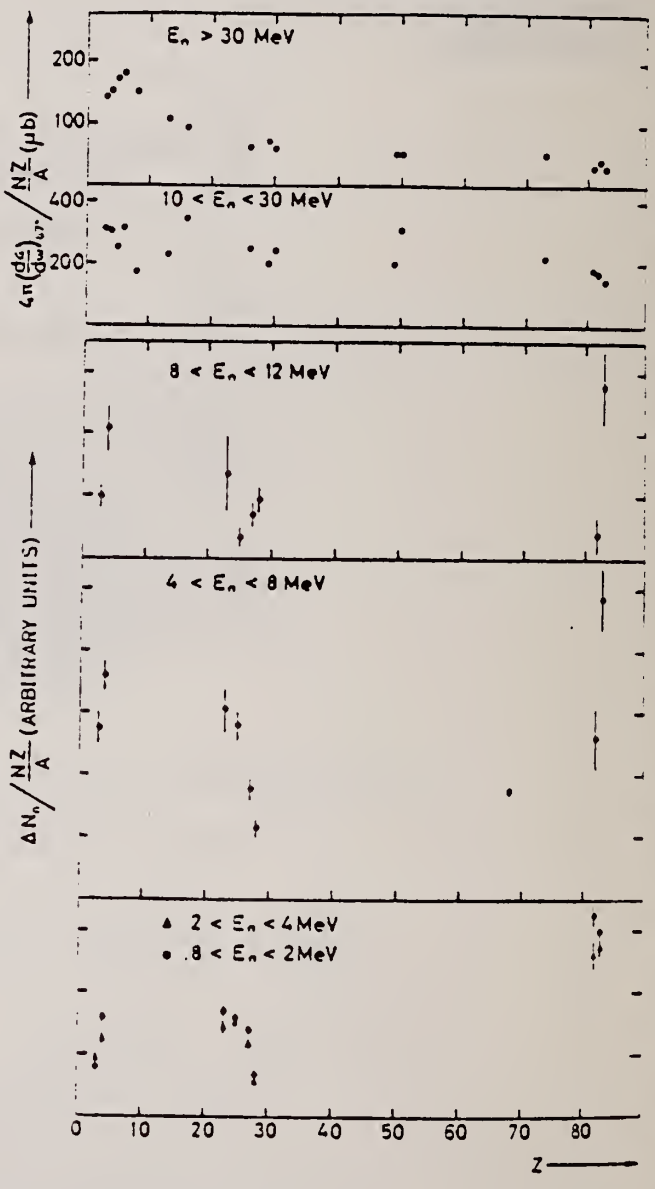

Fig. 2. – Number of photoneutrons emitted at 135°, normalized to the sum rule factor NZ/A, as a function of Z. In the upper part is reported the effective cross section divided by NZ/A for photoproduction of fast neutron by 55–85 MeV bremsstrahlung photons as deduced by Kaushal *et al.* [1]

[1] N.N. Kaushal et al., Phys. Rev. 175, 1330 (1968).

REF. J. Ahrens, H. Borchert, H.B. Eppler, H. Gimm, H. Gundrum, P. Riehn, G. Sita Ram, A. Zieger, and B. Ziegler
Elba-71, Tagungsbericht Elektronen Beschleuniger Arbeits Gruppen (Sept. 1971) Justus Liebig-Universitat Giessen. p.359

ELEM. SYM.	A	Z
Be	9	4

METHOD

REF. NO.	
71 Ah 1	hmg

REACTION	RESULT	EXCITATION ENERGY	SOURCE		DETECTOR		ANGLE
			TYPE	RANGE	TYPE	RANGE	
G,MU-T	ABX	THR-150	C	10-150	MGC-D		4PI

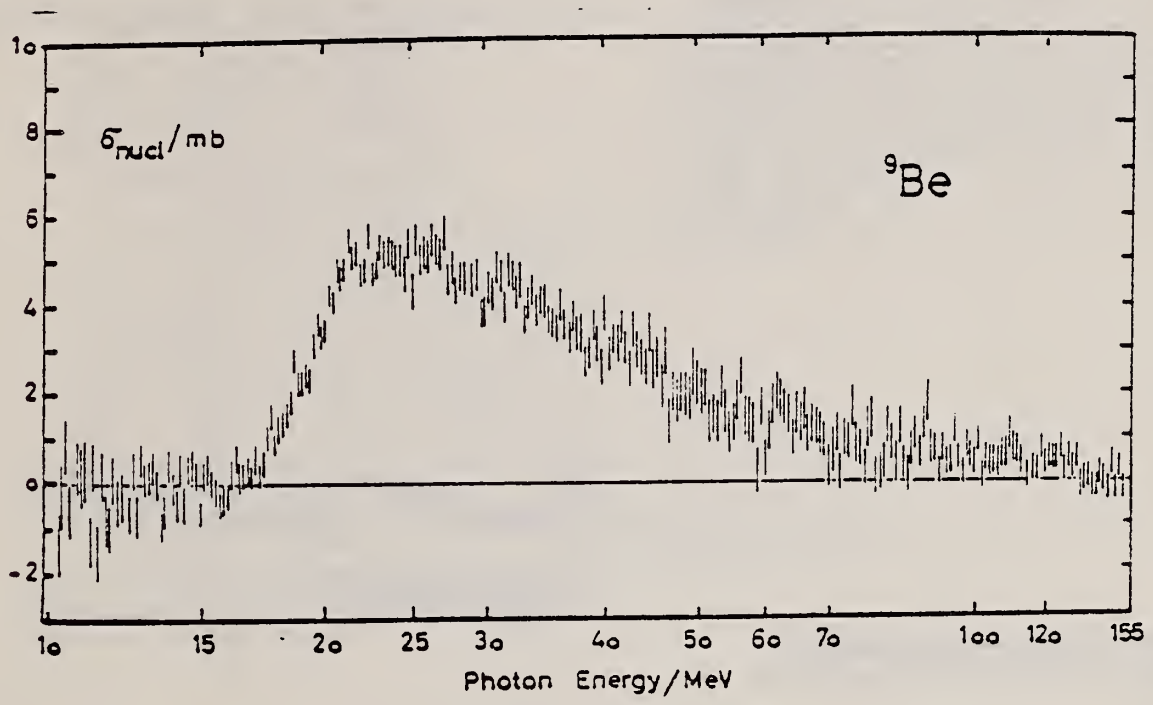

fig. 3

Yu. P. Antuf'ev, V. L. Agranovich, V. B. Ganenko, V. S. Kuz'menko, I. I. Miroshnichenko, and P. V. Sorokin
Yad. Fiz. 13, 473 (1971); Sov. J. Nucl. Phys. 13, 265 (1971)

ELEM. SYM.	A	Z
Be	9	4

METHOD

REF. NO. 71 An 1 hmg

REACTION	RESULT	EXCITATION ENERGY	SOURCE TYPE	SOURCE RANGE	DETECTOR TYPE	DETECTOR RANGE	ANGLE
G,P	SPC	51-999	C	700,999	TEL-D	25-400	DST
G,D	SPC	55-999	C	700,999	TEL-D	25-400	DST

999=1.2 GEV, REL D/P

Yield of protons 30-400 MeV, deuterons 30-200 MeV.

Table I. Values of the parameter τ, MeV

Target	E_0 = 700 MeV										E_0 = 1200 MeV					
	Protons					Deuterons					Protons			Deuterons		
	40°	60°	80°	100°	120°	40°	60°	80°	100°	120°	30°	60°	120°	30°	60°	120°
Li	46	42	34	30	27	28	24	22	21	20		45	28		27	24
Be	48	43	36	30	27	28	26	24	22	19		45	28		27	24
C	50	44	38	30	26	34	33	29	23	19	60	48	35	37	34	22
Si		43			28		27			22		46	35		28	25
Cu												45	29		27	24
Ta					28					21		45	34		27	24
Pb											51		29	36		22

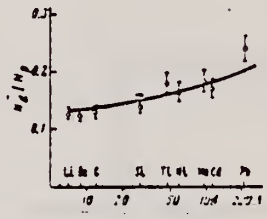

FIG. 4. The ratios N_d/N_p as a function of target-nucleus mass number A at an angle $\theta = 60°$ for E_0 = 1200 MeV. Solid curve—$A^{0.13}$.

The measured secondary-particle spectra for kinetic energies T > 80 MeV are well described by the expression

$$d^2\sigma / d\Omega dTQ = \text{const}\, T \exp(-T/\tau), \qquad (1)$$

which is identical to the formula for the evaporation process.[4] In Table I we have given the values of the parameter τ for the nuclei studied, at various angles. The accuracy in determination of τ is about 10%.

REF.

Yu. P. Antuf ev, V.L. Agranovich, V.B. Ganenko, V.S. Kuz menko, I.I. Miroshnichenko, and P.V. Sorokin
Yad. Fiz. 14, 898 (1971)
Sov. J. Nucl. Phys. 14, 502 (1972)

ELEM. SYM.	A	Z
Be	9	4

METHOD

REF. NO.	
71 An 2	hmg

REACTION	RESULT	EXCITATION ENERGY	SOURCE		DETECTOR		ANGLE
			TYPE	RANGE	TYPE	RANGE	
G,XD	ABX	107-620	C	620	MAG-D		DST

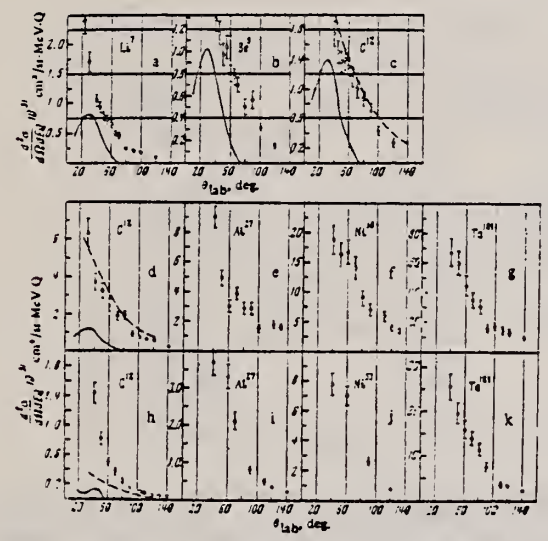

FIG. 1. Angular distributions of deuterons in (γ, d) reactions in nuclei for E_0 = 620 MeV (a–c) and E_0 = 1140 MeV (d–k). The statistical errors are shown. a–g–angular distributions of deuterons with energies of 90 MeV, h–k–with energy 160 MeV.

REF. S. Costa, L. Ferrero, L. Pasqualini, M. Sanzone
Lettere al Nuovo Cimento 1, 448 (1971)

ELEM. SYM.	A	Z
Be	9	4

METHOD

REF. NO. 71 Co 1 egf

REACTION	RESULT	EXCITATION ENERGY	SOURCE		DETECTOR		ANGLE
			TYPE	RANGE	TYPE	RANGE	
G,XP	ABY	17-90	C	50-90	TEL-D	11-40	60

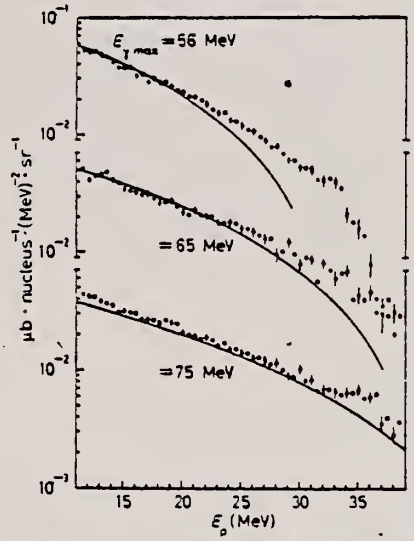

Fig. 2. – Photoproton spectra from ^{9}Be at 60° for some bremsstrahlung top energies. The curves represent the quasi-deuteron model predictions calculated as explained in the text.

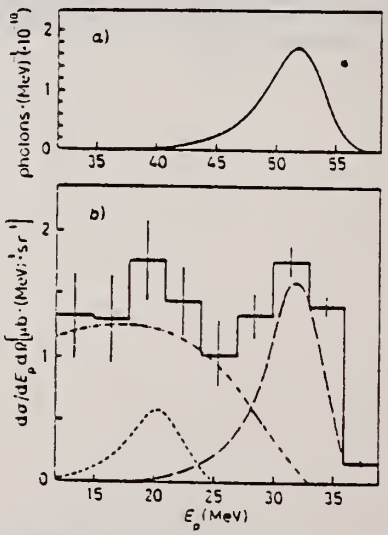

Fig. 3. – a) Photon spectrum, measured as described in the text. b) Doubly differential cross-section for the emission of photoprotons of energy E_p at 60° in the laboratory, measured with the photon spectrum shown in a). The hystogram represents the experimental data with the statistical errors given by the vertical bars: the dot-dashed line is the quasi-electron cross-section. The long-dashed (– – –) and short-dashed (– – –) lines represent the calculated shapes of the single-particle cross-sections due to the emission of 1p and 1s shell protons, respectively, supposed to have 16.5 and 29.5 MeV separation energies. The results of SHKLYAREVSKIJ (ref. [23]) have been used to perform these calculations, which, as well as the Q.D. one does, account for the actual photon spectrum used.

[23] G.M. Shklyarevskij: Zurn. Eksp. Teor. Fiz. 9, 1057 (1959).

REF.

V.I. Noga, Yu. N. Ranyuk, P.V. Sorokin, V.A. Tkachenko
Ukr. Fiz. Zh. 16, 1850 (1971)

ELEM. SYM.	A	Z
Be	9	4

METHOD

REF. NO.	
71 No 1	egf

REACTION	RESULT	EXCITATION ENERGY	SOURCE		DETECTOR		ANGLE
			TYPE	RANGE	TYPE	RANGE	
G, 2N	ABY	THR-999	C	80-999	ACT-I		4PI

999=1.2 GEV

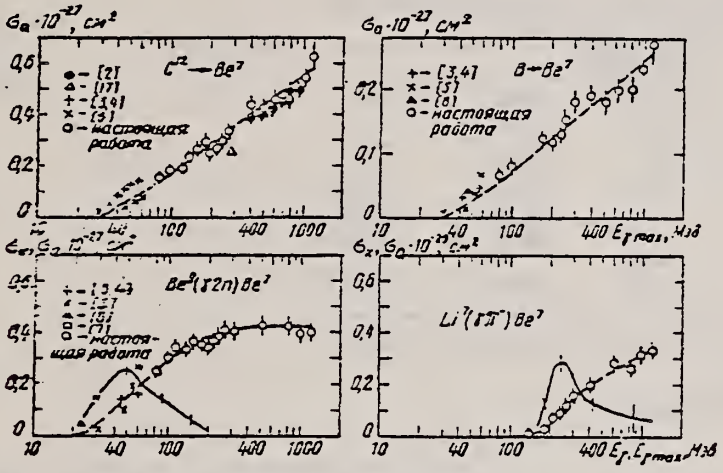

Рис. 3. Энергетическая зависимость сечений и выходов реакций: О — экспериментальные зависимости выхода от $E_{\gamma max}$; сплошная кривая — σ_k — функция возбуждения, вычисленная по способу наименьших квадратов по экспериментальным данным; пунктирная — σ_Q — выход, соответствующий функции возбуждения.

REF.

M. Schaeffer, M. Suffert, D. Magnac-Valette
Nucl. Phys. A175, 217 (1971)

ELEM. STM.	A	Z
Be	9	4

METHOD

REF. NO. 71 Sc 2 egf

REACTION	RESULT	EXCITATION ENERGY	SOURCE		DETECTOR		ANGLE
			TYPE	RANGE	TYPE	RANGE	
D,G	SPC	17	D	0	NAI-D		135

17 = 16.97 MEV
0 = .361 MEV

Tableau 1

Récapitulation de l'ensemble des résultats obtenus lors de l'étude de la désexcitation électromagnétique de l'état de 16.97 MeV vers les états inférieurs dans ^{9}Be

Résultats réf. [5])		Nos résultats				
$E_x(^9Be)$ (MeV)	ρ (%)	$E_x(^9Be)$ (MeV)	E_γ (MeV)	Γ (MeV)	surface SE_γ	ρ (%)
0	100	0	16.97	0	849995	100
1.7	8.5±4.3	1.75	15.22		97386	11.8±0.6
2.43	10.6±5.3	2.43	14.54	0	27691	3.3±0.7
		2.82	14.15	1.7	109049	13.3±4.2
3.04	≦ 4.5	3.03	13.94	0.265	0	
4.74	9.6±4.8	4.64	12.33	0.95	101330	12.9±1.3

Γ – Largeur du niveau assimilé à une Lorentzienne à l'exception du niveau à 1.75 MeV dont la forme a été tirée de la réf. [5]).
SE_γ – Surface du pic relatif à la transition vers E_γ.
ρ - Rapport des intensités γ en pourcent, toutes corrections faites.

[5] C. Gerardin, R. Seltz et D. Magnac-Valette, Nucl. Phys. A169 (1971) 521.

REF.

M. Schaeffer, A. Degre and M. Suffert
J. de Physique 32, C5B-223 (1971)

ELEM. SYM.	A	Z
Be	9	4

METHOD

REF. NO. 71 Sc 3 egf

REACTION	RESULT	EXCITATION ENERGY	SOURCE		DETECTOR		ANGLE
			TYPE	RANGE	TYPE	RANGE	
T,G	ABX	18- 20	D	1- 3	NAI-D		90

1045

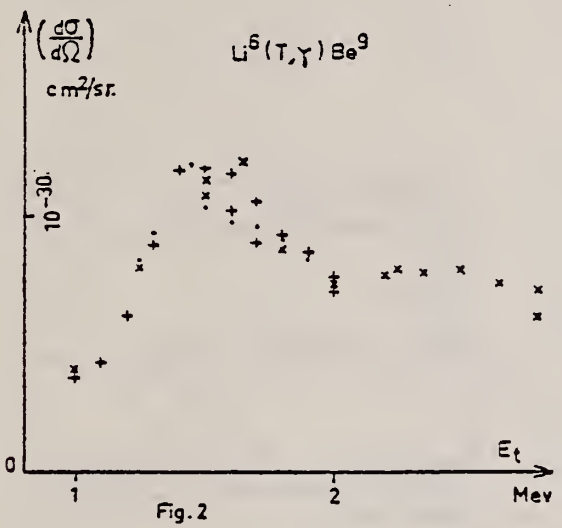

Fig. 2

REF. J. Ahrens, H. Borchert, H. B. Eppler, H. Gimm, H. Gundrum, P. Riehn, G. Sita Ram, A. Zieger, M. Kroning, B. Ziegler
Proc. International Conference on Nuclear Structure Studies Using Electron Scattering and Photoreaction, Sendai, Japan p. 213 (1972).

ELEM. SYM.	A	Z
Be	9	4

METHOD

REF. NO. 72 Ah 7 egf

REACTION	RESULT	EXCITATION ENERGY	SOURCE		DETECTOR		ANGLE
			TYPE	RANGE	TYPE	RANGE	
G,MUT	ABX	16-140	C	140	MGC-D		4PI

592

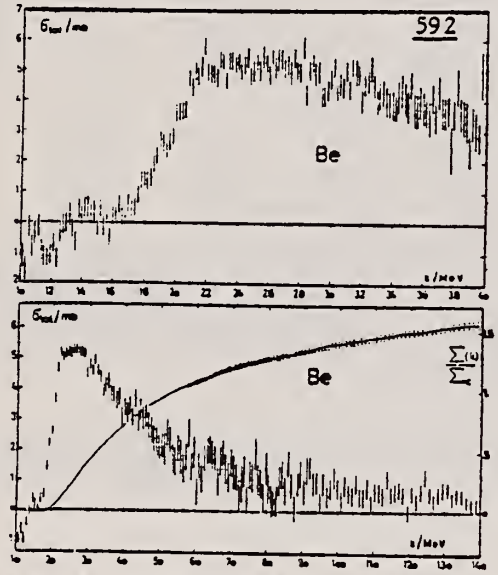

Fig. 5. Total nuclear cross-sections for Be.

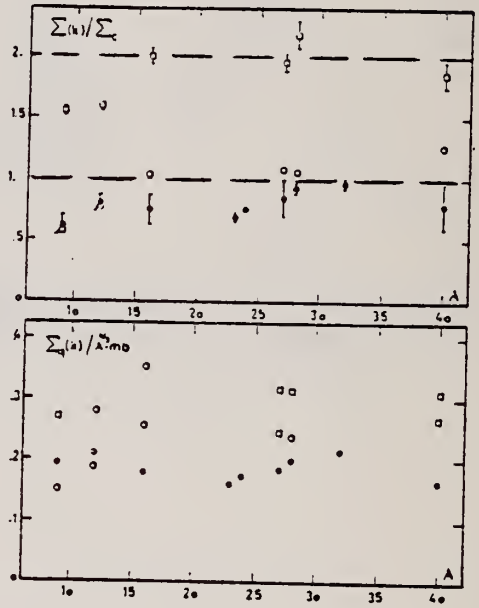

$\Sigma_c = 60\frac{NZ}{A}$, $\Sigma(k) = \int_0^k \delta(\tilde{k})\,d\tilde{k}$, $\Sigma_1(k) = \int_0^k \delta(\tilde{k})\,\frac{d\tilde{k}}{\tilde{k}}$

• NBS k=35 MeV, ○ k=35 MeV, ○ k=40 MeV

Fig.11 Integrated cross-sections

REF. D. Hiramatsu, T. Kamae, H. Muramatsu, K. Nakamura, N. Izutsu, and Y. Watase
PICNS-72, p.429 Sendai (see 73 Hi 5)

ELEM. SYM.	A	Z
Be	9	4

METHOD

REF. NO. 72 Hi 8 hvm

REACTION	RESULT	EXCITATION ENERGY	SOURCE TYPE	SOURCE RANGE	DETECTOR TYPE	DETECTOR RANGE	ANGLE
E,E/P	NOX	10*35	D	700	MAG-D		DST

* SEP ENERGY RANGE

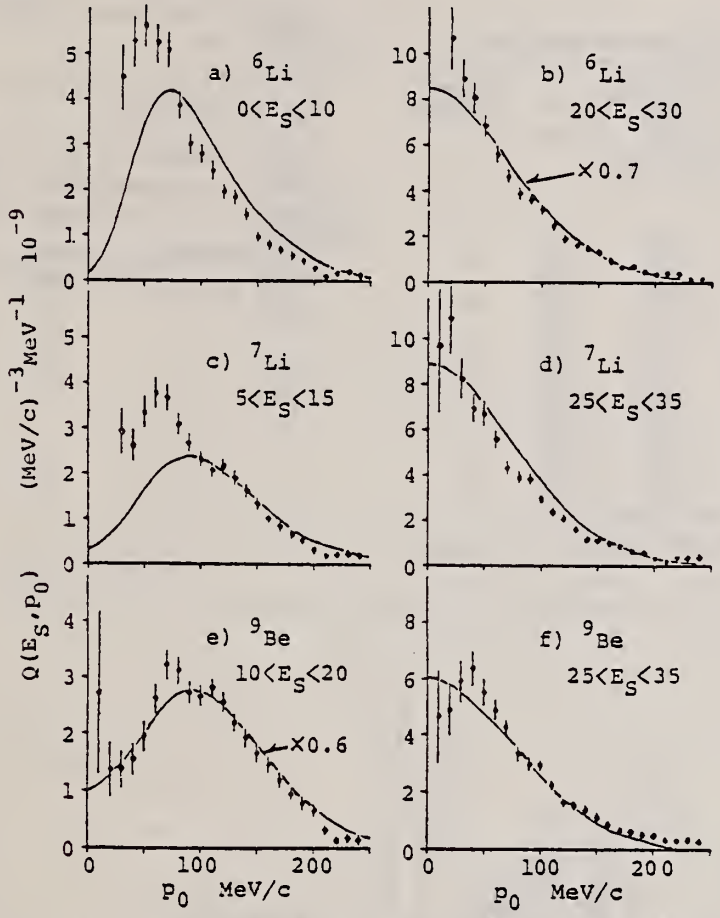

Fig. 4. Momentum distributions for ^{6}Li, ^{7}Li, and ^{9}Be the 1p state.

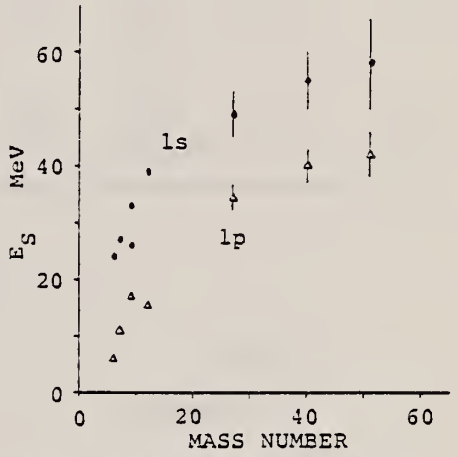

Fig. 6. The separation energy of 1s and 1p states as a function of the mass number.

REF.

B.W. Thomas, D.M. Crawford and H. H. Thies
Nucl. Phys. A196, 89 (1972)

ELEM. SYM.		
Be	9	4

METHOD

REF. NO. 72 Th 2 egf

REACTION	RESULT	EXCITATION ENERGY	SOURCE		DETECTOR		ANGLE
			TYPE	RANGE	TYPE	RANGE	
G,XN	ABX	6-28	C	7-28	BF3-I		4PI

S41

TABLE 2

Comparison between theoretical and experimental data on photo-excitation of ^{9}Be

J	P	Ref. [1] E_γ (MeV)	Ref. [1] $\int \sigma dE$ level (MeV · mb)	Ref. [1] Γ (MeV)	Present exp. E_γ (MeV)	Present exp. $\int \sigma dE$ level (MeV · mb)	Present exp. Γ (MeV)	Apparent correlation
1/2	2	6.30	3.38	2.73				
1/2	2	6.63	1.04	1.03	6.66	2.94	1.00	×
3/2	2	7.33	0.89	1.44	7.40	0.59	0.40	×
					8.48	1.06	0.70	
3/2	3	9.57	0.02	4.46	9.45	1.22	0.60	×
					10.10	0.72	0.37	
1/2	3	10.65	3.66	4.11	10.76	1.03	0.30	×
1/2	3	11.53	1.22	4.55	11.20	0.84	0.37	×
					12.18	1.80	0.60	
					13.20	0.90	0.40	
					14.12	1.78	0.60	
5/2	4	15.10	0.64	7.24	15.10	0.91	0.40	×
3/2	4	15.17	0.61	7.71	15.87	0.75	0.30	×
			sum = 11.46			sum = 14.54		

[1] F.C. Barker, Nucl. Phys. 28 (1961) 96.

[6] G. J. Vanpraet et al. Z. Phys. 211 (1968) 213.

[12] A. S. Penfold et al., Analysis of photo cross sections. Phys. Res. Lab., U. of Illinois, 1958,

[21] F. Ajzenberg-selove et al. Nucl. Phys. A116 (1968) 481.

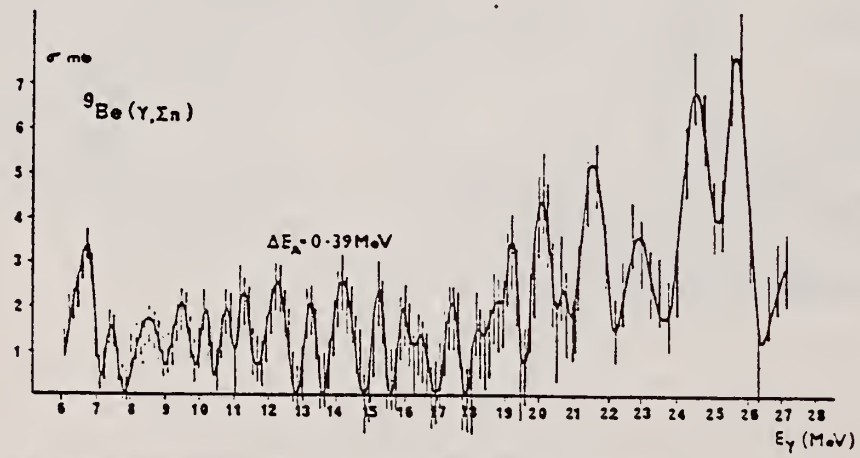

Fig. 2. Photoneutron production cross section in ^{9}Be, deduced from bremsstrahlung yield data on ^{9}Be(γ, Σn) using a Leiss-Penfold analysis [12]). Analysis bin width ΔE_A = 0.39 MeV; 3 sets of data interlaced. Cross sections were smoothed by treating unsmoothed Leiss-Penfold data using as resolution-function formula: $\sigma(E_i) = 0.15\,\sigma(E_{i-1}) + 0.70\,\sigma(E_i) + 0.15\,\sigma(E_{i+1})$.

(over)

TABLE 1

Information from experiments on excited states in ^{9}Be

Energy (MeV)			Relative strength		Apparent correlation
(a) present exp. (±0.02 MeV)	(b) ref. [6]) (±0.2 MeV)	(c) ref. [21])	present exp. (%)	ref. [6]) (%)	
6.66	6.8	6.66 ($\frac{7}{2}^-$) $\frac{1}{2}$	6.4	2.3	a, b, c
7.40			1.3		
	8.0	7.94		6.6	b, c
8.48			2.3		
	9.10			5.9	
9.45			2.7		
10.10	10.2		1.6	4.7	a, b
10.76			2.7		
11.20		11.28±0.05	1.9		a, c
	11.8	11.81		7.7	b, c
12.18			3.8		
13.20	13.2		2.0	1.7	a, b
		13.78			
14.12	14.2		3.9	7.4	a, b
		14.38			
		14.392 ($\frac{5}{2}^-$) $\frac{3}{2}$			
15.10			2.0		
15.87			1.6		
	16.3			6.2	possibly a, b
16.46			1.4		
		16.674			
	16.9	16.973 $T = \frac{3}{2}$		5.2	b, c
17.30		17.28 ($\frac{1}{2}^-$)	2.0		a, c
		17.48 $\leq \frac{7}{2}^+$			
18.10		18.1	1.1		a, c
18.60	18.5	18.6	1.8	8.1	a, b, c
19.06		18.94	3.4		(a, c)
		19.6			
19.98			5.8		
20.49		20.5	2.0		a, c possibly
	20.7	20.7		11.7	b, c a, b, c
		21.1			
21.68	21.6		10.0	8.0	a, b
	22.5	22.4		8.2	b, c
23.02			7.4		
	23.5			3.4	
		23.9			
24.58	24.5		16.3	4.7	a, b
25.62	25.7		14.2	8.0	a, b

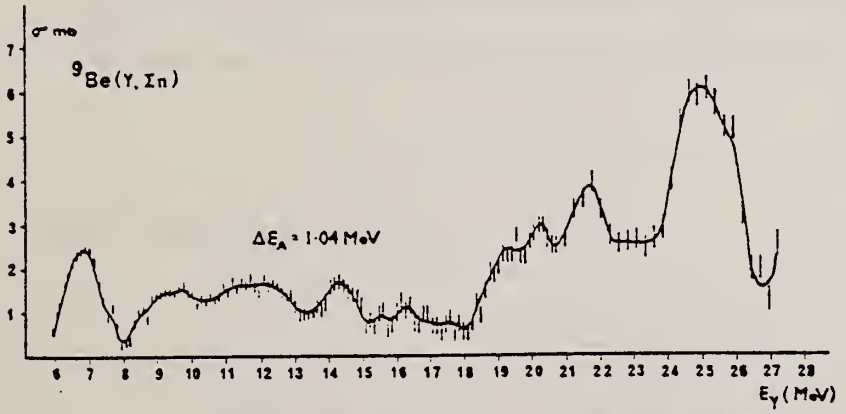

Fig. 4. Same as fig. 2. Analysis bin width ΔE_A = 1.04 MeV; 8 sets of data interlaced.

REF. J. Ahrens, H.B. Eppler, H. Gimm, H. Gundrum, M. Kroning, P. Riehn, G. SitaRam, A. Zieger, and B. Ziegler
PICNS-73, Vol.I, p.23 Asilomar

ELEM. SYM.	A	Z
Be	9	4

METHOD

REF. NO. 73 Ah 4 - hmg

REACTION	RESULT	EXCITATION ENERGY	SOURCE		DETECTOR		ANGLE
			TYPE	RANGE	TYPE	RANGE	
G,MU-T	ABX	10-140	C	140	MGC-D		4PI

Statistics may have been improved over those of 72Ah7.

See figure on other side.

(OVER)

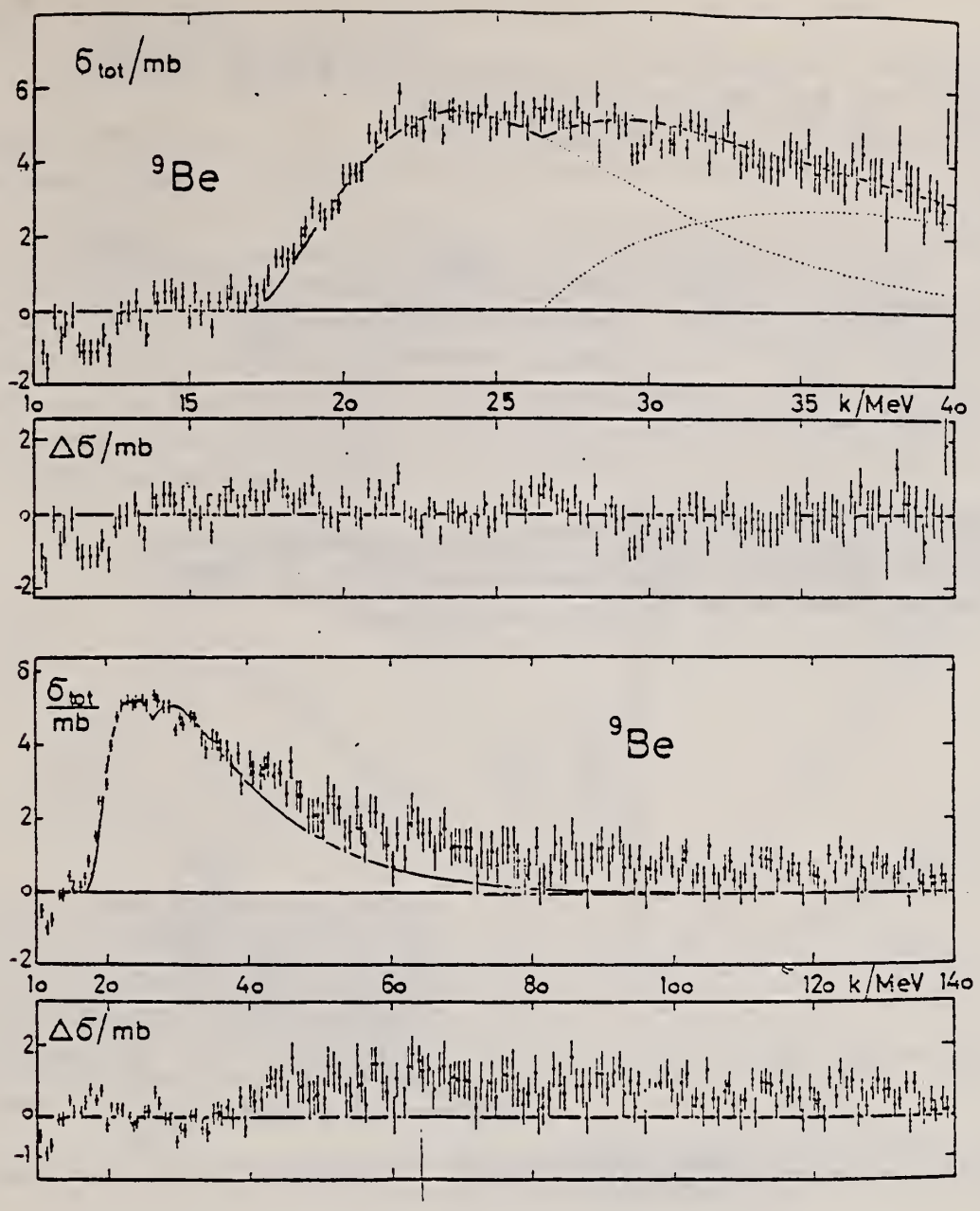

Fig. 3. Same as Fig. 2 for Be

REF.

G.P. Antropov, V.A. Vakhlamov, I.E. Mitrofanov, V.S. Russkikh
Izv. Akad. Nauk SSSR. Ser. Fiz. 37, 2657 (1973)
Bull. Acad. Sci. USSR, Phys. Ser. 37, 172 (1974)

ELEM. SYM.	A	Z
Be	9	4

METHOD

REF. NO. 73 An 16 hmg

REACTION	RESULT	EXCITATION ENERGY	SOURCE		DETECTOR		ANGLE
			TYPE	RANGE	TYPE	RANGE	
G,N	ABX	1- 17	C	1- 17	BF3-I		4PI

The cross section of the ^{9}Be photoneutron reaction has been measured from the threshold to 15.5 MeV in the bremsstrahlung beam of a betatron. The energy dependence of the cross section has a complicated resonance structure. Possible values of the spin and parity of the ^{9}Be levels are discussed.

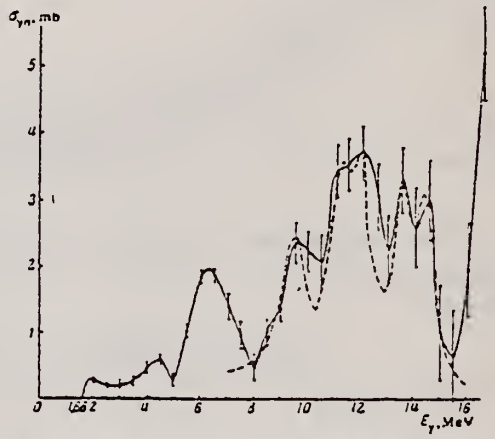

Cross section for the (γn) reaction of ^{9}Be. The dashed curve is calculated (see the text).

Table 1

E, MeV	8.3	9.5	11.2	12.0	13.5	14.5
Γ, MeV	1,75	1,01	0,9	1	0,7	1
Γ_γ (E1, M1), eV	35	52	73	116	78	154
($I_{max} = 3/2$)						
Γ_γ (E2), eV ($I_{max} = 7/2$)	28	38	54	86	58	115
$\Gamma_{\gamma n}$ (E1), eV	116	400	655	905	1146	1301
$\Gamma_{\gamma n}$ (E2), eV	0,022	0,17	0,40	0,56	1,01	1,39
$\Gamma_{\gamma n}$ (M1), eV	5	18	30	36	52	63
(Γ_γ (E1), eV) / E^3, MeV	1,14	0,061	0,052	0,067	0,032	0,052

REF. J.C. Bergstrom, I.P. Auer, M. Ahmad, F.J. Kline, J.H. Hough H.S. Caplan and J.L. Groh
Phys. Rev. C7, 2228 (1973)

EL.EM. SYM.	A	Z
Be	9	4

METHOD

REF. NO. 73 Be 4 hmg

REACTION	RESULT	EXCITATION ENERGY	SOURCE TYPE	SOURCE RANGE	DETECTOR TYPE	DETECTOR RANGE	ANGLE
E,E/	FMF	14- 18	D	62-122	MAG-D		DST

5 LEVELS

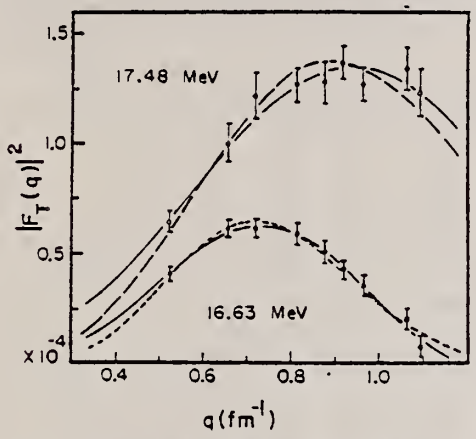

FIG. 4. Transverse form factors for the 16.63- and 17.48-MeV levels. The solid curve through the 16.63-MeV data represents the generalized Helm model fit for an $M1$ transition, and the short-dashed curve is the $E2$ (spin-flip) fit, which is slightly poorer. The $E1$ and $M2$ fits to the 16.63-MeV data are nearly indistinguishable from the solid curve. The solid curve through the 17.48-MeV data represents an $M1$ fit, while the long-dashed curve represents $E1$ and $M2$ fits, which are nearly identical.

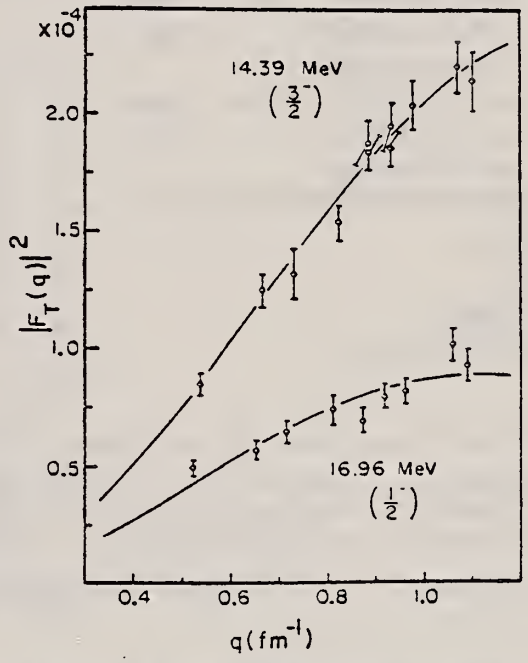

FIG. 3. Transverse form factors for the $T=\frac{3}{2}$ levels in ^{9}Be. The solid lines represent generalized Helm model fits for $M1$ transitions.

TABLE I. Transverse form factors for levels in ^{9}Be as measured in the present experiment.

q (fm^{-1})	14.39 $\lvert F_T(q)\rvert^2\times10^5$	q (fm^{-1})	E_x (MeV) 16.63	16.96 $\lvert F_T(q)\rvert^2\times10^5$	17.48
0.53	8.51 ± 0.5	0.52	4.06 ± 0.28	4.93 ± 0.32	6.40 ± 0.47
0.66	12.5 ± 0.7	0.65	6.12 ± 0.40	5.71 ± 0.42	9.99 ± 0.86
0.73	13.2 ± 1.1	0.72	6.12 ± 0.41	6.49 ± 0.45	12.2 ± 1.1
0.82	15.4 ± 0.8	0.81	5.84 ± 0.48	7.42 ± 0.64	12.7 ± 0.8
0.89	18.4 ± 0.8	0.87	5.04 ± 0.49	6.97 ± 0.53	12.8 ± 1.0
0.89	18.8 ± 1.0	0.92	4.26 ± 0.42	8.00 ± 0.50	13.7 ± 0.8
0.93	18.6 ± 0.8	0.96	3.50 ± 0.43	8.23 ± 0.53	12.7 ± 0.8
0.93	19.5 ± 1.1	1.06	2.03 ± 0.48	10.22 ± 0.68	13.4 ± 1.0
0.97	20.4 ± 0.9	1.09	0.78 ± 0.46	9.32 ± 0.69	12.3 ± 1.1
1.07	22.1 ± 1.1				
1.10	21.5 ± 1.3				

(over)

TABLE II. Summary of ground-state radiation widths from the present experiment and other work. The statistical factor g is defined by $g = (2J_0+1)/(2J+1)$, with $J_0 = \frac{1}{2}$. Γ_w is the single-particle Weisskopf unit.

E_x (MeV)	J^π		Γ_{γ_0} (eV) Experiment	Theory[a]	$\Gamma_{\gamma_0}/\Gamma_w$
14.39	$\frac{1}{2}^-$	($M1$)	6.2 ± 0.6[b]	5.3	
			8.1 ± 0.8[c]		
			6.7 ± 1.4[d]		
			6.9 ± 0.5[e]		0.11
16.96	$\frac{1}{2}^-$	($M1$)	11.5 ± 1.4[b]	15	0.11
			8.6 ± 0.9[c]		
16.63	$\leq\frac{3}{2}^-$	($M1$)	$(2.0 \pm 0.5)\,g$[b]	2.4[f]	$0.021\,g$
	$\leq\frac{1}{2}^+$	($M2$)	$(0.26 \pm 0.02)\,g$[b]		$3.2\,g$
		($M2$)	$(0.32 \pm 0.08)\,g$[c]		
(17.28	$\leq\frac{3}{2}^-$	($M1$)	$(7.3 \pm 1.3)\,g$[b]	0.92[g]	$0.065\,g$
17.48)	$\leq\frac{1}{2}^+$	($M2$)	$(0.40 \pm 0.03)\,g$[b]		$3.8\,g$
		($M2$)	$(0.42 \pm 0.10)\,g$[c]		

[a] Reference 1.
[b] Present results.
[c] Reference 5.
[d] Reference 8.
[e] Weighted average.
[f] $JT = \frac{1}{2}\,\frac{1}{2}$ (15.3 MeV).
[g] $\frac{5}{2}\,\frac{1}{2}$ (17.6 MeV) + $\frac{1}{2}\,\frac{1}{2}$ (17.9 MeV).

[1] F. C. Barker, Nucl. Phys. 83, 418 (1966).

[5] H. G. Clerc, K. J. Wetzel, and E. Spamer, Phys. Letters 20, 667 (1966); H. Theissen, Institute for Nuclear Physics, Darmstadt Report, 1972 (unpublished).

[8] I. C. Nascimento, I. D. Goldman, C. F. Wong, and H. S. Caplan, unpublished.

REF. P. Dougan and W. Stiefler
Z. Physik 265, 1 (1973)

ELEM. SYM.	A	Z
Be	9	4

METHOD

REF. NO. 73 Do 9 egf

REACTION	RESULT	EXCITATION ENERGY	SOURCE TYPE	SOURCE RANGE	DETECTOR TYPE	DETECTOR RANGE	ANGLE
G,XP	ABY	97-400	C	400	TEL-D		DST

Table 3. Beryllium. Bremsstrahlung endpoint energy: 400 MeV. Differential cross-sections in microbarns/sterrad · MeV · eq. quantum. Quoted errors: statistical in percent

Energy	Angle								
	14	22	30	40	50	60	74	90	110
89.4		2.26 2.0	1.79 1.8	1.40 1.7	1.03 1.7	0.832 2.0	0.629 2.1	0.458 1.9	0.333 2.5
106.3		1.88 2.4	1.47 2.2	1.05 2.2	0.792 2.1	0.664 2.4	0.528 2.6	0.359 2.3	0.244 3.2
109.3	1.84 2.3	1.62 2.3	1.35 2.4	0.946 2.3	0.744 2.6	0.612 2.4	0.509 2.1	0.337 2.1	0.219 2.8
122.5		1.28 2.9	0.979 2.6	0.773 2.5	0.563 2.5	0.494 2.8	0.369 3.0	0.253 2.7	0.137 4.2
131.4	1.21 2.9	1.05 3.0	0.844 3.1	0.666 2.9	0.549 3.2	0.443 3.0	0.340 2.7	0.208 2.8	0.107 4.2
152.3	0.876 3.5	0.622 3.9	0.530 4.0	0.464 3.5	0.372 3.9	0.293 3.7	0.219 3.4	0.111 3.9	0.0482 6.3
174.2	0.544 2.9	0.453 2.6	0.386 2.6	0.347 2.3	0.275 2.3	0.217 2.6	0.129 2.7	0.0610 4.7	
190.9	0.386 3.6	0.331 3.2	0.295 3.1	0.270 2.8	0.190 2.9	0.147 3.3	0.0750 3.7	0.0315 6.9	
207.5	0.264 4.3	0.215 3.9	0.222 3.6	0.181 3.4	0.131 3.5	0.0953 4.0	0.0344 5.4	0.0113 11.3	
226.1	0.257 4.4	0.201 3.7	0.183 4.4	0.132 4.1	0.0969 4.8	0.0485 6.5	0.0219 9.4	0.00692 14.9	0.0015 17.8
242.3	0.162 5.8	0.141 4.6	0.128 5.5	0.0850 5.3	0.0600 6.3	0.0259 9.2	0.00715 37.1		
253.7	0.121 6.4	0.107 4.2	0.0857 4.8	0.0542 6.1	0.0306 7.4				
258.5	0.113 6.8	0.102 5.3	0.0757 7.0	0.0428 7.4	0.0275 9.2	0.0111 13.9	0.00387 22.9		
268.8	0.0747 8.5	0.0560 5.9	0.0600 5.9	0.0287 8.6	0.0126 11.9				
284.5	0.0457 11.0	0.0434 6.8	0.0254 9.2	0.0136 12.7	0.00513 18.9				

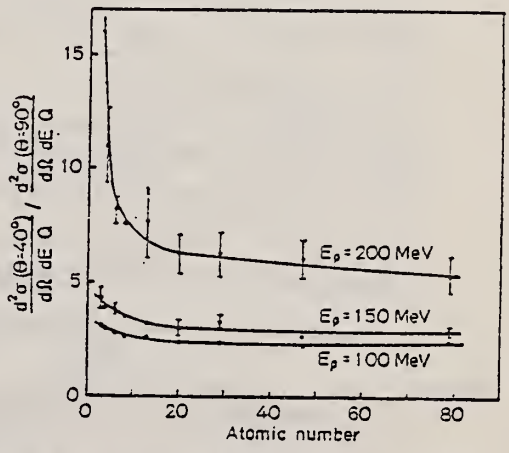

Fig. 6. The ratios of the experimental cross-sections at 40 and 90 degrees for selected proton energies as a function of atomic number

(over)

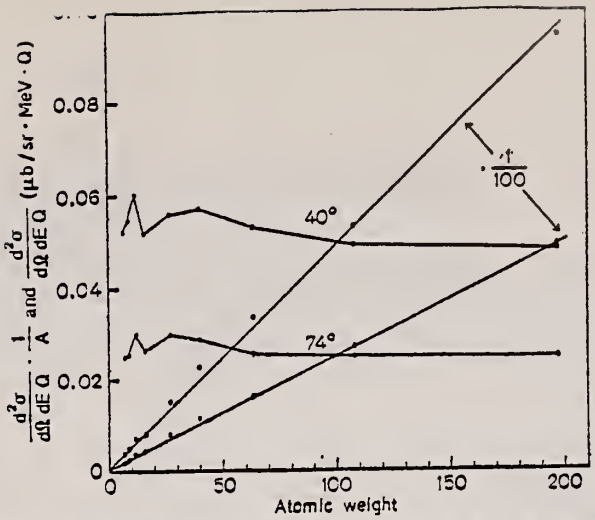

Fig. 9. In this figure, the straight lines show the experimental cross-sections at 40° and 74° for $E_p = 150$ MeV. The other curves are the same cross-sections divided by atomic weight

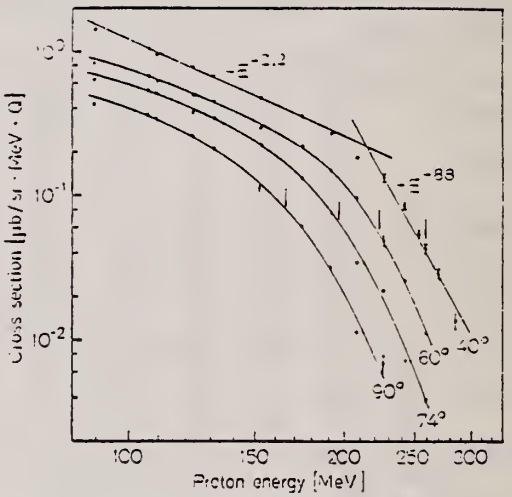

Fig. 7. Log-log plot of the energy distributions at selected laboratory angles for beryllium irradiated with bremsstrahlung of 400 MeV maximum energy. The vertical lines indicate the position of the kinematical cut-off in the proton spectrum from deuteron photodisintegration. A typical result obtained by fitting two straight lines to experimental data at 40° laboratory is shown

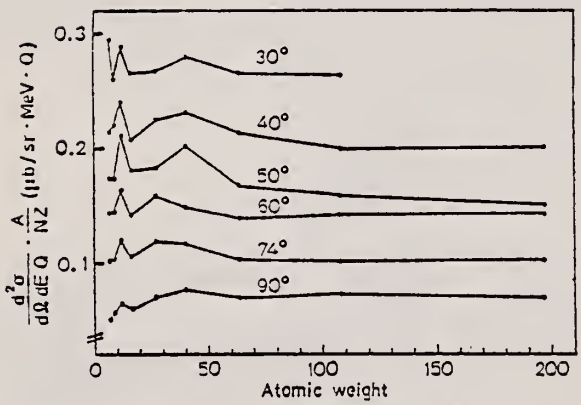

Fig. 8. Experimental cross-sections at various angles for $E_p = 150$ MeV divided by NZ/A plotted as a function of atomic weight

REF. H. Hiramatsu, T. Kamae, H. Muramatsu, K. Nakamura, N. Izutsu, and Y. Watase
Phys. Letters 44B, 50 (1973)

ELEM. SYM.	A	Z
Be	9	4

METHOD

REF. NO. 73 Hi 5 egf

REACTION	RESULT	EXCITATION ENERGY	SOURCE TYPE	SOURCE RANGE	DETECTOR TYPE	DETECTOR RANGE	ANGLE
E,E/P	SPC	0*70	D	700	MAG-D		UKN

*SEP ENERGY RANGE

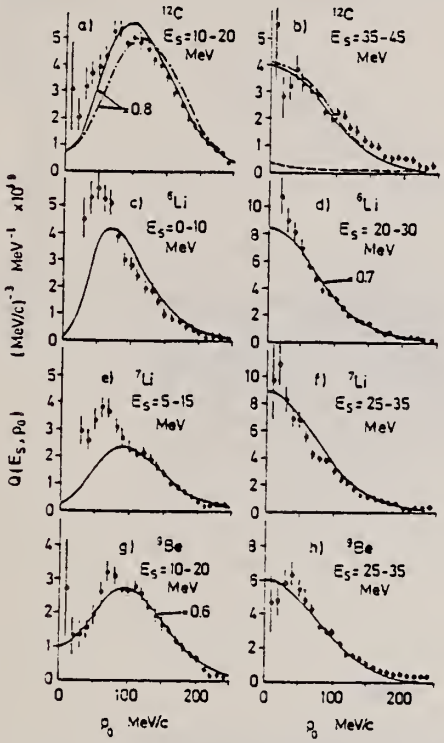

Fig. 2. Proton momentum distributions. See fig. 1 for the meaning of the curves in a) and b).

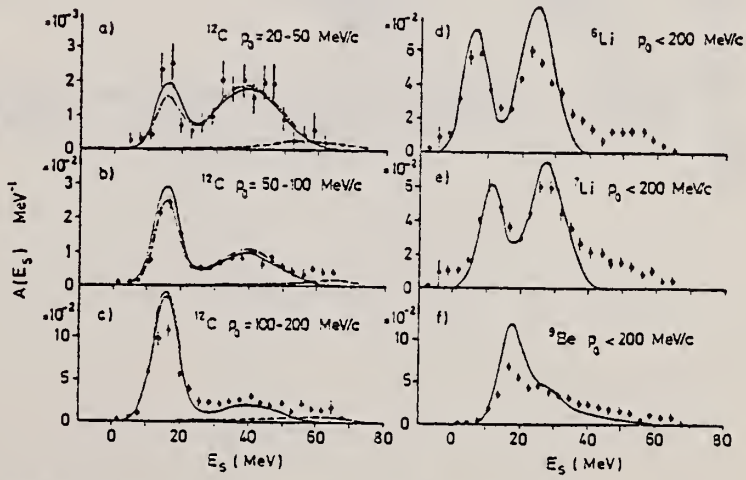

Fig. 1. Separation energy spectra. The solid curves show the DWIA results with the Woods-Saxon potentials. In a), b) and c) the dot-dashed curves represent the DWIA calculation with the harmonic oscillator potential given in ref. [5], and the dashed curves show the multiple collision background calculated by the Monte Carlo method.

[5] C. Ciofi degli Atti, Nucl. Phys. A166 (1968) 215.

REF. R.J. Hughes, R.H. Sambell and B.M. Spicer
PICNS-73, Vol.I, p.151 Asilomar

ELEM. SYM.	A	Z
Be	9	4

METHOD

REF. NO. 73 Hu 11 hmg

REACTION	RESULT	EXCITATION ENERGY	SOURCE		DETECTOR		ANGLE
			TYPE	RANGE	TYPE	RANGE	
G,XN	ABX	1- 28	C	1- 28	MOD-I		4PI

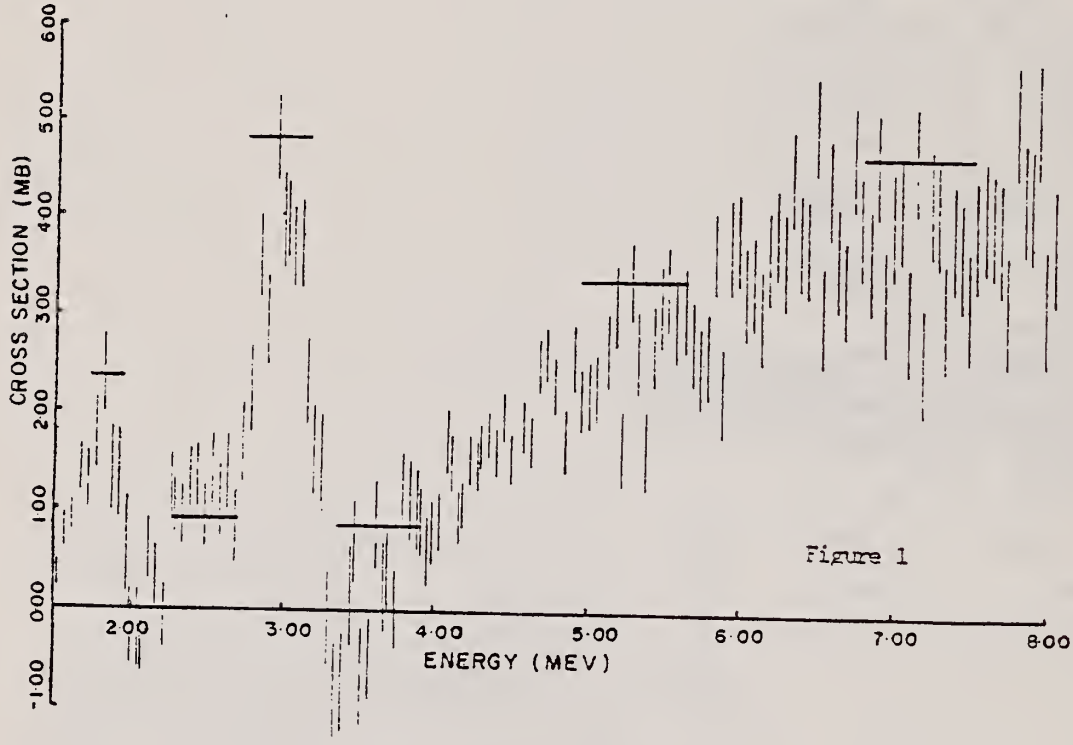

Figure 1

(over)

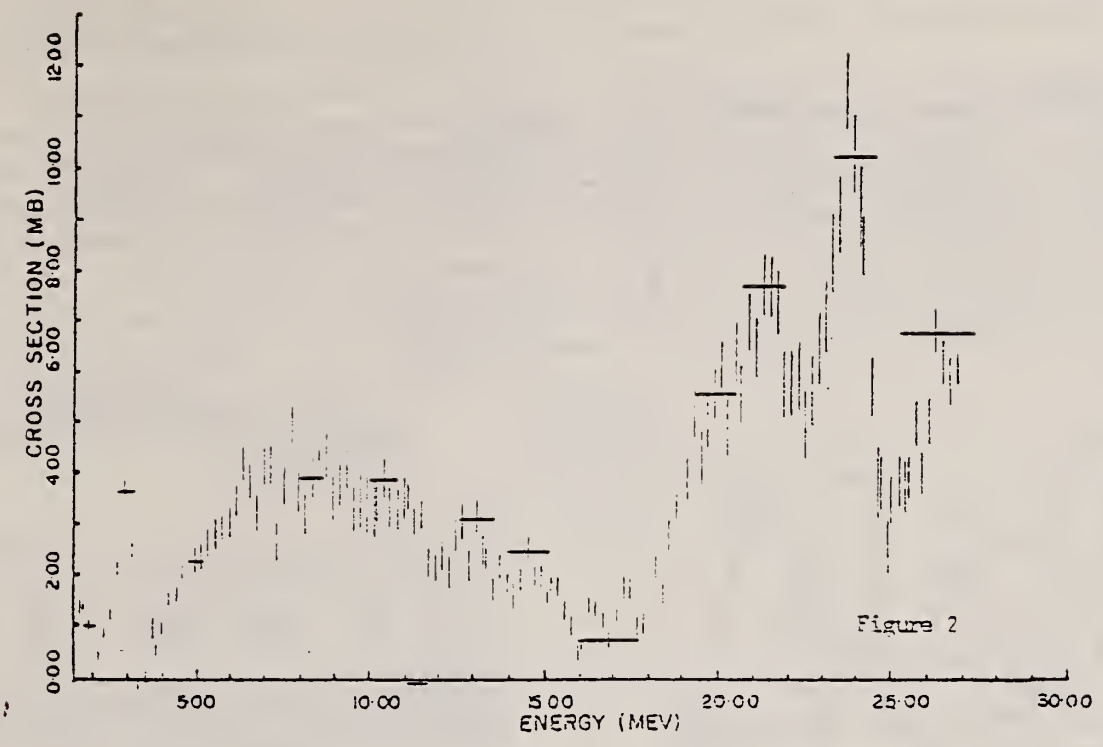
CROSS SECTION (MB)
000
200
400
600
800
1000
1200
5·00
10·00
15·00
20·00
25·00
30·00
ENERGY (MEV)

Figure 2

REF. E.L. Kuplennikov, N.G. Afanas'ev, V.A. Gol'dshtein, V.I. Ogurtsov, and V.G. Vlasenko
Yad. Fiz. 18, 20 (1973)
Sov. J. Nucl. Phys. 18, 10 (1974)

ELEM. SYM.	A	Z
Be	9	4

METHOD

REF. NO. 73 Ku 7 - hmg

REACTION	RESULT	EXCITATION ENERGY	SOURCE TYPE	SOURCE RANGE	DETECTOR TYPE	DETECTOR RANGE	ANGLE
E,E/	ABX	84-284	D	1*	MAG-D		DST

10

* 1=1.184 MEV

H. Überall, Electron Scattering from Complex Nuclei, Academic Press, New York, 1971.

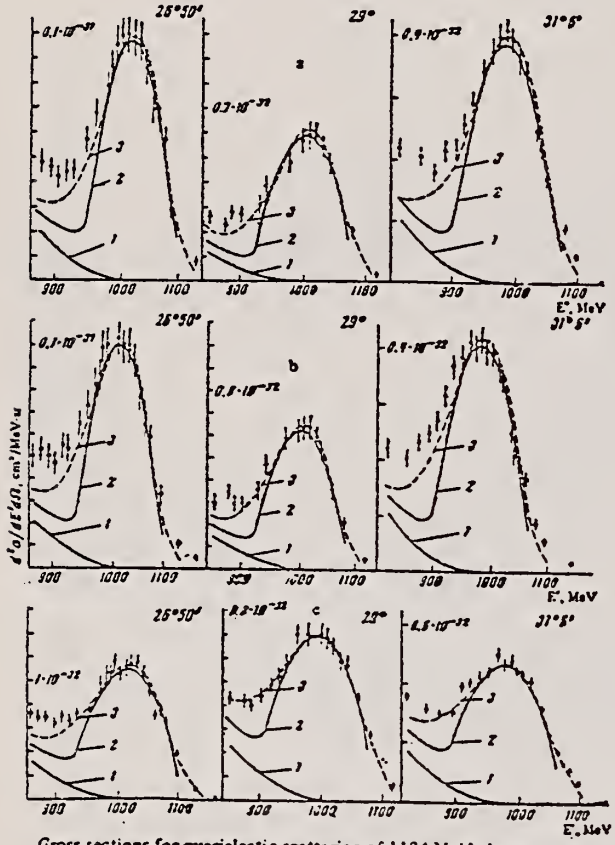

Cross sections for quasielastic scattering of 1184-MeV electrons on Li^6 (a), Li^7 (b), and Be^9 (c) vs energy E' of electrons scattered at 26°50', 29°, and 31°6'. The curves 1, 2, 3 represent calculations based, respectively, on allowance for the pion contribution, on the Fermi gas model, and on the single-particle shell model.

Nucleus	P_0, MeV/c	$\langle r^2\rangle^{1/2}_{qu.elast}$, F	$\langle r^2\rangle^{1/2}_{elast}$, F	P_F, MeV/c	$\bar{\varepsilon}$, MeV
Li^6	115±4	2.46±0.09	2.54±0.05	157±6	13±3
Li^7	116±4	2.43±0.09	2.37±0.03	160±6	14±3
Be^9	126±5	2.35±0.09	2.43±0.08	180±8	18±3

Remark. P is the oscillator parameter, $\langle r^2\rangle^{1/2}_{qu.elast}$ is the rms charge radius of the nucleus, P_F is the Fermi momentum, $\bar{\varepsilon}$ is the mean nucleon binding energy for $q \gtrsim 300$ MeV/c; all these experimental values were obtained for quasielastic electron scattering on the light nuclei Li^6, Li^7, and Be^9; $\langle r^2\rangle^{1/2}_{elast}$ is the experiment rms radius derived from elastic electron scattering on the same nuclei. [10]

REF. A. G. Slight, T. E. Drake and G. R. Bishop
Nucl. Phys. A208, 157 (1973)

ELEM. SYM.	A	Z
Be	9	4

METHOD

REF. NO. 73 S1 6 egf

REACTION	RESULT	EXCITATION ENERGY	SOURCE TYPE	SOURCE RANGE	DETECTOR TYPE	DETECTOR RANGE	ANGLE
E,E/	FMF	1- 10	D	60- 106	MAG-D		DST

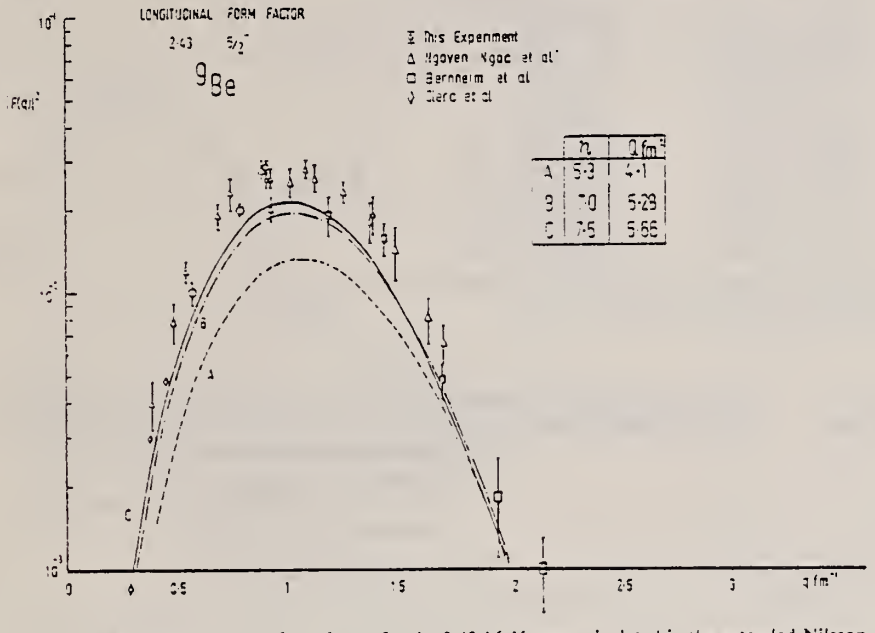

Fig. 11. The longitudinal (C2) form factor for the 2.43 MeV state calculated in the extended Nilsson model for different values of η.

1.67, 2.43, CONT.

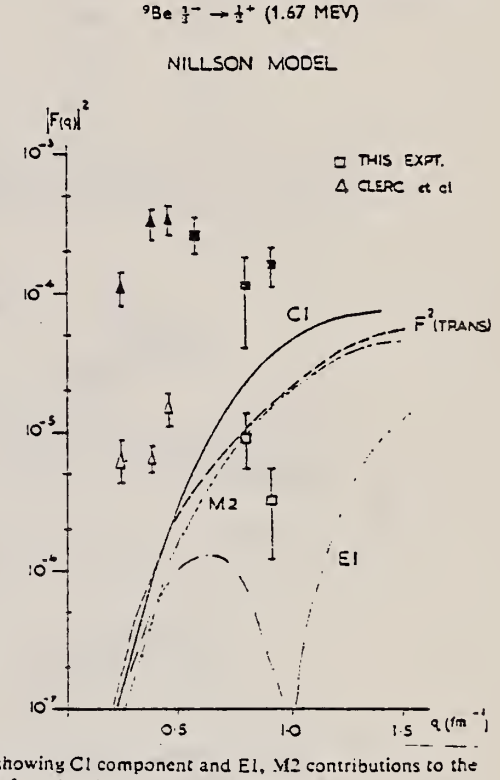

Fig. 13. Form factor for the 1.67 MeV state showing C1 component and E1, M2 contributions to the transverse form factor. Closed data points refer to longitudinal measurements, open to transverse.

TABLE 7

Continuum form factors obtained from the present experiment

Elastic q (fm^{-1})	Scattering angle (deg)	E_x region (MeV) 3–4	4–5	5–6	6–7	7–8	8–9	9–10
0.583	120	3.3 ±0.65	4.9 ±0.8	4.8 ±1.1	2.7 ±0.6	1.8±0.4	1.5±0.5	1.1±0.3
0.584	154	5.4 ±0.6	5.4 ±0.75	5.4 ±0.75	4.3 ±0.65	3.2±0.5	3 ±0.5	2.7±0.45
0.804	120	2.50±0.3	4 ±0.45	5.4 ±0.5	4.9 ±0.5	3.7±0.4	2.8±0.3	2.3±0.25
0.805	154	4.3 ±0.5	5.75±0.6	8.55±0.95	9.25±1.0	7 ±0.6	6.0±0.6	5.8±0.6
0.924	120	3.3 ±0.3	5.0 ±0.5	6.4 ±0.6	6.1 ±0.6	4.8±0.5	5.9±0.6	4.2±0.4
0.930	154	5 ±0.3	5.0 ±0.7	6.8 ±0.9	8.0 ±1.0	6.5±0.7	6.2±0.8	5.8±0.8

The table entries represent $F^2(q) \times 10^3$ for a bin of width 1 MeV.

Experimental results on the prominent levels observed in the present experiment

(a) Elastic

E_i (MeV)	θ (deg)	q(fm^{-1})	FWHM (keV)	σ(Be)/σ(C)	F^2(Be)
66.85±0.01	120	0.583	148	1.025±0.05	5.24±0.25×10^{-1}
59.50	154	0.584	220	1.056±0.055	5.4 ±0.3
92.40	120	0.804	252	1.025±0.04	2.82±0.11
82.25	154	0.805	246	1.073±0.05	2.96±0.15
106.18	120	0.924	193	1.05 ±0.05	1.84±0.09
94.52	154	0.930	240	1.094±0.066	1.92±0.12

(b) Inelastic

E_x (MeV)	θ (deg)	q (fm^{-1})	σ/σ(el)	F^2
1.67	120	0.575	(5.55±1.15)×10^{-4}	(2.9 ±0.6)×10^{-4}
	154		(6.67±1.1) ×10^{-4}	(3.6 ±0.6)
	120	0.796	(5.30±1.95)×10^{-4}	(1.5 ±0.55)
	154		(10.1 ±2.0) ×10^{-4}	(3 ±0.6)
	120	0.917	(9.5 ±1.9) ×10^{-4}	(1.75±0.3)
	154		(11.7 ±2.3) ×10^{-4}	(2.25±0.3)
2.43	120	0.572	(2.04±0.14)×10^{-2}	(1.05±0.07)×10^{-2}
	154		(2.81±0.07)×10^{-2}	(1.43±0.04)×10^{-2}
	120	0.793	(7.55±0.23)×10^{-2}	(2.08±0.06)×10^{-2}
	154		(9.8 ±0.3) ×10^{-2}	(2.63±0.08)×10^{-2}
	120	0.912	(17 ±0.7) ×10^{-2}	(2.96±0.12)×10^{-2}
	154		(19.6 ±1.0) ×10^{-2}	(3.44±0.17)×10^{-2}

The data on the 6.4 MeV level were scaled to the 2.43 MeV state as described in the text.

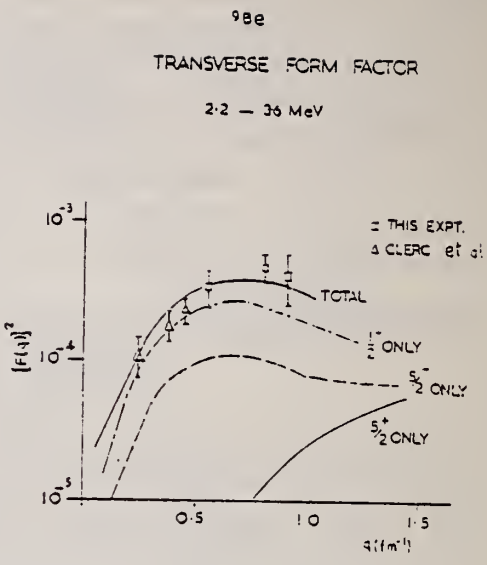

Fig. 15. Comparison of the transverse form factors measured in the present experiment and in ref. [8] with the extended Nilsson model calculations. Both data were integrated to include the 2.43 MeV state and the region up to 3.6 MeV.

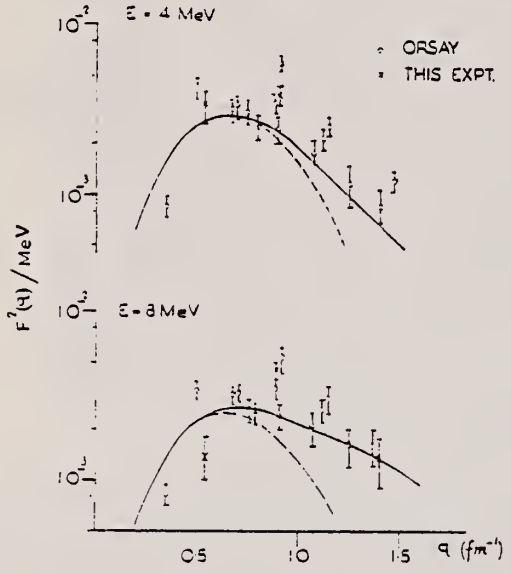

Fig. 14. Comparison of continuum cross-section measurements at Orsay [56]) and in this experiment. The data plotted are averaged over 4 MeV wide bins about the central energy (E). The solid line shows the Orsay fits obtained using the data in table 3, and the dotted line shows the j_1 component of the fit.

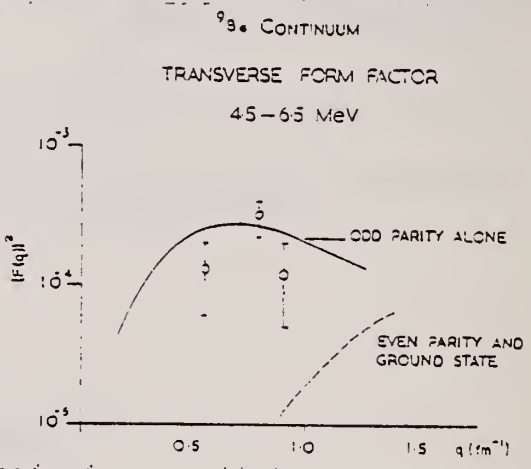

Fig. 16. Transverse form factor measured in the continuum, integrated from 4.5 to 6.5 MeV, compared with the sum of expected contributions calculated in the extended Nilsson model.

[7] M. Bernheim, T. Stovall, D. Vinciguerra, Nucl. Phys. A97 (1967) 480.

[8] H.G. Clerc, K.J. Wetzel, E. Spamer, Nucl. Phys. A120 (1968) 441.

[56] H. Nguyen-Ngoc and J. Perez-y-Jorba, Orsay internal report LAL 1108 (1964).

REF. J. Ahrens, H.B. Eppler, H. Gimm, M. Kroning, P. Riehn, A. Zieger and B. Ziegler
Phys. Lett. 52B, 43 (1974)

ELEM. SYM.	A	Z
Be	9	4

METHOD

REF. NO. 74 Ah 8 egf

REACTION	RESULT	EXCITATION ENERGY	SOURCE		DETECTOR		ANGLE
			TYPE	RANGE	TYPE	RANGE	
G,MUT	ABX	15-220	C	300	MGC-D		4PI

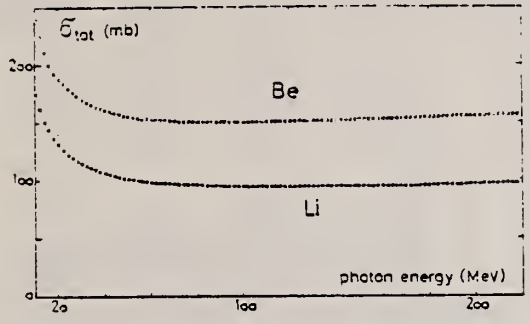

Fig. 1. The total photon absorption cross section σ_{tot} for Li and Be. One standard deviation of the statistical error is by far smaller than the size of the symbols.

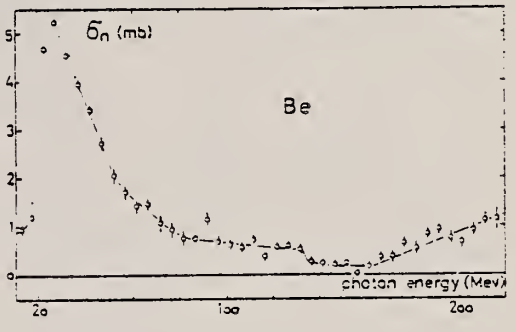

Fig. 3. Same as fig. 2 for Be.

Table 1
Absorber characteristics and relevant errors

	Li	Be
diameter (cm)	1.983 ± 0.002	2.029 ± 0.001
weight (g)	331.40 ± 0.15	718.340 ± 0.03
length (cm)	200.1	120.72
density (g/cm^3)	0.53618	1.843
impurities	0.024 %	0.448 %

REF. P. Dougan and W. Stiefler
Z. Phys. 269, 97 (1974)

ELEM. SYM.	A	Z
Be	9	4

METHOD

REF. NO. 74 Do 5 egf

REACTION	RESULT	EXCITATION ENERGY	SOURCE		DETECTOR		ANGLE
			TYPE	RANGE	TYPE	RANGE	
G,XP	ABX	100-999	C	125-999	TEL-D		DST

Tables of yield curves are given. 999=1 GEV

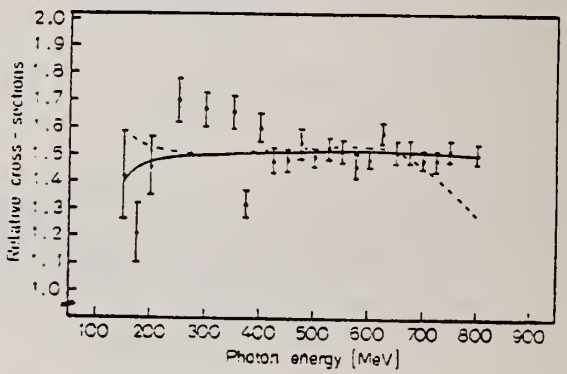

Fig. 3. Ratios of the experimental yields of protons of 82 MeV from carbon and 86 MeV from beryllium at 40° laboratory. The curves are the ratios of 4th-order fits σ_Q (full line) and σ_A (dashed line) as defined in the text

[5] Antuf'ev,Yu.P., Agranovich,V.L., Ganenko,V.B., Kuz'menko,V.S., Miroschnichenko,I.I., Sorokin,P.V., Sanin,V.M.: Sov.Jour.Nucl.Phys. 9,538 (1969).

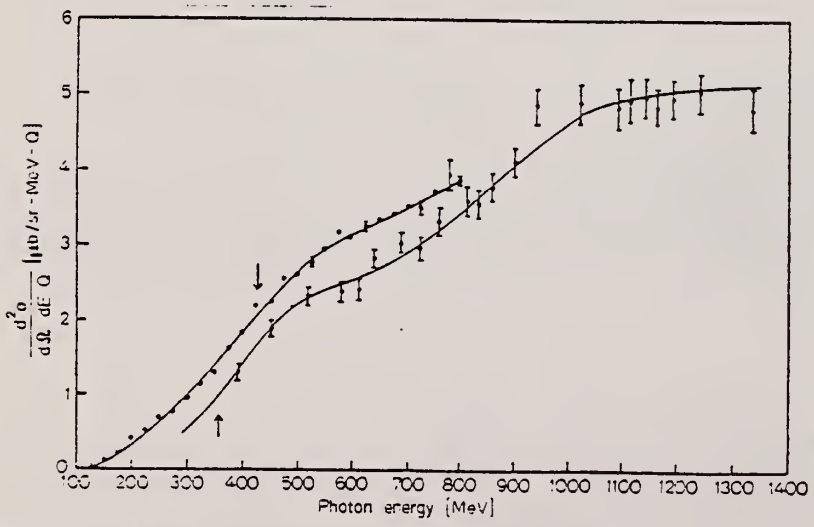

Fig. 2. Comparison of the yields of protons of energy 99 MeV at 40° laboratory (this experiment: open circles) with the yields of proton of energy 97 MeV at 30° laboratory (Ref. 5: full circles). The vertical arrows indicate the mean photon energies for detecting protons from π^0-photoproduction from hydrogen for identical kinematical conditions

REF.

N. Ensslin, W. Bertozzi, S. Kowalski, C.P. Sargent, W. Turchinetz, C.F. Williamson, S.P. Fivozinsky, J.W. Lightbody,Jr., S. Penner Phys. Rev. C9, 1705 (1974)

Be	9	4

METHOD

REF. NO. 74 En 1 hmg

REACTION	RESULT	EXCITATION ENERGY	SOURCE TYPE	SOURCE RANGE	DETECTOR TYPE	DETECTOR RANGE	ANGLE
E,E/	FMF	2	C	60-120	MAG-D		DST

TABLE V. Electron scattering form factors for ^{9}Be.

2.429 MEV LEVEL

Energy (MeV)	Angle (deg)	q [a] (fm^{-1})	$F^2(q)$ elastic [b]	$F^2(q)\times10^3$ 2.429-MeV level Be_3N_2 target	$F^2(q)\times10^3$ 2.429-MeV level Be metal target
60.65	163.66	0.604	0.4885	22.9±0.6	
73.06	163.44	0.727	0.3447	26.1±1.7	
39.82	110.79	0.744	0.3257	20.8±0.9	20.6±0.7
86.31	163.44	0.857	0.2207	30.5±1.2	
90.08	145.92	0.865	0.2144	27.4±0.4	
				26.1±0.7	
104.95	110.79	0.863	0.2118	25.8±0.9	24.9±0.5
104.62	145.71	1.002	0.1218	30.4±0.5	30.5±0.4
122.00	110.51	1.006	0.1202	30.6±1.0	28.5±0.6
117.62	145.65	1.125	0.0676	31.2±0.7	
120.01	145.97	1.148	0.0598	29.8±0.9	27.0±0.3

[a] Calculated for elastic scattering.
[b] Calculated from the parameters of Ref. 56.

56 H.G. Clerc, K.J. Wetzel, E. Spamer, Nucl. Phys. A120, 441 (1968).

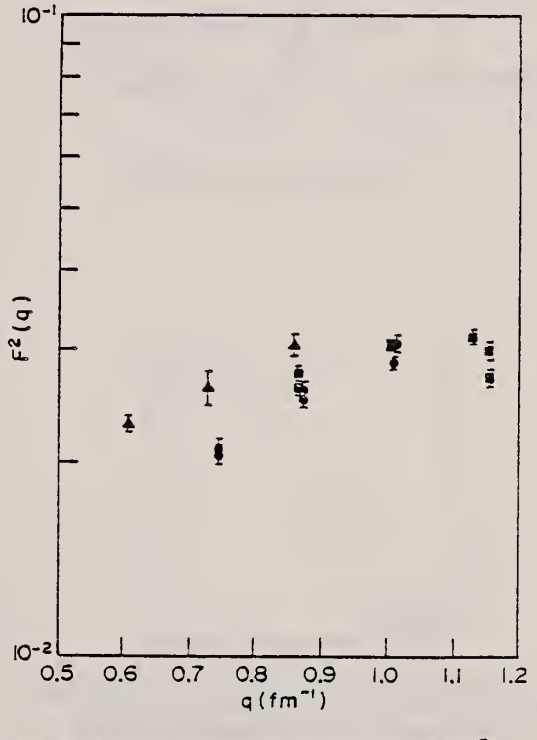

FIG. 9. Form factor squared of the 2.429-MeV ($\frac{5}{2}^-$) state in ^{9}Be. The data are shown before the separation into transverse and longitudinal parts was carried out: ▲— data taken at 163°, ■— data taken at 145°, ●— data taken at 110°.

REF. N.V. Goncharov, S.G. Tonapetyan, and V.M. Khvorostyan
Yad. Fiz. 19, 21 (1974)
Sov. J. Nucl. Phys. 19, 10 (1974)

ELEM. SYM.	A	Z
Be	9	4

METHOD

REF. NO.	
74 Go 1	hmg

REACTION	RESULT	EXCITATION ENERGY	SOURCE		DETECTOR		ANGLE
			TYPE	RANGE	TYPE	RANGE	
G,PI+	ABY	150-400	C	400	BBL -D		90
G,PI-	ABY	150-400	C	400	BBL -D		90
G,P	ABY	17-400	C	400	BBL -D		90

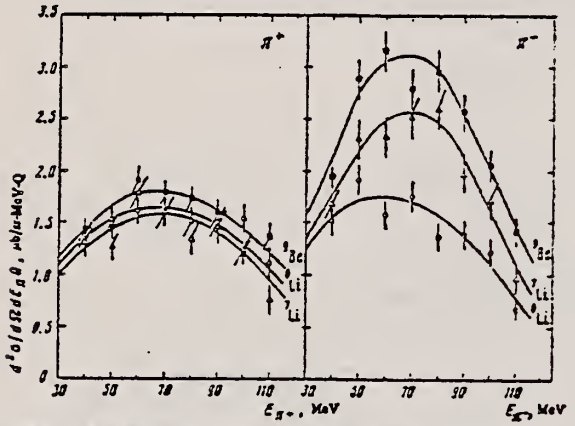

FIG. 1. Energy spectra of π^+ and π^- mesons. $E_\gamma^{max} = 400$ MeV, $\theta_{lab} = 90 \pm 7°$.

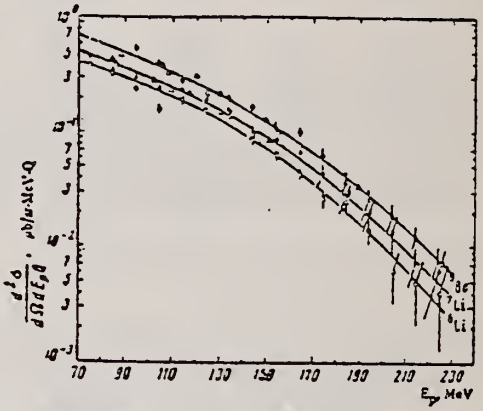

FIG. 2. Energy spectra of protons. $E_\gamma^{max} = 400$ MeV, $\theta_{lab} = 90 \pm 7°$. Points: circles—data of the present work, triangles—ref. 11.

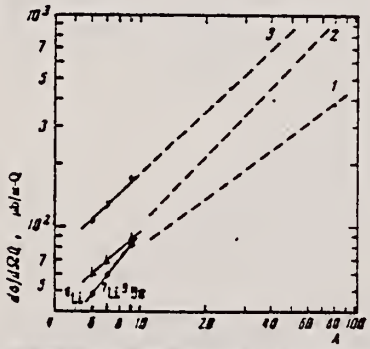

FIG. 3. Mass-number dependence of the yields of π mesons (points ▲, curve 1), protons (points ■, curve 2), and the sum of the π-meson and proton yields (points ●, curve 3). The dashed lines are the data from ref. 6.

[6] N.V. Goncharov et al., Yad. Fiz. 17, 242 (1973); Sov. J. Nucl. Phys. 17, 125 (1973).

[11] P. Dougan and W. Stiefler, Preprint LUSU, 1002-1005, 1970.

REF. V.A. Gol'dshtein, V.B. Shostak, N.G. Afanas'ev, V.G. Vlasenko, E.L. Kuplennikov, and V.I. Startsev
ZhETF Pis. Red. 19, 695 (1974)
JETP Lett. 19, 358 (1974)

ELEM. SYM.	A	Z
Be	9	4

METHOD

REF. NO. 74 Go 10 - hmq

REACTION	RESULT	EXCITATION ENERGY	SOURCE		DETECTOR		ANGLE
			TYPE	RANGE	TYPE	RANGE	
E,E/P	ABX	10* 50	D	801	MAG-D		30

*SEP ENERGY

A beam of 801-MeV electrons from the LUÉ-2000 accelerator was used to measure the cross section of the reaction $Be^9(e, e'p)Li^8$ as a function of the proton detachment energy. The values obtained for the detachment energies of the $1S$- and $1P$-protons are 28.7 and 16.9 MeV, respectively.

B, MeV	Width at half height, MeV	$\frac{d^3\sigma_{exp}}{d\Omega_e d\Omega_p dE_p} \cdot 10^{31}$, cm²/sr²-MeV
17.4 ± 1	7.1 ± 0.8	0.41 ± 0.14
26.4 ± 1	7.1 ± 0.8	0.41 ± 0.16
33.3 ± 1	11.2 ± 3.4	0.44 ± 0.20

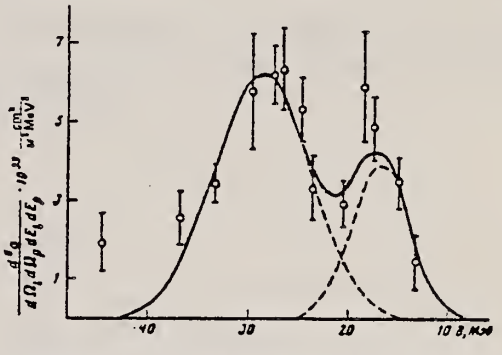

Dependence of the cross section of the reaction $Be^9(e, e'p)Li^8$ on the proton detachment energy.

REF. U. Kneisl, G. Kuhl, K.H. Leister and A. Weller
Z. Naturforsch, 29a, 1688 (1974)

ELEM. SYM.	A	Z
Be	9	4

METHOD

REF. NO. 74 Kn 10 egf

REACTION	RESULT	EXCITATION ENERGY	SOURCE		DETECTOR		ANGLE
			TYPE	RANGE	TYPE	RANGE	
G,XN	ABX	17- 25	D	17- 25	MOD-I		4PI

We measured the ^{9}Be photoneutron production cross section $\sigma(\gamma, T.n) = \sigma(\gamma, n) + 2\,\sigma(\gamma, 2n) + \sigma(\gamma, pn)$ in the energy range from 17–25 MeV with quasimonoenergetic photons from positron annihilation in flight. In contrast to experiments of Thomas, Crawford and Thies (1972) and Hughes (1973), performed with bremsstrahlung photon sources we found no pronounced structure in this energy range.

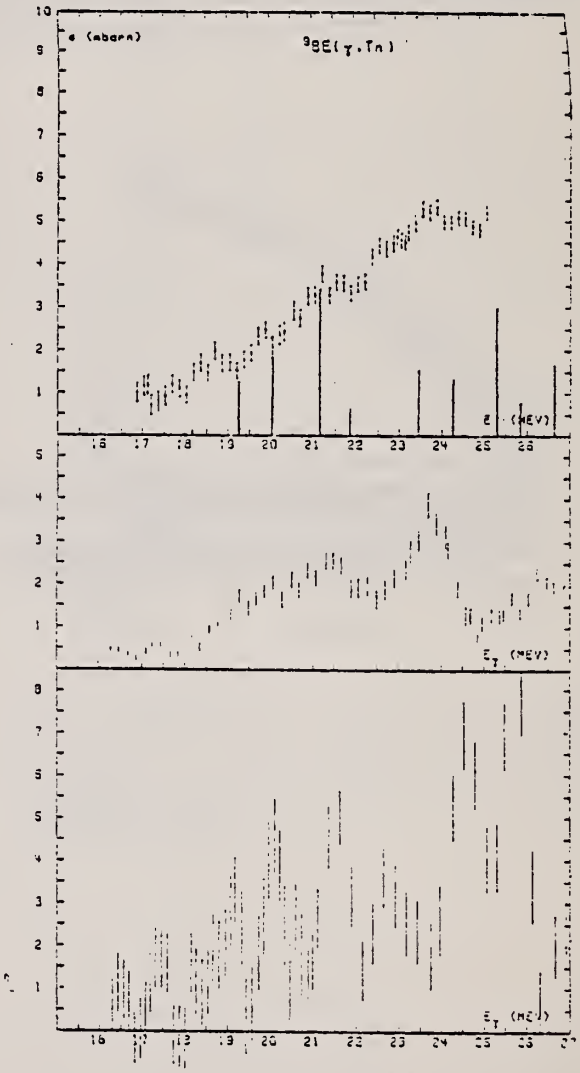

Fig. 1. Upper part: Present experiment with dipole strengths according to Majling [7]. Second curve: Results of the bremsstrahlung experiment of Hughes [4]. Below: Data given by Thomas et al. [1].

[1] B.W. Thomas, D.M. Crawford, and H.H. Thies, Nucl. Phys. A196, 89 (1972)

REF. Yu. I. Titov, E.V. Stepula, N.G. Afanas'ev, R.V. Akhmerov, and N.F. Severin
Yad. Fiz. 19, 479 (1974)
Sov. J. Nucl. Phys. 19, 240 (1974)

EL EM. SYM.	A	Z
Be	9	4

METHOD

REF. NO.	
74T13	hmg

REACTION	RESULT	EXCITATION ENERGY	SOURCE		DETECTOR		ANGLE
			TYPE	RANGE	TYPE	RANGE	
E,E/	ABX	0-600	D	1*	MAG-D		DST

* 1=1.2 GEV

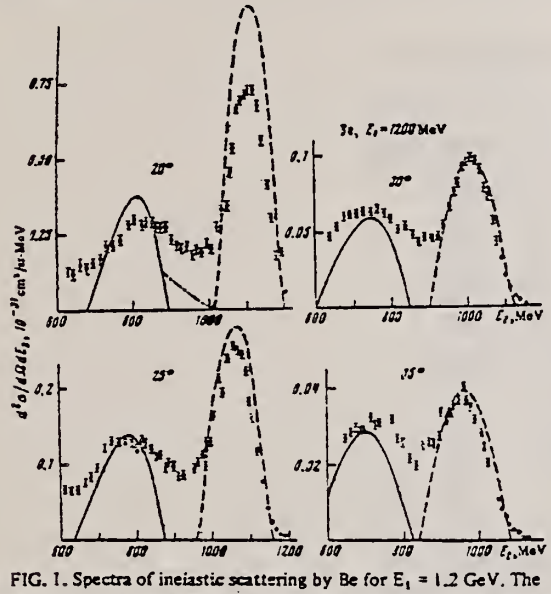

FIG. 1. Spectra of inelastic scattering by Be for E_1 = 1.2 GeV. The dashed curve is the quasielastic-scattering cross section, the solid curve is the electroproduction cross section calculated according to ref. 7, and the dot-dash curve is the electro-production cross section at threshold. [12] A radiation correction has been made to the experimental data.

[7] E.J. Moniz, Phys. Rev. 184, 1154 (1969).

[12] W. Czyz and J.D. Walecka, Nucl. Phys. 51, 312 (1964).

REF.		ELEM. SYM.	A	Z
	J. Ahrens, H. Borchert, K.H. Czock, H.B. Eppler, H. Gimm, H. Gundrum, M. Kroning, P. Riehn, G. Sita Ram, A. Zieger, and B. Ziegler Nucl. Phys. A251, 479 (1975)	Be	9	4

METHOD	REF. NO.	
	75 Ah 3	egf

REACTION	RESULT	EXCITATION ENERGY	SOURCE		DETECTOR		ANGLE
			TYPE	RANGE	TYPE	RANGE	
G,MU-T	ABX	10-210	C	140-275	MGC-D		4PI

918+

TABLE 2

The moments of the experimental nuclear cross section distributions integrated from 10 MeV to the energy $\mathcal{E}$, and their statistical errors

	$\mathcal{E}$ (MeV)	$\sum_{-2}$ (mb/MeV)	±(%)	$\sum_{-1}$ (mb)	±(%)	$\sum_{0}$ (mb·MeV)	±(%)	$\sum_{+1}$ (b·MeV^{1})	±(%)	$\sum_{+2}$ (b·MeV^{2})	±(%)
Li	100	0.196	1.1	4.64	1.0	143	1.7	5.82	3.1	305	5
	140	0.197	1.1	4.79	1.0	161	1.9	8.03	3.4	577	5
	210	0.198	1.1	5.03	1.0	206	2.0	16.60	3.7	2220	5
Be	100	0.192	2.5	5.19	1.5	173	2.0	7.11	3.4	362	5
	140	0.194	2.5	5.33	1.5	189	2.1	9.09	3.6	600	6
	210	0.195	2.5	5.58	1.5	236	2.1	17.80	3.5	2240	5
C	100	0.313	1.7	8.81	1.1	291	1.6	12.00	2.9	630	4
	140	0.316	1.7	9.18	1.2	334	2.2	17.10	5	1250	7
O	100	0.580	1.6	14.50	1.3	432	2.0	16.00	4	748	8
	140	0.585	1.6	15.10	1.3	508	2.5	25.20	5	1880	8
Al	100	1.10	1.8	25.70	1.5	739	2.6	27.9	5	1400	8
	140	1.11	1.8	26.3	1.7	807	3.9	36.4	9	2450	16
Ca	100	2.22	1.2	45.5	1.5	1120	3.6	34.9	9	1430	18
	140	2.23	1.2	46.8	1.7	1290	4.6	56.6	11	3710	19

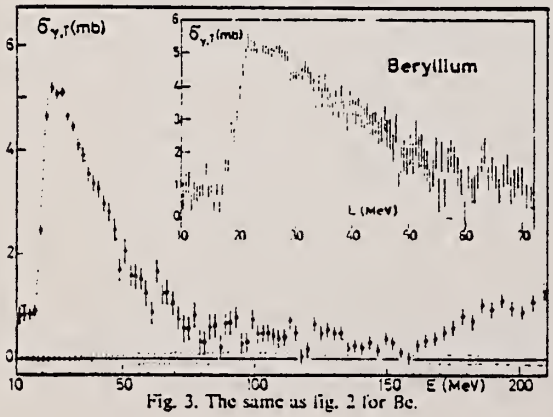

Fig. 3. The same as fig. 2 for Be.

Fig. 2. Total photonuclear cross section for natural Li. The error bars indicate one standard deviation of counting statistics from the main spectrometer. The dashed lines along the abscissa indicate the uncertainty due to counting statistics in the normalizing spectrometer. Oscillations of the base line within this area are possible, the period of these oscillations, however, must not be smaller than 10% in photon energy. The dashed and dotted lines through the cross section values have been drawn to guide the eye.

REF. R.J. Hughes, R.H. Sambell, E.G. Muirhead and B.M. Spicer
Nucl. Phys. A238, 189 (1975)

ELEM. SYM.	A	Z
Be	9	4

METHOD

REF. NO. 75 Hu 1 egf

REACTION	RESULT	EXCITATION ENERGY	SOURCE TYPE	SOURCE RANGE	DETECTOR TYPE	DETECTOR RANGE	ANGLE
G,XN	ABX	1- 28	C	1- 28	BF3-I		4PI

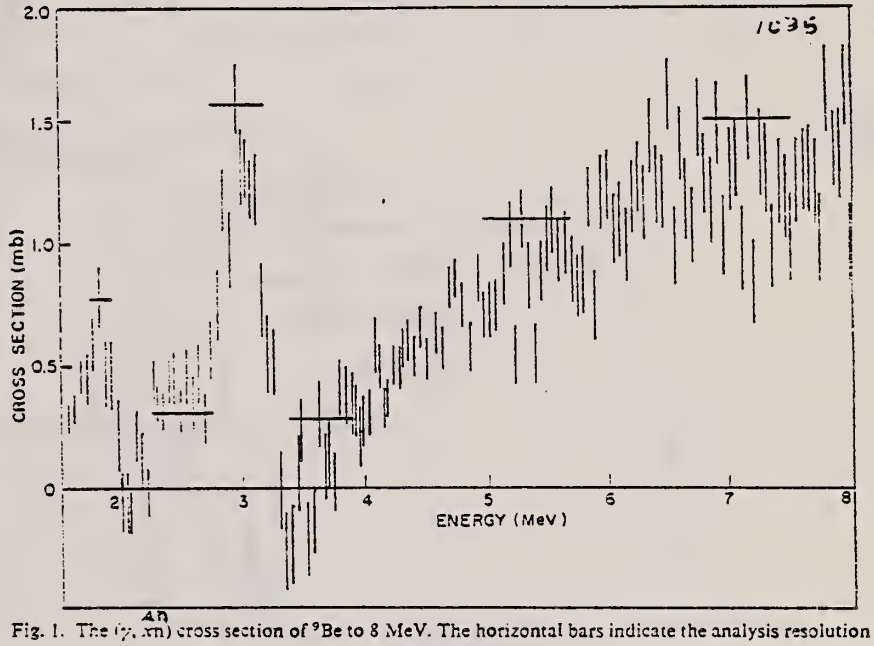

Fig. 1. The (γ, xn) cross section of ^{9}Be to 8 MeV. The horizontal bars indicate the analysis resolution at various energies.

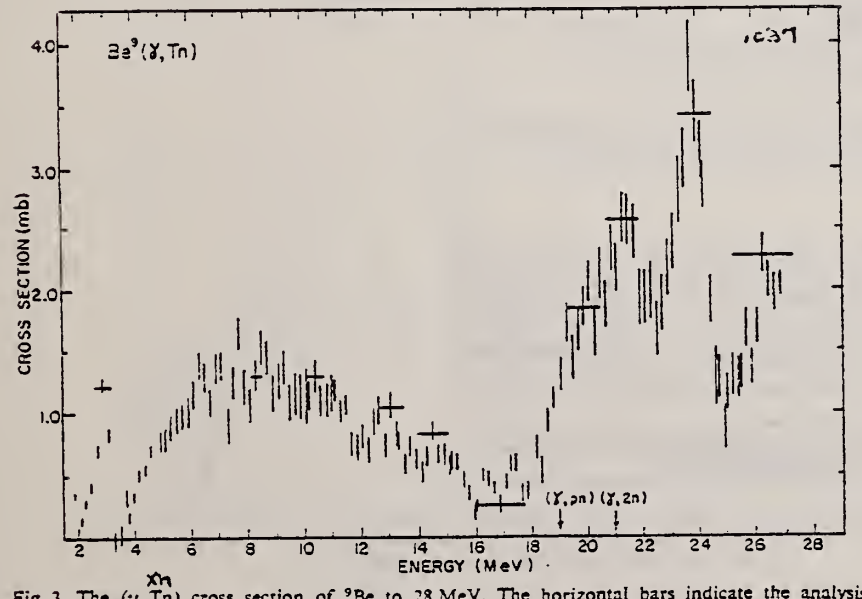

Fig. 3. The (γ, Tn) cross section of ^{9}Be to 28 MeV. The horizontal bars indicate the analysis resolution at various energies. The thresholds for the (γ, pn) and the (γ, 2n) reactions are indicated by arrows.

In this paper

$$\sigma(\gamma,Tn)=\sigma(\gamma,n)+\sigma(\gamma,pn)+2\sigma(\gamma,2n)$$
$$=\sigma(\gamma,xn)$$

and

$$\sigma(\gamma,xn)=\sigma(\gamma,n)+\sigma(\gamma,pn)+\sigma(\gamma,2n)$$
$$=\sigma(\gamma,An)$$

(over)

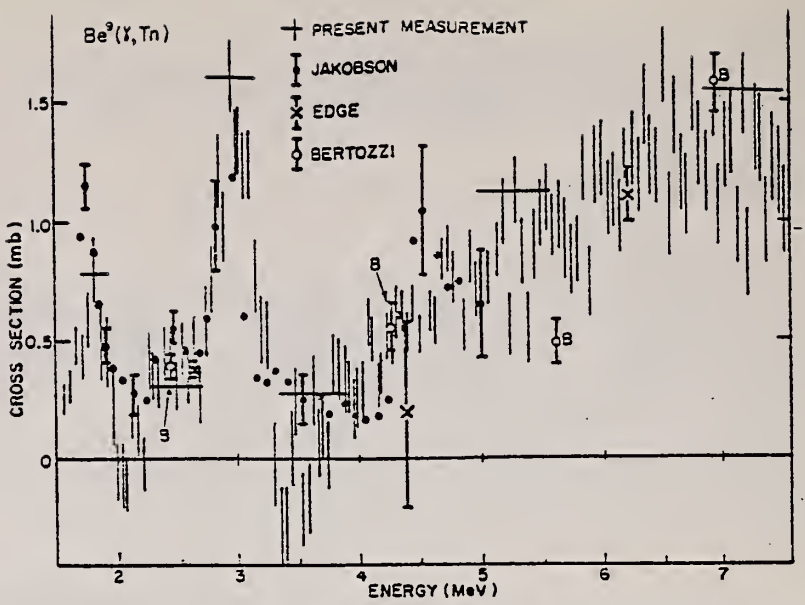

Fig. 4. A comparison between the present measurement of the ^{9}Be photoneutron cross section and the measurements of Edge [15]), Bertozzi *et al.* [16]) and Jakobson [17]).

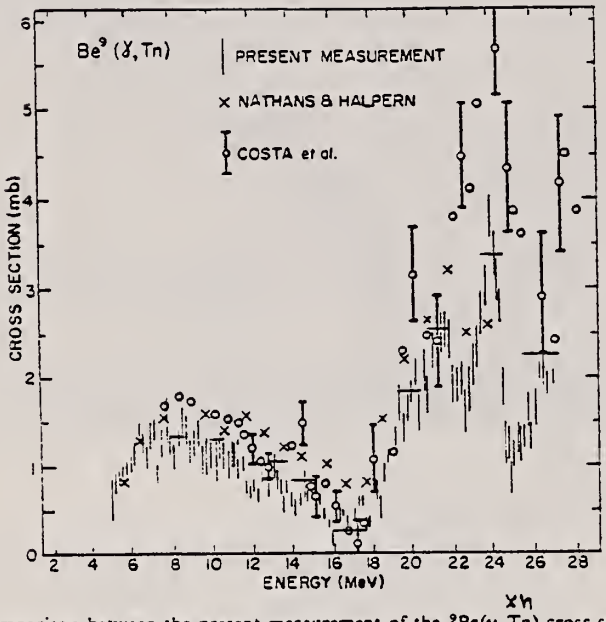

Fig. 5. A comparison between the present measurement of the ^{9}Be(γ, Tn) cross section from 5 to 28 MeV and the measurements of Nathans and Halpern [19]), and Costa *et al.* [18]).

15) R.D. Edge, Nucl.Phys. 2, 485 (1956)
16) W. Bertozzi et al., Karlsruhe Conf. on photonuclear reactions, 1960
17) M.K. Jakobson, Phys. Rev. 123, 229 (1961)
18) S. Costa et al., Nuovo Cim. B42, 306 (1966)
19) R. Nathans et al., Phys. Rev. 92, 940 (1953).

Abstract: The absolute total cross section for photoneutron production from ^{9}Be has been deduced from bremsstrahlung yield curves measured from threshold to 28 MeV. Neutron yields were measured using direct neutron counting and were analysed using the variable-bin Penfold-Leiss method. The integrated cross section to 17.8 MeV is 13 ± 1 MeV · mb; and to 27.5 MeV is 28.3 ± 3 MeV · mb. Detailed comparison between experiment and various shell model calculations show some points of agreement either at lower energies or in the GDR but there is no one overall satisfactory detailed version. More refined and detailed calculations are required.

E NUCLEAR REACTIONS ^{9}Be(γ, xn), $E < 28$ MeV; measured neutron yields; deduced total and integrated σ. ^{9}Be deduced resonances.

REF. U. Kneissl, G. Kuhl, K. H. Leister, A. Weller
Nucl. Phys. A247, 91 (1975)

ELEM. SYM.	A	Z
Be	9	4

METHOD

REF. NO. 75 Kn 5 egf

REACTION	RESULT	EXCITATION ENERGY	SOURCE TYPE	SOURCE RANGE	DETECTOR TYPE	DETECTOR RANGE	ANGLE
G,XN *	ABX	17- 38	D	17- 38	MOD-I		4PI
G,2N **	ABX	20- 38	D	17- 38	MOD-I		4PI

*1041
**1042+

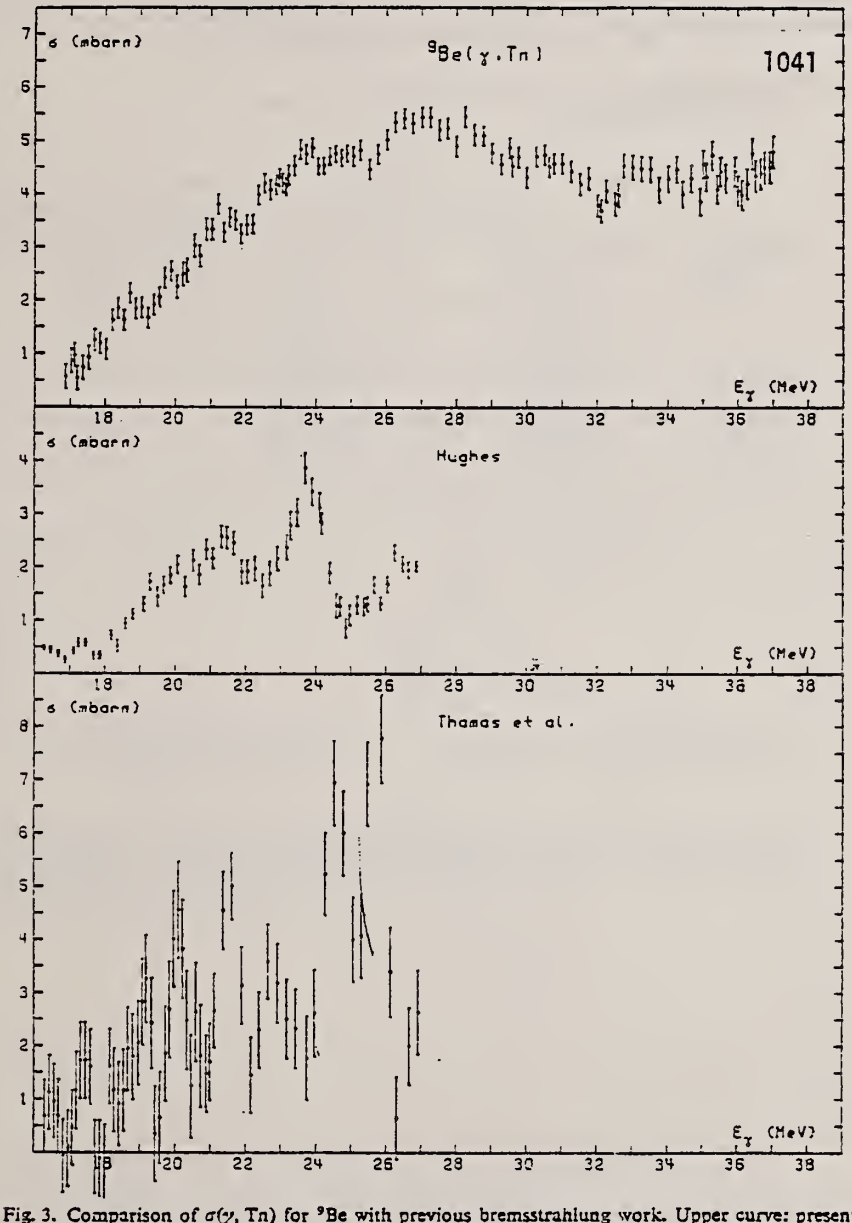

Fig. 3. Comparison of $\sigma(\gamma, Tn)$ for ^{9}Be with previous bremsstrahlung work. Upper curve: present results obtained with quasimonoenergetic photons. Second curve: results reported by Hughes *et al.* [10]). Third curve: results reported by Thomas *et al.* [9]).

[9] B.W. Thomas et al. Nucl. Phys. A196 (1972) 89

[10] R.J. Hughes et al. Ph.D. thesis, Univ. Melbourne 1973

(over)

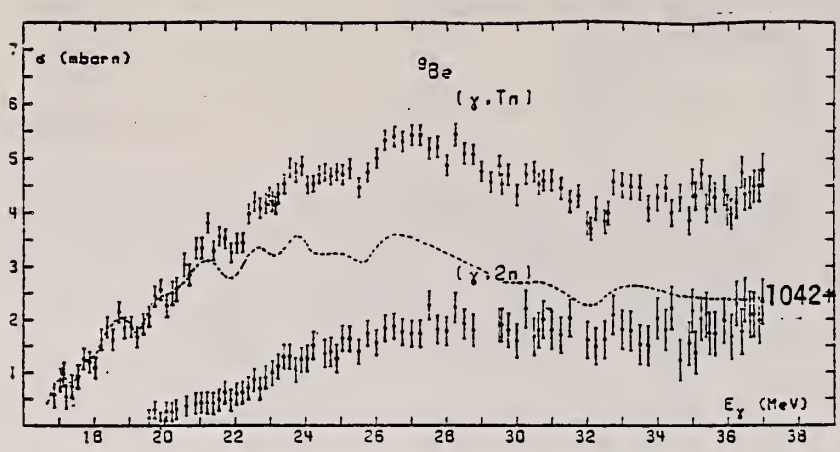

Fig. 4. Plot of $\sigma(\gamma, \mathrm{Tn}) = \sigma(\gamma, \mathrm{n}) + \sigma(\gamma, \mathrm{pn}) + 2\sigma(\gamma, 2\mathrm{n})$ and $\sigma(\gamma, 2\mathrm{n})$. Dotted line: $\sigma(\gamma, \mathrm{n}_{\mathrm{tot}}) = \sigma(\gamma, \mathrm{n}) + \sigma(\gamma, \mathrm{pn}) + \sigma(\gamma, 2\mathrm{n})$.

REF. H. Schier and B. Schoch
Nuovo Cimento Lett. 12, 334 (1975)

ELEM. SYM.	A	Z
Be	9	4

METHOD

REF. NO. 75 Sc 7 — egf

REACTION	RESULT	EXCITATION ENERGY	SOURCE		DETECTOR		ANGLE
			TYPE	RANGE	TYPE	RANGE	
G,N	ABX	62- 66	D	62- 66	TOF-D		DST

62.7-65.7 MEV

TABLE I. – *Measured cross-sections obtained from Fig.* 1-5. The photon energy corresponds to the maximum value of the difference spectrum.

Nucleus	Photon energy (MeV)	Excitation energy (MeV)	$d\sigma/d\Omega$ (40.2°) (μb/sr)	$d\sigma/d\Omega$ (90°) (μb/sr)
^{16}O	63.0	ground state	5.0 ± 0.75	
		$0 \div 6.18$	20.7 ± 3.1	
^{12}C	62.75	ground state	11.1 ± 0.8	7.8 ± 0.36
		$0 \div 4.79$	22.5 ± 1.1	17.1 ± 0.56
^{9}Be	61.25	ground state	0.8 ± 0.13	0.85 ± 0.1
		$0 \div (\gamma, np)$ threshold	3.4 ± 0.3	4.1 ± 0.22

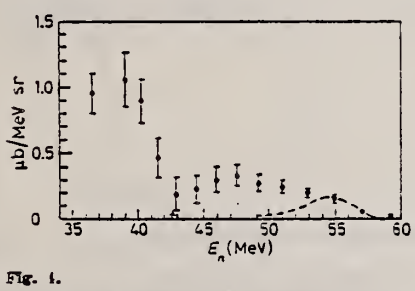

Fig. 4.

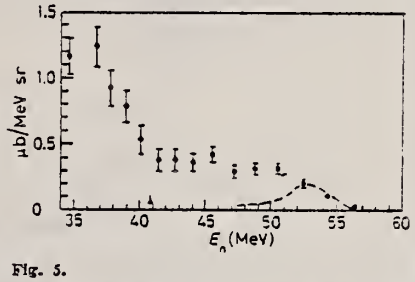

Fig. 5.

Fig. 4. – Cross-sections for the photoproduction of neutrons in ^{9}Be by quasi-monochromatic photons. The dashed line shows the photon spectrum fitted to the ground state in ^{9}Be. The arrow gives the threshold for the (γ, np) reaction. (65.25 ÷ 61.25) MeV, $\theta_n = 40.2°$.

Fig. 5. – The same as Fig. 4 for $\theta_n = 90°$.

REF.

J. L. Matthews, D. J. S. Findlay, S. N. Gardiner, R. O. Owens
Nucl. Phys. A267, 51 (1976)

EL EM. SYM.	A	Z
Be	9	4

METHOD

REF. NO.: 76 Ma 8 egf

REACTION	RESULT	EXCITATION ENERGY	SOURCE		DETECTOR		ANGLE
			TYPE	RANGE	TYPE	RANGE	
G,P	ABX	60-100	D	60-100	MAG-D		45

Cross section table given.

TABLE 1

Cross sections for the ^{6}Li, ^{7}Li, ^{9}Be and ^{12}C(γ, p) reactions at E_γ(lab) = 60 MeV, θ_p(lab) = 45° populating the excitation energy regions E_x = 0–9 MeV and 9–26 MeV in the residual nuclei

Target nucleus	$(d\sigma/d\Omega)^{45°}_{lab}$ (μb/sr) residual nucleus excitation energy E_x 0–9 MeV	9–26 MeV
^{6}Li	5.5±0.6	12.2±2.0
^{7}Li	9.5±0.8	14.7±3.0
^{9}Be	31.8±3.0	
^{12}C	36.4±3.9	

Only statistical errors are tabulated; there is an additional common systematic error of ±22%.

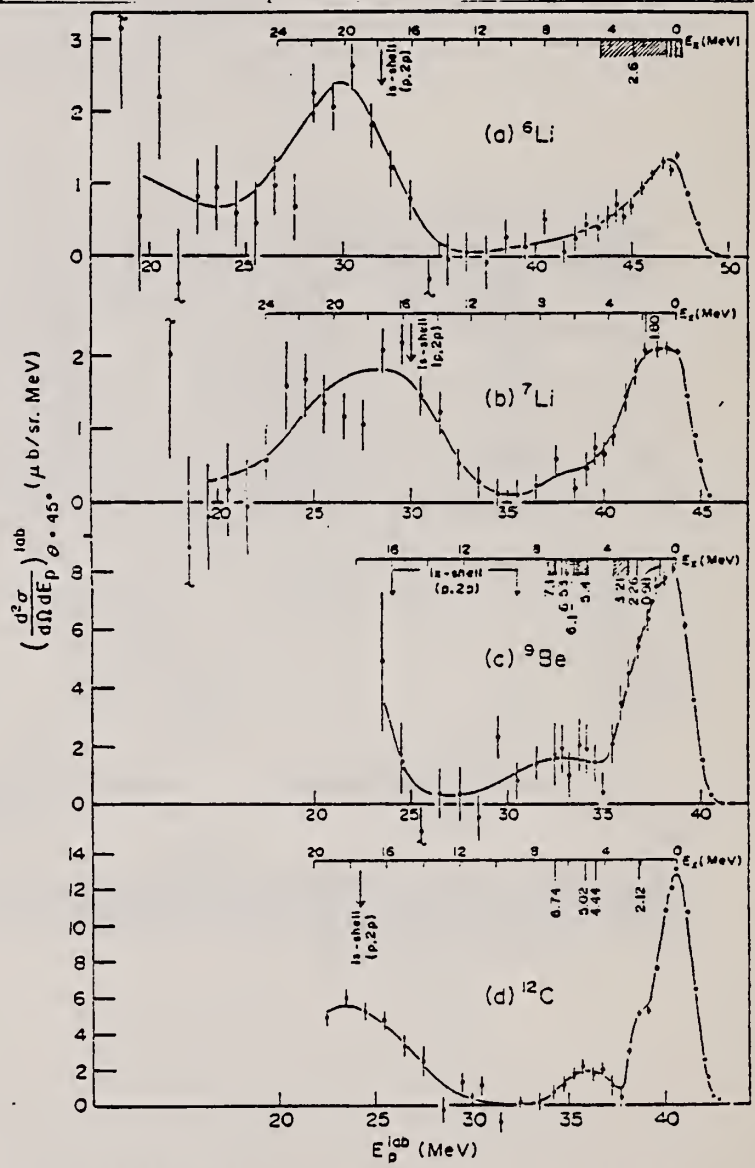

Fig. 8. Photoproton spectra for $E_\gamma = 60 \pm 1$ MeV, $\theta = 45°$ derived as described in the text from data such as those shown in fig. 7: (a) ^{6}Li(γ, p)^{5}He; (b) ^{7}Li(γ, p)^{6}He; (c) ^{9}Be(γ, p)^{8}Li; (d) ^{12}C(γ, p)^{11}B. The scale above each spectrum gives the excitation energy in the residual nucleus, with lines indicating the positions of known excited states. The location of the 1s shell peak observed in the (p, 2p) reaction is also marked.

REF. A. Buchnea, R. G. Johnson, and K. G. McNeill
Can. J. Phys. 55, 364 (1977)

ELEM. SYM.	A	Z
Be	9	4

METHOD

REF. NO. 77 Bu 4 hmg

REACTION	RESULT	EXCITATION ENERGY	SOURCE		DETECTOR		ANGLE
			TYPE	RANGE	TYPE	RANGE	
G,N1	ABX	17- 26	C	22- 29	TOF-D		DST

The $^{9}Be(\gamma,n_0)^{8}Be$ and $^{9}Be(\gamma,n_1)^{8}Be$ reactions were studied in the photon energy region 18 to 26 MeV. The integrated cross section of the (γ,n_0) reaction was found to be less than 0.1 MeV mb in this energy region. The integrated cross section for the (γ,n_1) reaction in the energy region is 2.4 ± 0.4 MeV mb, which is 10 to 15% of the total photoneutron cross section. The measured angular distributions for the (γ,n_1) reaction are consistent with the population of $3/2^+$ and $5/2^+$ states of ^{9}Be. These results are consistent with slightly re-interpreted predictions of Majling, Kukulin, and Smirnov.

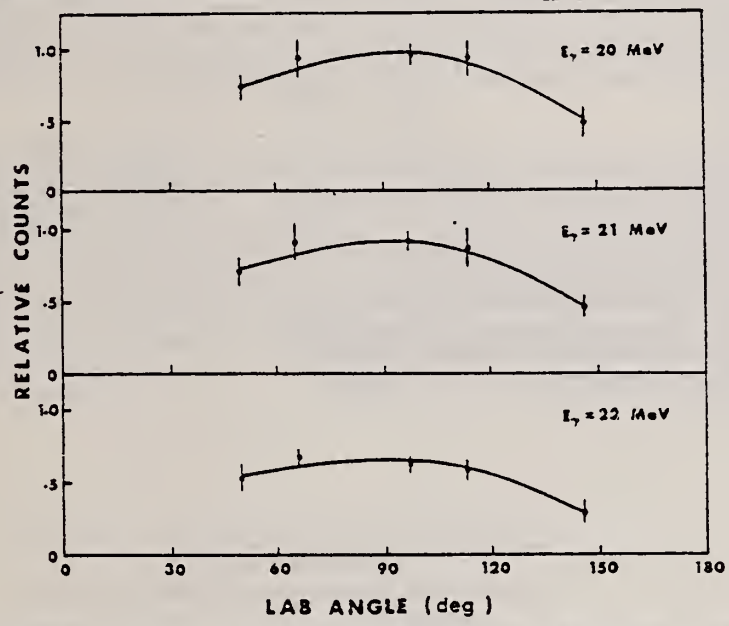

FIG. 2. Angular distributions of photoneutrons from the reaction $^{9}Be(\gamma,n_1)^{8}Be$ at an endpoint energy of 22.5 MeV and at the indicated photon energies.

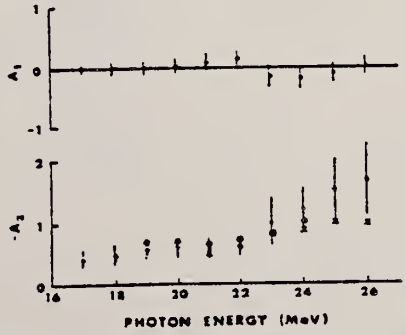

FIG. 3. Angular distribution coefficients for the reaction $^{9}Be(\gamma,n_1)^{8}Be$ from the expression, $W(0) = A_0(1 + A_1P_1(\cos\theta) + A_2P_2(\cos\theta))$. Data are as follows: + 22.5 MeV endpoint; ○ 24.5 MeV endpoint; × 26.5 MeV endpoint; and ● 28.5 MeV endpoint.

over

FORM NBS-418
(REV. 7-1-64)
USCOMM-NBS-DC

U.S. DEPARTMENT OF COMMERCE
NATIONAL BUREAU OF STANDARDS

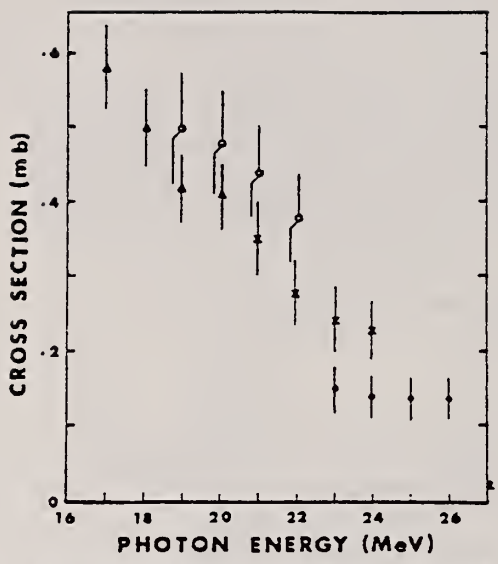

FIG. 4. Total cross section for the reaction $^{9}Be(\gamma,n_1)^{8}Be$. Data are as follows: Δ 22.5 MeV endpoint; ○ 24.5 MeV endpoint; × 26.5 endpoint; and ● 28.5 MeV endpoint.

REF. A. Buchnea, R.G. Johnson, & K.G. McNeill
Can. J. Phys. 56, 47 (1978)

ELEM. SYM.	A	Z
Be	9	4

METHOD

REF. NO. 78 Bu 15 hmg

REACTION	RESULT	EXCITATION ENERGY	SOURCE TYPE	SOURCE RANGE	DETECTOR TYPE	DETECTOR RANGE	ANGLE
G, N A	ABI	17-26	C	20-26	SCD-D		4PI

G,N to 8Be(16.6)

Alpha particles from the $^{9}Be(\gamma,n)^{8}Be(16.6)$ and $^{9}Be(\gamma,\alpha_0)^{5}He$ reactions were studied in the photon energy region 18 to 26 MeV; the results yielded a combined integrated cross section of 13.1 ± 2 MeV mb and an upper limit on the integrated (γ,α_0) cross section of 4.0 MeV mb. This agrees within error with the integrated cross section of Becchi, Meneghetti, Sanzone, and Vitale, 10 ± 2 MeV mb, which would contain about 50% of any contribution from the (γ,α_0) reaction. These reactions together with the $^{9}Be(\gamma,n_1)^{8}Be$ reaction (which has an integrated cross section of 2.4 ± 0.4 MeV mb) are the major reaction channels contributing to the total photoneutron cross section in this energy region. Their sum, 15.5 MeV mb, agrees well with the results of Nathans and Halpern and Hughes, Sambell, Muirhead, and Spicer but disagrees with that of Costa, Pasqualini, Piragino, and Roasio.

Les particules α émises lors des réactions $^{9}Be(\gamma,n)^{8}Be(16.6)$ et $^{9}Be(\gamma,\alpha_0)^{5}He$ ont été étudiées dans la gamme d'énergie 18 à 26 MeV pour les photons; les résultats ont fourni une section efficace totale combinée de 13.1 ± 2 MeV mb et une limite supérieure de la section efficace totale (γ,α_0) de 4.0 MeV mb. Ceci est en accord, compte tenu de l'erreur experimentale, avec la section efficace totale de Becchi, Meneghetti, Sanzone et Vitale, 10 ± 2 MeV mb, dans laquelle interviendrait une contribution d'environ 50% de la réaction (γ,α_0). Ces réactions, avec la réaction $^{9}Be(\gamma,n_1)$ ^{8}Be, (qui a une section efficace totale de 2.4 ± 0.4 MeV mb) sont les principaux canaux de réaction qui contribuent à la section efficace totale photon-neutron dans cette région d'énergie. Leur somme, 15.5 MeV mb, est en bon accord avec les résultats de Nathans et Halpern et Hughes, Sambell, Muirhead et Spicer mais sont en désaccord avec ceux de Costa, Pasqualini, Piragino et Roasio.

[Traduit par le journal]

Can. J. Phys., 56, 47 (1978)

TABLE 2. The average and integrated cross sections above 18 MeV photon energy

Photon energy interval (MeV)	Average cross section (mb)	Cumulative integrated cross section: Value (MeV mb)	Cumulative integrated cross section: Energy interval (MeV)
18–20	0.15	0.3	18–20
20–22	1.9	4.1	18–22
22–24	2.8	9.7	18–24
24–26	1.7	13.1	18–26

REF. S. V. Dementii, V. I. Ogurtsov, N. G. Afanas'ev
Yad. Fiz. 28, 865 (1978)
Sov. J. Nucl. Phys. 28, 443 (1978)

EL EM. SYM.	A	Z
Be	9	4

METHOD

REF. NO. 78De11 hg

REACTION	RESULT	EXCITATION ENERGY	SOURCE TYPE	SOURCE RANGE	DETECTOR TYPE	DETECTOR RANGE	ANGLE
E,E/	ABX	50-200	D	1*2	MAG-D		DST
				(799-1178)			

*GEV, QUASIELASTIC

Measurements were made of quasielastic scattering of electrons in the (e, e') reaction by the nuclei ^{9}Be, ^{12}C, ^{14}N, ^{16}O, and ^{27}Al. An experimental estimate is obtained of the effective mass of an intranuclear nucleon. At excitation energies up to 80 MeV, a ratio $M^*/M = 0.6$ is obtained, corresponding to a linear potential $V(E) = V_0 + 0.4E$ and in good agreement with the data on proton scattering by nuclei [C. M. and F. G. Perey, Atomic Data and Nuclear Tables 13, 294 (1974)]. At excitation energies above 120 MeV the nucleon effective mass turned out to be close to that of the free nucleon, $M^*/M = 0.9$.

PACS numbers: 25.30.Cg, 27.20. + n, 27.30. + t

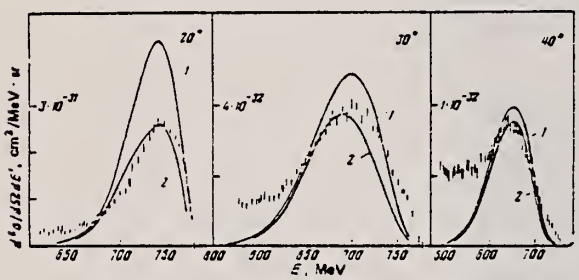

FIG. 1. Differential cross sections measured on the ^{9}Be nucleus at an initial electron energy 799 MeV. The scattering angle is marked on each plot. Curves 1 and 2 show the theoretical cross sections calculated in the impulse approximation using the real nucleon mass (1) and the effective nucleon mass (2).

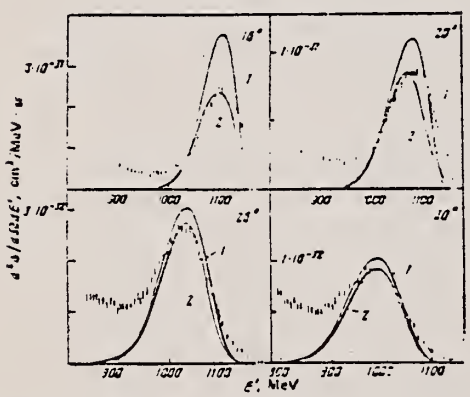

FIG. 3. The same as Fig. 1, but at an initial electron energy 1178 MeV.

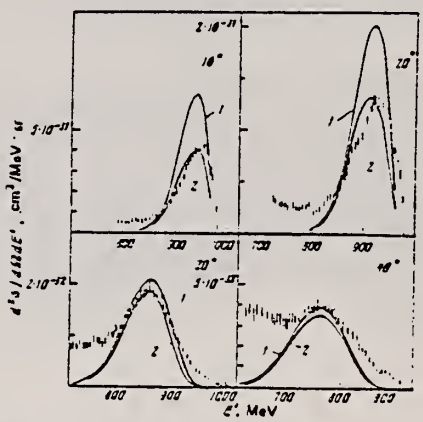

FIG. 2. The same as Fig. 1, but at an initial electron energy 996 MeV.

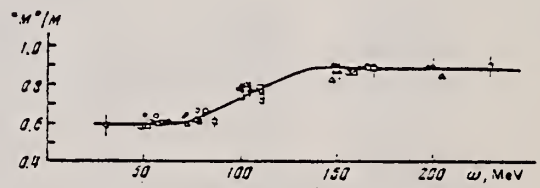

FIG. 4. Reduction coefficient M^*/M as a function of energy transfer: ●—^{9}Be, ▲—^{12}C, ○—^{14}N, △—^{16}O, □—^{27}Al. The curve has been drawn through the experimental points by hand.

REF. P. Dougan
Z. Physik A284, 165 (1978)

ELEM. SYM.	A	Z
Be	9	4

METHOD

REF. NO. 78 Do 1 egf

REACTION	RESULT	EXCITATION ENERGY	SOURCE		DETECTOR		ANGLE
			TYPE	RANGE	TYPE	RANGE	
G,P	ABX	67-600	C	100-600	TEL-D		DST

PROTONS OVER 50 MeV

Data on the differential cross-sections for the emission of photo-protons from beryllium irradiated with bremsstrahlung of various end-point energies up to a maximum of 600 MeV are presented and discussed. Particular attention has been paid to the photon energy-region around 150 MeV, where a dip in the total cross-sections for photon absorption has been reported. No evidence of anomalous structure is observed.
The data are compared with the predictions of the intra-nuclear cascade model PICA. Good fits can be obtained with a value of 7.2 ± 1.0 for the quasi-deuteron constant.

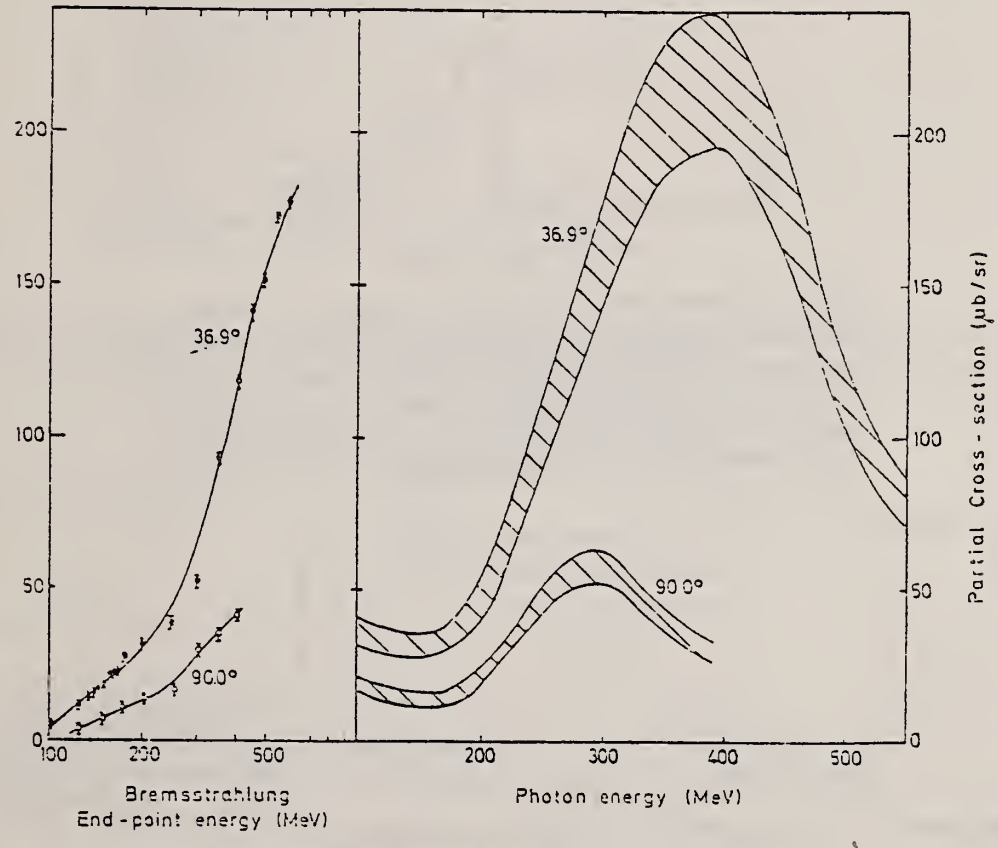

Fig. 1. The yields of photo-protons (integrated over energies from about 50 to about 100 MeV) observed at 36.9 and 90.0 degrees lab. and the values of partial cross-sections derived from them using the data-smoothing method. The solid curves in Figure 1a show the fifth-order polynomials fitted to the experimental data and which are unfolded to give the values shown in Figure 1b. The permissible ranges of variation of the (partial) cross-sections are as indicated. This is discussed in the text

over

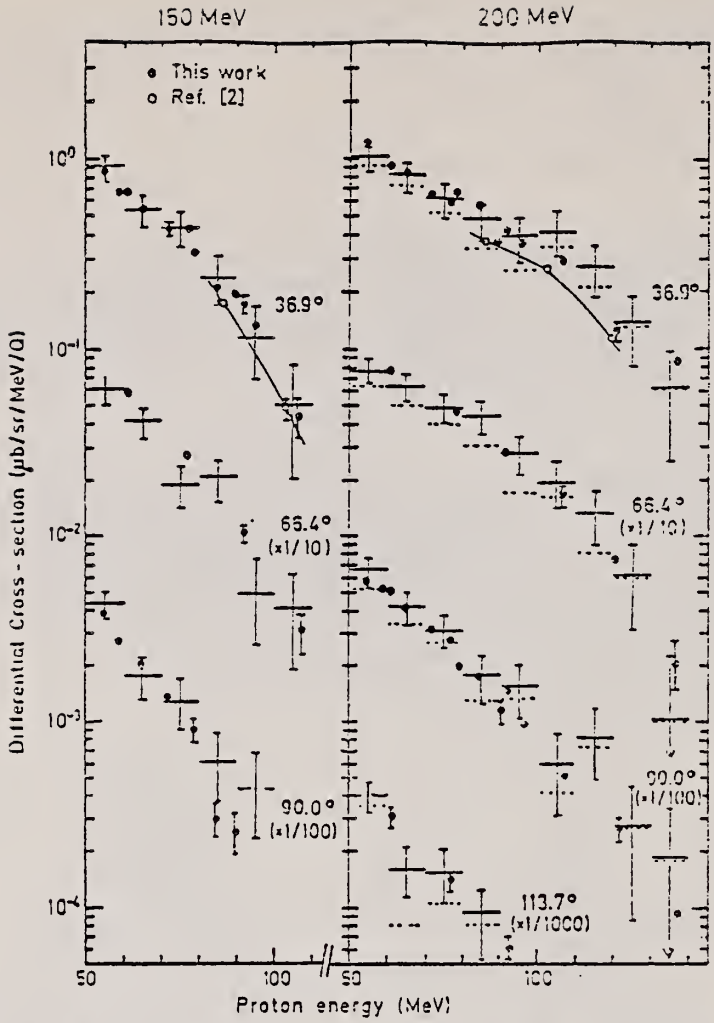

Fig. 2. Experimental values of the differential cross-sections for photo-proton production for beryllium irradiated with bremsstrahlung of maximum energy 150 and 200 MeV are compared with PICA predictions with $L = 7.2$. The energy-resolution of the experimental data varies from ≃25 MeV at 50 MeV to ≃15 MeV at 160 MeV. The PICA results are averaged over intervals of ten degrees on either side of the mean values. The experimental values at different angles have been shifted by the stated scale-factors to improve the legibility of the drawing. The dotted lines in the 200 MeV diagram show the effect of completely excluding photons of energies between 140 and 160 MeV in PICA

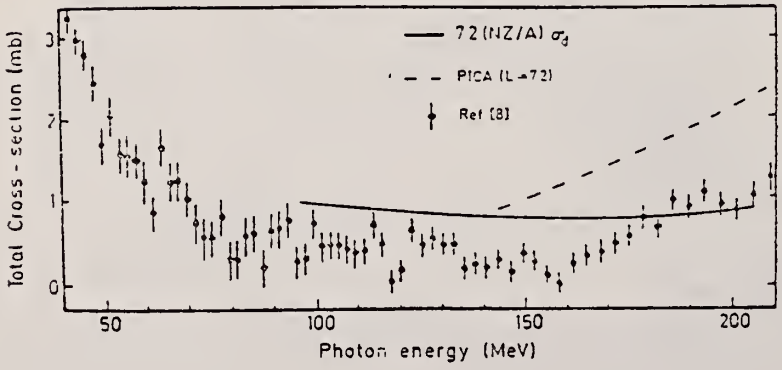

Fig. 4. Experimental values of the total cross-sections for the absorption of photons in beryllium nuclei as reported in [8] are compared with results calculated using PICA with $L = 7.2$ and with those given by $\sigma_{tot} = 7.2\,(NZ/A)\,\sigma_d$. As can be seen, the experimental values are considerably lower than expected

[8] Ahrens, J., Borchert, H., Czock, K.H., Eppler, H.B., Gimm, H., Gundrum, H., Kroning, M., Riehn, P., Sita Ram, G., Ziegler, A., Ziegler, B.: Nucl. Phys. A251, 479 (1975)

REF. K. Nakamura, S. Hiramatsu, T. Kamae, H. Muramatsu, N. Izutsu, Y. Watase
Nucl. Phys. A296, 431 (1978)

ELEM. SYM.	A	Z
Be	9	4

METHOD

REF. NO. 78 Na 3 hg

REACTION	RESULT	EXCITATION ENERGY	SOURCE TYPE	SOURCE RANGE	DETECTOR TYPE	DETECTOR RANGE	ANGLE
E,E/P	SPC	0*60	D	700	MAG-D		52

Abstract: The proton spectral functions of ^{6}Li, ^{7}Li, ^{9}Be and ^{10}B obtained from the (e, e'p) reactions at 700 MeV are presented. The results were analyzed in the distorted-wave impulse approximation, using the shell-model single-particle wave functions consistent with the elastic electron scattering results. The observed 1p proton momentum distributions for the nuclei ^{6}Li, ^{7}Li and ^{9}Be show significant disagreement with the shell-model momentum distributions. The occupation probabilities of the proton single-particle states are around 0.7, with a few exceptions.

*SEPARATION ENERGY

E NUCLEAR REACTIONS ^{6}, ^{7}Li, ^{9}Be, ^{10}B(e, e'p), E = 700 MeV; measured $\sigma(E_p, \theta_p)$; deduced proton spectral functions. DWIA calculations. Enriched ^{6}, ^{7}Li, ^{10}B and natural ^{9}Be targets.

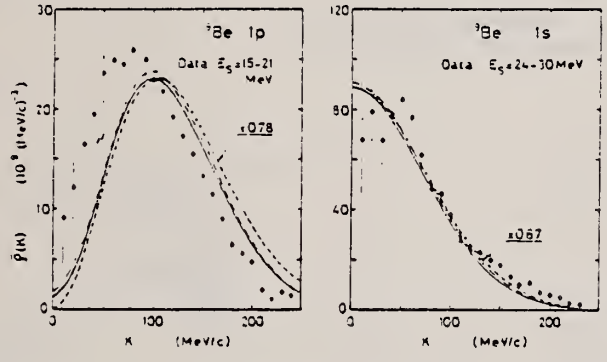

Fig. 5. The distorted momentum distributions corresponding to the optical potentials A (the solid curves) and B (the dot-dashed curves), and the undistorted momentum distributions (the dashed curves), calculated from the shell-model single-particle wave functions used in the DWIA analysis (a) ^{6}Li, (b) ^{7}Li, (c) ^{9}Be and (d) ^{10}B. For comparison, data points in the appropriate separation energy ranges are shown. They are arbitrarily normalized to the calculated distorted momentum distributions.

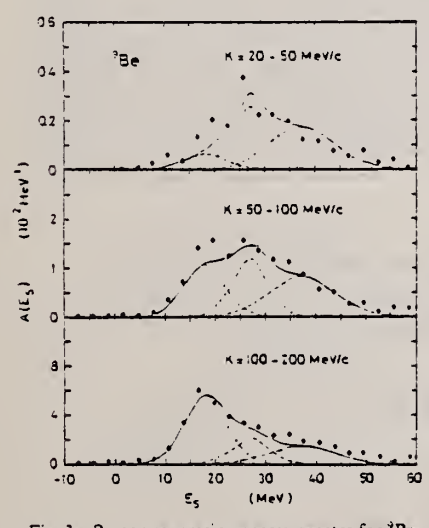

Fig. 3a. Proton separation energy spectra for ^{9}Be. The curves are as in fig. 1a.

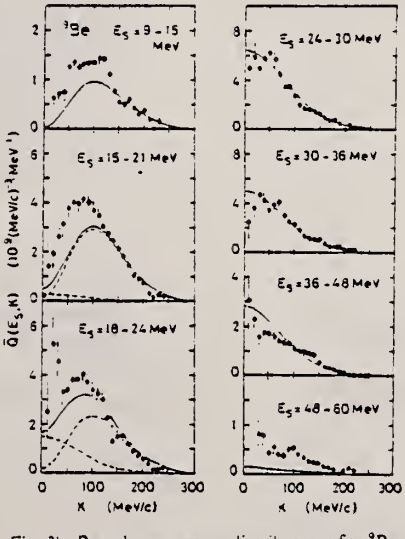

Fig. 3b. Recoil momentum distributions for ^{9}Be. The curves are as in fig. 1b.

REF. E.C. Gooth, B. Chasan, F.L. Milder, B.L. Roberts, J. Comuzzi
Phys. Rev. C20, 1603 (1979)

ELEM. SYM.	A	Z
Be	9	4

METHOD

REF. NO. 79 Bo 2 hg

REACTION	RESULT	EXCITATION ENERGY	SOURCE		DETECTOR		ANGLE
			TYPE	RANGE	TYPE	RANGE	
G,PI+	ABX	150-170	C	150-170	ACT-I		90

The total cross sections relative to photoproduction off the proton have been measured for the reactions $^{16}O(\gamma,\pi^-)^{16}N$ and $^{9}Be(\gamma,\pi^+)^{9}Li$ over the energy region from the production threshold up to 12 MeV over threshold. A distorted wave impulse approximation calculation has been performed for the $^{16}O(\gamma,\pi^-)^{16}N$ reaction and is seen to be $\simeq 30\%$ higher than the observed cross section from threshold to 10 MeV. The $^{9}Be(\gamma,\pi^-)^{9}Li$ reaction represents the first (γ,π^-) measurement near threshold in which the cross section is not dominated by the $\vec{\sigma}\cdot\vec{\epsilon}$ term in the production Hamiltonian.

[NUCLEAR REACTIONS $^{16}O(\gamma,\pi^+)^{16}N$, $^{9}Be(\gamma,\pi^+)^{9}Li$, bremsstrahlung end point energies to 175 MeV, measured $\sigma(E)$; calculated $\sigma(E)$, DWIA.]

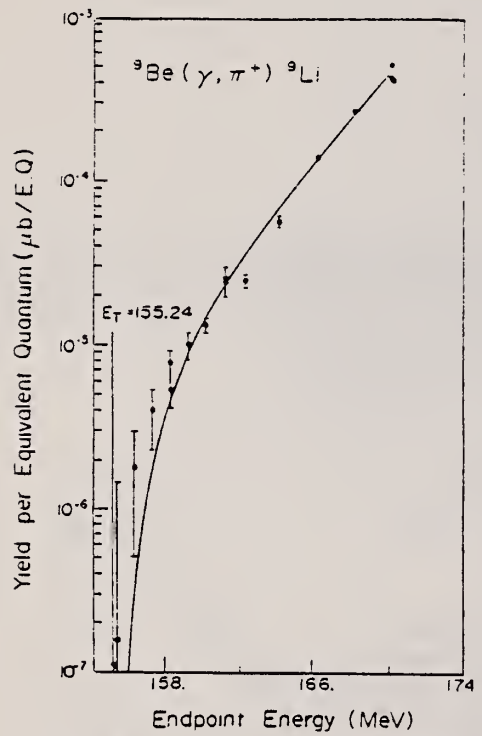

FIG. 2. The $^{9}Be(\gamma,\pi^+)^{9}Li$ yield per equivalent quantum. The solid curve is a fit as described in the text.

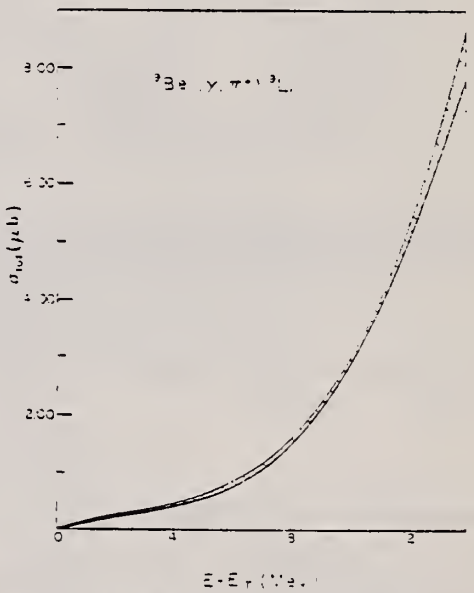

FIG. 5. The measured total cross section for the $^{9}Be(\gamma,\pi^-)^{9}Li$ reaction. The shaded region represents the statistical error on the cross section. The systematic error is an additional 7%.

REF. A.Yu. Buki, N.G. Shevchenko, V.N. Polishchuk, A.A. Khomich, I.I. Chkalov
Yad. Fiz. 30, 5 (1979)
Sov. J. Nucl. Phys. 30, 2 (1979)

ELEM. SYM.	A	Z
Be	9	4

METHOD

REF. NO.	
79 Bu 12	hg

REACTION	RESULT	EXCITATION ENERGY	SOURCE		DETECTOR		ANGLE
			TYPE	RANGE	TYPE	RANGE	
E,E/	FMF	10-80	C	135-237	MAG-D		DST

As the result of measurements of the spectra of electrons scattered by ^{9}Be, the transverse and longitudinal form factors for electrodisintegration are obtained in the region of the quasielastic scattering peak. In both the longitudinal and transverse components of the form factor, giant-resonance peaks are observed up to an excitation energy 63 MeV. Hindrance coefficients are obtained for the quasielastic scattering cross section for the transverse and longitudinal form-factor components. The ratio of the transverse form factor for quasielastic scattering to the longitudinal form factor is measured.

QUASI-ELASTIC SCATT

PACS numbers: 25.30.Cq, 27.20. + n

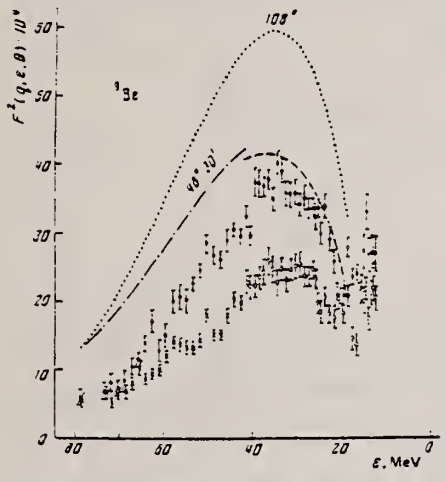

FIG. 2. Form factors for electrodisintegration of the ^{9}Be nucleus, measured at various scattering angles. The lines are the result of calculation of the form factors for quasielastic electron scattering[1] with values of θ and E_0 at which the measurements were made. The solid circles and the dotted line correspond to the experimental results and calculation at θ = 108°; the hollow circles and the dashed line are for θ = 52°30′; the crosses and the dot-dash line are for θ = 48°30′ (the measurements at θ = 48° are given for the portion of the spectrum 42 MeV < ε < 80 MeV).

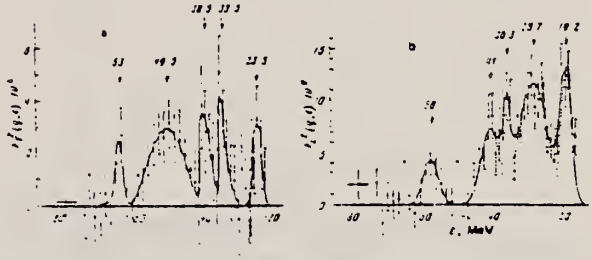

FIG. 4. Transverse and longitudinal spectra of the differential form factors of excited states of the ^{9}Be nucleus as the result of subtraction from the electrodisintegration spectra of the quasielastic electron-scattering continuum pedestal. The solid line in Fig. a has been drawn by eye through the points, and that in Fig. b is the result of variation by the method of least squares of the locations, heights, and half-widths of the sum of the Gaussian distributions shown by the dotted curves.

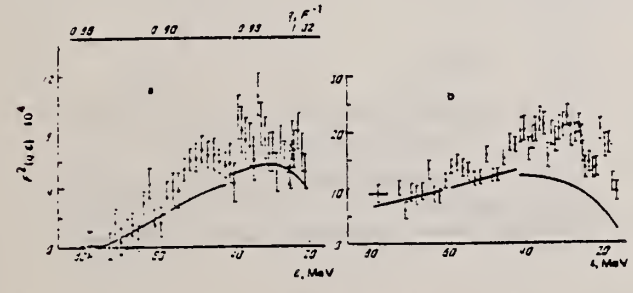

FIG. 3. Spectra of the transverse differential form factor $F_T^2(q, \varepsilon)$ (a) and of the longitudinal differential form factor $F_T^2(q, \varepsilon)$ (b) for electrodisintegration of ^{9}Be. The solid line is the calculated quasielastic electron scattering normalized to the experimental data.

REF. S. Homma, M. Kanazawa, K. Maruyama, Y. Murata, H. Okuno, A. Sasaki, T. Taniguchi
Phys. Rev. Lett. 45, 706 (1980)

ELEM. SYM.	A	Z
Be	9	4

METHOD

REF. NO. 80 Ho 1 hg

REACTION	RESULT	EXCITATION ENERGY	SOURCE		DETECTOR		ANGLE
			TYPE	RANGE	TYPE	RANGE	
G,P	ABX	200-400	D	200-400	MAG-D		25

Momentum spectra of protons in the reaction of γ + Be $\rightarrow p$ + anything in the incident energy range from 180 to 420 MeV were measured. The spectrum obtained shows two peaks which are interpreted to be due to the protons in reactions γ + "N" $\rightarrow p + \pi$ and γ + "d" $\rightarrow p + n$, where "N" and "d" are the quasifree nucleons and neutron-proton systems, respectively, in the beryllium nucleus.

COIN WITH CHARGED PART.

PACS numbers: 25.20.+y, 21.60.Gx, 27.20.+n

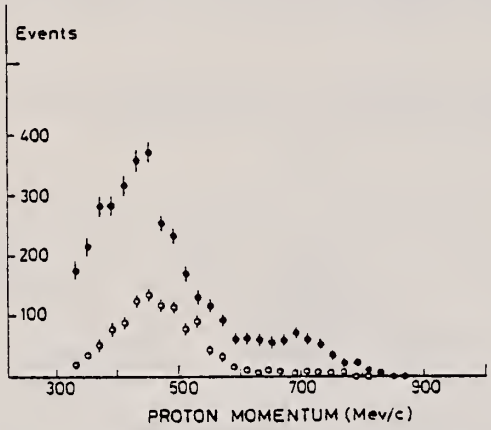

FIG. 2. Momentum spectrum of the protons at $E_\gamma = 360 \pm 20$ MeV. The solid circles represent the reaction γ + Be $\rightarrow p$ + (charged particle) + anything.

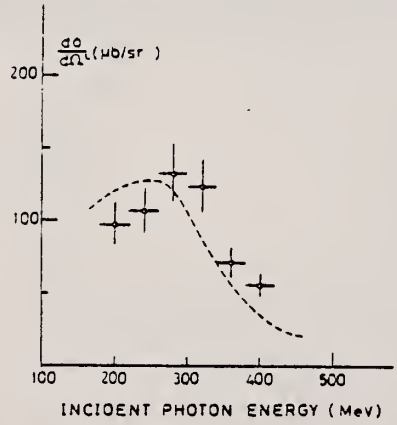

FIG. 3. The integrated cross sections $d\sigma(\gamma + \text{"}d\text{"} \rightarrow p + n)/d\Omega|_{Be}$ as a function of incident energy. The dotted curve is $13 \times d\sigma(\gamma + d \rightarrow p + n)/d\Omega|_{free}$ for similar kinematical conditions. The errors indicated are the quadratic sum of statistical and systematic uncertainties.

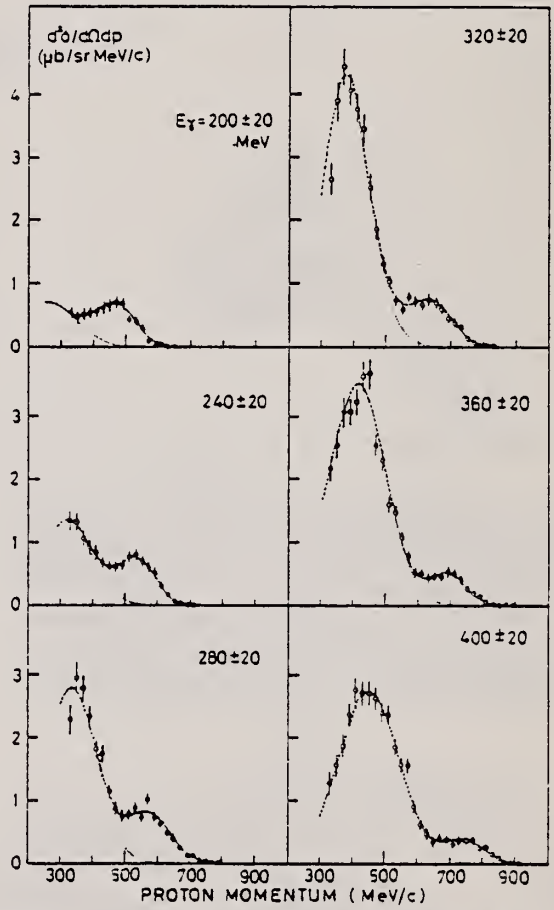

FIG. 1. Momentum spectra of the protons at the laboratory angle 25° ± 5° in the reaction γ + Be $\rightarrow p$ + anything. The dotted curves are Gaussian fits of the first peak.

REF. M. Nilsson, B. Schröder, B. Bülow, J. Grintals, G.G. Jonsson, B. Lindner, K. Srinivasa Rao, S. Susila
Zeit. Phys. A294, 253 (1980)

ELEM. SYM.	A	Z
Be	9	4

METHOD

REF. NO. 80 Ni 4 hg

REACTION	RESULT	EXCITATION ENERGY	SOURCE		DETECTOR		ANGLE
			TYPE	RANGE	TYPE	RANGE	
G,PI+	ABX	150-800	C	100-800	ACT-I		4PI

The reaction $^{9}Be(\gamma,\pi^{+})^{9}Li$ has been studied with bremsstrahlung in the energy range 100-800 MeV employing the radioactivity method. The cross section curve deduced is compared with an impulse approximation calculation including a volume and a surface production model. In the energy region 200-300 MeV the experimental cross section, approximately 7 μb, is best reproduced by the surface production model with a cut-off parameter r_0 equal to 2.8 fm, i.e. somewhat larger than the r.m.s. radius of ^{9}Be.

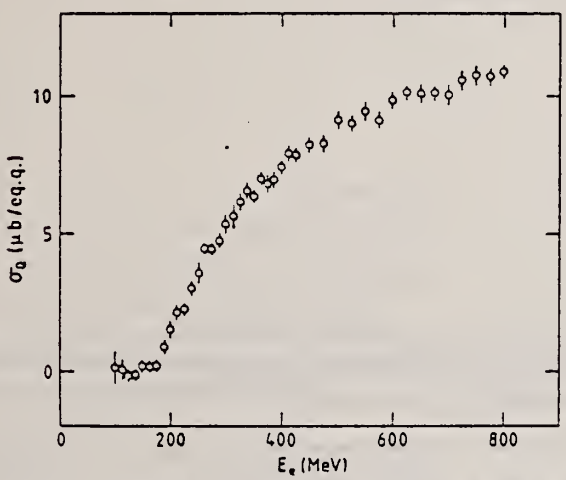

Fig. 2. Total bremsstrahlung yield for the reaction $^{9}Be(\gamma,\pi^{+})^{9}Li$ as a function of electron energy

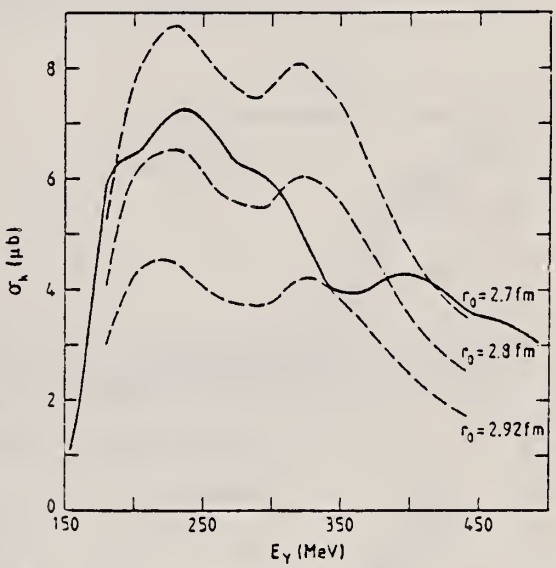

Fig. 4. *Solid curve:* Total experimental cross section for the reaction $^{9}Be(\gamma,\pi^{+})^{9}Li$ as a function of photon energy. *Dashed curves:* Theoretical cross sections for the same reaction assuming a surface production model for the pions with different values of r_0

REF. P. Stoler, E.J. Winhold, F. O'Brien, P.F. Yergin, D. Rowley, K. Min, J. LeRose, A.M. Bernstein, K.I. Blomqvist, G. Franklin, N. Paras, M. Pauli
Phys. Rev. C22, 911 (1980)

ELEM. SYM.	A	Z
Be	9	4

METHOD

REF. NO. 80 St 3 hg

REACTION	RESULT	EXCITATION ENERGY	SOURCE		DETECTOR		ANGLE
			TYPE	RANGE	TYPE	RANGE	
E,PI+	RLY	182-184	C	185	MAG-D		90
G,PI+	RLY	182-184	C	185	MAG-D		90

TEST VIRTUAL PHOTONS

The virtual photon spectrum shape and intensity within several MeV of the kinematic limit was measured for $^{9}Be(e,\pi^{+})^{9}Li,e'$ and $^{16}O(e,\pi^{+})^{16}N,e'$ ($T_{\pi}=28$ MeV, $\theta_{\pi}=90°$). The intensity over this interval is 1.25 ± 0.10 times plane-wave virtual photon theory predictions; the shape agrees with theory within errors. Measurements on the proton 30 to 55 MeV below the end point agree with the intensity predictions of virtual photon theory within the errors ($\pm 8\%$).

[NUCLEAR REACTIONS $^{16}O(e,\pi^{+})$, $E=180.4$ MeV; $^{9}Be(e,\pi^{+})$, $E=184.3$ MeV; measured $\sigma(E_{\pi},90°_{lab})$ relative to (γ,π^{+}), near $E_{\pi}=28$ MeV. $^{1}H(e,\pi^{+})$, $E=230$ MeV; measured $\sigma(E_{\pi},90°_{lab})$ relative to (γ,π^{+}), near $E_{\pi}=18$, 30 MeV. Compared to PWBA virtual photon theory.]

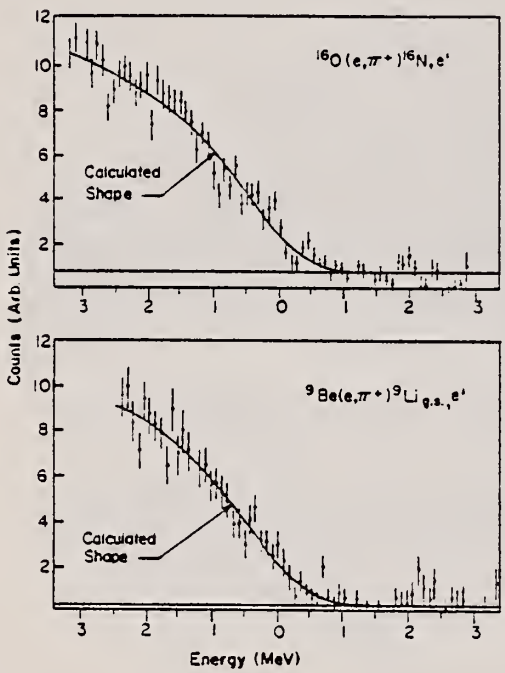

FIG. 1. Number of pions as a function of virtual photon energy. The zero on the abscissa corresponds to the virtual photon spectrum end point, 179.9 MeV for ^{16}O and 184.3 MeV for ^{9}Be. The solid curves were obtained as described in the text and normalized to the experimental data.

TABLE I. Results for R/V, the real-to-virtual ratio as defined in the text. The quantity E_0 is the incident electron total energy, T_{π} the pion kinetic energy, k the virtual photon energy, and ΔT_{π} the averaging interval over pion energy in the experiment (corresponding to the range of k). Note that k is close to the end point for ^{16}O and ^{9}Be but 30 to 55 MeV below for ^{1}H.

	$^{16}O(e,\pi^{+})$	$^{9}Be(e,\pi^{+})$	$^{1}H(e,\pi^{+})$	
E_0(MeV)	180.4	184.3	230	230
T_{π}(MeV)	28	28	18	30
k(MeV)	176.8–179.9	182.2–184.3	174.7–181.7	188.3–199.4
ΔT_{π}(MeV)	3.0	2.0	4.9	7.6
$(R/V)_{expt}$	78 ± 9	72 ± 8	71 ± 6	80 ± 6
$(R/V)_{theor}$	91	96	70	77
$(R/V)_{theor}/(R/V)_{expt}$	1.17 ± 0.14	1.33 ± 0.15	0.99 ± 0.08	0.96 ± 0.08

REF. J. Arends, J. Eyink, A. Hegerath, K.G. Hilger, B. Mecking, G. Nöldeke, H. Rost
Phys. Lett. 98B, 423 (1981)

ELEM. SYM.	A	Z
Be	9	4

METHOD

REF. NO. 81 Ar 1 hg

REACTION	RESULT	EXCITATION ENERGY	SOURCE		DETECTOR		ANGLE
			TYPE	RANGE	TYPE	RANGE	
G,MU-T	ABX	215-386	D	215-386	TOF-D		4PI

DATA ALSO IN 81AR3

Double differential cross sections for the photo-emission of protons and charged pion production were investigated for a number of target nuclei (He, Be, C, O, Al, Ti, Cu, Sn, Pb) in the photon energy range k = (215–386) MeV. On the basis of these experimental results the total hadronic cross section was determined.

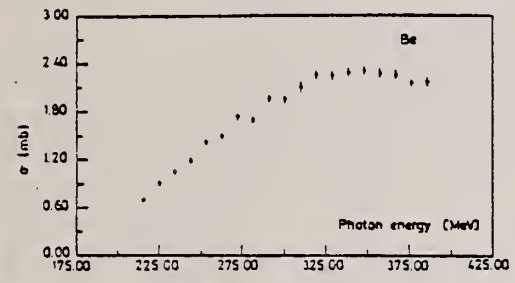

Fig. 4. Cross section for the photo emission of at least one charged particle of energy $T_p > T_p^{min}$ or $T_\pi > T_\pi^{min}$ off Be in a single hadronic process. (Statistical errors only.)

The total hadronic cross sections for all measured elements can be parametrized in the form

$$\sigma(k,A) = \sigma_0(k) \cdot A^x ,$$

A being the atomic number, with a constant exponent x = 1.1. The photon energy dependence of σ_0 is shown in fig. 7. Compared to the mean cross section for a free nucleon (the solid line in fig. 7) the excitation of the Δ-resonance is suppressed. Such a suppression is expected in the Δ-hole model [11].

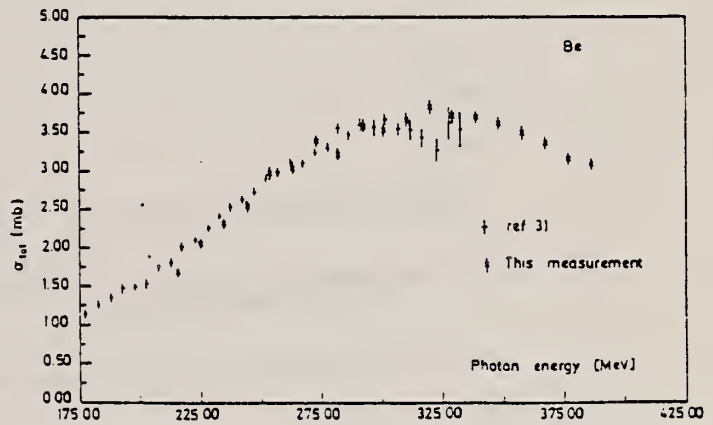

Fig. 5. Total hadronic cross section for Be. Our data are compared to ref. [3]. (Statistical errors only.)

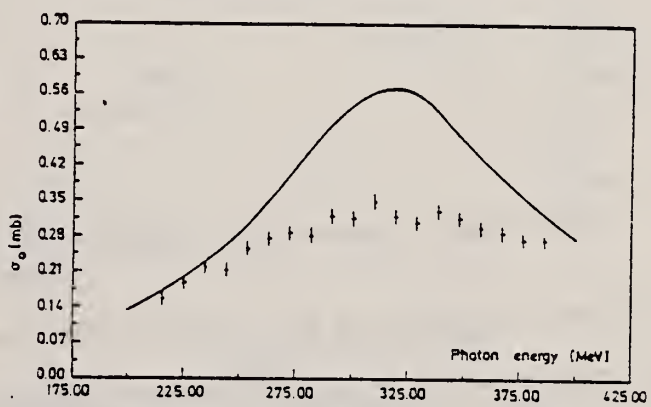

Fig. 7. Parameter σ_0 as a function of photon energy (data points) compared to the mean cross section for a free nucleon (solid line

REF. J. Arends, J. Eyink, A. Hegerath, K.G. Hilger, B. Mecking, G. Nöldeke, H. Rost
Nucl. Phys. A358, 367c (1981)

ELEM. SYM.	A	Z
Be	9	4

METHOD

REF. NO. 81 Ar 3 hg

REACTION	RESULT	EXCITATION ENERGY	SOURCE TYPE	SOURCE RANGE	DETECTOR TYPE	DETECTOR RANGE	ANGLE
G,MU-T	ABX	215-386	D	215-386	TOF-D		4PI

Abstract: Double differential cross sections for the photoemission of protons and charged pion photoproduction were investigated for a number of target nuclei (He, Be, C, O, Al, Ti, Cu, Sn, Pb) using the tagged bremsstrahlung beam at the Bonn 500 MeV-Synchrotron in the photon range k = (215-386)MeV. On the basis of these experimental results the total hadronic cross section was determined.

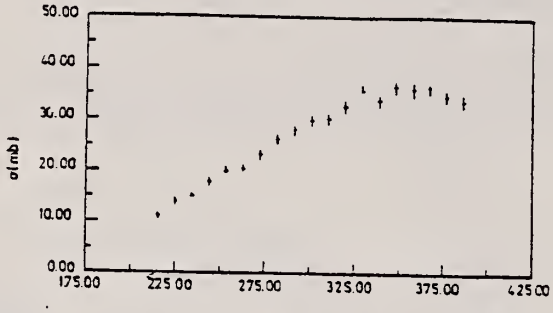

Fig. 2. Cross section for the process: $\gamma + Pb \rightarrow p + X$. The proton threshold is 58 MeV.

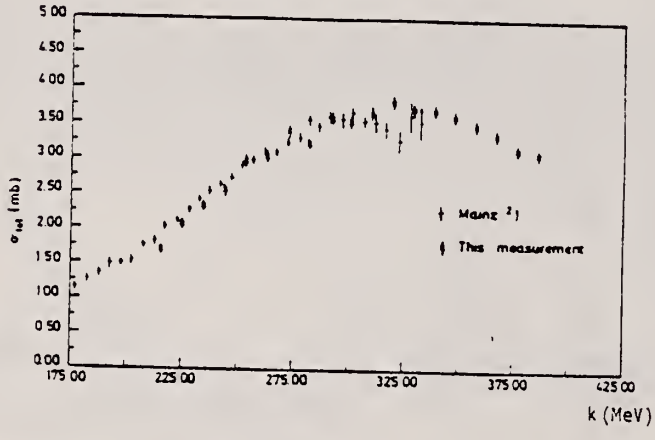

Fig. 3. Total hadronic cross section for Be. The data are compared to the cross section taken from ref.[2]).

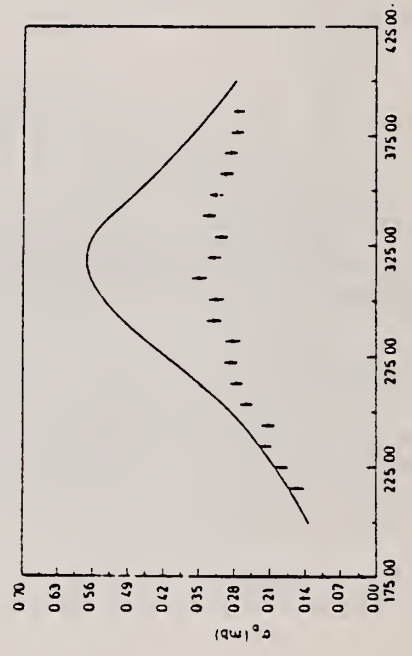

Fig. 4. Parameter σ_0 compared to the cross section for a free nucleon (full line).

The photon energy dependence of the total cross sections for heavier nuclei are similar to the Be results. The complete data set can be parametrized in the form

$$\sigma(k,A) = \sigma_0(k) \cdot A^x.$$

The exponent is constant $x = 1.1$. The photon energy dependence of σ_0 is shown in fig. 4. Compared to the mean cross section for a free nucleon, the excitation of the Δ-resonance is suppressed.

REF. B. Bellinghausen, A. Christ, H.J. Gassen, G. Goerigk, R. Müller
G. Nöldeke, T. Reichelt, H. Stanek and P. Stipp
Nucl. Phys. A358, 373c (1981)

ELEM. SYM.	A	Z
Be	9	4

METHOD

REF. NO. 81 Be 3 HG

REACTION	RESULT	EXCITATION ENERGY	SOURCE		DETECTOR		ANGLE
			TYPE	RANGE	TYPE	RANGE	
G,PIO	ABX	280-386	C	300-450	MGP-D		0

Abstract: π^0 photoproduction on ^{3}He, Li(nat) and ^{9}Be has been measured under small angles in the P_{33} resonance region.

Table 1

Cross sections as function of energy and momentum transfer

K_{max}	K	q	$d\sigma/d\Omega^*$ in ub/sterad		
MeV	MeV	fm^{-1}	^{3}He	Li(nat)	^{9}Be
300	280	0.27	12.4 ± 1.5	21.0 ± 2.4	23.6 ± 2.7
320	296	0.27	14.6 ± 1.5	26.9 ± 2.1	34.4 ± 2.7
370	334	0.26	14.3 ± 1.5	24.9 ± 2.0	31.0 ± 2.6
390	361	0.23	10.0 ± 1.1	21.1 ± 1.6	24.5 ± 1.8
450	386	0.27	7.7 ± 1.1	22.7 ± 2.3	22.8 ± 2.3

REF. M. Fujishiro, T. Tabata, K. Okamoto, T. Tsujimoto
Can. J. Phys. 60, 1672 (1982)

ELEM. SYM.	A	Z
Be	9	4

METHOD	REF. NO.	
	82 Fu 1	egf

REACTION	RESULT	EXCITATION ENERGY	SOURCE		DETECTOR		ANGLE
			TYPE	RANGE	TYPE	RANGE	
G,N	ABX	THR-2	D	1-2	BF3-I		4PI

RADIOISOTPE SOURCES

Six kinds of radioisotopes were used to measure cross sections of the ^{9}Be(γ, n) reaction near its threshold. The results obtained were 0.88 ± 0.16, 1.33 ± 0.24, 1.10 ± 0.20, 0.73 ± 0.13, 0.47 ± 0.09, and 0.18 ± 0.04 mb at 1674.7, 1705.2, 1724.9, 1778.9, 1836.0, and 2167.6 keV, respectively. The cross sections measured show a sharp peak near the threshold, and its width is narrower than that observed by Jakobson with Bremsstrahlung X-rays. Comparison of the present results with theories based on the valence neutron model indicates that the agreement is only qualitative.

On a utilisé six sortes de radioisotopes pour mesurer les sections efficaces de la réaction ^{9}Be(γ, n) près de son seuil. Les résultats obtenus sont 0.88 ± 0.16, 1,33 ± 0,24, 1,10 ± 0,20, 0.73 ± 0.13, 0,47 ± 0.09 et 0,18 ± 0.04 mb, à 1674.7, 1705.2, 1724.9, 1778.9, 1836.0 et 2167.6 keV, respectivement. Les sections efficaces mesurées présentent un pic prononcé au voisinage du seuil, et la largeur de ce pic est plus étroite que celle qu'a observée Jakobson avec des rayons X de freinage. La comparaison de ces résultats avec les théories basées sur le modèle du neutron de valence indique que l'accord est seulement qualitatif.

[Traduit par le journal]

Can. J. Phys., 60, 1672 (1982)

TABLE 3. Results of present measurements

E_γ (keV)	$\sigma(E_\gamma)$ (mb)
1674.7	0.88±0.16
1705.2	1.33±0.24
1724.9	1.10±0.20
1778.9	0.73±0.13
1836.0	0.47±0.09
2167.6	0.18±0.04

TABLE 4. Optimum values for the parameters $A_i (i = 1 \rightarrow 4)$ in the fitting function for the cross section [4.1]

A_1	A_2	A_3	A_4
2.515	0.295	−0.231	0.0257

$$[4.1] \quad \sigma(E_\gamma) = \frac{A_1(E_\gamma - 1666)^{A_2}}{1 + A_3\sqrt{E_\gamma - 1666} + A_4(E_\gamma - 1666)}$$

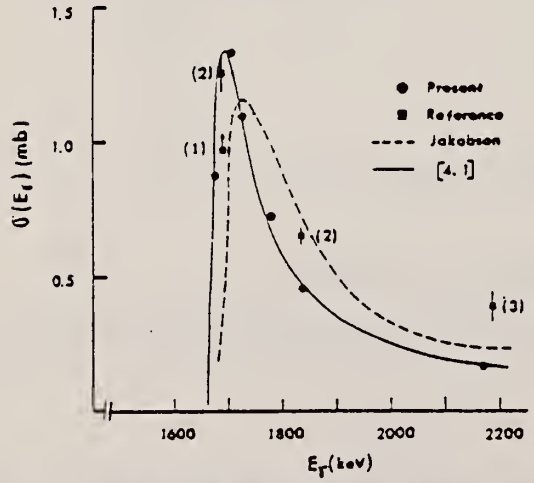

FIG. 4. Comparison of present results with previous data.

1. B. RUSSEL, D. SACHS, A. WATTENBERG, and R. FIELDS, Phys. Rev. 73, 545 (1948).
2. J. H. GIBBONS, R. L. MACKLIN, J. B. MARION, and H. W. SCHMITT, Phys. Rev. 114, 1319 (1959).
3. B. HAMERMESH and C. KIMBALL, Phys. Rev. 90, 1063 (1953).

BE
A=10

BE
A=10

REF. K.M. Subotic, B. Lalovic and B.Z. Stepancic
Nucl. Phys. A296, 141 (1978)

ELEM. SYM.	A	Z
Be	10	4

METHOD

REF. NO. 78 Su 1 rs

REACTION	RESULT	EXCITATION ENERGY	SOURCE TYPE	SOURCE RANGE	DETECTOR TYPE	DETECTOR RANGE	ANGLE
T,G	LFT	18	D	0- 1	SCD-D		DST

Abstract: The ^{7}Li(^{3}H, γ)^{10}Be radiative capture reaction has been studied for ^{3}H energies of 0.4–1.1 MeV. Gamma transitions to the ground and first excited states are observed. Their excitation functions at 0° and 90° and angular distributions at 0.8 MeV and 1.1 MeV are measured. The excitation curves show a peak at E_t = 0.8 MeV corresponding to an excitation energy in ^{10}Be of 17.79 MeV. This peak is interpreted as a resonance and the assignment J^{π} = 2^{+} is determined. The resonance structure observed in the capture reactions at 0° is much more pronounced than at 90°, indicating sizeable contributions of the direct capture process to the radiative transition strength.

18=17.79
Jπ=2+

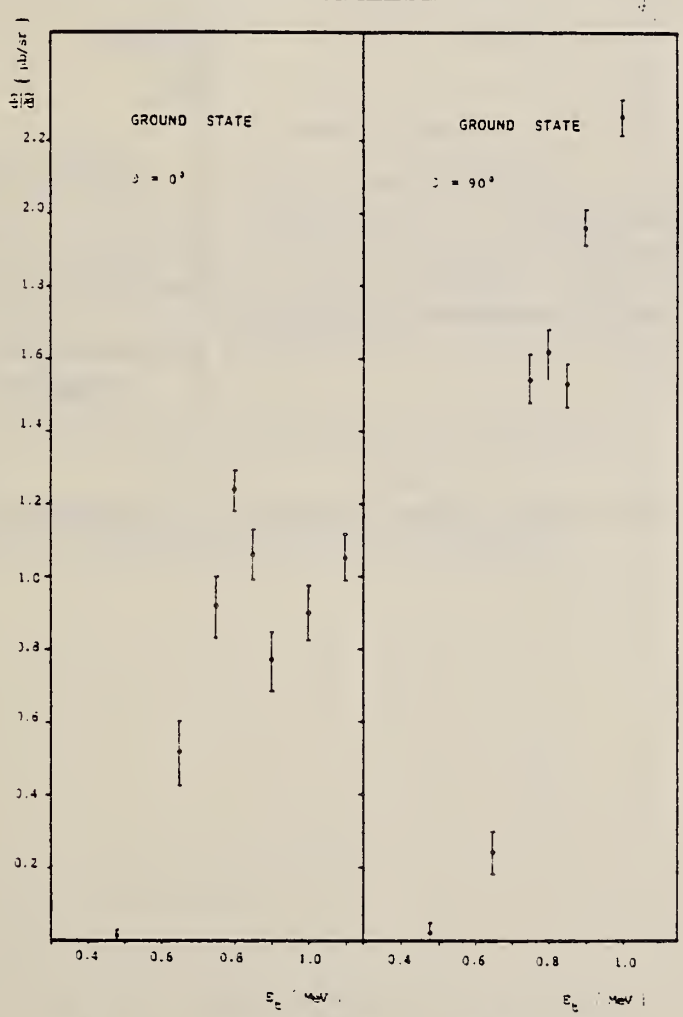

Fig. 3. Excitation curves for the reaction ^{7}Li(^{3}H, γ_0)^{10}Be at 0° and 90°.

over

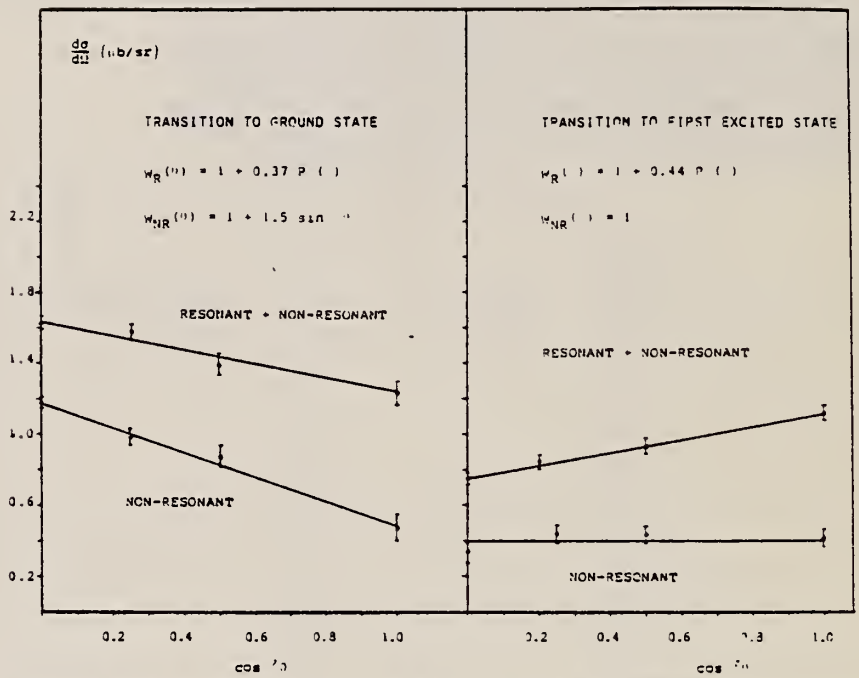

Fig. 5. The angular distributions of γ-rays from the 17.79 MeV level and non-resonant radiation from this energy region. The least-squares fits to the experimental points are shown.

BORON
Z=5

The name boron, analogous to carbon, was coined by Sir Humphry Davy. As borax, it was known to ancient peoples (Arabic, *buraq*; Persian, *borah*;) but was often confused by medieval writers. The boron hydrides (boranes) range from compounds so reactive as to be employed as rocket fuels, to materials so inert as to be promising in the field of heat-resistant plastics.

B

B

Ref. L. Cohen, R.A. Tobin, J. McElhinney
Phys. Rev. 114, 590 (1959)

Elem. Sym.	A	Z
B		5

Method: Betatron; photon scattering; NaI spectrometer; ion chamber

Ref. No.: 59 Co 5 — NVB

Reaction	E or ΔE	E_0	Γ	$\int \sigma dE$	Jπ	Notes
B(γ,γ)	Bremss.					Detector at 130°.
	5.0	4.46				ξ = Γ/Δ
	6.5	5.03				

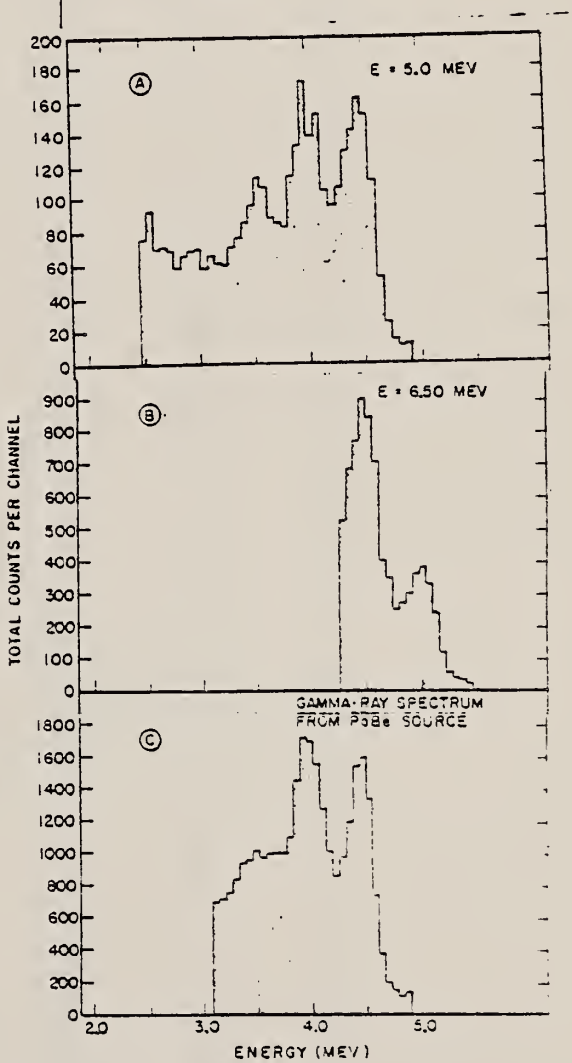

FIG. 2. Pulse-height distributions from the NaI crystal gamma rays scattered by B_4C at betatron energies of 5.0 and 6.5 Mev. The pulse-height distribution of a Mev gamma ray from Po-Be is given by the lowest curve (bottom).

TABLE I. The transmission measurements and the calculated resonance integrals.

Energy (Mev)	Transmission	$\sigma_n\xi$ (barns)	Δ (ev)	$\sigma_0\Gamma$ (Mev-barns)
4.46	0.76±0.04	5.7±1.5	13.9	(0.79±0.21)×10⁻³
5.03	0.75±0.03	6.2±1.1	15.7	(0.98±0.17)×10⁻³

Ref. V.P. Chizhov
Zhur. Eksp. i Teoret. Fiz. 38, 809 (1960)
Soviet Phys. JETP 11, 587 (1960)

Elem. Sym.	A	Z
B		5

Method: 90 MeV Bremsstrahlung; scintillator counter telescope

Ref. No.: 60 Ch 1 — JHH

Reaction	E or ΔE	E_o	Γ	$\int \sigma dE$	J π	Notes
B (γ,p)						Energy Range of particles detected:
B (γ,d)						E_d - 15.5-30 MeV
B (γ,t)						E_p - 15.5-30 MeV
						E_t - 17-30 MeV
						Ratios:
						$\sigma(\gamma,d)/\sigma(\gamma,p)$ } at $\theta = 90^\circ$
						$\sigma(\gamma,t)/\sigma(\gamma,d)$

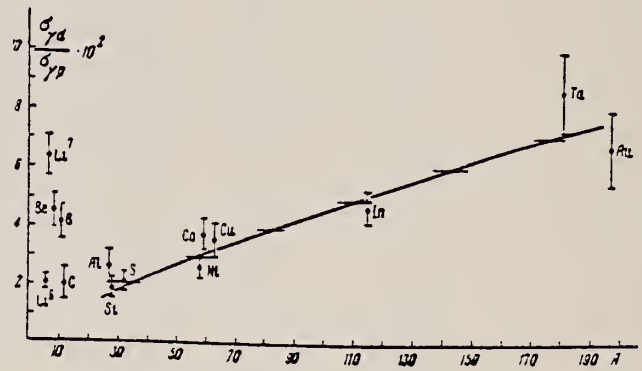

FIG. 3. Ratio of (γ, d) to (γ, p) cross sections for protons and deuterons of energies 15.5–30 Mev as function of atomic weight A. The solid curve shows the dependence given by Eq. (2), arbitrarily normalized.

TABLE I

Element	$100N_t/N_d$	Element	$100N_t/N_d$	Element	$100N_t/N_d$	Element	$100N_t/N_d$
Li^6	30±3	B	39±8	Ni	10±4	In	5±2.5
Li^7	22.5±2.5	Si	10±4	Co	2.5±2	Ta	10±4
Be	13±2.6	S	8±4	Cu	2.2±2	Au	3±3

Ref. K. Reibel, A.K. Mann
Phys. Rev. 118, 701 (1960)

Elem. Sym.	A	Z
B		5

Method
γ's from $F^{19}(\gamma,\alpha\gamma)$ reaction; protons from Van de Graaff; NaI

Ref. No. 60 Re 1 JHH

Reaction	E or ΔE	E_0	Γ	$\int \sigma dE$	Jπ	Notes
$B(\gamma,\gamma)$	~ 7					$\langle \bar{\sigma} \rangle$ (E_p = 2.05 MeV) = < 0.027 mb $\langle \bar{\sigma} \rangle$ (E_p = 2.40 MeV) = < 0.027 mb Assuming dipole angular distribution 90° measurement.

Ref. W. R. Dodge, W. C. Barber
Phys. Rev. 127, 1746 (1962)

Elem. Sym.	A	Z
B		5

Method
Magnetic analysis of proton psectrum produced by electron bombardment

Ref. No. 62 Do 1 — BG

Reaction	E or ΔE	E_o	Γ	$\int \sigma dE$	Jπ	Notes
(e,p)	30	5 (broad Max.) E_p=				Correspondence between (e,pe') reaction and (γ,p) reaction. Assumed electron has associated with it a virtual photon spectrum. Electron production yields were analyzed by use of E1 virtual photon spectrum to obtain σ(γ,p). $25\text{MeV-mb} < \int_{E_p=3.5}^{E_p=15} \sigma(\gamma,p)dE_\gamma < 42\text{MeV-mb}$

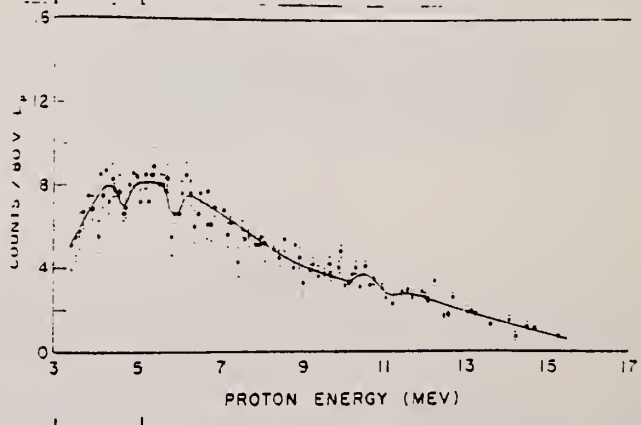

Ref. F.D. Seward
Phys. Rev. 125, 335 (1962)

Elem. Sym.	A	Z
B		5

Method
Linac; NaI; detector at 90°.

Ref. No.
62 Se 1 JHH

Reaction	E or ΔE	E_o	Γ	$\int \sigma dE$	Jπ	Notes
$B^{11}(\gamma,\gamma)$	Bremss; 13	4.4 5.0 7.3 8.8				

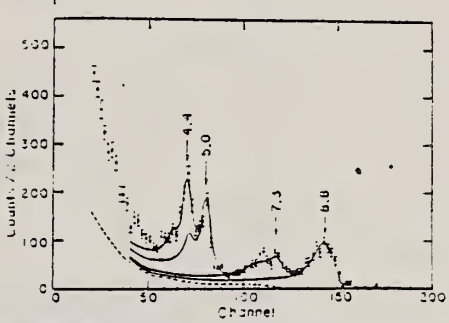

FIG. 3 Pulse-height spectrum for γ rays scattered from a ...ural B sample. The dashed line is the sample-out background. ...he solid lines are KS response functions for the indicated γ ray ...ergies

FORM NBS-418
(8-1-63)
USCOMM-DC 18556-P63

U.S. DEPARTMENT OF COMMER...
NATIONAL BUREAU OF STANDAR...

Ref. S. Costa, F. Ferrero, S. Ferroni, B. Minetti, C. Molino, R. Malvano
Phys. Letters 6, 226 (1963)

Elem. Sym.	A	Z
B		5

Method 100 MeV synchrotron; 4 π neutron detector; calcaulted integrated cross sections; fitted with polynomial of degree 7

Ref. No. 63 Co 3 — EGF

Reaction	E or ΔE	E_0	Γ	$\int \sigma dE$	Jπ	Notes
B(γ,xn)						

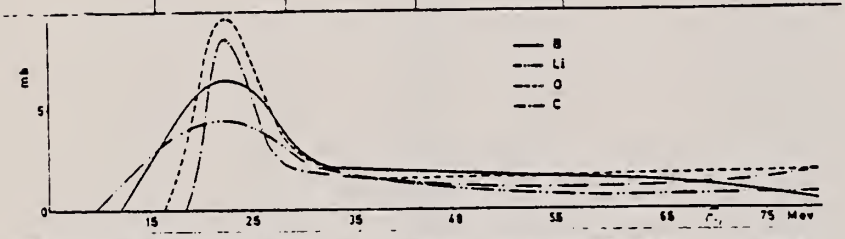

Fig. 1. Photoneutron cross sections for several light elements versus γ-ray energy.

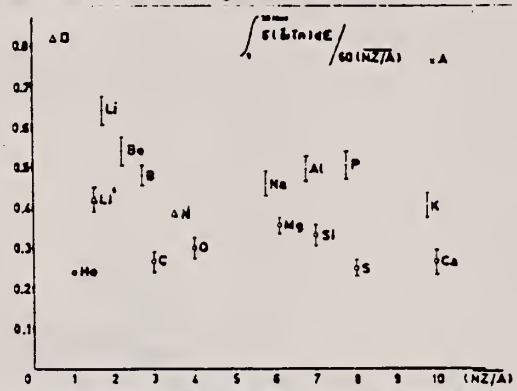

Fig. 2. 0 - 30 MeV integrated cross sections.

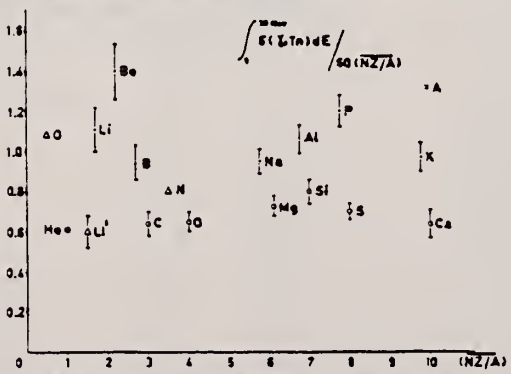

Fig. 3. 0 - 80 MeV integrated cross sections.

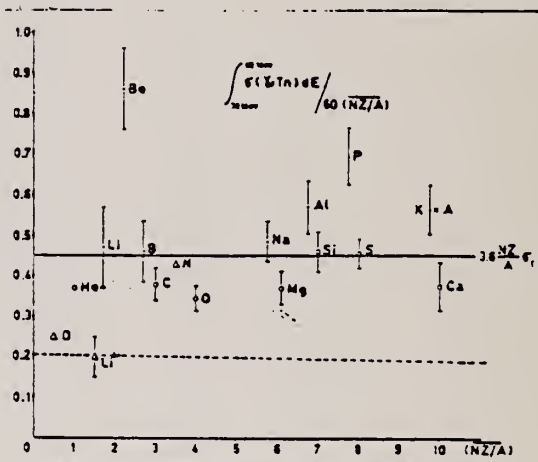

Fig. 4. 30 - 80 MeV integrated cross sections.

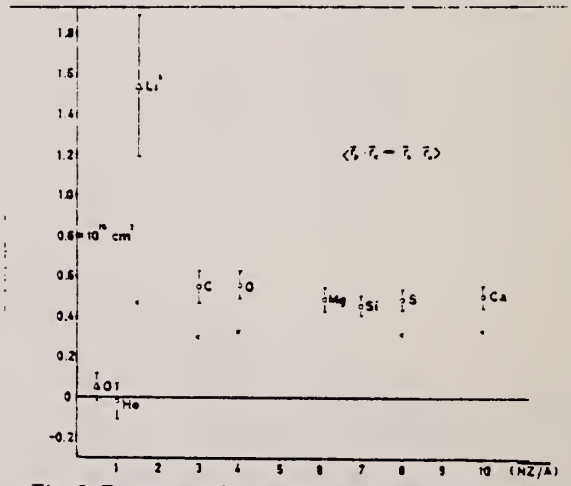

Fig. 5. Experimental value for the ground state expectation value of $(\vec{r}_p \cdot \vec{r}_n - \vec{r}_n \cdot \vec{r}_{n'})$.

Ref. F.S.Kim, F.F.Liu, F.J.Loeffler, T.R.Palfrey,Jr.

Phys.Rev. 129, 1362 (1963)

Elem. Sym.	A	Z
B		5

Method

335 MeV Synchrotron-scintillation counter telescope

Ref. No. 63Kil

BG

Reaction	E or ΔE	E_o	Γ	$\int \sigma dE$	Jπ	Notes
(γ,p)	$E_{\gamma max}$ 335					Data corrected for: nuclear absorption, γ attenuation, multiple scattering in target, multiple scattering in counter, pion contamination. Photoproton cross section found proportional to NZ/A (NZ is the probability of having np pair) over angular and energy region examined. (Z= 3,4,5,6). Differential cross section data given. T_p = proton energy (Fig. 3)

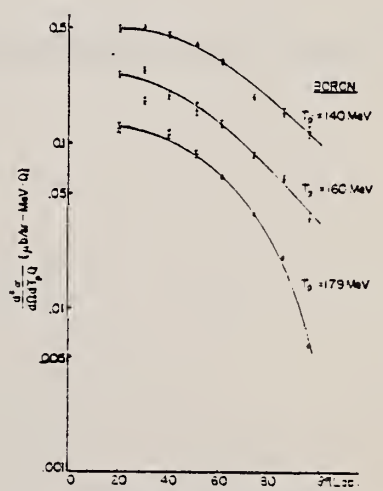

FIG. 3. Differential cross sections for photoproton production from beryllium.

METHOD	REF. NO.	
Van de Graaff; resonance fluorescence	64 Bo 1	NVB

REACTION	RESULT	EXCITATION ENERGY	SOURCE		DETECTOR		FIGURE
			TYPE	RANGE	TYPE	RANGE	
B,G	LFT	1-3	G	1 - 3	NAI-D		100
		(0.5 - 3.0)		(0.5 - 3.0)			

ABS

Table 1
Cases of observed resonance fluorescence

Nucleus multipol.	State (MeV)	Spin	Γ_0/Γ	$\tau(g\omega\Gamma_0/\Gamma^2)^{-1}$ (sec).	Mean lifetime τ DCW (sec)	Mean lifetime τ other (sec)	Ref.	Γ_0/Γ_W DCW
B^{11}	0.00	$\frac{3}{2}^-$						
M1	2.14	$\frac{1}{2}^-$	1	$12\pm4\times10^{-15}$	$6\pm2\times10^{-15}$	$4.7\pm0.6\times10^{-15}$	3)	0.55

REF. O. L. Garzon and G. G. Rocco
J. Inorg. Nucl. Chem. 29, 1 (1967)

B		5

METHOD

REF. NO. 67 Ga 1 JOC

REACTION	RESULT	EXCITATION ENERGY	SOURCE		DETECTOR		ANGLE
			TYPE	RANGE	TYPE	RANGE	
G,BE7	RLY	THR-23	C	23	ACT-I		4PI

TABLE 1.—PHOTOPRODUCTION OF ^{7}Be

Isotope	Foster and Voigt[1] Max. energy (45 MeV)	Yield of ^{7}Be relative to ^{11}C (%) Artus *et al.*[2] 44	Artus *et al.*[2] 56·5	Artus[3] 31·8–57	This work 23	Integrated cross section MeV-mbarn Nefkens *et al.*[4] 45–275	Lokan[5] 30	This work 23	Calculated mass threshold $-Q$(MeV)
^{9}Be	8 ± 2	7·6 $^{+0·5}_{-1}$	8·2 $^{+0·5}_{-1·3}$		1·88 ± 0·38	10	1·2 ± 0·2	0·47 ± 0·09	20·56
^{10}B		7·1 $^{+0·5}_{-0·9}$	8·3 $^{+0·6}_{-1·4}$						18·67
^{11}B		0·54 $^{+0·13}_{-0·17}$	0·84 $^{+0·17}_{-0·25}$						30·12
Natural B	2 ± 0·6	1·8 $^{+0·2}_{-0·3}$	2·3 $^{+0·2}_{-0·4}$		2·1 ± 0·42				
Enriched B		6·9 $^{+0·5}_{-0·9}$	8·0 $^{+0·5}_{-1·3}$						
^{12}C	12 ± 4	4·5 $^{+0·3}_{-0·4}$	5·8 $^{+0·3}$			13			26·3
^{16}O				[6]					

[6] Several experimental yields reported from 31·8–57 MeV.

[1] M. S. Foster and A. F. Voigt, *J. inorg. nucl. Chem.* 24, 343 (1962).
[2] H. Artus, G. Fricke and D. E. von Stein, *Z. Phys.* 178, 109 (1964).
[3] H. Artus, *Z. Naturf.* 20A, 320 (1965).
[4] B. M. K. Nefkins, G. Moscati and J. Todoroff, Abstract 4d/C421 of Contributed Papers to the Congress International de Physique Nucleaire, Paris, July, 1964.
[5] K. H. Lokan, *Proc. phys. Soc.* 70A, 836 (1957).

REF.	ELEM. SYM.	A	Z
N. N. Kaushal, E. J. Winhold, P. F. Yergin, H. A. Medicus and R. H. Augustson Phys. Rev. 175, 1330 (1968)	B		5

METHOD	REF. NO.	
	68 Ka 1	HMG

REACTION	RESULT	EXCITATION ENERGY	SOURCE		DETECTOR		ANGLE
			TYPE	RANGE	TYPE	RANGE	
G,N	ABX	50-85	C	55,85	TOF-D	10-85	67
							(67.5)

NEUT ENGY SPEC

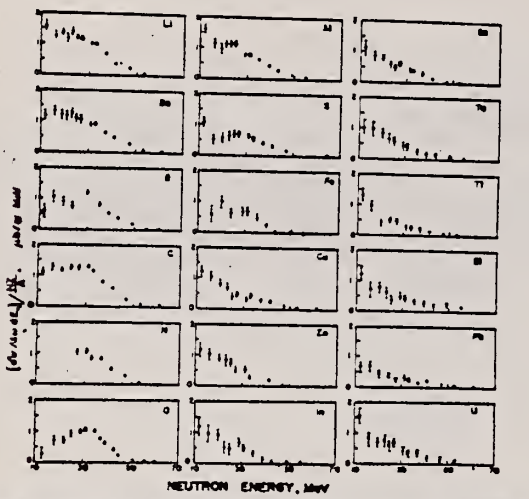

FIG. 6. Observed neutron spectra due to 55–85-MeV difference photon spectra. The effective cross sections have been divided by NZ/A.

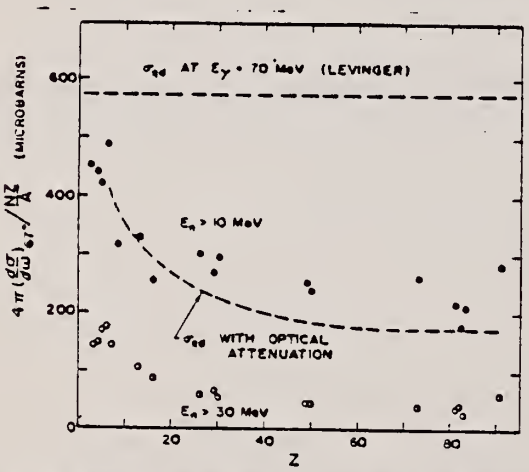

FIG. 7. Effective cross sections for production of fast neutrons with energies greater than 10 MeV (solid circles) and 30 MeV (open circles) by the 55–85-MeV photon difference spectrum. The dashed curves are modified quasideuteron model predictions as discussed in the text.

TABLE I. Comparison of present cross-section values in mb for production of high-energy photoneutrons by 55–85-MeV photons with measured cross sections $\sigma(\gamma,Tn)$, also in mb, for total photoneutron production. The present cross-section values are uncertain by 8 to 10% because of counting statistics and normalization errors; in addition all values depend on an absolute normalization in terms of the deuteron photodisintegration cross section, which is known to about 10% at these energies.

Target	$4\pi(d\sigma/d\omega)_{90°}$ (E_n>10 MeV) [Present experiment]	$\sigma(\gamma,Tn)$ Jones and Terwilliger[a]	Costa *et al.*[b]	Other results
Li	0.75		1.0	
Be	1.0	2.7	2.3	2.3[c]
B	1.0		1.4	
C	1.5	1.3	1.4	2.4[d]
O	1.3		1.6	
Al	2.8	5.5	4.6	8[d]
S	2.1		4.4	6.5[d]
Fe	4.2	16	12	
Cu	4.3	20	19	
Zn	4.4		15	
In	7.4			
Sn	7.0			
Ta	10.7	95		
Tl	10.7			
Pb	8.3	100		
Bi	13			
U	16	65		

[a] Average cross sections between 55 and 85 MeV, as read from Figs. 4 and 5 of Ref. 4.
[b] $\int_0^{85}\sigma dE - \int_0^{55}\sigma dE/50$, as taken from Fig. 4 of Ref. 5 and Table I of Ref. 6.
[c] S. Costa, L. Pasqualini, G. Piragino, and L. Roasio, Nuovo Cimento 42, 306 (1966).
[d] G. Bishop, S. Costa, S. Ferroni, R. Malvano, and G. Ricco, Nuovo Cimento 42, 148 (1966).

S. Costa, L. Ferrero, L. Pasqualini and E. Mancini
Lettere al Nuovo Cimento 2, 665 (1971)

B		5

METHOD

REF. NO. 71 Co 2 egf

REACTION	RESULT	EXCITATION ENERGY	SOURCE		DETECTOR		ANGLE
			TYPE	RANGE	TYPE	RANGE	
G,XN	ABI	36-64	C	10-64	BF3-I		4PI

FAST N YIELD

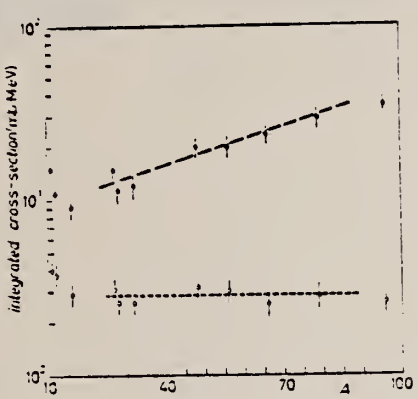

Fig. 2.

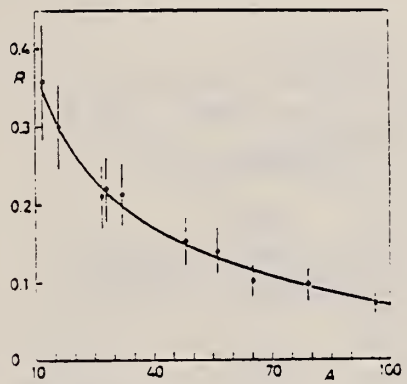

Fig. 3.

Fig 2. – Experimental photoneutron cross-sections integrated over photon energy between 36 and 64 MeV and divided by NZ/A are plotted as a function of the mass number. Black dots are total cross-sections not corrected for neutron multiplicity; open circles represent fast neutron cross-sections (see text). The dashed lines are drawn only to guide the eye.

Fig. 3. – The ratio between «fast» and total photoneutron integrated cross-sections as a function of the mass number A. The solid line represents a fit of the ratios calculated for some nuclei by taking into account the theoretical neutron energy spectra given by GABRIEL and ALEKSILLER (*) and the efficiencies of our detector (see Fig. 1).

REF.

V.I. Noga, Yu. N. Ranyuk, P.V. Sorokin, V.A. Tkachenko
Ukr. Fiz. Zh. 16, 1850 (1971)

ELEM. SYM.	A	Z.
B		5

METHOD

REF. NO.	
71 No 1	egf

REACTION	RESULT	EXCITATION ENERGY	SOURCE		DETECTOR		ANGLE
			TYPE	RANGE	TYPE	RANGE	
G,BE7	ABY	THR-999	C	80-999	ACT-I		4PI

999=1.2 GEV

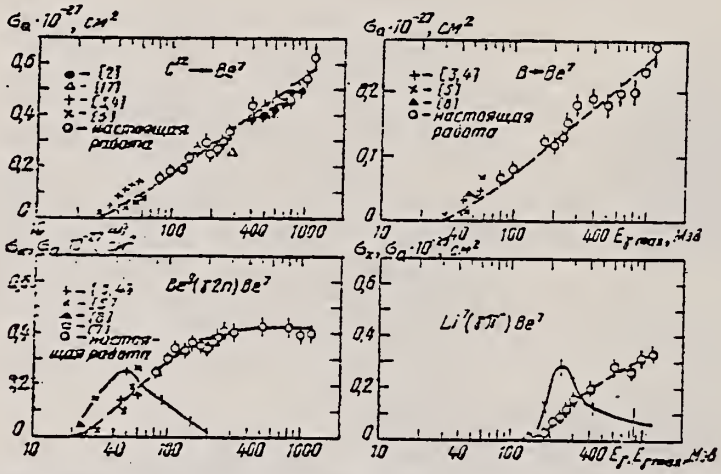

Рис. 3. Энергетическая зависимость сечений и выходов реакций: О — экспериментальные зависимости выхода от $E_{\gamma max}$; сплошная кривая — σ_k — функция возбуждения, вычисленная по способу наименьших квадратов по экспериментальным данным; пунктирная — σ_Q — выход, соответствующий функции возбуждения.

B
A=8

B
A=8

B
A=8

REF.

P. D. Parker
Phys. Rev. 150, 851 (1966)

ELEM. SYM.	A	Z
B	8	5

METHOD

Detection of delayed alphas.

REF. NO. 66 Pa 4 JDM

REACTION	RESULT	EXCITATION ENERGY	SOURCE TYPE	SOURCE RANGE	DETECTOR TYPE	DETECTOR RANGE	ANGLE
P,G	ABX	1 - 2	D	1 - 2	SCD - D		

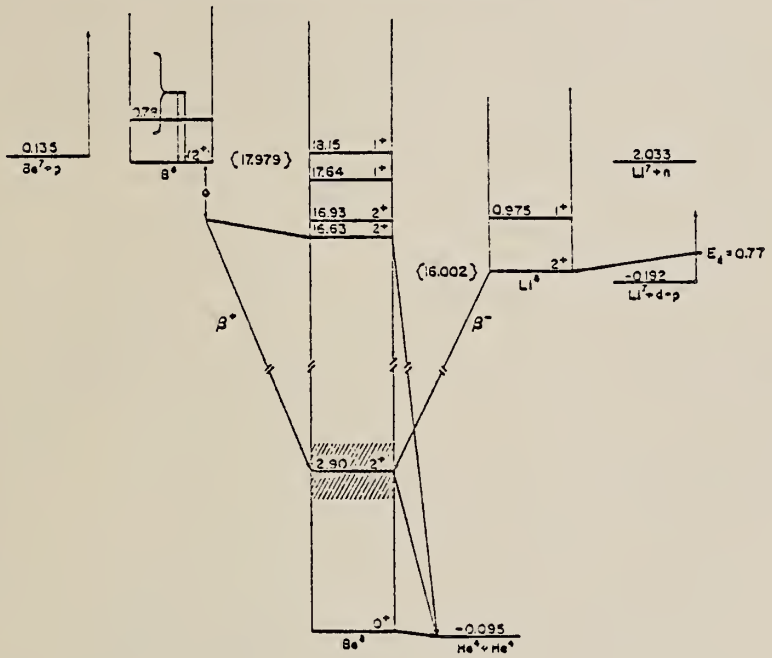

FIG. 1. Level diagram for the $A=8$ triad, indicating the energetics and decay schemes for the various reactions studied in this experiment.

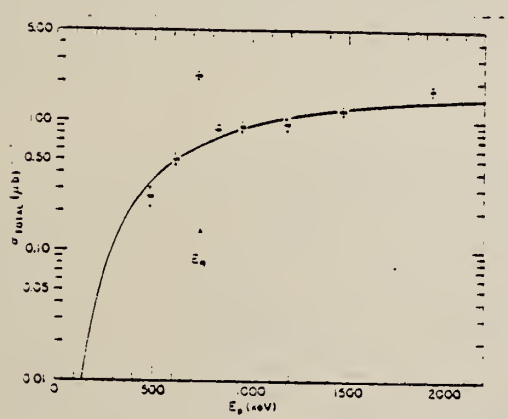

FIG. 5. The total capture cross section for the $Be^7(p,\gamma)B^8$ reaction as a function of proton energy. The solid curve indicates the energy dependence expected from the Coulomb barrier. The arrow indicates the expected position of a resonance corresponding to the first excited state of B^8.

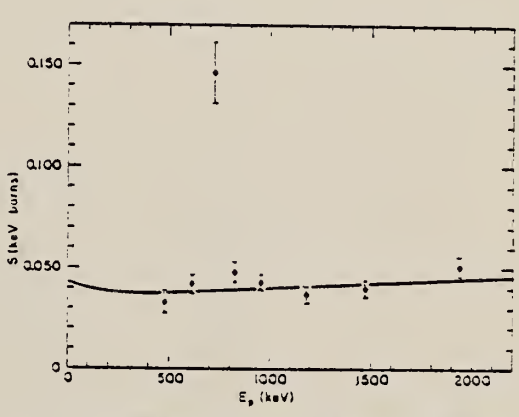

FIG. 6. The cross-section factor S for the $Be^7(p,\gamma)B^8$ reaction as a function of proton energy. The solid curve is a renormalization of the direct-capture calculation of Ref. 6 to the present data. At the intercept, $S_0=0.043\pm0.004$ keV b, and $(dS/dE)_0 = -4\times10^{-4}$ b.

$$S=\sigma E_{c.m.}\exp[31.28Z_0Z_1A^{\frac{1}{2}}/E_{c.m.}^{\frac{1}{2}}(\text{keV})]$$

B
A=10

B
A=10

B
A=10

REF. W. E. Meyerhof and C. M. Hudson
Phys. Rev. 115, 1227 (1959)

ELEM. SYM.	A	Z
B	10	5

METHOD

REF. NO. 59 Me 3 hmg

REACTION	RESULT	EXCITATION ENERGY	SOURCE TYPE	SOURCE RANGE	DETECTOR TYPE	DETECTOR RANGE	ANGLE
P,G	ABX	6- 8	D	0- 2	NAI-D		DST

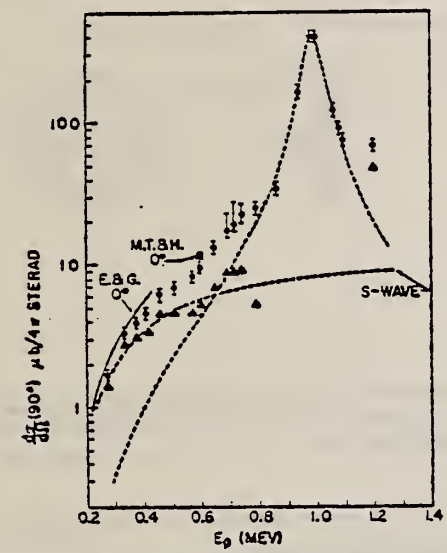

FIG. 5. Excitation curve of gamma ray to ground state ($J^\pi=3^+$, $T=0$) of B^{10} in Be^9+p at 90° to proton beam. Measurements at 0° are from reference 4 (E. and G.) and one point from the present work (M.T. and H.). The calculated Breit-Wigner resonance curve for the 0.99-Mev resonance is indicated. After subtraction of this curve from the experimental values, the points marked by triangles are obtained. An s-wave penetrability curve is indicated. See text for discussion.

TABLE II. Resonant gamma-ray yields in $Be^9(p,\gamma)$ reaction at $E_p=1.086$ Mev.

B^{10} state (Mev) to which γ ray goes		Y (90°)[a] (relative)	Y[b] (γ/10⁹)	Γ_γ[c] (ev)	$\Gamma_W(M1)$[d] (ev)
0	(3⁺)	≤0.03		≤0.2	9.1
0.72	(1⁺)	1.00[e]	0.98±0.2	6.0[e]	6.7
1.74	(0⁺)	≤0.08(0.04+0.02)[f]		(0.2±0.1)[f]	4.2
2.15	(1⁺)	≤0.08(0.04±0.02)[f]	≤0.05	(0.2±0.1)[f]	3.3
3.58[g]	(2⁺)	≤0.04		≤0.2	1.3
5.16	(2⁻?)	0.23±0.02[h]	0.15±0.05	1.3±0.1	0.29
Secondary γ-ray (Mev)					
0.41			≤0.008		
0.72		1.5±0.4	1.08±0.2		
1.02		0.07±0.02	≤0.04		
1.43		0.03±0.01	~0.05		
2.15		≤0.07			
3.01		~0.03			

[a] Relative differential cross section at 90° with respect to proton beam from present work.
[b] Absolute total yield from reference 5, calculated from yield at 90°, assuming isotropic cross section.
[c] Calculated assuming spin 0 for this resonance. For spin 1 the widths would be ⅓ of the values given.
[d] $M1$ widths calculated from Weisskopf estimate. See reference 13 for definitions. For B^{10} the estimates for $E1$ widths are 25 times the $M1$ widths.
[e] Normalized to this value.
[f] The values without parentheses are calculated from the capture gamma-ray intensities, the values in parentheses from the intensity balance of secondary gamma rays.
[g] The intensity of the capture transition to the 4.77-Mev state is less than or equal to that to the 3.58-Mev state.
[h] A small transition probability to the 5.11-Mev state is not excluded by our results.

(over)

TABLE I. Resonant gamma-ray yields in $Be^9(p,\gamma)$ reaction at $E_p = 0.33$ and 0.99 Mev (E_p = proton energy).

B^{10} state (Mev) to which γ ray goes	$(d\sigma/d\Omega)(90°)$[a] ($\mu b/4\pi$ sterad)	$E_p = 0.33$ Mev (1^-) Relative total yields[b]			Γ_γ[f] (ev)	$\lvert M\rvert^2$[g]
		[c]	[d]	[e]		
0 (3^+)	$\leqslant 0.7$	2.4	2.3		$\leqslant 0.08$	$\leqslant 8(M2)$
0.72 (1^+)	6.4 ± 2	6	6	6	0.7 ± 0.2	$0.6\times 10^{-4}(E1)$
1.74 (0^+)	15 ± 4	15[h]	15[h]	15[h]	1.7 ± 0.5	$2.5\times 10^{-4}(E1)$
2.15 (1^+)	4.5 ± 1.5	3	6.7	3	0.5 ± 0.2	$0.9\times 10^{-4}(E1)$
3.58[i] (2^+)	~ 1	5			~ 0.1	$\sim 0.5\times 10^{-4}(E1)$
5.16 (2^-?)	$\leqslant 2.9$[j]	3.6		3.7	$\leqslant 0.32$	$\leqslant 3(M1?)$
Secondary γ-ray (Mev)						
0.72	$39+8$					
1.02	20 ± 5					
1.43	~ 10					
2.15	$\leqslant 1$					
2.8	$\leqslant 1$					

B^{10} state (Mev) to which γ ray goes	$(d\sigma/d\Omega)(90°)$[a] ($\mu b/4\pi$ sterad)	$E_p = 0.99$ Mev (2^-)[k] Relative resonant yield (90°)[l]	Γ_γ[f] (ev)	$\lvert M\rvert^2$[g]
0 (3^+)	400[h]	400	23[h]	11×10^{-4} $(E1)$[m]
0.72 (1^+)	$\leqslant 10$	$\leqslant 30$	$\leqslant 0.6$	$\leqslant 0.4\times 10^{-4}(E1)$[m]
1.74 (0^+)	19 ± 14	$\leqslant 7$	0.7 ± 0.5[a]	40 ± 30 $(E2)$[n]
2.15 (1^+)	22 ± 13	$\leqslant 12$	1.3 ± 0.8	$\sim 2\times 10^{-4}$ $(E1)$[m]
3.58[i] (2^+)	$\leqslant 7$		$\leqslant 0.4$	$\leqslant 1\times 10^{-4}$ $(E1)$[m]
5.16 (2^-?)	$\leqslant 13$[j]		$\leqslant 0.8$	$\leqslant 3$ $(M1?)$[m]
Secondary γ-ray (Mev)				
0.41		5.5 ± 0.6		
0.72	27 ± 15	49 ± 5		
1.02	22 ± 8	13 ± 2		
1.43	10 ± 8	~ 6		
2.15	$\leqslant 2.5$			
2.8	$\leqslant 3$			

[a] Differential cross section at 90° to proton beam from present work, normalized to 400 $\mu b/4\pi$ sterad, i.e., $\Gamma_\gamma = 23$ ev (see reference 5), for the ground-state gamma ray at $E_p = 0.99$ Mev (see reference 6).
[b] These yields include the nonresonant as well as the resonant contributions. For a comparison of our results with those of reference 4, see Figs. 5 to 8.
[c] See reference 7.
[d] See reference 11.
[e] See reference 3.
[f] Calculated from present work assuming the partial and total level widths given in reference 1.
[g] Ratio of gamma-ray width to Weisskopf estimate. See reference 13 for definitions. The assumed multipolarity of the gamma ray is given in parentheses.
[h] Normalized to this value.
[i] The intensity of the capture transition to the 4.77-Mev state of B^{10} is less than or equal to that to the 3.58-Mev state.
[j] The major part of this transition appears to go to the 5.16-Mev state; a small transition probability to the 5.11-Mev state is not excluded by our results.
[k] The existence of an additional 2^+ state near $E_p = 0.98$ Mev is postulated in reference 9 and appears to be indicated by the transition to the 1.74-Mev state. See text.
[l] See reference 5. We assumed that the relative errors in intensity are one-half of the absolute errors given for the yields in this reference.
[m] This value of $\lvert M\rvert^2$ does not take into account possible transitions from the 2^+ state at 7.5 Mev.
[n] Γ_γ and $\lvert M\rvert^2$ calculated for a transition from the 2^+ state, assuming the widths for this state given in reference 9, but neglecting a possible angular anisotropy (which would not affect the value within the stated error).

E.D. Makhnovsky, Yu.M. Volkov
Nuclear Phys. 34, 562 (1962)

B	10	5

Method: 90 MeV Synchrotron; magnetic spectrometer; emulsions; NaI counter telescope

Ref. No.: 62 Ch 2 JHH

Reaction	E or ΔE	E_0	Γ	$\int \sigma dE$	Jπ	Notes
(γ,d) (γ,p)	Bremss. 30-90					$E_{(p,d)} > 15$ MeV. $\theta = 90°$

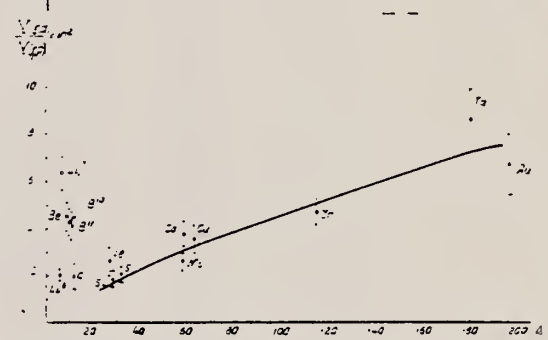

Fig. 4. The ratio of the yields of deuterons and protons with energies 13.5 to 30 MeV dependin... on the mass number of nuclei A for $E_{\gamma max} = 90$ MeV. The solid line stands for the normaliz... dependence ~A...

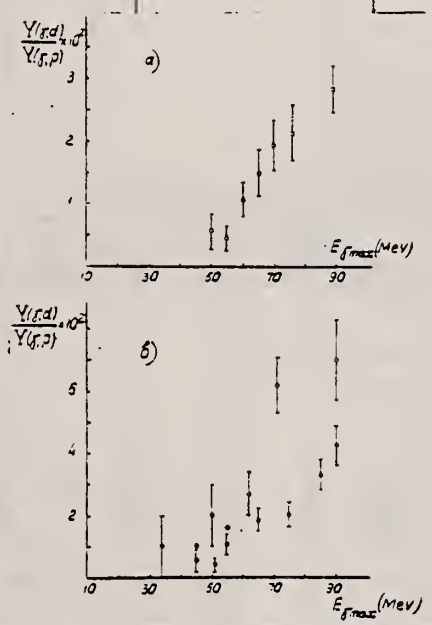

Figure 6: The ratio of deuteron and proton yields with E > 15 MeV plotted against $E_{\gamma max}$. a) Open circles denote Li^6. b) Open circles denote Be and black circles B.

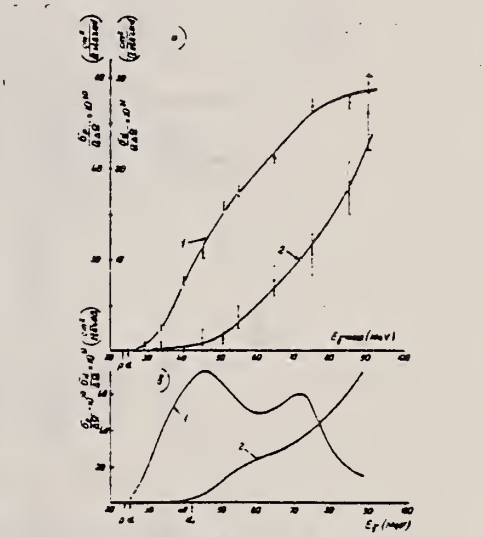

Fig. 10. Excitation functions for the reactions B^{10} (γ, p) and B^{11}(γ, d) for particles with energies E > 18 MeV (): protons and 2: deuterons). a) Cross sections are related for effective quantum b) Cross sections are related for incident quantum. The arrows p and d give the thresholds of the reactions B^{10} (γ, p) Be^9 and B^{11}(γ, d) Be^9 for the particle with kinetic energy of 18 MeV. d, is the energy equal to the sum of the energy of the threshold d and binding energy of the most weakly bound nucleon in the residual nucleus Be^9

Ref. R.D. Edge, G.A. Peterson
Phys. Rev. 128, 2750 (1962)

Elem. Sym.	A	Z
B	10	5

Method: Linac; counter telescope

Ref. No.: 62 Ed 1 BG

Reaction	E or ΔE	E_o	Γ_γ(eV)	$\int \sigma dE$(MeV-mb) J π	Notes
B^{10} (e,e')	41.5	7.9		0.75±0.15	Nuclear states excited by 180° electron scattering; M1 transitions assumed.
		11.8		0.75±0.38	
		14.0		0.5±0.25	Inelastic electron scattering cross sections obtained by comparing inelastic peaks to e-p elastic scattering peak.
					Γ_γ from virtual photon theory.
					Limits not given for cross sections.

TABLE I. Parameters of nuclear states excited by 180° electron scattering, assuming transitions are $M1$.

Isotope	Excitation energy, h (MeV)	Spin and parity: Ground state I_0	Spin and parity: Excited state I_n	Inelastic cross section $d\sigma/d\Omega$ (10^{-28} cm² sr^{-1})	$\int \sigma_n dh$ (MeV-mb)	Percentage experimental error	Ground-state radiation widths, Γ_{0n}(eV): This experiment	Weisskopf units	Other experiments
Be^9	2.4	3/2⁻	5/2⁻	1.1	0.12	15	0.12	0.30	0.13[a]
	14.7	3/2⁻	1/2⁻	0.042	0.3	50	36	67	
			3/2⁻				18		
			5/2⁻				12		
B^{10}	7.9	3⁺	2⁺	1.9	0.75	20	17	10	9.5[b]
			3⁺				12		
			4⁺				10		
	11.8	3⁺	2⁺	1.2	0.75	50	39	34	
			3⁺				15		
			4⁺				12		
	14.0	3⁺	2⁺	0.6	0.5	50	34	38	
			3⁺				24		
			4⁺				15		
B^{11}	2.1	3/2⁻	1/2⁻	0.72	0.72	20	0.17	0.21	0.15[a]
	4.4	3/2⁻	5/2⁻	1.5	0.34	40	1.1	1.8	0.602[c]
	6.9	3/2⁻	1/2⁻	2.4	0.59	40	1.7	2.5	
	7.3	3/2⁻	5/2⁻	0.4	0.12	50	1.0	8.1	
	9.1[e]	3/2⁻	7/2⁻	1.9	0.0097	20	0.10	4×10^{-3}	0.1[a]
	12.9	3/2⁻	1/2⁻	1.4	1.0	30	70	45	
			3/2⁻				36		
			5/2⁻				24		
C^{12}	15.1	0⁺	1⁺	1.82	1.95	10	39	73	40[a], 54.5[f], 59.5[g]
N^{14}	9.2	1⁺	0⁺	1.3	0.65	30	43	17	
			1⁺				16		
			2⁺				9		
	10.5	1⁺	0⁺	1.9	1.2	30	100	24	
			1⁺				34		
			2⁺				30		
O^{16}	No resonances detected below 16 MeV.								
S^{32}	11.6	0⁺	1⁻	3.5	2.8	40	33	33	47[a], 68[h]

[a] W. C. Barber, F. Bertrand, G. Fricke, and F. E. Gudden, Phys. Rev. 120, 2081 (1960).
[b] G. Fricke (private communication).
[c] F. R. Metzger, C. P. Swann, and V. K. Rasmussen, Phys. Rev. 110, 906 (1958).
[d] This transition is assumed to be $M2$.
[e] L. Meyer-Schützmeister and S. S. Hanna, Bull. Am. Phys. Soc. 3, 188 (1958).
[f] E. Hayward and S. Fultz, Phys. Rev. 106, 991 (1957).
[g] E. L. Garwin, Phys. Rev. 114, 143 (1959).
[h] A. B. De Nancy, Thesis, University of Paris, Orsay Center, 1962 (unpublished).

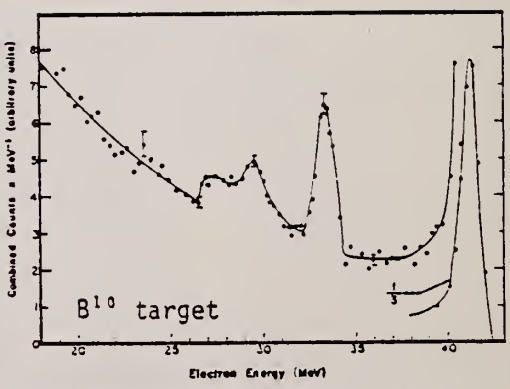

FIG. 2. Energy distribution of electrons, which were initially 41.5 MeV, after scattering through 180° from a B^{10} target.

Ref. R.J. Ellison, B. Dickinson
Nuclear Phys. 35, 606 (1962)

Elem. Sym.	A	Z
B	10	5

Method: 2 MeV Van de Graaff; NaI

Ref. No.: 62 Ell 1 — JHH

Reaction	E or ΔE	E_o	Γ	$\int \sigma dE$	Jπ	Notes
$Be^9(p,\gamma)$	0.85-1.11					
		7.42			$1^+,2^+$	
		7.47			$1^+,2^+$	
		7.48			2^-	

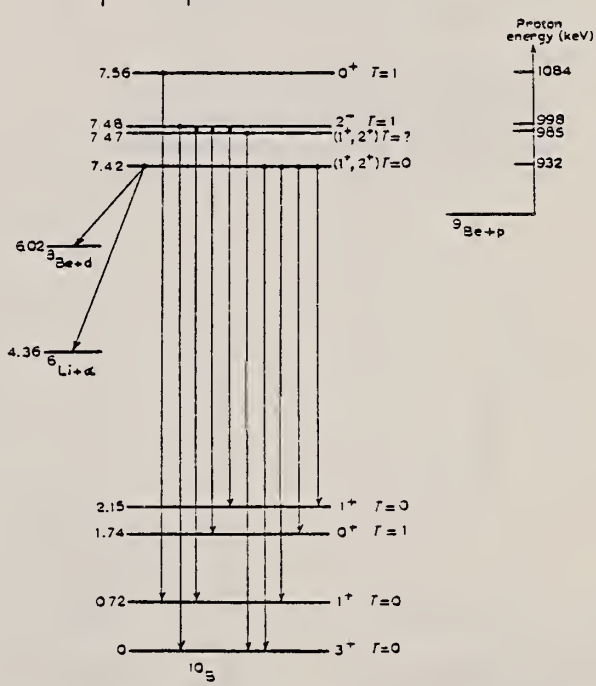

Fig. 1. Proposed level scheme for ^{10}B. The region near 7.5 MeV is expanded in energy by a factor of 10 in order to show details. Where a decay is shown from a point between two levels it indicates that either or both of these levels decay in this way. Only levels referred to in the text are shown. The decay schemes for the 1.74 and 2.15 MeV levels are given in ref. [14]).

[14] F. Ajzenberg-Selove and T. Lauritsen, Nuclear Physics 11 (1959) 1

Ref. Yu. M. Volkov, A.V. Kulikov, V.P. Chizov
Zhur. Eksp. i Teoret. Fiz. 42, 61 (1962)
Soviet Phys. JETP 15, 42 (1962)

Elem. Sym.	A	Z
B	10	5

Method: Synchrotron; scintillator counter telescope

Ref. No.: 62 Vo 2 | JHH

Reaction	E or ΔE	E_o	Γ	$\int \sigma dE$	Jπ	Notes
(γ,p)	Bremss.					E_d, E_p > 1.5 MeV
(γ,d)	90					

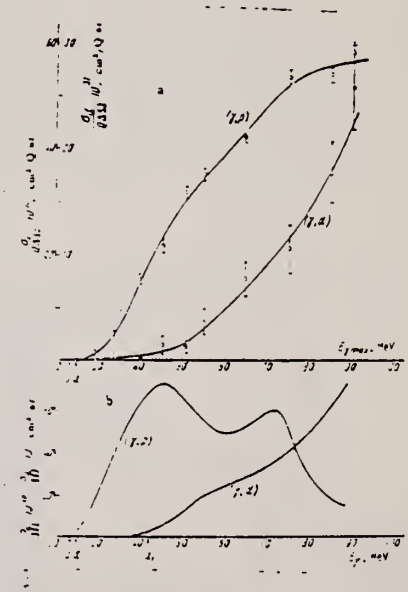

Figure 2: (b) cross section of the reactions $B^{10}(\gamma,d)$ and $B^{10}(\gamma,p)$ normalized per effective photon; (a) excitation functions of the same reactions for particles of energies > 15 MeV.

B. Furubayashi, E. Teranishi, M. Kageyama
J. Phys. Soc. Japan 18, 1235 (1963)

B	10	5

METHOD: Van de Graaff; inverse; NaI spectrometer

REF. NO.: 63 Fu 3 NVB

REACTION	RESULT	EXCITATION ENERGY	SOURCE TYPE	SOURCE RANGE	DETECTOR TYPE	DETECTOR RANGE	ANGLE
P,G	ABX	7-9	D	1-2	NAI-D		DST
		(7.8)		(700-1900			
				keV)			

G-WDTH, J-PI, T

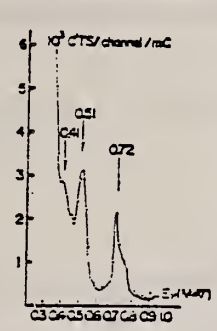

Fig. 3. Low energy gamma ray spectrum of $Be^9 + p$ at 1330 keV resonance. 0.72 and 0.41 MeV (from 2.15 to 1.74 MeV state) gamma rays are seen to occur along with 0.51 MeV annihilation gamma ray.

Table I. Observed partial gamma widths for transitions from 7.78 MeV level.

Transition from	to	Partial gamma width	Γ^2 exp
MeV	MeV	eV	
7.78	0.00	12.1±0.8	0.39±0.03
7.78	0.72	<1.4	<0.06
7.78	3.58	<3.1	<0.13

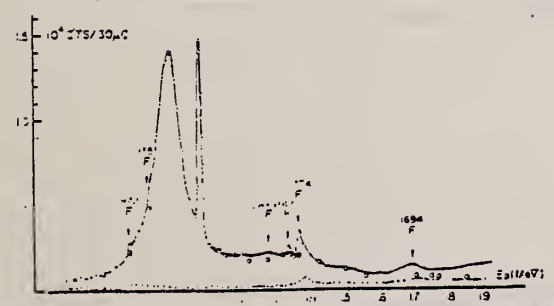

Fig. 1. Excitation curve of high energy gamma rays ($E>2.6$ MeV) from $Be^9(p,\gamma)B^{10}$ reaction. Six points marked "F" correspond to resonances of $F^{19}(p,\alpha\gamma)O^{16}$ reaction due to fluorine contamination. The yield of gamma ray to the ground state of $B^{10}(\gamma_0)$ are normalized at 991 keV resonance and shown by circles. Gamma ray yield from proton bombardment of blank tantalum is also shown at the lowest bottom.

3) R. D. Edge and D. S. Gemmel: Proc. Phys. Soc. (London) 71 (1958) 925.
4) W. E. Meyerhof, N. W. Tanner and C. M. Hudson: Phys. Rev., 115 (1959) 1227.

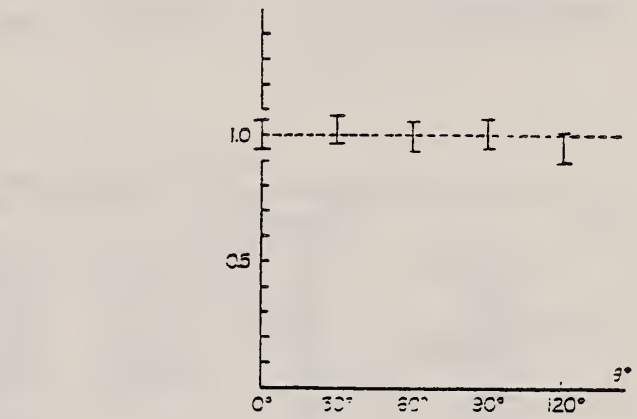

Fig. 4. Angular distribution of γ_0 at 1330 keV resonance. The second order coefficient of Legendre polynomial expansion is estimated to be less than 0.04 after correction of the finite solid angle effect.

Fig. 2. High energy gamma ray spectrum of $Be^9 + p$ at 1330 keV resonance. Transition to the first (0.72 MeV) and to the fourth (3.53 MeV) excited states of B^{10} and subsequent decay to the 0.72 MeV state are clearly identified in addition to γ_0.

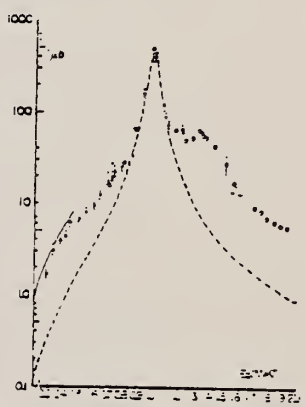

Fig. 5. γ_0 excitation curve. The result of present measurements are shown by circles whose absolute errors are typically such as is denoted by a bar at E_p=1.5 MeV. Filled circles with flags and solid line are taken from ref. 4) and 3), respectively. The calculated Breit-Wigner resonance curve for the 991 keV resonance is indicated by a broken line.

REF.

L. Green, D. J. Donahue
Phys. Rev. 135, B701-05 (1964)

ELEM. SYM.	A	Z
B	10	5

METHOD

Reactor; neutron capture gamma rays

REF. NO.

64 Gr 2 NVB

REACTION	RESULT	EXCITATION ENERGY	SOURCE		DETECTOR		ANGLE
			TYPE	RANGE	TYPE	RANGE	
G,N	ABX	9-11	D	9-11	BF3-I		4PI

WIDTH

Enriched to 93% B^{10}.
Ground-state radiative width of 8.89 MeV level,

$$\Gamma_\gamma^o \gtrsim 0.6 \text{ eV}$$

TABLE II. Summary of measured cross sections (millibarns).

Source	Energy[a] (MeV)	Targets Ta^{181}	Li^7	Li^6	C^{13}	B^{10}
Aluminum	7.72	4.1± 0.4	0.06 ±0.01	1.13±0.12	1.7 ±0.2	...
Copper	7.91	10.8±1.0	0.07 ±0.01	1.1 ±0.2	0.97±0.13	...
Chlorine	8.56	29 ± 6	0.17 ±0.12	...	...	...
Nickel	9.00	44 ± 6	0.16 ±0.06	1.6 ±0.3	0.6 ±0.1	0.11±0.01
Nitrogen	10.83	121 ±12	1.07 ±0.25	...	4 ±2	0.9 ±0.2
Chromium	9.72	84 ±25	0.55 ±0.25	...	...	0.23±0.05
Iron	7.64	0.0± 0.9	0.079±0.014	1.3 ±0.2	0.23±0.05	...
Iron	9.30	...	...	...	...	0.09±0.03
Lead	7.38	...	0.068±0.035	1.2 ±0.2	0.3 ±0.3	...
Sulphur	5.43	...	...	0.42±0.07		
Sodium	6.41	...	...	0.6 ±0.1		
Titanium	6.75	...	...	1.3 ±0.2	...	...
Titanium	6.61[b]	...	...	...	0.32±0.04	...
Manganese	7.16[c]	...	...	0.9 ±0.1	0.4 ±0.1	
Zinc	7.88	...	...	1.0 ±0.2	1.2 ±0.2	

[a] Energies taken from Refs. 4 and 5.
[b] Weighted average of 6.75-, 6.55-, and 6.41-MeV γ rays.
[c] Weighted average of 7.26-, 7.15-, and 7.05-MeV γ rays.

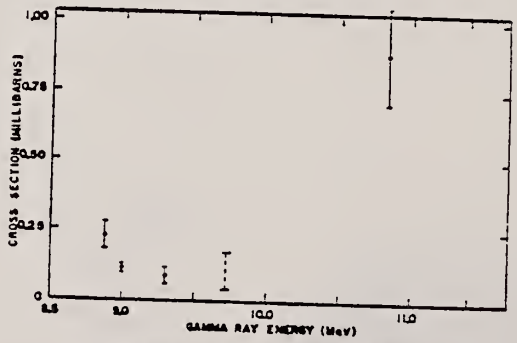

FIG. 6. Energy versus cross section, $B^{10}(\gamma,n)$.

REF.

J. M. Loiseaux, M. Langevin and J. M. Maison
Proc. Paris Conf. 1048 (1964)

ELEM. SYM.	A	Z
B	10	5

METHOD

Betatron

REF. NO.: 64 Lo 3 JDM

REACTION	RESULT	EXCITATION ENERGY	SOURCE		DETECTOR		ANGLE
			TYPE	RANGE	TYPE	RANGE	
G,G	ABX	10-30	C	10-30	NAI-D		140

The effective differential scattering cross section remains quite constant from 20-30 MeV.

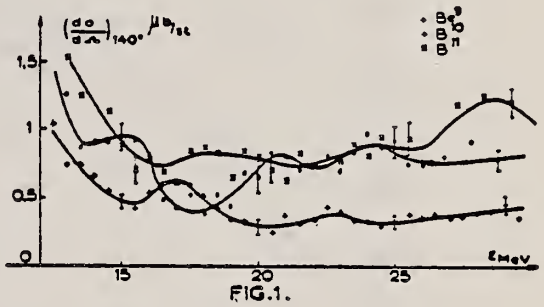

FIG.1.

REF.

G. Fricke, G. R. Bishop and D. B. Isabelle
Nuclear Phys. 67, 187 (1965)

ELEM. SYM.	A	Z
B	10	5

METHOD

REF. NO. 65 Fr 2 EGF

REACTION	RESULT	EXCITATION ENERGY	SOURCE		DETECTOR		ANGLE
			TYPE	RANGE	TYPE	RANGE	
E,E/	FMF	6	D	100-220	MAG-D	90-220	DST
		(6.02)					

Absolute values obtained relative to elastic form factor.

Concludes spin in 4^+.

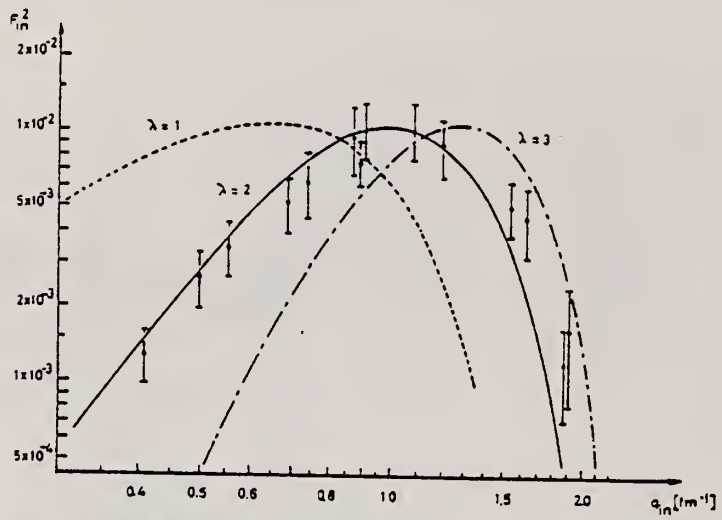

Fig. 2. The inelastic form factor for excitation of the studied level. The three curves are the theoretical form factors for $E_1(\lambda = 1)$, $E_2(\lambda = 2)$ and $E_3(\lambda = 3)$ transition.

TABLE 1

Experimental form factors

E_0 (MeV)	θ^0	q_{1n} (fm^{-1})	A_{1n}/A_{01}	$F_{01}^2(q^2)$	$F_{1n}^2(q^2)$	$\frac{\Delta(F_{1n}^2)}{F_{1n}^2}$ (%)
98.6	50	0.410	1.83×10^{-3}	7.05×10^{-1}	1.29×10^{-3}	25
119.6	50	0.499	4.31×10^{-3}	6.02×10^{-1}	2.59×10^{-3}	25
98.7	70	0.556	6.60×10^{-3}	5.24×10^{-1}	3.46×10^{-3}	25
119.5	70	0.690	1.31×10^{-2}	3.95×10^{-1}	5.18×10^{-3}	25
150.1	60	0.740	1.86×10^{-2}	3.35×10^{-1}	6.24×10^{-3}	30
99.6	130	0.872	4.62×10^{-2}	2.05×10^{-1}	9.46×10^{-3}	30
98.6	135	0.895	4.02×10^{-2}	1.88×10^{-1}	7.53×10^{-3}	20
183.1	60	0.908	5.23×10^{-2}	1.97×10^{-1}	1.03×10^{-2}	25
119.3	135	1.08	1.10×10^{-1}	9.33×10^{-2}	1.03×10^{-2}	25
211.1	70	1.20	1.47×10^{-1}	6.01×10^{-2}	8.80×10^{-3}	25
221.1	90	1.54	5.21×10^{-1}	9.66×10^{-3}	5.03×10^{-3}	25
210.4	105	1.63	8.2×10^{-1}	5.51×10^{-3}	4.53×10^{-3}	30
221.2	120	1.88	9.0×10^{-1}	1.31×10^{-3}	1.18×10^{-3}	40
209.9	135	1.90	1.3	1.24×10^{-3}	1.62×10^{-3}	50

See the text for the definitions of quantities which label the columns.

E. Hayward and T. Stovall
Nuclear Phys. 69, 241 (1965)

B	10	5

METHOD

REF. NO. 65 Ha 1 EGF

REACTION	RESULT	EXCITATION ENERGY	SOURCE TYPE	SOURCE RANGE	DETECTOR TYPE	DETECTOR RANGE	ANGLE
G,XN	ABX	THR - 30	C	6-30	BF3-I		4PI

573

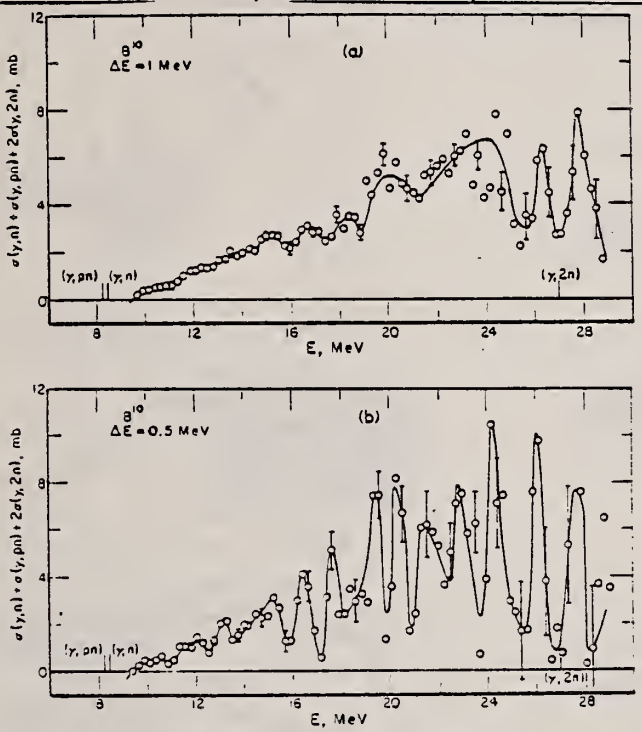

Fig. 5. The neutron production cross section for B^{10} where the analysis has been made using a 1 MeV grid (a) and 0.05 MeV grid (b). Thresholds for the neutron producing cross sections are indicated by vertical lines at the bottom. The indicated errors are standard deviations based only on the number of counts.

TABLE 3

Neutron emission cross sections integrated to 29 MeV

Target	$\int \sigma dE$ (MeV · mb)	$\int \sigma dE/(60NZ/A)$	$\int^{30} \sigma dE/(60NZ/A)$ [a]
Li^6	36.1	0.40±0.03 [b]	0.42
Li^7	50.1	0.49±0.04	0.64
B^{10}	66.7	0.44±0.03	
B^{11}	68.6	0.42±0.03	0.47 [c]
O^{16}	61.9	0.26±0.02	0.30

[a]) Ref. [17]).
[b]) This value is for natural boron.
[c]) Estimated systematic errors.

REF.

P. Paul, S. L. Blatt, and D. Kohler
Phys. Rev. 137, B493-498 (1965)

ELEM. SYM.	A	Z
B	10	5

METHOD

Van de Graaff; NaI plus plastic scintillator detector. [Page 1 of 2]

REF. NO. 65 Pa 1 NVB

REACTION	RESULT	EXCITATION ENERGY	SOURCE		DETECTOR		ANGLE
			TYPE	RANGE	TYPE	RANGE	
HE3,G	ABX	18 - 19		0-3	NAI-D	10-30	DST

Target 99.7% Li^7.

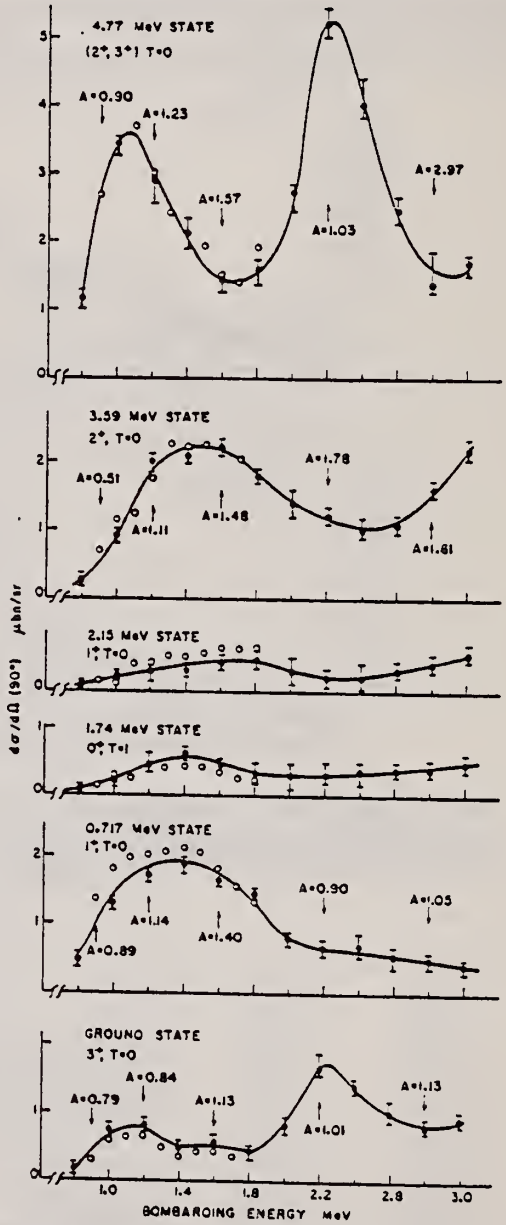

FIG. 6. Excitation functions at 90° of gamma rays observed in $Li^7(He^3,\gamma)$. Each curve is marked by the final state in B^{10} and its quantum numbers. Target thickness is 150 keV for 1-MeV He^3. Open circles represent results from an independent run in 100 keV steps with a target 50-keV thick. A gives the intensity ratio $Y(0°)/Y(90°)$ measured at the indicated energy. Error bars are estimated from the gamma-ray unpeeling procedure. The systematic error on the cross-section scale is ±10%.

METHOD | REF. NO.

Van de Graaff; NaI plus plastic scintillator detector. [Page 2 of 2] | 65 Pa 1 | NVB

REACTION	RESULT	EXCITATION ENERGY	SOURCE TYPE	SOURCE RANGE	DETECTOR TYPE	DETECTOR RANGE	ANGLE

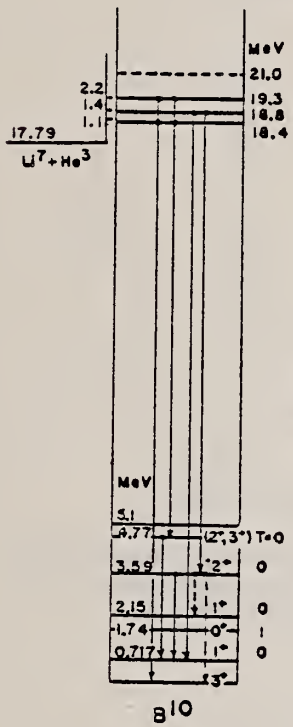

FIG. 5. Simplified level scheme of B^{10}. Vertical arrows are resonant gamma transitions. Horizontal lines above 18 MeV indicate position of resonances observed in the present experiment.

TABLE I. Resonances observed in radiative capture of He^3 by Li^7.

E_{res} (lab) (MeV)	Γ_{tot} (c.m.) (keV)	Final states in B^{10} (MeV) and their spins		$\frac{d\sigma}{d\Omega}$ (90°) (μb/sr)	Possible spin-parity assignments[a,b]
1.1	<500	0	3+	0.8	(1+), 2±, 3+
		4.77	(2+,3+)	3.6	
1.4	<600	0.717	1+	2.0	(0+), 1±, 2±, (3+)
		3.59	2+	2.2	
2.2	280<Γ<420	0	3+	1.8	(1+), 2±, 3±
		4.77	(2+,3+)	5.3	

[a] Incoming s- and p-waves considered for all resonances; d-waves also considered for 1.4- and 2.2-MeV resonances.
[b] Assignments in parentheses require $E2$ transition.

TABLE II. Radiative strengths and He^3 single-particle widths estimated for observed resonances in $Li^7(He^3,\gamma)$.

E_{res} (lab) (MeV)	$\Gamma_{l\pi}$ (He^3)[a] $= 2P_l(\gamma^3)_\pi$			Lower limit[b] of $(2J+1)\Gamma_\gamma$ (eV) for transitions to states in B^{10} at			
	$l=0$	$l=1$	$l=2$	0	0.717	3.59	4.77
1.1	130	25	1	35	···	···	140
1.4	400	100	2	···	100	100	···
2.2	1500	600	50	85	···	···	200

[a] $(\gamma^3)_\pi = (3/2)\hbar^2/\mu R^2$, $R = 4.7$ F.
[b] Assuming isotropy and $\Gamma_{He^3} = \Gamma_{tot}$.

E. Spamer and F. Gudden
Phys. Letters 14, 210 (1965)

B	10	5

METHOD

Linac

REF. NO.

65 Sp 1 EGF

REACTION	RESULT	EXCITATION ENERGY	SOURCE		DETECTOR		ANGLE
			TYPE	RANGE	TYPE	RANGE	
E,E/	FMF	7.	D	55	MAG-D	15-55	DST
		7.48 ± 0.02					

J-PI, WIDTH

Inelastic cross section relative to elastic.
At const. $q_T = 0.47$ fm^{-1} ang. dist. consistent with magnetic transition.
Corrected for 2^- T = 1 level at 7.48 MeV.
Fig. 1 analysis assumes M1.
Reduced transition probably corresponds to $\Gamma_\gamma^o = 11 \pm 2$ eV ($I_f = 2^+$).
Target 96% B^{10}.

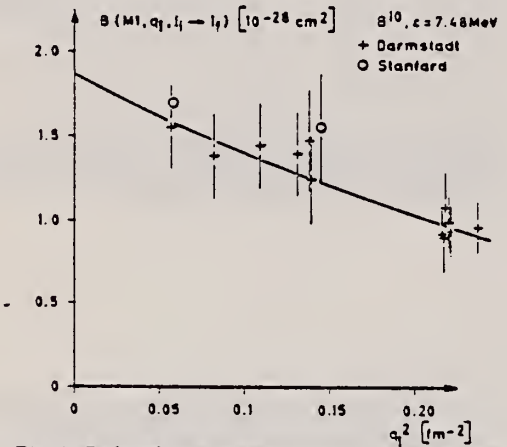

Fig. 1. Reduced transition probability versus momentum transfer squared.
Stanford: Edge and Peterson (ref. 2).

REF.

P. D. Forsyth, H. T. Tu and W. F. Hornyak
Nucl. Phys. 82, 33 (1966)

ELEM. SYM.	A	Z
B	10	5

METHOD

[Page 1 of 3]

REF. NO. 66 Fo 2 JDM

REACTION	RESULT	EXCITATION ENERGY	SOURCE		DETECTOR		ANGLE
			TYPE	RANGE	TYPE	RANGE	
A,G	SPC	5-7	D	1-3	NAI-D	2-7	90

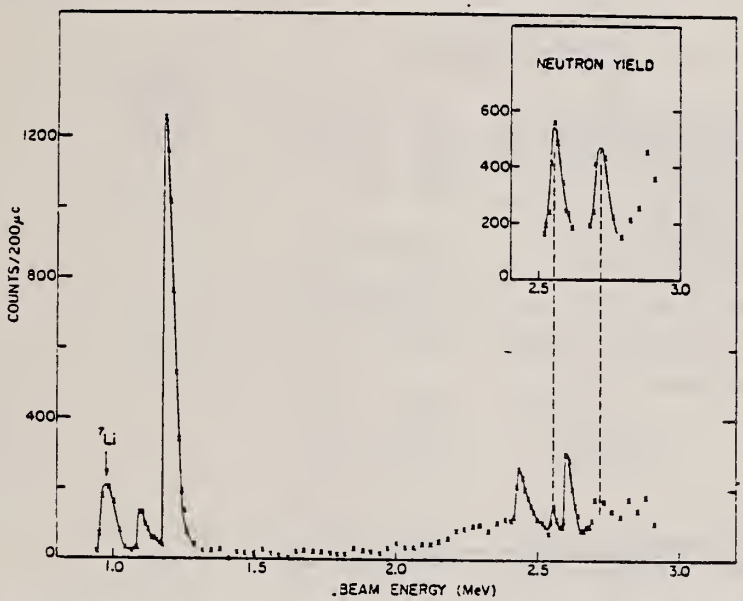

Fig. 1. Excitation function for the $^6Li(\alpha,\gamma)^{10}B$ reaction with a 30 keV enriched ^6Li target and accepting γ-ray scintillations corresponding to an energy range 2 MeV $< E_\gamma <$ 4 MeV. The simultaneously obtained neutron yield using a moderated BF_3 counter is also shown.

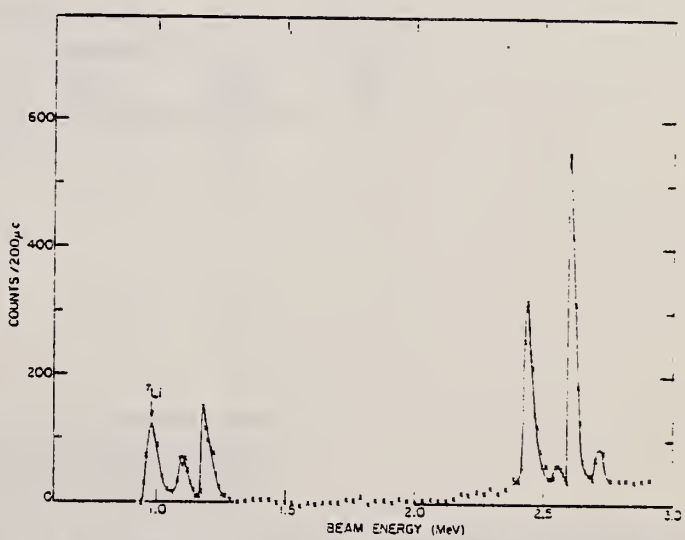

Fig. 2. Excitation function obtained simultaneously with the data shown in fig. 1, however, with the γ-ray energy range set to 4 MeV $< E_\gamma <$ 7 MeV.

REACTION	RESULT	EXCITATION ENERGY	SOURCE TYPE	SOURCE RANGE	DETECTOR TYPE	DETECTOR RANGE	ANGLE

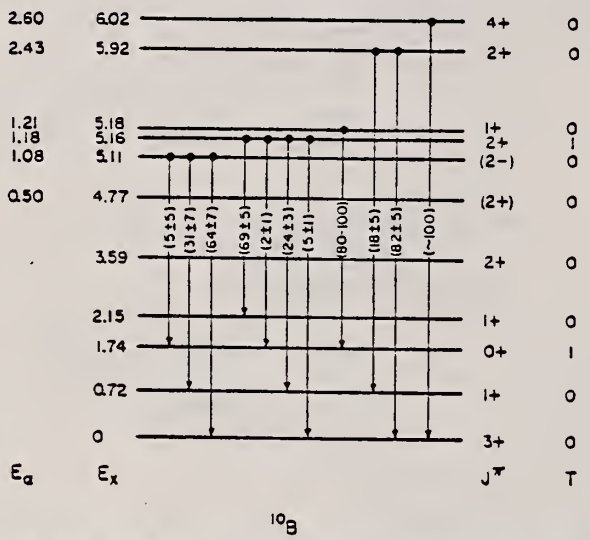

Fig. 7. The relevant levels of ^{10}B indicating the present determination for γ-decay branching ratios and implied level characters.

TABLE 1

Radiative widths and branching ratios

E_x (MeV)	Excitation in ^{10}B (MeV)	$\Gamma_{(lab)}$ (keV)	Primary radiation $E_{\gamma'}$ (MeV)	Primary radiation Branching ratio [b] (%)	$\omega\gamma$ [c] (eV)
1.09	5.11	2 [a]	5.11	64±7	0.059±0.012
			4.39	31±7	0.028±0.008
			3.37	5±5	0.005±0.005
1.18	5.16	< 0.5 [a]	5.16	5±1	0.035±0.007
			4.43	24±3	0.17 ±0.04
			3.42	2±1	0.017±0.008
			3.01	69±5	0.47 ±0.09
2.43	5.92	10±1	5.92	82±5	0.31 ±0.06
			5.20	18±5	0.07 ±0.02
			4.18		< 0.02
2.60	6.02	< 1.5 [a]	6.02	100	0.57 ±0.08
			5.30		< 0.02

[a]) Taken from Meyerhof and Chase [3]).
[b]) Only relative errors are given for the branching ratios.
[c]) Errors given related to absolute errors.

REACTION	RESULT	EXCITATION ENERGY	SOURCE TYPE	SOURCE RANGE	DETECTOR TYPE	DETECTOR RANGE	ANGLE

TABLE 3
Radiative matrix elements

Excitation in ^{10}B (MeV)	J^π	E_γ (MeV)	$\omega\gamma$ (eV)	Γ_γ^0 (eV)	$\lvert M\rvert^2_{M1}$	$\lvert M\rvert^2_{E2}$	$\lvert M\rvert^2_{E1}$	$\lvert M\rvert^2_{M2}$	Assumed multipole mixture
5.11	2^-	5.11	0.059	0.035			9×10^{-4}	1.5	$\frac{M2}{E1} = 0.01$
		4.39	0.028	0.017			6×10^{-4}	1.5	$\frac{M2}{E1} = 0.01$
		3.37	0.005	0.003				100 ± 100	–
5.16 a)	2^+	5.16	0.035	0.16	0.06	0.8			$\frac{E2}{M1} = 0.02$
		4.44	0.17	0.78	0.4	4			$\frac{E2}{M1} = 0.01$
		3.42	0.017	0.08		160 ± 80			–
		3.01	0.47	2.2	3.8	80			$\frac{E2}{M1} = 0.01$
5.92	2^+	5.92	0.31	0.21	0.05	0.27			$\frac{E2}{M1} = 0.01$
					5×10^{-6}	25			$\frac{E2}{M1} = 10$
		5.20	0.07	0.04	0.015	0.1			$\frac{E2}{M1} = 0.01$
					1.5×10^{-6}	9			$\frac{E2}{M1} = 10$
6.02	4^+	6.02	0.57	0.19	4×10^{-6}	20			$\frac{E2}{M1} = 9$

a) In calculating Γ_γ^0 we have taken $\Gamma_\gamma/\Gamma = 0.87$.

REF.

P. Kossanyi-Demay and G. J. Vanpraet
Nucl. Phys. 81, 529 (1966)

ELEM. SYM.	A	Z
B	10	5

METHOD

Stanford Mark II; Linac

[Page 1 of 4]

REF. NO. 66 Ko 1 JDM

REACTION	RESULT	EXCITATION ENERGY	SOURCE		DETECTOR		ANGLE
			TYPE	RANGE	TYPE	RANGE	
E,E/	ABX	0 - 18	D	50,60	MAG-D	30 - 60	180

TABLE 1

Excited states observed in $^{10}B(J^\pi = 3^+)$ by inelastic scattering at 180° of electrons of primary energy 50 MeV

1	2	3	4	5	6	7	8	9	10		
exp. ±0.2 MeV	$d\sigma/d\Omega$ [a] (nb · sr^{-1})	J^π	Transition	$\frac{F^2(qr)}{F^2(kr)}$	$\frac{dN}{d\Omega} \cdot 10^{+4}$	$\int \sigma_\gamma dk$ (MeV · μb)	Γ^0_γ (eV)	Γ_ω (eV)	$\Gamma^0_\gamma/\Gamma_\omega$	Percentage experimental error	References
2	1.5	1+	E2	0.615	2.19	16	$3.7 \cdot 10^{-2}$	$4.8 \cdot 10^{-6}$	770	50	
3.58	1.9	2+	M1	0.377	1.29	52.5	0.25	0.96	0.26	50	
5.1	2.0		M1	0.396	1.32	74.8	0.65	2.80	0.15		$\Gamma^0_\gamma(5.16) \approx 100$ meV ref. [16])
		2+	E2	0.64	2.13	46.1	0.41	$9 \cdot 10^{-6}$	25	50	
			M2	0.64	735	0.125	$1.12 \cdot 10^{-3}$	$3.4 \cdot 10^{-4}$	1.8		$\Gamma^0_\gamma(4.16) \approx 20$ meV ref. [17])
		2−	E1	0.396	0.004	27800	248	68	18.5		$\Gamma^0_\gamma(4.77) \approx 3$ meV ref. [17])
5.9	1.2		M1	0.408	1.33	54.1	0.71	4.53	0.16		
6.0		2+	E2	0.65	2.11	34	0.45	$2 \cdot 10^{-6}$	22.5	50	
			M2	0.65	519	0.14	$1.8 \cdot 10^{-4}$	$7.8 \cdot 10^{-4}$	2.3		
		2−	E1	0.408	0.005	13200	174	110	1.7		
7.5	15	2+	M1	0.426	1.34	829	17.05	8.49	2.0	25	$\Gamma \leq 7$ eV ref. [18]) $\Gamma = 12 \pm 2$ eV ref. [16])
8.9	6		M1	0.445	1.36	392	8.15	15.3	0.53		
		3+	E2	0.67	2.05	260	5.38	0.154	35	25	
			M2	0.67	215	2.5	0.05	$5.9 \cdot 10^{-6}$	8.5		
			E1	0.445	0.013	41000	850	372	2.28		
10.7	5		M1	0.465	1.37	390	16.3	25.7	0.63		
		2+	E2	0.68	2.01	266	11.1	0.36	30.8	25	
			M2	0.68	140	3.8	0.16	$1.39 \cdot 10^{-5}$	11.5		$J^\pi = 2^+$ ref. [17])
			E1	0.465	0.019	27100	1130	630	1.8		

TABLE 1

Excited states observed in $^{10}B(J^\pi = 3^+)$ by inelastic scattering at 180° of electrons of primary energy 50 MeV

1	2	3	4	5	6	7	8	9	10		
exp. ±0.2 MeV	$d\sigma/d\Omega$ [a]) (nb · sr^{-1})	J^π	Transition	$\frac{F^2(qr)}{F^2(kr)}$	$\frac{dN}{d\Omega} \cdot 10^{+4}$	$\int \sigma_\gamma dk$ (MeV · μb)	Γ_γ^0 (eV)	Γ_ω (eV)	$\Gamma_\gamma^0/\Gamma_\omega$	Percentage experimental error	References
11.25	5		M1	0.472	1.37	425	18.8	29.9	0.62		
		2$^+$	E2	0.69	1.99	281	13.0	0.45	2.9	25	
			M2	0.69	124	4.4	0.208	$1.75 \cdot 10^{-2}$	11		
		2$^-$	E1	0.472	0.022	25400	1170	720	1.66		
11.9	5.9		M1	0.48	1.37	510	26.4	35.4	0.74		
		2$^+$	E2	0.69	1.98	354	18.3	0.62	29	25	
			M2	0.69	108	6.47	0.334	$2.38 \cdot 10^{-2}$	14		
		2$^-$	E1	0.48	0.025	27900	1440	860	1.7		
12.7	5.8		M1	0.49	1.37	530	30.8	42.0	0.74		
		2$^+$	E2	0.70	1.96	372	21.6	0.82	25.5	25	
			M2	0.70	34	7.73	0.45	$3.18 \cdot 10^{-2}$	14		
		2$^-$	E1	0.49	0.028	25500	1480	1020	1.45		
13.5	3.4		M1	0.50	1.37	340	23.4	54.6	0.42		
		2$^+$	E2	0.70	1.93	242	16.7	1.25	13.4	25	
			M2	0.70	76.1	6.1	0.42	$4.8 \cdot 10^{-2}$	8.7		
		2$^-$	E1	0.50	0.035	11300	920	1300	0.7		
14.5	2.9		M1	0.508	1.37	302	22.7	62.0	0.37		
		2$^+$	E2	0.71	1.92	217	16.3	1.55	10.5	30	
			M2	0.71	68.3	6.1	0.45	$6 \cdot 10^{-2}$	7.55		
		2$^-$	E1	0.508	0.038	10700	809	1500	0.53		
16.2	6		M1	0.526	1.37	692	64.0	84.4	0.76		
		2$^+$	E2	0.72	1.87	506	47.0	2.6	18.0	25	
			M2	0.72	52.5	5.6	1.67	0.1	16.7		
		2$^-$	E1	0.526	0.049	19500	1790	2000	0.87		
17±0.15	5.2		M1	0.54	1.37	660	70.2	105	0.66		
		2$^+$	E2	0.73	1.84	482	52	3.8	13.6	25	
			M2	0.73	43	7.8	2.21	0.15	14.8		
		2$^-$	E1	0.54	0.058	15200	1630	2500	0.65		

[a]) Note that the differential cross section in column 2 is measured in nanobarn/steradian.

REACTION	RESULT	EXCITATION ENERGY	SOURCE		DETECTOR		ANGLE
			TYPE	RANGE	TYPE	RANGE	

TABLE 3

Magnetic transitions in ^{11}B and ^{10}B

(1)	(2)		(3)		(4)		(5)	(6)	(7)	(8)	(9)			
			$d\sigma/d\Omega$		$\Lambda_{M1}(q)$						$(2I_1+1)\Lambda_{M1}$	$(a/K = 4.5)$		
exp.	I_2	T_2	50 MeV	60 MeV	50 MeV	60 MeV	F_I^{*2}	$(2I_1+1)\Lambda_{M1}(0)$	F^{-2}	$(2I_1+1)\Lambda_{M1}$	Inglis (a/k)	(8.16) POT	(8.16) 2BME	(6.16) 2BME
^{11}B														
2.15	$\frac{1}{2}$	$\frac{1}{2}$	3.95±0.4		1.06		0.358	11.8±1.2	0.58	7.3 ±0.7				
				2 ±1		0.53			0.44	4.8 ±2.4	9.28	16.8	15.7	15.1
4.45	$\frac{1}{2}$	$\frac{1}{2}$	5.1 ±1.5		1.42		0.388	14.6±4.3	0.6	9.5 ±2.8				
				3.8±1.1		1.05			0.46	9.1 ±2.7	20.1	13.3	13.4	13.1
5.03	$\frac{1}{2}$	$\frac{1}{2}^+$	9.6 ±2.8		2.71		0.395	27.4 ±8.2	0.615	17.6 ±5.2				
				5.8±1.7		1.61			0.475	13.5 ±4	28.5	22.1	23.1	22.7
8.92	$\frac{1}{2}$	$\frac{1}{2}^{**}$	5.6 ±1.4		1.72		0.444	15.5±3.8	0.63	10.9 ±2.7				
				4.5±1.1		1.34			0.495	10.8 ±2.7	6.05	6.52	7.77	9.35
12.65	$\frac{1}{2}$	$\frac{3}{2}$	3.7		1.24		0.488	10.2±0.3	0.655	7.65±2.3				
				3.4		1.08			0.53	8.15±2.4	13.5	10.0	11.5	12.5
^{10}B														
3.59	2^+	0	1.9 ±0.4		0.47		0.377	8.9±1.8	0.59	5.7 ±1.1				
				0.7±0.35		0.17			0.45	2.6 ±1.3	0.31	0.13	0.04	0.000
5.16	2^+	1	2 ±0.4		0.5		0.396	8.8±1.7	0.615	5.7 ±1.1				
				1.7±0.3		0.42			0.475	6.1 ±1.1	4.46	8.32	5.93	1.09
7.5	2^+	1^*	16 ±4		4.8		0.426	77.0±19	0.62	58 ±13	81.7	103	103	102
				11 ±2		3.15			0.505	44 ±9				
8.9	3^+	1	6 ±1.5		1.81		0.445	28.4±5.6	0.63	20 ±5				
				4 ±1		1			0.51	14 ±3.5	44.6	33.9	33.6	29.6
10.7	2^+	1^{**}	5 ±1.25		1.76		0.452	24 ±5.75	0.635	17.7 ±4				
				6.5±1.5		1.9			0.51	26.0 ±4	19.5	6.46	10.6	16.3

REF.
P. Kossanyi-Demay and G. J. Vanpraet
Nucl. Phys. 81, 529 (1966)

ELEM. SYM.	A	Z
B	10	5

METHOD

REF. NO. 66 Ko 1

JDM

REACTION	RESULT	EXCITATION ENERGY	SOURCE		DETECTOR		ANGLE
			TYPE	RANGE	TYPE	RANGE	

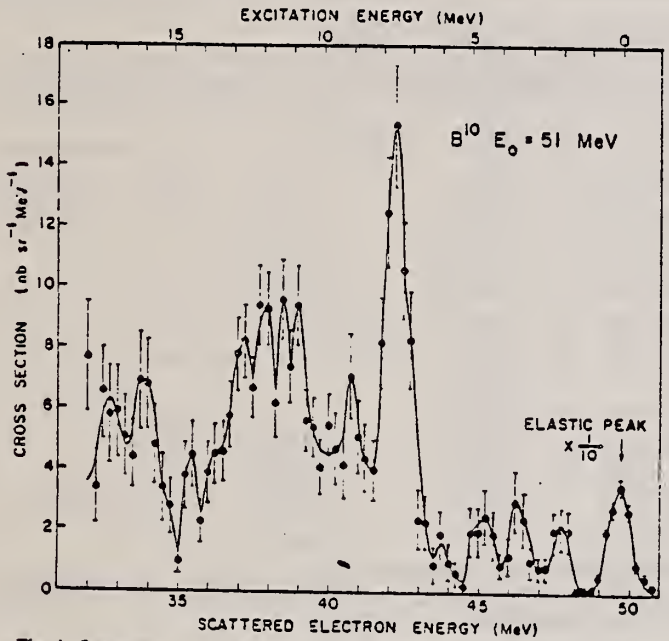

Fig. 1. Spectrum of 51 MeV electrons scattered from a ^{10}B target at 180°.

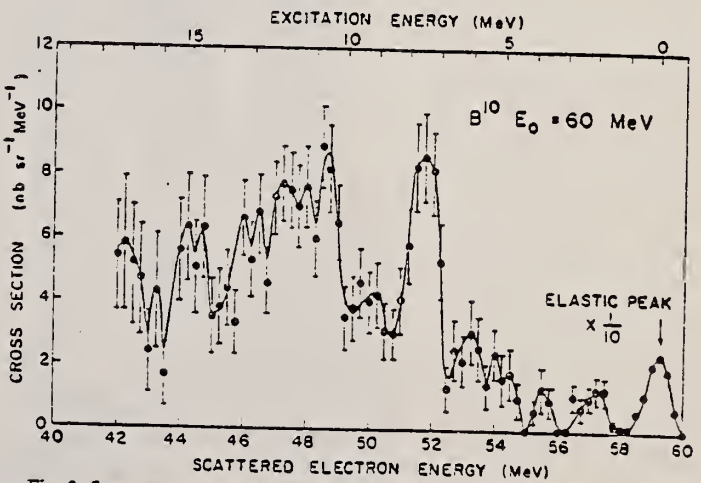

Fig. 2. Spectrum of 60 MeV electrons scattered from a ^{10}B target at 180°.

REF.

E. Spamer
Z. Physik, 191, 24 (1966)

ELEM. SYM.	A	Z
B	10	5

METHOD

60 MeV Linac; MAG.

[Page 1 of 2]

REF. NO. 66 Sp 1 JDM

REACTION	RESULT	EXCITATION ENERGY	SOURCE		DETECTOR		ANGLE
			TYPE	RANGE	TYPE	RANGE	
E,E/	ABX	6.7	D	32 - 57	MAG-D		DST

Tabelle 2. *Meßergebnisse für die untersuchten Kernniveaus*

Die in der vorliegenden Arbeit bestimmten Anregungsenergien stehen in der Spalte 2. Zum Vergleich sind in Klammern die Werte nach LANDOLT-BÖRNSTEIN (Neue Serie 1961) angegeben. Mit den in Spalte 3 gegebenen Spins wurden die Strahlungsbreiten Γ_γ^0 berechnet. Γ_ω in Spalte 8 sind die von WILKINSON — in F. AJZENBERG-SELOVE: Nuclear Spectroscopy, Part B. New York and London: Academic Press 1960 — benutzten Weisskopfeinheiten (mit $R = 1{,}2$ fm).

1. Isotop	2. Anregungsenergie (MeV)	3. I_f	4. Übergang	5. $B(\lambda, k, I_i \to I_f)$ (a)	6. R_{tr} (fm)	7. Γ_γ^0 (eV)	8. $\Gamma_\gamma^0/\Gamma_\omega$	9. Andere Autoren Γ_γ in eV
B^{10}	$6{,}014 \pm 0{,}020$ $(6{,}04 \pm 0{,}02)$	4^+	$C2$	$2{,}44 \pm 0{,}25$ $2{,}34 \pm 0{,}25$ [c]	$3{,}70 \pm 0{,}30$ $3{,}40 \pm 0{,}30$ [c]	$0{,}122 \pm 0{,}020$ [b] $0{,}116 \pm 0{,}020$ [c]	14	0,120 [2]
$(I_i = 3^+)$	$7{,}477 \pm 0{,}020$ [d] (7,47)	2^+	$M1$	$1{,}97 \pm 0{,}26$	$2{,}70 \pm 0{,}20$	$12{,}0 \pm 2{,}2$	1,4	17 [e]
B^{11}	$2{,}120 \pm 0{,}030$ $(2{,}138 \pm 0{,}006)$	$\frac{1}{2}^-$	$M1$		$2{,}60 \pm 0{,}20$			s. Text
$(I_i = \frac{3}{2}^-)$	$8{,}561 \pm 0{,}020$ $(8{,}568 \pm 0{,}007)$	$\frac{3}{2}^-$	$M1$ $C2$	$1{,}08 \pm 0{,}16$	$3{,}90 \pm 0{,}50$	$0{,}72 \pm 0{,}30$ $0{,}40 \pm 0{,}10$	0,055 7,3	
	$8{,}926 \pm 0{,}020$ $(8{,}923 \pm 0{,}004)$	$\frac{5}{2}^-$	$M1$ $C2$	$0{,}81 \pm 0{,}08$	$2{,}65 \pm 0{,}21$	$4{,}0 \pm 0{,}6$ [f] $\left(16^{+8}_{-16}\right) 10^{-3}$	0,27 0,24	0,06 [27]; 7,9 [g]

a) Einheit 10^{-51} cm^4 bei $C2$, 10^{-28} cm^2 bei $M1$. — b) Mit $\Gamma_\gamma^0(E2)/\Gamma_\gamma^0(M1) = 9$ nach [28] ergibt sich $\Gamma_\gamma^0(M1) = 0{,}014$ eV. — c) Daten Darmstadt und Orsay (s. Fig. 8). — d) $\Gamma_{tot} \approx 40$ keV. — e) Daten von [1] mit $\varepsilon = 7{,}48$ MeV anstatt $\varepsilon = 7{,}9$ MeV ergibt $\Gamma_\gamma^0 = 14$ eV. — f) Mit Daten von [27] folgt $\Gamma_\alpha \approx 0{,}03$ eV. — g) Daten von [1] mit $\varepsilon = 8{,}93$ MeV wie $M1$ ausgewertet.

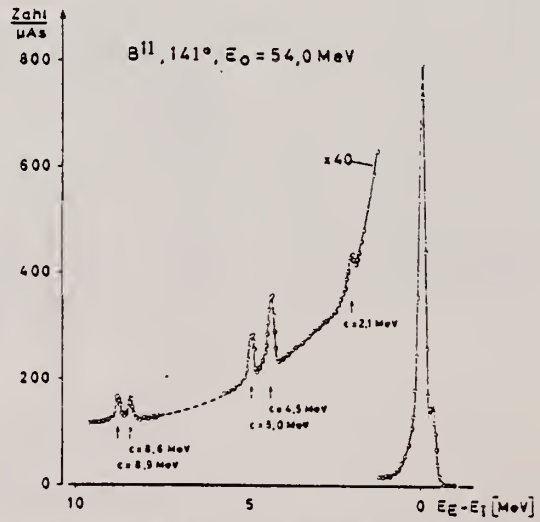

Fig. 1. Energieverteilung der von einem B^{11}-Target gestreuten Elektronen. Diese Übersichtsmessung wurde nicht ausgewertet. Die relative Energieunschärfe von Primärstrahl und Spektrometer betrug $(\Delta E/E)_A = (\Delta E/E)_S = 0{,}3\%$

REACTION	RESULT	EXCITATION ENERGY	SOURCE		DETECTOR		ANGLE
			TYPE	RANGE	TYPE	RANGE	

Tabelle 1. *Experimentelle Parameter und Meßwerte*

	θ (°)	E_0 (MeV)	q^2 (fm^{-2})	$A_i/h\,A_E$ (10^{-3}) (± Fehler in %)	$(d\sigma/d\Omega)\,R^*$ (10^{-32} cm^2/sr)	$B(\lambda, q)$ (a)	$B(\lambda, q)$ (a) (b)
B^{10}	104,98	31,85	0,054	0,149 ± 18	1,58 ± 0,29	2,09 ± 0,38	
6,01 MeV	104,98	36,01	0,071	0,269 ± 15	2,16 ± 0,32	2,13 ± 0,32	
$C2$	129,02	34,98	0,086	0,423 ± 12	1,04 ± 0,13	2,19 ± 0,26	
	104,98	44,10	0,109	0,529 ± 15	2,92 ± 0,44	1,81 ± 0,27	
	129,02	44,10	0,141	1,070 ± 12	1,48 ± 0,18	1,82 ± 0,22	
	92,91	54,54	0,143	1,190 ± 10	6,60 ± 0,66	1,95 ± 0,20	
	117,04	57,80	0,223	2,234 ± 12	3,14 ± 0,38	1,43 ± 0,17	
	141,11	54,88	0,244	3,560 ± 10	1,30 ± 0,13	1,64 ± 0,17	
	141,11	53,07	0,227	2,900 ± 12	1,17 ± 0,14	1,61 ± 0,18	
B^{10}	129,02	29,20	0,057	0,676 ± 20	2,39 ± 0,48	1,65 ± 0,37	1,89
7,477 MeV	129,02	34,98	0,081	0,871 ± 18	2,14 ± 0,39	1,38 ± 0,27	1,74
$M1$	129,02	39,83	0,109	1,225 ± 15	2,23 ± 0,34	1,44 ± 0,24	1,65
	129,02	44,10	0,136	1,591 ± 15	2,20 ± 0,33	1,41 ± 0,23	1,58
	153,15	41,78	0,139	5,870 ± 17	2,10 ± 0,36	1,63 ± 0,29	1,97
	92,91	54,54	0,140	0,518 ± 20	3,23 ± 0,65	1,17 ± 0,29	2,00
	165,05	50,26	0,216	21,200 ± 10	1,25 ± 0,13	0,98 ± 0,10	1,14
	117,04	57,80	0,217	1,290 ± 12	1,64 ± 0,20	0,92 ± 0,12	1,10
	129,02	55,28	0,220	2,060 ± 12	1,53 ± 0,18	0,98 ± 0,12	1,16
	153,15	51,73	0,221	7,280 ± 15	1,35 ± 0,20	1,01 ± 0,15	1,27
	141,11	53,07	0,220	3,484 ± 10	1,41 ± 0,14	0,99 ± 0,10	1,24
	141,11	54,88	0,237	3,720 ± 12	1,36 ± 0,16	0,95 ± 0,12	1,28
B^{11}	141,11	53,90	0,242	1,210 ± 20	0,49 ± 0,10	0,34 ± 0,07	
2,12 MeV	129,02	54,15	0,282	0,810 ± 20	0,63 ± 0,13	0,33 ± 0,07	
$M1$							
B^{11}	129,02	32,55	0,067	0,130 ± 50	0,37 ± 0,18	0,60 ± 0,55	
8,56 MeV	117,04	40,55	0,099	0,280 ± 20	0,92 ± 0,19	0,86 ± 0,22	
$C2+M1$	129,02	42,59	0,123	0,450 ± 14	0,68 ± 0,10	0,81 ± 0,16	
	141,11	45,05	0,151	0,830 ± 20	0,53 ± 0,11	0,87 ± 0,24	
	141,11	51,56	0,203	1,340 ± 12	0,59 ± 0,07	0,75 ± 0,12	
	165,05	49,26	0,203	2,790 ± 30	0,18 ± 0,06	0,65 ± 0,65	
	117,04	57,08	0,206	1,040 ± 10	1,37 ± 0,14	0,65 ± 0,08	
	129,02	54,15	0,207	1,230 ± 10	0,97 ± 0,10	0,72 ± 0,09	
	153,15	52,23	0,221	1,940 ± 19	0,35 ± 0,07	0,76 ± 0,23	
	141,11	53,90	0,223	1,230 ± 18	0,47 ± 0,09	0,52 ± 0,15	
	153,15	56,93	0,267	2,240 ± 20	0,31 ± 0,07	0,53 ± 0,16	
B^{11}	129,02	32,55	0,066	0,268 ± 24	0,78 ± 0,19	0,62 ± 0,15	0,63
8,93 MeV	117,04	40,55	0,098	0,283 ± 20	0,92 ± 0,18	0,63 ± 0,14	0,66
$M1$	129,02	42,59	0,122	0,529 ± 14	0,81 ± 0,11	0,59 ± 0,09	0,61
	141,11	45,05	0,149	1,125 ± 14	0,72 ± 0,16	0,56 ± 0,08	0,57
	141,11	51,56	0,201	1,339 ± 12	0,59 ± 0,07	0,44 ± 0,06	0,45
	165,05	49,26	0,202	8,792 ± 12	0,55 ± 0,07	0,45 ± 0,06	0,45
	117,04	57,08	0,206	0,503 ± 15	0,66 ± 0,10	0,41 ± 0,07	0,45
	129,02	54,15	0,206	0,834 ± 10	0,66 ± 0,07	0,44 ± 0,09	0,47
	153,15	52,23	0,220	3,460 ± 18	0,62 ± 0,11	0,48 ± 0,09	0,48
	141,11	53,90	0,221	1,132 ± 20	0,44 ± 0,09	0,31 ± 0,07	0,33
	153,15	56,93	0,265	3,942 ± 15	0,54 ± 0,08	0,41 ± 0,08	0,42

a) Einheit 10^{-28} cm^2 für $M1$; 10^{-51} cm^4 für $C2$. — b) Andere Auswertung: totale Fläche statt Anpassung für 7,477 MeV, ohne Korrektur des longitudinalen Anteils für 8,93 MeV.

* R ist der Rückstoßfaktor [s. Text zu Gl. (1a); (1b)].

REF.

J. M. Loiseaux, J. M. Maison and M. Langevin
J. de Physique 28, 11 (1967)

ELEM. SYM.	A	Z
B	10	5

METHOD

REF. NO.	
67 Lo 1	JOC

REACTION	RESULT	EXCITATION ENERGY	SOURCE		DETECTOR		ANGLE
			TYPE	RANGE	TYPE	RANGE	
G,G/	ABX	12-30	C	34	NAI-D		DST

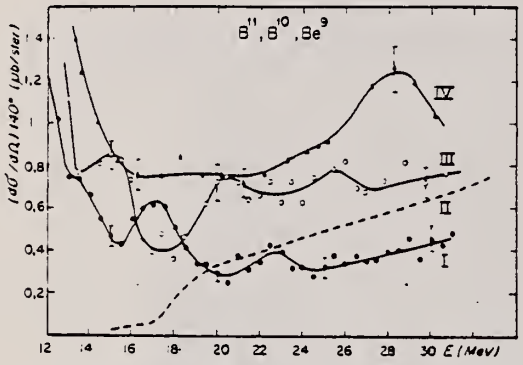

FIG. 5.

Sections efficaces différentielles de diffusion à 140° pour ^{9}Be (I), ^{10}B (III) et ^{11}B (IV).
Section efficace prévue par la relation de dispersion pour ^{9}Be (courbe II).

REF. S. C. Ling, A. M. Young and S. L. Blatt
Nucl. Phys. A108, 221 (1968)

ELEM. SYM.	A	Z
B	10	5

METHOD

REF. NO. 68 Li 1 EGF

REACTION	RESULT	EXCITATION ENERGY	SOURCE		DETECTOR		ANGLE
			TYPE	RANGE	TYPE	RANGE	
HE3,G	ABX	21-27	D	3-6	NAI-D		DST

962

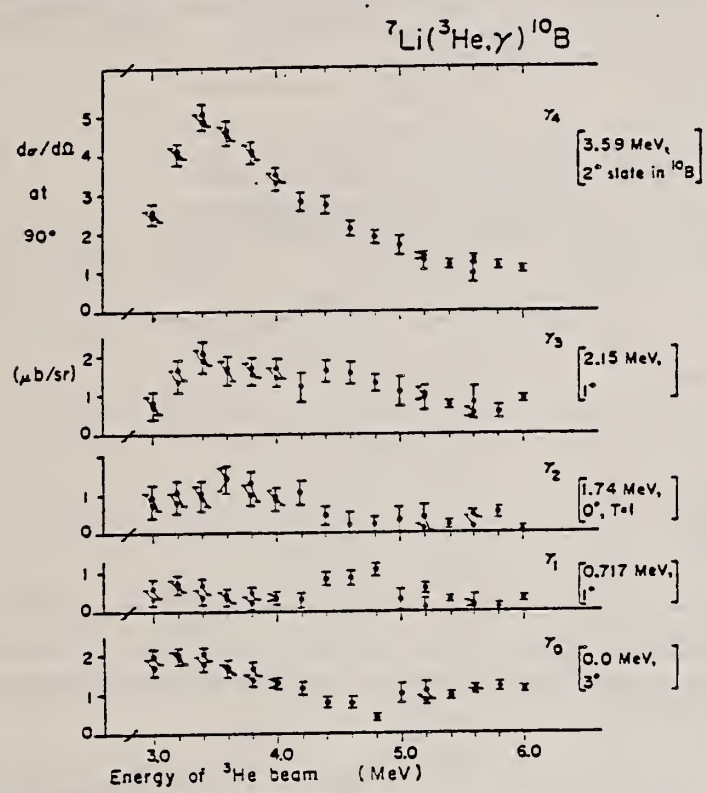

Fig. 5. Measured 90° differential cross sections for $^{7}Li(^{3}He,\gamma)^{10}B$ from 3.0 to 6.0 MeV bombarding energy. The curves are labeled according to the final states in ^{10}B involved in the transitions.

TABLE 1

Angular distribution coefficients a obtained from least-squares fit to the data assuming a distribution of the form $W(\theta) = 1 + aP_2(\cos\theta)$

Transition \ ^{3}He energy	2.8 MeV	3.4 MeV	4.2 MeV	5.0 MeV
γ_0	-0.09 ± 0.03	$+0.11 \pm 0.09$	-0.26 ± 0.09	-0.05 ± 0.15
γ_1	-0.08 ± 0.06	-0.01 ± 0.02	3 ± 6	-0.20 ± 0.57
γ_2	$+0.09 \pm 0.11$	$+0.81 \pm 0.50$	-0.42 ± 0.28	$+0.24 \pm 0.17$
γ_3	$+0.08 \pm 0.03$	$+0.01 \pm 0.06$	-0.21 ± 0.33	-0.36 ± 0.22
γ_4	$+0.10 \pm 0.07$	$+0.01 \pm 0.04$	-0.29 ± 0.09	-0.08 ± 0.11

REF.

A. Kh. Shardanov and B. A. Yur'ev
Yad. Fiz. 8, 424 (1968)
Sov. J. Nucl. Phys. 8, 245 (1969)

ELEM. SYM.	A	Z
B	10	5

METHOD

REF. NO.	
68 Sh 6	HMG

REACTION	RESULT	EXCITATION ENERGY	SOURCE		DETECTOR		ANGLE
			TYPE	RANGE	TYPE	RANGE	
G,P	ABX	6-13	C	13	EMU-D		DST
		(6.6-12.5)		(12.5)			

13=12.5 MEV

Table I. Experimental data on resonances in the cross section for the reaction $B^{10}(\gamma, p)Be^{9}$ and theoretical values of the radiation widths of B^{10} levels

E_{res}, MeV	σ_{max}, mb	σ_{int}, MeV-mb	Γ_γ^{exp}, eV			$\Gamma_{\gamma,p}^{theor}$, eV (ref. 3)			$\Gamma_{\gamma int}^{theor}$, eV						
									M1						E2***
			$l=2$	$l=3$	$l=4$	E1	M1	E2	$l=2$;	$T=1$;	$l=3$;	$T=1$;	$l=4$;	$T=1$	
8.8±0.1	5.7±0.8	1.8±0.25	50	35	26	215	14	0.05	5.5*	1.7—4.5**	12*	8**	1.8*	0.7**	0.01—0.20
9.2±0.1	5.4±0.8	1.6±0.25	40	30	23	245	16	0.07	6*	2—5**	15*	10**	2*	0.8**	0.02—0.3
(10.5)	0.5±0.15	0.25±0.1	>11	>8	>6	904	25	0.13	9*	3—7.5**	21*	14**	3*	1.2**	0.03—0.5

*Estimates according to ref. 4; **Estimates according to ref. 5; ***Estimates according to ref. 6.

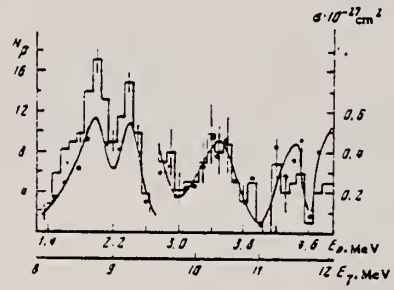

FIG. 1. Energy distribution of photoprotons (histogram) and cross-section curve for the reaction $B^{10}(\gamma, p)Be^{9}$ (solid curve). The cross-section values and the number of protons in the region below 2.75 MeV have been reduced by a factor of 10.

σ calculated on assumption that the final nucleus Be^{9} is left in the ground state.

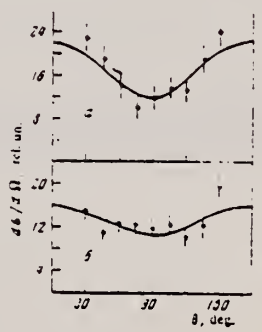

FIG. 2. Angular distributions of photoprotons: a – for the proton group with energy 1.5 2.15 MeV; b – for the proton group with energy 2.25 2.55 MeV. Solid curves – results of a calculation on the assumption of M1 transitions to levels with spin $I = 2$ (a) and $I = 3$ (b).

REF.

S.C. Ling and S.L. Blatt
Nucl. Phys. A174, 375 (1971)

EL EM. SYM.	A	Z
B	10	5

METHOD

REF. NO. 71 Li 3 hmg

REACTION	RESULT	EXCITATION ENERGY	SOURCE TYPE	SOURCE RANGE	DETECTOR TYPE	DETECTOR RANGE	ANGLE
T,G	LFT	18.19	D	1-2	SCD-D		DST
		(18.4,19.3)		(1.1-2.2)			

See 65Pa1.

J-PI, 18.4,19.3 MEV

TABLE 1

Resonances in the $^7Li(\tau,\gamma)^{10}B$ reaction

E_{res}(lab) (MeV)	Γ(c.m.) (keV)	E_{ex} in ^{10}B (MeV)	Final states in ^{10}B (MeV)	J^π	Γ_γ (eV)	J^π
0.92	140	18.4	0.0	3^+	$\geqq$ 3	2^-
			4.77	3^+	$\geqq$ 17	
1.4	<600	18.8	0.717	1^+	$\geqq$ 20	$(1^+, 2^+)$
			3.59	2^+	$\geqq$ (20) *)	
2.1	280	19.3	0.0	3^+	$\geqq$ 12	2^-
			4.77	3^+	$\geqq$ 49	
3.4	910	20.2	3.59	2^+	$\geqq$ 350	1^-

*) Assumes isotropy; angular distribution not determined in present experiment.

Abstract: Existing data on four resonances seen in $^7Li+\tau$ reactions have been re-examined, and additional measurements of the reaction $^7Li(\tau,\gamma)^{10}B$ have been made, in order to better establish the spins and parities of the ^{10}B compound states involved. The excitation energies of these states and their most likely assignments are: 18.4 MeV, 2^-; 18.8 MeV, $(1^+, 2^+)$; 19.3 MeV, 2^-; and 20.2 MeV, 1^-. All appear to be $T = 1$ states.

E NUCLEAR REACTIONS $^7Li(^3He,\gamma)$, $E = 1.1$, 1.4, 2.2 MeV; measured $\sigma(E_\gamma, \theta_\gamma)$. ^{10}B deduced levels, J, π. Enriched target.

REF. R. J. Hughes and B. M. Spicer
PICNS-73, Vol.I, p.153 Asilomar

ELEM. SYM.	A	Z
B	10	5

METHOD

REF. NO. 73 Hu 12 - hmg

REACTION	RESULT	EXCITATION ENERGY	SOURCE		DETECTOR		ANGLE
			TYPE	RANGE	TYPE	RANGE	
G,XN	ABX	8- 28	C	8- 28	MOD-I		4PI

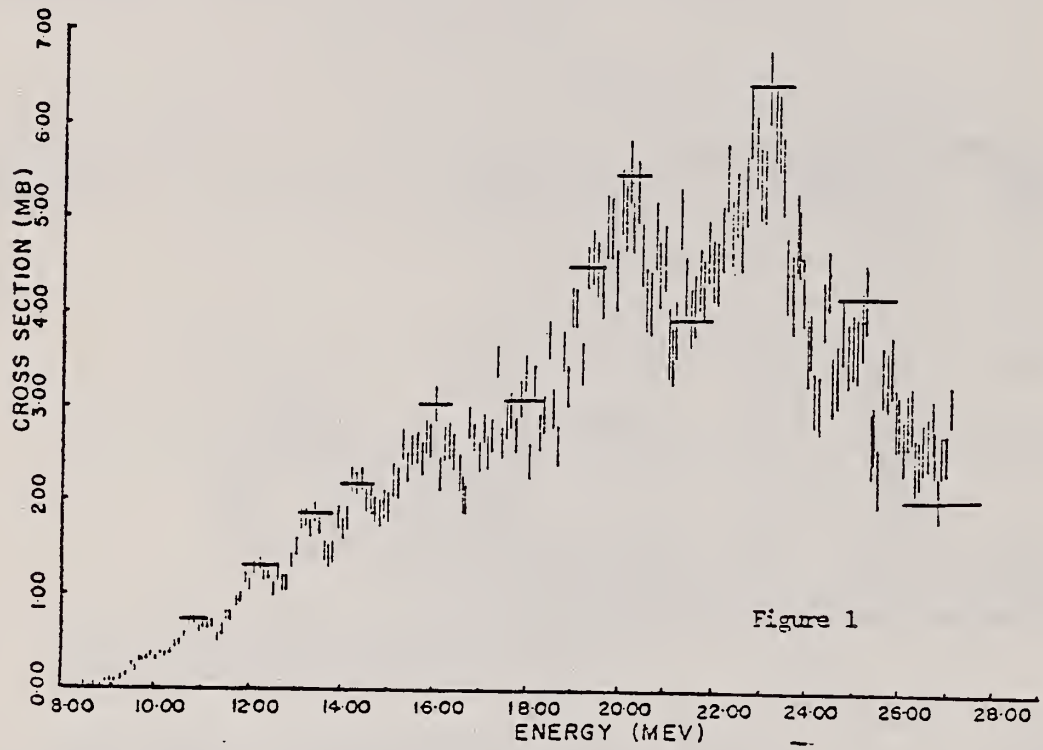

Figure 1

REF.

R. J. Hughes and E.G. Muirhead
Nucl. Phys. A215, 147 (1973)

B	10	5

METHOD

REF. NO. 73 Hu 14 egf

REACTION	RESULT	EXCITATION ENERGY	SOURCE		DETECTOR		ANGLE
			TYPE	RANGE	TYPE	RANGE	
G,XN	ABX	8- 28	C	8- 28	BF3-I		4PI

831

Figures also give comparison with theory.

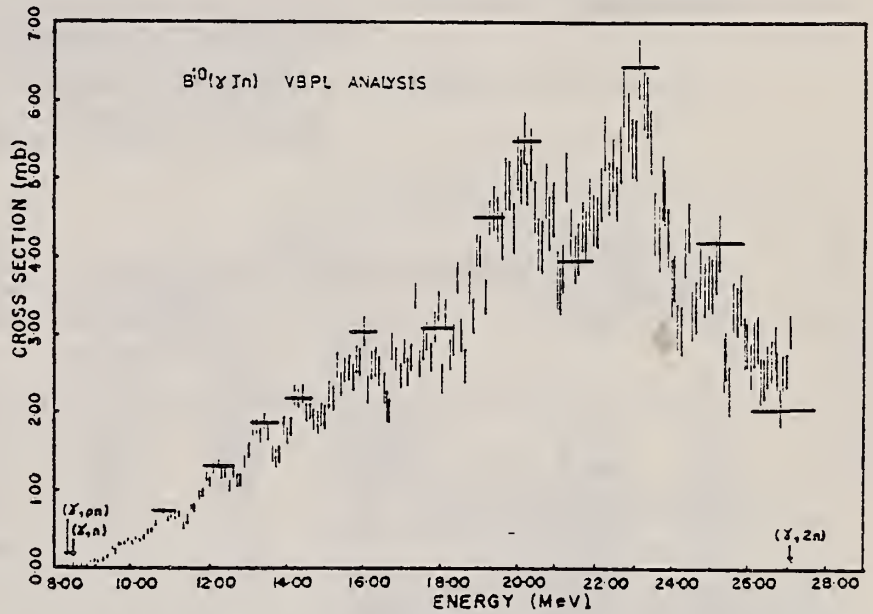

Fig. 1. The total photoneutron cross section of ^{10}B. The horizontal bars indicate the analysis resolution at various energies.

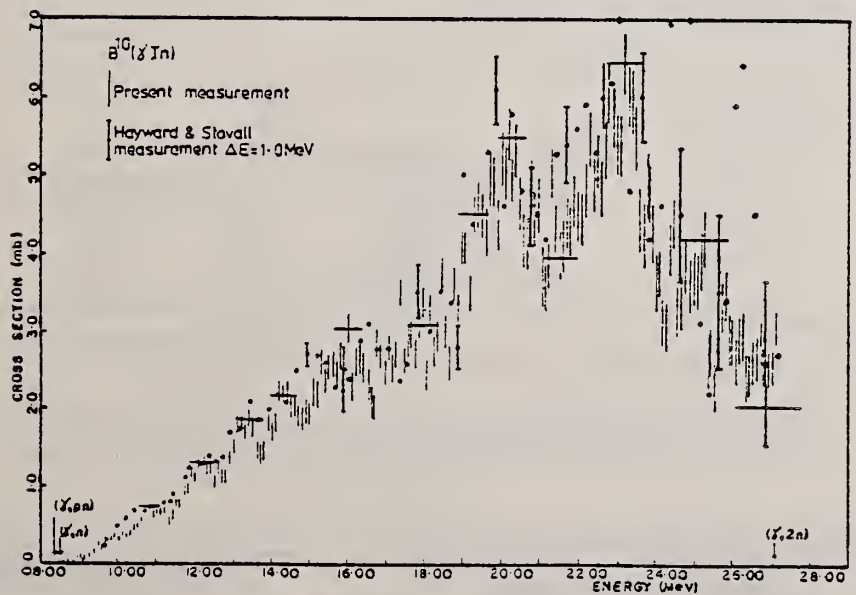

Fig. 3. The photoneutron cross section of ^{10}B.

REF. W. Auwarter and V. Meyer
Nucl. Phys. A242, 129 (1975)

ELEM. SYM.	A	Z
B	10	5

METHOD

REF. NO. 75 Au 8 - egf

REACTION	RESULT	EXCITATION ENERGY	SOURCE TYPE	SOURCE RANGE	DETECTOR TYPE	DETECTOR RANGE	ANGLE
P,G	ABX	7- 8	D	0- 1	SCD-D		0
A,G	ABX	7- 8	D	4- 5	SCD-D		0

LEVELS 6.88,7.44 MEV

6.88 1^- level $d\sigma/d\Omega(\theta=0)$ = 0.17±0.04 μb/sr α-capture
= 1±0.2 μb/sr p-capture

7.44 2^-(?) level $d\sigma/d\Omega(\theta=0)$ = 0.07±0.03 α-capture

TABLE 1
Gamma-ray transitions from the 6.88 MeV level

Final state E_x	Final state J^π, T	Relative intensity (p,γ) $\theta = 0°$	(α,γ) $\theta = 0°$ exp.	(α,γ) $\theta = 55°$ calc.	(p,γ) [a] $\theta = 55°$
g.s.	(3⁺, 0)	< 4.6	4.5±2	5.5±2	
0.72	(1⁺, 0)	20±2	13±3	19±4	24±4
1.74	(0⁺, 1)	53±2	66±4	53±3	62±4
2.15	(1⁺, 0)	13±1	8±3	13±4	8±4
3.59	(2⁺, 0)	< 1			
5.11	(2⁻, 0)	4±1			
5.17	(2⁺, 1)	3±1	not seen		not given
5.18	(1⁺, 0)	< 1			
5.92	(2⁺, 0)	3.5±1			

[a]) Renan *et al.* [9]).

[9] M.J. Renan, J.P.F. Sellschop, R.J. Keddy, and D.W. Mingay, Phys. Rev. C6, 12 (1972).

TABLE 2
Gamma-ray transitions from the 7.44 MeV level

Final state	Relative intensity
g.s. (3⁺, 0)	50±12
0.72 MeV (1⁺, 0)	50±12

REF.

L.W. Fagg, R.A. Lindgren, W.L. Bendel, E.C. Jones,Jr.
Phys. Rev. C14, 1727 (1976)

ELEM. SYM.	A	Z
B	10	5

METHOD

REF. NO. 76 Fa 5 hmg

REACTION	RESULT	EXCITATION ENERGY	SOURCE		DETECTOR		ANGLE
			TYPE	RANGE	TYPE	RANGE	
E,E/	ABX	5- 12	D	40- 61	MAG-D		180

6 LEVELS, 5.11-11.56

Peaks at excitations of 5.11, 6.02, 7.48, 8.90, 10.79, and 11.56 MeV were observed in spectra of ^{10}B produced by 180° inelastic scattering of electrons at 40.5, 50.6, and 60.6 MeV. The transitions at 6.02 and 8.90 MeV appear to be $E2$ and $M2$ or $E2$, respectively. There is evidence for $M1$ transition strength to at least one level in the 11 MeV excitation region. The model-dependent radiative widths of the levels at 5.11 and 7.48 MeV were determined to be: $\Gamma_0(M2) = (6.9 \pm 1.4) \times 10^{-4}$ eV and $\Gamma_0(M1) = 11.3 \pm 2.0$ eV, respectively. Subject to qualifications cited in the text, radiative widths for some of the other transitions are also given.

TABLE I. Values of cross sections for excitation of the nuclear states studied at the three incident energies of 40.5, 50.6, and 60.6 MeV.

Excitation energy (MeV)	Cross section (nb/sr) 40.5 MeV	50.6 MeV	60.6 MeV
5.11	0.52 ± 0.08	1.03 ± 0.15	1.24 ± 0.17
6.02	0.97 ± 0.15	1.08 ± 0.16	0.83 ± 0.12
7.48	15.99 ± 1.74	14.18 ± 1.55	9.72 ± 0.95
8.90	0.30 ± 0.08	0.39 ± 0.09	0.38 ± 0.08
10.79	2.62 ± 0.33	2.52 ± 0.33	2.02 ± 0.26
11.56	3.72 ± 0.46	3.70 ± 0.46	2.57 ± 0.33

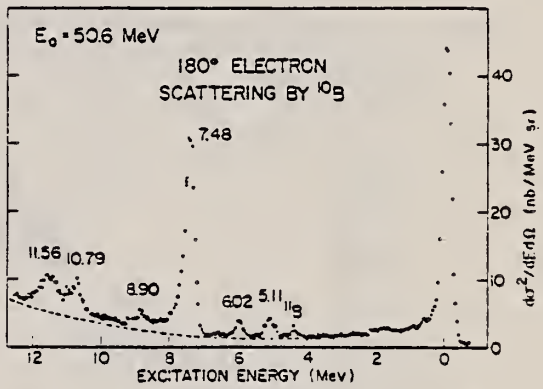

FIG. 1. Spectrum of 50.6-MeV electrons scattered at 180° from ^{10}B. The base line used is indicated by the dashed curve. An indication of the statistical errors involved is given by the error bars on the point on the left hand side of the 7.48-MeV peak.

TABLE II. Multipolarities, transition radii, and ground state transition widths for states in ^{10}B electroexcited at 180°.

Excitation energy (MeV)	J^π, T [a]	Multipolarity	R (fm)	Γ_0 (eV)
5.11	$2^-, 0$	$M2$		$(6.9 \pm 1.4) \times 10^{-4}$ [b]
			4.3 ± 1.1	$(10.2 \pm 2.2) \times 10^{-4}$ [c]
6.02	4^+	$E2$	(4.6 ± 1.0)	(0.3 ± 0.07) [c,d]
7.48	$2^+, 1$	$M1$		11.3 ± 2.0 [b]
			2.4 ± 0.4	10.1 ± 1.9 [c]
8.90	$(2^+, 1)$	$(E2)$		(0.5 ± 0.2) [c]
	$(3^-, 1)$	$(M2)$		$[(6 \pm 2) \times 10^{-3}]$ [c]
10.79		$M1$ or $E2$		
11.56		$(M1)$		(11.4 ± 2.3) [b]

[a] Spin assignments are taken from Ref. 17.
[b] Result obtained by direct comparison with DWBA oscillator model; oscillator parameter, 1.88.
[c] Result obtained using DWBA corrected PWBA generalized Helm model expressions.
[d] Due to other levels in this region there may be some question as to whether all of this strength is due to a transverse $E2$ transition to the 4^+ state. A DWBA oscillator model calculation was not available for electric transitions.

17 F. Ajzenberg-Selove, T. Lauritsen, Nucl. Phys. A227, 1 (1974).

REF. U. Kneissl, K. H. Leister, H. O. Neidel, A. Weller
Nucl. Phys. A264, 30 (1976)

ELEM. SYM.	A	Z
B	10	5

METHOD

REF. NO. 76 Kn 3 egf

REACTION	RESULT	EXCITATION ENERGY	SOURCE		DETECTOR		ANGLE
			TYPE	RANGE	TYPE	RANGE	
G,XN *	ABX	10- 35	D	10- 35	MOD-I		4PI
G,2N **	ABX	16- 35	D	16- 35	MOD-I		4PI

$\sigma_o(35)_{xn}$ = 83.1±1.2 MeV-mb *1048

$\sigma_o(35)_{sn}$ = 80.8±1.4 MeV-mb **1049

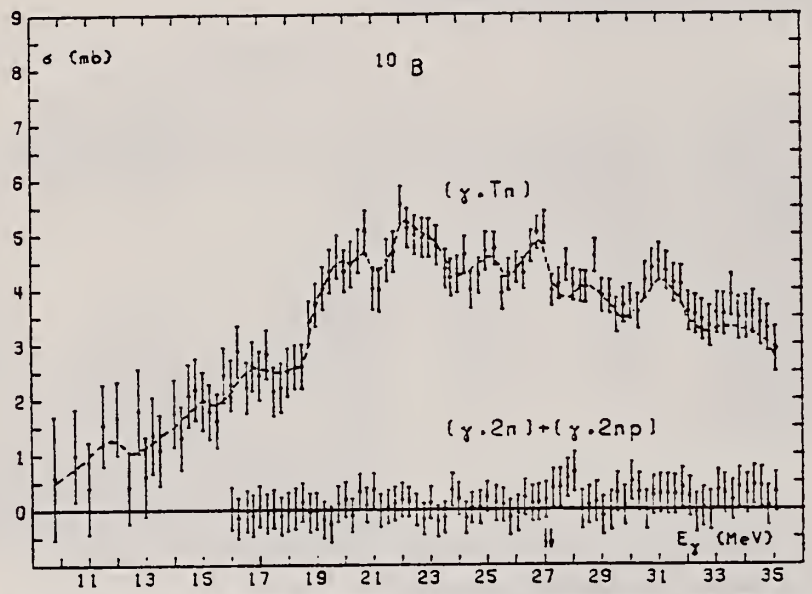

Fig. 2. The $\sigma(\gamma, Tn)$ and the double neutron cross section $\sigma(\gamma, 2n)+\sigma(\gamma, 2np)$ for ^{10}B. [The (2n) and (2n, p) thresholds at 27.0 and 27.2 MeV respectively are indicated by arrows.] The dashed line represents $\sigma(\gamma, n_{tot}) = \sigma(\gamma, n)+\sigma(\gamma, np)+\sigma(\gamma, 2n)+\sigma(\gamma, 2np)$.

REF. V. Di Napoli, J. B. Martins, G. Rosa, F. Salvetti, O. A. P. Tavares, M. L. Terranova and H. G. De Carvalho
J. Inorg. Nucl. Chem. 40, 1619 (1978)

ELEM. SYM.	A	Z
B	10	5

METHOD

REF. NO. 78 Di 10 hg

REACTION	RESULT	EXCITATION ENERGY	SOURCE		DETECTOR		ANGLE
			TYPE	RANGE	TYPE	RANGE	
G,Be7	ABY	18(18.67)-999	C	300-999	ACT-I		4PI

Abstract—Mean cross sections for the photoproduction of ^{7}Be and ^{11}C from ^{19}F, ^{27}Al, ^{28}Si and ^{32}S targets, ^{7}Be from ^{10,11}B, and ^{11}C from ^{14}N and ^{16}O targets have been measured using bremsstrahlung beams in the energy range 0.3–1.0 GeV. The results have been compared with previous measurements and an excellent agreement has been found. In most cases, the values obtained turned out to be much larger than those expected from a simple spallation mechanism. A fragmentation and/or a fission-like process has been suggested in explaining the mechanism of such reactions.

999=1 GEV

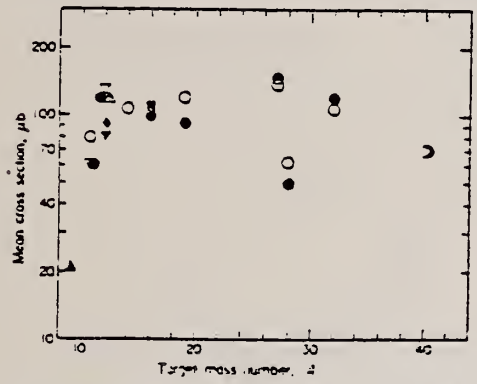

Fig. 2. The same as in Fig. 1 for ^{7}Be photoproduction. Experimental data are taken from: ▲, Refs. [6, 7]; ▽, Ref. [8]; ●, Ref. [9]; △, Ref. [10]; ◆, Ref. [11]; ▼, Ref. [12]; □, Ref. [13]; ■, Ref. [14]; ◇, Ref. [2]; ○, present work.

Table 2. Cross sections per equivalent quantum of ^{7}Be photoproduction

E_0 (GeV)	Cross Section, σ_Q (μb) $^{10,11}B$	^{14}N	^{16}O	^{19}F	^{27}Al	^{28}Si	^{32}S
0.30	150±20	200±20	111±20	152±20	40±20	20±20	50±20
0.32	160±20	200±20	120±20	150±20	45±20	30±20	54±20
0.35	160±20	210±20	130±20	159±20	42±20	30±20	60±20
0.40	175±20	226±20	145±20	170±20	98±20	28±20	70±20
0.48	190±20	245±20	161±20	186±20	100±20	50±20	140±20
0.55	200±20	260±20	187±20	200±20	93±20	48±20	90±20
0.65	220±21	280±20	197±20	214±20	140±20	68±20	130±20
0.75	225±20	300±20	215±20	227±20	160±20	70±20	130±20
0.90	240±20	318±20	230±20	245±20	186±20	88±20	165±20
1.01	250±20	330±20	242±20	260±20	200±20	97±20	190±20

Table 3. Comparison between experimentally determined and calculated cross sections of ^{7}Be and ^{11}C photoproduction and indication of the dominant reaction channels

Target Nucleus	Product Nucleus	Nominal Nucleon Loss, ΔA	$\Delta A/A_t$ (x100)	$\bar{\sigma}_{exp}$(*) (μb)	$\bar{\sigma}_{CDNO}$ (**) (μb)	$\bar{\sigma}_{exp}/\bar{\sigma}_{CDNO}$	Apparent Threshold (Exp.) E_{th}(MeV)	Possible Mechanism of Production
$^{10,11}B$	^{7}Be	(3)	(30);.16	67	28	2	≤ 50	Spallation
^{12}C	^{7}Be	5	42	110	20	5	≤ 50	Spallation
^{14}N	^{7}Be	7	50	108	12	9	≤ 50	Fission Spallation
^{14}N	^{11}C	3	21	130	60	2	≤ 50	Spallation
^{16}O	^{7}Be	9	56	107	8	13	$50<E_{th}<200$	Fission Fragmentation
^{16}O	^{11}C	5	31	117	33	3	≤ 50	Spallation
^{19}F	^{7}Be	12	63	106	5	21	$50<E_{th}<200$	Fission Fragmentation
^{19}F	^{11}C	8	42	105	16	7	$50<E_{th}<200$	Fission Fragmentation Spallation
^{27}Al	^{7}Be	20	74	142	2	71	> 200	Fragmentation
^{27}Al	^{11}C	16	59	70	5	14	$50<E_{th}<200$	Fission Fragmentation
^{28}Si	^{7}Be	21	75	56	2	28	> 200	Fragmentation
^{28}Si	^{11}C	17	61	68	4	17	$50<E_{th}<200$	Fission Fragmentation
^{32}S	^{7}Be	25	78	114	2	57	> 200	Fragmentation
^{32}S	^{11}C	21	66	68	3	23	$50<E_{th}<200$	Fission Fragmentation
$^{35,37}Cl$	^{11}C	24,(25)	69,(70)	59	3	20	$50<E_{th}<200$	Fission Fragmentation
^{40}Ca	^{7}Be	33	83	70	1	70	> 200	Fragmentation
^{40}Ca	^{11}C	29	73	70	2	35	> 200	Fragmentation

(*) Mean values of the different measurements (see Figs. 1 and 2).

(**) Calculated values according to Ref. [9].

U.S. DEPARTMENT OF COMMERCE
NATIONAL BUREAU OF STANDARDS

USCOMM-NBS-DC

REF. K. Nakamura, S. Hiramatsu, T. Kamae, H. Muramatsu, N. Izutsu, Y. Watase
Nucl. Phys. A296, 431 (1978)

ELEM. SYM.	A	Z
B	10	5

METHOD

REF. NO. 78 Na 3 hg

REACTION	RESULT	EXCITATION ENERGY	SOURCE TYPE	SOURCE RANGE	DETECTOR TYPE	DETECTOR RANGE	ANGLE
E,E/P	SPC	0*60	D	700	MAG-D		53

Abstract: The proton spectral functions of ^{6}Li, ^{7}Li, ^{9}Be and ^{10}B obtained from the (e, e'p) reactions at 700 MeV are presented. The results were analyzed in the distorted-wave impulse approximation, using the shell-model single-particle wave functions consistent with the elastic electron scattering results. The observed 1p proton momentum distributions for the nuclei ^{6}Li, ^{7}Li and ^{9}Be show significant disagreement with the shell-model momentum distributions. The occupation probabilities of the proton single-particle states are around 0.7, with a few exceptions.

*SEPARATION ENERGY

E NUCLEAR REACTIONS ^{6}, ^{7}Li, ^{9}Be, ^{10}B(e, e p), E = 700 MeV; measured $\sigma(E_p, \theta_p)$; deduced proton spectral functions. DWIA calculations. Enriched ^{6}, ^{7}Li, ^{10}B and natural ^{9}Be targets.

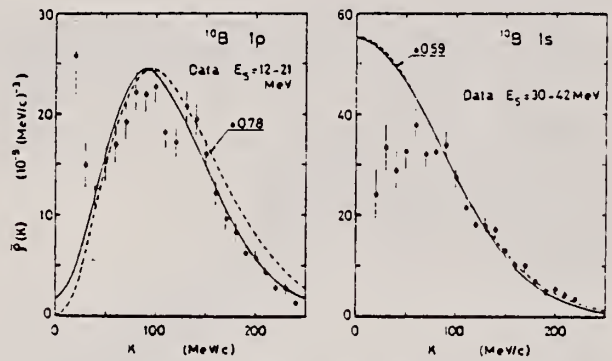

Fig. 5. The distorted momentum distributions corresponding to the optical potentials A (the solid curves) and B (the dot-dashed curves), and the undistorted momentum distributions (the dashed curves), calculated from the shell-model single-particle wave functions used in the DWIA analysis. (a) ^{6}Li, (b) ^{7}Li, (c) ^{9}Be and (d) ^{10}B. For comparison, data points in the appropriate separation energy ranges are shown. They are arbitrarily normalized to the calculated distorted momentum distributions.

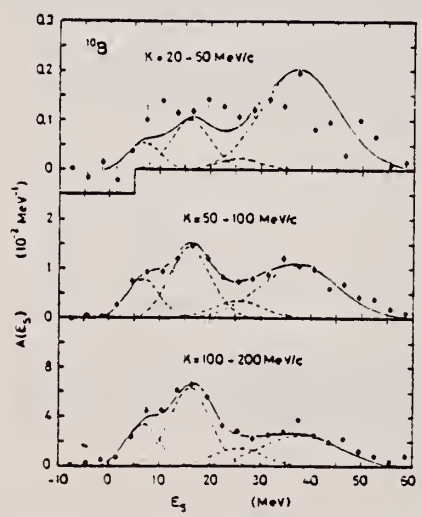

Fig. 4a. Proton separation energy spectra for ^{10}B. The curves are as in fig. 1a.

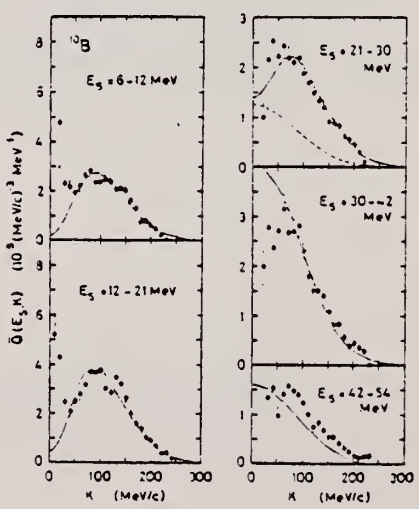

Fig. 4b. Recoil momentum distributions for ^{10}B. The curves are as in fig. 1b.

REF. N. G. Shevchenko, A. Yu. Buki, B. V. Mazan'ko, V. N. Polishchuk, A. A. Khomich
Yad. Fiz. 28, 12 (1978)
Sov. J. Nucl. Phys. 28, 5 (1978)

ELEM. SYM.	A	Z
B	10	5

METHOD

REF. NO.	
78Sh8	hg

REACTION	RESULT	EXCITATION ENERGY	SOURCE		DETECTOR		ANGLE
			TYPE	RANGE	TYPE	RANGE	
E,E/	SPC	8-10	D	140	MAG-D		DST
		(8.26-9.7)					

Energy spectra of 140-MeV electrons are measured after scattering by ^{10}B and ^{12}C nuclei. Peaks above the nucleon emission threshold are observed in the ^{10}B spectra at energies 8.26, 9.0, and 9.7 MeV, and at 18.1 MeV in the ^{12}C spectra. The existence of these peaks and their energy location is predicted by calculations based on inclusion of the contribution of triangle Feynman diagrams to the reaction amplitude.

PACS numbers: 25.30.Cg, 27.20.+n

EX 8.26, 9., 9.7 MEV

Examines levels above the nuclear threshold

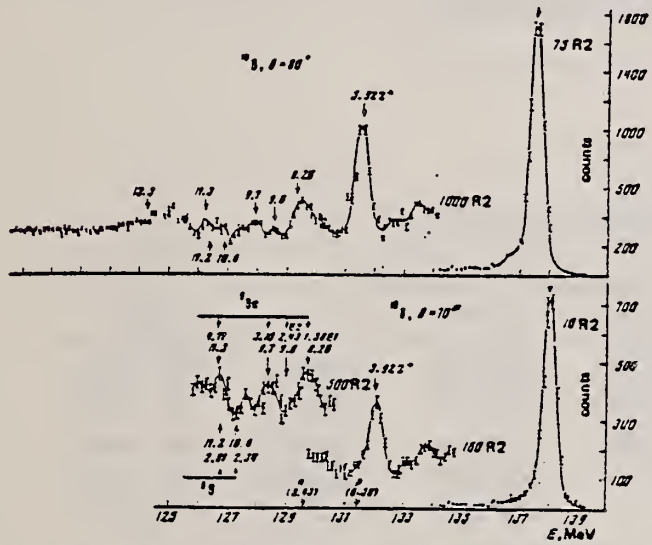

FIG. 2. Spectra of 140-MeV electrons after scattering by ^{10}B nucleus at angles 70 and 80°. We have indicated in the figure the energies of the discrete levels of ^{9}B and ^{9}Be and also the proton and neutron binding energies in ^{11}B. In each spectrum we have shown the exposure in units of the second monitor range R2, equal to 3.7×10^{-8} Coulomb.

REF. E. J. Ansaldo, J. C. Bergstrom, R. Yen, H. S. Caplan
Nucl. Phys. A322 , 237 (1979)

ELEM. SYM.	A	Z
B	10	5

METHOD

REF. NO. 79An5 hg

REACTION	RESULT	EXCITATION ENERGY	SOURCE TYPE	SOURCE RANGE	DETECTOR TYPE	DETECTOR RANGE	ANGLE
E,E/	FMF	1-9	D	67-194	MAG-D	61-192	DST
		(1.74-8.9)					

Abstract: Electron scattering form factors were measured for six transitions in ^{10}B in the momentum transfer range 0.61 to 1.81 fm^{-1}. Ground state radiative widths were extracted by means of the generalized Helm model for the levels at 1.74 MeV (M3), 5.17 MeV (M1+M3), 6.03 MeV (C2+C4), 7.48 MeV (M1), 8.07 MeV (C2) and 8.9 MeV (M1+M3 or M2). The transverse form factors for the 1.74 and 5.17 MeV levels agree well with predictions based on Cohen–Kurath wave functions. The longitudinal form factor for the 6.03 MeV state shows effects due to the deformation of ^{10}B and is in good agreement with the deformed Hartree–Fock shell model prediction of Bouten and Bouten. Estimates are presented for the ratios of radiative pion capture rates leading to analogue states in ^{10}Be.

6 LEVELS 1.74-8.9 MEV

E NUCLEAR REACTIONS ^{10}B(e, e'), E = 67–194 MeV; measured $\sigma(E; E_e; \theta)$. ^{10}B deduced form factors, reduced widths, multipolarities, (π^-, γ) rates. Helm model. Enriched targets.

TABLE 1

Longitudinal and transverse form factors obtained in this work

E_0 (MeV)	θ (deg)	q (fm^{-1})	F_L^2(×10^3) 6.03 MeV	F_L^2(×10^3) 8.07 MeV	F_T^2(×10^3) 1.74 MeV	F_T^2(×10^3) 5.17 MeV	F_T^2(×10^3) 7.48 MeV	F_T^2(×10^3) 8.9 MeV
67	145	0.62	3.45±0.40	1.2±0.5	—	0.056±0.030	0.18±0.05	0.0058±0.005
78	145	0.72	5.20±0.50	1.2±0.2	0.041±0.010	0.093±0.008	0.14±0.05	0.015 ±0.007
107	101	0.82	6.50±0.60	1.5±0.4	0.075±0.040	0.155±0.035	0.085±0.010	0.028 ±0.007
92 113	141 100	0.86	7.10±0.40	2.2±0.4	0.051±0.020	0.185±0.080	0.076±0.010	0.034 ±0.008
107	146	1.00	9.20±0.30	1.9±0.4	0.125±0.010	0.260±0.030	0.011±0.008	0.056 ±0.005
120 130	120 105	1.03	8.72±0.77	1.8±0.4	—	0.350±0.070	0.005±0.015	0.047 ±0.015
134 146	125 110	1.19	8.66±0.55	1.3±0.3	0.200±0.040	0.490±0.130	0.011±0.015	0.050 ±0.010
160 188	130 105	1.44	6.63±0.40	0.6±0.3	0.240±0.030	0.540±0.120	0.055±0.015	0.075 ±0.015
170 188	139 120	1.58	5.10±0.70	1.0±0.3	0.200±0.040	0.480±0.070	0.086±0.015	0.110 ±0.040
194	130	1.81	2.56±0.50	0.5±0.3	0.180±0.050	0.420±0.070	0.070±0.030	0.077 ±0.017

The momentum transfer is for 6 MeV excitation energy.

Plotted form factors:
Longitudinal: 8.07 MeV Fig. 4
Transverse: 1.74 MeV(0+) Figs. 5,7; 5.17 MeV (2+) Fig. 6; 5.17 MeV (2+) Fig. 8; 8.9 MeV (2+,3-) Fig. 10

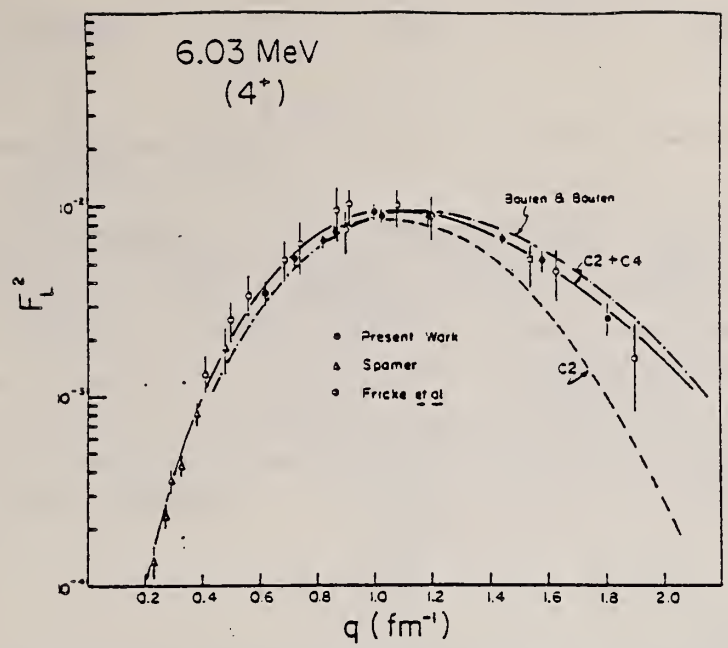

Fig. 3. Longitudinal form factor for the 6.03 MeV state. All the data from this work plus that of Spamer [6]) and Fricke *et al.* [7]) were fit by the C2-C4 Helm model (R = 2.3 fm) admixture shown by the solid line. Also shown (dash-dotted line) is the theoretical form factor of Bouten and Bouten [20]).

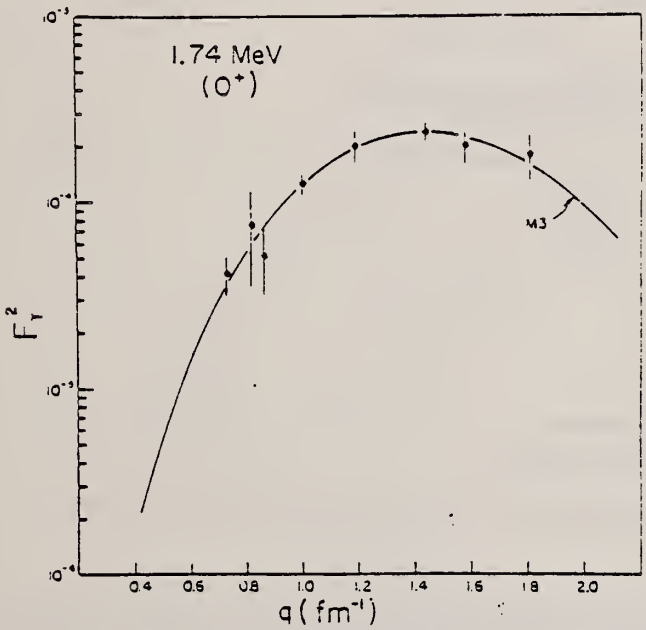

Fig. 5. Transverse form factor for the 1.74 MeV transition. The solid curve is the M3 generalized Helm model fit with R = 2.31 fm.

TABLE 2

Properties of the longitudinal transitions observed in this work

E_x (MeV)	J^π	CA	Γ_γ^0 (eV)	B(CA↑) (e^2·fm^{2A})	Γ_γ^0 (eV) other work
6.03	4⁺	C2	0.106 ± 0.005	21.2 ± 1.0	0.122 ± 0.020[a,b]
		C4	(3.3 ± 0.8) × 10^{-7}	(3.6 ± 0.9) × 10^3	
8.07	2⁺	C2	0.19 ± 0.02	4.9 ± 0.5	

[a]) Ref. [6]).
[b]) Ref. [7]).

TABLE 3

Properties of the magnetic transitions observed in this work

E_x (MeV)	J^π	MA	Γ_γ^0 (eV)	B(MA↑) (e^2·fm^{2A})	Γ_γ^0 (eV) other work
1.74	0⁺	M3	(1.05 ± 0.25) × 10^{-7}	6.0 ± 1.4	
5.17	2⁺	M1	0.05 ± 0.05	(2.5 ± 2.5) × 10^{-4}	
		M3	(1.1 ± 0.10) × 10^{-6}	21.6 ± 2.2	
		M2	(3.5 ± 0.3) × 10^{-4}	(1.92 ± 0.12) × 10^{-2}	(6.9 ± 1.4) × 10^{-4}[a])
7.48	2⁺	M1	11.75 ± 0.75		11.3 ± 2.0[a])
					12.0 ± 2.2[b])
8.9	2⁺	M1	0.3 ± 0.1	(2.9 ± 1.0) × 10^{-4}	
		M3	(1.0 ± 0.1) × 10^{-3}	4.3 ± 0.4	
	3⁻	M2	(1.2 ± 0.1) × 10^{-3}	1.5 ± 0.2	(6 ± 2) × 10^{-3}[a])

[a]) Ref. [5]).
[b]) Ref. [6]).

ELEM. SYM.	A	Z
B	10	5

METHOD

REF. NO. 79An5 hg

REACTION	RESULT	EXCITATION ENERGY	SOURCE		DETECTOR		ANGLE
			TYPE	RANGE	TYPE	RANGE	
E,E/	FMF	1-9	D	67-194	MAG-D	61-192	DST
		(1.74-8.9)					

6 LEVELS 1.74-8.9 MEV

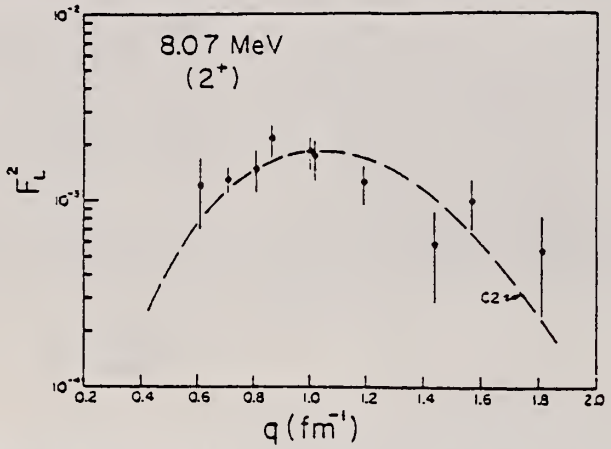

Fig. 4. Longitudinal form factor for the 8.07 MeV transition. The dashed line is the C2 Helm model fit using $R = 2.3$ fm as obtained from the analysis of the 6.03 MeV form factor.

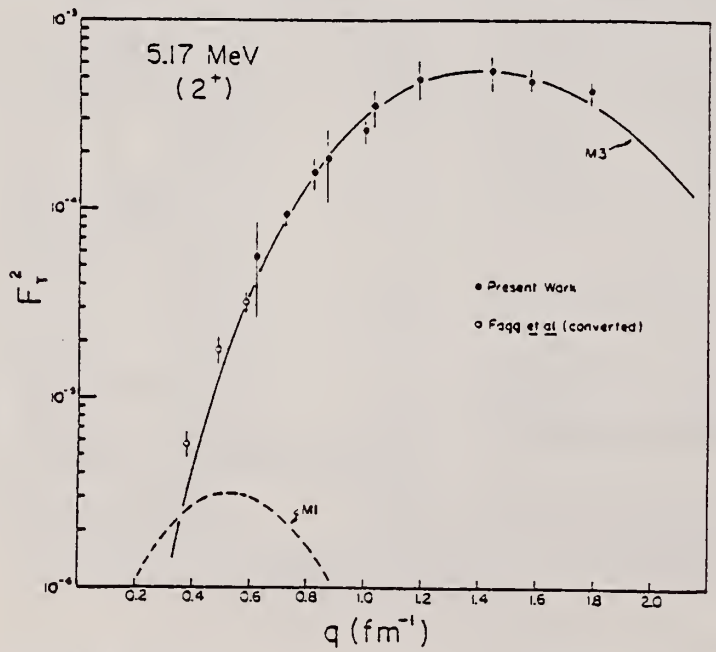

Fig. 6. Transverse form factor for the excitation at 5.16 ± 0.04 MeV. The 180° cross sections of Fagg *et al.* [5]) were converted to form factors and are also shown. The curves represent the M1-M3 Helm model fit to all the data using $R = 2.27$ fm.

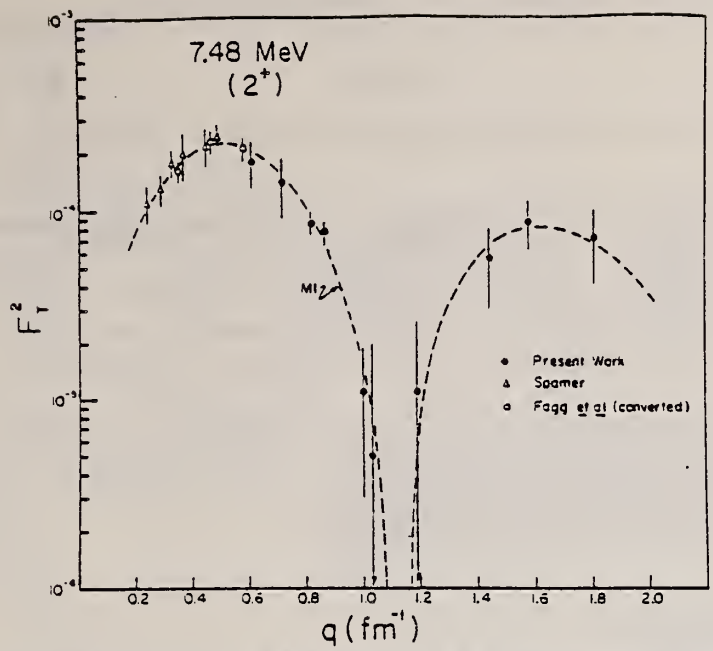

Fig. 9. Transverse form factor for the 7.48 MeV excitation from the present work plus that of Spamer [6]) and Fagg *et al.* [5]) (converted to form factors from 180° cross sections). The dashed curve represents the M1 Helm model fit with $R = 2.27$ fm.

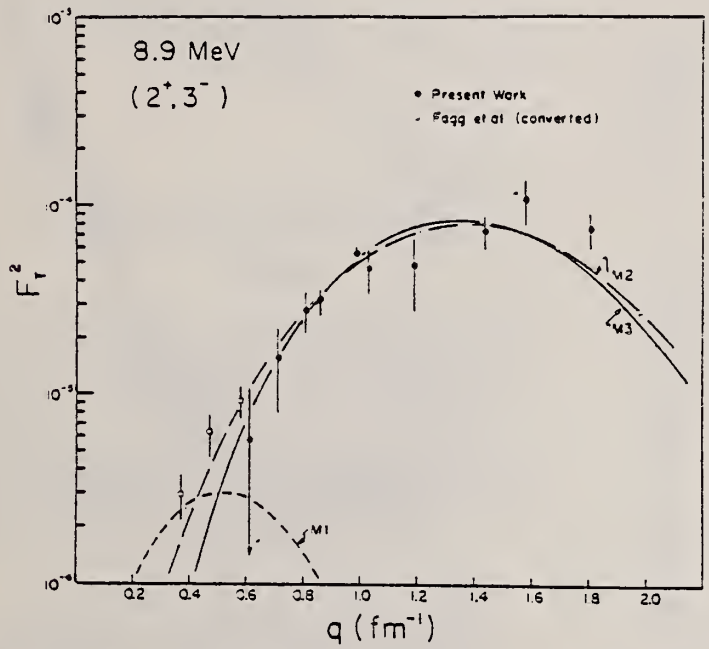

Fig. 10. Transverse form factor for the 8.9 MeV transition from this work and the 180° cross sections of Fagg *et al.* [5]) (converted to form factors). The dash-dotted line is the Helm model fit for an M2 transition ($J^\pi = 3^-$), while the solid and dashed lines are the M1-M3 admixture corresponding to $J^\pi = 2^+$. The radius parameter is $R = 2.27$ fm.

REF. P.E. Bosted, K.I. Blomqvist, A.M. Bernstein, S.A. Dytman, R.A. Miskimen
Phys. Rev. Lett. 45, 1544 (1980)

ELEM. SYM.	A	Z
B	10	5

METHOD

REF. NO. 80 Bo 2 hg

REACTION	RESULT	EXCITATION ENERGY	SOURCE		DETECTOR		ANGLE
			TYPE	RANGE	TYPE	RANGE	
G,PI+	ABX	150-360	C	220-360	CKV-I		DST

Differential cross sections for $^{10}B(\gamma,\pi^+)^{10}Be$ to the ground and first excited states of ^{10}Be separately and $^{16}O(\gamma,\pi^+)^{16}N$ to the sum of the four lowest-lying states in ^{16}N have been measured at laboratory angles of 45° and 90° for pions with kinetic energies from 30 and 210 MeV. The results, which are the first to discrete nuclear final states in the Δ(1236) region, are in qualitative agreement with several distorted-wave impulse-approximation calculations.

PACS numbers: 25.20.+y

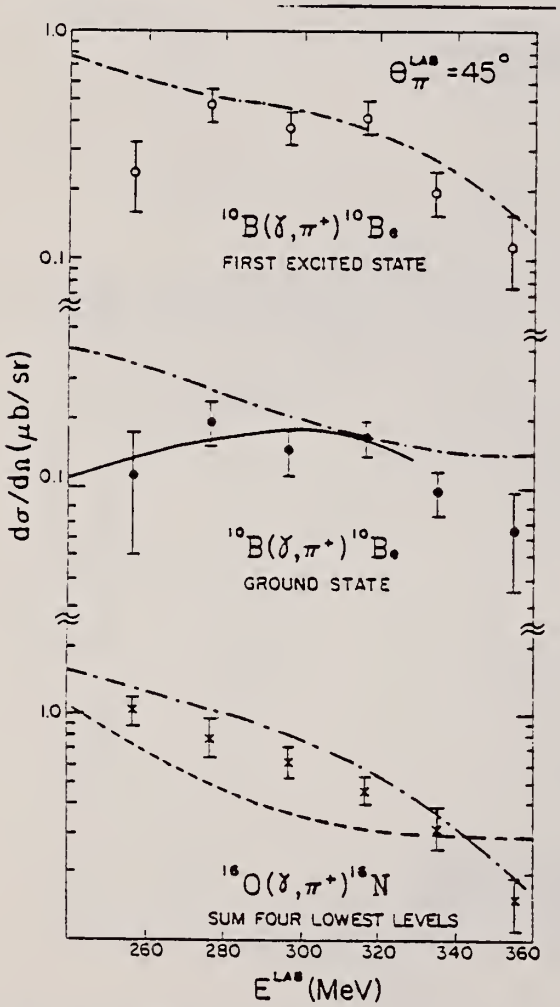

FIG. 3. Same as for Fig. 2, but at a pion laboratory angle of 45°.

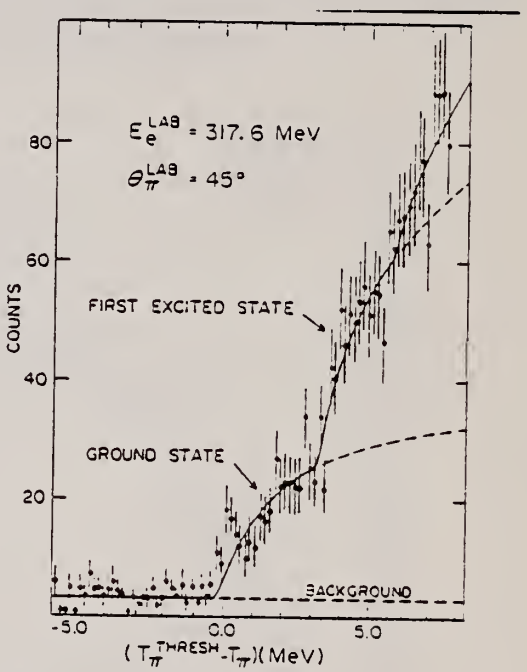

FIG. 1. Typical pion-energy spectrum for $^{10}B(\gamma,\pi^+)^{10}Be$ showing the contributions to the ground, first, and second excited states of ^{10}Be. Most of the background events shown come from pions that decay in flight into muons.

(OVER)

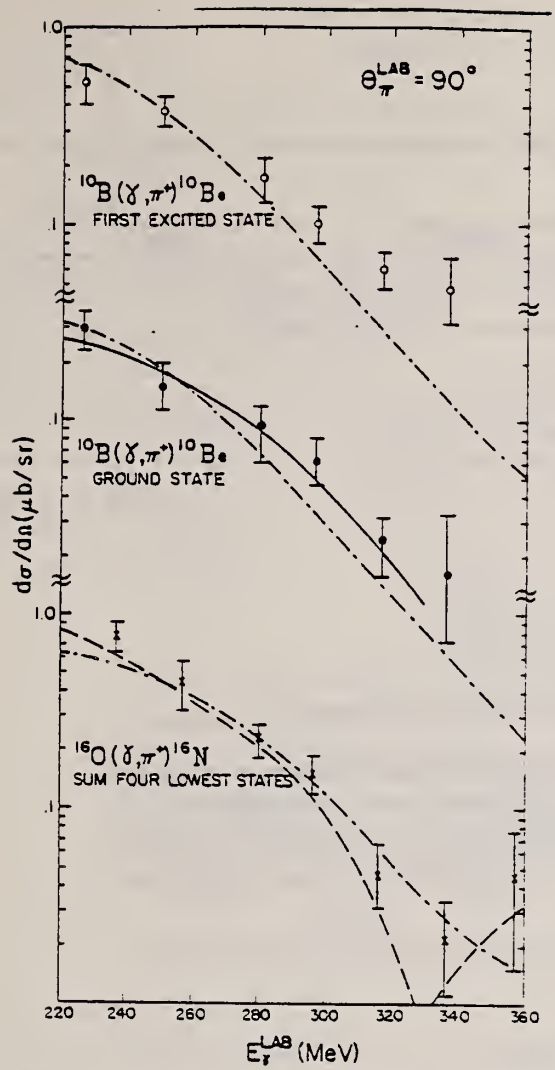

FIG. 2. Differential cross sections for $^{16}O(\gamma,\pi^+)^{13}Be$ at 90°. The solid circles represent the contributions from the ground state of ^{10}Be, the open circles are for the first excited state of ^{10}Be, and the crosses are for the sum of the four lowest-lying levels in ^{16}N. The solid line is the calculation of Singham and Tabakin (Ref. 8), the dashed line that of Devanathan *et al.* (Ref. 9), and the dot-dashed lines are from Nagl and Uberall (Ref. 10). Pion energies can approximately be found by subtracting 140 MeV from the photon energies.

REF. D. Rowley, J. LeRose, K. Min, B.O. Sapp, P. Stoler, E.J. Winhold, P.F. Yergin, A.M. Bernstein, K.I. Blomqvist, H.S. Caplan, S.A. Dytman, G. Franklin, M. Pauli
Phys. Rev. C25, 2652 (1982)

ELEM. SYM.	A	Z
B	10	5

METHOD

REF. NO. 82 Ro 1 — egf

REACTION	RESULT	EXCITATION ENERGY	SOURCE TYPE	SOURCE RANGE	DETECTOR TYPE	DETECTOR RANGE	ANGLE
G,PI+	ABX	17*42	C	150-200	MAG-D		90

Measurements were made of $d\sigma/d\Omega$ [θ_γ=90°(lab)] for $^{10}B(\gamma,\pi^+)^{10}Be$ (g.s.) at T_γ=17, 29, and 42 MeV, for $^{10}B(\gamma,\pi^+)^{10}Be$ (E_x=3.37 MeV) at T_γ=29 and 42 MeV, and for $^{10}B(\gamma,\pi^-)^{10}C$ (g.s.) at T_γ=29 MeV. The results disagree significantly with several recent distorted-wave impulse approximation calculations.

17*42 PION ENERGY

[NUCLEAR REACTIONS $^{10}B(\gamma,\pi^+)^{10}Be$ (E_x=0, 3.37 MeV), $^{10}B(\gamma,\pi^-)^{10}C(E_x=0)$, θ_γ=90° (lab), E_γ=17, 29, 42 MeV, measured $d\sigma/d\Omega$, compared with DWIA calculations.]

TABLE I. Experimental differential cross section results (in nb/sr) for $^{10}B(\gamma,\pi)$ at θ_γ=90° (lab). The uncertainties quoted for the present results are statistical only (see text).

	$\frac{d\sigma}{d\Omega}(\gamma,\pi^+)$ (g.s.)			$\frac{d\sigma}{d\Omega}(\gamma,\pi^+)(E_x=3.37$ MeV)		$\frac{d\sigma}{d\Omega}(\gamma,\pi^-)$(g.s.)
	T_γ=17 MeV	T_γ=29 MeV	T_γ=42 MeV	T_γ=29 MeV	T_γ=42 MeV	T_γ=29 MeV
Present Results	41±3	62±2	104±7	136±4	254±13	117±10
Yamazaki[a] ($T_\gamma\simeq$40 MeV)			117±27		256±65	

[a]Reference 20.

TABLE II. $^{10}B(\gamma,\pi)$ differential cross section ratios at θ_γ=90° (lab).

	$\frac{\frac{d\sigma}{d\Omega}(\gamma,\pi^+)(E_x=3.37\text{MeV})}{\frac{d\sigma}{d\Omega}(\gamma,\pi^+)\text{(g.s.)}}$		$\frac{\frac{d\sigma}{d\Omega}(\gamma,\pi^-)\text{(g.s.)}}{\frac{d\sigma}{d\Omega}(\gamma,\pi^+)\text{(g.s.)}}$
	T_γ=29 MeV	T_γ=42 MeV	T_γ=29 MeV
Experiment:			
Present results	2.19±0.11	2.44±0.21	1.39±0.18
Yamazaki[a] ($T_\gamma\simeq$40 MeV)		2.19±0.75	
Theory:			
Nagl-Überall code [b](NU)	2.44	2.38	1.80
Maleki[c] (M)	2.16	1.96	1.55
DeCarlo-Freed[d] (DF)	2.45	2.16	

[a]Reference 20.
[b]Reference 28.
[c]Reference 31.
[d]Reference 30.

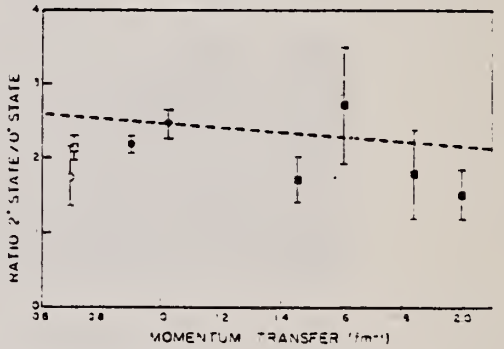

FIG. 8. Ratio of $^{10}B(\gamma,\pi^+)$ differential cross sections to the 2⁺ 3.37 MeV and 0⁺ states of ^{10}Be as a function of momentum transfer. The solid circles are the present results and the solid squares are the results of Bosted *et al.* (Ref. 34). Also shown is the form factor ratio for the analogs of these two states in ^{10}B obtained from (*e,e'*) (Ref. 18), and the ratio of $^{10}B(\gamma,\pi^-,\gamma)$ branching ratios for the two states (open circle: Ref. 33; open square: Ref. 32).

(OVER)

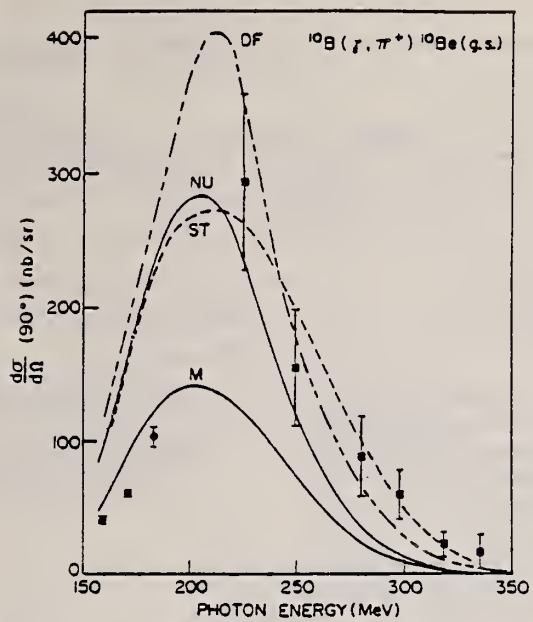

FIG. 9. Differential cross section at 90° for $^{10}B(\gamma,\pi^+)^{10}Be(g.s.)$ at photon energies up to 340 MeV. The solid circles are the present results and the solid squares are the higher energy results of Bosted *et al.* (Ref. 34). The curves are the results of four different theoretical calculations as described in the text.

REF. B.W. Zulkoskey, R.M. Sealock, H.S. Caplan, J.C. Bergstrom
Phys. Rev. C26, 1610 (1982)

ELEM. SYM.	A	Z
B	10	5

METHOD

REF. NO. 82 Zu 1 egf

REACTION	RESULT	EXCITATION ENERGY	SOURCE		DETECTOR		ANGLE
			TYPE	RANGE	TYPE	RANGE	
E,PI+	ABX	12*	D	159-165	TEL-D		DST

The electroproduction of 12.3±0.7 MeV positive pions from ^{10}B, leading to low-lying states in ^{10}Be, has been measured in the angular range $\theta_\pi = 30° - 140°$ for incident electron energies $E_e = 158.5 - 165.0$ MeV. The unique character of $M3$ transitions in the p shell permits a direct comparison of $d^2\sigma/dE_\pi d\Omega_\pi$ with the analog electron scattering form factors in ^{10}B, assuming the strong π-nucleus interaction can be neglected. For the two lowest $T=1$ states, the (e,π^+) angular distributions agree with the $M3$ form factors. The convective term in the $M1$ form factor for the third $T=1$ state is deduced from a comparison of the (e,π^+) and (e,e') data and is in good agreement with recent radiative pion capture results. The photoproduction cross section leading to the ^{10}Be ground state is estimated.

[NUCLEAR REACTIONS ^{10}B$(e,\pi^+)e'$ ^{10}Be; $E_e = 158.5 - 165.0$ MeV; $E_\pi = 12.3$ MeV; measured $\sigma(E_\pi,\theta_\pi)$; $\theta_\pi = 30° - 140°$; compare to electron scattering, radiative pion capture, and photoproduction.]

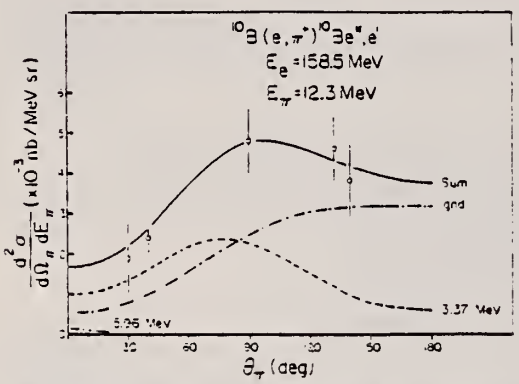

FIG. 2. Double differential cross sections for the (e,π^+) reaction leading to the ground plus first excited states of ^{10}Be, for an incident energy $E_e = 158.5$ MeV and detected pion energies of 12.3±0.7 MeV. The curves are predictions based directly on the experimental $M3$ form factors for the 1.74 MeV (0^+) and 5.17 MeV (2^+) states of ^{10}B as discussed in the text. The gradual decrease in the 3.37 MeV curve is due to the kinematic cutoff for excitation of this state which does not occur simultaneously in all detectors.

12*=12.3±.7 MEV PI+

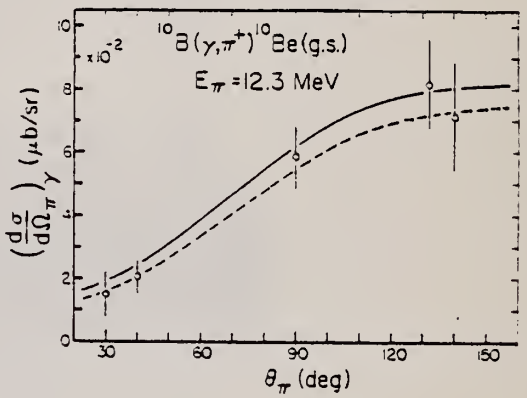

FIG. 6. Photopion angular distribution leading to the ^{10}Be ground state as deduced from the data in Fig. 2. The solid curve is based on the $M3$ form factor for the 1.74 MeV state of ^{10}B. For the dashed curve some allowance was made for Coulomb distortion of the (e,e') data by using the effective-q approximation.

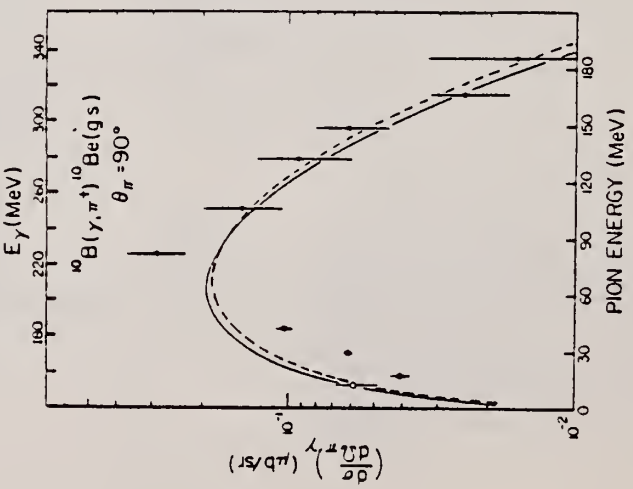

FIG. 7. The 90° photopion cross section leading to the ^{10}Be ground state, as a function of the pion kinetic energy. The open-circle point is from this work, the closed-circle points are from Rowley *et al.* (Ref. 11), and the triangle points are from Bosted *et al.* (Ref. 12). The curves are as in Fig. 6.

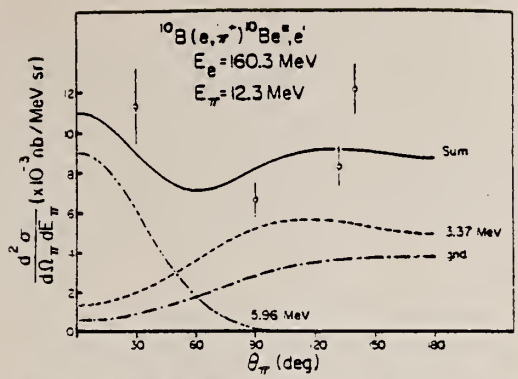

FIG. 3. Same as Fig. 2, but for $E_e = 160.3$ MeV. The threshold for population of the 5.96 MeV state has now been crossed causing an increase in the forward-angle cross section, consistent with the behavior expected for an $M1$ transition.

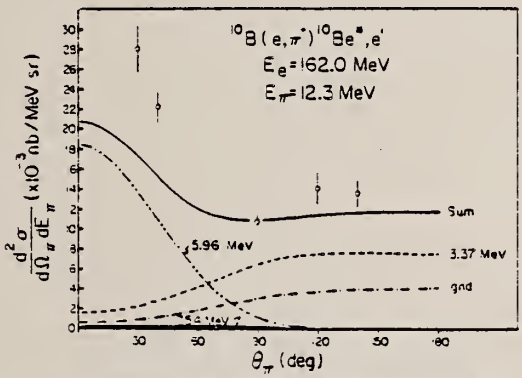

FIG. 4. Same as Fig. 2, but for $E_e = 162.0$ MeV. Excitation of the 7.54 MeV state is now possible. As in Fig. 3, the 5.96 MeV prediction is based directly on the 7.48 MeV $M1$ form factor in ^{10}B. The discrepancy with the forward-angle data is interpreted as a destructive interference between the spin and convection terms in the $M1$ form factor.

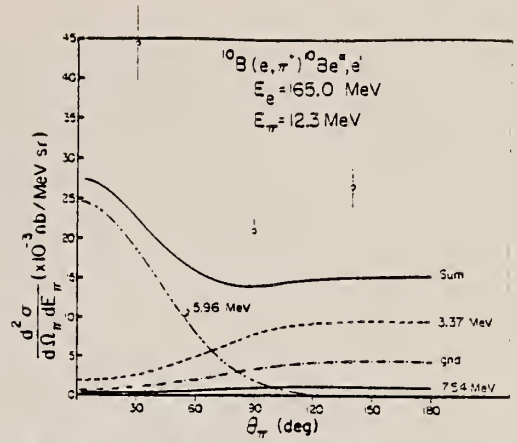

FIG. 5. Same as Fig. 2, but for $E_e = 165.0$ MeV. At this energy it is possible for ^{10}Be to be excited somewhat above 7.54 MeV.

B
A=11

B
A=11

B
A=11

Ref. F.R. Metzger, C.P. Swann, V.K. Rasmussen
Phys. Rev. 110, 906 (1958)

Elem. Sym.	A	Z
B	11	5

Method Van de Graaf; photon scattering, absorption; NaI spectrometer

Ref. No. 58 Me 1 NVB

Reaction	E or ΔE	E_o	Γ	$\int \sigma dE$	Jπ	Notes
$B^{11}(\gamma,\gamma)$	2.14	2.14				Mean life: $\tau = (4.7 \pm 0.6)\ 10^{-15}$ sec. Assumed spin = 1/2.

Ref. V.K. Rasmussen, F.R. Metzger, C.P. Swann
Phys. Rev. 110, 154 (1958)

Elem. Sym.	A	Z
B	11	5

Method: Van de Graaf; photon scattering, absorption; NaI spectrometer

Ref. No.: 58 Ra 1 — NVB

Reaction	E or ΔE	E_o	Γ	$\int \sigma dE$	Jπ	Notes
$B^{11}(\gamma,\gamma)$	4.46	4.46				Mean life: $\tau = (1.17 \pm 0.17)\ 10^{-15}$ sec. Assumed spin = 5/2.

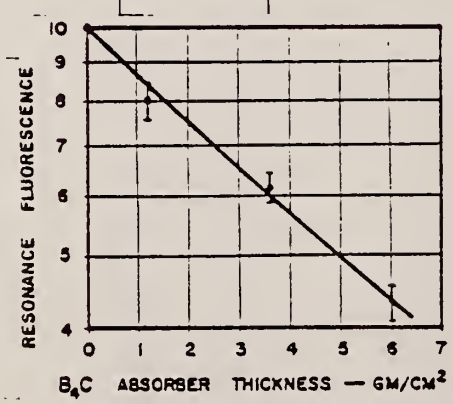

FIG. 6. Attenuation of the resonance radiation from the 4.46-Mev level of B^{11} by B_4C absorbers.

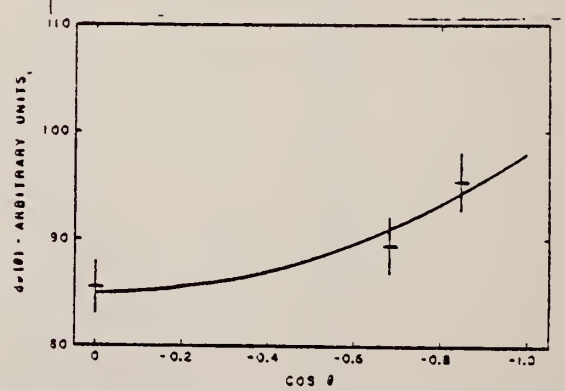

FIG. 5. Angular distribution of the resonance radiation from the 4.46-Mev level of B^{11}. The curve drawn is the distribution $89+8.7P_2(\cos\theta)$.

Ref. G.W. Tautfest
Phys. Rev. 110, 708 (1958)

Elem. Sym.	A	Z
B	11	5

Method Li^9 delayed neutrons; BF_3 counters; Purdue University synchrotron; ion chamber.

Ref. No. 58 Ta 1 EH

Reaction	E or ΔE	E_o	Γ	$\int \sigma dE$	Jπ	Notes
(γ,2p)	Bremss.			$\int_{}^{320}$ 2.0±0.3 MeV-mb		E_{th} = 31.3 MeV

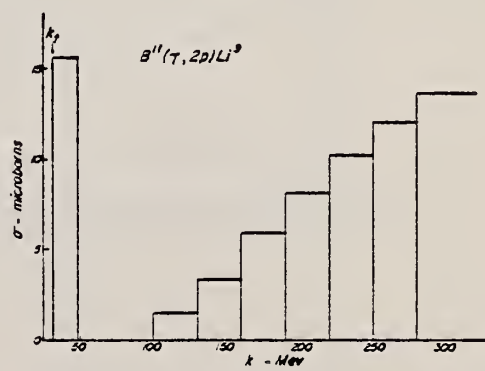

FIG. 8. Photon cross section for the reaction $B^{11}(\gamma,2p)Li^9$ obtained by the photon difference method from the yield points of Fig. 6. The photon cross section below 100 Mev was chosen arbitrarily.

Ref. E.C. Booth
Nuclear Phys. 19, 426 (1960)

Elem. Sym.	A	Z
B	11	5

Method: Van de Graaff; electron bremss.; Ring scatterer; NaI

Ref. No.: 60 Bo 3 — JHH

Reaction	E or ΔE	E_o	Γ	$\int \sigma dE$	Jπ	Notes
(γ,γ)	Bremss. 0.5-2.2	2.14			3/2	Mean lifetime t/g: $=(0.064)10^{-13}$ sec ± 50% [resonance scattering] where $g = (1+2I)/(1+2I_o)$.

REF.

H. H. Knitter and H. Wäffler
Proc. Ruth. Int. Conf. Man. 823 (1961)

EL EM. SYM.	A	Z
B	11	5

METHOD

REF. NO.	
61 Kn 1	JDM

REACTION	RESULT	EXCITATION ENERGY	SOURCE		DETECTOR		ANGLE
			TYPE	RANGE	TYPE	RANGE	
D,G	ABX	16-18	D	0-2	THR-I		4PI

σ_{res} = (6.5 ± 2.0) μb for 1.29 MeV deuteron energy.

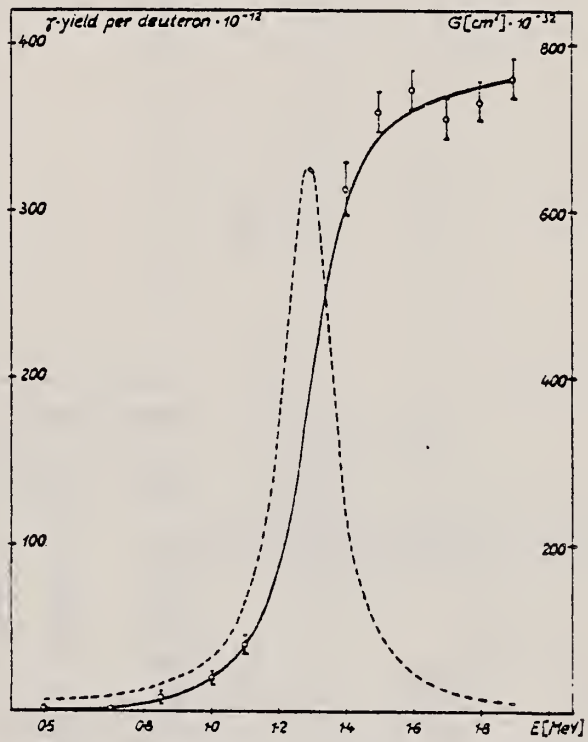

The figure shows the absolute thick-target yield of high-energy gamma-quanta from Be^9 (full line) as well as the cross-section deduced from it (dotted line)

Ref. E.C. Booth, K.A. Wright
Nuclear Phys. 35, 472 (1962)

Elem. Sym.	A	Z
B	11	5

Method 4 MeV electron Van de Graaff; bremss.; nuclear resonance scattering, ring scatterer; NaI

Ref. No. 62 Bo 6 — JHR

Reaction	E or ΔE	E_0	Γ	$\int \sigma d_e E$	Jπ	Notes
$B^{11}(\gamma,\gamma)$	Bremss. 0 - 4					$p = 0.53 \times 10^{-14}$ sec.

TABLE 2
Comparison of mean lifetime measurements

Nucleus	Energy	%	Spins	g	Γ_0/Γ	$W'(\theta)$	$\tau \times 10^{14}$ sec		
							This work	Other	
Li^6	3.56	7	$1^+ - 0$	$\frac{1}{2}$	(1)	1	0.012	0.0072	$^{+0.0015}_{-0.0013}$ [12]
								0.0105	± 0.001 [13]
B^{11}	2.14	81	$\frac{1}{2}^- - (\frac{1}{2})$	$\frac{1}{2}$	1	1	0.53	0.47	± 0.06 [14]
Al^{27}	2.21	100	$\frac{1}{2}^+ - \frac{1}{2}^-$	$\frac{1}{2}$	(1)	1	3.2	2.7	± 0.3 [15]
Al^{27}	1.01	100	$\frac{1}{2}^+ - \frac{3}{2}^+$	$\frac{2}{3}$	0.98	1	520	170	± 50 [15]
Si^{28}	1.78	92	$0^+ - 2^+$	5	1	0.63	88	73	± 22 [16]
S^{32}	2.24	95	$0^+ - 2^+$	5	1	0.63	26	≈ 16	[16]
Mg^{24}	1.37	78.6	$0^+ - 2^+$	5	1	0.63	220	155	± 40 [15]
Mg^{25}	1.61	25	$\frac{1}{2}^+ - \frac{3}{2}^+$	$\frac{1}{2}$	(1)	1	3.6	2.5	$^{+0.6}_{-0.4}$ [17]
Cu^{65}	0.963	69	$\frac{3}{2} - \frac{1}{2}$	$\frac{1}{2}$	1	0.92	230	72	± 18 [18]
								90	± 15 [19]
Cu^{65}	0.67	69	$\frac{1}{2} - \frac{1}{2}$	$\frac{1}{2}$	1	1	100	31	± 3 [18]

The factor g equals $(2I+1)(2I_0+1)^{-1}$.

10) R. C. Heim, Phys. Rev. 140 (1966) 1466
11) S. Vegors, L. Marsden and R. Heath, IDO-16370
12) Leone Cohen and Ralph Tobes, Nuclear Physics 14 (1960) 243
13) W. C. Barber, F. Berthold, G. Fraeis and F. E. Gedden, Phys. Rev. 120 (1960) 2123
14) F. R. Metzger, C. P. Swann and V. K. Rasmussen, Phys. Rev. 110 (1958) 906
15) F. R. Metzger, C. P. Swann and V. K. Rasmussen, Nuclear Physics 16 (1960) 568
16) S. Ofer and A. Schwarzschild, Phys. Rev. Lett. 3 (1959) 284
17) V. K. Rasmussen, F. R. Metzger and C. P. Swann, Phys. Rev. 123 (1961) 1366
18) J. B. Cummings, A. Schwarzschild, A. W. Sunyar and N. T. Porile, Phys. Rev. 120 (1960) 2128
19) T. Rothen, F. R. Metzger and C. P. Swann, Nuclear Physics 22 (1961) 506

Ref. V.P. Chizhov, A.P, Komar, L.A. Kulchitsky, A.V. Kulikov, E.D. Makhnovsky, Yu.M. Volkov
Nuclear Phys. 34, 562 (1962)

Elem. Sym.	A	Z
B	11	5

Method: 90 MeV Synchrotron; magnetic spectrometer; emulsions; NaI counter telescope

Ref. No.: 62 Ch 2 | JHH

Reaction	E or ΔE	E_0	Γ	$\int \sigma dE$	Jπ	Notes
	Bremss.					$E_{(p,d)}$ = 7.5 - 19.
(γ,d)	40					θ = 90°
(γ,p)						

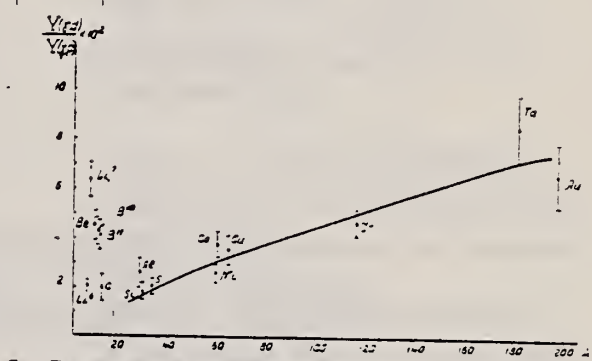

Fig. 4. The ratio of the yields of deuterons and protons with energies 13.5 to 30 MeV depending on the mass number of nuclei A for $E_{\gamma max}$ = 90 MeV. The solid line stands for the normalized dependence (3).

TABLE 1

Experimental data

Elements	$E_{\gamma max}$ (MeV)	Particle energy interval (MeV)	$\frac{Y(\gamma,d)}{Y(\gamma,p)}$	θ	
Li^6	30	7.5 to 15	0.003 ± 0.006		
	43		0.007 ± 0.005	90°	I
	90		0.007 ± 0.014		
Li^7	25		0.029 ± 0.030		
	43	7.5 to 15	0.056 ± 0.009	90°	I
	90		0.150 ± 0.054		
B^{11}	40	7.5 to 19	0.006 ± 0.002	90°	I
Al^{27}	35	2.0 to 10	0.009 ± 0.007	90° – 150°	II
Ca^{40}	35	3.7 to 10	0.038 ± 0.017	90° – 150°	II
$Cu^{63, 65}$	34	4.5 to 15	0.007 ± 0.003	90°	I
	34	7.5 to 15	0.007 ± 0.003	90°	I
	70	3 to 10	0.05 ± 0.01	90° – 150°	II
	70	4 to 10	0.04 ± 0.01	90° – 150°	II
	90	7 to 19	0.021 ± 0.005	90°	I

I: Scintillation telescope method.
II: Method of deflecting charged particles in magnetic field.

Ref. R.D. Edge, G.A. Peterson
Phys. Rev. 128, 2750 (1962)

Elem. Sym.	A	Z
B	11	5

Method: Linac; counter telescope

Ref. No.: 62 Ed 1 | BG

Reaction	E or ΔE	E_o	Γ_γ(eV)	$\int \sigma dE$(MeV-mb) Jπ	Notes
$B^{11}(e,e')$	41.5	2.1	0.17	0.72±0.15	Nuclear states excited by 180° electron scattering; M1 transitions assumed.
		4.4	1.1	0.34±0.14	
		4.9	3.7	0.59±0.24	Inelastic electron scattering cross sections obtained by comparing inelastic peaks to e-p eleastic scattering peak.
		7.3	1.0	0.12±0.06	
		9.1	0.10	0.0097±0.0012	Γ_γ from virtual photon theory.
		12.9		1.0±0.3	Limits not given for cross sections.
					E_o = 9.1 assumed to be M2

TABLE I. Parameters of nuclear states excited by 180° electron scattering, assuming transitions are M1.

Isotope	Excitation energy, k (MeV)	Spin and parity: Ground state I_0	Spin and parity: Excited state I_k	Inelastic cross section $d\sigma_k/d\Omega$ (10^{-28} cm²sr⁻¹)	$\int \sigma_k dk$ (MeV-mb)	Percentage experimental error	Ground-state radiation width, Γ_{γ_0}(eV): This experiment	Weisskopf units	Other experiments
B^{9}	2.4	3/2⁻	5/2⁻	1.3	0.12	15	0.12	0.30	0.13[a]
	14.7	3/2⁻	1/2⁻	0.042	0.3	50	56	67	
			3/2⁻				18		
			5/2⁻				12		
B^{10}	7.9	3⁺	2⁺	1.9	0.75	20	17	10	9.5[b]
			3⁺				12		
			4⁺				10		
	11.8	3⁺	2⁺	1.2	0.75	50	39	34	
			3⁺				28		
			4⁺				22		
	14.0	3⁺	2⁺	0.6	0.5	50	34	58	
			3⁺				24		
			4⁺				15		
B^{11}	2.1	3/2⁻	1/2⁻	0.72	0.72	30	0.17	0.21	0.15[c]
	4.4	3/2⁻	5/2⁻	1.5	0.54	60	1.1	1.6	0.602[d]
	4.9	3/2⁻	3/2⁻	2.4	0.59	60	3.7	2.5	
	7.3	3/2⁻	5/2⁻	0.4	0.12	50	1.0	1.1	
	9.1[e]	3/2⁻	7/2⁻	1.9	0.0097	20	0.10	4×10^{-3}	0.1[e]
	12.9	3/2⁻	1/2⁻	1.4	1.0	30	70	45	
			3/2⁻				36		
			5/2⁻				24		
C^{12}	15.1	0⁺	1⁺	1.82	1.95	10	39	73	40[f], 54.5[g], 39.2[h]
N^{14}	9.2	1⁺	0⁺	1.3	0.65	30	43	17	
			1⁺				14		
			2⁺				9		
	10.5	1⁺	0⁺	1.9	1.2	30	100	24	
			1⁺				34		
			2⁺				20		
O^{16}	No resonances detected below 16 MeV.								
S^{32}	11.6	0⁺	1⁺	3.5	2.8	40	33	33	47[i], 68[j]

[a] W. C. Barber, F. Berthold, G. Fricke, and F. E. Gudden, Phys. Rev. 128, 2081 (1960).
[b] G. Fricke (private communication).
[c] F. R. Metzger, C. P. Swann, and V. K. Rasmussen, Phys. Rev. 110, 906 (1958).
[d] This transition is assumed to be M1.
[e] L. Meyer-Schützmeister and S. S. Hanna, Bull. Am. Phys. Soc. 2, 168 (1958).
[f] E. Hayward and E. Fuller, Phys. Rev. 106, 991 (1957).
[g] G. L. Guthrie, Phys. Rev. 116, 1482 (1959).
[h] A. B. De Neroy, Thesis, University of Paris, Orsay Center, 1962 (unpublished).

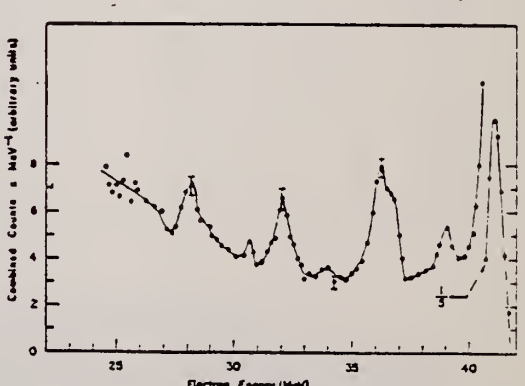

FIG. 3. Energy distribution of electrons, which were initially 41.5 MeV, after scattering through 180° from a B^{11} target.

Ref. F.F.Liu, F.J.Loeffler, T.R.Palfrey, Y.S.Kim

Phys.Rev. 128, 2764 (1962)

Elem. Sym.	A	Z
B	11	5

Method: Synch-defining counter telescope, proton counter telescope - C analyser

Ref. No.: 62Lil

BG

Reaction	E or ΔE	E_o	Γ	$\int \sigma dE$	Jπ	Notes
(γ,p)	$E_{\gamma max}$ = 335					Polarization of high energy photo-protons given in %. Mean proton production energy = 154 MeV θ_p = 45° +12.4±15 θ_p = 56° 7.5±15 Postulates identical γ absorption process for each kind of nucleus (quasi-deuteron). Fig.2: combined results of Li^7, Be^9, B^{11}, C^{12} at 3 angles of measurement. θ_{plab} = 90° only for Carbon data. Fig. 2 A: Only E1 transitions considered. C-M1 transitions from $^3S_1 - {}^1S_0$ also taken into account. Results are consistent both with a zero value for the polarization and also with theory.

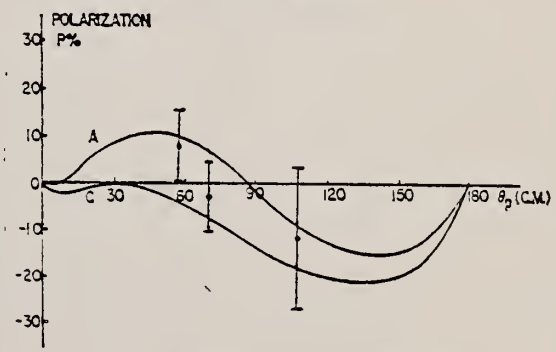

FIG. 2. Comparison of the experimental results with the predicted polarization.

REF.

M. Suffert, G. Costa and D. Magnac-Valette
Proc. Padua Conf. 842 (1962)

ELEM. SYM.	A	Z
B	11	5

METHOD

REF. NO.	
62 Su 2	JDM

REACTION	RESULT	EXCITATION ENERGY	SOURCE		DETECTOR		ANGLE
			TYPE	RANGE	TYPE	RANGE	
D,G	RLX	16-20	D	1-5	NAI-D		90

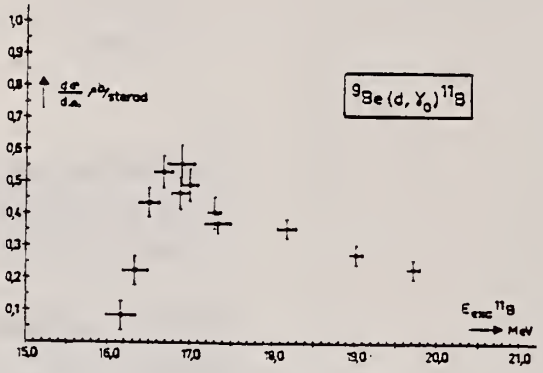

Fig. 1. The differential cross-section at 90° for the ground state γ-transition from the reaction $Be^9(d, \gamma_0)B^{11}$ versus excitation energy in B^{11}.

Circles and squares are measurements taken with two different Beryllium targets. The horizontal bars represent the energy loss of the deuterons in the target. The indicated errors on the differential cross-section are only statistical and do not include a possible systematic error on the absolute calibration.

Ref. Yu.M.Volkov, L.A.Kul'chitskii
Zhur.Eksptl. i Teoret.Fiz. 42, 108 (1962);
Soviet Phys.JETP 15, 77 (1962)

Elem. Sym.	A	Z
B	11	5

Method
— scintillation counter telescope

Ref. No. 62Vol BG

Reaction	E or ΔE	E_o	Γ	$\int \sigma dE$	Jπ	Notes
(γ,d) (γ,t) (γ,p)	$E_{\gamma max}$= 40					Particle energy interval is 7.5 - 19 MeV. $Y(\gamma,d)/Y(\gamma,p) = .006 \pm 0.002$ $Y(\gamma,t)/Y(\gamma,p) = .036 \pm 0.005$

Ref. B. M. K. Nefkens
Phys. Rev. Letters 10, 243 (1963)

Elem. Sym.	A	Z
B	11	5

Method: Synchrotron; β^- activity of He^8

Ref. No.: 63 Ne 2 JHH

Reaction	E or ΔE	E_o	Γ	$\int \sigma dE$	Jπ	Notes
$B^{11}(\gamma,3p)$	Bremss					σ = >6μb (ABY)
	320					1/2 life of He^8 = 30±20 m sec.

REF.

M. Suffert, G. Costa, D. Magnac-Valette
J. de Physique 24, 1029 (1963)

EL EM. SYM.	A	Z
B	11	5

METHOD

Van de Graaff; inverse; NaI spectrometer

REF. NO. 63 Su 2 NVB

REACTION	RESULT	EXCITATION ENERGY	SOURCE		DETECTOR		ANGLE
			TYPE	RANGE	TYPE	RANGE	
D,G	ABX	16 - 20	D	1 - 4	NAI - D		DST

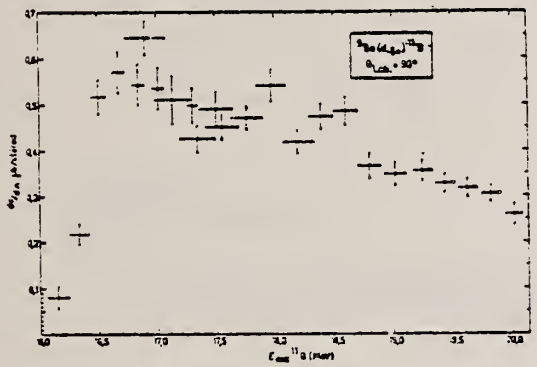

FIG. 4. — Section efficace différentielle à 90° de la réaction $^{9}Be(d, \gamma_0)^{11}B$, en fonction de l'énergie d'excitation dans le ^{11}B au centre de la cible. Les barres horizontales indiquent la dispersion d'énergie due à l'épaisseur de la cible. L'erreur indiquée pour la section efficace ne comprend pas une erreur possible sur le calibrage absolu de l'ensemble.

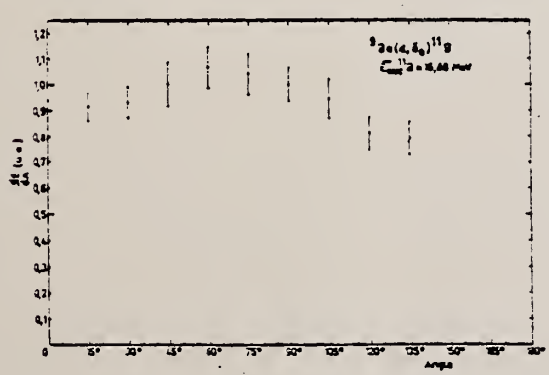

FIG. 5. — Distribution angulaire de la réaction $^{9}Be(d, \gamma_0)^{11}B$ à $\overline{E_{exc}} = 16{,}88$ MeV ($E_{d\ inc} = 1{,}43$ MeV).

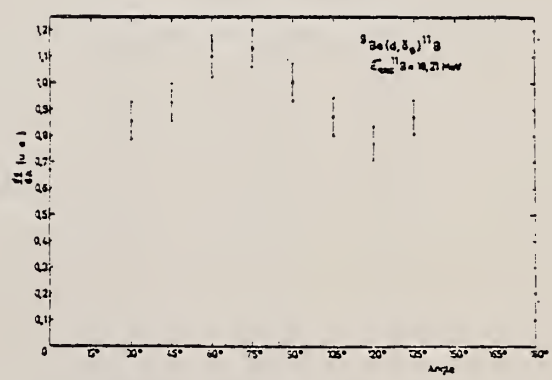

FIG. 6. — Distribution angulaire de la réaction $^{9}Be(d, \gamma_0)^{11}B$ à $\overline{E_{exc}} = 18{,}21$ MeV ($E_{d\ inc} = 3{,}00$ MeV).

Ref. V.J.Vanhuyse, G.J.Vanpraet

Nuclear Phys. 43, 344 (1963)

Elem. Sym.	A	Z
B	11	5

Method
linac - NaI(Tl)

Ref. No.
63Val

BG

Reaction	E or ΔE	E_o	Γ	$\int \sigma dE$	Jπ	Notes
$B^{11}(\gamma,\gamma)$	bremss. spectrum of 3 MeV electrons	2.14	.22±.06eV			

REF.

P. Brix, H. G. Clerc, R. Engfer, G. Fricke, F. Gudden, H. Liesem and E. Spamer
Proc. Paris Conf. 372 (1964)

ELEM. SYM.	A	Z
B	11	5

METHOD

REF. NO. 64 Br 2 JDM

REACTION	RESULT	EXCITATION ENERGY	SOURCE		DETECTOR		ANGLE
			TYPE	RANGE	TYPE	RANGE	
E,E/	SPC	0-10	D	54	SCI-D		141

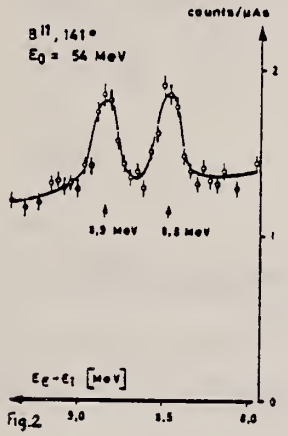

Fig.2

FIG. 2. — Electrons scattered inelastically from a boron target ($d_{eff} = 0.14$ g/cm² with 97 per cent B^{11}). $q_1 = 0.47$ fm^{-1}.

REF.

J. M. Loiseaux, M. Langevin and J. M. Maison
Proc. Paris Conf. 1048 (1964)

ELEM. SYM.	A	Z
B	11	5

METHOD

Betatron

REF. NO.	
64 Lo 3	JDM

REACTION	RESULT	EXCITATION ENERGY	SOURCE		DETECTOR		ANGLE
			TYPE	RANGE	TYPE	RANGE	
G,G	ABX	10-30	C	10-30	NAI-D		140

The effective differential scattering cross section remains quite constant from 20-30 MeV.

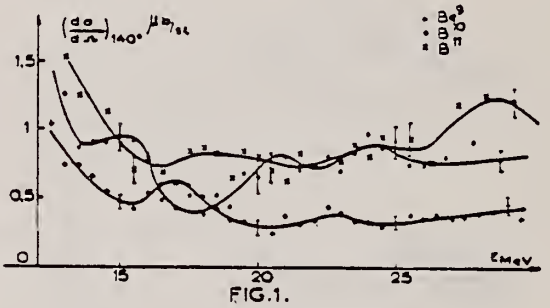

FIG.1.

REF.

M. Suffert, G. Costa and D. Magnac-Valette
Proc. Paris Conf. 1054 (1964)

ELEM. SYM.	A	Z
B	11	5

METHOD

REF. NO.: 64 Su 1 JDM

REACTION	RESULT	EXCITATION ENERGY	SOURCE		DETECTOR		ANGLE
			TYPE	RANGE	TYPE	RANGE	
D,G	ABX	18-23	D	0-5	NAI-D		DST

At Excitation Energy, E_{exc} = :

16.88 MeV : $W(\theta) = 1 + 0.18\ P_1 - 0.18\ P_2$
18.21 MeV : $W(\theta) = 1 + 0.05\ P_1 - 0.09\ P_2 - 0.27\ P_3$
19.83 MeV : $W(\theta) = 1 + 0.06\ P_1 - 0.33\ P_2 - 0.19\ P_3$

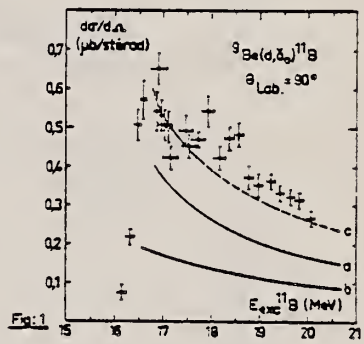

Fig:1

E. Hayward and T. Stovall
Nuclear Phys. 69, 241 (1965)

B	11	5

METHOD

REF. NO. 65 Ha 1 EGF

REACTION	RESULT	EXCITATION ENERGY	SOURCE		DETECTOR		ANGLE
			TYPE	RANGE	TYPE	RANGE	
G,XN	ABX	THR - 30	C	6-30	BF3-I		4PI

574

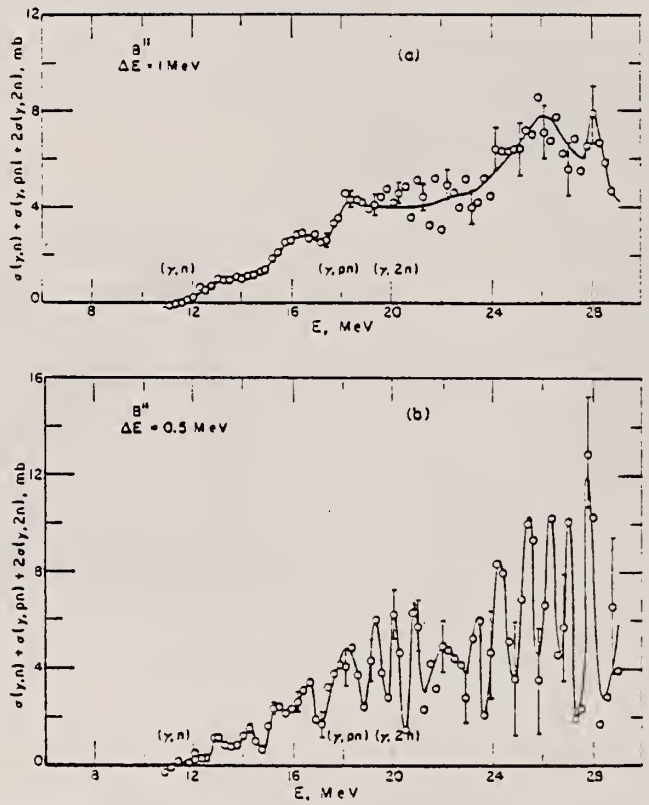

Fig. 6. The neutron production cross section for B^{11} where the analysis has been made using a 1 MeV grid (a) and a 0.5 MeV grid (b). Thresholds for the neutron producing cross sections are indicated by the dotted vertical lines at the bottom. The indicated errors are standard deviations based only on the number of counts.

TABLE 3

Neutron emission cross sections integrated to 29 MeV

Target	$\int \sigma dE$ (MeV · mb)	$\int \sigma dE/(60NZ/A)$	$\int^{30} \sigma dE/(60NZ/A)$ [a]
Li^6	36.1	0.40±0.03 [b]	0.42
Li^{7}	50.1	0.49±0.04	0.64
B^{10}	66.7	0.44±0.03	
B^{11}	68.6	0.42±0.03	0.47 [c]
O^{16}	61.9	0.26±0.02	0.30

[a]) Ref. [17]).
[b]) This value is for natural boron.
[c]) Estimated systematic errors.

REF.

E. F. Kennedy and W. C. Miller
Nuclear Phys. 63, 634 (1965)

ELEM.	A	Z
B	11	5

METHOD

Self-absorption

REF. NO.	
65 Ke 1	EGF

REACTION	RESULT	EXCITATION ENERGY	SOURCE		DETECTOR		ANGLE
			TYPE	RANGE	TYPE	RANGE	
G,G	LFT	2	C	4.5	NAI-D	0-2.5	135
		(2.13)					

$\Gamma = 4.8 \pm 0.7 \times 10^{-15}$ sec. for 2.13 MeV

0.137 eV ± 13.9% state in B^{11}.

REF. H. Artus, P. Brix, H. G. Clerc, F. Eigenbrod, A. Goldmann, F. Gudden, E. Spamer, P. Strehl, M. Stroetzel, O. Titze, and K. J. Wetzel
Proc. Gatlinburg Conference, 314 (1966)

ELEM. SYM.	A	Z
B	11	5

METHOD

REF. NO. 66 Ar 2 hmg

REACTION	RESULT	EXCITATION ENERGY	SOURCE TYPE	SOURCE RANGE	DETECTOR TYPE	DETECTOR RANGE	ANGLE
E,E/	LFT	4.5	D	30-60	MAG-D		DST
		(4.46,5.04)					

4=4.46, 5=5.04 MEV

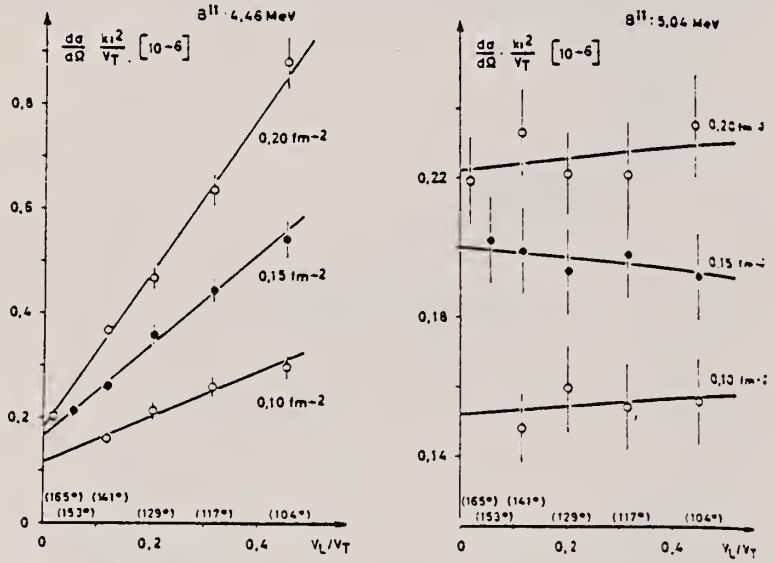

Fig. 2. Angular distributions at various constant inelastic momentum transfers q (indicated in the diagrams) for two transitions in ^{11}B. $d\sigma/d\Omega$ is the differential inelastic cross section, $k_i = E_x/\hbar c$, and V_L, V_T are functions of the scattering angle ϑ (see, e.g., Ref. 2 or 4). The slope of the straight lines gives the longitudinal part; the intersection with the ordinate scale the transverse part of the cross sections. The figure shows that the 4.46 MeV transition is mixed, whereas the 5.04 MeV transition is purely magnetic within experimental errors. The multipolarity, Γ_γ^0, and R_σ, are determined from the q dependence of the cross sections (see, e.g., Ref. 4).

[2] Barber, W.C., Ann. Rev. Nucl. Sci. 12, 1 (1962).
[4] Spamer, E., Z. Physik 191, 24 (1966).

TABLE 1

Summary of Experimental Results[a]

Nuclide	E_x (MeV)	Type	Γ_γ^0 (eV)	Γ_γ^0/Γ_w	R_σ (F)
^{6}Li	2.18	E2	(3.9 ± 0.5) × 10^{-3}	14.4	3.77 ± 0.48
	3.56	M1	8.9 ± 0.4	9.4	2.96 ± 0.11
^{7}Li	11.28 ± 0.05	(M1) or	(1.3 ± 0.4)/g[b]	0.043/g	—
		(M2)	(0.028 ± 0.008)/g	2.6/g	—
^{9}Be	15.97 ± 0.03	M1	(3.7 ± 0.8)/g	0.043/g	—
^{11}B	4.46	E2 and	0.0173 ± 0.0021	8.2	3.44 ± 0.50
		M1	0.64 ± 0.08	0.34	2.60 ± 0.35
	5.04	M1	1.34 ± 0.14	0.69	2.60 ± 0.11
^{12}C	4.43	E2	0.0122 ± 0.0008	5.30	3.14 ± 0.30
^{16}O	6.92	E2	0.100 ± 0.015	3.28	3.82 ± 0.46
	11.52	E2	0.52 ± 0.13	1.31	—
^{24}Mg	9.35 ± 0.04	M1	7.95 ± 1.2	0.38	3.50 ± 0.49
	9.97 ± 0.03				
	10.35 ± 0.03	E2	0.24 ± 0.05	0.58	5.05 ± 0.50
	10.70 ± 0.03	M1	22.2 ± 2.4	0.86	3.60 ± 0.36
	10.93 ± 0.04	E2	0.26 ± 0.11	0.50	—
^{28}Si	4.97 ± 0.02	C0	(2.0 ± 0.5) × 10^{-5}[c]	—	6.90 ± 1.20
^{40}Ca	6.89 ± 0.05	E2	0.29 ± 0.04	2.85	4.60 ± 0.50

[a] The Born approximation has been used except for ^{16}O and ^{40}Ca.
[b] $g = (2I_f + 1)/(2I_i + 1)$.
[c] Γ_0^2 equivalent to ME = (8.87 ± 1.00) F^2.

REF.

P. Kossanyi-Demay and G. J. Vanpraet
Nucl. Phys. 81, 529 (1966)

ELEM. SYM.	A	Z
B	11	5

METHOD

Stanford Mark II; Linac

REF. NO. 66 Ko 1 JDM

REACTION	RESULT	EXCITATION ENERGY	SOURCE		DETECTOR		ANGLE
			TYPE	RANGE	TYPE	RANGE	
E,E/	ABX	0 - 19	D	50,60	MAG-D	30-60	180

TABLE 2

Excited states observed in $^{11}B(J_0^\pi = \frac{3}{2}^-)$ by inelastic scattering at 180° of 50 MeV electrons

Exp. ±0.2 MeV	$d\sigma/d\Omega$ (nb · sr^{-1})	J^π	Transition	$\frac{F^2(qr)}{F^2(kr)}$	$\left(\frac{dN}{d\Omega}\right)\cdot 10^{+4}$	$\int \sigma_\gamma dk$ (MeV·μb)	Γ_γ^0 (eV)	Γ_w (eV)	Γ_γ^0/Γ_w	Percentage experimental error	References
2.13	3.95	$\frac{1}{2}^-$	M1	0.358	1.26	66.5	0.16	0.206	0.8	10	$\Gamma_{eV} = 0.16$ eV refs. [2, 20])
4.46	5.1	$\frac{1}{2}^-$	M1	0.388	1.31	175	0.60	1.86	0.32	30	$\Gamma_{eV} = 0.6$ eV refs. [2, 23])
5.03	9.6	$\frac{1}{2}^-$	M1	0.395	1.32	366	2.42	2.67	0.9	30	$\Gamma_{eV} = 0.11$ eV ref. [21])
6.8	1.25	$\frac{1}{2}^-$	M1	0.416	1.34	63	0.74	6.5	0.11		
			E2	0.655	2.09	40.4	0.48	0.036	13	20	
			M2	0.655	430	0.2	0.002	$1.42 \cdot 10^{-3}$	1.4		
			E1	0.416	0.007	12000	143	160	0.9		
7.9	1.5	$\frac{1}{2}^+$	M1	0.432	1.35	87.5	1.47	10.7	0.14		
			E2	0.66	2.07	57.7	0.96	0.098	9.75	30	
			M2	0.66	274	0.44	0.007	$3.56 \cdot 10^{-3}$	2.0		
			E1	0.432	0.01	11700	195	279	0.76		
8.92	5.6	$\frac{1}{2}^-$	M1	0.444	1.36	367	5.0	14.9	0.33	25	$\Gamma \geqq 0.18$ eV ref. [20]) $\Gamma = 0.6$ eV ref. [23]) $\Gamma = 4 \pm 0.6$ eV ref. [18])
9.5	2.9	$(\frac{3}{2})$	M1	0.452	1.36	204	4.85	18.5	0.26		
			E2	0.67	2.03	84.9	3.28	0.24	13.6	25	
			M2	0.67	180	0.96	0.037	$8.8 \cdot 10^{-3}$	4.2		
			E1	0.452	0.015	18000	435	485	0.9		

[Turn over for continuation]

TABLE 2

Excited states observed in $^{11}B(J_0^\pi = \frac{3}{2}^-)$ by inelastic scattering at 180° of 50 MeV electrons

Exp. ±0.2 MeV	$d\sigma/d\Omega$ (nb · sr^{-1})	J^π	Transition	$\frac{F^2(qr)}{F^2(kr)}\left(\frac{dN}{d\Omega}\right)\cdot 10^{+4}$	$\int \sigma_\gamma dk$ (MeV·μb)	Γ_γ^0 (eV)	Γ_w (eV)	Γ_γ^0/Γ_w	Percentage experimental error	References
10.6	1.7	($\frac{5}{2}$)	M1	0.464 1.37	131	5.83	25.0	0.154		
			E2	0.68 2.01	89.5	2.62	0.39	67	20	
			M2	0.68 143	1.26	0.037	$1.44 \cdot 10^{-3}$	2.6		
			E1	0.464 0.019	9340	274	650	0.42		
11.3	1.8	($\frac{5}{2}$)	M1	0.473 1.37	147	4.93	30.3	0.15		
			E2	0.69 1.99	101	3.40	0.538	6.3	25	
			M2	0.69 123	1.65	0.055	$1.98 \cdot 10^{-3}$	2.8		
			E1	0.473 0.022	9110	303.8	785	0.39		
12.2	3.1	($\frac{5}{2}$)	M1	0.480 1.37	269	10.0	360	0.28		
			E2	0.69 1.97	187	7.01	0.73	9.4	30	
			M2	0.69 107	3.46	0.129	$2.68 \cdot 10^{-3}$	4.8		
			E1	0.480 0.025	14500	545.2	940	0.58		
12.65	3.7	($\frac{5}{2}$)	M1	0.488 1.37	339	14.1	42.5	0.33		
			E2	0.70 1.96	23800	9.96	0.9	11	30	
			M2	0.70 93	5	0.21	$2.32 \cdot 10^{-3}$	9		
			E1	0.488 0.029	16100	676	1040	0.66		
13.2	2.7	($\frac{5}{2}$)	M1	0.496 1.37	259	11.9	48.8	0.24		
			E2	0.70 1.95	183	8.42	1.2	7	30	
			M2	0.70 83.4	4.28	0.196	$4.41 \cdot 10^{-3}$	4.5		
			E1	0.496 0.032	11100	509	1260	0.4		
14.55	3.5	($\frac{5}{2}$)	M1	0.51 1.37	369	20.4	64.7	0.31		
			E2	0.71 1.91	266	14.7	1.91	8.1	20	
			M2	0.71 66	7.72	0.42	$7.04 \cdot 10^{-3}$	6		
			E1	0.51 0.04	12700	704	1670	0.42		
15.55	4.5	($\frac{5}{2}$)	M1	0.522 1.376	510	32.2	78.9	0.52		
			E2	0.72 1.88	370	23.4	2.6	9.0	20	
			M2	0.72 55	12.5	0.795	$9.6 \cdot 10^{-3}$	8.2		
			E1	0.522 0.046	15000	950	2020	0.46		
16.9	8.5	($\frac{5}{2}$)	M1	0.54 1.37	1050	78.1	106	0.73		
			E2	0.73 1.84	780	57.9	3.8	15.3	25	
			M2	0.73 43	33.4	2.4	0.15	16		
			E1	0.54 0.058	24800	1880	2500	0.75		

REF.

P. Kossanyi-Demay and G. J. Vanpraet
Nucl. Phys. 81, 529 (1966)

ELEM. SYM.	A	Z
B	11	5

METHOD

Stanford Mark II; Linac

REF. NO. 66 Ko 1 JDM

REACTION	RESULT	EXCITATION ENERGY	SOURCE		DETECTOR		ANGLE
			TYPE	RANGE	TYPE	RANGE	
E,E/	ABX	0 - 19	D	50,60	MAG-D	30-60	180

TABLE 3

Magnetic transitions in ^{11}B and ^{10}B

(1)	(2)		(3)		(4)		(5)	(6)	(7)	(8)	(9)			
			$d\sigma/d\Omega$		$\Lambda_{M1}(q)$						$(2I_1+1)\Lambda_{M1}$		$(a/K = 4.5)$	
exp.	I_2	T_2	50 MeV	60 MeV	50 MeV	60 MeV	F_I^{*2}	$(2I_1+1)\Lambda_{M1}(0)$	F^{-2}	$(2I_1+1)\Lambda_{M1}$	Inglis (a/k)	(8.16) POT	(8.16) 2BME	(6.16) 2BME
^{11}B														
2.15	$\frac{1}{2}$	$\frac{1}{2}$	3.95±0.4	2 ±1	1.06	0.53	0.358	11.8±1.2	0.58 0.44	7.3 ±0.7 4.8 ±2.4	9.28	16.8	15.7	15.1
4.45	$\frac{1}{2}$	$\frac{1}{2}$	5.1 ±1.5	3.8±1.1	1.42	1.05	0.388	14.6±4.3	0.6 0.46	9.5 ±2.8 9.1 ±2.7	20.1	13.3	13.4	13.1
5.03	$\frac{1}{2}$	$\frac{1}{2}^*$	9.6 ±2.8	5.8±1.7	2.71	1.61	0.395	27.4±8.2	0.615 0.475	17.6 ±5.2 13.5 ±4	28.5	22.1	23.1	22.7
8.92	$\frac{1}{2}$	$\frac{1}{2}^{**}$	5.6 ±1.4	4.5±1.1	1.72	1.34	0.444	15.5±3.8	0.63 0.495	10.9 ±2.7 10.8 ±2.7	6.05	6.52	7.77	9.35
12.65	$\frac{1}{2}$	$\frac{1}{2}$	3.7	3.4	1.24	1.08	0.488	10.2±0.3	0.655 0.53	7.65±2.3 8.15±2.4	13.5	10.0	11.5	12.5
^{10}B														
3.59	2^+	0	1.9 ±0.4	0.7±0.35	0.47	0.17	0.377	8.9±1.8	0.59 0.45	5.7 ±1.1 2.6 ±1.3	0.31	0.13	0.04	0.000
5.16	2^+	1	2 ±0.4	1.7±0.3	0.5	0.42	0.396	8.8±1.7	0.615 0.475	5.7 ±1.1 6.1 ±1.1	4.46	8.32	5.93	1.09
7.5	2^+	1^*	16 ±4	11 ±2	4.8	3.15	0.426	77.0±19	0.62 0.505	58 ±13 44 ±9	81.7	103	103	102
8.9	3^+	1	6 ±1.5	4 ±1	1.81	1	0.445	28.4±5.6	0.63 0.51	20 ±5 14 ±3.5	44.6	33.9	33.6	29.6
10.7	2^+	1^{**}	5 ±1.25	6.5±1.5	1.76	1.9	0.452	24 ±5.75	0.635 0.51	17.7 ±4 26.0 ±4	19.5	6.46	10.6	16.3

REF.

P. Kossanyi-Demay and G. J. Vanpraet
Nucl. Phys. 81, 529 (1966)

ELEM. SYM.	A	Z
B	11	5

METHOD

Stanford Mark II; Linac

REF. NO. 66 Ko 1 JDM

REACTION	RESULT	EXCITATION ENERGY	SOURCE		DETECTOR		ANGLE
			TYPE	RANGE	TYPE	RANGE	

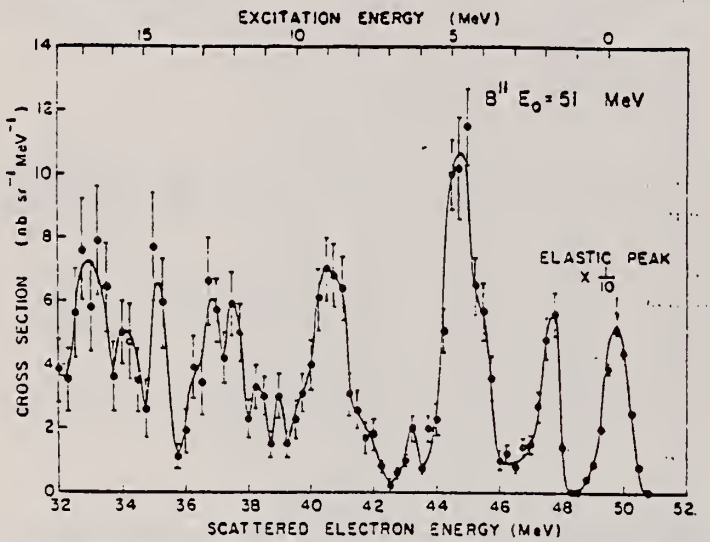

Fig. 3. Spectrum of 51 MeV electrons scattered from a ^{11}B target at 180°.

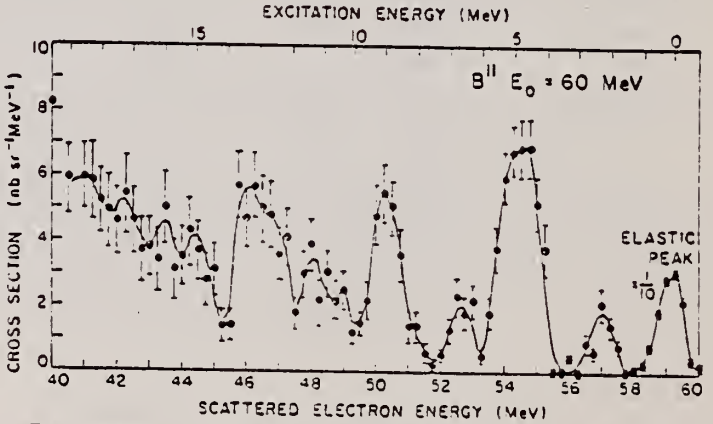

Fig. 4. Spectrum of 60 MeV electrons scattered from a ^{11}B target at 180°.

REF.

B. M. K. Nefkens, D. C. Sutton, and M. N. Thompson
Nucl. Phys. 88, 523 (1966)

ELEM. SYM.	A	Z
B	11	5

METHOD

Natural and enriched ^{10}B target

REF. NO. 66 Ne 1 egf

REACTION	RESULT	EXCITATION ENERGY	SOURCE		DETECTOR		ANGLE
			TYPE	RANGE	TYPE	RANGE	
G, 3P	ABY	45-250	C	250	ACT-I		4PI

TABLE I
Cross section per effective quantum

Reaction	J^{π}_{init}	J^{π}_{final}	Q (MeV)	Cross section (μb) per effective quantum
$^{12}C(\gamma, {}^{8}Li)$	0^+	$\frac{1}{2}^-$	—47	1.2
$^{11}B(\gamma, {}^{3}He)$	$\frac{1}{2}^-$	0^+	—45	0.09

REF.

R. Riskalla and D. Vinciguerra
J. Physique, Colloq. 1, 106 (1966)

ELEM. SYM.	A	Z
B	11	5

METHOD

REF. NO.	
66 Ri 1	JDM

REACTION	RESULT	EXCITATION ENERGY	SOURCE		DETECTOR		ANGLE
			TYPE	RANGE	TYPE	RANGE	
E,E/	FMF	2,4	D		MAG-D		DST

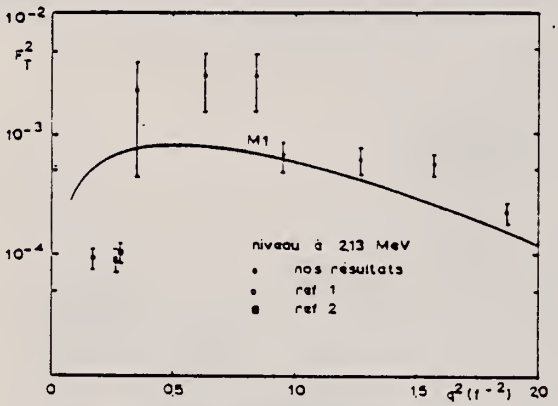

FIG. 1. — Facteur de forme transverse pour le niveau à 2,13 MeV du ^{11}B. La courbe théorique a été calculée pour une transition $M1$ entre deux états de proton $p\,\frac{3}{2}$ et $p\,\frac{1}{2}$.

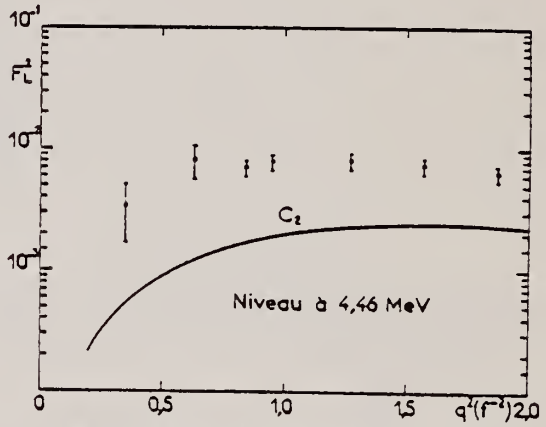

FIG. 2. — Facteur de forme longitudinal pour le niveau à 4,46 MeV du ^{11}B. La courbe theorique a ete calculée pour une transition $C2$ entre deux états de proton $p\,\frac{3}{2}$ et $p\,\frac{1}{2}$.

REF.

E. Spamer
Z. Physik, 191, 24 (1966)

ELEM. SYM.	A	Z
B	11	5

METHOD

60 MeV Linac; MAG.

[Page 1 of 2]

REF. NO. 66 Sp 1 JDM

REACTION	RESULT	EXCITATION ENERGY	SOURCE TYPE	SOURCE RANGE	DETECTOR TYPE	DETECTOR RANGE	ANGLE
E,E/	ABX	2 - 9	D	32 - 57	MAG-D		DST

Tabelle 2. *Meßergebnisse für die untersuchten Kernniveaus*

Die in der vorliegenden Arbeit bestimmten Anregungsenergien stehen in der Spalte 2. Zum Vergleich sind in Klammern die Werte nach LANDOLT-BÖRNSTEIN (Neue Serie 1961) angegeben. Mit den in Spalte 3 gegebenen Spins wurden die Strahlungsbreiten Γ_γ^0 berechnet. Γ_w in Spalte 8 sind die von WILKINSON — in F. AJZENBERG-SELOVE: Nuclear Spectroscopy, Part B. New York and London: Academic Press 1960 — benutzten Weisskopfeinheiten (mit $R = 1{,}2$ fm).

1. Isotop	2. Anregungsenergie (MeV)	3. I_f	4. Übergang	5. $B(\lambda, k, I_i \to I_f)$ (a)	6. R_{tr} (fm)	7. Γ_γ^0 (eV)	8. Γ_γ^0/Γ_w	9. Andere Autoren Γ_γ in eV
B^{10}	$6{,}014 \pm 0{,}020$ $(6{,}04 \pm 0{,}02)$	4^-	$C2$	$2{,}44 \pm 0{,}25$ $2{,}34 \pm 0{,}25$ [c]	$3{,}70 \pm 0{,}30$ $3{,}40 \pm 0{,}30$ [c]	$0{,}122 \pm 0{,}020$ [b] $0{,}116 \pm 0{,}020$ [c]	14	0,120 [2]
($I_i = 3^+$)	$7{,}477 \pm 0{,}020$ [d] (7,47)	2^+	$M1$	$1{,}97 \pm 0{,}26$	$2{,}70 \pm 0{,}20$	$12{,}0 \pm 2{,}2$	1,4	17 [e]
B^{11}	$2{,}120 \pm 0{,}030$ $(2{,}138 \pm 0{,}006)$	$\frac{1}{2}^-$	$M1$		$2{,}60 \pm 0{,}20$			s. Text
($I_i = \frac{1}{2}^-$)	$8{,}561 \pm 0{,}020$ $(8{,}568 \pm 0{,}007)$	$\frac{1}{2}^-$	$M1$ $C2$	$1{,}08 \pm 0{,}16$	$3{,}90 \pm 0{,}50$	$0{,}72 \pm 0{,}30$ $0{,}40 \pm 0{,}10$	0,055 7,3	
	$8{,}926 \pm 0{,}020$ $(8{,}923 \pm 0{,}004)$	$\frac{5}{2}^-$	$M1$ $C2$	$0{,}81 \pm 0{,}08$	$2{,}65 \pm 0{,}21$	$4{,}0 \pm 0{,}6$ [f] $\left(16^{+8}_{-16}\right) 10^{-3}$	0,27 0,24	0,06 [27]; 7,9 [g]

a) Einheit 10^{-51} cm^4 bei $C2$, 10^{-28} cm^2 bei $M1$. — b) Mit $\Gamma_\gamma^0(E2)/\Gamma_\gamma^0(M1) = 9$ nach [28] ergibt sich $\Gamma_\gamma^0(M1) = 0{,}014$ eV. — c) Daten Darmstadt und Orsay (s. Fig. 8). — d) $\Gamma_{tot} \approx 40$ keV. — e) Daten von [1] mit $\varepsilon = 7{,}48$ MeV anstatt $\varepsilon = 7{,}9$ MeV ergibt $\Gamma_\gamma^0 = 14$ eV. — f) Mit Daten von [27] folgt $\Gamma_\alpha \approx 0{,}03$ eV. — g) Daten von [1] mit $\varepsilon = 8{,}93$ MeV wie $M1$ ausgewertet.

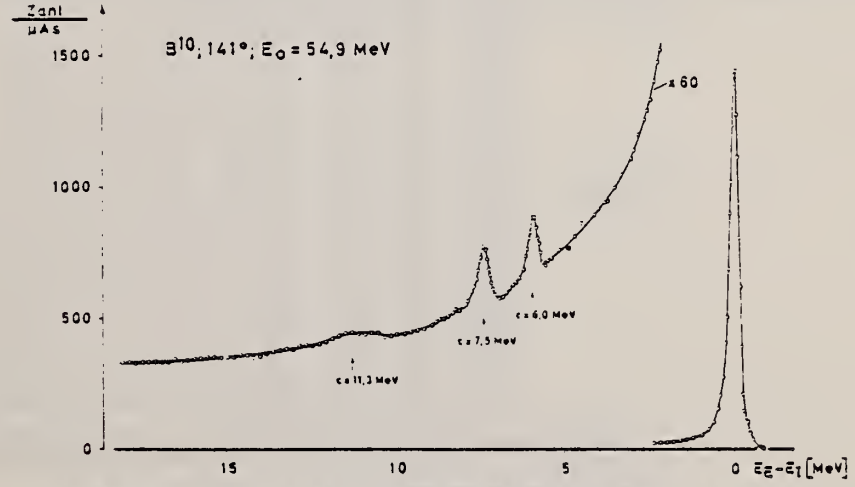

Fig. 2. Energieverteilung der von einem B^{10}-Target gestreuten Elektronen. Die Meßpunkte für $E_\varepsilon - E_f > 6$ MeV und $E_\varepsilon - E_f < 2$ MeV sind Mittelwerte aus mehreren Meßwerten. $(\Delta E/E)_A = 0{,}5\%$; $(\Delta E/E)_S = 0{,}2\%$

REACTION	RESULT	EXCITATION ENERGY	SOURCE		DETECTOR		ANGLE
			TYPE	RANGE	TYPE	RANGE	

Tabelle 1. *Experimentelle Parameter und Meßwerte*

	Θ (°)	E_0 (MeV)	q^2 (fm^{-2})	$A_{1/h}A_E$ (10^{-3}) (± Fehler in %)	$(d\sigma/d\Omega)\,R^*$ (10^{-31} cm^2/sr)	$B(\lambda, q)$ (a)	$B(\lambda, q)$ (a) (b)
B^{10}	104,98	31,85	0.054	0,149 ± 18	1,58 ± 0.29	2,09 ± 0,38	
6,01 MeV	104,98	36,01	0.071	0,269 ± 15	2,16 ± 0,32	2,13 ± 0,32	
$C2$	129,02	34,98	0.086	0,423 ± 12	1,04 ± 0,13	2,19 ± 0,26	
	104,98	44,10	0.109	0,529 ± 15	2,92 ± 0,44	1,81 ± 0,27	
	129,02	44,10	0,141	1,070 ± 12	1,48 ± 0,18	1,82 ± 0,22	
	92,91	54,54	0,143	1,190 ± 10	6,60 ± 0,66	1,95 ± 0,20	
	117,04	57,80	0,223	2,234 ± 12	3,14 ± 0,38	1,43 ± 0,17	
	141,11	54,38	0,244	3,560 ± 10	1,30 ± 0,13	1,64 ± 0,17	
	141,11	53,07	0,227	2,900 ± 12	1,17 ± 0,14	1,61 ± 0,18	
B^{10}	129,02	29,20	0.057	0,676 ± 20	2,39 ± 0,48	1,65 ± 0,37	1,89
7,477 MeV	129,02	34,98	0,081	0,871 ± 18	2,14 ± 0,39	1,38 ± 0,27	1,74
$M1$	129,02	39,83	0,109	1,225 ± 15	2,23 ± 0,34	1,44 ± 0,24	1,65
	129,02	44,10	0,136	1,591 ± 15	2,20 ± 0,33	1,41 ± 0,23	1,58
	153,15	41,78	0,139	5,870 ± 17	2,10 ± 0,36	1,63 ± 0,29	1,97
	92,91	54,54	0,140	0,518 ± 20	3,23 ± 0,65	1,17 ± 0,29	2,00
	165,05	50,26	0,216	21,200 ± 10	1,25 ± 0,13	0,98 ± 0,10	1,14
	117,04	57,80	0,217	1,290 ± 12	1,64 ± 0,20	0,92 ± 0,12	1,10
	129,02	55,28	0,220	2,060 ± 12	1,53 ± 0,18	0,98 ± 0,12	1,16
	153,15	51,73	0,221	7,280 ± 15	1,35 ± 0,20	1,01 ± 0,15	1,27
	141,11	53,07	0,220	3,484 ± 10	1,41 ± 0,14	0,99 ± 0,10	1,24
	141,11	54,88	0,237	3,720 ± 12	1,36 ± 0,16	0,95 ± 0,12	1,28
B^{11}	141,11	53,90	0,242	1,210 ± 20	0,49 ± 0,10	0,34 ± 0,07	
2,12 MeV	129,02	54,15	0,282	0,810 ± 20	0,63 ± 0,13	0,33 ± 0,07	
$M1$							
B^{11}	129,02	32,55	0,067	0,130 ± 50	0,37 ± 0,18	0,60 ± 0,55	
3,56 MeV	117,04	40,55	0,099	0,280 ± 20	0,92 ± 0,19	0,86 ± 0,22	
$C2+M1$	129,02	42,59	0,123	0,450 ± 14	0,68 ± 0,10	0,81 ± 0,16	
	141,11	45,05	0,151	0,830 ± 20	0,53 ± 0,11	0,87 ± 0,24	
	141,11	51,56	0,203	1,340 ± 12	0,59 ± 0,07	0,75 ± 0,12	
	165,05	49,26	0,203	2,790 ± 30	0,18 ± 0,06	0,65 ± 0,65	
	117,04	57,08	0,206	1,040 ± 10	1,37 ± 0,14	0,65 ± 0,08	
	129,02	54,15	0,207	1,230 ± 10	0,97 ± 0,10	0,72 ± 0,09	
	153,15	52,23	0,221	1,940 ± 19	0,35 ± 0,07	0,76 ± 0,23	
	141,11	53,90	0,223	1,230 ± 18	0,47 ± 0,09	0,52 ± 0,15	
	153,15	56,93	0,267	2,240 ± 20	0,31 ± 0,07	0,53 ± 0,16	
B^{11}	129,02	32,55	0,066	0,268 ± 24	0,78 ± 0,19	0,62 ± 0,15	0,63
8,93 MeV	117,04	40,55	0,098	0,283 ± 20	0,92 ± 0,18	0,63 ± 0,14	0,66
$M1$	129,02	42,59	0,122	0,529 ± 14	0,81 ± 0,11	0,59 ± 0,09	0,61
	141,11	45,05	0,149	1,125 ± 14	0,72 ± 0,16	0,56 ± 0,08	0,57
	141,11	51,56	0,201	1,339 ± 12	0,59 ± 0,07	0,44 ± 0,06	0,45
	165,05	49,26	0,202	3,792 ± 12	0,55 ± 0,07	0,45 ± 0,06	0,45
	117,04	57,08	0,206	0,503 ± 15	0,66 ± 0,10	0,41 ± 0,07	0,45
	129,02	54,15	0,206	0,834 ± 10	0,66 ± 0,07	0,44 ± 0,09	0,47
	153,15	52,23	0,220	3,460 ± 18	0,62 ± 0,11	0,48 ± 0,09	0,48
	141,11	53,90	0,221	1,132 ± 20	0,44 ± 0,09	0,31 ± 0,07	0,33
	153,15	56,93	0,265	3,942 ± 15	0,54 ± 0,08	0,41 ± 0,08	0,42

a) Einheit 10^{-28} cm^2 für $M1$; 10^{-51} cm^4 für $C2$. — b) Andere Auswertung: totale Fläche statt Anpassung für 7,477 MeV, ohne Korrektur des longitudinalen Anteils für 8,93 MeV.

* R ist der Rückstoßfaktor [s. Text zu Gl. (1a); (1b)].

REF.

M. Suffert
Nucl. Phys. 75, 226 (1966)

EL EM. SYM.	A	Z
B	11	5

METHOD

6 MeV Van de Graaff

[Page 1 of 2]

REF. NO.

66 Su 1 JDM

REACTION	RESULT	EXCITATION ENERGY	SOURCE		DETECTOR		ANGLE
			TYPE	RANGE	TYPE	RANGE	
D,G	ABX	16 - 21	D	1 - 6	NAI-D	0 - 25	DST

3 G+

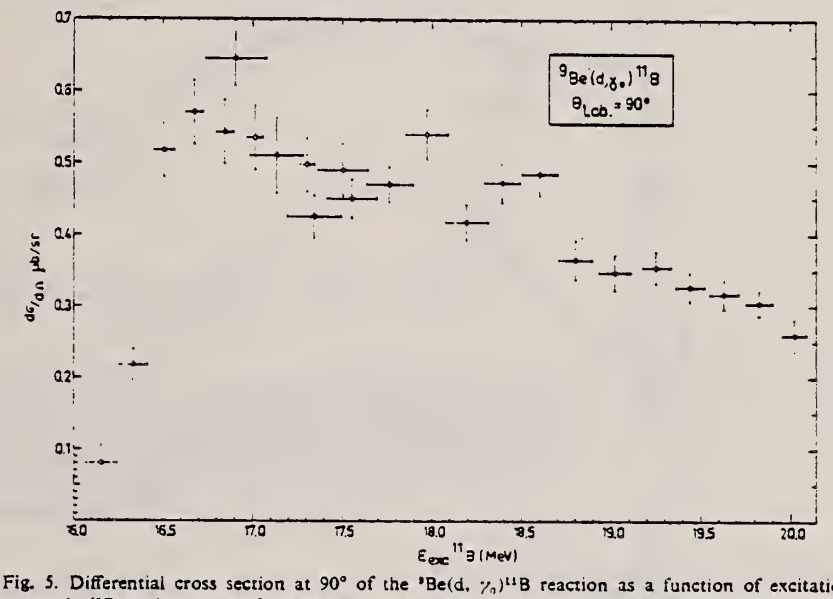

Fig. 5. Differential cross section at 90° of the $^{9}Be(d, \gamma_0)^{11}B$ reaction as a function of excitation energy in ^{11}B at the centre of the target. The horizontal bars show the energy spread due to the target thickness. The indicated errors for the cross section do not contain a possible error of the absolute calibration (estimated maximum value ±40 %).

REF.

M. Suffert
Nucl. Phys. 75, 226 (1966)

ELEM. SYM.	A	Z
B	11	5

METHOD

REF. NO. 66 Su 1

JDM

REACTION	RESULT	EXCITATION ENERGY	SOURCE		DETECTOR		ANGLE
			TYPE	RANGE	TYPE	RANGE	

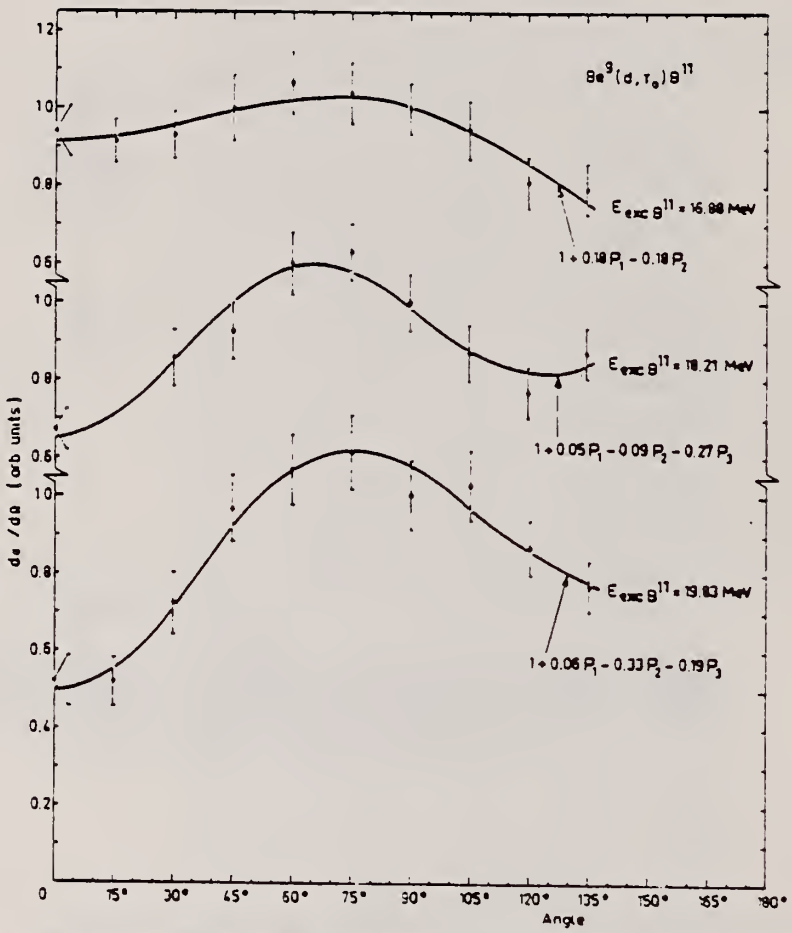

Fig. 6. Angular distributions of the ^{9}Be(d, γ_0)^{11}B reaction. The curves are the Legendre polynomial fits.

B. Ziegler, W. Buss and H. Wäffler
Nuclear Phys. 83, 145 (1966)

B	11	5

METHOD

1.5 MeV Cascade Accelerator

REF. NO. 66 Zi 1 JDM

REACTION	RESULT	EXCITATION ENERGY	SOURCE		DETECTOR		ANGLE
			TYPE	RANGE	TYPE	RANGE	
D,G	ABX	16-18	D	1-2	NAI-D		DST

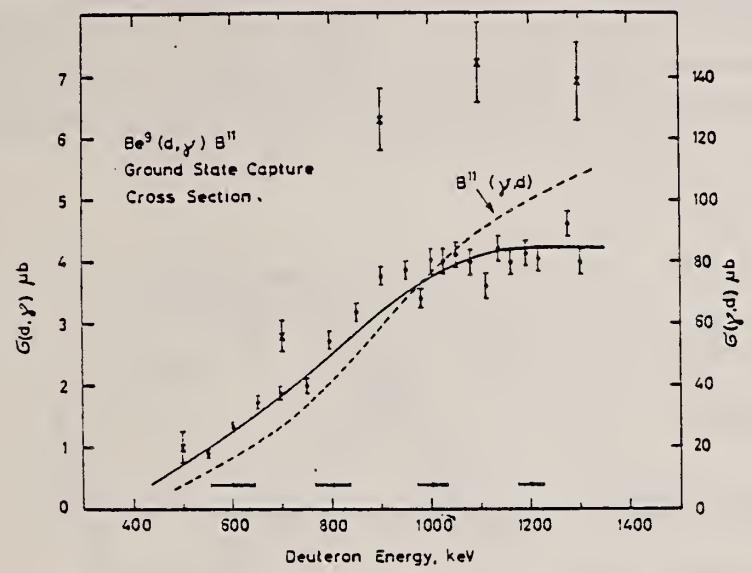

Fig. 5. The ground state transition cross section (scale on the left). The smooth curve is the result of all thick target runs (polynomial in fig. 4); the points result from the measurements with the thin target, the horizontal error bars marking the spread in energy due to target thickness. The results of Suffert *et al.* [4]) are marked by the crosses. The dashed curve (scale on the right) gives the $^{11}B(\gamma, d)$ cross section, calculated by detailed balance (sect. 4) from the experimental values.

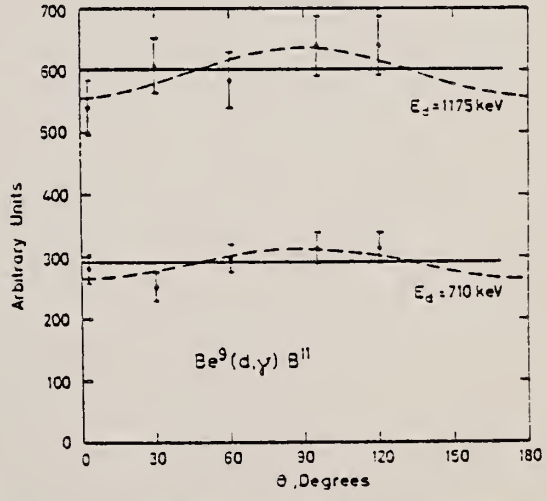

Fig. 6. Angular distributions of the ground state transition for two deuteron energies, thin target. The dashed curves are best fits to the distribution

$$d\sigma/d\Omega(\theta) = a \sin^2\theta + b\tfrac{1}{2}(1 + \cos^2\theta),$$

with

$$b/a = 1.5 \pm 0.5 \quad (E_d = 710 \text{ keV}),$$
$$b/a = 1.6 \pm 0.5 \quad (E_d = 1175 \text{ keV}).$$

REF.

J. M. Loiseaux, J. M. Maison, and M. Langevin
J. de Physique 28, 11 (1967)

ELEM. SYM.	A	Z
B	11	5

METHOD

REF. NO.	
67 Lo 1	JOC

REACTION	RESULT	EXCITATION ENERGY	SOURCE		DETECTOR		ANGLE
			TYPE	RANGE	TYPE	RANGE	
G,G/	ABX	12-30	C	34	NAI-D		DST

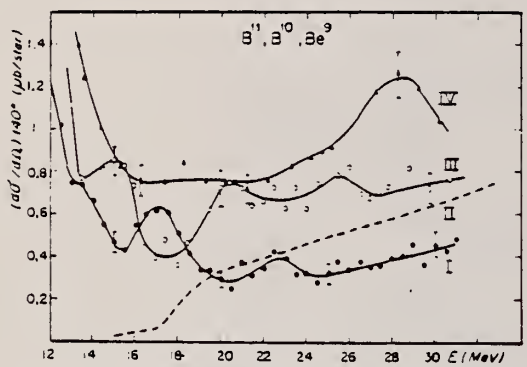

FIG. 5.

Sections efficaces différentielles de diffusion à 140° pour ^{9}Be (I), ^{10}B (III) et ^{11}B (IV).

Section efficace prévue par la relation de dispersion pour ^{9}Be (courbe II).

REF. P. Paul, N. G. Puttaswamy and D. Kohler
Phys. Rev. 164, 1332 (1967)

ELEM. SYM.	A	Z
B	11	5

METHOD

REF. NO. 67 Pa 3 egf

REACTION	RESULT	EXCITATION ENERGY	SOURCE		DETECTOR		ANGLE
			TYPE	RANGE	TYPE	RANGE	
A,G	ABX	9-11	D	1-4	NAI-D	2-10	90

Tries to fit both (A,G) and (A,A/) cross sections with resonances. Yes

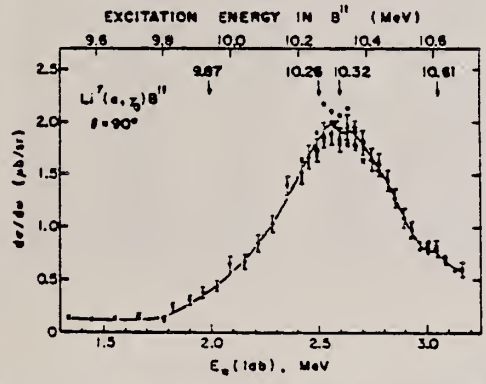

FIG. 5. Excitation function of the capture reaction $Li^7(\alpha,\gamma_0)B^{11}$, measured at 90° to beam axis. Arrows indicate position of previously reported states (Ref. 3) in B^{11}. The cross section calibration is described in the text. Typical errors shown contain statistics and analysis uncertainties. The data points for different target-spot positions are shown by different symbols. The solid line is a smooth curve drawn through the data points.

REACTION	RESULT	EXCITATION ENERGY	SOURCE		DETECTOR		ANGLE
			TYPE	RANGE	TYPE	RANGE	
E,E/	FMF	4,5	D	35-57	MAG-D		DST

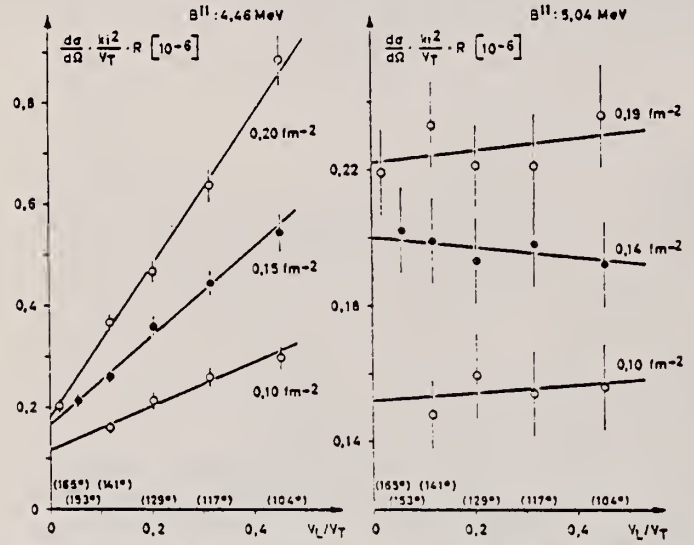

Fig. 1. Winkelabhängigkeit der Wirkungsquerschnitte bei verschiedenen Impulsübertragungen q für die Anregung des 4,46- und 5,04 MeV-Niveaus in B^{11}, $V_L(\Theta)$ und $V_T(\Theta)$ sind Funktionen vom Streuwinkel (siehe z.B. D), $d\sigma/d\Omega$ ist der differentielle Wirkungsquerschnitt, $k_1 = E_0/\hbar c$ und $R = 1 + 2(E_0/Mc^2)\sin^2\Theta/2$

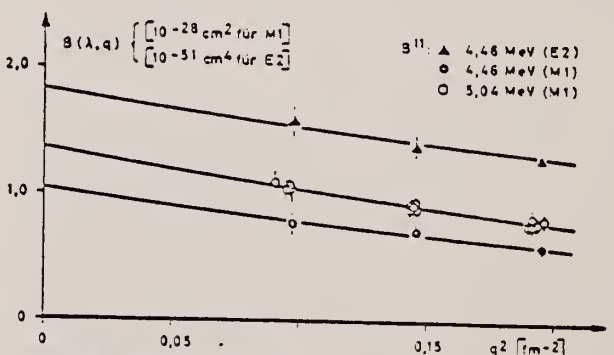

Fig. 2. Reduzierte Übergangswahrscheinlichkeit $B(\lambda, q)$ als Funktion von q^2

REACTION	RESULT	EXCITATION ENERGY	SOURCE		DETECTOR		ANGLE
			TYPE	RANGE	TYPE	RANGE	

Tabelle 1. *Experimentelle Parameter und Meßwerte. Die Abkürzung Q steht für* $\kappa A_I/hA_E=(d\sigma/d\Omega)/(d\sigma/d\Omega)_E$

		E_x=4,46 MeV			E_x=5,04 MeV		
Θ [°]	E_0 [MeV]	q^2 [fm^{-2}]	Q [10^{-3}]	$d\sigma/d\Omega$ [10^{-32} cm^2/sr]	q^2 [fm^{-2}]	Q [10^{-3}]	$d\sigma/d\Omega$ [10^{-32} cm^2/sr]
104,98	56,99	0,193	2,14 ± 0,13	5,39 ± 0,32	0,191	0,57 ± 0,06	1,44 ± 0,15
117,04	53,25	0,194	2,23 ± 0,11	3,53 ± 0,18	0,191	0,77 ± 0,07	1,22 ± 0,12
129,02	50,80	0,196	2,54 ± 0,13	2,37 ± 0,12	0,194	1,22 ± 0,07	1,14 ± 0,07
141,11	49,00	0,198	3,50 ± 0,17	1,76 ± 0,09	0,195	2,28 ± 0,13	1,14 ± 0,07
165,05	46,07	0,192	12,64 ± 0,74	0,94 ± 0,06	0,190	13,63 ± 0,82	1,02 ± 0,06
104,98	50,01	0,147	1,20 ± 0,08	4,32 ± 0,30	0,146	0,43 ± 0,03	1,54 ± 0,12
117,04	46,72	0,146	1,42 ± 0,09	3,19 ± 0,19	0,144	0,64 ± 0,04	1,43 ± 0,09
129,02	44,20	0,146	1,78 ± 0,11	2,41 ± 0,14	0,144	0,96 ± 0,07	1,30 ± 0,09
141,11	42,36	0,146	2,29 ± 0,13	1,66 ± 0,10	0,144	1,72 ± 0,12	1,27 ± 0,09
153,15	41,36	0,148	4,02 ± 0,28	1,32 ± 0,11	0,146	3,84 ± 0,31	1,27 ± 0,10
104,98	41,19	0,098	0,60 ± 0,05	3,50 ± 0,28	0,097	0,32 ± 0,03	1,83 ± 0,18
117,04	38,50	0,098	0,76 ± 0,06	2,76 ± 0,22	0,096	0,46 ± 0,04	1,64 ± 0,13
129,02	35,47	0,093	0,84 ± 0,06	1,97 ± 0,16	0,091	0,67 ± 0,07	1,57 ± 0,15
141,11	35,00	0,098	1,25 ± 0,07	1,50 ± 0,09	0,096	1,16 ± 0,09	1,39 ± 0,11

Tabelle 2. *Longitudinaler* $T_L(\lambda, q)$- *und transversaler* $T_T(\lambda, q)$- *Wirkungsquerschnitt*

	q^2 [fm^{-2}]	$T_L(\lambda, q)$ [10^{-1}]	$T_T(\lambda, q)$ [10^{-1}]
4,46 MeV	0,098	4,36 ± 0,35	1,14 ± 0,10
	0,146	8,76 ± 0,50	1,65 ± 0,10
	0,195	14,90 ± 0,60	1,80 ± 0,18
5,04 MeV	0,096	0,12 ± 0,22	1,52 ± 0,07
	0,144	−0,16 ± 0,20	2,00 ± 0,06
	0,191	0,18 ± 0,30	2,22 ± 0,07

Tabelle 3. *Meßergebnisse für das 4,46 und 5,04 MeV-Niveau in Bornscher Näherung. Die Weisskopfeinheiten* Γ_w *gelten für einen Kernradius* $R=1{,}2\,fm\cdot A^{\frac{1}{3}}$

E_x [MeV]	Übergang	$B(\lambda, k)$ a)	R_{tr} [fm]	Γ_γ^0 [eV]	Γ_γ^0/Γ_w
4,46	$C2$	1,83 ± 0,13	3,44 ± 0,50	$(17{,}1 \pm 1{,}6)\cdot 10^{-3}$	8,1
	$M1$	1,07 ± 0,10	2,60 ± 0,35	0,63 ± 0,07	0,34
5,04	$M1$	1,38 ± 0,05	2,60 ± 0,15	1,82 ± 0,08	0,68
	$C2$			$<3{,}4\cdot 10^{-3}$	

a) Einheit: 10^{-51}cm^4 für $C2$, 10^{-28}cm^2 für $M1$.

REF. G. Nydahl and B. Forkman
Nucl. Phys. B7, 97 (1968)

ELEM. SYM.	A	Z
B	11	5

METHOD

REF. NO. 68 Ny 1 egf

REACTION	RESULT	EXCITATION ENERGY	SOURCE		DETECTOR		ANGLE
			TYPE	RANGE	TYPE	RANGE	
G,PI-	ABX	140-700	C	140-700	ACT-I		4PI

C-11 ACT

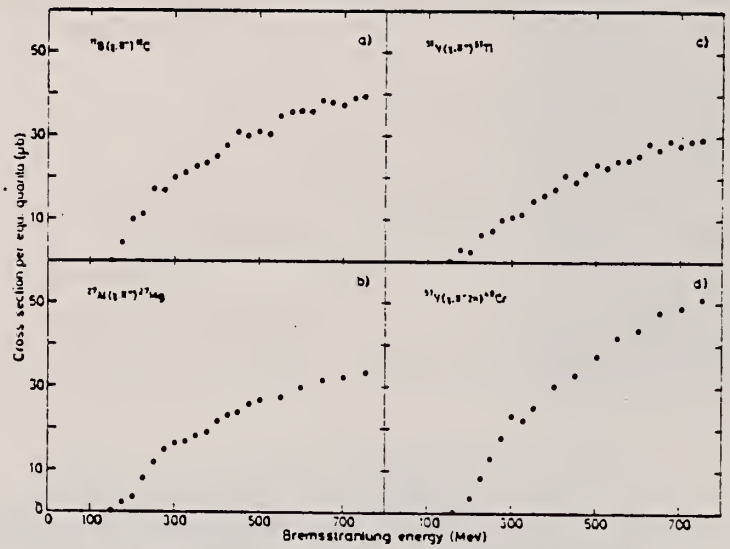

Fig. 3. Absolute yields for the measured reactions.

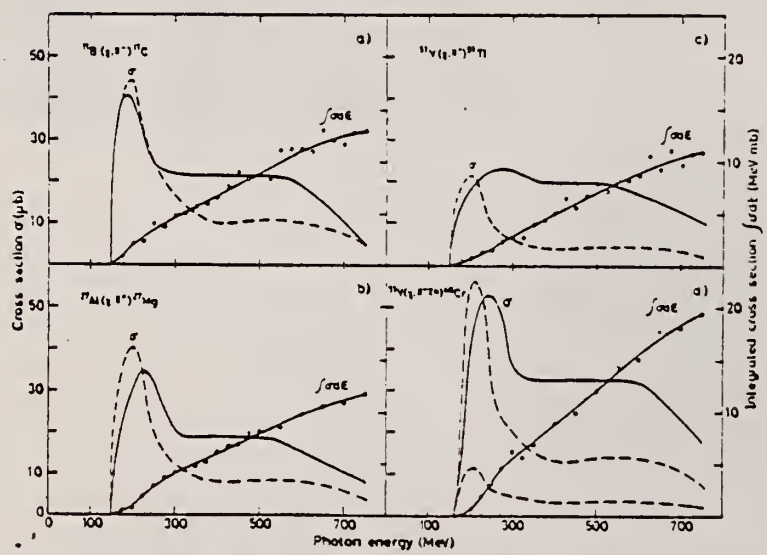

Fig. 4. Experimentally determined true and integrated cross sections. Theoretical calculations of the cross sections are marked with dashed lines.

REF. Kenneth M. Murray
Phys. Rev. Letters 23, 1461 (1969)
[See Evans Hayward, Robert B. Schwartz, and Kenneth M. Murray, Phys. Rev. C2, 761 (1970)]

EL EM. SYM.	A	Z
B	11	5

METHOD

REF. NO. 69 Mu 2 hmg

REACTION	RESULT	EXCITATION ENERGY	SOURCE TYPE	SOURCE RANGE	DETECTOR TYPE	DETECTOR RANGE	ANGLE
G,PG	SPC	11-35	C	24,35	SCD-D		
G,NG	SPC	11-35	C	24,35	SCD-D		

COMMENTS

Conclusions drawn in this paper were modified in a later paper. See Evans Hayward, Robert B. Schwartz, and Kenneth M. Murray, Phys. Rev. C2, 761 (1970).

GAMMA SPECTRUM

In summary: There is evidence for the (γ, n) reaction leaving B^{10} in an excited state (717 keV); there is no evidence of population of the $T = 1$ states in B^{10}; and the first excited state in Be^{10} at 3366 keV is seen clearly.

From these data it appears that the cross section integrated from threshold to 35 MeV for the $T = \frac{3}{2}$ giant resonance in B^{11} is considerably smaller than the cross section over the same range for the $T = \frac{1}{2}$ giant resonance.

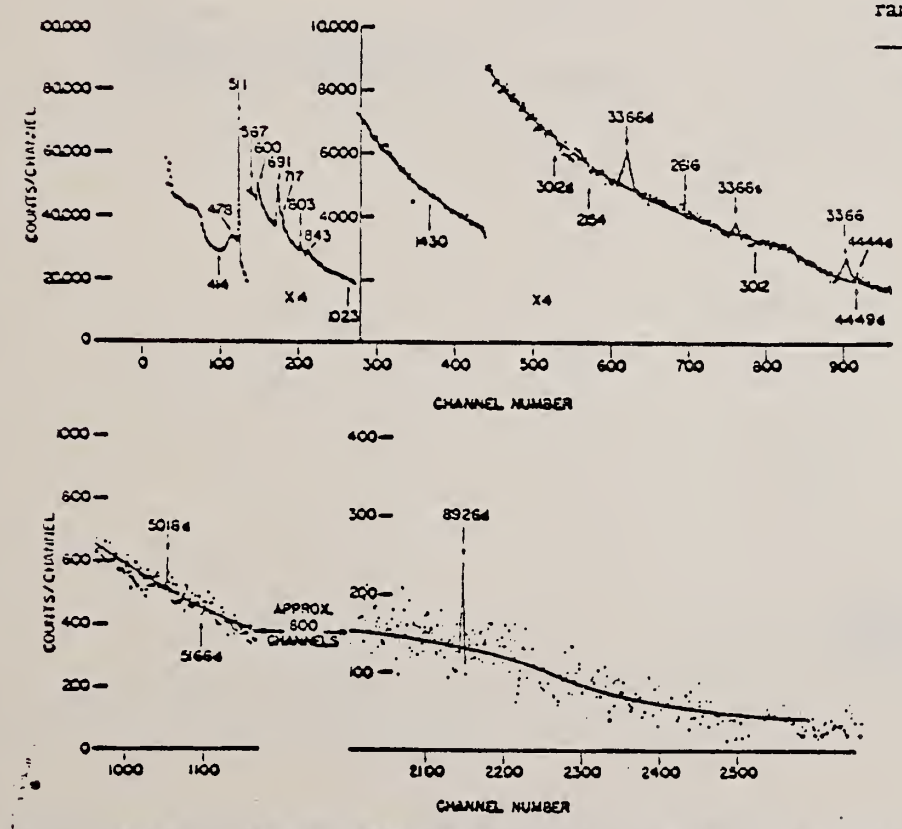

FIG. 3. Gamma-ray spectrum from B_4C target irradiated with 35-MeV bremsstrahlung.

over

Abstract of the paper referred to under "Comments" on reverse side of this sheet.

PHYSICAL REVIEW C VOLUME 2, NUMBER 2 AUGUST 1970

Comments on "Isospin of the B^{11} Giant Resonance"

Evans Hayward and Robert B. Schwartz
National Bureau of Standards, Washington, D. C. 20234
and
Kenneth M. Murray
Linac Branch, Nuclear Physics Division, U. S. Naval Research Laboratory, Washington, D. C. 20390

(Received 4 February 1970)

It was recently shown that in the photodisintegration of B^{11} certain expected γ rays were missing. A partial explanation is offered here for the failure to observe these transitions. It is also pointed out that no conclusions about the strength of the $T=\frac{3}{2}$ giant resonance can be drawn from this experiment.

Yu. I. Sorokin, V. G. Shevchenko, and B. A. Yur'ev
Yad. Fiz. 9, 254 (1969)
Sov. J. Nucl. Phys. 9, 149 (1969)

B	11	5

METHOD

REF. NO. 69 So 2 hmg

REACTION	RESULT	EXCITATION ENERGY	SOURCE TYPE	SOURCE RANGE	DETECTOR TYPE	DETECTOR RANGE	ANGLE
G,P	ABX	15-32	C	15-32	SCD-D		4PI
		(31.5)		(31.5)			

Cross sections include contributions from the (γ,d), (γ,t), and (γ,α) reactions.

316

σ(γ, p)*		σ(γ, n)**		σ(γ, p) + σ(γ, n)	Calculations based on the many-particle shell model***	
E, MeV	σ_{int}, MeV-mb	E, MeV	σ_{int}, MeV-mb	σ_{γ}, MeV-mb	E, MeV	σ_{int}, MeV-mb
					11.7	3.4
					14.15	4.3
(18.5)****	0.75	~16.5	2	3	16.9	18.5
					17.1	3.0
(~18.0)	3.6	~18.2	2.5	6.1	17.9	2.7
		19.2	4		18.2	18.4
(20.2	5.5	(20.1)	2	7.1	19.3	2.6
					21	7.8
21.6	10	21	2.5	12.5	21.5	7.6
					22.0	3.4
23.2	13.4	(23.3)	3	16.4	23	17.8
(24.5)	8.5	(24.2)	4.5	13	24.3	2.7
25.5	23	(25.4)	5	18		
		(26.2)	4	14		
27.7	26	27.3	4	30	28.1	10.4
					29.1	3.5
29.2	7				30.8	4.4

*Present work.
**From [11].
***From [5] (for transitions with $\sigma_{int} > 1$ MeV-mb).
****The parentheses indicate maxima whose reliability is not entirely obvious.

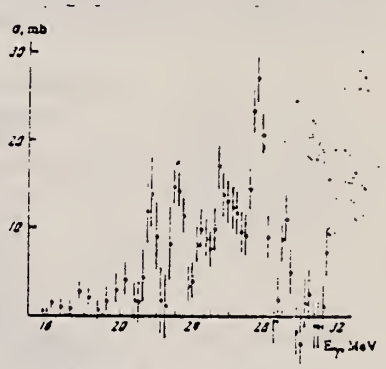

FIG. 2. $B^{11}(\gamma, p)$ cross sections.

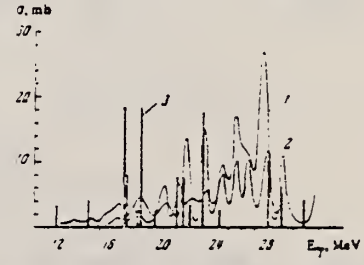

FIG. 3. Experimental and calculated cross sections for B^{11} photodisintegration. 1 – $B^{11}(\gamma, p)$ cross sections obtained in the present work; 2 – $B^{11}(\gamma, n)$ cross sections from [11]; 3 – vertical bars denote the calculated integral cross sections (MeV-mb) for dipole transitions, from [5].

REF. D. R. Goosman, E. G. Adelberger and K. A. Snover
Phys. Rev. C 1, 123 (1970) (See Erratum: Phys. Rev. C7, 1717 (1973).

ELEM. SYM.	A	Z
B	11	5

METHOD

REF. NO. 70 Go 2 hmg

REACTION	RESULT	EXCITATION ENERGY	SOURCE		DETECTOR		ANGLE
			TYPE	RANGE	TYPE	RANGE	
P,G	ABX	12-16	D	0-7	NAI-D	3-16	DST
				(0.6-6.3)			

J-PI. G-WIDTH 235 r

The differential cross section for the $^{10}Be(p,\gamma_0)^{11}B$ reaction has been measured at 90° for $0.6 \leq E_p \leq 6.3$ MeV. Compound resonances in ^{11}B have been located at (12.17±0.04)-, 12.55±0.03-, 12.91±0.02-, 14.33±0.02-, and 15.3±0.1-MeV excitation energy. The last four are probably analogs to the lowest four levels in ^{11}Be. Total widths and ground-state γ-ray widths of these levels are presented. The spins of the 12.55- and 14.33-MeV levels are shown to be $\frac{1}{2}^+(\frac{1}{2}^+)$ and $\frac{1}{2}^{(+)}(\frac{1}{2}^-)$, respectively.

TABLE I. Levels in ^{11}B from the $^{10}Be(p,\gamma_0)^{11}B$ reaction.

Excitation energy (MeV±keV)	Proton energy (MeV±keV)	$\Gamma_{c.m.}$ (keV)	$(J+\frac{1}{2})(\Gamma_p/\Gamma)\Gamma_{\gamma_0}$ (eV)	J^π	Γ_{γ_0} (eV)	$\Gamma_{\gamma_1}/\Gamma_{\gamma_0}$
(12.17±40)	(1.05±40)	230±90	$1.8_{-1.2}^{+1.2}$	...	...	
12.55±30	1.46±30	230±65	6_{-3}^{+4}	$\frac{1}{2}^+(\frac{1}{2}^+)$	6_{-3}^{+4}	0.25±0.08
12.91±20	1.85±20	235±27	17±5	$\frac{1}{2}^-$ [b]	17±5	≤0.06
14.33±20	3.41±20	255±36	17±5	$\frac{1}{2}^{(+)}(\frac{1}{2}^-)$	8.5±2.5	≤0.1
15.3±100	4.5±100	635±180	31_{-18}^{+28} [c]	...	...	

[a] These values assume that $J = \frac{1}{2}$. Γ_p/Γ has been estimated as described in the text.
[b] Reference 2.
[c] Assumes that $\sigma_{total} = 4\pi\, d\sigma/d\Omega\ (90°)$.

Cross sections and γ-ray widths should be increased by a factor of 1.7.

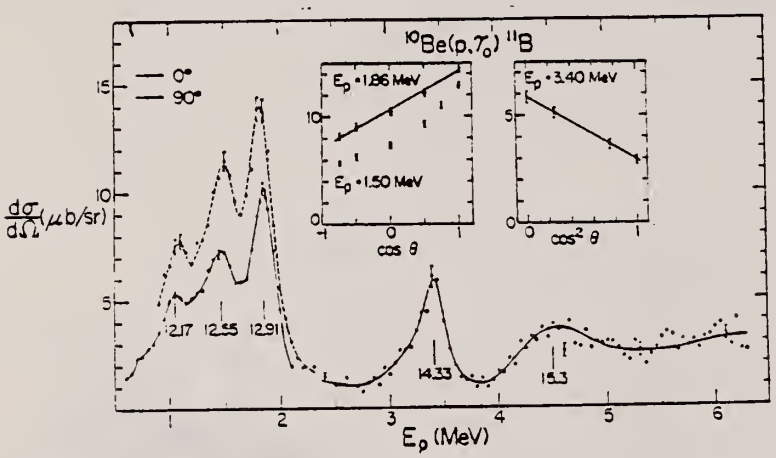

FIG. 5. Excitation function for $^{10}Be(p,\gamma_0)^{11}B$. Angular distributions at three beam energies are shown, and the fit for the distribution at $E_p = 3.4$ MeV is drawn for $J = \frac{1}{2}$. In addition to the relative error bars shown, there is a 30% uncertainty in the cross-section scale.

Cross sections and γ-ray widths should be increased by a factor of 1.7.

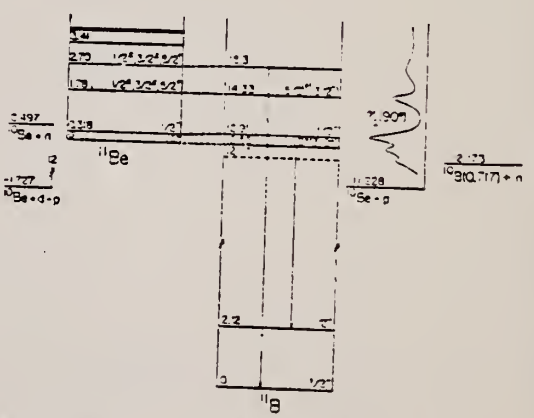

FIG. 6. Energy levels of ^{11}Be and ^{11}B that are relevant to the present work. The spins shown for the ground and first excited states of ^{11}Be are due to Auton *et al.* (Ref. 12) and Goosman and Kavanagh (Ref. 3), while the spins of higher levels are due to Pullen *et al.* (Ref. 5).

REF. Yu. I. Sorokin, A. Kh. Shardanov, V.G. Shevchenko, and B.A. Yur'ev
Yad. Fiz. 11, 8 (1970)
Sov. J. Nucl. Phys. 11, 4 (1970)

ELEM. SYM.	A	Z
B	11	5

METHOD

REF. NO. 70 So 1 hmg

REACTION	RESULT	EXCITATION ENERGY	SOURCE		DETECTOR		ANGLE
			TYPE	RANGE	TYPE	RANGE	
G,P	ABX	11-19	C	17,19	EMU-D		DST
		(11.2-18.5)		(16.5,18.5)			

279+

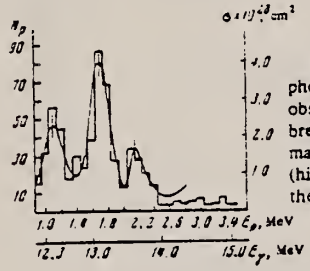

FIG. 1. Energy distribution of the photoprotons from the B^{11} nucleus, observed following irradiation with bremsstrahlung γ radiation having a maximum energy $E_{\gamma max}$ = 16.5 MeV (histogram) and the cross section of the $B^{11}(\gamma, p)Be^{10}$ reaction (solid line).

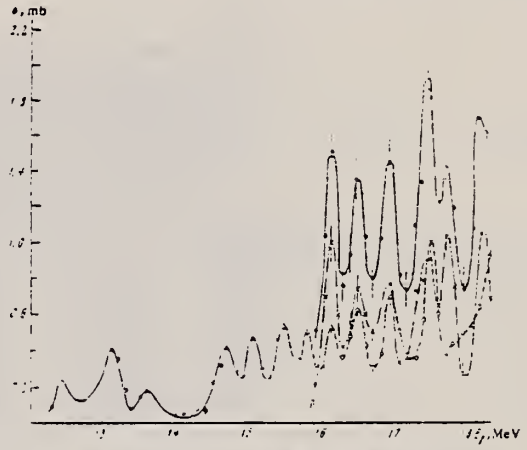

FIG. 3. Cross section of the reaction $B^{11}(\gamma, p)Be^{10}$. Solid line – total cross section of the reaction; dashed line – cross section of the reaction $B^{11}(\gamma, p)Be^{10}$ in the case when the Be^{10} nucleus remains in the ground state; dash-dot line – cross section in the case when the Be^{10} nucleus remains in the first excited state.

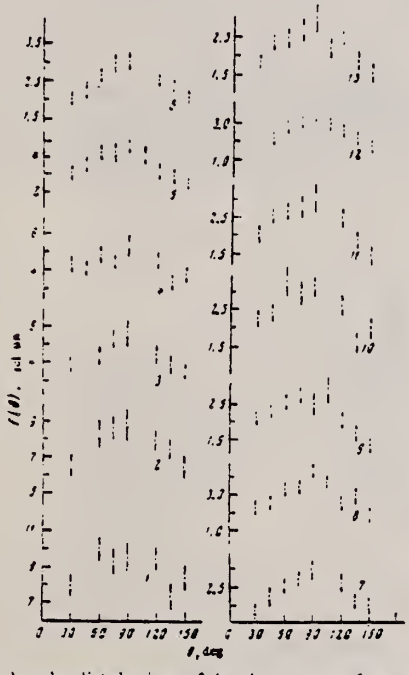

FIG. 4. Angular distributions of the photoprotons from the B^{11} nucleus following irradiation with $E_{\gamma max}$ = 18.5 MeV. Curves 1 – 13 pertain to photoproton groups with different energies (see Table I).

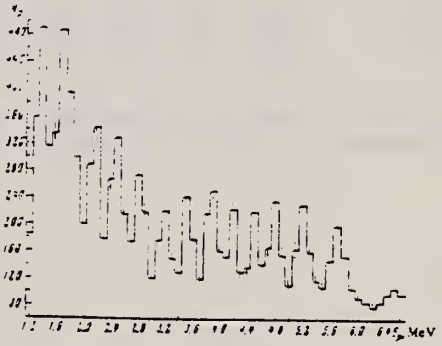

FIG. 2. Energy distribution of the photoprotons from the B^{11} nucleus, observed following irradiation at $E_{\gamma max}$ = 18.5 MeV.

over

Table I. Approximated angular distributions of the photoprotons from the reaction $B^{11}(\gamma, p)Be^{10}$

Group number	E_p, MeV	$I(\vartheta)$	Group number	E_p, MeV	$I(\vartheta)$
1	1.3—1.5	$1+0.3\ \sin^2\vartheta$	8	3.8—4.0	$1+0.8\ \sin^2\vartheta$
2	1.6—1.8	$1+0.6\ \sin^2\vartheta$	9	4.1—4.3	$1+0.9\ \sin^2\vartheta$
3	2.1—2.3	$1+0.65\ \sin^2\vartheta$	10	4.4—4.6	$1+0.75\ \sin^2\vartheta$
4	2.4—2.6	$1+0.6\ \sin^2\vartheta$	11	4.7—4.9	$1+0.85\ \sin^2\vartheta$
5	2.7—2.9	$1+0.8\ \sin^2\vartheta$	12	5.1—5.3	$1+1.5\ \sin^2\vartheta$
6	3.1—3.3	$1+0.7\ \sin^2\vartheta$	13	5.6—5.8	$1+\sin^2\vartheta$
7	3.4—3.6	$1+0.95\ \sin^2\vartheta$			

Table V. Levels of the B^{11} nucleus decaying by proton emission to the ground state (reaction (γ, p_0)) and first-excited state (reaction (γ, p_1)) of the final nucleus B^{10}, and integral cross sections σ_0 and σ_1 of the reactions (γ, p_0) and (γ, p_1) which proceed with excitation of these levels

E^*, MeV	$\sigma_0(\gamma, p_0)$, MeV-mb	$\sigma_1(\gamma, p_1)$, MeV-mb	$\sigma_0+\sigma_1$, MeV-mb
16.2±0.2	0.13±0.015 30% $(\sigma_0+\sigma_1)$	0.32±0.05 70% $(\sigma_0+\sigma_1)$	0.45±0.07
16.5±0.2	0.18±0.02 50% $(\sigma_0+\sigma_1)$	0.19±0.03 50% $(\sigma_0+\sigma_1)$	0.37±0.05
16.9±0.2	0.24±0.03 55% $(\sigma_0+\sigma_1)$	0.2±0.03 45% $(\sigma_0+\sigma_1)$	0.44±0.6
17.5±0.2	0.3±0.04 45% $(\sigma_0+\sigma_1)$	0.38±0.05 55% $(\sigma_0+\sigma_1)$	0.68±0.9

Table II

(γ, p)		(γ, n)			Γ_γ^{exp}, eV			(e, e') [17]		Γ_γ^{theor}, eV [18]			Γ_γ^{theor}, eV [19]		$E1$-transition [1]	
E^*, MeV	σ_{int}, MeV-mb	E^*, MeV	σ_{int}, MeV-mb	$\sigma_{int}(\gamma, p)^{[16]}+\sigma_{int}(\gamma, n)$, MeV-mb	$I=3/2$	$I=1/2$	$I=3/2$	E^*, MeV	$\Gamma_\gamma(M1)$, eV $(I=1/2)$	$E1$	$M1$	$E2$	$M1$	$E2$	E^*, MeV	σ_{int}^{γ}, MeV-mb
12.4	0.11	12.2	0.06	0.17	14	7	4.5	12.2	10	640	40	0.3			10.5	0.8
								12.65	14					0.05	11.5	3.4
13.1	0.25	13.0	0.25	0.5	43	22	14	13.2	12	760	47	0.45	2—50			
13.65	0.06			0.38	30	15	10			860	53	0.6		0.5	14.0	4.4
		14.3	0.3					14.55	20.4						14.2	0.3
14.75	0.04			0.34	47	23	16			1100	67	0.8			14.3	0.5
15.1	0.14	15.2	0.6	0.74	84	42	29			1160	72	0.9				
15.5	0.53		(0.65)	(1.2)	(140)	(70)	(47)	15.55	32.2	1250	78	1.1	1—100	0.1—1		
15.85	0.50		(0.70)	(1.2)	(150)	(75)	(50)			1340	83	1.2				
16.2	0.45		(0.75)	(1.2)	(155)	(77)	(52)			1430	90	1.3				
16.5	0.37	16.5	0.8	1.2	160	80	53			1510	94	1.5				
															17.0	18.5
16.9	0.44		(0.85)	(1.3)	(180)	(90)	(60)	16.9	78	1620	100	1.7			17.1	4.4
															17.7	2.4
17.5	0.66		(0.9)	(1.6)	(240)	(120)	(80)			1800	112	2.0	3—200	0.2—2	18.0	14.3

Note. The parentheses contain values that are not quite reliable.

K. Battleson and D. K. McDaniels
Phys. Rev. C4, 1601 (1971)

B	11	5

METHOD

REF. NO. 71 Ba 4 hmg

REACTION	RESULT	EXCITATION ENERGY	SOURCE TYPE	SOURCE RANGE	DETECTOR TYPE	DETECTOR RANGE	ANGLE
D,G	ABX	16-20	D	0-4	NAI-D		DST
		(16.4-19.4)		(0.56-3.56)			

3G-1

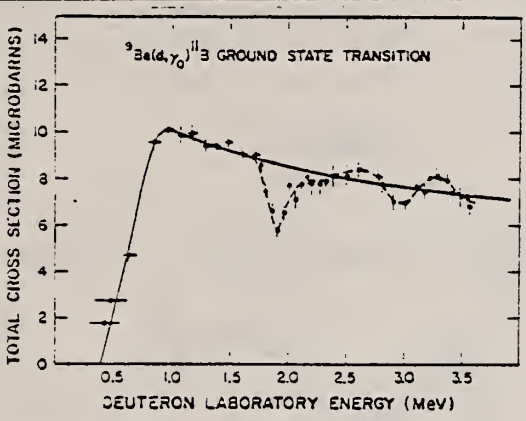

FIG. 4. Excitation function for the ground-state γ-ray transition in the reaction ^{9}Be(d,γ)^{11}B. Data points were obtained both from angular-distribution measurements and from runs at 55° to the incident beam as described in the text. Horizontal bars on the data points show the energy loss of the deuteron in passing through the target. The solid curve is meant to represent the over-all data behavior neglecting the resonance structure. The dashed curve is drawn through the actual data points.

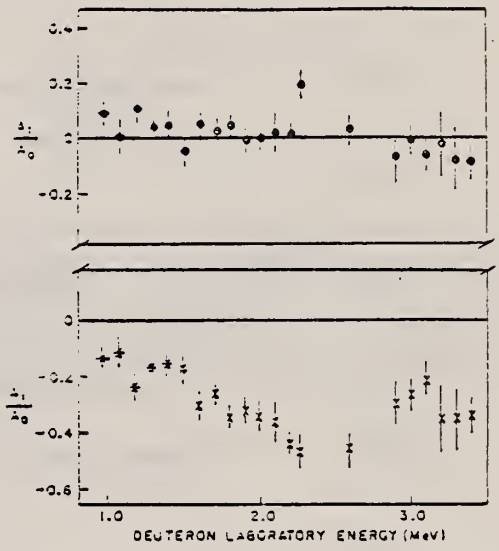

FIG. 5. Plots of the Legendre polynomial coefficients obtained from the angular-distribution measurements as a function of the incident deuteron energy for the γ-ray transition to the ground state of ^{11}B.

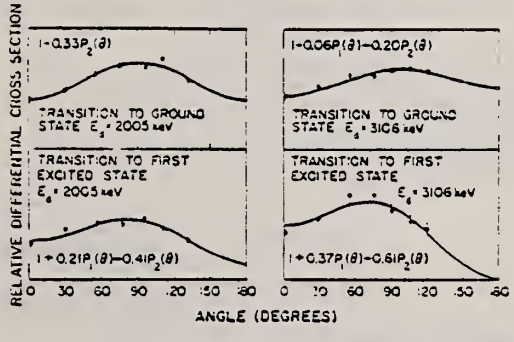

FIG. 7. Typical examples of angular-distribution data. The solid curve represents a least-squares fit to $A_0 + A_1P_1(\cos\theta) + A_2P_2(\cos\theta)$, with A_0 normalized to unity.

REF. B. H. Patrick, H. A. Medicus, G. K. Mehta, E. M. Bowey, and D. B. Gayther
Phys. Letters 34B, 488 (1971)

ELEM. SYM.	A	Z
B	11	5

METHOD

REF. NO. 71 Pa 1 egf

REACTION	RESULT	EXCITATION ENERGY	SOURCE		DETECTOR		ANGLE
			TYPE	RANGE	TYPE	RANGE	
G,PG	ABX	10-35	C	20-35	SCD-D		90
G,NG	ABX	10-35	C	20-35	SCD-D		90

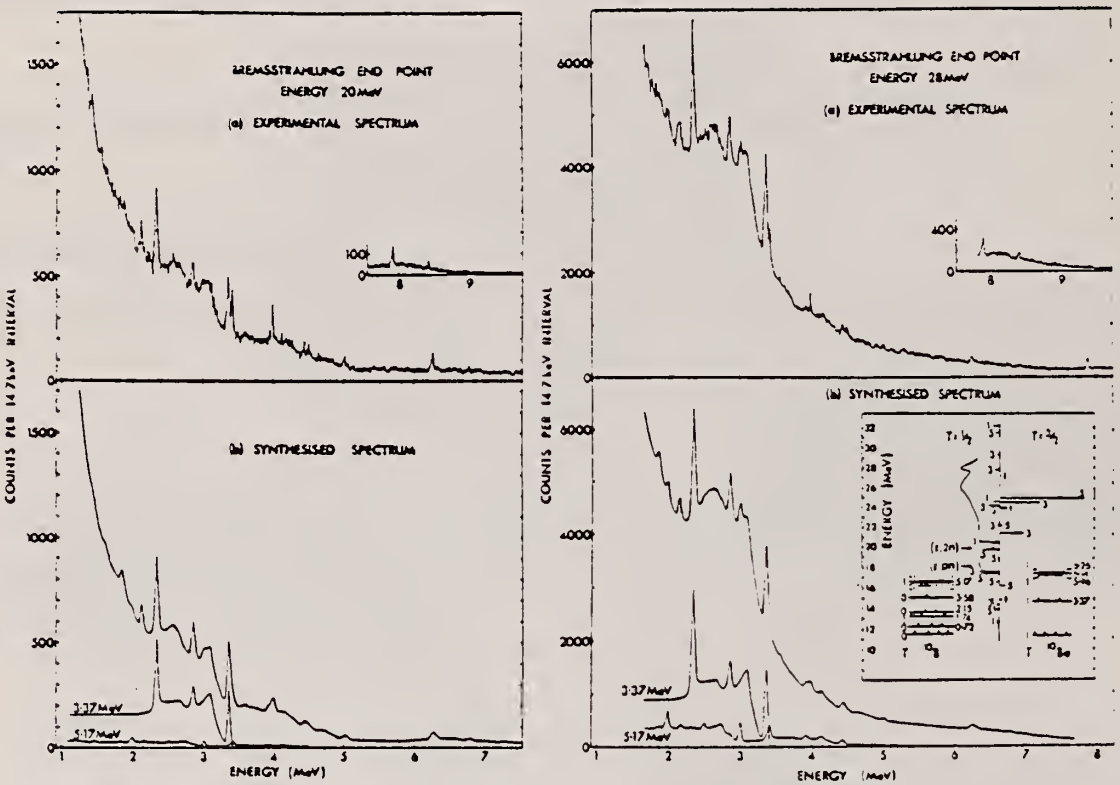

Fig. 1. Measured and computer-synthesized γ-ray spectra from the $(\gamma, \overset{n}{p}\gamma')$ reactions on ^{11}B with 20 and 28 MeV bremsstrahlung. The insert shows the results of the calculations by Fraser [4] in relation to the energy levels of ^{10}B and ^{10}Be. The lines emanating from the central vertical line represent the strength of the dipole states in ^{11}B calculated for a 50 MeV Gillet force, the $T = 1/2$ states to the left, the $T = 3/2$ states to the right. The spin (shown as $2J$ for clarity) of each state is also indicated. The curve shows the $(\gamma, n) + (\gamma, pn) + 2(\gamma, 2n)$ cross section as measured by Hayward and Stovall [13].

[13] E. Hayward and T. Stovall, Nucl. Phys. 69 (1965) 241.

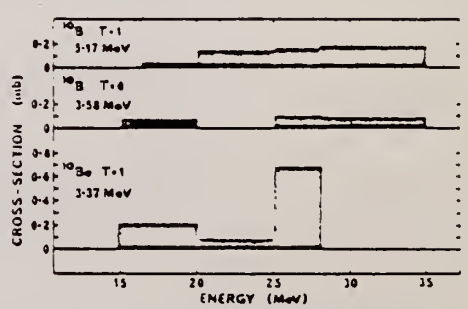

Fig. 2. Partial cross sections for some excited states in ^{10}B and ^{10}Be.

V. G. Vlasenko, N. G. Afanas'ev, V. A. Gol'dshtein, S. V. Dementii and E. L. Kuplennikov
Yad. Fiz. 13, 259 (1971); Sov. J. Nucl. Phys. 13, 144 (1971)

B	11	5

METHOD

REF. NO. 71 V1 1 hmg

REACTION	RESULT	EXCITATION ENERGY	SOURCE TYPE	SOURCE RANGE	DETECTOR TYPE	DETECTOR RANGE	ANGLE
E,E/	FMF	0-300	D	592- 999	MAG-D		DST

999 = 1143 QUASIELASTIC SCTNG

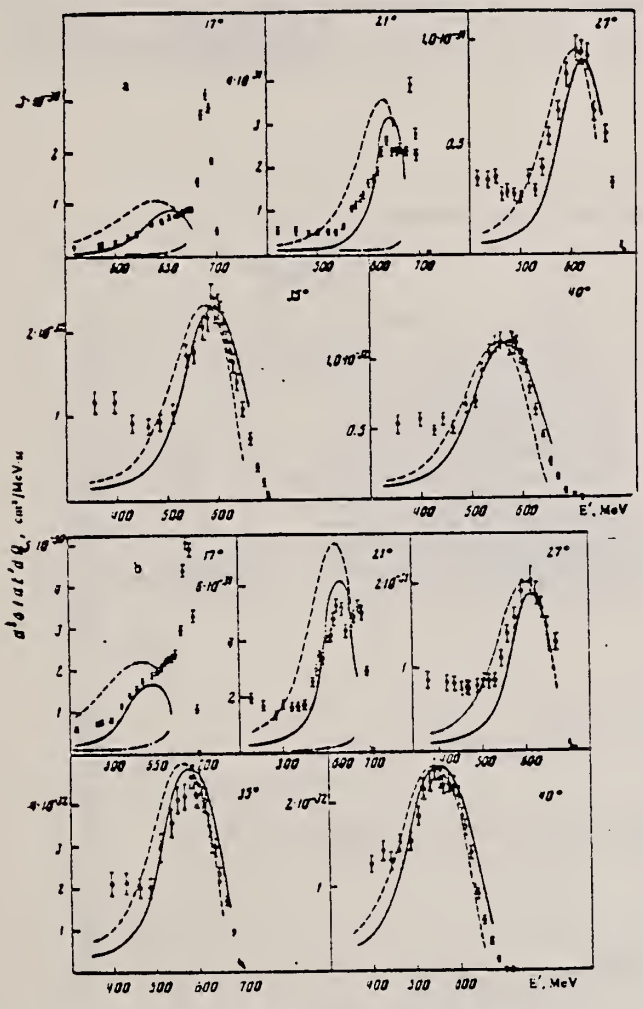

FIG. 1. Cross sections for scattering of 690-MeV electrons by B^{11} (a) and Al^{27} (b) at angles 17, 21, 27, 35, and 40°, as a function of scattered-electron energy. The dashed and solid curves have been calculated from Eqs. (1), (2), (4) and (1), (3), (4), respectively.

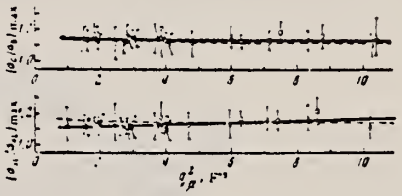

FIG. 2. Ratios of cross sections for scattering of electrons, $\sigma_{C^{12}}/\sigma_B$ and $\sigma_{Si^{28}}/\sigma_{Al^{27}}$ at the maximum of the continuum, as a function of squared momentum transfer. The solid lines are the result of fitting a linear function to the experimental points, and the dashed lines correspond to calculations using Eq. (5) for the cross section. The following designations are used for the experimental ratios at the various initial electron energies: ● – 592 MeV, ○ – 690 MeV, Δ – 802 MeV, □ – 969 MeV, X – 1143 Mev.

$$\left(\frac{d^2\sigma}{dE'\,d\Omega}\right)_{\max} = A\frac{M}{\sqrt{\pi}p_0 q}(z\sigma_p + n\sigma_n)\left(1+\frac{2E_0}{M}\sin^2\frac{\theta}{2}\right). \quad (5)$$

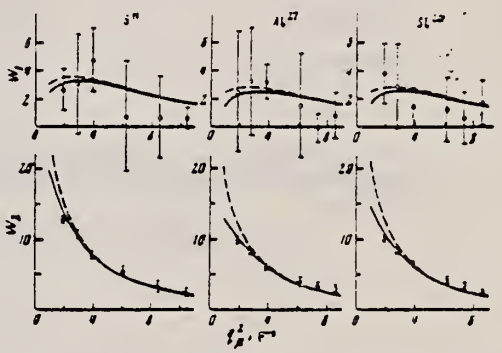

FIG. 3. Inelastic electromagnetic form factors of B^{11}, Al^{27}, and Si^{28}, measured in the region of the continuum. The dashed curves are the result of a calculation based on Eqs. (2), (7), and (8), and the solid curves based on Eqs. (3), (7), and (8).

Nucleus	Quasielastic electron scattering: Pauli principle not taken into account: p_m, MeV/c	$\frac{z\sigma_p}{N\sigma_n}$	$\langle r_Z^2\rangle^{1/2}$, F	Pauli principle taken into account: p_m, MeV/c	$\frac{z\sigma_p}{N\sigma_n}$	$\langle r_Z^2\rangle^{1/2}$, F	Elastic electron scattering: $\langle r_Z^2\rangle^{1/2}$, F	p_m, MeV/c
B^{11}	150±5	1,6	2,07±0,07	155±5	1,5	2,01±0,07	2,42±0,12 [11]	125±6
Al^{27}	145±4	1,4	2,39±0,07	149±4	1,2	2,33±0,07	2,90±0,09 [11]	114±3

REF.

V.I. Noga, Yu. N. Ranyuk, P.V. Sorokin, V.A. Tkachenko
Yad. Fiz. 14, 904 (1971)
Sov. J. Nucl. Phys. 14, 506 (1972)

B	11	5

METHOD

REF. NO. 72 No 3 hmg

REACTION	RESULT	EXCITATION ENERGY	SOURCE		DETECTOR		ANGLE
			TYPE	RANGE	TYPE	RANGE	
G,PI- *	ABX	150-999	C	150-999	ACT-I		4PI
E,PI- **	RLY	150-999	C	150-999	ACT-I		4PI

* 999=1.2 GEV
** 999=1.2 GEV RLY TO G

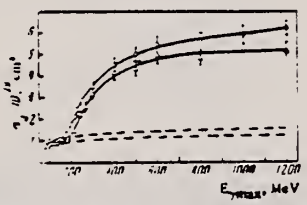

FIG. 2. Yields of C^{11} and Mg^{27} activities from B^{11} and Al^{27} targets. Points: O–$B^{11}(\gamma, \pi^-)C^{11}$; Δ–$Al^{27}(\gamma, \pi^+)Mg^{27}$. The dashed curves are the corresponding background activities.

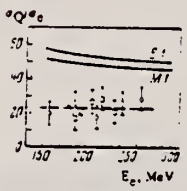

FIG. 5

FIG. 5. The ratio σ_Q/σ_0 as a function of electron energy. Solid curves–theoretical results; points–values obtained experimentally for the reactions:

$$O - B^{11}\left(\begin{matrix}\gamma, \pi^-\\ e, e'\pi^-\end{matrix}\right)C^{11};\ \square - Al^{27}\left(\begin{matrix}\gamma, \pi^+\\ e, e'\pi^+\end{matrix}\right)Mg^{27}$$

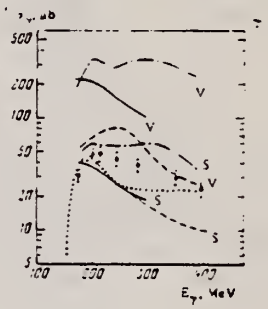

FIG. 3. Cross section per real photon $\sigma_\gamma(E_\gamma)$ for the reaction $B^{11}(\gamma, \pi^-)C^{11}$. Curves: solid–theory [1], dot-dash–theory [2], dashed–theory [4]. The curves with the letter v correspond to the mechanism of pion production over the entire nuclear volume, and with the letter s to the mechanism of pion production on the nuclear surface. Points: O–experimental data [5], ●–experimental data of the present work.

[1] E.V. Laing et al., Proc. Phys. Soc. (London) 70, 629 (1957).
[2] V. Devanathan et al., Phys. Letters 25B, 456 (1967).
[5] G. Nydahl et al., Nucl. Phys. B7, 97 (1968).

REF. D.M. Fleming, P.T. Kan, G.A. Peterson, D.V. Webb, S.P. Fivozinsky, J.W. Lightbody and S. Penner
PICNS-73, Vol.II, p.887 (1973) Asilomar

ELEM. SYM.	A	Z
B	11	5

METHOD

REF. NO. 73 F1 3 egf

REACTION	RESULT	EXCITATION ENERGY	SOURCE		DETECTOR		ANGLE
			TYPE	RANGE	TYPE	RANGE	
E,E/	SPC	0- 35	D	50- 90	MAG-D		DST

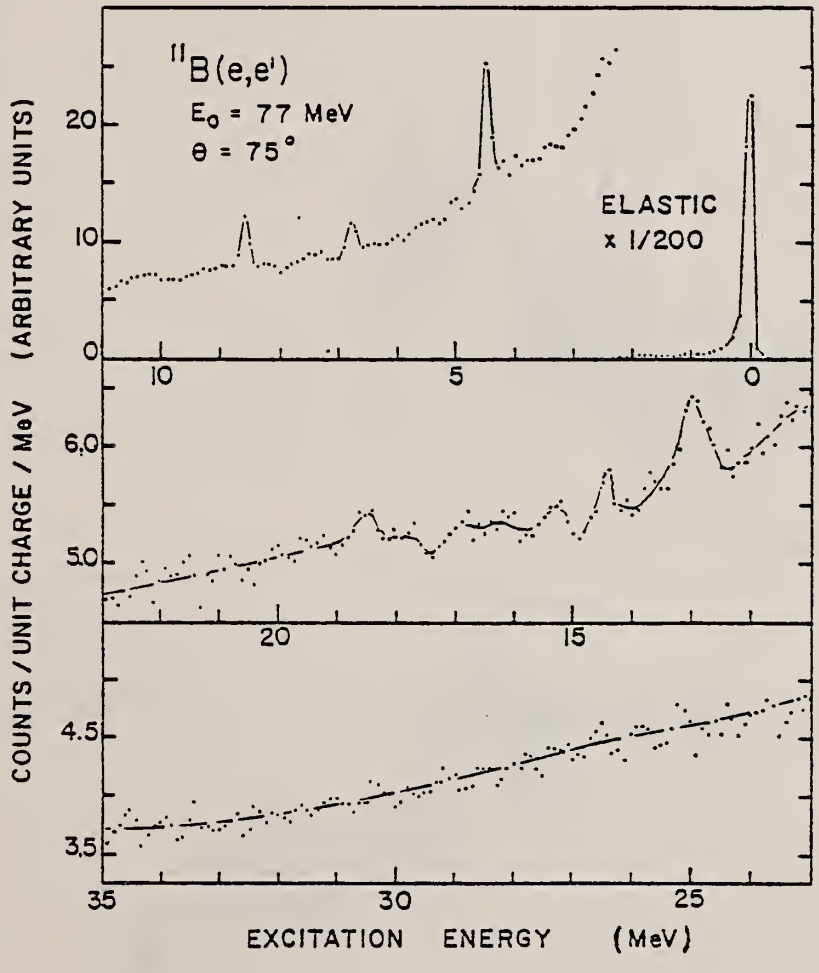

REF. R. J. Hughes and B. M. Spicer
PICNS-73, Vol.I, p.153 Asilomar

ELEM. SYM.	A	Z
B	11	5

METHOD

REF. NO. 73 Hu 12 - hmg

REACTION	RESULT	EXCITATION ENERGY	SOURCE		DETECTOR		ANGLE
			TYPE	RANGE	TYPE	RANGE	
G,XN	ABX	11- 28	C	11- 28	MOD-I		4PI

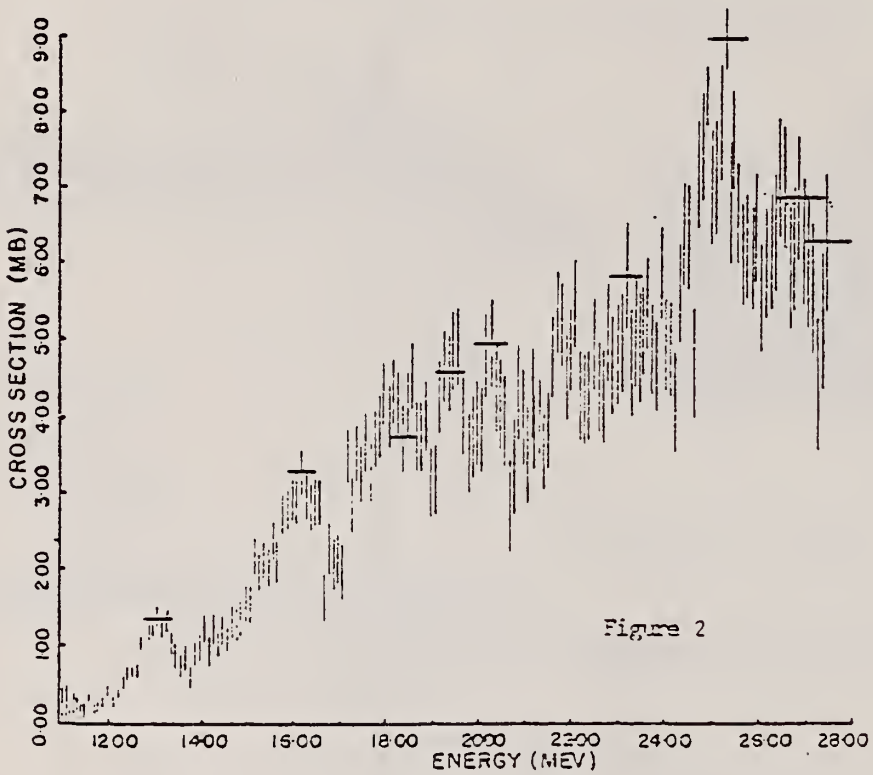

Figure 2

R.J. Hughes and E.G. Muirhead
Nucl. Phys. A215, 147 (1973)

B	11	5

METHOD

REF. NO. 73 Hu 14 egf

REACTION	RESULT	EXCITATION ENERGY	SOURCE		DETECTOR		ANGLE
			TYPE	RANGE	TYPE	RANGE	
G,XN	ABX	11- 28	C	11- 28	BF3-I		4PI

Figures also give comparison with theory. 832

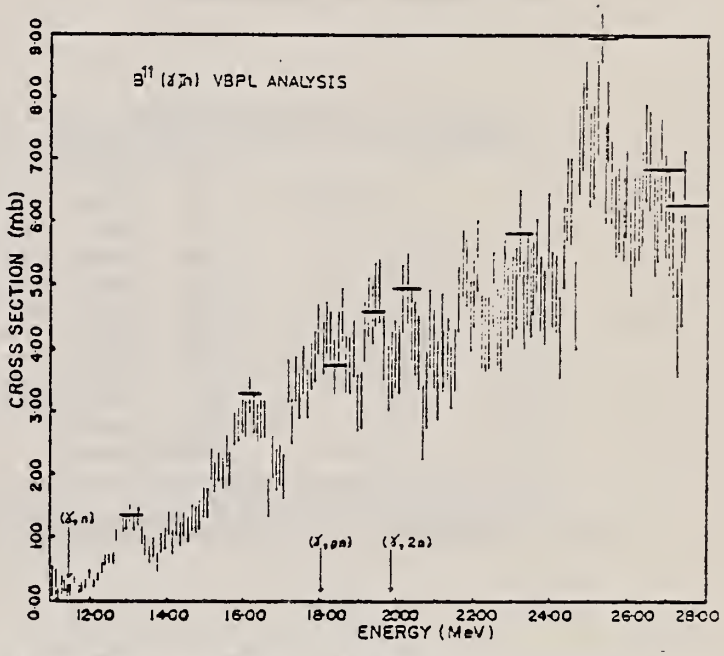

Fig. 2. The total photoneutron cross section of ^{11}B. The horizontal bars indicate the analys resolution at various energies.

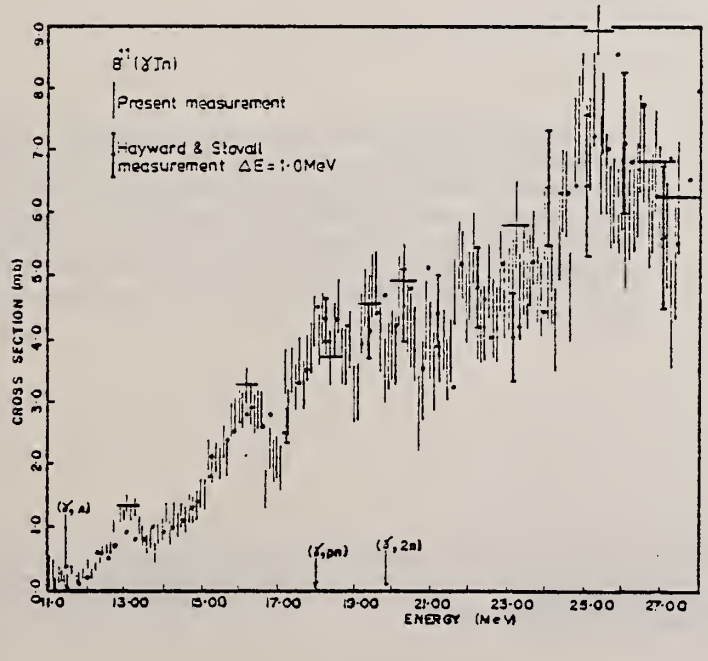

Fig. 5. The photoneutron cross section of ^{11}B.

U.S. DEPARTMENT OF COMMERCE
NATIONAL BUREAU OF STANDARDS

REF.

T. Saito
J. Phys. Soc. Japan 35, 1 (1973)

ELEM. SYM.	A	Z
B	11	5

METHOD

REF. NO. 73 Sa 14 egf

REACTION	RESULT	EXCITATION ENERGY	SOURCE		DETECTOR		ANGLE
			TYPE	RANGE	TYPE	RANGE	
G,G	LFT	2, 4	C	5	NAI-D		120

Self-absorption measurements

2=2.12, 4=4.44

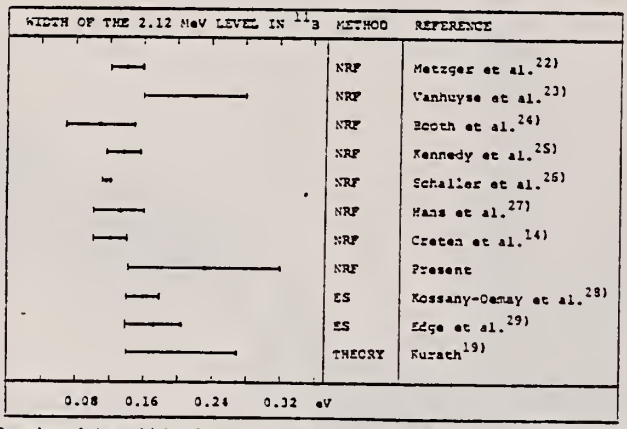

Fig. 7. Results of the width of the 2.12 MeV level in ^{11}B measured by different authors.

The bremsstrahlung beam from a 5 MeV electron linear accelerator was used to excite and study low-lying levels in ^{6}Li, ^{11}B and ^{27}Al. A self-absorption method was used to find the widths Γ of these levels. The following level widths are obtained: $\Gamma=(6.5^{+2.4}_{-1.7})$ eV for the 3.56 MeV level in ^{6}Li; $\Gamma=(0.23\pm0.09)$ eV for the 2.12 MeV level, and $\Gamma=(0.53\pm0.21)$ eV for the 4.44 MeV level in ^{11}B. For the 2.98 MeV level in ^{27}Al, the level width is found to be $\Gamma=(0.10\pm0.04)$ eV assuming that the lower energy member of the doublet at 3 MeV is excited.

REF.

W. Del Bianco, P. Boucher, S. Kundu, and B. Rouben
Can. J. Phys. 52, 92 (1974)

ELEM. SYM.	A	Z
B	11	5

METHOD

REF. NO. 74 De 1 hmg

REACTION	RESULT	EXCITATION ENERGY	SOURCE		DETECTOR		ANGLE
			TYPE	RANGE	TYPE	RANGE	
D,G	ABX	18- 26	D	3- 12	NAI-D		90

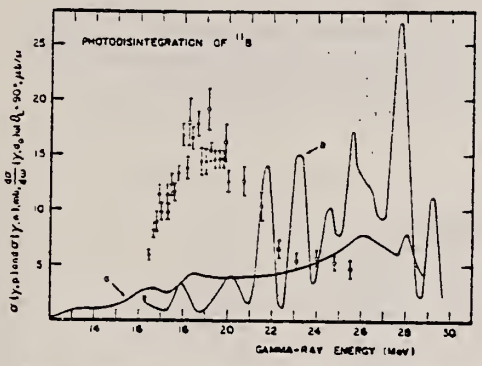

FIG. 1. Photodisintegration of ^{11}B: experimental results. Curve a is the ^{11}B(γ,n)^{10}B cross section of Hayward and Stovall analyzed in 1 MeV bins and curve b is the ^{11}B(γ,p)^{10}Be cross section of Sorokin *et al.* The ^{9}Be(γ,d_0)^{11}B differential cross section at $\theta = 90°$, calculated by means of the principle of detailed balance from the inverse reaction, is given by two sets of data. The closed symbols are the experimental points of Suffert and the open symbols represent the results of this experiment. Note the different units for the ordinate scale of the (γ,d_0) reaction.

W. Del Bianco, S. Kundu, and B. Rouben

REF. Nucl. Phys. A232, 333 (1974)

ELEM. SYM.	A	Z
B	11	5

METHOD

REF. NO. 74 De 4 egf

REACTION	RESULT	EXCITATION ENERGY	SOURCE TYPE	SOURCE RANGE	DETECTOR TYPE	DETECTOR RANGE	ANGLE
D,G	ABX	18- 26	D	3- 12	NAI-D		DST

868

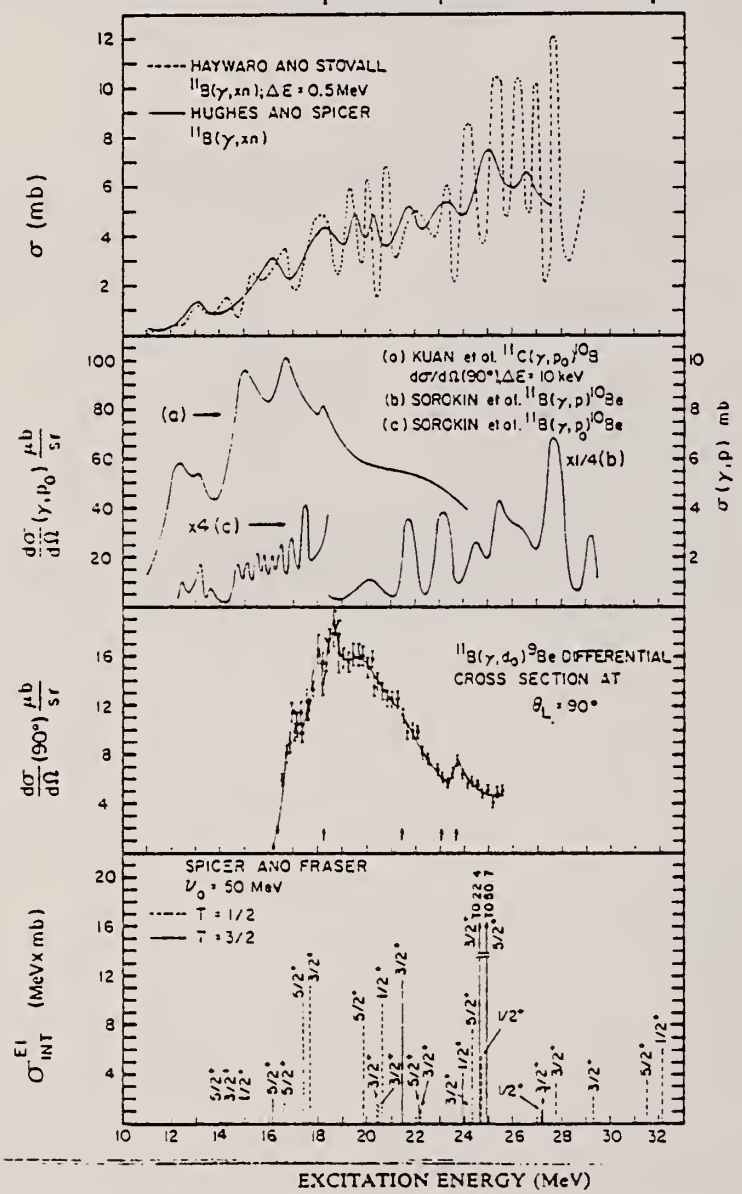

Fig. 9. Comparison of photonuclear cross sections and the particle-hole calculation of ref. [8]). The $^{11}C(\gamma, p_0)^{10}B$ data of Kuan *et al.* [29]) and the $^{11}B(\gamma, d_0)^9Be$ cross section were obtained from the inverse reactions by means of the principle of detailed balance. The $^{11}B(\gamma, d_0)^9Be$ differential cross section at $\theta_L = 90°$ consists of two sets of data. The closed symbols are the experimental points of Suffert [5]) and the open symbols represent the result of this experiment. The solid line was drawn by hand through the experimental points and is intended only as a guide to the eye. In the display of Spicer's calculation [8]) the J^π of the states are shown.

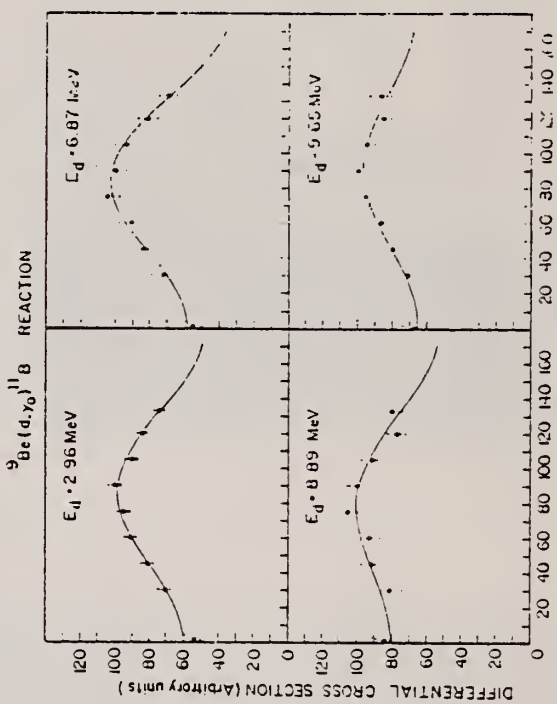

Fig. 6. Angular distributions of the $^9Be(d,\gamma_0)^{11}B$ reaction. The solid symbols are the experimental points and the curves are the results of the least-squares fits.

(over)

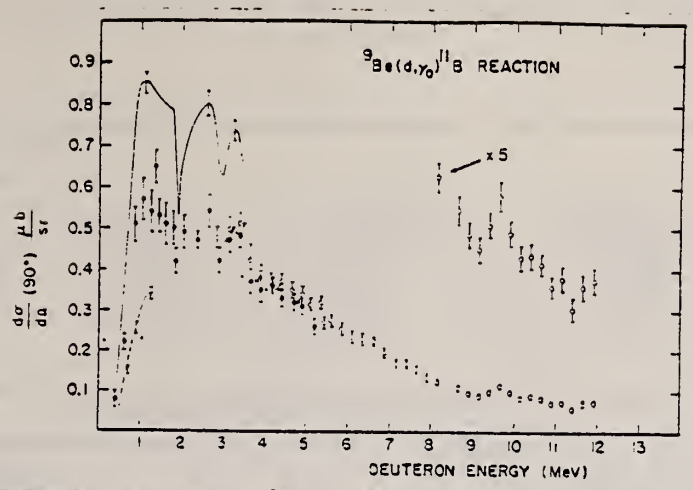

Fig. 5. Differential cross section of the $^{9}Be(d,\gamma_0)^{11}B$ reaction at $\theta_L = 90°$ as a function of deuteron energy. The open symbols are the results of this experiment and the solid symbols the data of Suffert [5]); the dashed and solid curves are average curves drawn through the experimental points of Ziegler *et al.* [6]) and Battleson and McDaniels [7]), respectively. In all instances only statistical errors are indicated and the deuteron energies are the average energies in the Be target.

TABLE 2

Coefficients A_l for the Legendre polynomial expansion of the $^{9}Be(d,\gamma_0)^{11}B$ reaction

E_d (MeV)	E_{exc} (MeV)	A_1/A_0	A_2/A_0
2.96	18.24	0.071±0.018	−0.350±0.026
6.87	21.44	0.136±0.021	−0.439±0.027
8.89	23.09	0.152±0.042	−0.239±0.055
9.65	23.71	−0.012±0.026	−0.231±0.032

[5] M. Suffert, Nucl. Phys. 75 (1966) 226

[6] B. Ziegler, W. Buss and H. Waefller, Nucl. Phys. 83 (1966) 145

[7] K. Battleson and D.K. McDaniels, Phys. Rev. C4 (1971) 1601

[8] B.M. Spicer and R.F. Fraser, Austral. J. Phys. 26 (1973) 729

H.M. Kuan et al. Nucl. Phys. A151 (1970) 129

REF. J. O. Adler, G. G. Jonsson, K. Lindgren
Nucl. Phys. A239, 440 (1975)

ELEM. SYM.	A	Z
B	11	5

METHOD

REF. NO. 75 Ad 2 eef

REACTION	RESULT	EXCITATION ENERGY	SOURCE		DETECTOR		ANGLE
			TYPE	RANGE	TYPE	RANGE	
G,PG	ABY	11-300	C	100-800	SCD-D		135

YIELD TO 3.4 MEV 2+

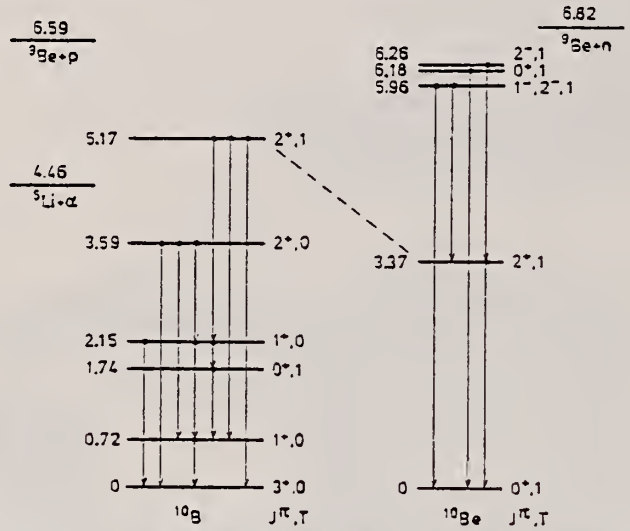

Fig. 2. Level diagrams for ^{10}B and ^{10}Be together with particle emission thresholds. Levels which decay predominantly by particle emission are not shown.

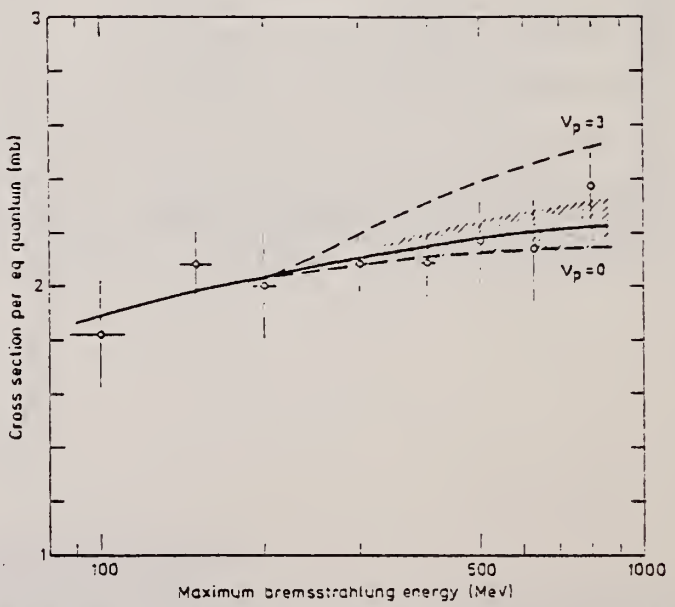

Fig. 3. Measured yields for the reaction ^{11}B(γ, p)^{10}Be* ($J_0^\pi = 2^+$; $E_0 = 3.37$ MeV). The solid curve is a least-squares fit to the experimental points. The shaded area shows the error in the fit of the pion contribution. The curves marked $\nu_p = 0$ and $\nu_p = 3$ give the yields corresponding to no and three effective protons, respectively.

REF. E. D. Arthur, D. M. Drake, I. Halpern
Phys. Rev. Lett. 35, 914 (1975)

ELEM. SYM.	A	Z
B	11	5

METHOD

REF. NO. 75 Ar 5 - hmg

REACTION	RESULT	EXCITATION ENERGY	SOURCE TYPE	SOURCE RANGE	DETECTOR TYPE	DETECTOR RANGE	ANGLE
N,G	NOX	25	D	14	NAI-D		DST
		(25.5)					

Relative yields of capture photons have been observed for four nuclei at angles of 55°, 90°, and 125° in bombardments with 14-MeV neutrons. The yields from ^{10}B, ^{29}Si, and ^{40}Ca show smaller fore-aft anisotropies than those observed in corresponding proton captures. This suggests that the forward peaking in (p,γ) reactions is due mainly to direct rather than collective capture amplitudes. Photons from $^{12}C(n,\gamma_0)^{13}C$ peak backward, but this peaking cannot be straightforwardly accounted for in terms of the interference between the collective excitations dominant in this energy region.

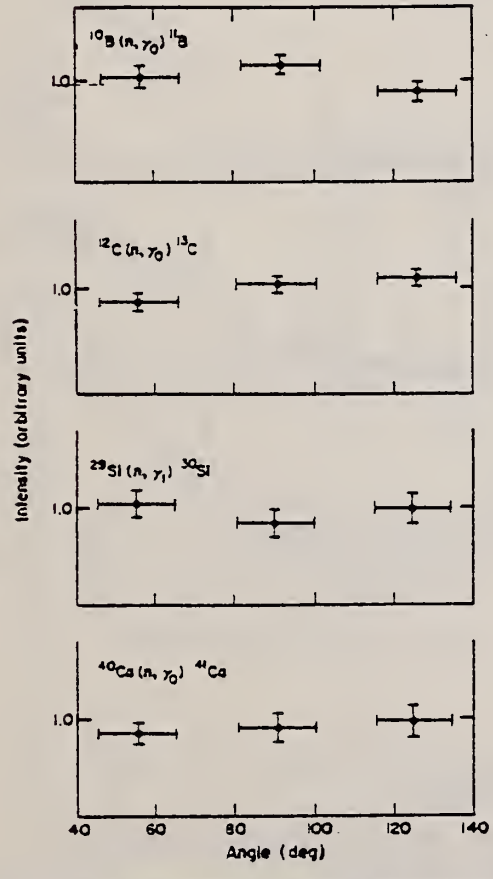

FIG. 3. Angular distributions obtained for 14-MeV neutron capture leading to the designated final states. The horizontal bars show the angular widths subtended by the capture targets.

TABLE I. Angular distribution coefficients.

Reaction	E^a (MeV)	a_2	$R_n = 0.57a_1 - 0.39a_3$	R_p
$^{10}B(n,\gamma_0)^{11}B$	25	-0.44 ± 0.28	0.05 ± 0.08	$^{10}B(p,\gamma_0)^{11}C \sim 0.3^a$
$^{12}C(n,\gamma_0)^{13}C$	18	-0.08 ± 0.18	-0.15 ± 0.06	$^{12}C(p,\gamma_0)^{13}N \sim 0.3^b$
$^{29}Si(n,\gamma_1)^{30}Si$	24	0.2 ± 0.24	0.02 ± 0.1	
$^{40}Ca(n,\gamma_0)^{41}Ca$	22	0.03 ± 0.20	-0.06 ± 0.08	$^{39}K(p,\gamma_0)^{40}Ca \sim 0.2^c$

[a]Ref. 13. [b]Ref. 14. [c]Ref. 15.

[13]H.M. Kuan, Nucl. Phys. A151, 129 (1970).

[14]M. Hasinoff, private communication.

[15]E.M. Diener et al., Phys. Rev. C7, 695 (1973); E.M. Diener et al., Phys. Rev. C7, 705 (1973).

$$W(\theta_{n\gamma}) \sim 1 + \sum_{n=1} a_n P_n.$$

U.S. DEPARTMENT OF COMMERCE
NATIONAL BUREAU OF STANDARDS

REF.

P.T. Kan, G.A. Peterson, D.V. Webb, S.P. Fivozinsky, J.W. Lightbody,Jr., and S. Penner
Phys. Rev. C11, 323 (1975)

ELEM. SYM.	A	Z
B	11	5

METHOD

REF. NO.	
75 Ka1	hmg

REACTION	RESULT	EXCITATION ENERGY	SOURCE		DETECTOR		ANGLE
			TYPE	RANGE	TYPE	RANGE	
E,E/	ABX	0- 34	D	52- 90	MAG-D		DST

LEVELS 2-13

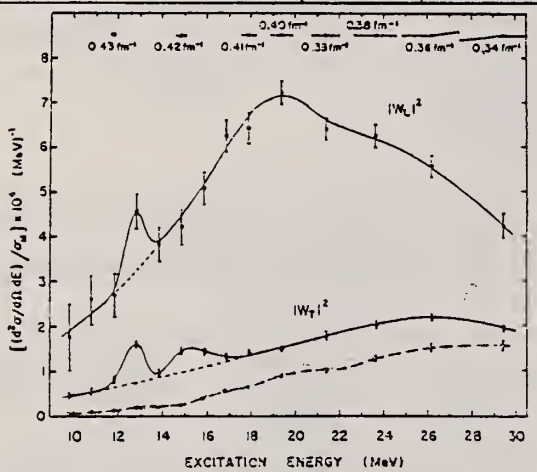

FIG. 5. Separated longitudinal W_L^2, and transverse W_T^2, differential form factors squared (solid circles) and the estimated non-spin-flip transverse component using Siegert's theorem (open circles). The transformed photoabsorption cross section is shown approximated by ^{11}B (γ, n) data (Refs. 5 and 6) normalized to 60% of the TRK dipole sum rule limit (dotted line). The indicated errors are purely statistical.

TABLE I. Bound state cross sections.

Level (MeV)	E_γ (MeV)	θ (deg)	$\frac{d\sigma}{d\Omega}$ (cm^2/sr)
2.12	77	75	$(3.38 \pm 1.6) \times 10^{-31}$
	90	75	$(4.45 \pm 1.7) \times 10^{-32}$
	52.3	145	$(4.95 \pm 0.9) \times 10^{-33}$
	58.9	145	$(5.38 \pm 1.9) \times 10^{-33}$
4.44	77	75	$(1.53 \pm 0.06) \times 10^{-31}$
	90	75	$(1.79 \pm 0.08) \times 10^{-31}$
	52.3	145	$(1.59 \pm 0.07) \times 10^{-32}$
	58.9	145	$(1.46 \pm 0.06) \times 10^{-32}$
5.02	77	75	$(1.99 \pm 0.03) \times 10^{-32}$
	90	75	$(1.42 \pm 0.52) \times 10^{-32}$
	52.3	145	$(1.03 \pm 0.05) \times 10^{-32}$
	58.9	145	$(7.89 \pm 0.42) \times 10^{-33}$
8.57	77	75	$(6.15 \pm 0.33) \times 10^{-32}$
	90	75	$(6.78 \pm 0.30) \times 10^{-32}$
	52.3	145	$(4.55 \pm 0.49) \times 10^{-33}$
	58.9	145	$(4.89 \pm 0.36) \times 10^{-34}$
8.93	77	75	$(1.12 \pm 0.24) \times 10^{-32}$
	90	75	$(1.02 \pm 0.19) \times 10^{-32}$
	52.3	145	$(5.98 \pm 0.52) \times 10^{-33}$
	58.9	145	$(5.43 \pm 0.38) \times 10^{-33}$

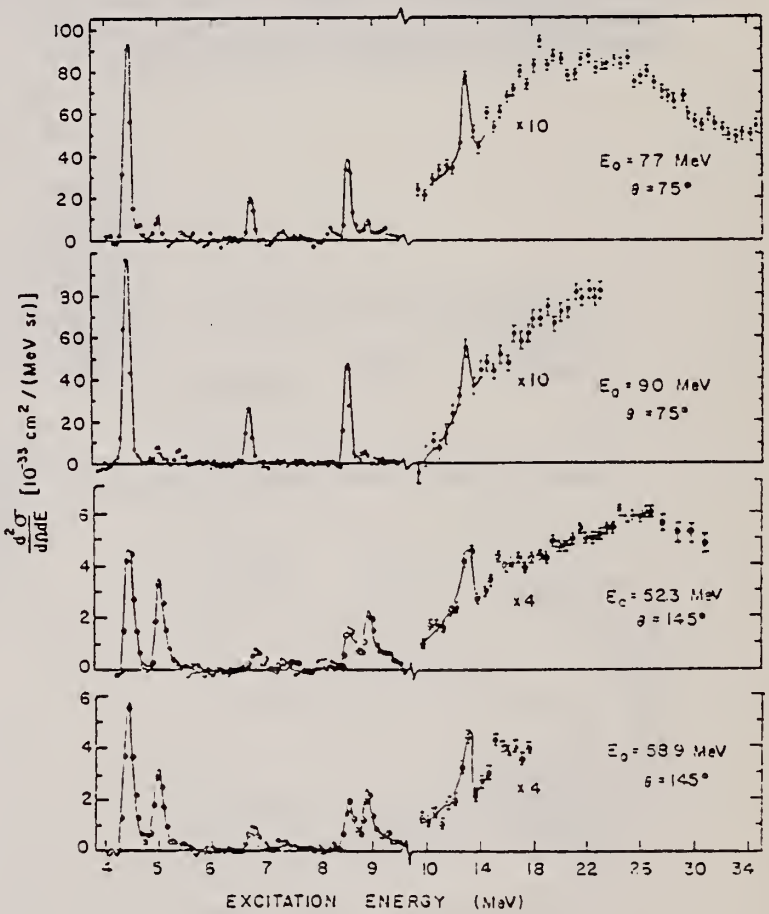

FIG. 3 The radiatively unfolded spectra.

[5] E. Hayward and T. Stovall, Nucl. Phys. 69, 241 (1965).

[6] R.J. Hughes and E.G. Muirhead, Nucl. Phys. A215, 147 (1973).

(over)

TABLE II. Level properties.

Energy (MeV)	J^π, T	Transitions	$B(E/ML\uparrow)$ (e^2 fm^{2L}) This expt.	Other expts.[a]	Γ_γ^0 (eV) This expt.	Γ_γ^0/Γ_W	Other expts.	Theory[b]
2.12	$\frac{1}{2}^-$, $\frac{1}{2}$	$M1$	$(6.8 \pm 2) \times 10^{-3}$		0.14 ± 0.04	0.70	0.16 ± 0.02[a]	0.09–0.11
							0.23 ± 0.09[c]	
1.41	$\frac{5}{2}^-$, $\frac{1}{2}$	$M1$	$(1.20 \pm 0.12) \times 10^{-2}$	$(1.07 \pm 0.10) \times 10^{-2}$	0.73 ± 0.07	0.39	0.63 ± 0.07[a]	0.79–0.81
							0.53 ± 0.21[c]	
							0.60 ± 0.20[d]	
		$E2$	21.3 ± 2.0	18.3 ± 1.3	$(2.0 \pm 0.2) \times 10^{-2}$	9.7	$(1.71 \pm 0.16) \times 10^{-2}$[a]	
5.02	$\frac{3}{2}^-$, $\frac{1}{2}$	$M1$	$(1.60 \pm 0.16) \times 10^{-2}$	$(1.38 \pm 0.05) \times 10^{-2}$	2.12 ± 0.21	0.80	1.82 ± 0.08[a]	1.9–2.0
							2.42 ± 0.76[d]	
8.57	$\frac{3}{2}^-$, $\frac{1}{2}$	$M1$	$(1.7 \pm 0.2) \times 10^{-3}$		0.73 ± 0.07	0.06	0.72 ± 0.30[a]	0.03–0.17
		$E2$	9.37 ± 0.15	10.05 ± 1.6	0.23 ± 0.03	4.2	0.4 ± 0.1[a]	
8.93	$\frac{5}{2}^-$, $\frac{1}{2}$	$M1$	$(9.9 \pm 1) \times 10^{-3}$	$(8.1 \pm 0.8) \times 10^{-3}$	4.93 ± 0.50	0.33	4.0 ± 0.6[a]	3.2–4.6
							5.0 ± 1.2[d]	
13.0[e]	$\frac{1}{2}^-$, $(\frac{1}{2})$	$M1$	$(7.9 \pm 2) \times 10^{-3}$		36 ± 7	0.78	29 ± 8[f]	15–19
	$\frac{1}{2}^-$, $(\frac{1}{2})$				18 ± 4	0.39		17–19
	$\frac{1}{2}^-$, $(\frac{3}{2})$	$E2$	3.6 ± 0.5		2.2 ± 0.2	5.0		
	$\frac{3}{2}^-$, $(\frac{3}{2})$				1.1 ± 0.1	2.5		

[a] Reference 17.
[b] Reference 26. Range of values resulting from different parametrizations of the two-body matrix elements.
[c] Reference 31.
[d] Reference 21.
[e] Above breakup thresholds.
[f] References 22 and 25.

[17] E. Spamer, Z. Phys. 191, 24 (1966); E. Spamer and H. Artus, ibid. 198, 445 (1967).

[21] P. Kossanyi-Demay and G.J. Vanpraet, Nucl.Phys. 81, 229 (1966).

[22] D.R. Goosman, E.G. Adelberger, and K.A. Snover, Phys. Rev. C1, 123 (1970).

[25] D.R. Goosman and R.W. Kavanagh, Phys. Rev. C7, 1717 (1973).

[26] S. Cohen and D. Kurath, Nucl. Phys. 73, 1 (1965).

[31] T. Saito, J. Phys. Soc. Jap. 35, 1 (1973).

REF. V. D. Epaneshnikov, V. M. Kuznetsov, O. I. Stukov
Yad. Fiz. 23, 249 (1976)
Sov. J. Nucl. Phys. 23, 129 (1976)

ELEM. SYM.	A	Z
B	11	5

METHOD

REF. NO. 76 Ep 4 hmg

REACTION	RESULT	EXCITATION ENERGY	SOURCE		DETECTOR		ANGLE
			TYPE	RANGE	TYPE	RANGE	
G,P-	ABX	150-400	C	180-400	ACT-I		4PI

The activation method has been used to measure the yields of the reactions $^{28}Si(\gamma,\pi^-)^{28}P$ and $^{11}B(\gamma,\pi^-)^{11}C$ from the π-meson production threshold to 400 MeV. The results obtained are in satisfactory agreement with theoretical calculations based on the model of surface production of mesons.

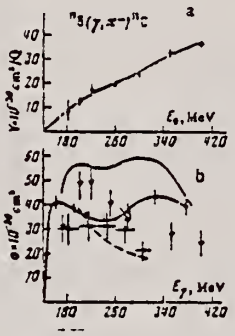

FIG. 2. Yield curve (a) and total cross sections (b) for the reaction $^{11}B(\gamma,\pi^-)^{11}C$. The dashed curve shows the theory of Ref. 10, and the solid curve that of Ref. 11; the solid circles are the data obtained by us (they are joined by a smooth curve), the hollow circles are the data of Ref. 2, and the triangles are data from the Ukrainian Physicotechnical Institute at Khar'kov.

[2] I .S. Hughes et al., Proc. Phys. Soc. (London) A72, 259 (1958).
[10] E.W. Laing and R.G. Moorhouse, Proc. Phys. Soc. (London) 70, 629 (1957).
[11] V. Devanathan et al., Phys. Lett. 25B, 456 (1967).

REF. U. Kneissl, K. H. Leister, H. O. Neidel, A. Weller
Nucl. Phys. A264, 30 (1976)

ELEM. SYM.	A	Z
B	11	5

METHOD

REF. NO. 76 Kn 3 - egf

REACTION	RESULT	EXCITATION ENERGY	SOURCE		DETECTOR		ANGLE
			TYPE	RANGE	TYPE	RANGE	
G,XN *	ABX	10- 35	D	10- 35	MOD-I		4PI
G,2N **	ABX	16- 35	D	16- 35	MOD-I		4PI

$\sigma_o(35)_{xn}$ = 84±0.7 MeV-mb *1050

$\sigma_o(35)_{sn}$ = 69.1±8 MeV-mb **1051

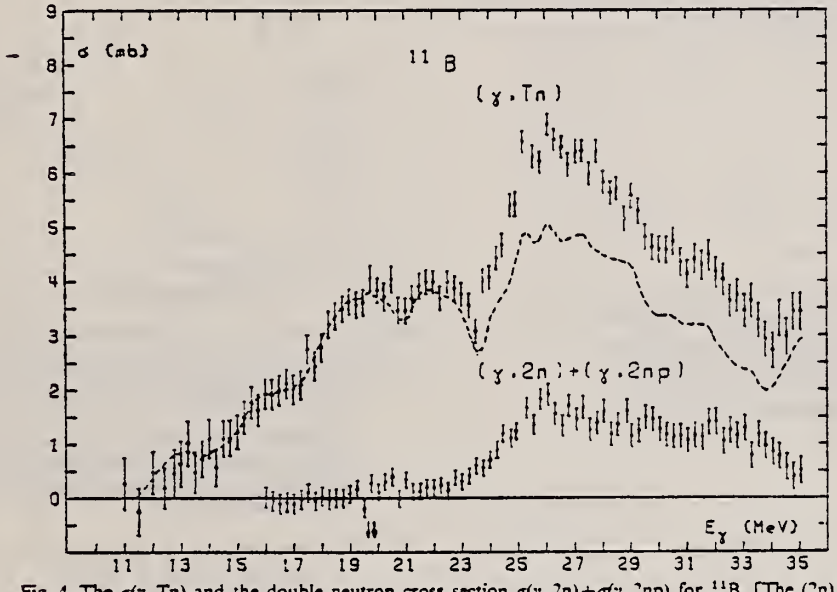

Fig. 4. The $\sigma(\gamma, Tn)$ and the double neutron cross section $\sigma(\gamma, 2n)+\sigma(\gamma, 2np)$ for ^{11}B. [The (2n) and (2n, p) thresholds at 19.9 and 19.6 MeV respectively are indicated by arrows.] The dashed line represents $\sigma(\gamma, n_{tot}) = \sigma(\gamma, n)+\sigma(\gamma, np)+\sigma(\gamma, 2n)+\sigma(\gamma, 2np)$.

REF.		ELEM. SYM.	A	Z
	K. Min, P. Stoler, S. Trentalange, E.J. Winhold, P.F. Yergin, A.M. Bernstein, W. Turchinetz, K.S.R. Sastry Phys. Rev. C14, 807 (1976)	B	11	5

METHOD	REF. NO.	
	76 Mi 7	hmg

REACTION	RESULT	EXCITATION ENERGY	SOURCE		DETECTOR		ANGLE
			TYPE	RANGE	TYPE	RANGE	
G,PI-	ABX	142-169	C	120-170	ACT-I		4PI

Yields for the $^{11}B(\gamma,\pi^-)$ reaction have been measured between its threshold at 142.0 MeV and 169 MeV by observing the residual ^{11}C activity. The reaction was initiated by thin-radiator bremsstrahlung. Measurements were made in 1 MeV steps up to 150 MeV, and in larger steps above this. The present results are consistent with previous data for this reaction obtained at higher energies. The cross section values near threshold deduced from the data are compared to recent preliminary theoretical values.

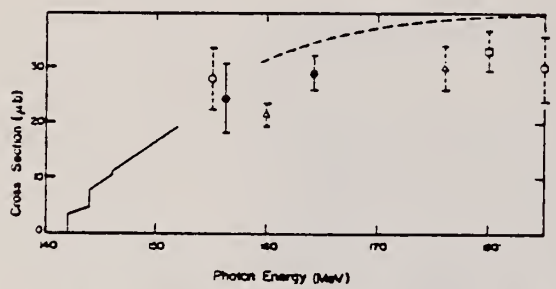

FIG. 9. The solid line and solid points are the present cross section results. The two open circle points are the results of Hughes and March (Ref. 3), the two open triangle points are the results of Dyal and Hummel (Ref. 4), the dashed curve is from the work of Nydahl and Forkman (Ref. 6), while the open square point is due to Noga *et al*. (Ref. 7).

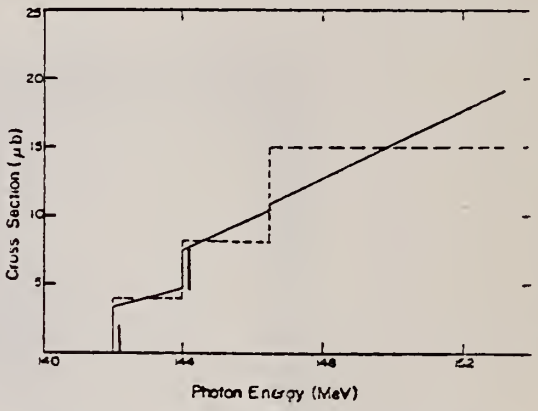

FIG. 8. The solid curve is the best-fit three-step cross section taking the same slope per unit height as that measured (Ref. 11) for the $^{12}C(\gamma,\pi^-)$ ground state transition. The vertical bars are the preliminary theoretical results of Koch and Donnelly (Ref. 21). The dashed curve is the best-fit three-step cross section with horizontal steps.

[3] I.S. Hughes and P.V. March, Proc. Phys. Soc. (London) 72, 259 (1958).

[4] P. Dyal and J.P. Hummel, Phys. Rev. 127, 2217 (1962).

[6] G. Nydahl and B. Forkman, Nucl. Phys. B7, 97 (1968).

[7] V.I. Noga et al., Yad. Fiz. 14, 904 (1971) (Sov. J. Nucl. Phys. 14, 506 (1972).

[11] A.M. Bernstein et al., Phys. Rev. Lett. (to be published).

[21] J.H. Koch and T.W. Donnelly (priv.comm.).

REF. V. Di Napoli, J. B. Martins, G. Rosa, F. Salvetti, O. A. P. Tavares, M. L. Terranova and H. G. De Carvalho
J. Inorg. Nucl. Chem. 40, 1619 (1978)

ELEM. SYM.	A	Z
B	11	5

METHOD

REF. NO. 78 Di 10 - hg

REACTION	RESULT	EXCITATION ENERGY	SOURCE		DETECTOR		ANGLE
			TYPE	RANGE	TYPE	RANGE	
G,Be7	ABY	33(33.02)-999	C	300-999	ACT-I		4PI

999=1 GEV

Abstract—Mean cross sections for the photoproduction of ^{7}Be and ^{11}C from ^{19}F, ^{27}Al, ^{28}Si and ^{32}S targets, ^{7}Be from ^{10,11}B, and ^{11}C from ^{14}N and ^{16}O targets have been measured using bremsstrahlung beams in the energy range 0.3–1.0 GeV. The results have been compared with previous measurements and an excellent agreement has been found. In most cases, the values obtained turned out to be much larger than those expected from a simple spallation mechanism. A fragmentation and/or a fission-like process has been suggested in explaining the mechanism of such reactions.

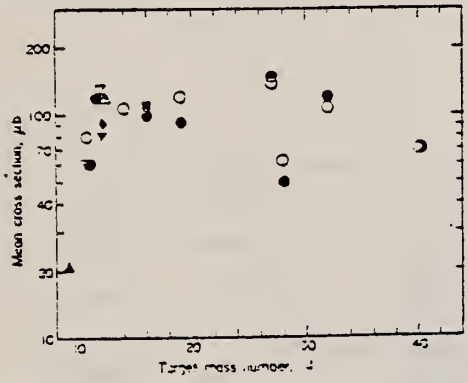

Fig. 2. The same as in Fig. 1 for ^{7}Be photoproduction. Experimental data are taken from: ▲, Refs. [6,7]; ▽, Ref. [8]; ●, Ref. [9]; △, Ref. [10]; ◆, Ref. [11]; ▼, Ref. [12]; □, Ref. [13]; ■, Ref. [14]; ◇, Ref. [2]; ○, present work.

Table 2. Cross sections per equivalent quantum of ^{7}Be photoproduction

ε_0 (GeV)	Cross Section, σ_Q (μb)						
	^{10,11}B	^{14}N	^{16}O	^{19}F	^{27}Al	^{28}Si	^{32}S
0.30	150±20	200±20	113±20	152±20	40±20	20±20	50±20
0.32	160±20	200±20	120±20	150±20	45±20	30±20	54±20
0.35	160±20	210±20	130±20	159±20	42±20	30±20	60±20
0.40	175±20	226±20	145±20	170±20	98±20	20±20	70±20
0.48	190±20	245±20	163±20	186±20	100±20	50±20	140±20
0.55	200±20	260±20	187±20	200±20	93±20	48±20	90±20
0.65	220±20	280±20	197±20	214±20	140±20	68±20	130±20
0.75	225±20	300±20	215±20	227±20	180±20	70±20	130±20
0.90	240±20	318±20	230±20	245±20	166±20	88±20	165±20
1.01	250±20	330±20	242±20	260±20	200±20	97±20	190±20

Table 3. Comparison between experimentally determined and calculated cross sections of ^{7}Be and ^{11}C photoproduction and indication of the dominant reaction channels

Target Nucleus	Product Nucleus	Nominal Nucleon Loss, ΔA (x100)	$\bar{\sigma}_{exp}$ (*) (μb)	$\bar{\sigma}_{CDHO}$ (**) (μb)	$\frac{\bar{\sigma}_{exp}}{\bar{\sigma}_{CDHO}}$	Apparent Threshold (Exp.) ε_{th} (MeV)	Possible Mechanism of Production
^{10,11}B	^{7}Be	(1).	(20).35	67	28	2	≤ 50	Spallation
^{12}C	^{7}Be	5	42	110	20	5	≤ 50	Spallation
^{14}N	^{7}Be	7	50	108	12	9	≤ 50	Fission Spallation
^{14}N	^{11}C	3	21	130	60	2	≤ 50	Spallation
^{16}O	^{7}Be	9	56	107	8	13	50<ε_{th}<200	Fission Fragmentation
^{16}O	^{11}C	5	31	117	33	3	≤ 50	Spallation
^{19}F	^{7}Be	12	63	106	5	21	50<ε_{th}<200	Fission Fragmentation
^{19}F	^{11}C	8	42	105	16	7	50<ε_{th}<200	Fission Fragmentation Spallation
^{27}Al	^{7}Be	20	74	142	2	71	> 200	Fragmentation
^{27}Al	^{11}C	16	59	70	5	14	50<ε_{th}<200	Fission Fragmentation
^{28}Si	^{7}Be	21	75	56	2	28	> 200	Fragmentation
^{28}Si	^{11}C	17	61	68	4	17	50<ε_{th}<200	Fission Fragmentation
^{32}S	^{7}Be	25	78	114	2	57	> 200	Fragmentation
^{32}S	^{11}C	21	66	68	3	23	50<ε_{th}<200	Fission Fragmentation
^{35,37}Cl	^{11}C	24.(26)	69.(70)	59	3	30	50<ε_{th}<200	Fission Fragmentation
^{40}Ca	^{7}Be	33	83	70	1	70	> 200	Fragmentation
^{40}Ca	^{11}C	29	73	70	2	35	> 200	Fragmentation

(*) Mean values of the different measurements (see Figs. 1 and 2).

(**) Calculated values according to Ref. [9].

REF. N. Kumagai, G. Isoyama, E. Tanaka, K. Kageyama, T. Ishimatsu
Nucl. Inst. Meth. 157, 423 (1978)

ELEM. SYM.	A	Z
B	11	5

METHOD

REF. NO. 78Ku13 hg

REACTION	RESULT	EXCITATION ENERGY	SOURCE TYPE	SOURCE RANGE	DETECTOR TYPE	DETECTOR RANGE	ANGLE
G,G	LFT	2-9 (2.125-8.920)	C	15	SCD-D		125

RESONANCE SELF-ABSOR

The radiative widths of the 2.125, 4.445, 5.020, 7.285 and 8.920 MeV levels in ^{11}B were determined rather accurately by the resonance fluorescence self-absorption method using bremsstrahlung from a betatron. The results are very useful for the calibration of the bremsstrahlung spectrum multiplied by the detection efficiency $N(E_\gamma)\cdot\varepsilon(E_\gamma)$, which is necessary in the determination of level widths by the resonance fluorescence scattering method which is far more versatile than the self-absorption method. An example using such a procedure is given of determining the 8.091 MeV level of ^{52}Cr.

TABLE I
Level widths of ^{11}B determined by the present experiment[a].

Level energy (MeV ± keV)	J^π	$\Gamma_{\gamma_0}/\Gamma_\gamma$	Transmission	Γ_γ (eV)	Γ_γ (eV)
2.125 ± 0.4	1/2⁻	1.0	0.642 ± 0.053	0.10 ± 0.03	
			0.622 ± 0.070	0.11 ± 0.04	0.11 ± 0.02
			0.780 ± 0.049	0.11 ± 0.04	
4.445 ± 0.5	5/2⁻	1.0	0.511 ± 0.025	0.58 ± 0.06	
			0.530 ± 0.030	0.55 ± 0.06	0.58 ± 0.04
			0.694 ± 0.028	0.65 ± 0.09	
5.020 ± 0.6	3/2⁻	0.83 ± 0.01	0.477 ± 0.024	$1.88^{+0.22}_{-0.17}$	
			0.516 ± 0.031	$1.58^{+0.24}_{-0.19}$	1.80 ± 0.13
			0.680 ± 0.027	$1.92^{+0.31}_{-0.26}$	
7.285 ± 1.5	5/2⁻	0.87 ± 0.02	0.746 ± 0.059	$1.06^{+0.41}_{-0.34}$	
			0.728 ± 0.065	$1.20^{+0.46}_{-0.43}$	1.17 ± 0.26
			0.849 ± 0.054	$1.23^{+0.66}_{-0.58}$	
8.920 ± 2.0	5/2⁻	0.95 ± 0.01	0.574 ± 0.036	$4.52^{+0.84}_{-0.72}$	
			0.620 ± 0.049	$3.66^{+0.96}_{-0.88}$	4.20 ± 0.52
			0.768 ± 0.37	$4.20^{+1.15}_{-1.00}$	

[a] The level energy, spin, parity and branching ratio ($\Gamma_{\gamma_0}/\Gamma_\gamma$) were taken from ref. 4 except for the branching ratio of the 5.020 MeV level obtained from our measurement.

REF. I.M. Kapitonov, E.V. Lazutin, V.I. Mokeev, E.S. Omarov, I.M. Piskarev
Yad. Fiz. 30, 1175 (1979)
Sov. J. Nucl. Phys. 30, 609 (1979)

ELEM. SYM.	A	Z
B	11	5

METHOD

REF. NO.	-
79 Ka 8	hg

REACTION	RESULT	EXCITATION ENERGY	SOURCE		DETECTOR		ANGLE
			TYPE	RANGE	TYPE	RANGE	
G,NG	SPC	THR-30	C	30	SCD-D		135
G,PG							

DE-EXCIT GAMMA RAYS

The inelastic scattering of gamma rays by the ^{11}B nucleus is studied experimentally with a Ge(Li) detector, in order to investigate the wave function of highly excited states of a nucleus with an unfilled shell. The 1.02-MeV gamma line is observed for the first time in this reaction. It is suggested that states with isospin $T_<$ and $T_>$ can both contribute to the photoneutron cross section.

PACS numbers: 25.20. + y, 27.20. + n

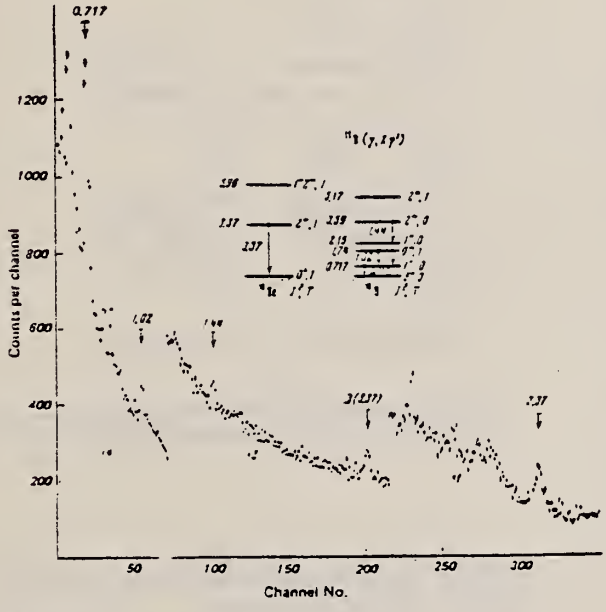

FIG. 1.

REF. V. N. Polishchuk, N. G. Shevchenko, N. G. Afanas'ev, A. Yu. Buki, A. A. Khomich
Yad. Fiz. 29, 582 (1979)
Sov. J. Nucl. Phys. 29, 297 (1979)

ELEM. SYM.	A	Z
B	11	5

METHOD

REF. NO. 79Po8 - hg

REACTION	RESULT	EXCITATION ENERGY	SOURCE		DETECTOR		ANGLE
			TYPE	RANGE	TYPE	RANGE	
E,E/	FMF	4-13	D	121-250	MAG-D	108-246	DST
		(4.4-13.)					

Inelastic electron scattering has been used to measure the Coulomb form factors of the excited states of the ^{11}B nucleus at excitation energies ω = 4.4, 6.7, 8.5, 8.9, and 13 MeV. The measurements were made at initial electron energies E_0 = 121, 186, and 250 MeV in the momentum-transfer region q' = 0.7–1.6 F^{-1}. The data obtained for discrete low-lying levels are discussed in terms of the excited-core model, and the resonances beyond threshold are discussed in terms of a diagram model of nuclear excitation.

DEL Q 0.7-1.6 FM-1

PACS numbers: 25.30.Cg, 27.20. + n

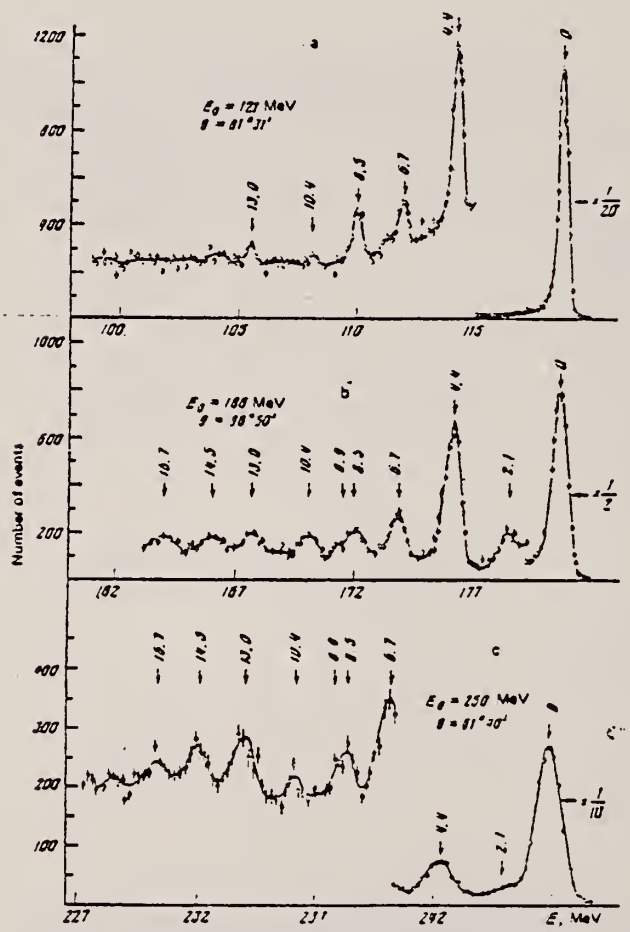

FIG. 1. Spectra of electrons inelastically scattered by ^{11}B at initial energies E_0 and scattering angles θ.

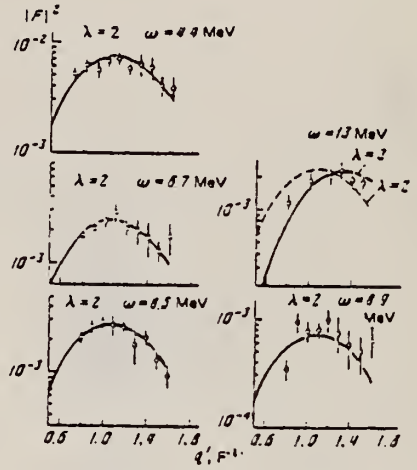

FIG. 2. Inelastic form factors for excited states of the ^{11}B nucleus as a function of momentum transfer.

TABLE I. Reduced probabilities $B(E\lambda)\uparrow$ and level widths Γ_γ for excited states in the ^{11}B nucleus.

E, MeV	J^π	λ	$B(E\lambda)\uparrow$, $e^2F^{2\lambda}$			Γ_γ, eV		
			Our data	Ref. 12	Ref. 11	Our data	Ref. 11	Ref. 12
4.44	1/2⁻	2	23.1±1.8	21.3±2.0	18.3±1.3	(2.14±0.07)·10⁻³	(1.71±0.16)·10⁻³	(2.0±0.2)·10⁻³
6.77	3/2⁻	2	7.81±0.32			(4.44±0.18)·10⁻³		
8.56	5/2⁻	2	8.80±0.36	9.37±0.15	10.08±1.6	0.32±0.02	0.4±0.1	0.23±0.03
8.92	1/2⁻	2	2.35±0.09			(7.16±0.08)·10⁻³	(16⁺⁴₋₆)·10⁻³	
		3	22.4±2.4					

DEFINITIONS OF ABBREVIATIONS AND SYMBOLS

Note: In this list definitions are given for various photoneutron reactions in which the following symbols are used: N, NL, nN, SN and XN. Corresponding definitions apply for reactions involving other nuclear particles where the symbols N (neutron) is replaced by, e.g. P, D, T, HE, A etc. Where unknown reactions result in the production of a specific radionuclide, the chemical symbol and mass number is listed as the reaction product, e.g. a G,NA22 reaction in ^{59}Co.

A	alpha particle
ANAL	analysis
ABI	absolute integrated cross-section data
ABX	absolute cross-section data
ABY	absolute yield data. Often means cross-section per equivalent quantum is listed.
ACT	measurement of induced radioactivity of the target
ASM	asymmetric, asymmetry
AVG	average
BBL	bubble chamber
BEL B(EL)	reduced electric radiative transition probability
BF3	BF_3 neutron counter with moderator e.g., Halpern detector, long counter
BML	reduced magnetic radiative transition probability, B(ML)
BREAKS	levels located by "breaks" in the yield curve
BRKUP	breakup
BRMS	bremsstrahlung
BTW	between
C	continuous. Used to describe a photon source or a detector response function. Contrast with D = discrete.
CCH	cloud chamber
CF	compared with
CHRGD	charged
CMPT	Compton
COIN COINC	coincidence, coincide
COH	coherent
CK	Cerenkov
D	deuteron or discrete. When discrete, it is used to describe a photon source or a detector response function. Contrast with C = continuous.
DLTE	energy loss
DLTQ	momentum transfer
DST	distribution
DT BAL	detailed balance
E	electron
E/	inelastically scattered electron
E+	positron
EDST	energy distribution or spectrum
E/N	used only to indicate a coincidence experiment as in (E,E/N).

	N stands for any outgoing particle measured in coincidence with an inelastically scattered electron. Distinguish from eg., (E,N) which is used to represent an electron induced reaction when only the outgoing particle N is detected.
EMU	emulsions (photographic plates)
EXCIT	excited
F	fission
FMF	form factor
FM-1	inverse femtometers
FRAG	fragment
G	photon
G/	inelastically scattered photon
G-WIDTH	gamma-ray transition width
HAD	hadrons, hadron production
HE He3	^{3}He particle
INT	interaction, integral, intensity
INC	includes
ION	ionization chamber
ISOB	isobaric
ISM	isomer
J	multiplicity of particle defined by following symbol e.g. (G,PJN) with remark J = 2,3,5,7
JPI J-PI	spin and parity of a nuclear state
K	second multiplicity index, e.g. (G,JPKN) with both J & K positive integers greater than 1
KE	kinetic energy
L	may be an integer or zero that always follows a reaction product symbol. This is used to indicate transitions to specific states in the residual nuclide. When the letter is used as in (G,NL) the cross section given is that for the sum of transitions to two or more specific final states.
LFT	excited state lifetime
LIM	limit
LV,LVS	level, levels
LQD	liquid
MAG	magnetic spectrometer
MEAS	measurement(s)
MGC	magnetic Compton spectrometer
MGP	magnetic pair spectrometer
MOD	moderated neutron detector not employing a BF_3 counter, e.g. rhodium foil, Szilard-Chalmers reaction, ^{3}He, ^{6}Li reactions, GD loaded liquid scintillator, etc.
MSP	mass spectrometer
MULT	multiple, multipole, multiplicity
MU-T	used only in combination with G to indicate a total photon absorption cross section measurement, i.e. (G,MU-T)
N	neutron (see also XN and SN). The notation (G,N) is used to indicate a reaction in which only a single neutron is emitted, i.e. the reaction that can, in many cases, be measured by observing the radioactive decay of the residual nuclide.

nN	where n is any integer. (G,nN) indicates the sum over all reaction cross sections in which n neutrons are emitted.
NAI	NaI(Tl) spectrometer
NEUT	neutron(s)
NOX	no cross-section data
P	proton (see also XP)
PART	particle(s)
PHOT	photon(s)
PI	pion, usually written as PI+, PI-, PI0 to indicate charge
POL	polarized or polarization
Q-SQUAR	momentum transfer squared (q^2)
RCL	recoil
REL	relative
RLI	relative integrated cross-section data
RLX	relative cross-section data
RSP	reaction spectrometer
RLY	relative yield data
SCTD	scattered
SCD	semiconductor (solid state) detector
SCI	scintillator detector other than NaI, e.g., CsI, KI, organic (liquid or solid), stilbene, He
SEP	separation
SEP ISOTP	separated isotope used
SIG	SIGMA (cross section)
SN	sum of neutron producing reactions, $\sigma(\gamma,SN)=\sigma(\gamma,N) + \sigma(\gamma,NP) + \sigma(\gamma,2N) + \sigma(\gamma,3N)$ + etc.
SPC	photon or particle energy spectrum
SPK	spark chamber
SPL	spallation
STAT	statistical
SYM	symetric, symmetry
T	triton
TEL	counter telescope
THR	threshold for reaction or threshold detector, e.g., $^{29}Si(n,p)^{29}Al$.
TOF	time-of-flight detector
TRK	tracks of particles or fragments observed in solid materials (glass, mylar, etc.)
TRNS	transition
UKN UNK	unknown
VIB	vibrational
VIR PHOT	virtual photon(s)
XN	all neutrons, total neutron yield, $\sigma(\gamma,XN) = \sigma(\gamma,N) + 2\sigma(\gamma,2N) + 3\sigma(\gamma,3N) + \sigma(\gamma,NP)$ + etc.
XP	all protons, total proton yield $\sigma(\gamma,XP) = \sigma(\gamma,P) + \sigma(\gamma,NP) + 2\sigma(\gamma,2P)$ + etc.
XX XXX	reaction products defined in REMARKS
YLD	yield

4PI	a 4π geometry was used or a method like radioactivity or a total absorption measurement		products was determined. The polarized particle is indicated in REMARKS.
999	energy defined in REMARKS	* or @	symbols used to indicate that the units associated with the numerals on one or both sides of the symbol in a specific column are not MeV. The units are defined in REMARKS.
$	indicates the measurement involved beams or targets that were either polarized or aligned, or that the polarization of the reaction		

NBS-114A (REV. 2-8C)

U.S. DEPT. OF COMM. BIBLIOGRAPHIC DATA SHEET (See instructions)	1. PUBLICATION OR REPORT NO. NBSIR 83-2742	2. Performing Organ. Report No.	3. Publication Date October 1983

4. TITLE AND SUBTITLE

Photonuclear Data-Abstract Sheets
1955-1982

5. AUTHOR(S)

E.G. Fuller and Henry Gerstenberg

6. PERFORMING ORGANIZATION (If joint or other than NBS, see instructions)

NATIONAL BUREAU OF STANDARDS
DEPARTMENT OF COMMERCE
WASHINGTON, D.C. 20234

7. Contract/Grant No.

8. Type of Report & Period Covered

9. SPONSORING ORGANIZATION NAME AND COMPLETE ADDRESS (Street, City, State, ZIP)

10. SUPPLEMENTARY NOTES

☐ Document describes a computer program; SF-185, FIPS Software Summary, is attached.

11. ABSTRACT (A 200-word or less factual summary of most significant information. If document includes a significant bibliography or literature survey, mention it here)

These abstract sheets cover most classes of experimental photonuclear data leading to information of the electromagnetic matrix element between the ground and excited states of a given nucleus. This fifteen volume work contains nearly 7200 abstract sheets and covers 89 chemical elements from hydrogen through americium. It represents a twenty-seven year history of the study of electromagnetic interactions. The sheets are ordered by target element, target isotope, and by an assigned bibliographic reference code. Information is given on the type of measurement, excitation energies studied, source type and energies, detector type, and angular ranges covered in the measurement. For a given reference, the relevant figures and tables are mounted on a separate sheet for each nuclide studied.

12. KEY WORDS (Six to twelve entries; alphabetical order; capitalize only proper names; and separate key words by semicolons)

data-abstract sheets, elements, experimental, isotopes, nuclear physics, photonuclear reactions

13. AVAILABILITY

☐ Unlimited

☒ For Official Distribution. Do Not Release to NTIS

☐ Order From Superintendent of Documents, U.S. Government Printing Office, Washington, D.C. 20402.

☐ Order From National Technical Information Service (NTIS), Springfield, VA. 22161

14. NO. OF PRINTED PAGES

(2) 581 pgs

15. Price

USCOMM-DC 6043-P80